Reference
NBS PUBLICATIONS
NAT'L INST. OF STAND & TECH
A11106 262749

NBSIR 83-2742 (R)

Photonuclear Data - Abstract Sheets 1955 - 1982 Volume VIII (Scandium - Manganese)

U.S. DEPARTMENT OF COMMERCE
National Bureau of Standards
National Measurement Laboratory
Center for Radiation Research
Gaithersburg, MD 20899

May 1985

U.S. DEPARTMENT OF COMMERCE
BUREAU OF STANDARDS

QC
100
.U56
83-2742
1985

NATIONAL BUREAU
OF STANDARDS
LIBRARY

NBSIR 83-2742

PHOTONUCLEAR DATA - ABSTRACT SHEETS 1955 - 1982 VOLUME VIII (SCANDIUM - MANGANESE)

E. G. Fuller, Henry Gerstenberg

U.S. DEPARTMENT OF COMMERCE
National Bureau of Standards
National Measurement Laboratory
Center for Radiation Research
Gaithersburg, MD 20899

May 1985

U.S. DEPARTMENT OF COMMERCE, Malcolm Baldrige, *Secretary*
NATIONAL BUREAU OF STANDARDS, Ernest Ambler, *Director*

TABLE OF CONTENTS

Table of Contents	i
Introduction	1
Scandium (A=41)	3
Scandium (A=43)	7
Scandium (A=45)	11
Scandium (A=47)	33
Scandium (A=49)	37
Titanium (Natural)	47
Titanium (A=44)	65
Titanium (A=46)	71
Titanium (A=47)	87
Titanium (A=48)	97
Titanium (A=49)	117
Titanium (A=50)	129
Titanium (A=52)	143
Vanadium (A=49)	145
Vanadium (A=51)	151
Chromium (Natural)	221
Chromium (A=50)	237
Chromium (A=52)	245
Chromium (A=53)	279
Manganese (A=51)	293
Manganese (A=53)	297
Manganese (A=55)	303
Manganese (A=56)	361

Iron (Natural) 365
Iron (A=54) 407
Iron (A=56) 431
Iron (A=57) 469
Iron (A=58) 481
Cobalt (A=55) 485
Cobalt (A=57) 497
Cobalt (A=58) 509
Cobalt (A=59) 513
Cobalt (A=60) 597
Definition of Abbreviations and Symbols 603

Photonuclear Data-Abstract Sheets
1955-1982

I. Introduction

As used in connection with this collection of data-abstract sheets, the term photonuclear data is taken to mean any data leading to information on the electromagnetic matrix element between the ground state and excited states of a given nuclide. The most common types of reactions included in this compilation are: (e,e'), (γ,γ), (γ,γ'), (γ,n), (γ,p), etc. as well as ground-state particle capture reactions, e.g. (α,γ_0). Two reactions which fit the matrix element criterion are not included in the compilation because of their rather special nature. These are heavy particle Coulomb excitation and the thermal neutron capture reaction (n,γ_0). While the energy region of particular interest extends from 0 to 150 MeV, papers are indexed which report measurements in the region from 150 MeV to 4 GeV. Most of the experiments listed are concerned with the excitation energy range from 8 to 30 MeV, the region of the photonuclear giant resonance.

The hierarchical grouping of the photonuclear data-abstract sheets within the file is by: 1. Target Element, 2. Target Isotope, and 3. by the Bibliographic Reference Code assigned to the paper from which the data on the sheet were abstracted. In this file, colored pages are used to mark the beginning and end of the sheets for each chemical element. A brief historical sketch of the element is given on the divider sheet marking the start of each section; the information for this sketch was derived from references such as the Encyclopaedia Britannica. In those cases where the sheets for a given element make up a major part of a volume, colored pages are also used to delineate sections pertaining to the individual isotopes of the element. Each of the sections of the file, as delineated by two colored divider sheets, represents a 27 year history of the study of electromagnetic interactions in either a specific nuclide or a specifc element.

The data-abstract sheets are filed under the element and/or isotope in which the ground-state electromagnetic transition takes place. For example, the abstract sheet for a total neutron yield measurement for a naturally occurring copper sample would appear in the elemental section of the copper file. On the other hand, a measurement of the ^{62}Cu 9.73 minute positron activity produced in the same sample by photons with energies below the three-neutron separation energy for ^{65}Cu (28.68 MeV) would be filed with the sheets for ^{63}Cu. Similarly a measurement of the ground-state neutron capture cross section in ^{12}C would be filed under ^{13}C while the corresponding ground-state alpha-particle capture cross section would be filed under ^{16}O.

At the end of this volume there is a master list of the abbreviations that have been used in the index section of the abstract sheets. The listings are those used in the final published index, Photonuclear Data Index, 1973-1981, NBSIR 82-2543, issued in August 1982 by the U. S. Department of Commerce, National Bureau of Standards, Washington, DC 20234. In some cases two notations are entered for the same quantity. The second entry is the abbreviation that was used in one or more of the earlier published editions of the index.

# SCANDIUM
Z=21

Scandium is a metallic element found mainly in rare ores of Scandinavia from which it derived its name. The oxide, scandia, was discovered by L. F. Nilson in 1879. The event was of great scientific interest because this and other compounds of scandium had properties as predicted by Mendel'eyev in 1869 for the derivatives of a hypothetical element ekaboron. This element was needed to fill a gap in the periodical classification of the chemical elements.

Sc
A=41

Sc
A=41

Ref. J.W. Butler
Phys. Rev. 123, 873 (1961)

Elem. Sym.	A	Z
Sc	41	21

Method: Van de Graaff; NaI for promt γ's; thin "pilot-B" plastic scintillator for $Sc^{41} \rightarrow Ca^{41}$ positrons

Ref. No.: 61 Bu 1 JHH

Reaction	E or ΔE	E_o	Γ	$\int \sigma dE$	Jπ	Notes
$Ca^{40}(p,\gamma)$	650±5kev	1.723± 0.011	< 5 kev	0.02 ev-barns		E_γ = 1.71 ± 0.03 MeV
	1550±15? kev	2.590 ±0.018	< 10? kev	0.03? ev-barns		
	1630±15? kev	2.669 ±0.018?	< 10? kev	0.03? ev-barns		
	1850±10 kev	2.883 ±0.014	< 10 kev	0.3 ev-barns		E_{γ_o} = 2.89±0.02 MeV.

Assuming 2.89 MeV γ is to ground state, Q-value for reaction $Ca^{40}(p,\gamma)Sc^{41}$ is calculated to be 1.09±0.02 MeV.

Question marks indicate doubtful assignment as Ca^{40} resonances.

Integrated cross sections $\int \sigma dE$ refer to (p,γ) rather than (γ,p).

REF.

R.L. Kozub, B.E. Cooke, J.R. Leslie, and B.C. Robertson
Phys. Rev. C 16, 132 (1977)

ELEM. SYM.	A	Z
Sc	41	21

METHOD

REF. NO.: 77 Ko 4 | hmg

REACTION	RESULT	EXCITATION ENERGY	SOURCE TYPE	SOURCE RANGE	DETECTOR TYPE	DETECTOR RANGE	ANGLE
$P,G	LFT	3,5	D	1,5	SCD-D		DST
		(2.883,5.037)		(1.84,4.05)			

Proton and γ-ray decay widths for the $7/2^-$ resonance at 2883 keV excitation in ^{41}Sc have been deduced from measurements of Γ_γ/Γ and the (p,γ) resonance strength. Our results are $\Gamma_\gamma = 0.058 \pm 0.007$ eV and $\Gamma = 0.090 \pm 0.011$ eV. Angular distributions measured for the 5037 $(9/2^-)$—2883 keV and 2883→0 $(7/2^-)$ keV transitions confirm the $J = 7/2$ assignment for the 2883-keV level. The linear polarization was measured for the 2883→0 keV transition and confirms the positive parity assignment. In addition, the (p,γ) strength for the 5037-keV level was measured, and our strength results for both resonances are lower than those of Youngblood, Wildenthal, and Class by a factor of 1.4.

Pol scat G's, 2.8MeV

TABLE II. Summary of angular distribution results and comparisons with other work.

E_p (keV)	E_i (keV)	E_f (keV)	E_γ[a] (keV)	$J_i^\pi \to J_f^\pi$	Normalized Legendre coefficients a_2	a_4	Mixing ratio δ	Branching ratio (%)	Ref.
4051.2 ± 1.4	5036.9 (R)	0	5036.9	$\frac{9^+}{2} \to \frac{7^-}{2}$	−0.285 ± 0.039	−0.031 ± 0.039	$-0.017^{+0.015}_{-0.008}$	72 ± 2	b
	5036.9 (R)	2883.1	2153.9	$\frac{9^+}{2} \to \frac{7^+}{2}$	−0.270 ± 0.042	−0.024 ± 0.043	$-0.017^{+0.297}_{-0.022}$	26 ± 2	b
	5036.9 (R)	3358.1	1678.8	$\frac{9^+}{2} \to (\frac{11^+}{2})$	−0.169 ± 0.179	0.066 ± 0.191		2.7 ± 0.5	b
	2883.1	0	2883.1	$\frac{7^+}{2} \to \frac{7^-}{2}$	0.467 ± 0.054	0.017 ± 0.064	$-0.035^{+0.072}_{-0.035}$	100	b, c
	5036 (R)	0	5036	$\frac{9^+}{2} \to \frac{7^-}{2}$	−0.215 ± 0.021	−0.069 ± 0.025	(−)0.035		d
1643.1 ± 1.0	2883.1 (R)	0	2883.1	$\frac{7^+}{2} \to \frac{7^-}{2}$	0.517 ± 0.034	−0.060 ± 0.046	$-0.052^{+0.043}_{-0.030}$	100	b
	2879 (R)	0	2879	$\frac{7^+}{2} \to \frac{7^-}{2}$	0.507 ± 0.023	−0.025 ± 0.031	(−)0.035		d
	2882.1 (R)	0	2882.1	$\frac{7^+}{2} \to \frac{7^-}{2}$	0.498 ± 0.034	0.008 ± 0.040	$-0.28^{+0.47}_{-0.30}$	100	e

[a] Results from the present work have ±0.5 keV uncertainty.
[b] Present work.
[c] Primary mixing ratio was taken to be −0.017.
[d] See Ref. 2.
[e] See Ref. 16.

[2] D.H. Youngblood, B.H. Wildenthal, and C.M. Class, Phys. Rev. 169, 859 (1968)

[16] B. Rabin, Ph.D. thesis, Strasbourg-1 University, 1973 (unpublished)

Sc
A=43

Sc
A=43

Sc
A=43

REF. A. E. Vlieks, C. W. Cheng and J. D. King
Nucl. Phys. A309, 506 (1978)

ELEM. SYM.	A	Z
Sc	43	21

METHOD

REF. NO. 78 V1 2 rs

REACTION	RESULT	EXCITATION ENERGY	SOURCE		DETECTOR		ANGLE
			TYPE	RANGE	TYPE	RANGE	
P,G	ABX	6- 11	D	1- 6	NAI-D		4PI

Abstract: The cross section for the $^{42}Ca(p,\gamma)^{43}Sc$ reaction has been measured over the lab energy range from 0.7 to 5.5 MeV using a positron spectrometer to measure the annihilation radiation from the decay of 3.9 h ^{43}Sc. Stellar reaction rates $N_A\langle\sigma v\rangle$ have been calculated from the experimental cross section curve for a series of three temperatures of interest for explosive oxygen and silicon burning in stars. The calculated rates are compared with the theoretical predictions of Woosley *et al.* and found to be in agreement within the experimental errors and the quoted validity of the theoretical calculation.

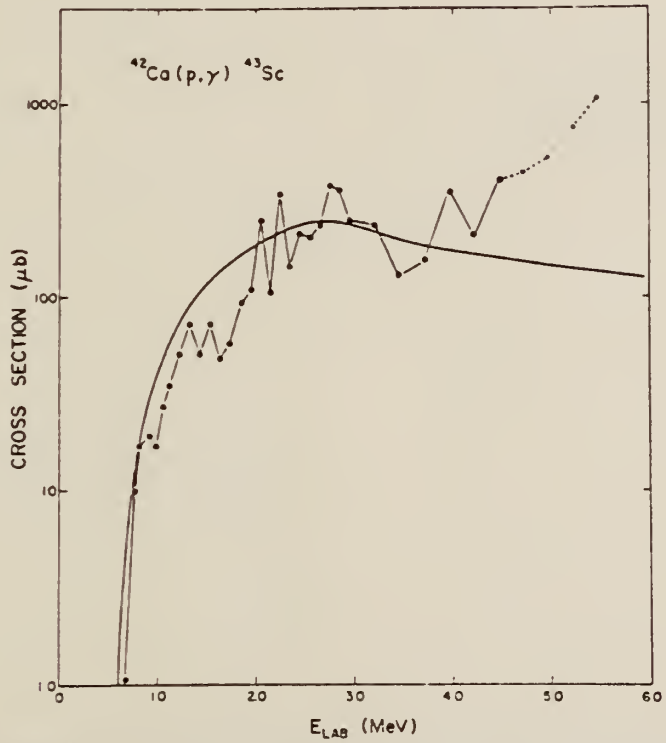

Fig. 1 The cross section for the $^{42}Ca(p,\gamma)^{43}Sc$ reaction. The solid curve is the calculated cross section from ref. [4]) as estimated from a graph. The magnitude of the cross section is somewhat uncertain above 4.5 MeV due to contributions to the observed yield from the $^{44}Ca(p,n)$ reaction.

[4]S. E. Woosley, W. A. Fowler, J. A. Holmes and B. A. Zimmerman, Caltech preprint OAP422 (1975)

Sc
A=45

Sc
A=45

REF.

J. R. Tatarczuk and H. A. Medicus
Phys. Rev. 143, B818 (1966)

ELEM. SYM.	A	Z
Sc	45	21

METHOD

Bremsstrahlung from Linac

REF. NO.	
66 Ta 1	JDM

REACTION	RESULT	EXCITATION ENERGY	SOURCE		DETECTOR		ANGLE
			TYPE	RANGE	TYPE	RANGE	
G,N	RLY	THR - 48	C	24-48	ACT-I		4PI

Level density $\rho(J) = \rho(0)(2J + 1) \exp [-(J + \frac{1}{2})^2 / 2\sigma^2]$
Measured relative yield to g.s. and .27 MeV isomer.

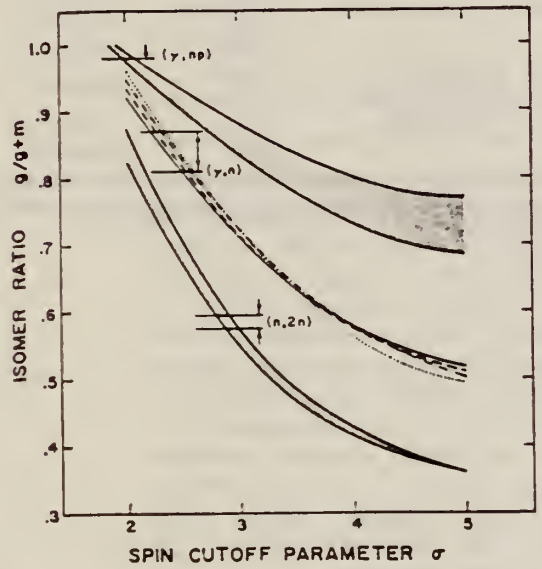

FIG. 6. Calculated isomer ratios versus spin cutoff parameter σ. The top shaded area shows typical calculated results as a function of σ for the (γ,np) reaction. The horizontal line at $g/(g+m) = 0.98$ is the experimental value. The bottom area shows results obtained for the $(n,2n)$ reaction with the two horizontal lines indicating the experimental result. The middle set of curves are results for the (γ,n) reaction. Each line corresponds to a different assumption which is given in the text.

TABLE I. Isomer ratios for ^{44}Sc, ground-state yield/total yield $g/(g+m)$.

	Reaction		
	^{45}Sc(γ,n)	^{46}Ti(γ,np)	^{45}Sc$(n,2n)$
Bremsstrahlung endpoint energy (MeV)			
24	0.86±0.02		
36	0.84±0.02		
48	0.84±0.03	>0.98	
X-radiation energy range (MeV)			
Threshold-24	0.86±0.02		
24–36	0.79±0.13		
36–48	0.84±0.40		
Neutron energy 13.9 MeV			
From measurement of the 1.16-MeV γ line			0.581±0.025
From measurement of the annihilation radiation			0.586±0.[illegible]

W. B. Walters and J. P. Hummel
Phys. Rev. 150, 867 (1966)

Sc	45	21

METHOD

Betatron

REF. NO. 66 Wa 1 JDM

REACTION	RESULT	EXCITATION ENERGY	SOURCE		DETECTOR		ANGLE
			TYPE	RANGE	TYPE	RANGE	
G,N	RLY	THR-300	C	50-300	ACT-I		4PI

Measured isomeric yield ratios.

TABLE II. Summary of the results for the photoproduction of the Sc^{44} isomers (spins 2 and 6).

Target isotope and spin	Bremsstrahlung energy (MeV)	Fraction of yield to high-spin isomer
Sc^{45} ($I=\frac{7}{2}$)	50	0.21±0.04
	75	0.21±0.03
	175	0.20±0.02
	223	0.18±0.01
	264	0.17±0.02
	300	0.21±0.02
$Fe^{54,56}$ ($I=0$)[a]	250	0.38±0.02
Mn^{55} ($I=\frac{5}{2}$)	225	0.42±0.04
	300	0.39±0.02

[a] It is assumed that most of the yield is due to reactions involving the two lightest isotopes present in natural iron (Fe^{54} and Fe^{56}).

H. Bernatowicz and H. A. Medicus
PICNS-67 Contributions, International Conference on Nuclear Structure, Tokyo, Japan 1967 (Institute for Nuclear Study, University of Tokyo, Tanashi-shi, Tokyo, Japan) 10.20, p. 384

ELEM. SYM.	A	Z
Sc	45	21

METHOD

REF. NO. 67 Be 8 EGF

REACTION	RESULT	EXCITATION ENERGY	SOURCE TYPE	SOURCE RANGE	DETECTOR TYPE	DETECTOR RANGE	ANGLE
G,N	ABY	11-48	C	48	ACT-I		4PI
G,2N	ABY	21-48	C	48	ACT-I		4PI
G,2P	ABY	19-48	C	48	ACT-I		4PI

Photonuclear Reactions with Emission of Several Nucleons

H. Bernatowicz and H. A. Medicus
Rensselaer Polytechnic Institute, Troy, N.Y., U.S.A.

Photonuclear reactions were induced on scandium and vanadium by bremsstrahlung at the Rensselaer Electron Linac. The activity of the residual nuclei was measured. The approximate energy dependence of the photonuclear reactions was either estimated by rough application of the photon difference method or calculated. This permitted determination of integrated cross sections by comparison with the activity of a beam monitor with known cross section.

Competing reactions, especially those involving emission of more than one particle, are a sensitive test of evaporation theory. Detailed calculations were therefore performed using various level density formulas. The Fermi gas formula, $\rho \sim e^{2\sqrt{aU}}/U^{5/4}$, (where $a = A/8$ Mev^{-1} and U is the excitation energy minus pairing energy), Weisskopf's formula, $\rho \sim e^{2\sqrt{aU}}$, and the constant temperature formula $\rho \sim e^{(E - E_0)/T}$ were tried. Corrections to the Fermi gas formula for shell effects have been made by Newton[1] and by Gilbert and Cameron[2]. Gilbert and Cameron also proposed a composite formula which joins the Fermi gas expression smoothly to a constant temperature formula below 8 Mev. The calculated integrated cross sections using these formulas were found to differ by as much as several orders of magnitude. The composite formula with Gilbert and Cameron's parameters gave the best overall agreement with our experimental data. The composite formula results with optical model inverse cross sections[3] and giant resonance data from Fultz, et al.,[4] are given in the table. Results using the constant temperature, Fermi gas, and Fermi gas formula with shell corrections by Newton have been included in one case. Integrated cross sections are in Mev-mb.

Target	End Point	Results	(γ,n)	(γ,2n)	(γ,3n)	(γ,2p)	(γ,α)	(γ,Cm)
^{45}Sc	48 Mev	Composite	310	78		2.0×10^{-1}		
		Experiment	430 ± 70	68 ± 12		3.0 ± 0.8		
^{51}V	37 Mev	Composite		140	1.4	6.3×10^{-1}	3.1	1.6
		Constant T		99	2.0	3.8	1.3	0.37
		Fermi Gas		97	1.3	3.5×10^{-2}	1.0	30
		Newton		101	2.1	3.2×10^{-3}	0.44	8.6
		Experiment		124 ± 35	2.5 ± 0.5	$(2.4 \pm 0.5) \times 10^{-1}$	7.1 ± 1.5	3.0 ± 2.
^{51}V	29 Mev	Composite		106		4.9 ± 10^{-2}	2.9	
		Experiment		115 ± 30		$(1.7 \pm 0.3) \times 10^{-2}$	6.8 ± 1.4	
^{51}V	25 Mev	Composite		60		3.0 ± 10^{-4}	2.4	
		Experiment		62 ± 12		$(2.6 \pm 0.3) \times 10^{-4}$	4.9 ± 1.2	

When the parameters of Newton were used in a composite level density formula agreement improved but remained significantly poorer than obtained with Gilbert and Cameron's parameters. The large disparity found in the ^{45}Sc(γ,2p) result would be eliminated by a 15 percent increase in the level density parameter of ^{44}Ca which has a closed proton shell. Our work indicates that this type of experiment can be of significant value in the study of nuclear level densities.

References: 1. Newton, T. D. Can. J. Phys. 34, 804 (1956).
2. Gilbert, A. and Cameron, A. G. W. Can. J. Phys. 43, 1449 (1965).
3. Maldner, H. and Lindner, A. Z. Physik 180, 362 (1964).
4. Fultz, S. C., Bramblett, R. L., Caldwell, J. T., Hansen, N. E., and Jupiter, C. P. Phys. Rev. 128, 2345 (1962).

FORM NBS-418 (REV. 7-14-64) USCOMM-DC 26010-P64
PARTMENT OF COMMERCE - BUREAU OF STANDARDS

REF. R. G. Arnold, E. C. Booth, and W. J. Alston, III
Phys. Rev. C7, 1490 (1973)

ELEM. SYM.	A	Z
Sc	45	21

METHOD

REF. NO. 73 Ar 1 hmg

REACTION	RESULT	EXCITATION ENERGY	SOURCE TYPE	SOURCE RANGE	DETECTOR TYPE	DETECTOR RANGE	ANGLE
G,G	LFT	0-. 3	C	0- 3	SCD-D		125

13 LEVELS

Absolute values come from normalizing to know total widths. $\overline{W}$ is angular distribution factor to correct for difference in unknown and standard distribution. Assumed = 1 to get Γ_o values.

TABLE II. $M1$ strengths and mixing ratios in ^{45}Sc.

Level energy (keV)	$B(E2)\uparrow$ Previous work (e^2 fm^4)	$g\Gamma_0(E2)$ [a] (meV)	$g\Gamma_0(M1+E2)$ This work (meV)	δ^2 Deduced	$g\Gamma_0(M1)$ Deduced (meV)	$\Gamma_0(M1)/\Gamma_W(M1)$ [b]
720	72(10) [c]	0.0113(16)	1.58(16)	0.0072(13)	1.57(16)	0.27
1237	154(21) [c]	0.36(5)	0.38(2)	>4.0	<0.08	...
1663	69(21) [d]	0.71(21)	3.87(41)	0.22(7)	3.16(45)	0.033 [e]

[a] Derived from column 2.
[b] Transition strength in W.u.
[c] Average of values listed in Table 1 of Ref. 3 plus results from Ref. 2 with the results of M. D. Goldberg and B. W. Hooton, Nucl. Phys. A132, 369 (1969) omitted from the average.
[d] R. J. Peterson and D. M. Perlman, Nucl. Phye. A117, 185 (1968). Estimated 30% uncertainty not explicitly given by the authors.
[e] Assuming g=1.0.

[1] M.B. Lewis, Nucl. Data B4(Nos.3,4) 237 (1970).
[2] P. Blasi et al., Nuovo Cimento 68, 49 (1970).
[3] D.A. Eastham et al., Nucl. Phys. A146, 112 (1970).

(over)

TABLE I. ^{45}Sc levels and results.

Level energy [a] (keV)	$J\pi$ [a]	E_γ This work (keV)	Γ_0/Γ or Γ_1/Γ	$g\overline{W}\Gamma_0\Gamma_0/\Gamma$ This work (meV)	Γ_0 Deduced (meV)
g.s.	$\frac{7}{2}^-$	...			
12.4(2)	$\frac{3}{2}^+$	...	1.0 [b]	c	...
376.7(6) [d]	$\frac{5}{2}^-$	...	0.92 [d]	c	...
543.1(6) [d]	$\frac{1}{2}^+$	531(2) [e]	0.58(1) [d, e]	0.019(4) [e]	...
		543(2)	0.42(1) [d]	0.011(3)	0.039(8)
720.5(5) [d]	$\frac{5}{2}^-$	720(1)	1.0 [b]	1.58(16)	2.11(21)
939.1(9) [d]	$\frac{1}{2}^+$	...	0.0	...	...
974.3(7) [d]	$\frac{3}{2}^+$ [d]	962(2) [e]	0.32(1) [d, e]	0.062(9) [e]	...
		974(2)	0.58(1) [d]	0.08(1)	0.17(3)
1068.4(10) [d]	$\frac{3}{2}^-$	...	0.0 [d]	...	...
1237.4(9) [d]	$(\frac{1}{2})^-$ [f]	1237(2)	1.0 [d]	0.38(2)	0.58(3)
1409.0(10) [d]	$(\frac{3}{2})^-$ [d]	1409(1)	0.91(4) [d]	1.36(11)	1.87(16)
1433.5(10) [d]	$(\frac{1}{2})^+$ [d]	...	0.10(2) [d]	<0.2	...
1474(3)	...	...	...	<0.2	...
1557(3)	$(\frac{1}{2}, \frac{3}{2})^-$	...	0.0 [b]	<0.2	...
1661.8(7) [d]	$(\frac{5}{2}-\frac{9}{2})^-$ [d]	1663(2)	0.83(4) [d]	3.2(3)	3.9(4) g^{-1}
1799(5)	...	1798(2)	0.23(3) [g]	0.22(5)	0.94(21) g^{-1}
1897(5)	...	...	1.0 [g]	<1.0	...
1936(5)	...	...	...	c	...
2031.0(10) [d]	$(\frac{11}{2})^+$ [d]	...	...	<0.5	...
2095(5)	...	2093(2)	0.78(12) [g]	47(2)	60(9) g^{-1}
2106(5)	...	...	...	<0.5	...
2223(5)	...	...	...	<0.5	...
2291(5)	...	2291(3)	...	1.28(8)	...
2303(5)	...	...	0.0 [g]	<0.5	...
2341(5)	$(\frac{3}{2})^-$ [f]	2341(2)	...	16(1)	...
2351(5)	...	...	0.02 [b, h]	<0.5	...
2531(5)	...	...	0.0	<2	...
2562(5)	...	...	...	<2	...
2590(5)	...	2592(2)	0.64(9) [g]	8.9(5)	14(2) g^{-1}

[a] Except where noted Ref. 1.
[b] Reference 1.
[c] No data taken for these levels.
[d] Reference 2.
[e] Branch to the first excited state. Transition strength in column 5 is $g\overline{W}\Gamma_0\Gamma_1/\Gamma$.
[f] See discussion in the text.
[g] Private communication from J. C. Manthuruthil of preliminary results related to work reported in Ref. 4. He estimates 10 to 20% uncertainty in branching ratios.
[h] Manthuruthil (see footnote d) reports a level at 2355 ± 2 keV with $\Gamma_0/\Gamma = 0.63$ which may be the same as the level at 2351.

REF. M. Eriksson and G. G. Jonsson
PICNS-73, Vol.II, p.995 (1973) Asilomar

ELEM. SYM.	A	Z
Sc	45	21

METHOD

REF. NO. 73 Er 1 egf

REACTION	RESULT	EXCITATION ENERGY	SOURCE TYPE	SOURCE RANGE	DETECTOR TYPE	DETECTOR RANGE	ANGLE
G,N	NOX	0-800	C	100-800	ACT-I		4PI

SC-44 ISOMER RATIO

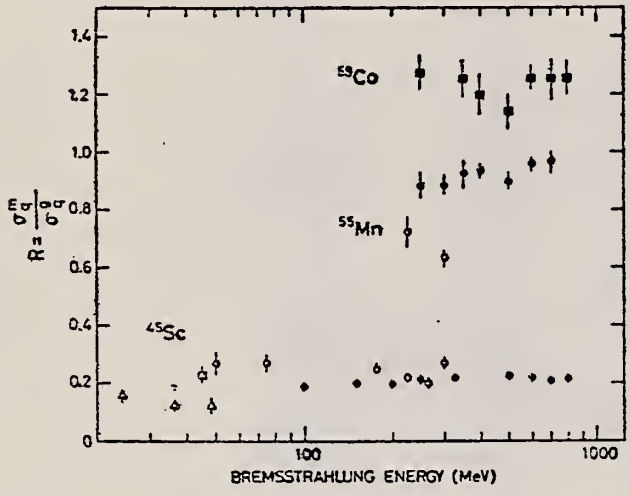

Isomeric yield ratio, $^{44}Sc^{m}(6+)/^{44}Sc^{g}(2+)$, versus bremsstrahlung end point energy.
●, ■ this work, Δ ref 1, O ref 2, □ ref 3.

[1] J.R. Tatarczuk and H.A. Medicus, Phys. Rev. 143 (1966) 818.
[2] W.B. Walters and J.P. Hummel, Phys. Rev. 150 (1966) 867.
[3] R. Völpel, Nucl. Phys. A182 (1972) 311.

REF. R.H. Sambell and B.M. Spicer
Nucl. Phys. A205, 139 (1973)

ELEM. SYM.	A	Z
Sc	45	21

METHOD

REF. NO. 73 Sa 5 egf

REACTION	RESULT	EXCITATION ENERGY	SOURCE TYPE	SOURCE RANGE	DETECTOR TYPE	DETECTOR RANGE	ANGLE
G,XN	ABX	10- 25	C	10- 25	BF3-I		4PI

589

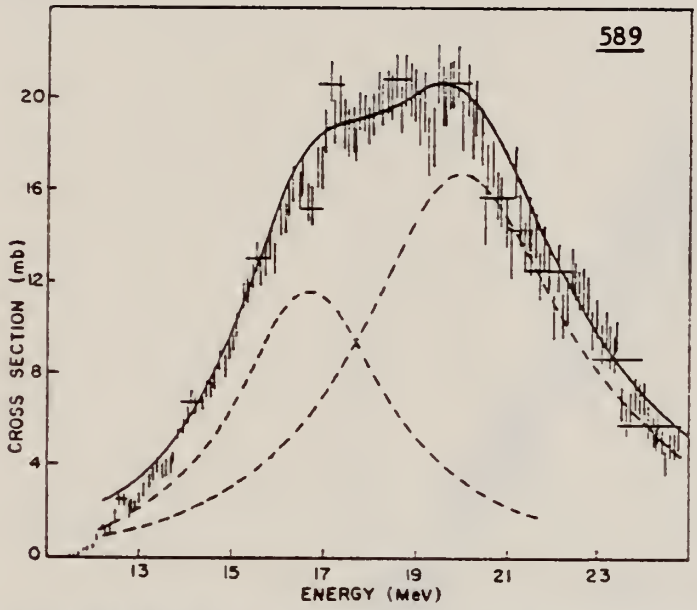

Fig. 1. The total photoneutron cross section $\sigma(\gamma, n)+\sigma(\gamma, np)+\sigma(\gamma, 2n)$ for ^{45}Sc. The horizontal bars indicate the resolution width. The smooth curve represents the Danos model fit which is the sum of the two dashed Lorentz curves.

Yields corrected by using statistical model with 20% direct reactions assumed.

TABLE I

Integrated cross section and moments from threshold to 25 MeV

σ_0 (mb · MeV)	σ_{-1} (mb)	σ_{-2} (mb · MeV^{-1})
158±24	8.4±1.3	0.46±0.07

$$\sigma_a = \int_{thres}^{25\ MeV} \sigma E^{-a} dE.$$

REF. R. H. Sambell and B. M. Spicer
PICNS-73, Vol. I, p. 541 Asilomar

ELEM. SYM.	A	Z
Sc	45	21

METHOD

REF. NO.	
73 Sa 8	hmg

REACTION	RESULT	EXCITATION ENERGY	SOURCE		DETECTOR		ANGLE
			TYPE	RANGE	TYPE	RANGE	
G,XN	ABX	11- 25	C	11- 25	BF3-I		4PI

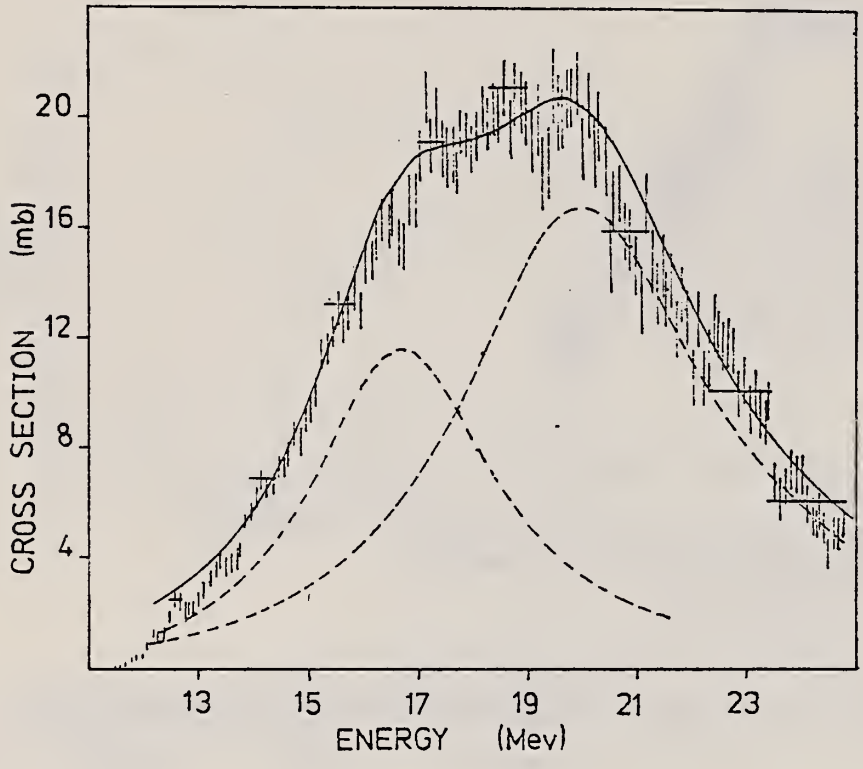

The total photoneutron cross section $\sigma(\gamma,n) + \sigma(\gamma,np) + \sigma(\gamma,2n)$ for ^{45}Sc. The horizontal bars indicate the resolution width. The smooth curve represents the Danos model fit which is the sum of the two dashed Lorentz curves.

A. Veyssiere, H. Beil, R. Bergere, P. Carlos, A. Lepretre, and A. De Miniac
Nucl. Phys. A227, 513 (1974)

ELEM. SYM.	A	Z
Sc	45	21

METHOD

REF. NO.: 74 Ve 1 | egf

REACTION	RESULT	EXCITATION ENERGY	SOURCE TYPE	SOURCE RANGE	DETECTOR TYPE	DETECTOR RANGE	ANGLE
* G,N	ABX	11- 28	D	11- 28	BF3-I		4PI
** G,2N	ABX	21- 28	D	21- 28	BF3-I		4PI

* 906+
** 907

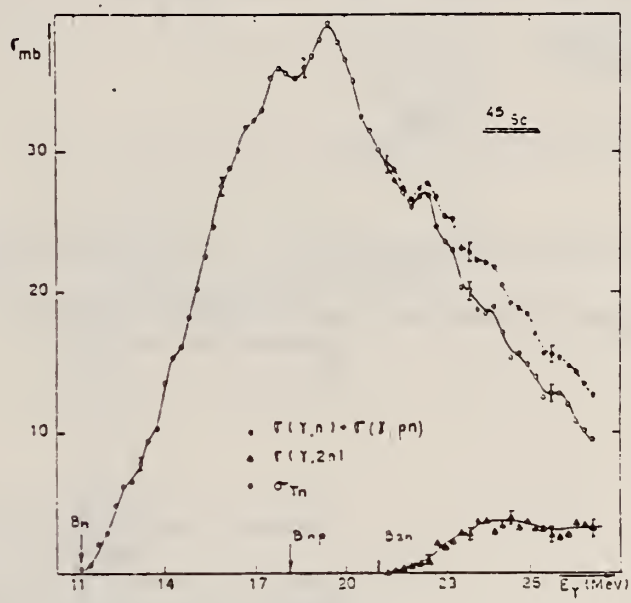

Fig. 13. Photoneutron cross sections σ_{Tn}, $[\sigma(\gamma, n)+\sigma(\gamma, 2n)]$ and $\sigma(\gamma, 2n)$ of ^{45}Sc.

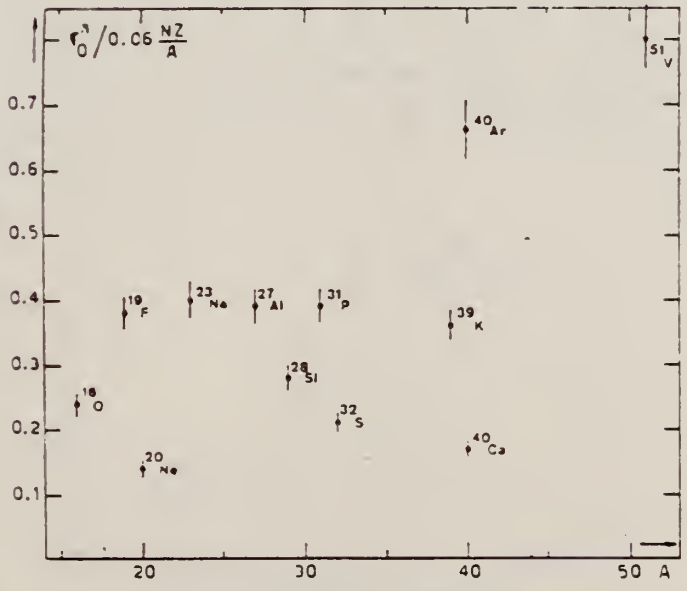

Fig. 22. Ratio of experimental integrated photoneutron cross section σ_0^n over the Thomas, Reiche and Kuhn sum rule $[0.06\,NZ/A]$. Numerical values and upper integration limits E_M are taken from table 3. Also $\Delta\sigma_0^n = \pm 7\%$ for all nuclei.

(over)

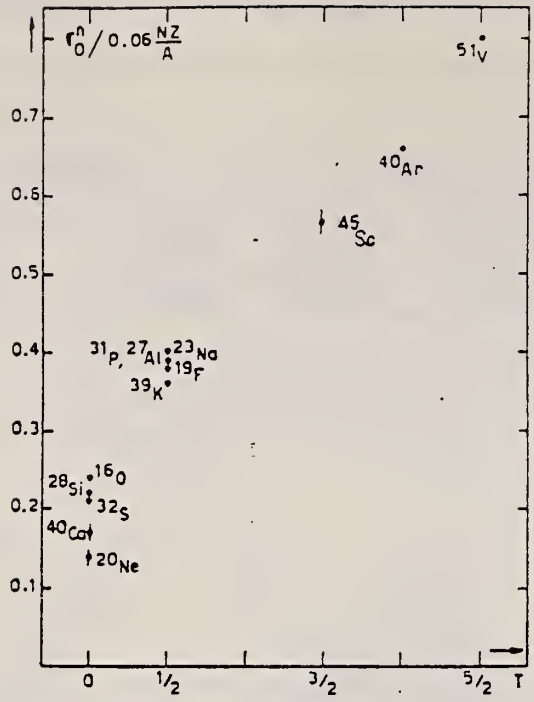

Fig. 24. The $[\sigma_0^n/(0.06\,NZ/A)]$ ratio as a function of isospin T. Possible overall errors of ± 7% are to be applied to all nuclei shown.

TABLE 3

Experimental integrated photoneutron cross sections $\sigma_0^n = \int_0^{E_M} \sigma_{Tn}(E)\mathrm{d}E$ compared with the classical sum rule [0.06 NZ/A] of Thomas, Reich and Kuhn

	$T = 0$					$T = \frac{1}{2}$					$T = \frac{3}{2}$	$T = 2$	$T = \frac{5}{2}$
Nucleus	^{16}O	^{20}Ne	^{28}Si	^{32}S	^{40}Ca	^{19}F	^{23}Na	^{27}Al	^{31}P	^{39}K	^{45}Sc	^{40}Ar	^{51}V
σ_0^n (MeV · mb)	58 ±4	42 ±3	94 ±7	98 ±7	100 ±7	108 ±7	137 ±9	158 ±10	182 ±12	210 ±14	383 ±25	393 ±28	602 ±42
$\sigma_0^n/(0.06NZ/A)$	0.24	0.14	0.22	0.21	0.17	0.38	0.40	0.39	0.39	0.36	0.57	0.66	0.3
E_M (MeV)	30	26.7	30	30	29.5	29	30	30	29	30	28.1	26.7	28

REF. M. Eriksson and G. G. Jonsson
Nucl. Phys. A242, 507 (1975)

ELEM. SYM.	A	Z
Sc	45	21

METHOD

REF. NO. 75 Er 2 egf

REACTION	RESULT	EXCITATION ENERGY	SOURCE		DETECTOR		ANGLE
			TYPE	RANGE	TYPE	RANGE	
G,N	ABY	THR-800	C	100-800	ACT-I		4PI

ISOMER RATIO

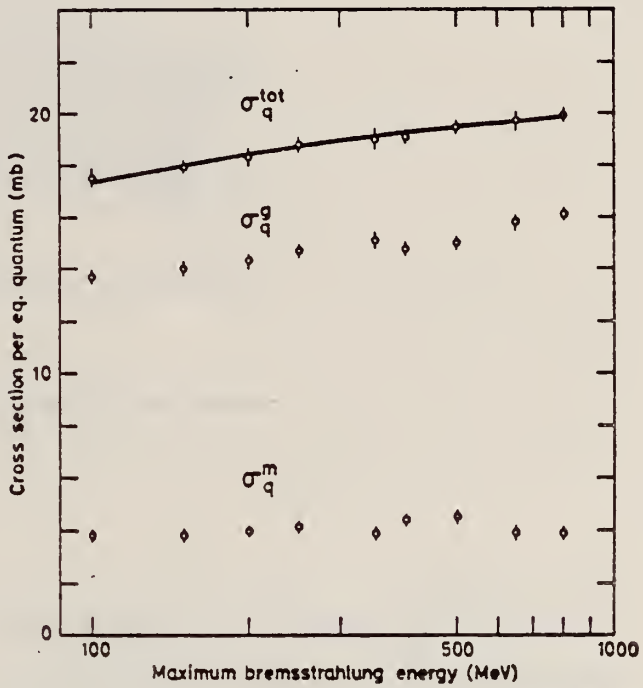

Fig. 2. Yield curves for the reactions $^{45}Sc(\gamma, n)^{44g}Sc$, $^{45}Sc(\gamma, n)^{44m}Sc$ and $^{45}Sc(\gamma, n)^{44}Sc$. The solid curve shows the result calculated from giant resonance data plus the contribution from pion production processes.

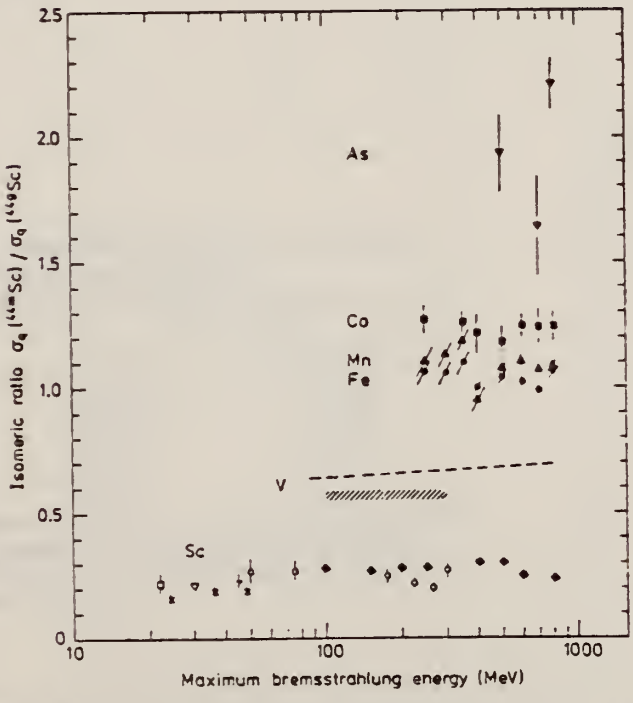

Fig. 6. Isomeric ratio $\sigma_q(^{44m}Sc)/\sigma_q(^{44g}Sc)$ versus bremsstrahlung end-point energy for the different targets. Sc target: ◆ – this work, □ – ref. [15]), × – ref. [16]), ▽ – ref. [17]), + – ref. [18]), ○ – ref. [19]); V target: dashed curve – ref. [20]), dashed area – ref. [21]); Fe target: ● – this work; Mn target: ▲ – this work; Co target: ■ – this work; As target: ▼ – this work.

(over)

TABLE 2

Comparison between experimental and calculated cross sections and isomeric ratios

Target	$\bar{\sigma}_{exp}$ (mb) 250–800 MeV	σ_{MC} (mb) 400 MeV	$\bar{\sigma}_{SE}$ (mb) 250–800 MeV	$\sigma(m)/\sigma(g)_{exp}$ 250–800 MeV	$\sigma(m)/\sigma(g)_{calc}$ 400 MeV
^{45}Sc	≈ 0.5	0.58 ± 0.05		≈ 0	0.05
^{51}V	≈ 0.5	0.48 ± 0.05	0.47	0.7	0.72
^{55}Mn	0.40 ± 0.14	0.59 ± 0.05	0.28	1.08 ± 0.04	1.04
Fe	0.40 ± 0.14		0.26	1.00 ± 0.05	
^{59}Co	0.26 ± 0.10	0.34 ± 0.04 0.65 ± 0.07 [a])	0.18	1.26 ± 0.06	1.12 1.15 [a])
^{75}As		0.01 ± 0.01	0.044	1.9 ± 0.3	

[a]) 325 MeV.

15) S. A. Steinberg, B. Sc. thesis, Univ. of Illinois, 1963, unpublished (value taken from ref. [19]))
16) J. R. Tatarczuk and H. A. Medicus, Phys. Rev. 143 (1966) 818
17) T. Kato and Y. Oka, Talanta 19 (1972) 515
18) R. Völpel, Nucl. Phys. A182 (1972) 411
19) W. B. Walters and J. P. Hummel, Phys. Rev. 150 (1966) 867
20) B. Bülow, Lund, private communication (preliminary results)
21) R. A. Meyer, thesis, Univ. of Illinois, 1963, unpublished

REF. F. R. Metzger
Phys. Rev. C12, 312 (1975)

ELEM. SYM.	A	Z
Sc	45	21

METHOD

REF. NO. 75 Me 4 hmg

REACTION	RESULT	EXCITATION ENERGY	SOURCE TYPE	SOURCE RANGE	DETECTOR TYPE	DETECTOR RANGE	ANGLE
G,G	LFT	1- 3	C	0- 3	SCD-D		DST
		(.72-2.092)		(.8-2.2)			

5 LEVELS .72-2.09 MEV

TABLE II. Comparison of the mean lifetimes determined in the resonance fluorescence experiments with the results of the Doppler shift attenuation measurements.

E_{level} (keV)	$I_{exc.}$	Γ_0/Γ	Res. Fl.	Mean lifetimes (fs) DSAM (Ref. 1)	DSAM (Ref. 2)
720	$\frac{5}{2}^{-}$ [a]	1.00	320 ± 30	···	220 ± 60
1237	$\frac{11}{2}^{-}$ [b]	1.00	2630 ± 200	···	1100 ± 200
1409	$\frac{7}{2}^{-}$ [c]	0.89	400 ± 30	< 170 [e]	600 ± 300
1662	$\frac{9}{2}^{-}$ [b]	0.74	151 ± 13	···	110 ± 30
2092	$\frac{5}{2}^{-}$ [d]	0.83	8 ± 1	12 ± 3	···

[a] Reference 5.
[b] References 5, 6.
[c] References 3, 5.
[d] References 7–9.
[e] This value differs from the limit given in the abstract of Ref. 1; it takes into account the error quoted in Table I of Ref. 1.

TABLE I. Comparison of the results of the nuclear resonance fluorescence experiments.

E_{level} (keV)	$g\Gamma_0^2/\Gamma$ (meV) Ref. 2	Present work
720	1.58 ± 0.16	1.50 ± 0.20
1237	0.38 ± 0.02 [a]	0.35 ± 0.07
1409	1.36 ± 0.11 [a]	1.27 ± 0.12
1663	3.2 ± 0.3	2.8 ± 0.3
2095	47 ± 2	40 ± 4

[a] The Γ_0's deduced in Table I of Ref. 2 from the $g\Gamma_0^2/\Gamma$ values are incorrect. The authors apparently multiplied by g instead of dividing by g.

1 R.L. Schulte et al., Phys. Rev. C9, 1436 (1974).
2 R.G. Arnold et al., Phys. Rev. C7, 1490 (1973).
3 N.J.A. Rust et al., Nucl. Phys. A219, 232 (1974).
5 W.M. Zuk et al., Aust. J. Phys. 24, 13 (1971).
6 Z.P. Sawa et al., Nucl. Phys. A205, 257 (1973).
7 G. Bergdolt et al., Nucl. Phys. A211, 486 (1973).
8 R.L. Schulte et al., Can. J. Phys. 52, 131 (1974).
9 G. Hardie et al., Phys. Rev. C10, 1829 (1974).

REF.

C. O. Wene
Z. Phys. A272, 77 (1975)

ELEM. SYM.	A	Z
Sc	45	21

METHOD

REF. NO. 75 We 4 egf

REACTION	RESULT	EXCITATION ENERGY	SOURCE		DETECTOR		ANGLE
			TYPE	RANGE	TYPE	RANGE	
G,P	ABX	18	D	18	SCD-D		90

18 = 17.6 MEV

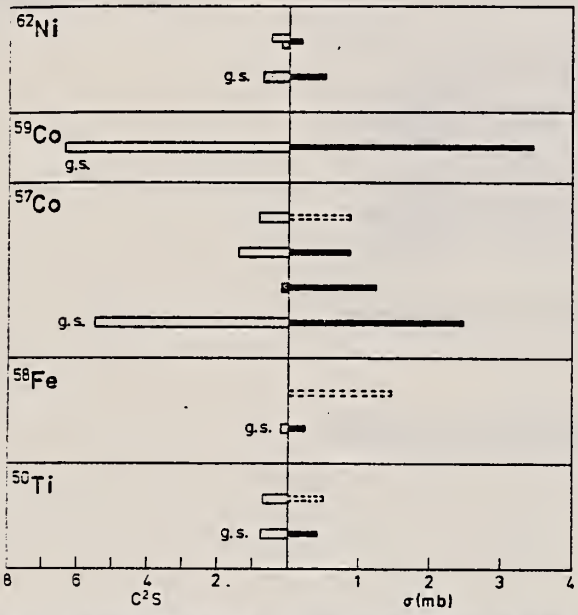

Fig. 5. Correlation between the spectroscopic factors and the cross-sections measured in this work. Open staples indicate $\ell_p = 3$ pick-up and cross hatched staples $\ell_p = 1$ pick-up. Dashed staples indicate that the cross section is uncertain due to the subtraction of a large back-ground

Table 2

Daughter nucleus	Level (MeV)	J^π	σ^a (mb)
^{44}Ca	0	0^+	$\leqq 0.2^b$
	1.16	2^+	$\leqq 0.5^b$
^{50}Ti	0	0^+	0.41 ± 0.05
	2.68	4^+	$(0.5)^c$
^{58}Fe	0	0^+	0.23 ± 0.08
	3.24?	0^+?	$(1.5)^c$
^{57}Co	0	$7/2^-$	2.5 ± 0.2^d
	1.76	$3/2^-$	1.2 ± 0.3
	1.90	$7/2^-$	0.9 ± 0.2
	2.31	$7/2^-$	$(0.9)^c$
^{59}Co	0	$7/2^-$	3.5 ± 0.8
^{62}Ni	0	0^+	0.51 ± 0.09
	1.18	2^+	0.2 ± 0.1

[a] The quoted errors are only those due to counting statistics.
[b] Confidence level 95%.
[c] Uncertain because of large background.
[d] $\sigma = 2.4$ mb from [43].

43. Miyase, H., Oikawa, S., Suzuki, A., Uegaki, J., Saito, T., Sugawara, M., Shoda, K.: The photoproton reactions of Ni-isotopes. In: Proc. Int. Conf. Photonuclear Reactions and Applications, Vol. I, p. 553. Livermore, USA 1973 (see Ref. 13)

REF.		ELEM. SYM.	A	Z
	N. M. Bachschi, P. David, J. Debrus, F. Lubke, H. Mommsen, R. Schoenmackers, G. G. Jonsson, K. Lindgren Nucl. Phys. A264, 493 (1976)	Sc	45	21

METHOD	REF. NO.	
	76 Ba 7	egf

REACTION	RESULT	EXCITATION ENERGY	SOURCE		DETECTOR		ANGLE
			TYPE	RANGE	TYPE	RANGE	
G,JPKN	ABY	THR* 2	C	* 2	ACT-I		4PI

*GEV,J=1-10,K=1-19

Abstract: Yields and isomeric yield ratios of nuclei produced in the irradiation of ^{45}Sc and ^{nat}Cu with bremsstrahlung of E_γ^{max} = 2 GeV have been measured by the activation method. The experimental yields are compared to predictions with a Rudstam formula modified to photonuclear reactions.

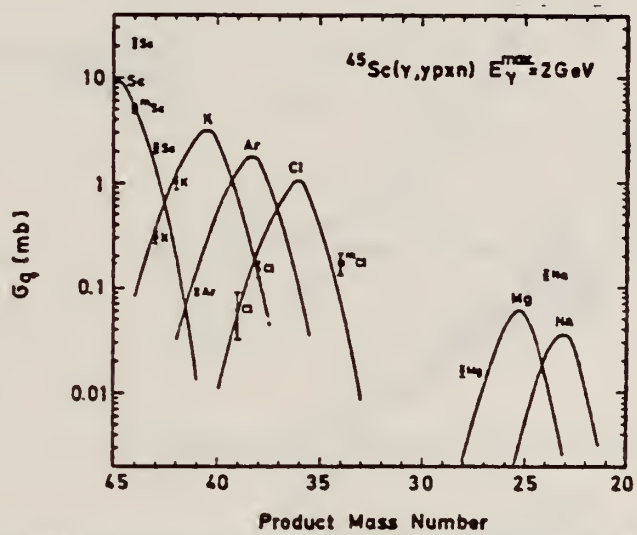

Fig. 1. Yields of nuclei produced in the irradiation of ^{45}Sc with bremsstrahlung of E_γ^{max} = 2 GeV. The curves are calculated with eq. (1).

TABLE 1

Cross section and isomeric ratios

Target	σ_q (ground state)	σ_q (isomer)	$\frac{\sigma_q^{(m)}}{\sigma_q^{(g)}}$
^{45}Sc	^{44g}Sc (2$^+$): 21.4 ± 1.8 mb	^{44m}Sc (6$^+$): 5.08 ± 0.50 mb	0.24 ± 0.03
^{nat}Cu	^{52g}Mn(6$^+$): 250 ± 25 μb	^{52m}Mn(2$^-$): 63 ± 8 μb	0.25 ± 0.04
^{nat}Cu	^{44g}Sc (2$^+$): 66.5 ± 6.8 μb	^{44m}Sc (6$^+$): 129 ± 13 μb	1.9 ± 0.3

REF. S. Oikawa and K. Shoda
Nucl. Phys. A277, 301 (1977)

ELEM. SYM.	A	Z
Sc	45	21

METHOD

REF. NO. 77 0i 1 egf

REACTION	RESULT	EXCITATION ENERGY	SOURCE		DETECTOR		ANGLE
			TYPE	RANGE	TYPE	RANGE	
E,P	ABX	14-25	D	14-25	MAG-D		90

Abstract: The cross sections of the (e, e'p) reaction on ^{44}Ca, ^{45}Sc and ^{46}Ti have been measured and used to deduce (γ, p) cross sections. Together with (γ, n) cross sections from others, these data allow an estimate of the $T_<$ and $T_>$ GDR cross sections. The experimental results seem to be consistent with the theory on the isospin splitting. The (γ, p_0) or (γ, p_0+p_1) and (γ, n_0) cross sections have also been measured. The ratio $\sigma(\gamma, p_0)/\sigma(\gamma, p)$ indicates a contribution of a statistical nature in the $T_<$ GDR region and some additional direct modes in the $T_>$ GDR region. The contribution of one (^{45}Sc) or two (^{46}Ti) extra protons is discussed and it is found that the valence nucleons contribite to GDR in an independent way.

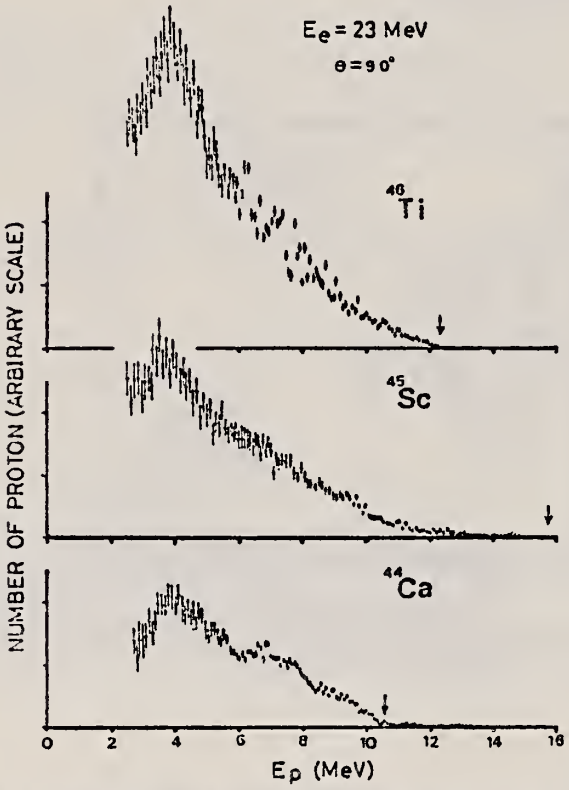

Fig. 4. Example of proton energy distribution obtained with 23 MeV electron beam. Arrows show the proton end point energy.

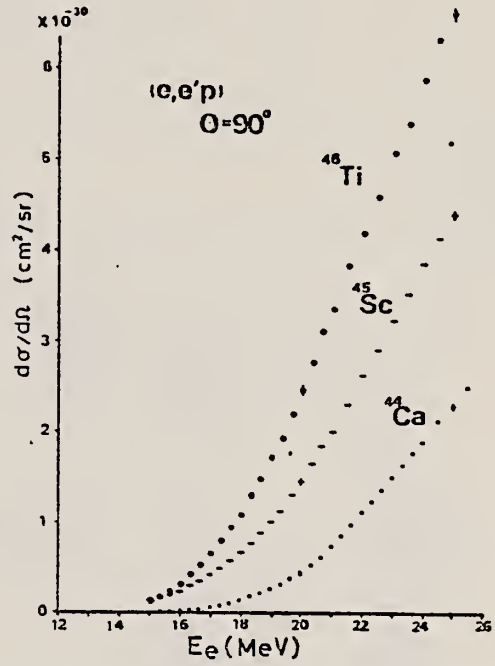

Fig. 5. The differential cross sections at $\theta = 90°$ of the (e, e'p) reaction.

(over)

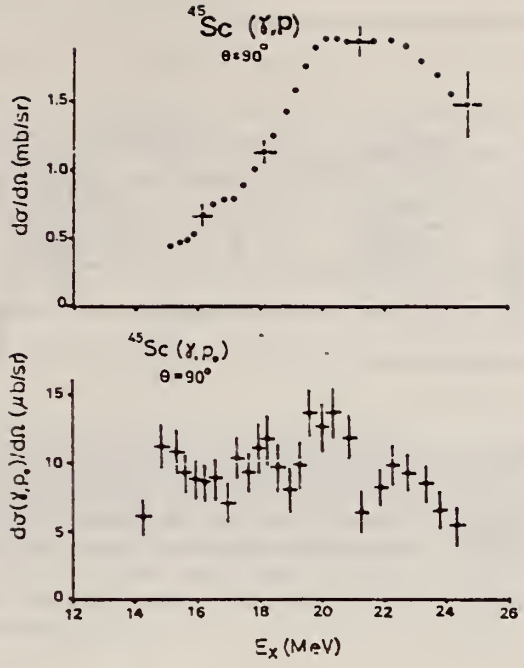

Fig. 7. The differential cross sections at $\theta = 90°$ of the (γ, p) and (γ, p_0) reactions of ^{45}Sc.

REF. V.I. Noga, S.A. Pashchuk, Yu.N. Ranyuk, P.V. Sorokin
Yad. Fiz. 34, 1431 (1981)
Sov. J. Nucl. Phys. 34, 792 (1981)

ELEM. SYM.	A	Z
Sc	45	21

METHOD

REF. NO. 81 No 1 egf

REACTION	RESULT	EXCITATION ENERGY	SOURCE		DETECTOR		ANGLE
			TYPE	RANGE	TYPE	RANGE	
G,N	RLY	11-260	C	165-260	ACT=I		4PI
E,N	RLY	11-259	D	165-260	ACT-I		4PI

BRMS/E YIELD

The induced-activity method has been used to study the reaction $^{45}Sc(\gamma,pn)^{44m}Sc$. The targets were bombarded by an electron beam at energies 165, 195, 225, and 260 MeV. The use of paired targets of scandium, separated by a converter of tantalum, permitted determination of the ratio of the cross sections for photo- and electrodisintegration of the nuclei. Comparison of the experimental data with theoretical calculations indicates a dominant role of $E1$ transitions and a small admixture of $E2$ transitions in the reactions studied.

PACS numbers: 25.20. + y, 25.30. − c, 27.40. + z

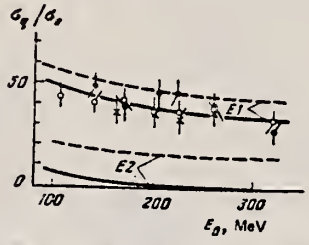

FIG. 2. The ratio σ_q/σ_γ as a function of the electron energy.
Points: o—$^{63}Cu-^{62}Cu$, ●—$^{12}C-^{11}C$, ×—$^{45}Sc-^{44m}Sc$.

REF. D. Ryckbosch, E. Van Camp, R. Van de Vyver, E. Kerkhove, P. Van Otten, P. Berkvens, H. Ferdinande
Phys. Rev. C26, 448 (1982)

ELEM. SYM.	A	Z
Sc	45	21

METHOD

REF. NO. 82 Ry 4 egf

REACTION	RESULT	EXCITATION ENERGY	SOURCE		DETECTOR		ANGLE
			TYPE	RANGE	TYPE	RANGE	
G,PØ	ABX	15-25	C	17-25	SCD-D		DST
G,PL	ABX	15-25	C	17-25	SCD-D		DST

The absolute (γ,p_0) differential cross sections for ^{45}Sc were measured at bremsstrahlung end point energies between 17 and 25 MeV. Using an artificially constructed pseudo-monoenergetic photon spectrum, absolute cross sections for various semidirect photoproton reaction channels were also determined. The general structure in the total (γ,p) cross section is discussed in terms of isospin and deformation effects. The direct, preequilibrium and equilibrium contributions to the photoproton decay of the giant dipole resonance equal about 35, 20, and 45%, respectively, of the total energy-integrated (γ,p) cross section. Comparison is made with the predictions of the exciton model.

[NUCLEAR REACTIONS ^{45}Sc(γ,p), $E=15.6-25$ MeV, $\theta=37°-143°$; measured $\sigma(E;\theta)$ absolutely. Deduced $\sigma(E;p_i)$, $\sigma(E)$, direct-semidirect cross section, isospin splitting, preequilibrium decay. Natural target.]

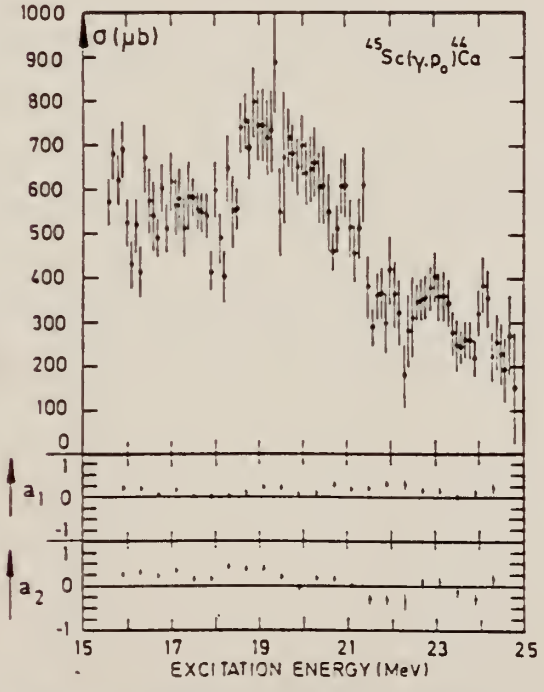

FIG. 2. The upper part of the figure shows the absolute ^{45}Sc$(\gamma,p_0)^{44}$Ca cross section, while in the lower part the angular distribution coefficients $a_1(E)$ and $a_2(E)$, as a function of excitation energy are depicted.

L=S,D,F P-HOLE STATES

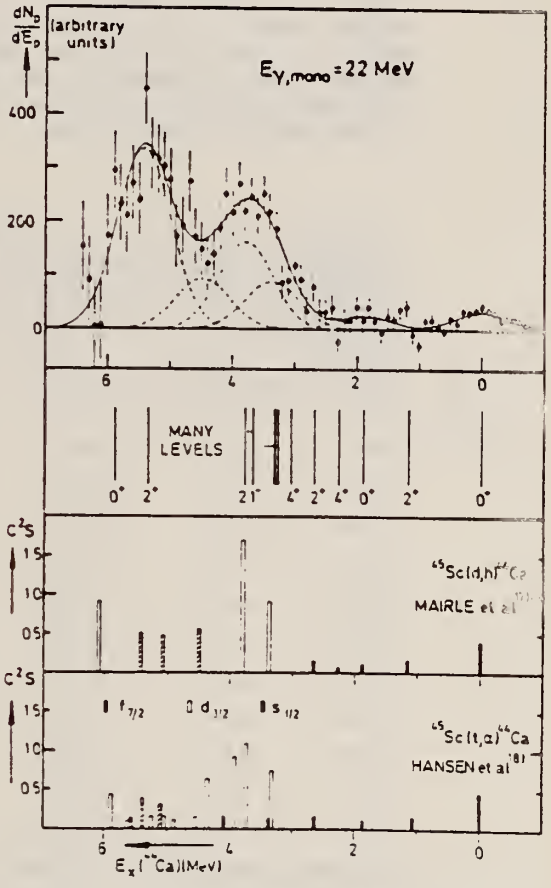

FIG. 3. The ^{45}Sc photoproton energy distribution corresponding to a monoenergetic photon spectrum with $E_{\gamma,mono}=22$ MeV; the energy scale represents excitation energy in the residual nucleus ^{44}Ca. In the lower part of the figure the ^{44}Ca level scheme is shown, together with the experimentally determined (Refs. 17 and 18) values of the spectroscopic factors for proton-hole states.

(OVER)

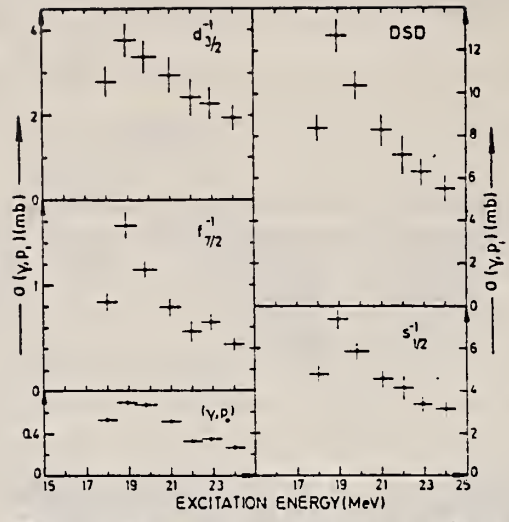

FIG. 4. The absolute cross sections for the $^{45}Sc(\gamma,p)$ reaction, leading to $f_{7/2}$, $d_{3/2}$, and $s_{1/2}$ proton-hole states in ^{44}Ca, together with their sum which represents the direct-semidirect photoproton cross section. The (γ,p_0) cross section, on which the other cross sections are normalized, is also shown explicitly.

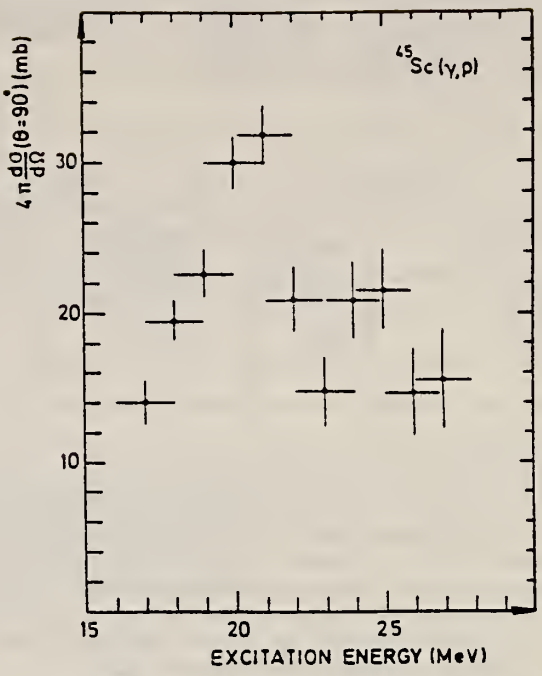

FIG. 5. The 90° differential total (γ,p) cross section, multiplied by 4π, as a function of excitation energy.

TABLE I. Comparison of our integrated cross sections, leading to specific proton-hole states in ^{44}Ca, with the spectroscopic factors as determined by Mairle *et al.*[17]

E_x (^{44}Ca) (MeV)	(l,j) (from Ref. 17)	c^2S (from Ref. 17)	$\int_{18}^{24}\sigma(\gamma,p_i)dE$ (mb MeV)
0.0	$3,\frac{7}{2}$	0.40	3.35±0.05
1.16	$3,\frac{7}{2}$	0.15	(0.24±0.06)
1.88	$3,\frac{7}{2}$	0.11	2.42±0.18
2.29	$3,\frac{7}{2}$	0.07	
2.66	$3,\frac{7}{2}$	0.16	
3.37	$2,\frac{3}{2}$	0.92	10.52±0.59
3.78	$2,\frac{3}{2}$	1.70	8.89±0.76
4.48	$0,\frac{1}{2}$	0.55	9.49±0.62
5.07	$0,\frac{1}{2}$	0.46	
5.43	$0,\frac{1}{2}$	0.50	23.73±0.81
6.10	$2,\frac{3}{2}$	0.92	

Sc
A=47

Sc
A=47

REF.

G. B. Vingiani, M. De Poli, C. Rossi Alvarez, F. Folkmann
Nucl. Phys. A239, 221 (1975)

ELEM. SYM.	A	Z
Sc	47	21

METHOD

REF. NO. 75 Vi 2 egf

REACTION	RESULT	EXCITATION ENERGY	SOURCE TYPE	SOURCE RANGE	DETECTOR TYPE	DETECTOR RANGE	ANGLE
P,G	LFT	10	D	1- 2	NAI-D		55

PROTON E 1.82-1.90 MEV

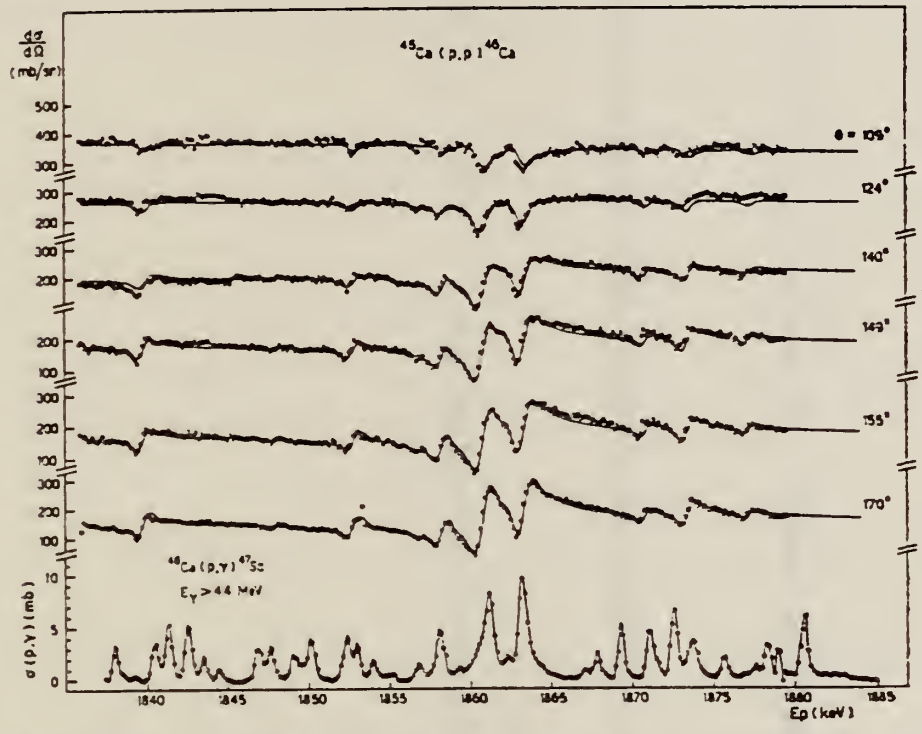

Fig. 2. Excitation function for protons elastically scattered from ^{46}Ca at six backward angles and for capture γ-rays ($E_\gamma > 4.4$ MeV) from the ^{46}Ca(p, γ)^{47}Sc reaction measured in steps of 160 eV. The solid lines in the (p, p) data are theoretical excitation functions with the parameters given in table 1 folded with a Gaussian energy distribution of 0.75 keV.

TABLE 2

Resonance widths and fine-structure parameters of ^{47}Sc(1) and ^{49}Sc(0) isobaric analogue states

Channel	J^π	E_A (keV)	Δ_A (keV)	Γ_s (keV)	γ_η^2 (keV)
^{46}Ca+p	$\frac{1}{2}^-$	1863	−77	5.3	0.02
^{48}Ca+p	$\frac{1}{2}^-$	1975	−8	1.5	0.03

(over)

TABLE 3

Partial Γ_γ from the $p_{\frac{1}{2}}$ IAS in $^{46}Ca(p,\gamma)$ for transitions to lower states in ^{47}Sc; $B(M1, IAS \rightarrow f)$ is calculated summing the partial widths for the three resonance components and multiplying with the proton width ratio 1.6 (from table 1)

$E_{res.}$	(keV)	1858	1861	1863	
Γ_p	(eV)	150	600	400	
Γ_γ total	(eV)	0.56	1.53	1.33	
E_f (keV)		Γ_γ (meV)	Γ_γ (meV)	Γ_γ (meV)	$B(M1, IAS \rightarrow f)$ $(10^{-3}\mu_0^2)$
0		10	241	49	
767		8	21	35	
808		9	67	73	24
1297		32	26	67	24
1391		10	135	74	
1405		18	23	31	14
1797		21	96	27	32
2003		6	31	40	
2207		12	21	62	
2499			18	20	11
2528			29	13	13
2650			33	15	15
2810		15	9	62	
2836		21	16	30	
2909		10	20	39	
2941		15	60	45	41
3133		28	28	31	32
3205		12	28	9	19
3262		6		38	
3290		11	24	19	22
3576		18	15	20	23
3728		9		11	10
4019		12	42	30	46
4085		9	13	31	30
4099		6	21	15	25
4408			8	11	13
4475		6	10	6	15
4553		44		14	
4609		18	37	26	62
4631			18	34	39
4690		8	31	22	47
4721		27	24		41
4792			38	18	45
4802			31	42	60
4831		5	36	21	53
4956		16	23	35	68
4998		15	15	20	46
5151		12	48	36	97
5509		12	37	30	100
5600		19	45	48	150
6383		20	58	42	275
6584		17	10	12	105
6724		28	24	26	234

Sc
A=49

Sc
A=49

REF.

J. Dubois, S. Maripuu and O. Almén
Ark. Fysik 31, 65 (1966)

ELEM. SYM.	A	Z
Sc	49	21

METHOD

REF. NO. 66 Du 2 JDM

REACTION	RESULT	EXCITATION ENERGY	SOURCE		DETECTOR		ANGLE
			TYPE	RANGE	TYPE	RANGE	
P,G	SPC	10-11	D	1	NAI-D	1-12	DST

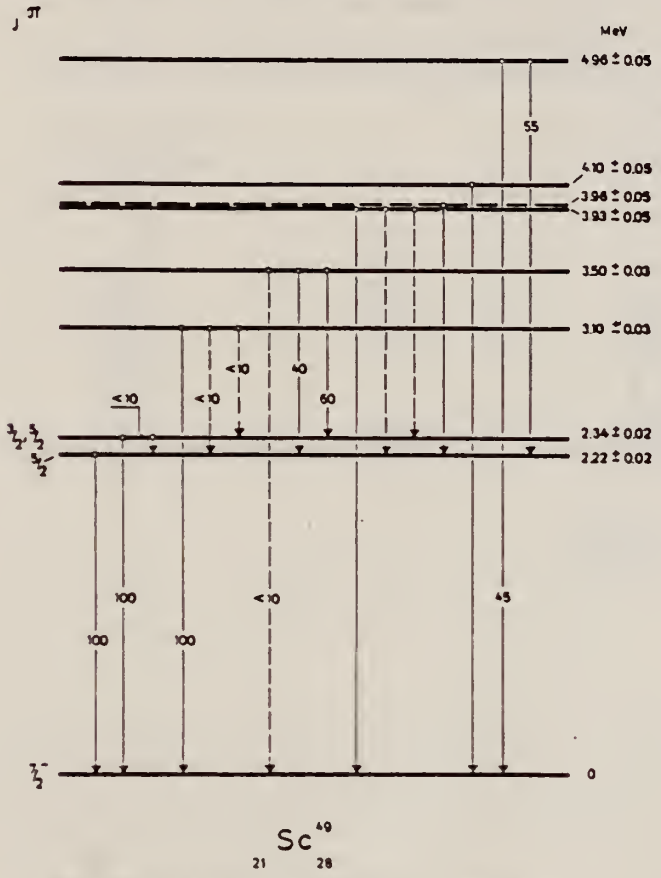

Fig. 7. The level scheme of Sc^{49} from the present work.

Table 2. Observed transitions at the 1012 keV resonance.

Gamma transition	Relative intensity
$r-0$	6 ± 1
$r-2.22$	100
$r-2.34$	< 7
$r-3.50$	37
$r-3.93$	40

Table 3. Observed transitions at the 1117 keV resonance.

Gamma transition	Relative intensity
$r-0$	< 4
$r-2.22$	52
$r-2.34$	100

Table 4. Observed transitions at the 1213 keV resonance.

Gamma transition	Relative intensity
$r-0$	< 6
$r-2.22$	< 10
$r-2.34$	100
$r-3.10$	24
$r-3.50$	32
$r-3.93$	34

Table 5. Observed transitions at the 1340 keV resonance.

Gamma transition	Relative intensity
$r-0$	< 4
$r-2.22$	100
$r-2.34$	20
$r-3.10$	14
$r-3.50$	58

REF. J. Dubois, S. Maripuu and O. Almén
Ark. Fysik 31, 65 (1966)

ELEM. SYM.	A	Z
Sc	49	21

METHOD

[Page 2 of 2]

REF. NO. 66 Du 2 JDM

REACTION	RESULT	EXCITATION	SOURCE	DETECTOR TYPE	DETECTOR RANGE	ANGLE

$Ca^{48}(p,\gamma)Sc^{49}$
$E_\gamma \geq 1.5$ MeV

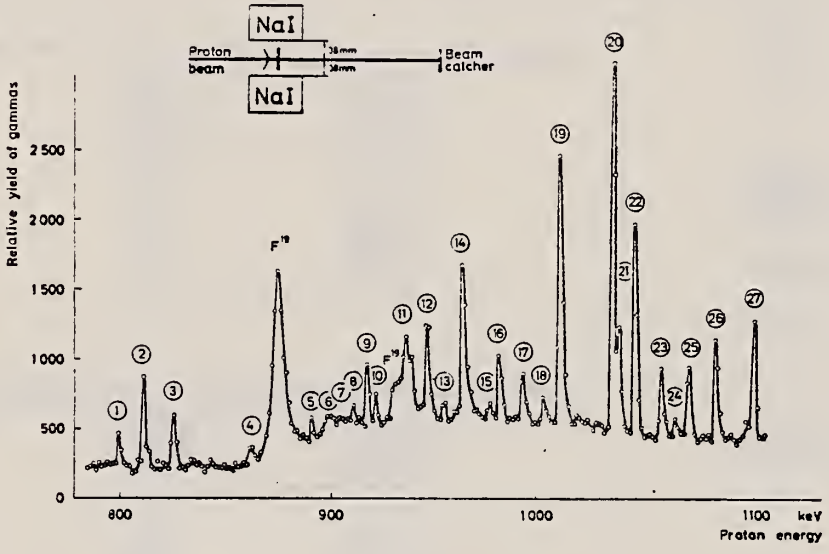

$Ca^{48}(p,\gamma)Sc^{49}$
$E_\gamma \geq 1.5$ MeV

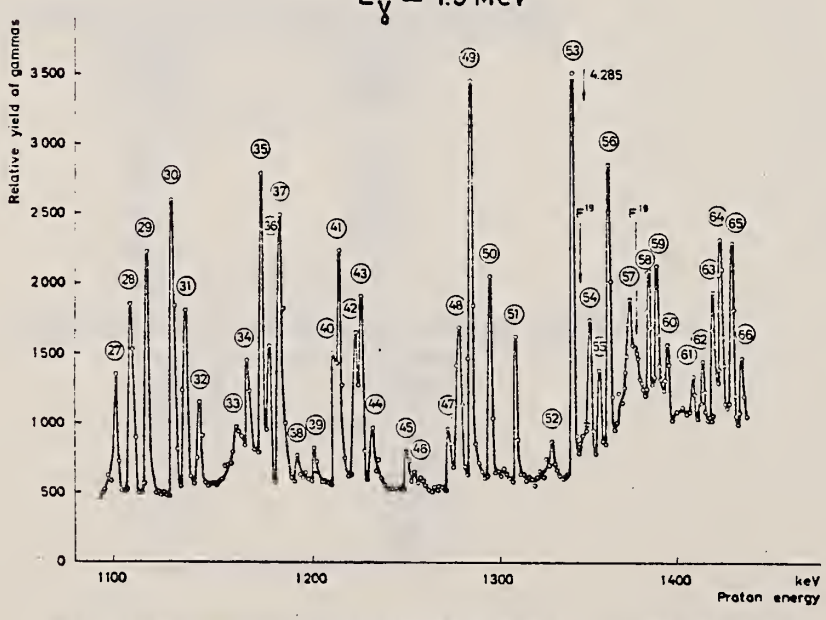

Fig. 1. The excitation curve of the $Ca^{48}(p,\gamma)Sc^{49}$-reaction. In the insert the detector arrangement is shown.

REF.

C. Chasman, K. W. Jones, R. A. Ristinen, and J. T. Sample
Phys. Rev. Letters 18, 219 (1967)

ELEM. SYM.	A	Z
Sc	49	21

METHOD

REF. NO.	
67 Ch 1	JDM

REACTION	RESULT	EXCITATION ENERGY	SOURCE		DETECTOR		ANGLE
			TYPE	RANGE	TYPE	RANGE	
P,G	LFT	12	D	2	SCD-D		90

Table I. Transitions from analogs of the Ca^{43} ground state in Sc^{43} to low-lying excited states in Sc^{49}.

Sc^{49} final-state[a] excitation energy (keV)	l[a]	J^{π}[a]	S[a]	Assumed multipolarity of gamma transition	Γ_{ω}[b] (eV)	E_p(lab) = 1.968 MeV Γ_{γ} (eV)	$\Gamma_{\gamma}/\Gamma_{\omega}$	E_p(lab) = 1.977 MeV Γ_{γ} (eV)	$\Gamma_{\gamma}/\Gamma_{\omega}$
0.0	3	$(7/2^-)$	1.0	$E2$	1.8	≤ 0.7	≤ 0.4	3.5	1.9
2233.0	(2)	$(3/2^+)$	0.05	$E1$	745.0	1.1	0.002	0.9	0.001
2382.0	(0)	$(1/2^+)$	0.005	$E1$	710.0	2.1	0.003	1.2	0.002
3092.0	1	$(3/2^-)$	0.68	$M1$	12.9	2.7	0.2	≤ 0.5	≤ 0.04
3819.0	3	$(5/2^-)$	0.15	$M1$	9.8	≤ 0.4	≤ 0.04	2.8	0.3
3923.0[c]	...					...		...	
4004.0[c]	...					...		...	
4080.0	3	$(5/2^-)$	0.20	$M1$	8.9	3.9	0.4	3.0	0.3

REF. P. Paul, J. F. Amann, and K. A. Snover
Phys. Rev. Letters 27, 1013 (1971)

EL EM. SYM.	A	Z
Sc	49	21

METHOD

REF. NO. 71 Pa 3 hmg

REACTION	RESULT	EXCITATION ENERGY	SOURCE		DETECTOR		ANGLE
			TYPE	RANGE	TYPE	RANGE	
P,G	REL	13-27	D	4-18	NAI-D		105

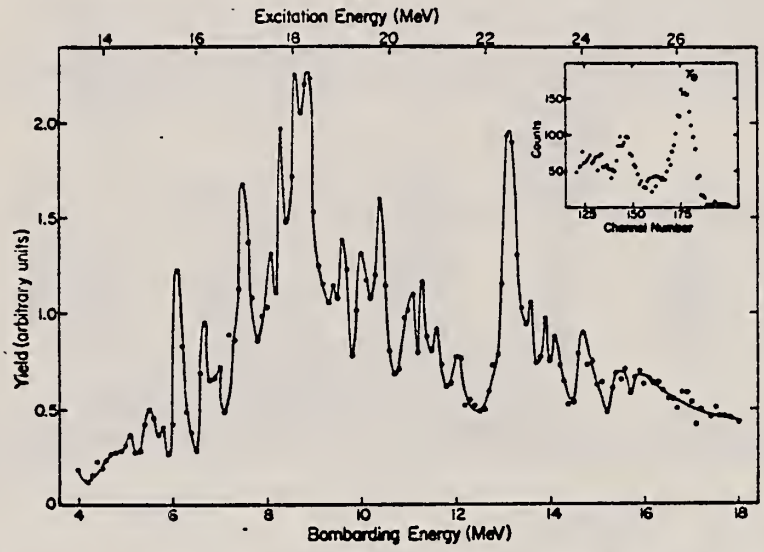

FIG. 1. Excitation function of the γ_0 yield obtained at 105° in the reaction $^{48}Ca(p,\gamma_0)^{49}Sc$. The insert shows the high-energy part of the γ-ray spectrum.

TABLE I. Separation energies $\Delta E = E_> - E_<$ of the $T+1$ and T components of the GDR observed from proton capture into various nuclei with ground-state isospin T. $\bar{V}$ is obtained from Eq. (2) in the text.

Nucleus	ΔE(MeV)	T	$\bar{V}$(MeV)	Ref.
^{42}Ca	3.0±0.2	1	63±4	13
^{49}Sc	4.8±0.2	7/2	52±2	Present
^{60}Ni	3.0±0.2	2	60±4	5
^{64}Zn	3.2±0.3	2	68±6	Present
$^{64}Zn^{*a}$	2.9±0.3	2	62±6	Present
^{88}Sr	3.7±0.5	6	47±6	1
^{89}Y	3.9±0.5	11/2	54±7	2
$^{89}Y^{*a}$	3.8±0.4	11/2	52±6	2
^{90}Zr	3.9±0.5	5	58±7	1
^{91}Nb	3.6±0.7	9/2	59±10	2

[a] First excited state.

REF. M. Adachi and H. Taketani
J. Phys. Soc. Jap. 35, 317 and 325 (1973)

ELEM. SYM.	A	Z
Sc	49	21

METHOD

REF. NO. 73 Ad 14 egf

REACTION	RESULT	EXCITATION ENERGY	SOURCE		DETECTOR		ANGLE
			TYPE	RANGE	TYPE	RANGE	
P,G	SPC	12	D	2	SCD-D		DST

12=11.559 MEV,J-PI

Table II. Partical Γ_γ (meV) to the excited states in ^{49}Sc.

Ex. (keV)	J^{π}***	E_p (keV)					SUM	Summed M1 strength (W.U.)
		1960	1964	1975	1982	1991		
0	7/2−	5 (meV)		127	4		0.136(eV)	E2
2226	1/2+	16	66	82	3	6	0.173	E1
2371	3/2+	25	36	59	4		0.124	E1
3082	3/2−	10	85	34	5	28	0.162	1.2×10^{-2}
3515	3/2−	23	81	58	16	29	0.207	1.9×10^{-2}
3804	5/2−, 7/2−	22	63	146	16	48	0.295	2.3×10^{-2}
3991		27	51	147	14	34	0.273	3.0×10^{-2}
4068	5/2−	25	156	259	39	54	0.533	6.2×10^{-2}
4491	1/2−, 3/2−	*	69	78	*	*	0.147	2.0×10^{-2}
4736	5/2−	40	80	182	43	30	0.375	5.7×10^{-2}
6305	5/2	38	71	67	42	40	0.258	8.6×10^{-2}
6412	3/2− (7/2−)	71	124	292	55	31	0.573	2.0×10^{-1}
6504	3/2−	58	196	538	66	53	0.911	3.4×10^{-1}
6723	3/2−	87	214	431	64	42	0.835	3.6×10^{-1}
6984	5/2−	69	303	593	40	36	1.041	5.3×10^{-1}
7062	1/2−	59	160	331	34	41	0.625	3.3×10^{-1}
7192	5/2	58	118	246	28	26	0.476	2.8×10^{-1}
7226	5/2	41	131	268	48	42	0.550	3.2×10^{-1}
Total		674	2004	3938	521	540		

* The transition to the 4491 keV state was obscured by the presence of Doppler-broadened lines from the reaction ^{19}F(p,$\alpha\gamma$)^{16}O due to a target contaminant.

** See ref. 7.

The uncertainties on the Γ_γ are dominated by the uncertainties on Γ_{p_0}, which sum up to ≈20% in the cases of 1960 and 1975 keV resonances. In other three resonances, the uncertainties on the Γ_γ are due to the uncertainties on Γ_{p_0} and intensities of gamma rays. The uncertainty on the individual Γ_γ ranged form 20 to 100%.

[7] M. Adachi and H. Taketani: J. Phys. Soc. Japan 35 (1973) 317.

(over)

Table I. Analyses of angular distribution data.

Final state (MeV)	A_2	Assumed spin	Mixing ratio				l-value*	Assigned spin
0	0.000 ±0.050	7/2	$-0.035^{+0.050}_{-0.049}$	or	$1.74^{+0.19}_{-0.21}$		3[7-12]	7/2
2222	−0.384 ±0.060	1/2	$-0.065^{+0.033}_{-0.032}$	or	$2.02^{+0.18}_{-0.16}$		0,[10 12] (2)[9]	
		3/2	$0.593^{+0.083}_{-0.068}$	or	$3.44^{-0.82}_{-0.63}$			1 2
2371	0.089 ±0.084	1/2	$-0.316^{0.045}_{-0.048}$	or	$4.53^{+1.13}_{-0.76}$		(0),[9 2[10 12]	
		3/2	$0.198^{+0.057}_{-0.954}$	or	$-17.6^{+8.5}_{-292.5}$			3/2
3082	−0.075±0.164	1/2	$-0.228^{+0.086}_{-0.088}$	or	$3.24^{+1.29}_{-0.75}$		1[7-10]	
		3/2	$0.311^{+0.132}_{-0.113}$	or	$-\ 17.6^{6.0}$			3/2
3515	0.389±0.376	1/2	$-0.497^{+0.222}_{-0.341}$	or	$-\ 5.9^{3.83}$		1[10]	
		3/2	$0.007^{+0.242}_{-0.279}$	or	$-3.99^{+2.24}_{-115.4}$			3/2
		5/2	$3.1 > \delta > 0.1$					
3804	0.502±0.446	5/2	$2.73 > \delta > 0.14$				3[8-10]	
		7/2	$1.75 > \delta > -0.09$					7/2, 5/2
4068	−0.006±0.063	5/2	$0.081^{+0.059}_{-0.055}$	or	$3.29^{+0.79}_{-0.57}$		3[8-10]	
		7/2	$-0.149^{+0.061}_{-0.060}$	or	$2.02^{+0.33}_{-0.27}$			5/2
4736	−0.029±0.095	5/2	$0.061^{+0.087}_{-0.081}$	or	$3.55^{+1.55}_{-0.90}$		3[9,10]	
		7/2	$-0.171^{+0.092}_{-0.090}$	or	$2.14^{+0.59}_{-0.42}$			5/2
6306	−0.153±0.149	1/2	$-0.187^{+0.078}_{-0.079}$	or	$2.84^{+0.86}_{-0.57}$			
		3/2	$0.371^{+0.131}_{-0.110}$	or	$9.76^{+377.3}_{-5.13}$			
		5/2	$-0.044^{+0.127}_{-0.125}$	or	$5.84^{+15.80}_{-2.57}$			5/2
		7/2	$0.288^{+0.141}_{-0.151}$	or	$2.96^{+2.16}_{-0.94}$			
6412	0.292±0.098	1/2	$-0.435^{+0.059}_{-0.063}$	or	$8.76^{+7.48}_{-2.73}$		1,[10] (4)[3]	
		3/2	$0.069^{+0.062}_{-0.063}$	or	$-5.37^{+1.40}_{-2.74}$			3/2(7/2)
		5/2	0.287		1.86			
		7/2	0.058		1.28			
6504	0.546±0.051	1/2	$-0.614^{+0.040}_{-0.044}$	or	$-37.0^{+}_{-}\ 19.8$		1[10]	
		3/2	$-0.098^{+0.035}_{-0.036}$	or	$-2.74^{+2.79}_{-0.33}$			3/2
6728	0.204±0.064	1/2	−0.382±0.037	or	$6.23^{+1.65}_{-1.08}$		(1),[9] (3)[10]	
		3/2	$0.124^{+0.041}_{-0.040}$	or	$7.72^{+1.85}_{-3.51}$			
		5/2	$0.299^{+0.093}_{-0.075}$	or	$1.81^{+0.35}_{-0.31}$			3/2
		7/2	$0.070^{+0.085}_{-0.073}$	or	$1.25\pm\ 0.20$			

REF. M. Adachi and H. Taketani
J. Phys. Soc. Jap. 35, 317 and 325 (1973)

ELEM. SYM.	A	Z
Sc	49	21

METHOD

REF. NO. 73 Ad 14 egf

REACTION	RESULT	EXCITATION ENERGY	SOURCE TYPE	SOURCE RANGE	DETECTOR TYPE	DETECTOR RANGE	ANGLE

Final state (keV)	A_2	Assumed spin	Mixing ratio			l-value*	Assigned spin
6984	-0.055 ± 0.055	1/2	-0.239 ± 0.029	or	$3.36^{+0.37}_{-0.31}$		
		3/2	$0.297^{+0.040}_{-0.039}$	or	13.8		
		5/2	$0.038^{+0.049}_{-0.046}$	or	$3.88^{+0.92}_{-0.65}$		5/2
		7/2	$-0.195^{+0.052}_{-0.053}$	or	$2.28^{+0.35}_{-0.28}$		
7062	-0.492 ± 0.094	1/2	$-0.005^{+0.056}_{-0.052}$	or	$1.75^{+0.24}_{-0.21}$	1?)(1)9)(4)10)	
		3/2	$0.758^{+0.310}_{-0.147}$	or	$2.39^{+0.89}_{-0.81}$		1/2
		5/2	$-0.345^{+0.091}_{-0.105}$	or	$-8.43^{+3.71}_{-20.3}$		
7192	-0.125 ± 0.091	1/2	-0.202 ± 0.048	or	$2.97^{+0.52}_{-0.40}$		
		3/2	$0.349^{+0.074}_{-0.067}$	or	$12.0^{+33.3}_{-5.3}$		5/2
		5/2	$-0.021^{+0.078}_{-0.076}$	or	$5.41^{+3.07}_{-1.80}$		
7226	-0.084 ± 0.054	1/2	$-0.223^{+0.023}_{-0.029}$	or	$3.19^{+0.33}_{-0.28}$		
		3/2	$0.318^{+0.041}_{-0.039}$	or	$18.1^{+33.2}_{-7.3}$		5/2
		5/2	0.014 ± 0.046	or	$4.32^{+1.11}_{-0.76}$		

* Deduced from stripping or pick up reaction, see ref. 7-12.

7) [illegible]
8) D.D. Armstrong and A.G. Blair: Phys. Rev. 140 (1965) B1226.
9) J.R. Erskine, A. Marinov and J.P. Schiffer: Phys. Rev. 142 (1966) 633.
10) G. Bruge, H. Faraggi, Ha Duc Long and P. Roussel: CEA-N-1232, p. 124.
11) J.L. Yntema and G.R. Satchler: Phys. Rev. 134 (1964) B974.
12) E. Newman and J.C. Hiebert: Nuclear Phys. A110 (1968) 366; F. Hinterberger, G. Mairle, V. Schmidt-Rohr, P. Turek and G.J. Wagner: Z. Phys. 202 (1967) 236.

REF. F. S. Dietrich, S. D. Bloom and D. W. Heikkinen
Nucl. Phys. A259, 75 (1976)

ELEM. SYM.	A	Z
Sc	49	21

METHOD

REF. NO. 76 Di 2 egf

REACTION	RESULT	EXCITATION ENERGY	SOURCE TYPE	SOURCE RANGE	DETECTOR TYPE	DETECTOR RANGE	ANGLE
P,G	LFT	15	D	6- 7	NAI-D		DST

Abstract: Gamma rays have been observed from the ^{48}Ca(p, γ) reaction de-exciting analogs of the 4.005 MeV ($f_{\frac{7}{2}}$) and 4.024 MeV ($g_{\frac{9}{2}}$) states in ^{49}Ca. The resonances were observed at E_p(c.m.) = 5.933±0.005 and 5.992±0.005 MeV, respectively, with total widths 39±5 and 18±5 keV. The corresponding ground-state γ-widths were inferred to be 17±5 and 22^{+22}_{-11} eV. Decays of the lower resonance to excited states of ^{49}Sc were also observed. A tentative lower limit of 1.7 eV was placed on the width of the transition to the $\frac{3}{2}^-$ (3.08 MeV) level. The upper ($\frac{3}{2}^+$) γ-ray (g.s.) resonance is depleted by a factor of 10–20 by the giant dipole resonance and cannot be used easily to extract structural information. The (tentative) lower limit on the M1 decay of the lower ($\frac{5}{2}^-$) resonance to the $\frac{3}{2}^-$ state (E_x = 3.08 MeV) implies a strong $1f_{\frac{5}{2}}$ neutron admixture in the lower state which is not borne out by theoretical estimates of the effects of the core polarization. The M1 decay of this same resonance to the ground state is calculated to be 9–13 eV, with the Arima-Horie estimate for the effects of core polarization, and 16 eV in a three-particle, two-hole configuration mixing shell-model calculation. Both figures are consistent with the measurement and confirm the existence of strong magnetic moment renormalization effects.

EXC 15.55,15.61 MEV

TABLE 1

Angular distribution coefficients for the ground-state transition expressed in the form $d\sigma/d\Omega = \Sigma^2_{L=0} A_L P_L(\cos\theta)$

E_p(lab) (MeV)	A_0	A_1	A_2
5.982	10.0±1.2	1.7±0.5	4.8±1.0
6.040	15.1±1.8	2.0±0.5	3.6±0.8
6.063	29.0±4.0	7.2±1.0	2.4±1.0
6.080	23.0±3.0	1.2±1.0	−1.2±1.6
6.097	16.6±2.0	−1.0±0.2	−1.1±0.2
6.120	31.0±4.0	−1.9±0.5	−3.1±0.9
6.160	12.6±1.5	−1.3±0.3	−0.2±0.4

Values of A_L are given in μb/sr.

TABLE 3

Radiation widths extracted from the data

Transition	$\Gamma_p\Gamma_\gamma$ [a] (keV · eV)	Γ_p [b] (keV)	Γ_γ (eV)	$S\Gamma_{s.p.\ IAS}$ [c] (eV)
$\frac{5}{2}^- \to \frac{7}{2}^-(0)$	420±63	24 ±5	17 ±5	33 (M1)
$\frac{5}{2}^- \to \frac{3}{2}^+(2.37)$	34±10	24 ±5	1.4±0.5	
$\frac{5}{2}^- \to \frac{3}{2}^-(3.08)$	>40	24 ±5	>1.7	0 (M1)
$\frac{3}{2}^+ \to \frac{7}{2}^-(0)$	58^{+58}_{-29}	2.7±0.8	22^{+22}_{-11}	254 (E1)

The single-particle estimate is discussed in the text. See table 4 also.
[a]) This work.
[b]) Ref. [4]).
[c]) Values of S from (d, p) reaction [15]).

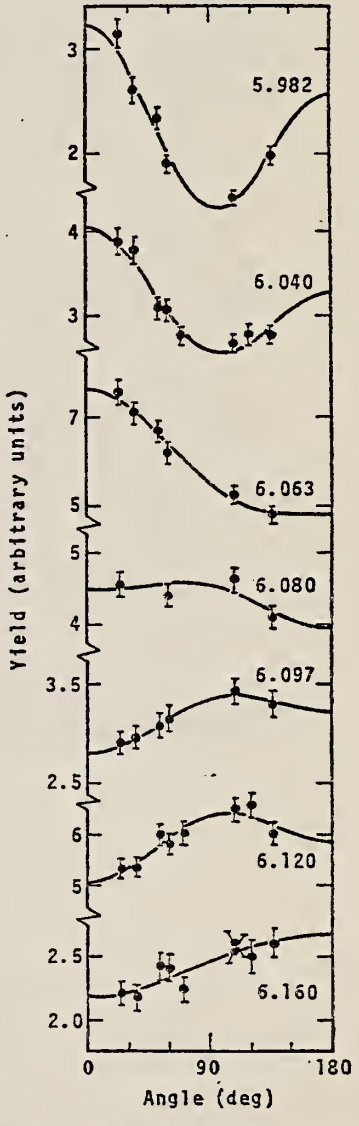

Fig. 4. Angular distributions of the ground-state γ-decays in the ^{48}Ca(p, γ)^{49}Sc reaction. The distributions are labeled by the lab proton energy in MeV. The curves are Legendre-polynomial fits to the data with parameters listed in table 1.

[4] K.W. Jones et al., Phys. Rev. 145, 894 (1966).
[15] E. Kashy et al., Phys. Rev. 135, B865 (1965).

U.S. DEPARTMENT OF COMMERCE
NATIONAL BUREAU OF STANDARDS

# TITANIUM
Z=22

Titanium was discovered in 1790 by William Gregor, an English clergyman who was also a mineralogist and an amateur chemist. Gregor's analysis of the black sand found in his own parish along the beach in the county of Cornwall showed 45.26 percent of a white metallic oxide, up to that time unrecognized. A few years later, Martin Klaproth found a new element in rutile found in Boinile, Hungary. Klaproth acknowledged Gregor's priority and suggested the name "titanic earth" or titanium, from the Titans of Greek Mythology. Almost 100 years passed before Lars Nilson and Otto Pettersson finally prepared a metal, 95 percent pure, by reducing titanium tetrachloride with sodium in an airtight cylinder.

Ti

Ref. O.M.M. Mitchell, K.G. McNeill
Can. J. Phys. 41, 871 (1963)

Elem. Sym.	A	Z
Ti		22

Method: Betatron; proton yield; angular distribution; scintillator; ion chamber

Ref. No.: 63 Mi 5 NVB

Reaction	E or ΔE	E_o	Γ	$\int \sigma dE$	Jπ	Notes
Ti(γ,xp)	Bremss. 22					Angular distribution: $Y(\theta) = a + b \sin^2\theta (1 + p \cos\theta)^2$ where a = 51±0, b = 47±15, p = 0.0±0.2, and b/a = 0.9±0.4. Yield ($E_p > 8$ MeV): (0.44±0.1) 10^5 protons/mole-r Yield ($3.7 < E_p < 14$): (5.4±0.5) 10^5

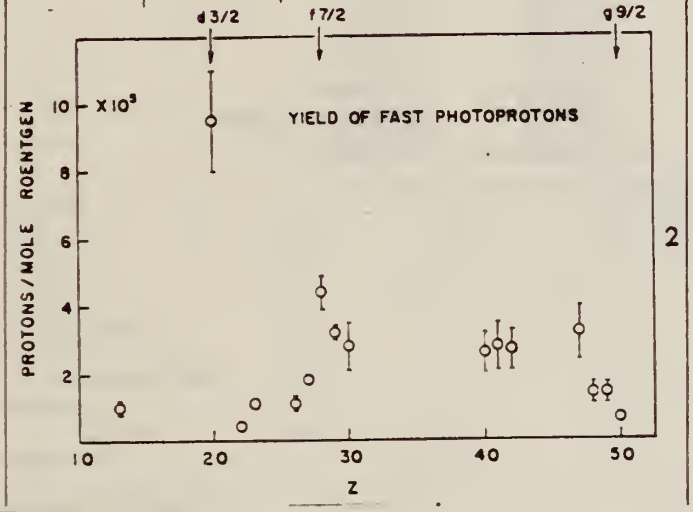

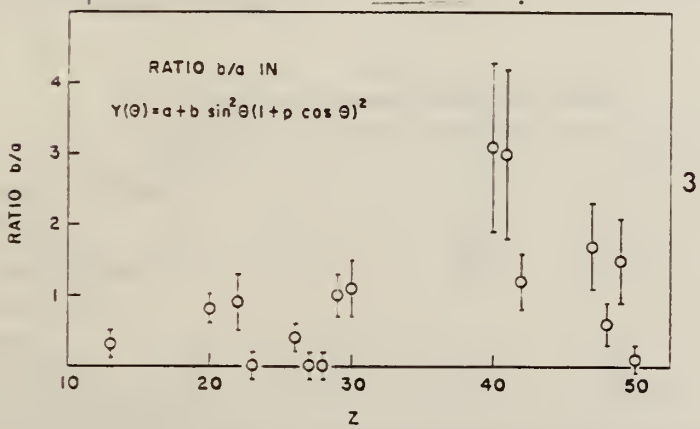

FIG. 2. The yields of fast photoprotons ($E_p > 8$ Mev) obtained from targets of various elements when irradiated with 22-Mev bremsstrahlung. The target thicknesses range from 351 to 572 mg/cm² (about 8 Mev for protons). The errors noted are statistical.

FIG. 3. The anisotropy coefficient b/a for fast photoprotons ($E_p > 8$ Mev) from 16 elements. The errors noted are statistical.

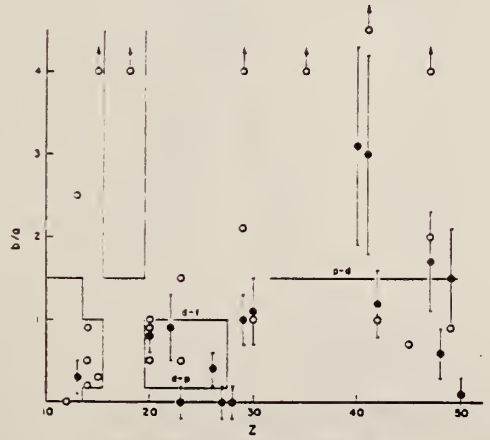

FIG. 4. The values of the fast photoproton anisotropy coefficient b/a found by the present authors ● and other workers (○) in the region of the periodic table $10 \leq Z \leq 50$. Arrows indicate off-scale points. The references to the results of other workers are given in Table II. The demarcations are explained in the text.

FORM NBS-418
(8-1-63)
USCOMM-DC 18556-P63

U.S. DEPARTMENT OF COMMERCE
NATIONAL BUREAU OF STANDARDS

F.R. Allum, T.W. Quirk, and B.M. Spicer
Nucl. Phys. 53, 545 (1964)

Ti		22

METHOD

REF. NO. 64 Al 5 JOC

REACTION	RESULT	EXCITATION ENERGY	SOURCE		DETECTOR		ANGLE
			TYPE	RANGE	TYPE	RANGE	
G,XN	NØX	THR-34	C	34	THR-I	6-	DST

TABLE 1

Summary of present experimental data at 34 MeV bremsstrahlung

Element		$-\frac{a_2}{a_0}$	$\frac{a_1}{a_0}$
$_{4}$Be		0.43±0.02	0.05±0.01
$_{6}$C		0.61±0.04	0.09±0.02
$_{13}$Al		0.39±0.03	0.05±0.01
$_{22}$Ti		0.34±0.02	0.06±0.01
$_{24}$Cr	34 MeV	0.33±0.02	0.02±0.01
	22 MeV	0.13±0.07	−0.02±0.03
$_{29}$Cu		0.36±0.02	0.10±0.01
$_{50}$Sn		0.38±0.02	0.11±0.01
$_{56}$Ba		0.39±0.03	0.11±0.02
$_{73}$Ta	Before installation of iron shielding	0.26±0.04	0.13±0.02
	After installation of iron shielding	0.27±0.02	0.12±0.01
$_{82}$Pb	target diameter 3.0 cm	0.39±0.03	0.15±0.02
	target diameter 1.5 cm	0.40±0.03	0.19±0.02
$_{83}$Bi		0.42±0.03	0.17±0.02

† $a_0 + a_1 \cos\theta + a_2 \cos^2\theta$

REF.

J. A. Scheer, K. Schlupmann und F. Triantafyllidis
Nucl. Phys. 56, 113-116 (1964)

ELEM. SYM.	A	Z
Ti		22

METHOD: Betatron

REF. NO.: 64 Sc 1 | JOC

REACTION	RESULT	EXCITATION ENERGY	SOURCE TYPE	SOURCE RANGE	DETECTOR TYPE	DETECTOR RANGE	ANGLE
G,A	SPC	THR - 33	C	33	SCD	4-13	90

ABS YIELD

Tabelle 1
Meßdaten und Ergebnisse

	Ti	Ni	Cu	Nb
Targetdicke (mg/cm²)	2.08	1.52	9.90	8.87
Bestrahlungsdauer (h)	52.5	55.5	18.0	84.5
Registrierte Teilchenanzahl ($4 \leq E_x \leq 12.6$ MeV)	1861	2376	2333	1987
Lage des Maximums E_{max} der Energieverteilung (MeV)	6.4	8.2	8.5	11
Halbwertsbreite des Maximums (MeV)	2.8	2.8	4.0	3.5
Mittlerer Energieverlust im Target bei $E_x = E_{max}$ (MeV)	0.4	0.25	1.7	1.1
Ausbeute in μb/MeV [a]	22±3.5	45±7	23±3.5	5.5±0.8

[a]) Vgl. Bemerkung [a]) in Tabelle 2.

Tabelle 2
Vergleich der Ergebnisse verschiedener Autoren

	E_0(MeV)	Ti	Ni	Cu	Nb
Ausbeute ($10^3 \times N_a$/Mol. r)					
Boulègue	31		58.7	50.8	
Diese Arbeit [a])	32.5	48±7	98±15	50±7.5	12±1.8
Toms und McElhinney	21.5		39.4	26	4.6 [b])
Relative Ausbeute					
Boulègue	31		1	0.87	
Kregar und Povh	30		1	0.54	
Diese Arbeit	32.5	0.49±0.08	1	0.51±0.08	0.12±0.02
Toms und McElhinney	21.5		1	0.66	0.12 [b])

[a]) Die Fehlerangaben beinhalten auch die Unsicherheit in der Absoluteichung der Intensität des γ-Strahles.

[b]) Dieser Wert wurde aus nur 14 beobachteten Ereignissen bestimmt.

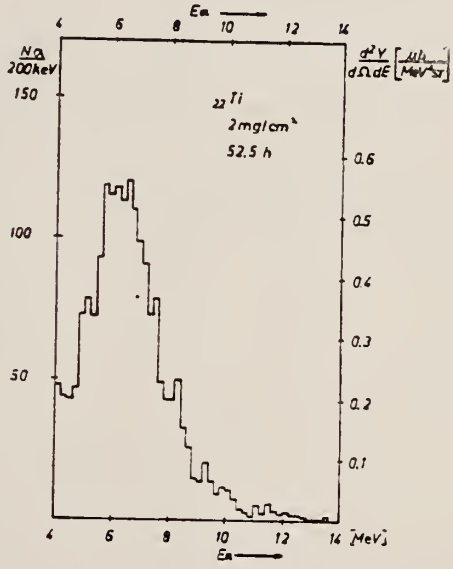

Abb. 1. Die erhaltenen Energie-Spektren der Photoalphateilchen aus Ti, Ni, Cu und Nb.

REF.	ELEM. SYM.	A	Z
G. Ben-David, B. Arad, J. Balderman, and Y. Schlesinger Phys. Rev. 146, B852 (1966)	Ti		22

METHOD	REF. NO.	
Nuclear Resonance Scattering using N,G reactions.	66 Be 3	JDM

REACTION	RESULT	EXCITATION ENERGY	SOURCE TYPE	SOURCE RANGE	DETECTOR TYPE	DETECTOR RANGE	ANGLE
G,G	RLX	5 - 10	D	5 - 10	NAI-D	5 - 10	135

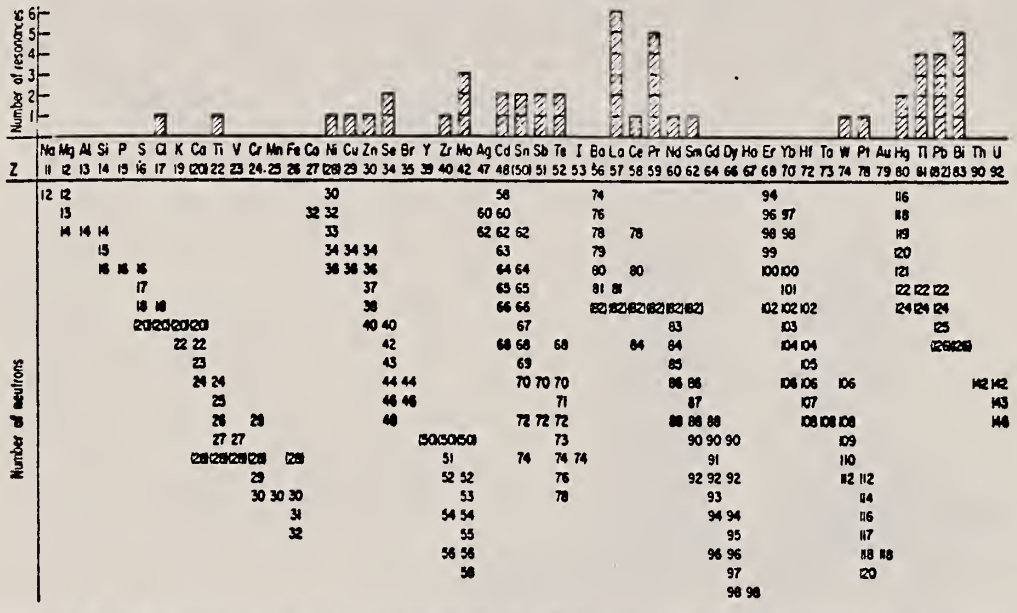

FIG. 3. Histogram of distribution of observed resonances among the different targets. The atomic number is given directly beneath the chemical symbol followed by the neutron numbers of the naturally occurring isotopes. Magic numbers are shown in brackets.

TABLE III. List of effective cross sections.

Scatterer	Energy (MeV)	Gamma source	δ (mb)	Scatterer	Energy (MeV)	Gamma source	δ (mb)
Sm^{144}	8.997	Ni	100	Sn	7.01	Cu	110
Pr^{141}	8.881	Cr	9	Nd	6.867	Co	30
La	8.532	Ni	6	Pr^{141}	6.867	Co	3
Te	8.532	Ni	3[a]	Te	6.7	Ni	...
Cu	8.499	Cr	24	La	6.54	Ag	12
Zr	8.496	Se	3050	Cd	6.474	Co	110
Zn	8.119	Ni	13	Mo	6.44	Hg	25[g]
Se	7.817	Ni	50	La	6.413	Ti	72
Se	7.76	K	90	Mo	6.413	Ti	10
Sb	7.67	V	...[b]	Tl	6.413	Ti	25
Cd	7.64	Fe	40[c]	W	~6.3	Ti	...[b]
Ni	7.64	Fe	7[c]	Sb	6.31	Hg	6[c]
Pr^{141}	7.64	Fe	12[c]	Ti	6.31	Hg	2[c]
Tl	7.64	Fe	370[c]	Sn	6.27	Ag	75
La	7.634	Cu	7	Pb^{206}	6.15	Gd	...[e]
Mo	7.634	Cu	11	Te	5.8	Ni	...[f]
Bi^{209}	7.634	Cu	4	La	6.12	Cl	35
Te	7.528	Ni	66[d]	Pr^{141}	6.12	Cl	110
Bi^{209}	7.416	Se	100	Pt	5.99	Hg	40[a,g]
Bi^{209}	7.300	As	80[c]	Tl	5.99	Hg	5[g]
Pb^{206}	7.285	Fe	4100	Pb^{206}	5.9	Sr	...[b]
Cl	7.285	Fe	34	Ce	5.646	Co	17
Pr^{141}	7.185	Se	80	Bi^{209}	5.646	Co	55
Tl	7.16	Cu	120	Pb^{206}	5.53	Ag	70
La	7.15	Mn	50	Hg	5.44	Hg	75[g]
Bi^{209}	7.149	Ti	2000	Hg	4.903	Co	385

[a] High-energy component of a complex spectrum.
[b] A broad scattered spectrum with no observable peak structure.
[c] There are actually two lines of energies 7.647 and 7.633 MeV having equal intensities in the iron capture gamma spectrum. The cross section has therefore been corrected, although there is no possibility at present of deciding which line is responsible for each resonance.
[d] Is probably an independent level in the complex spectrum of Ni γ rays on Te.
[e] Rough estimate.
[f] May be inelastic component from 7.528 level in Te.
[g] The relative line intensities in this case are due to Groshev and co-workers.
[h] No line is known for the source at this energy.
[i] Difficult to resolve among the many source lines present at this energy.

REF.

S. Costa, F. Ferrero, C. Manfredotti, L. Pasqualini and G. Piragino and H. Arenhovel
Nuovo Cimento 48B, 461 (1967)

ELEM. SYM.	A	Z
Ti		22

METHOD

Betatron; NBS ionization chamber

REF. NO.	
67 Co 1	JDM

REACTION	RESULT	EXCITATION ENERGY	SOURCE		DETECTOR		ANGLE
			TYPE	RANGE	TYPE	RANGE	
G,XN	ABX	12-24	C	24	BF3-I		4PI

434

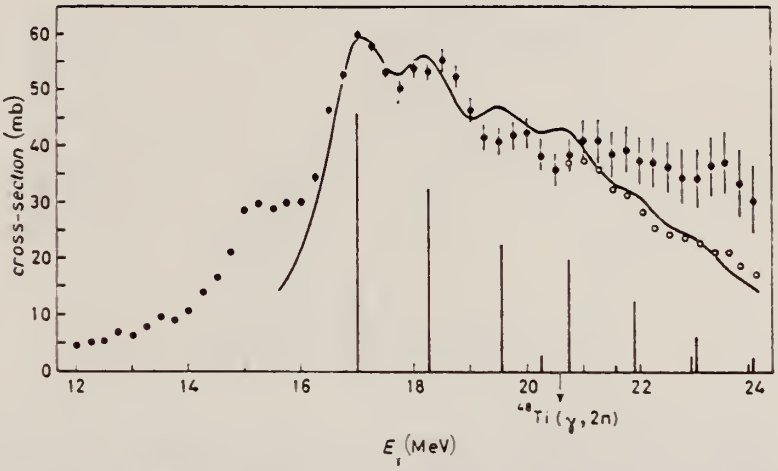

Fig. 1. – (γ, Tn) cross-section for Ti. The dipole strengths, calculated for ^{48}Ti, are indicated by the vertical bars. Open circles represent the (γ, Tn) cross-section corrected for neutron multiplicity. The level density parameter used has been taken from ref. (*).

Y. Oka, T. Kato and N. Sato
Bull. Chem. Soc. Japan 42, 387 (1969)

Ti		22

METHOD

REF. NO.	
69 Ok 1	hmg

REACTION	RESULT	EXCITATION ENERGY	SOURCE		DETECTOR		ANGLE
			TYPE	RANGE	TYPE	RANGE	
G,TI 45	RLY	THR-60	C	30-60	NAI-D		4PI
G,SC 44	RLY	THR-60	C	30-60	NAI-D		4PI
G,P	RLY	THR-60	C	30-60	NAI-D		4PI
G,CA 47	RLY	THR-60	C	30-60	NAI-D		4PI

YLD REL 12C(G,N)

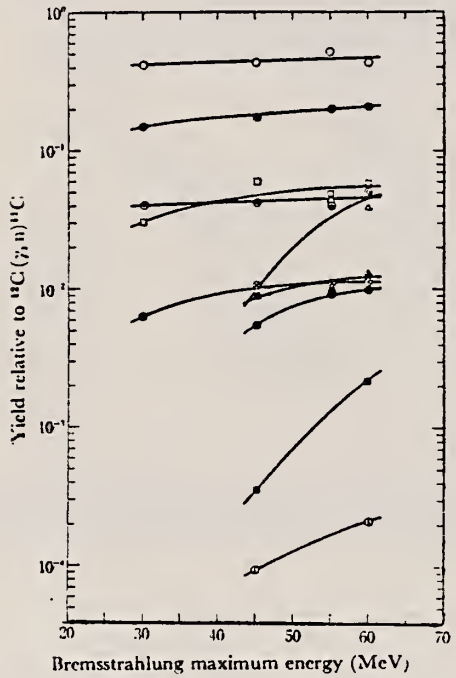

Fig. 6. The yield relative to $^{12}C(\gamma,n)^{11}C$ as a function of bremsstrahlung maximum energy.

○ : ^{45}Ti from titanium
● : ^{41}Sc from titanium
◎ : ^{48}Sc from titanium
⊙ : ^{47}Sc from titanium
⊗ : ^{48}Sc from titanium
△ : ^{48}V from vanadium
▲ : ^{46}Sc from vanadium
□ : ^{47}Sc from vanadium
◪ : ^{48}Sc from vanadium
⓵ : ^{47}Ca from titanium

TABLE 6. THE RELATIVE YIELDS FOR (γ, p) REACTIONS ON TITANIUM NUCLEI EXPRESSED AS THOSE PER MOLE

Reaction	Yield per mole relative to $^{12}C(\gamma, n)^{11}C$			
	30 MeV	45 MeV	55 MeV	60 MeV
$^{47}Ti(\gamma, p)^{46}Sc$	5.4×10^{-1}	5.8×10^{-1}	5.4×10^{-1}	6.3×10^{-1}
$^{48}Ti(\gamma, p)^{47}Sc$	2.0×10^{-1}	2.4×10^{-1}	2.8×10^{-1}	2.8×10^{-1}
$^{49}Ti(\gamma, p)^{48}Sc$	1.2×10^{-1}	2.1×10^{-1}	2.2×10^{-1}	2.1×10^{-1}

REF. H. Arenhovel, J. M. Maison
Nucl. Phys. A147, 305 (1970)

ELEM. SYM.	A	Z
Ti		22

METHOD

REF. NO. 70 Ar 1 egf

REACTION	RESULT	EXCITATION ENERGY	SOURCE		DETECTOR		ANGLE
			TYPE	RANGE	TYPE	RANGE	
G,G	ABX	.12-30	C	32	NAI	12-30	DST

GETS G,G/ TO 2+

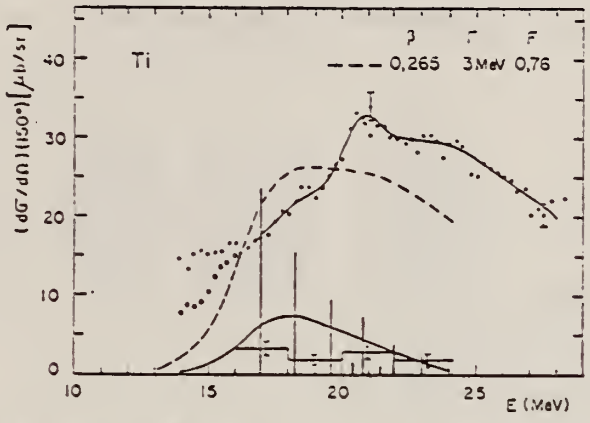

Fig. 4. Differential total scattering cross section at 150° for natural Ti. The full curve through experimental points is only a guide for the eyes. The vertical bars represent the relative strength of dipole levels calculated by the D.C.M. with parameters of table 1. Theoretical elastic plus inelastic scattering is computed from these levels with a common width Γ (dashed curve). Experimental inelastic scattering (histogram) and theoretical inelastic scattering to the first 2^+ (full curve) are shown in the lower part of the figure. Open circles give the cross section after background subtraction.

TABLE 4
Integrated inelastic scattering cross section

Nucleus	Limits of integration (in MeV)	Experimental [a] $\int \sigma_i(E)dE$ (MeV · μb)	Theoretical [a] 2^+	$2^{+\prime}$ (MeV · μb)	Total
Ti(^{48}Ti)	16 −24	250 ± 50	425	109	534
^{51}V(^{52}Cr)	16.4−24.9	492 ± 50	509	116	579
Cr	16.4−23.4	431 ± 50	509	116	579
^{75}As(^{76}Se)	14.1−23.6	1254 ± 120	1373	414	1787
Se(^{80}Se)	14.1−24.6	1035 ± 100	1066	353	1419
^{89}Y					364
Cd(^{112}Cd)	13.6−23.3	3264 ± 240	1894	370	2264
In(^{114}Cd)	13.6−23.6	2840 ± 220	2173	388	2561
Sn(^{110}Sn)	14.2−24.2	2363 ± 220			643

[a]) We assume an angular distribution of the form $1 + \frac{1}{13}\cos^2\theta$.

S. Costa, L. Ferrero, L. Pasqualini, and E. Mancini
Lettere al Nuovo Cimento 2, 665 (1971)

	T1	22
METHOD	REF. NO.	
	71 Co 2	egf

REACTION	RESULT	EXCITATION ENERGY	SOURCE		DETECTOR		ANGLE
			TYPE	RANGE	TYPE	RANGE	
G,XN	ABI	36-64	C	10-64	BF3-I		4PI

FAST N YIELD

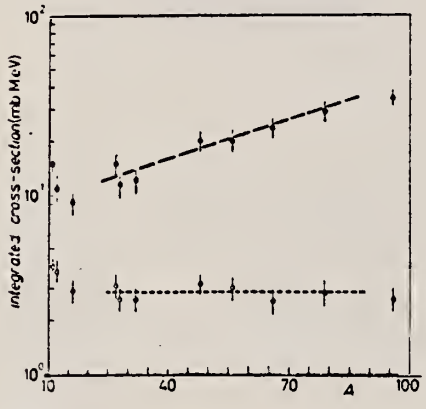

Fig. 2.

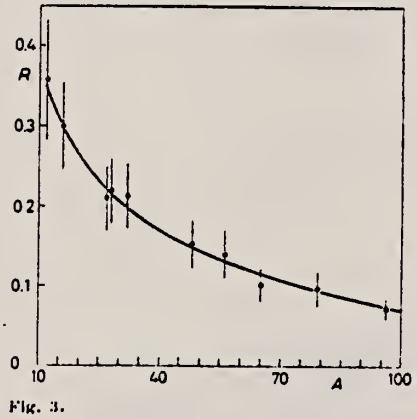

Fig. 3.

Fig 2. – Experimental photoneutron cross-sections integrated over photon energy between 36 and 64 MeV and divided by NZ/A are plotted as a function of the mass number. Black dots are total cross-sections not corrected for neutron multiplicity; open circles represent fast neutron cross-sections (see text). The dashed lines are drawn only to guide the eye.

Fig. 3. – The ratio between «fast» and total photoneutron integrated cross-sections as a function of the mass number A. The solid line represents a fit of the ratios calculated for some nuclei by taking into account the theoretical neutron energy spectra given by GABRIEL and ALSMILLER (4) and the efficiencies of our detector (see Fig. 1).

REF.

N. A. Keller and D. B. McConnell
Can. J. Phys. 50, 1554 (1972)

ELEM. SYM.	A	Z
Ti		22

METHOD

REF. NO.	
72 Ke 4	hmg

REACTION	RESULT	EXCITATION ENERGY	SOURCE		DETECTOR		ANGLE
			TYPE	RANGE	TYPE	RANGE	
G,A	RLY	7-32	C	32	SCD-D		DST

TABLE 3. Observed angular distribution parameters for 32 MeV electron energy

Element	A_0	A_1/A_0	A_2/A_0
Ti	7.03 ± 0.15	0.073 ± 0.052	−0.286 ± 0.073
V	2.58 ± 0.06	0.037 ± 0.042	−0.126 ± 0.069
Fe	10.22 ± 0.30	0.006 ± 0.043	−0.333 ± 0.072
Co	6.80 ± 0.20	0.022 ± 0.048	+0.016 ± 0.077
Ni	15.95 ± 0.49	0.051 ± 0.048	−0.213 ± 0.074
Cu	8.37 ± 0.28	0.076 ± 0.056	−0.035 ± 0.081
Zn	17.87 ± 0.61	0.004 ± 0.045	−0.270 ± 0.073
Ag	0.39 ± 0.01	0.115 ± 0.049	+0.093 ± 0.074

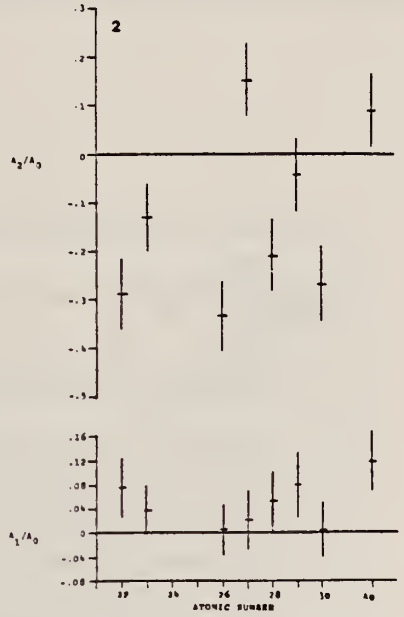

FIG. 2. Angular distributions for 32 MeV electron energy.

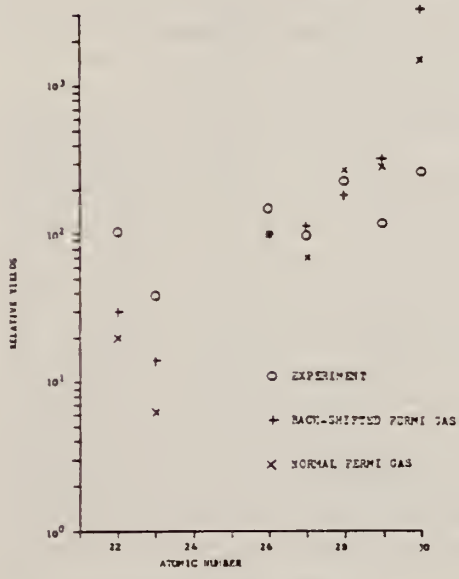

FIG. 13. Experimental and theoretical relative photo-alpha yields for 32 MeV electron beam energy.

REF. V.P. Kovalev, V.P. Kharits, V.V. Gordeev, V.I. Isaev (USSR)
Atomnaya Energiya 32, 496 (1972)

ELEM. SYM.	A	Z
Ti		22

METHOD

REF. NO. 72 Ko 8 hmg

REACTION	RESULT	EXCITATION ENERGY	SOURCE		DETECTOR		ANGLE
			TYPE	RANGE	TYPE	RANGE	
G,N	NOX	8- 22	C	22	THR-I		DST

Мишень	Энергия электронов, Мэв	Детектор	Угол, град							B/A
			30	50	70	90	110	130	150	
Al	22,5	$P^{31}(n,p)$	1,05±0,08	1,03±0,08	0,97±0,08	1,0±0,08	0,98±0,08	1,02±0,08	1,04±0,08	Изотропное
	22,5	$Al^{27}(n,p)$	0,90±0,15	0,95±0,15	1,02±0,15	1,00±0,14	0,96±0,13	1,07±0,13	1,01±0,13	»
Ti	22,5	$P^{31}(n,p)$	1,04±0,07	0,96±0,07	1,03±0,07	1,00±0,07	0,98±0,07	1,05±0,07	1,03±0,07	»
	22,5	$Al^{27}(n,p)$	1,06±0,13	0,94±0,13	1,04±0,12	1,00±0,12	0,95±0,11	0,98±0,11	1,02±0,10	»
Cu	12,8	$P^{31}(n,p)$	0,97±0,10	1,04±0,10	1,02±0,10	1,00±0,10	1,01±0,10	0,90±0,10	0,96±0,10	»
	17,0	$P^{31}(n,p)$	1,03±0,07	0,97±0,07	1,00±0,07	1,00±0,07	1,06±0,07	0,95±0,07	0,88±0,07	»
	22,5	$P^{31}(n,p)$	0,87±0,05	0,94±0,05	0,97±0,05	1,00±0,05	0,99±0,05	0,93±0,05	0,91±0,05	0,18±0,04
	22,5	$Al^{27}(n,p)$	0,75±0,09	0,86±0,07	0,93±0,06	1,00±0,05	1,02±0,05	0,94±0,04	0,90±0,04	0,28±0,06
Mo	22,5	$P^{31}(n,p)$	0,90±0,05	0,93±0,05	0,98±0,05	1,00±0,05	0,99±0,05	0,92±0,05	0,84±0,05	0,21±0,04
	22,5	$Al^{27}(n,p)$	0,80±0,08	0,95±0,08	0,95±0,07	1,00±0,06	0,94±0,05	0,83±0,04	0,72±0,04	0,44±0,08
	22,5	$Al^{27}(n,\alpha)$	0,72±0,08	0,84±0,08	0,89±0,08	1,00±0,08	0,95±0,08	0,87±0,08	0,63±0,08	0,78±0,18
W	22,5	$P^{31}(n,p)$	0,85±0,04	0,90±0,04	0,98±0,04	1,00±0,04	0,98±0,04	0,92±0,04	0,087±0,04	0,25±0,04
	22,5	$Al^{27}(n,p)$	0,78±0,06	0,84±0,06	0,89±0,05	1,00±0,05	0,97±0,04	0,86±0,04	0,75±0,04	0,54±0,06
Pb	22,5	$P^{31}(n,p)$	0,79±0,04	0,85±0,04	0,96±0,04	1,00±0,04	0,98±0,04	0,88±0,04	0,84±0,04	0,36±0,05
	22,5	$Al^{27}(n,p)$	0,70±0,09	0,81±0,08	0,94±0,07	1,00±0,06	0,94±0,06	0,80±0,05	0,69±0,05	0,69±0,12

(over)

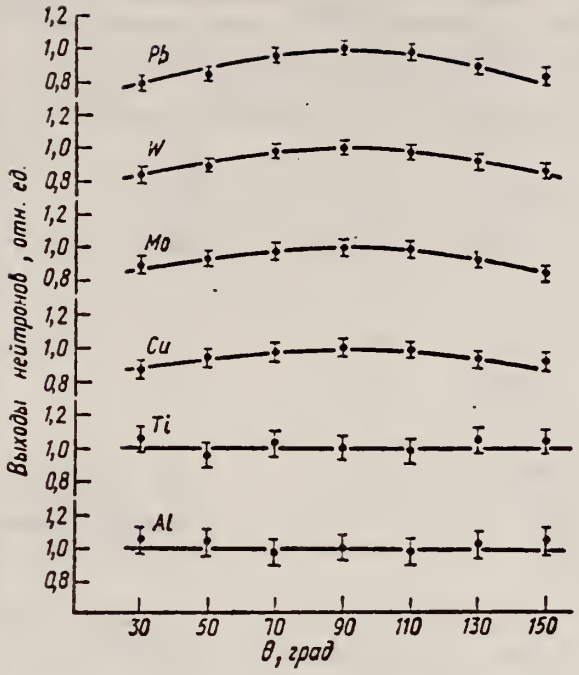

Угловые распределения быстрых фотонейтронов из Al, Ti, Cu, Mo, W, Pb, облучаемых электронами с энергией 22,5 *Мэв*. Детектор I^{131} (n, γ) Si^{31}.

R.F. Barrett, J.R. Birkelund, B.J. Thomas, K.S. Lam, and H.H. Thies
Nucl. Phys. A210, 355 (1973)

Ti		2

METHOD

REF. NO. 73 Ba 20

REACTION	RESULT	EXCITATION ENERGY	SOURCE TYPE	SOURCE RANGE	DETECTOR TYPE	DETECTOR RANGE	ANGLE
G,N	NOX	THR- 27	C	10- 27	BF3-I		4P

MEAN NEUT ENERGY

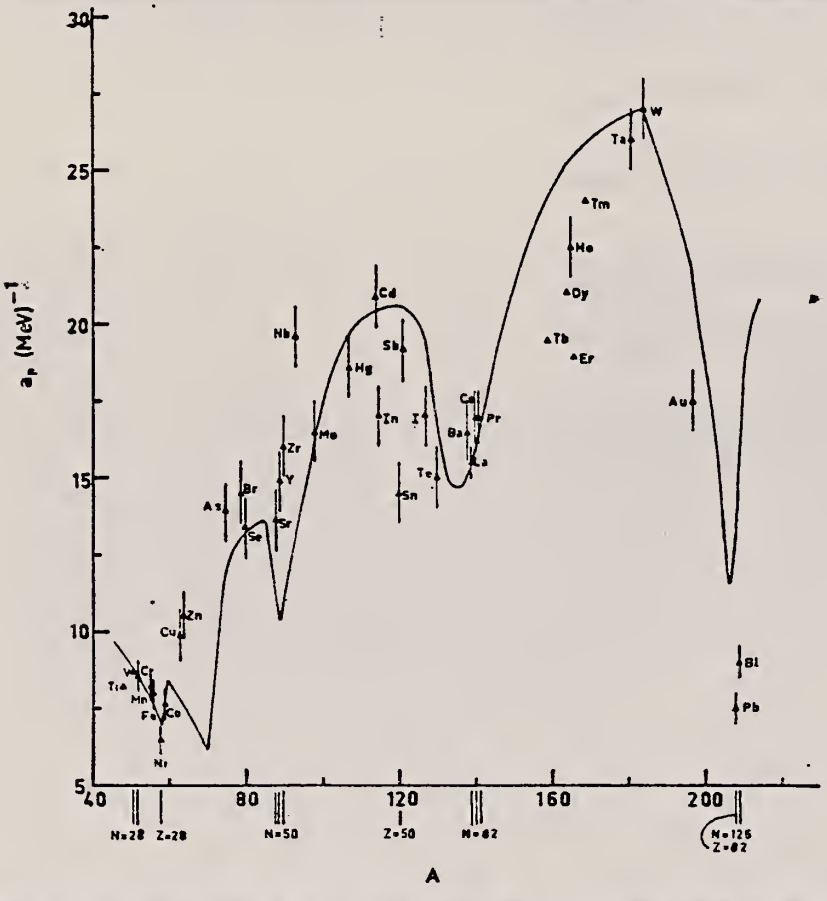

Fig. 12. Experimental values of the level density parameter a_p (Fermi gas formula plus pairing correction) versus atomic number A. The continuous curve is a least-squares fit to the data of a theoretical calculation from Newton [15].

1
H. Baba and S. Baba, Japan Atomic Energy Research Institute report JAERI-1183 (1969).

2
H. Baba, Nucl. Phys. A159, 625 (1970).

15
T.D. Newton, Can. J. Phys. 34, 804 (1956).

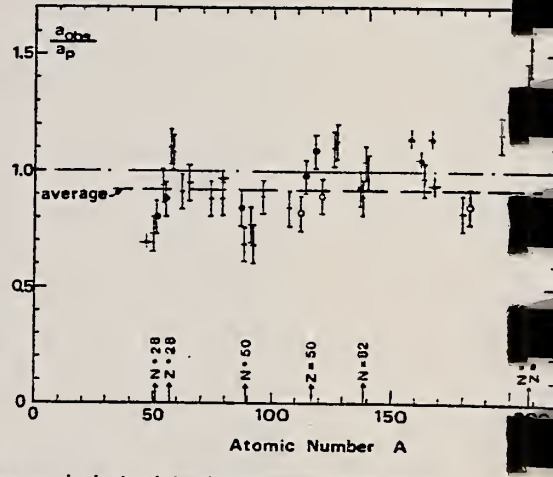

Fig. 15. Ratio a_{obs}/a_p versus atomic number A. Here a_{obs} is the level density parameter taken from the neutron resonance work of refs. [1,2]), and a_p is the level density parameter derived from the present (γ, n) work. Filled circles represent points where nuclei in the neutron resonance and in the (γ, n) experiment were the same. Open circles represent points where the respective nuclei were approximately matched. Triangles represent points which are based on measurement of neutron mean energies at two bremsstrahlung energies only.

(over)

TABLE 3

Comparison of experimental and theoretical data on nuclear level densities with Fermi gas formulae, and comparison of nuclear level density parameters from (γ, n) and n-resonance absorption experiments

Target	N (residual nucleus) [a]		Goodness of fit [b]		$\hat{E}_s(24)$ (MeV) [c]	T (MeV) [d]	a_p (MeV^{-1}) [e]	a_{obs} (MeV^{-1}) [f]	a_{obs}/a_p
			no p.c.	with p.c.					
Ti [g]	23	8%			1.93		8.1–^{47}Ti	6.41–^{47}Ti	0.79
	24	8%							
	25	73%							
	26	5%							
	27	5%							
V [g]	27	100%			1.96		8.7–^{50}V	6.35–^{51}V	0.73
Cr	25	4%	P	G	1.89		8.6–^{51}Cr	6.9 –^{51}Cr	0.80
	27	84%							
	28	10%							
	29	2%							
Mn	29	100%	V.P.	G	2.1		8.2–^{54}Mn	7.82–^{56}Mn	0.94
Fe	27	6%	F	G	1.96		8.0–^{55}Fe	7.06–^{55}Fe	0.88
	29	92%							
	30	2%							
Co	31	100%	P	F	2.12		7.7–^{58}Co	8.35–^{60}Co	1.08
Ni	29	68%	V.P.	P	2.04	1.4	6.5–^{57,7}Ni	7.19–^{59}Ni	1.10
($Z = 28$)	31	26%							
	32	1%							
	33	4%							
	35	1%							
Cu	33	69%	V.P.	P	1.78	1.0	9.8–^{62}Cu	8.90–^{64}Cu	0.91
	35	31%							
Zn	33	49%	F	F	1.61		10.5–^{64,4}Zn	10.0–^{65}Zn	0.95
	35	28%							
	36	4%							
	37	19%							
As	41	100%	V.P.	F	1.44		14.5–^{74}As	12.81–^{76}As	0.88
Se [g]	41	9%			1.39		13.3–^{78}Se	12.8 –^{78}Se	0.97
	42	8%							
	43	24%							
	45	50%							
	47	9%							
Br	43	45%	V.P.	V.P.	1.41		14.5–^{79}Br	12.69–^{80}Br	0.88
	45	49%							
Sr	47	10%	F	G	1.31		13.6–^{87}Sr	11.4 –^{87}Sr	0.84
	48	7%							
	49	83%							

[a]) Neutron numbers and abundances of respective residual nuclei in (γ, n) experiments.

[b]) These give an assessment of the goodness of fit of a calculated $\hat{E}_s$ versus E_0 curve to the observed data, using the Fermi gas level density formula both without and with pairing corrections.

[c]) Bremsstrahlung photoneutron mean energies $\hat{E}_s$ for peak bremsstrahlung energy $E_0 = 24$ MeV.

[d]) Nuclear temperature from fit with constant-temperature formula.

[e]) Level density parameter a_p derived from the present (γ, n) experiment, using a Fermi gas formula plus pairing correction, and corresponding residual nucleus (the atomic weight shown is the weighted average of atomic weights of the respective isotopes present).

[f]) As column 7, but using data on n-resonance absorption from refs. [1,2]).

[g]) Measurements of $\hat{E}_s(E_0)$ for these nuclei were made only for $E_0 = 21$, 23 and 24 MeV.

REF. J. Arends, J. Eyink, A. Hegerath, K.G. Hilger, B. Mecking, G. Nöldeke, H. Rost
Phys. Lett. 98B, 423 (1981)

ELEM. SYM.	A	Z
Ti		22

METHOD

REF. NO. 81 Ar 1 hg

REACTION	RESULT	EXCITATION ENERGY	SOURCE		DETECTOR		ANGLE
			TYPE	RANGE	TYPE	RANGE	
G,MU-T	ABX	215-386	D	215-386	TOF-D		4PI

DATA ALSO IN 81AR3

Double differential cross sections for the photo-emission of protons and charged pion production were investigated for a number of target nuclei (He, Be, C, O, Al, Ti, Cu, Sn, Pb) in the photon energy range k = (215–386) MeV. On the basis of these experimental results the total hadronic cross section was determined.

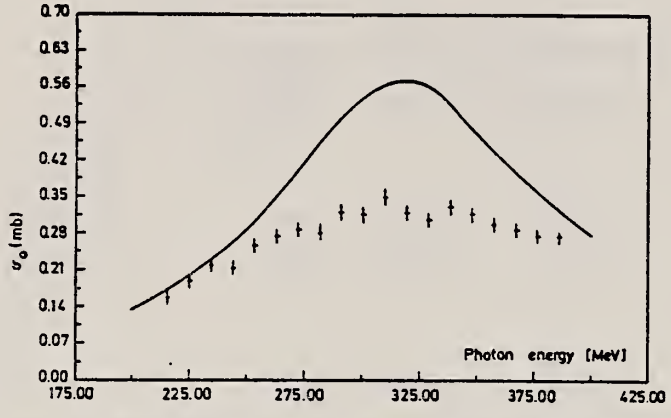

Fig. 7. Parameter σ_0 as a function of photon energy (data points) compared to the mean cross section for a free nucleon (solid line).

The total hadronic cross sections for all measured elements can be parametrized in the form

$$\sigma(k,A) = \sigma_0(k) \cdot A^x ,$$

A being the atomic number, with a constant exponent $x = 1.1$. The photon energy dependence of σ_0 is shown in fig. 7. Compared to the mean cross section for a free nucleon (the solid line in fig. 7) the excitation of the Δ-resonance is suppressed. Such a suppression is expected in the Δ-hole model [11].

REF. J. Arends, J. Eyink, A. Hegerath, K.G. Hilger, B. Mecking, G. Nöldeke, H. Rost
Nucl. Phys. A358, 367c (1981)

ELEM. SYM.	A	Z
Ti		22

METHOD

REF. NO.	
81 Ar 3	hg

REACTION	RESULT	EXCITATION ENERGY	SOURCE		DETECTOR		ANGLE
			TYPE	RANGE	TYPE	RANGE	
G,MU-T	ABX	215-386	D	215-386	TOF-D		4PI

Abstract: Double differential cross sections for the photoemission of protons and charged pion photoproduction were investigated for a number of target nuclei (He, Be, C, O, Al, Ti, Cu, Sn, Pb) using the tagged bremsstrahlung beam at the Bonn 500 MeV-Synchrotron in the photon range k = (215-386)MeV. On the basis of these experimental results the total hadronic cross section was determined.

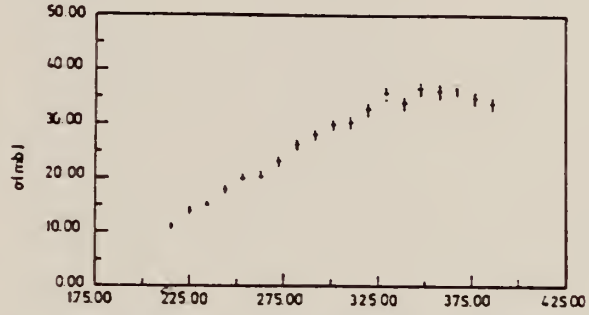

Fig. 2. Cross section for the process: $\gamma + Pb \rightarrow p + X$. The proton threshold is 58 MeV.

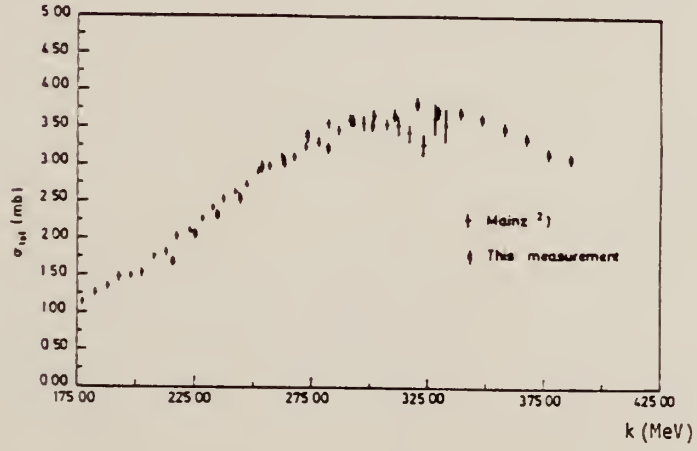

Fig. 3. Total hadronic cross section for Be. The data are compared to the cross section taken from ref.[2]).

The photon energy dependence of the total cross sections for heavier nuclei are similar to the Be results. The complete data set can be parametrized in the form

$$\sigma(k,A) = \sigma_0(k) \cdot A^x.$$

The exponent is constant x = 1.1. The photon energy dependence of σ_0 is shown in fig. 4. Compared to the mean cross section for a free nucleon, the excitation of the Δ-resonance is suppressed.

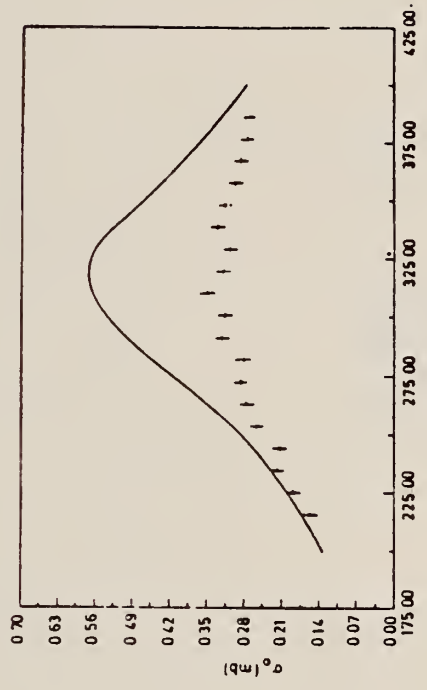

Fig. 4. Parameter σ_0 compared to the cross section for a free nucleon (full line).

Ti
A=44

Ti
A=44

Ti
A=44

REF.
J.J. Simpson, W.R. Dixon, and R.S. Storey
Phys. Rev. C4, 443 (1971)

ELEM. SYM.	A	Z
Ti	44	22

METHOD

REF. NO.	
71 Si 1	hmg

REACTION	RESULT	EXCITATION ENERGY	SOURCE		DETECTOR		ANGLE
			TYPE	RANGE	TYPE	RANGE	
A,G	LFT	8-9	D	4-5	SCD-D		DST
		(8.754-9.227)		(4.2-4.5)			

4 LEVELS

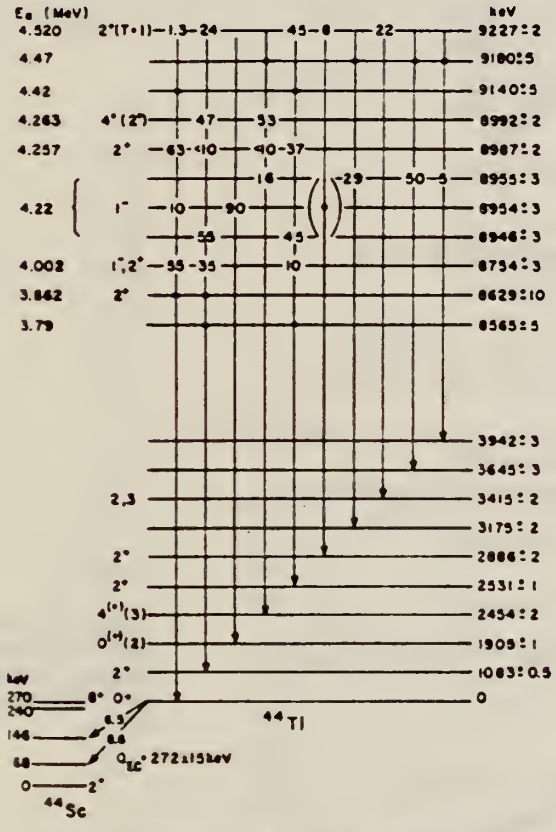

FIG. 3. The main decay branches of resonances examined in the ^{40}Ca(α,γ)^{44}Ti reaction. Resonances for which branching ratios are not given were studied at one angle only. A bracket is used to indicate that no clear choice exists for the resonance at E_α = 4.22 MeV feeding the 2886-keV level.

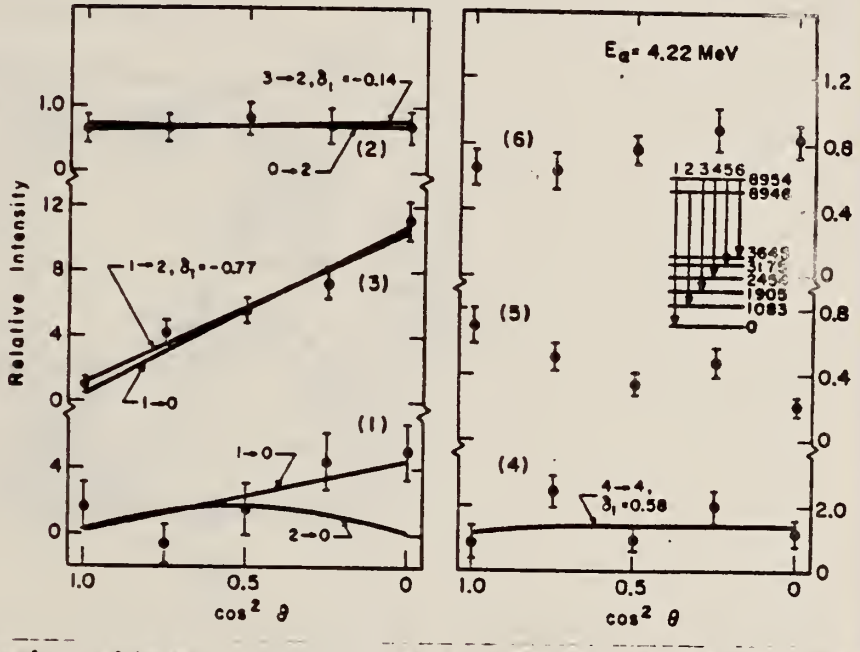

FIG. 4. Angular distributions of some of the primary γ rays from the E_α = 4.22 MeV resonance. The number beside each angular distribution corresponds to the number of the transition in the decay scheme also shown.

(over)

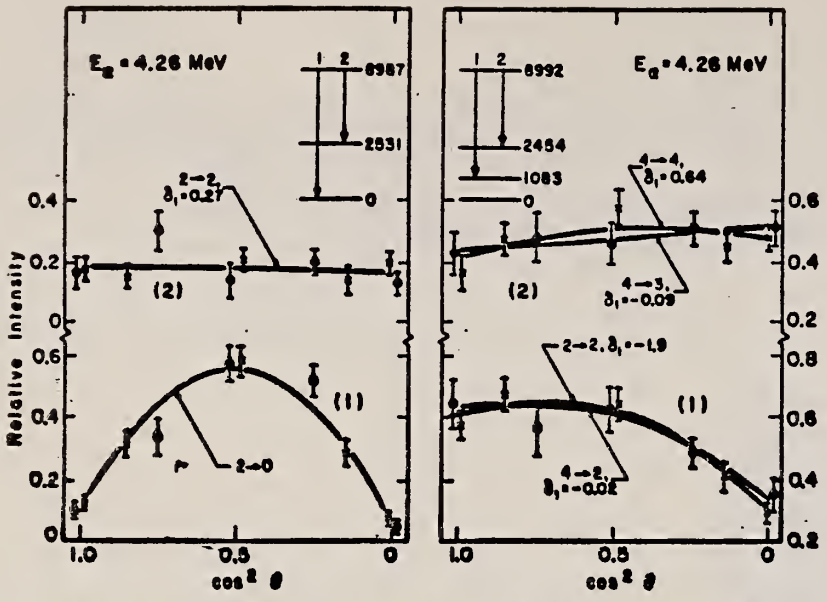

FIG. 7. Angular distributions of primary γ rays from the E_α = 4.26 MeV resonance (see caption for Fig. 4).

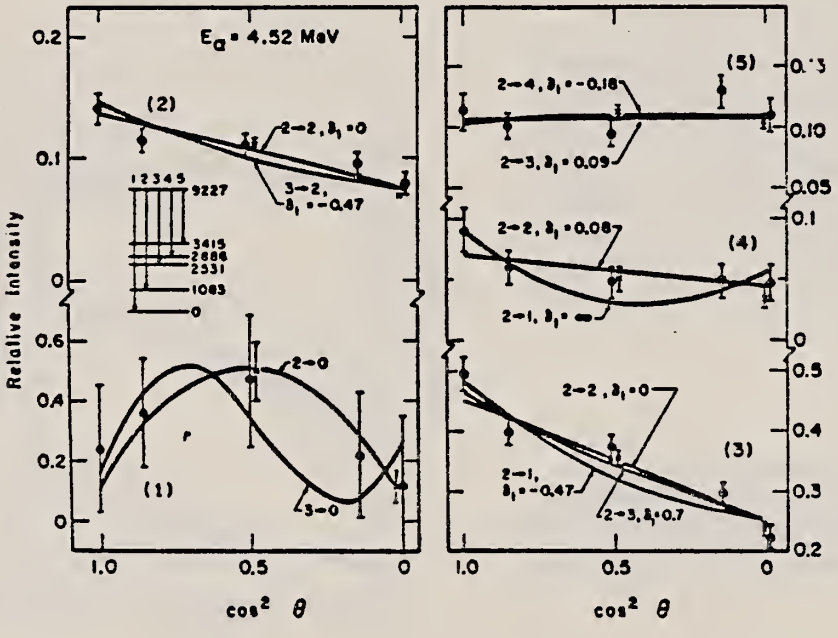

FIG. 11. Angular distributions of primary γ rays from the E_α = 4.52 MeV resonance (see caption for Fig. 4).

REF. R.E. Peschel, J.M. Long, H.D. Shay, and D.A. Bromley
Nucl. Phys. A232, 269 (1974)

ELEM. SYM.	A	Z
Ti	44	22

METHOD

REF. NO. 74 Pe 3 egf

REACTION	RESULT	EXCITATION ENERGY	SOURCE		DETECTOR		ANGLE
			TYPE	RANGE	TYPE	RANGE	
A,G	ABX	11- 21	D	7- 17	NAI-D		DST

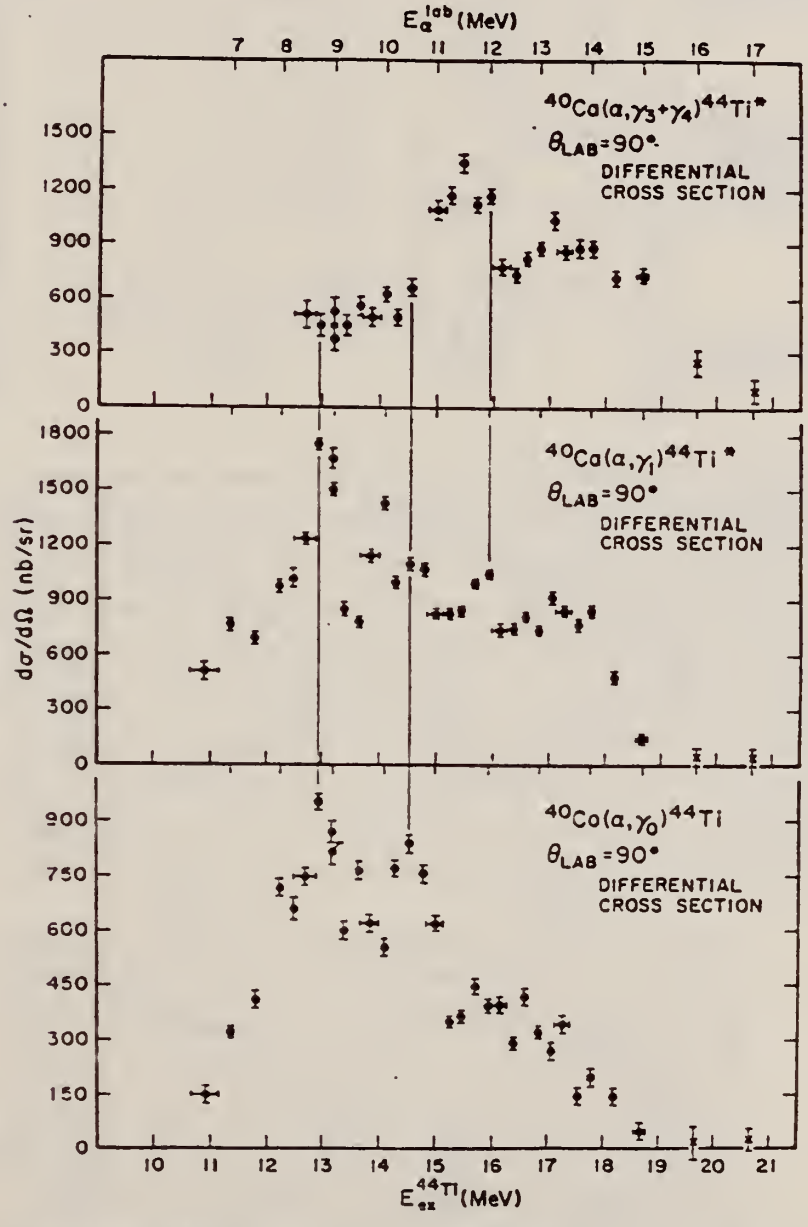

Fig. 3. The 90° differential cross sections for the reactions $^{40}Ca(\alpha,\gamma_0)$, $^{40}Ca(\alpha,\gamma_1)$ and $^{40}Ca(\alpha,\gamma_3+\gamma_4)$. Points represented by solid dots were obtained with a target 1 mg/cm² thick. Points represented by crosses were obtained with a slightly thicker target. Error bars include only statistical errors.

(over)

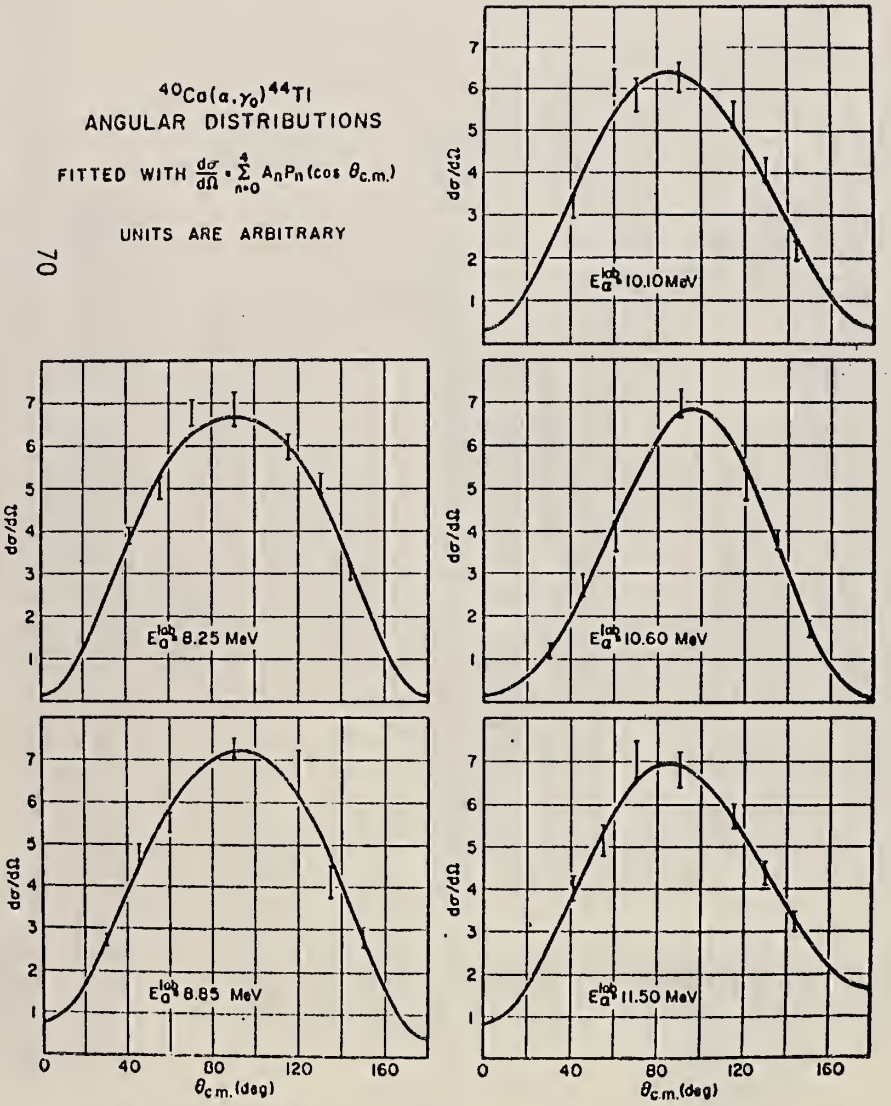

Fig. 4. Angular distributions of the reaction $^{40}Ca(\alpha,\gamma_0)^{44}Ti$. Data are shown as bars, the height of which represents the statistical errors. The solid lines are the Legendre polynomial fits.

TABLE I

The E1 and E2 transition strengths extracted from the $^{40}Ca(\alpha,\gamma_0)$ angular distributions

E_α^{lab}(MeV)	A_2^{exp}	a^2	$(1-a^2)$	A_4^{exp}
8.25	−0.80±0.08	0.88±0.09	0.10±0.04	−0.16±0.07
8.85	−0.77±0.04	0.86±0.05	0.06±0.04	−0.11±0.07
10.10	−0.86±0.10	0.92±0.11	0.03±0.01	−0.057±0.01
10.60	−1.06±0.04	1.03±0.04	0.04±0.05	+0.06±0.08
11.50	−0.73±0.12	0.84±0.13	0.01±0.08	−0.02±0.14

$d\sigma/d\Omega_{exp} = (\sigma_T/4\pi)(1+\Sigma^4_{n=1} A_n P_n)$.

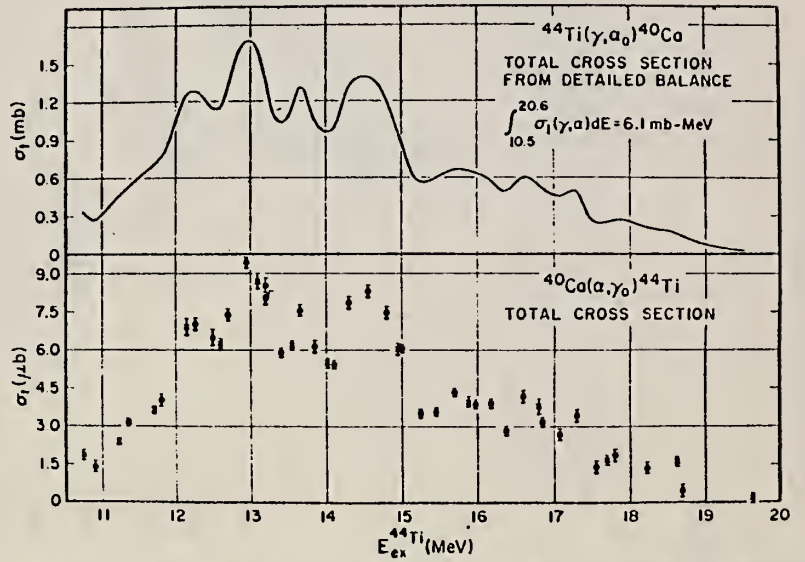

Fig. 7. Total cross section for the reaction $^{40}Ca(\alpha,\gamma_0)^{44}Ti$ obtained from the 90° differential cross section by assuming a $\sin^2\theta$ function for the angular distribution. The points represented by solid dots were obtained with a target 1 mg/cm² thick. The points represented by crosses were obtained with a slightly thicker target. The upper curve is the $^{44}Ti(\gamma,\alpha_0)^{40}Ca$ total cross section obtained from detailed balance.

Ti
A=46

Ti
A=46

Ti
A=46

REF.

E. Silva, J. Goldemberg
An. Acad. Brasil. Cienc. 30, 51 (1958)

ELEM. SYM.	A	Z
Ti	46	22

METHOD

Betatron

REF. NO. 58 Si 4 NVB

REACTION	RESULT	EXCITATION ENERGY	SOURCE		DETECTOR		ANGLE
			TYPE	RANGE	TYPE	RANGE	
G,N	RLX	13-22	C	THR-22	ACT-I		4PI

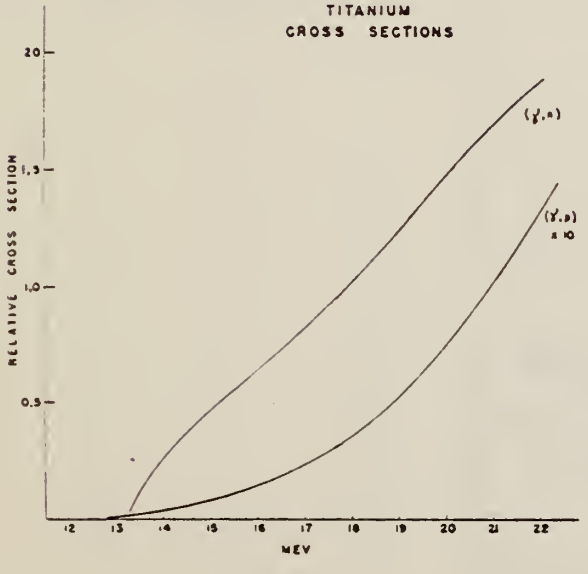

Fig. 4

Ref. T.R. Sherwood, W.E. Turchinetz
Nuclear Phys. 29, 292 (1962)

Elem. Sym.	A	Z
Ti	46	22

Method
Bremss.; Canberra electron synchrotron; activity

Ref. No.
62 Sh 5

EGF

Reaction	E or ΔE
$Ti^{46}(\gamma,n)$	Bremss.
$Ti^{46}(\gamma,np)$	14-31

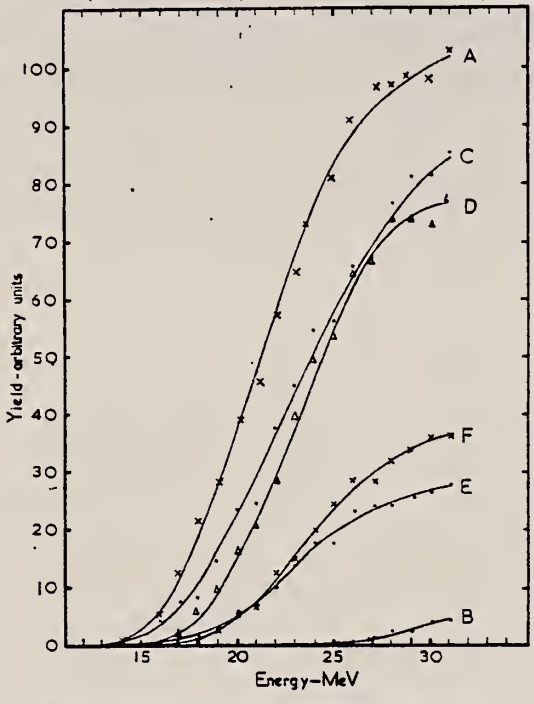

Fig. 1. Activation curves for the photo-disintegration of titanium. A: ^{46}Ti; B: ^{44}Sc (ground state decay); C: ^{44}Sc; D: ^{47}Sc; E: ^{48}Sc; F: ^{49}Sc.

Notes

Table 3: $Cu^{63}(\gamma,n)$ by Berman and Brown [Phys. Rev. 96, 83 (1954)] used as standard.

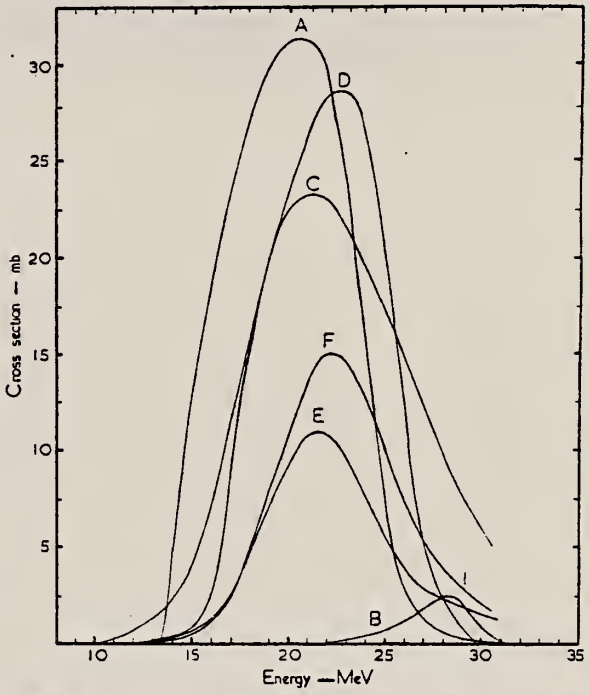

Fig. 2. Excitation function for the photo-disintegration of titanium. A: ^{46}Ti(γ, n) + 1.09 ^{47}Ti(γ, 2n); B: ^{44}Ti(γ, np); C: ^{47}Ti(γ, p) + 10.1 ^{48}Ti(γ, np); D: ^{48}Ti(γ, p) + 0.07 ^{49}Ti (γ, np); E: ^{49}Ti(γ, p) + 0.96 Ti (γ, np); F: ^{50}Ti(γ, p).

TABLE 4

Comparison of experimental results with statistical theory predictions for gamma rays of 22 MeV

Ratio of cross sections	Experimental	Theoretical
$\frac{^{47}Ti(\gamma, p)}{^{48}Ti(\gamma, p)}$	0.81	1.40
$\frac{^{49}Ti(\gamma, p)}{^{48}Ti(\gamma, p)}$	0.39	0.63
$\frac{^{50}Ti(\gamma, p)}{^{48}Ti(\gamma, p)}$	0.45	0.56
$\frac{^{43}Ti(\gamma, p)}{^{44}Ti(\gamma, n)}$	0.98	0.34

TABLE 3

Integrated (to 31 MeV) cross sections

Reactions	Relative weights	Integrated cross section (MeV · mb)
^{44}Ti(γ, n) : ^{47}Ti(γ, 2n)	1 : 1.09	260±34
^{44}Ti(γ, np)		8.8±1.4 [a])
^{47}Ti(γ, p) : ^{48}Ti(γ, np)	1 : 10.1	246±38
^{48}Ti(γ, p) : ^{49}Ti(γ, np)	1 : 0.07	217±32
^{49}Ti(γ, p) : ^{50}Ti(γ, np)	1 : 0.96	86±13
^{50}Ti(γ, p)		113±32

[a]) Upper limit. The partial cross section from the ^{44}Sc formed in the ground state is 4.4 MeV · mb.

(8-1-63)
USCOMM-DC 18556-P63

Ref. D.K. Kaipov, R.B. Begzhanov, A.V. Kuz'minov, Yu.K. Shubnyĭ
Zhur. Eksp. i Teoret. Fiz. 44, 1811 (1963)
Soviet Phys. JETP 17, 1217 (1963)

Elem. Sym.	A	Z
Ti	46	22

Method: Gaseous radioactive source; resonance scattering; NaI

Ref. No.: 63 Ka 1 | JHH

Reaction	E or ΔE	E_o	Γ	$\int \sigma dE$	Jπ	Notes
$Ti^{46}(\gamma,\gamma)$	0.890	0.890				Mean resoance scattering cross section: $\bar{\sigma}(0.890\ MeV) = (1.91\pm0.16)10^{-26} cm^2$ Lifetime: $\tau_\gamma = (1.42\pm0.20)10^{-11}$ sec. for 0.890 MeV state. Detector at 108°.

REF.

J. R. Tatarczuk and H. A. Medicus
Phys. Rev. 143, B818 (1966)

ELEM. SYM.	A	Z
Ti	46	22

METHOD

Bremsstrahlung from Linac

REF. NO. 66 Ta 1 JDM

REACTION	RESULT	EXCITATION ENERGY	SOURCE		DETECTOR		ANGLE
			TYPE	RANGE	TYPE	RANGE	
G,NP	RLY	THR - 48	C	24-48	ACT-I	0-1.4	4PI

Level density $\rho(J) = \rho(0)(2J + 1) \exp [-(J + \frac{1}{2})^2/2\sigma^2]$
Measured relative yield to g.s. and .27 MeV isomer.

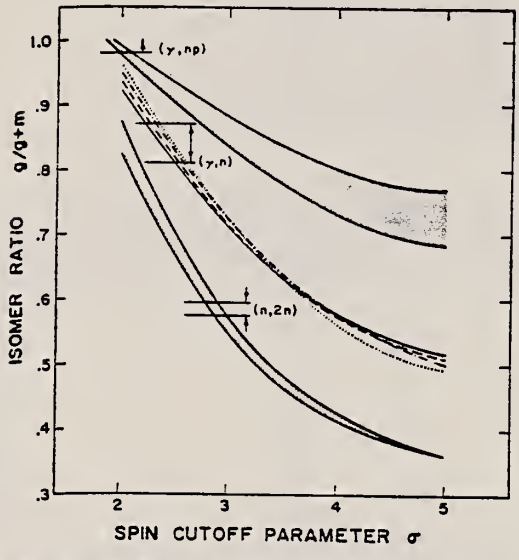

FIG. 6. Calculated isomer ratios versus spin cutoff parameter σ. The top shaded area shows typical calculated results as a function of σ for the (γ,np) reaction. The horizontal line at $g/(g+m)=0.98$ is the experimental value. The bottom area shows results obtained for the $(n,2n)$ reaction with the two horizontal lines indicating the experimental result. The middle set of curves are results for the (γ,n) reaction. Each line corresponds to a different assumption which is given in the text.

TABLE I. Isomer ratios for ^{46}Sc, ground-state yield/total yield $g/(g+m)$.

	Reaction		
	^{46}Sc(γ,n)	^{46}Ti(γ,np)	^{46}Sc$(n,2n)$
Bremsstrahlung endpoint energy (MeV)			
24	0.86±0.02		
36	0.84±0.02		
48	0.84±0.03	>0.98	
X-radiation energy range (MeV)			
Threshold-24	0.86±0.02		
24–36	0.79±0.13		
36–48	0.84±0.40		
Neutron energy 13.9 MeV			
From measurement of the 1.16-MeV γ line			0.581±0.025
From measurement of the annihilation radiation			0.586±0.010

REF. D. B. Gayther, J. W. McMillan, and H. A. Medicus
International Conference on Clustering Phenomena in Nuclei.
Bochum, 21-24 July 1969. International Atomic Energy Agency,
Vienna, 1969)

ELEM. SYM.	A	Z
Ti	46	22

METHOD

REF. NO.	
69 Ga 2	egf

REACTION	RESULT	EXCITATION ENERGY	SOURCE		DETECTOR		ANGLE
			TYPE	RANGE	TYPE	RANGE	
G,NP	ABX	30,34	C	31-39	ACT-I		4PI
G,2N	ABX	30,34	C	31-39	ACT-I		4PI

Difference spectra Bremsstrahlung energies (MeV)	σ(γ, np) (mb)	σ(γ, 2n) (mb)	σ(γ, np)/σ(γ, 2n)	
			observed	calculated
31 - 35	1.6 ± 0.2	0.53 ± 0.08	2.9 ± 0.6	1.1
35 - 39	2.3 ± 0.5	0.37 ± 0.08	6.1 ± 1.1	2.2

REF. J. Heisenberg, J. S. McCarthy and I. Sick
Nucl. Phys. A164, 353 (1971)

ELEM. SYM.	A	Z
Ti	46	22

METHOD

REF. NO. 71 He 1 egf

REACTION	RESULT	EXCITATION ENERGY,	SOURCE		DETECTOR		ANGLE
			TYPE	RANGE	TYPE	RANGE	
E,E/	FMF	1,2	D	198-300	MAG-D		DST

1=0.885, 2=2.0

TABLE 3

Inelastic parameters

Isotope	E^* (MeV)	L	Shape	c_{tr} [a]) (fm)	z_{tr} [a]) (fm)	G [b]) (s.p.u.)	R_{tr} [a]) (fm)	G(s.p.u.) heavy-particle scattering [19])
^{40}Ca	3.740	3	2	3.536±0.030	1.483±0.020	24.9 ±1.0	4.835±0.030	23.6±3.5
	4.480	5	2	3.538±0.050	1.260±0.035	9.7 ±0.6	4.810	17.7±2.7
			3			17.7 ±1.5	5.467±0.060	11.3±1.7
^{42}Ca	3.440	3	2	3.565±0.018	1.383±0.014	12.4 ±0.5	4.719±0.023	12.0±1.8
	4.100	5	2	3.231±0.030	1.404±0.025	3.4 ±0.3	4.816±0.044	9.0±1.4
^{44}Ca	3.30	3	2	3.555±0.018	1.313±0.013	6.95±0.28	4.618±0.023	8.0±1.2
	2.28	4	2	4.091±0.030	1.268±0.016	2.66±0.15	5.135±0.030	1.3±0.3
	3.91	5	2	3.268±0.030	1.397±0.024	2.30±0.20	4.832±0.045	4.4±0.7
^{46}Ti	2.00	4	2	4.264±0.021	1.229±0.013	7.61±0.30	5.226±0.026	
^{48}Ti	2.286	4	2	4.330±0.021	1.196±0.013	3.37±0.15	5.237±0.026	
^{50}Ti	4.42	3	2	3.645±0.017	1.244±0.012	3.76±0.15	4.600±0.023	5.4±0.8
								5.9 [20])
	2.50	4	2	3.865±0.017	1.347±0.012	4.7 ±0.15	5.064±0.026	3.3±0.7
								2.7 [20])
	3.20	5	2	3.254±0.032	1.345±0.026	0.83±0.08	4.724±0.045	

Present experiment

[a]) Errors do not reflect any model dependence.
[b]) Given errors do not include the 6 % error of normalization.

[19] A. M. Bernstein, Adv. in Nucl. Phys. 3 (1969) 325.

13) J. Simpson, J. Cookson, D. Eccleshall and M. Yates, Nucl. Phys. 62 (1965) 385
14) G. M. Temmer and N. P. Heydenburg, Phys. Rev. 104 (1956) 967
15) D. S. Andreyev, A. P. Grinberg, K. I. Erokhina and I. Kh. Lemberg, Nucl. Phys. 19 (1960) 400
16) F. R. Metzger, Nucl. Phys. 27 (1961) 612
17) W. H. Kelly and G. B. Beard, Nucl. Phys. 27 (1961) 188
18) R. B. Begzhanov, A. A. Islamov, D. K. Kaipov and Yu. K. Shubnyi, JETP (Sov. Phys.) 17 (1963) 94

[over]

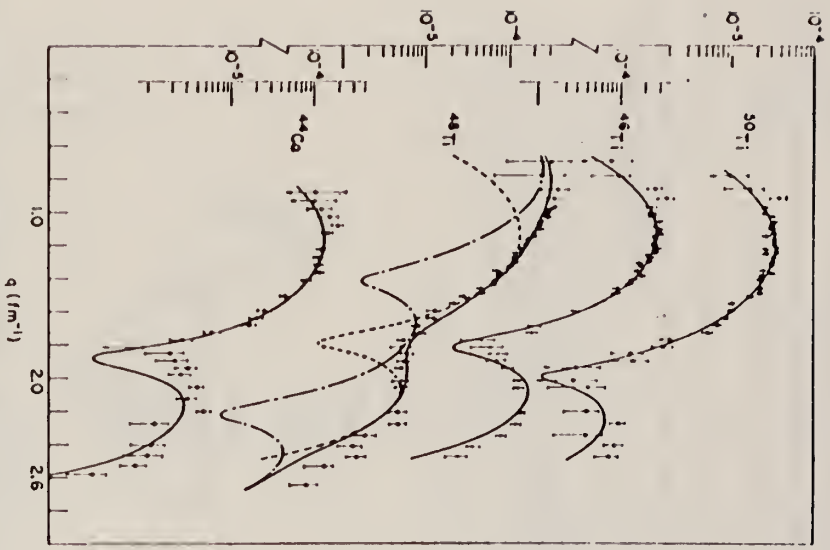

Fig. 6. Fits to ^{45}Ti, ^{46}Ti, ^{48}Ti and ^{44}Ca 4$^+$ levels. For ^{46}Ti we show the decomposition into contributions of the 2.42 MeV 2$^+$ level (dash-dot curve) and the 2.286 MeV 4$^+$ level (dashed curve).

TABLE 2

Inelastic parameters for 2$^+$ levels

Isotope	E^* (MeV)	B(E2) Coulomb Excit: ($e^2 \cdot fm^4$)	Shape	c_{tr} [a] (fm)	z_{tr} [a] (fm)	Fitted B(E2) ($e^2 \cdot fm^4$) [b]	R_{tr} [a] (fm)	B(E2)($e^2 \cdot fm^4$) heavy-particle scattering
^{42}Ca	1.520	364± 82 [9])	2	3.541±0.025	1.459±0.020	320±20	4.619±0.030	476± 74 [19])
^{44}Ca	1.160	350± 70 [10])	2	3.691±0.027	1.428±0.020	480±30	4.704±0.030	507±100 [19])
			1	3.454±0.025	0.690±0.010	1270±85	5.553±0.030	
	3.259		2			54±10		
^{46}Ti	0.885	830±170 [14])	2	3.807±0.014	1.397±0.010	740±20	4.763±0.017	867 [20])
		560±100 [13])	1	3.562±0.014	0.669±0.005	1680±50	5.510±0.020	738 [11])
^{48}Ti	0.984	700±140 [14])	2	3.777±0.014	1.340±0.010	537±15	4.671±0.017	788±120 [19])
		310± 70 [13])	1	3.539±0.014	0.633±0.005	1110±30	5.321±0.020	673 [11])
								659 [20])
	2.420		2			49± 8		57± 10 [19])
^{50}Ti	1.580	240± 20 [13])	2	3.768±0.014	1.255±0.010	307±10	4.567±0.017	349 [20])
			1	3.535±0.014	0.576±0.005	515±17	5.047±0.020	260 [21])
								431 [24])
	4.320		2			51± 8		72 [24])
^{56}Fe	0.880	877± 70 [c])	2	4.048±0.024	1.357±0.014	945±45	4.919±0.025	
			1	3.878±0.024	0.651±0.006	1570±70	5.454±0.030	
				Present experiment				

[a]) Errors do not reflect any model dependence.
[b]) Given errors do not include the 6 % error of normalization.
[c]) Average for B(E2) formed from values of refs. [13–18]).

REF.	ELEM. SYM.	A	Z
V. K. Rasmussen Phys. Rev. C13, 631 (1976)	Ti	46	22

METHOD	REF. NO.
	76 Ra 1 hmg

REACTION	RESULT	EXCITATION ENERGY	SOURCE		DETECTOR		ANGLE
			TYPE	RANGE	TYPE	RANGE	
G,G	LFT	3, 4	C	1- 5	SCD-D		DST
		(3.168,4.316)	(1.3-4.7)				

3168,4316 KEV

TABLE II. Mean lives of some levels in the titanium isotopes.

Mass no., ground state, spin, & abund.	Level energy (keV)	Level spin	Γ_0 (meV)	τ (pres. meas.) (fs)	τ (other) (fs)
46, 0^+	3168	1^-	7.3 ± 2.0	41 ± 12	71 ± 12 [a]
7.95%	4316	1	$(172 \pm 26)\Gamma/\Gamma_0$	0.96 ± 0.14 [b]	<44 [a]
47, $\frac{5}{2}^-$	2162	$\frac{3}{2}^-$	18 ± 5	38 ± 10	31 ± 8 [c]
7.75%	2297	$(\frac{5}{2}^-, \frac{7}{2}^-)$	$\begin{cases} 104 \pm 10 \text{ or} \\ 78 \pm 8 \end{cases}$ [d]	$\begin{cases} 4.7 \pm 0.5 \text{ or} \\ 6.3 \pm 0.7 \end{cases}$ [d]	11 ± 7 [c]
	2548	$\frac{3}{2}^-$	72 ± 8	9 ± 1	
48, 0^+	2421	2_2^+	0.74 ± 0.18	44 ± 12	35 ± 7 [e]
73.45%					$\begin{cases} \Gamma_0 = 0.66 \pm 0.11 \text{ meV and} \\ 0.77 \pm 0.14 \end{cases}$ [f]
	3371	2_3^+	5.5 ± 0.6	16.1 ± 2.1	18 ± 7 [e]
	3700	$1^{(+)}$	20.4 ± 2.3	15.1 ± 1.6	35 ± 3 [g]
	3739	1^+	101 ± 10	4.2 ± 0.4	16 ± 3 [g]
49, $\frac{7}{2}^-$	1623	$(\frac{3}{2}^-, \frac{5}{2}^-, \frac{7}{2}^-)$	11.4 ± 1.5 [h]	55 ± 7	
5.51%	1763	$\frac{5}{2}^-$	18.3 ± 2.2	36 ± 4.3	
50, 0^+	1554	2_1^+	0.52 ± 0.15	1300 ± 400	$\Gamma = 0.18 \pm 0.04$ meV [i]
5.34%	(4311)	2^+	85 ± 60	$1 < \tau < 6$	<80 [j]
(47,49)	3917		$(90 \pm 20)\Gamma/g\Gamma_0$ [k]		
	2810		$(29 \pm 4)\Gamma/g\Gamma_0$ [k]		

[a] Reference 11.
[b] Assuming $\Gamma_0/\Gamma = 0.50$.
[c] Reference 18.
[d] The larger width and shorter lifetime correspond to spin $\frac{5}{2}$.
[e] Reference 23.
[f] Coulomb excitation and (e, e'), J. Heisenberg, J. S. McCarthy, and I. Sick, Nucl. Phys. A164, 353 (1971).
[g] C. D. Kavaloski and W. J. Kossler, Phys. Rev. 180, 971 (1969).
[h] Assuming spin $\frac{9}{2}$.
[i] From Coulomb excitation results of C. W. Towsley, D. Cline, and R. Horoshko, Nucl. Phys. A250, 381 (1975).
[j] Reference 12.
[k] Calculated as if ^{49}Ti, g is the statistical factor.

[11] P.A. Assimakopoulos et al., Nucl. Phys. A180, 131 (1972).
[12] J.G. Pronko et al., Phys. Rev. C10, 1345 (1974).
[18] J.J. Weaver et al., Nucl. Phys. A196, 269 (1972).
[23] T.T. Bardin et al., Phys. Rev. C7, 190 (1973).

REF. S. Oikawa and K. Shoda
Nucl. Physics A277, 301 (1977)

ELEM. SYM.	A	Z
Ti	46	22

METHOD

REF. NO. 77 0i 1 egf

REACTION	RESULT	EXCITATION ENERGY	SOURCE		DETECTOR		ANGLE
			TYPE	RANGE	TYPE	RANGE	
E,P	ABX	13-25	D	13-25	MAG-D		90
E,A	ABY	12-19	D	12-19	MAG-D		90

Abstract: The cross sections of the (e, e'p) reaction on ^{44}Ca, ^{45}Sc and ^{46}Ti have been measured and used to deduce (γ, p) cross sections. Together with (γ, n) cross sections from others, these data allow an estimate of the $T_<$ and $T_>$ GDR cross sections. The experimental results seem to be consistent with the theory on the isospin splitting. The (γ, p_0) or (γ, $p_0 + p_1$) and (γ, α_0) cross sections have also been measured. The ratio $\sigma(\gamma, p_0)/\sigma(\gamma, p)$ indicates a contribution of a statistical nature in the $T_<$ GDR region and some additional direct modes in the $T_>$ GDR region. The contribution of one (^{45}Sc) or two (^{46}Ti) extra protons is discussed and it is found that the valence nucleons contribute to GDR in an independent way.

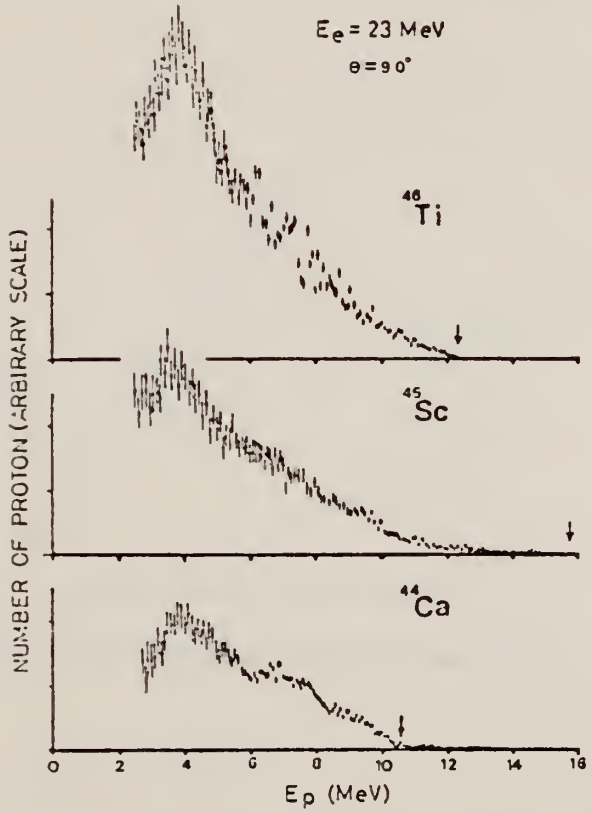

Fig. 4. Example of proton energy distribution obtained with 23 MeV electron beam. Arrows show the proton end point energy.

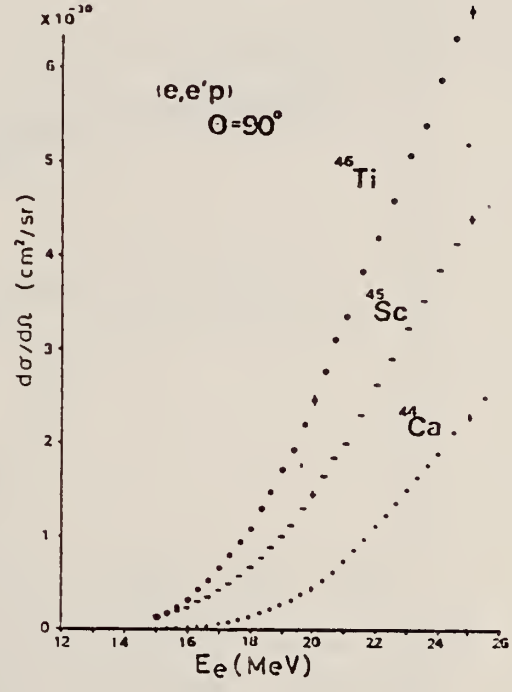

Fig. 5. The differential cross sections at $\theta = 90$ of the (e, e'p) reaction.

(over)

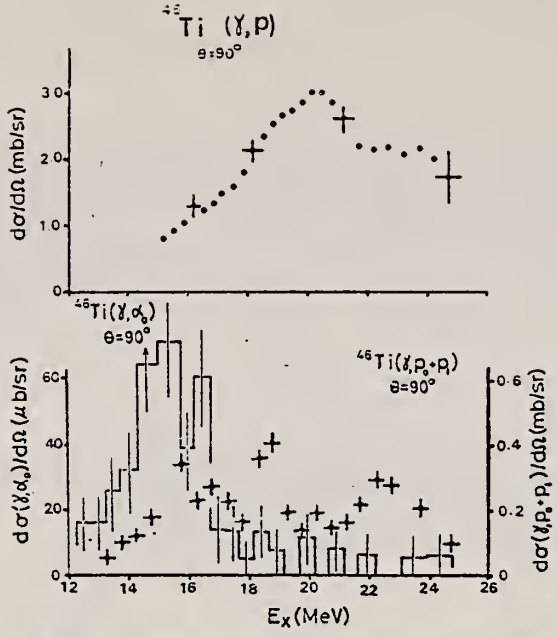

Fig. 8. The differential cross sections at $\theta = 90^{\circ}$ of the (γ, p), (γ, p_0+p_1) and (γ, α_0) reactions of ^{46}Ti.

REF. K. Masumoto, T. Kato, N. Suzuki
Nucl. Inst. Meth. 157, 567 (1978)

ELEM. SYM.	A	Z
Ti	46	22

METHOD

REF. NO. 78 Ma 10 hg

REACTION	RESULT	EXCITATION ENERGY	SOURCE		DETECTOR		ANGLE
			TYPE	RANGE	TYPE	RANGE	
G,N	ABY	13-68	C	30-68	ACT-I		4PI

Analysis is made of reactions interfering with photon activation analysis procedures.

The activation yield curves have been presented for a number of photonuclear reactions in the energy range from 30 to 68 MeV, in order to evaluate quantitatively the interferences due to competing reactions in multielement photon activation analysis. The general features of the yields as functions of both target mass number and excitation energy were elucidated from the data obtained, discussion being given on the results in terms of the reaction mechanism.

Simultaneous neutron activation due to appreciable neutron production from the converter and surrounding materials has also been studied, and, finally, the magnitudes of interferences in real multielement analysis were given in the form of their energy dependences.

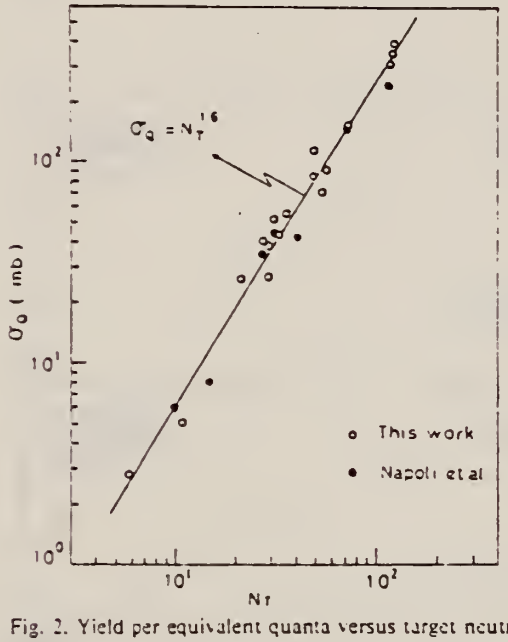

Fig. 2. Yield per equivalent quanta versus target neutron number.

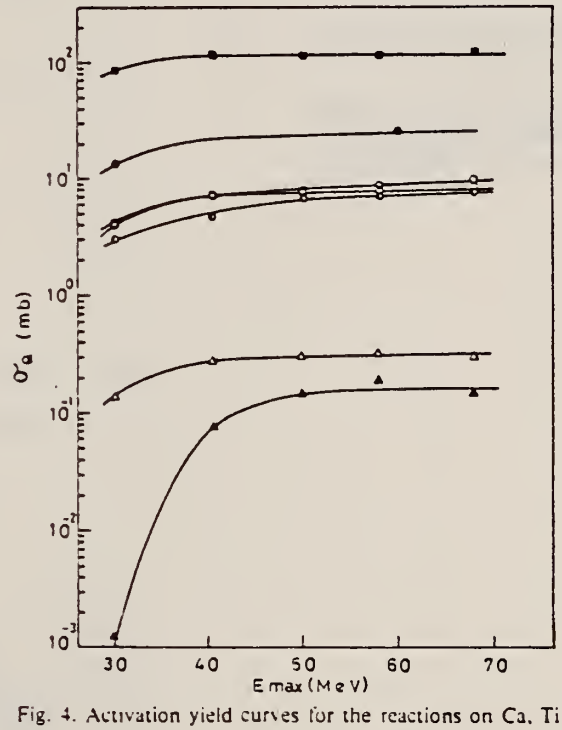

Fig. 4. Activation yield curves for the reactions on Ca, Ti and V.

■ $^{48}Ca(\gamma, n)^{47}Ca$, □ $^{44}Ca(\gamma, p)^{43}K$, ● $^{46}Ti(\gamma, n)^{45}Ti$,
○ $^{48}Ti(\gamma, p)^{47}Sc$, ◐ $^{49}Ti(\gamma, p)^{48}Sc$, △ $^{51}V(\gamma, \alpha)^{47}Sc$,
▲ $^{51}V(\gamma, xn)^{46}Sc$.

FORM NBS-418

U.S. DEPARTMENT OF COMMERCE

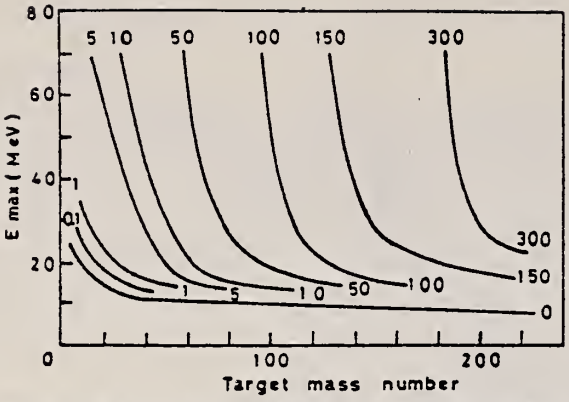

Fig. 9. Yields of the (γ, n) reactions as a function of bremsstrahlung maximum energy and target mass number. The numerical values in the figure are yields per equivalent quanta in mb.

REF. R.E. Pywell and M.N. Thompson
Nucl. Phys. A318, 461 (1979)

ELEM. SYM.	A	Z
Ti	46	22

METHOD

REF. NO. 79 Py 5 hg

REACTION	RESULT	EXCITATION ENERGY	SOURCE TYPE	SOURCE RANGE	DETECTOR TYPE	DETECTOR RANGE	ANGLE
G,N	ABX	12-25	C	12-26	ACT-I		4 PI

Abstract: The photoneutron cross section, $^{46}Ti(\gamma, n)$, has been studied in the photon energy range 12 to 25 MeV. Comparison of this cross section with the $^{46}Ti(\gamma, p)$ cross section shows evidence for isospin splitting of the giant dipole resonance. A detailed calculation for the (γ, n) and (γ, p) cross sections assuming a statistical decay process and taking into account the isospin selection rules and the predictions of Goulard and Fallieros for the energy separation and relative strengths of the two isospin components of the giant dipole resonance, agrees with the experimental results. The possibility of deformation splitting of the ^{46}Ti GDR is also discussed.

MIXED YIELDS MEASURED

COMMENTS

(1) Absolute scale of the yield curve normalized to that of the $^{63}Cu(\gamma,n)$ reaction reported in ref. 7,8.
Ref. 7 -- F. Dreyer, H. Dahmere, J. Staude and H.H. Thies, Nucl. Phys. A192 (1972) 433
Ref. 8 -- R.E. Sund, M.P. Baker, L.A. Kull and R.B. Walton, Phys. Rev. 176 (1968) 1366

(2) Integrated cross section to 25 MeV is 194±40 MeV mb.

(3) Actual cross section measured is $\sigma(^{46}Ti(\gamma,n))+1.09\sigma(^{47}Ti(\gamma,2n))+1.36\sigma(^{46}Ti(\gamma,np))$.

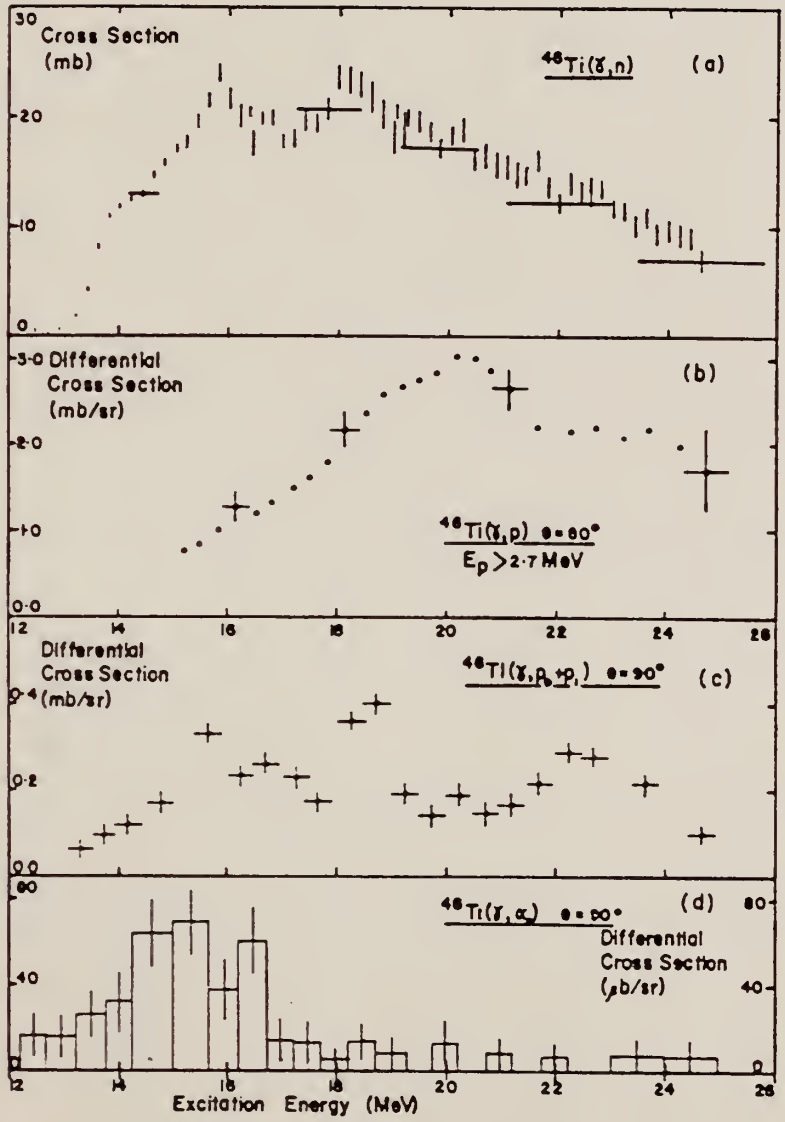

Fig. 2. (a) The $^{46}Ti(\gamma, n)$ cross section. Vertical error bars show statistical errors only. There is a 20 % uncertainty in the absolute cross section scale. Horizontal bars show the analysis bin width used. (b) The $^{46}Ti(\gamma, p)$. (c) The $^{46}Ti(\gamma, p_0+p_1)$. (d) The $^{46}Ti(\gamma, \alpha_0)$ differential cross sections of ref. [5]).

Ref. 5 -- S. Oikawa & K. Shoda, Nucl. Phys. A277 (1977) 301

Ti
A=47

Ti
A=47

Ref. T.R. Sherwood, W.E. Turchinetz
Nuclear Phys. 29, 292 (1962)

Elem. Sym.	A	Z
Ti	47	22

Method
Bremss.; Canberra electron synchrotron; activity

Ref. No.
62 Sh 5 | EGF

Reaction	E or ΔE
$Ti^{47}(\gamma,p)$	Bremss.
$Ti^{47}(\gamma,2n)$	14-31

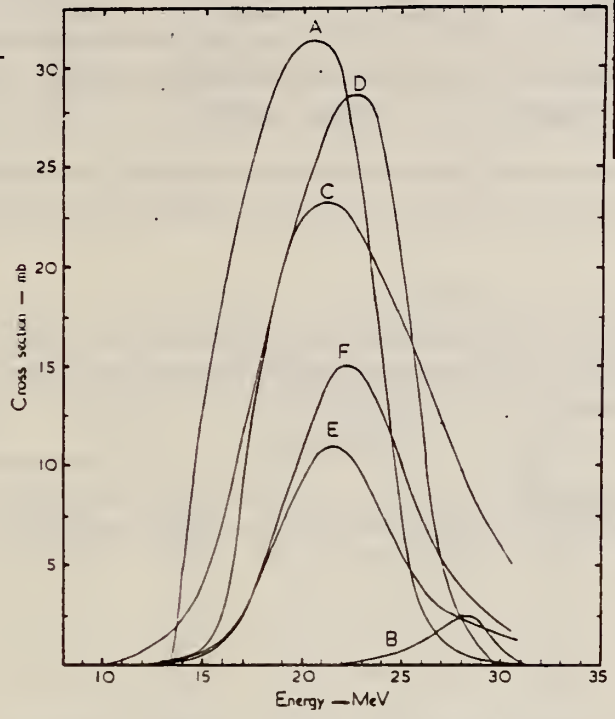

Fig. 2. Excitation function for the photo-disintegration of titanium. A: $^{49}Ti(\gamma, n) + 1.09\ ^{47}Ti(\gamma, 2n)$; B: $^{49}Ti(\gamma, np)$; C: $^{47}Ti(\gamma, p) + 10.1\ ^{49}Ti(\gamma, np)$; D: $^{48}Ti(\gamma, p) + 0.07\ ^{49}Ti(\gamma, np)$; E: $^{46}Ti(\gamma, p) + 0.96$ Ti (γ, np); F: $^{50}Ti(\gamma, p)$.

TABLE 3

Integrated (to 31 MeV) cross sections

Reactions	Relative weights	Integrated cross section (MeV · mb)
$^{46}Ti(\gamma, n) : {}^{47}Ti(\gamma, 2n)$	1 : 1.09	260 ± 34
$^{46}Ti(\gamma, np)$		8.8 ± 1.4 a)
$^{47}Ti(\gamma, p) : {}^{49}Ti(\gamma, np)$	1 : 10.1	246 ± 38
$^{49}Ti(\gamma, p) : {}^{49}Ti(\gamma, np)$	1 : 0.07	217 ± 32
$^{49}Ti(\gamma, p) : {}^{50}Ti(\gamma, np)$	1 : 0.96	86 ± 13
$^{50}Ti(\gamma, p)$		113 ± 32

a) Upper limit. The partial cross section from the ^{49}Sc formed in the ground state is 4.4 MeV · mb.

TABLE 4

Comparison of experimental results with statistical theory predictions for gamma rays of 22 MeV

Ratio of cross sections	Experimental	Theoretical
$\frac{^{47}Ti(\gamma, p)}{^{48}Ti(\gamma, p)}$	0.81	1.40
$\frac{^{46}Ti(\gamma, p)}{^{49}Ti(\gamma, p)}$	0.39	0.63
$\frac{^{50}Ti(\gamma, p)}{^{48}Ti(\gamma, p)}$	0.45	0.56
$\frac{^{49}Ti(\gamma, p)}{^{49}Ti(\gamma, n)}$	0.98	0.34

Notes

Table 3: $Cu^{63}(\gamma,n)$ by Berman and Brown [Phys. Rev. 96, 83 (1954)] used as standard.

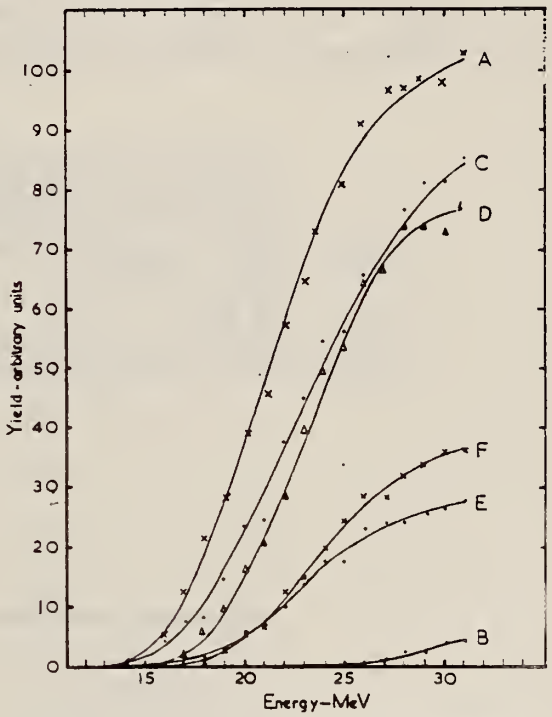

Fig. 1. Activation curves for the photo-disintegration of titanium. A: ^{48}Ti; B: ^{49}Sc (ground state decay) C: ^{46}Sc; D: ^{47}Sc; E: ^{48}Sc; F: ^{49}Sc.

FORM NBS-418
(9-1-63)
USCOMM-DC 18656-P63

REF. E. C. Booth, B. Chasan and K. A. Wright
Nucl. Phys. 57, 403-420 (1964)

ELEM. SYM.	A	Z
Ti	47	22

METHOD
Van de Graaff; resonance fluorescence

REF. NO. 64 Bo 1 NVB

REACTION	RESULT	EXCITATION ENERGY	SOURCE TYPE	SOURCE RANGE	DETECTOR TYPE	DETECTOR RANGE	ANGLE
G,G	LFT	1-3	C	1 - 3	NAI-D		100
		(0.5 - 3.0)		(0.5 - 3.0)			

ABI

TABLE 1
Cases of observed resonance fluorescence

Nucleus multipol.	State (MeV)	Spin	Γ_0/Γ	$T(gw\Gamma_0^2/\Gamma^2)^{-1}$ (sec).	Mean lifetime T BCW (sec)	Mean lifetime T other (sec)	Ref.	Γ_0/Γ_W BCW
Ti^{47}	0.00	$\frac{5}{2}^-$						
[M1]?	2.58	[$\frac{3}{2}^-$]	?	$45^{+80}_{-18}\times10^{-16}$				$1.0\Gamma/\Gamma_0$

REF. H. L. Pai and K. G. McNeill
Can. J. Phys. 45, 3235 (1967)

ELEM. SYM.	A	Z
Ti	47	22

METHOD

REF. NO. 67 Pa 2

EGF

REACTION	RESULT	EXCITATION ENERGY	SOURCE		DETECTOR		ANGLE
			TYPE	RANGE	TYPE	RANGE	
G,P	RLY	THR-30	C	22,30	ACT-I		4PI
G,NP	RLY	THR-30	C	22,30	ACT-I		4PI

TABLE I

Yields, Y, and cross sections, σ, of the proton reactions in Ti isotopes excited by photons or neutrons. (The yields and cross sections with primes are "first proton" yields and cross sections)

		1	2	3	4	5	6	7
		E_γ = 22 MeV				E_n = 13 MeV		
Compound nucleus	Target nucleus	$Y_{\gamma p}$	$Y_{\gamma pn}$	$Y_{\gamma np}$	$Y_{\gamma p}'$ (cols. 1 + 2)	σ_{np}	$\sigma_{n,pn}$	σ_{np}' (cols. 5 + 6)
^{47}Ti*	^{47}Ti ^{46}Ti	57	(<1)[a]	(<1)	~57	277	(<10)	~280
^{46}Ti*	^{46}Ti ^{47}Ti	20	E.I.[b]	E.I.	20	121	34	155
^{48}Ti*	^{48}Ti ^{48}Ti	9.2	<0.1	<0.1	9.2	69	<1	~70
^{49}Ti*	^{49}Ti ^{48}Ti	9.6	E.I.	E.I.	9.6	29	<1	~30

		1	2	3	4	5	6	7
		E_γ = 30 MeV				E_n = 19 MeV		
Compound nucleus	Target nucleus	$Y_{\gamma p}$	$Y_{\gamma pn}$	$Y_{\gamma np}$	$Y_{\gamma p}'$	σ_{np}	$\sigma_{n,pn}$	σ_{np}'
^{47}Ti*	^{47}Ti ^{46}Ti	5.5	(0.03)	(0.04)	5.5	167	47	214
^{46}Ti*	^{46}Ti ^{47}Ti	2.5	0.24	0.41	2,7	77	70	147
^{48}Ti*	^{48}Ti ^{48}Ti	1.5	0.29	0.57	1.8	42	31	73
^{49}Ti*	^{49}Ti ^{48}Ti	1.6	0.17	0.37	1.8	28	9	37

[a] Bracketed values are calculated from yields for production of ^{47}Ti, as ^{47}Sc is stable.
[b] E.I. = energetically impossible.

REF.	ELEM. SYM.	A	Z
H. L. Pai and K. G. McNeill Can. J. Phys. 45, 3235 (1967)	Ti	47	22

METHOD	REF. NO.	
[Page 2 of 2]	67 Pa 2	EGF

REACTION	RESULT	EXCITATION ENERGY	SOURCE		DETECTOR		ANGLE
			TYPE	RANGE	TYPE	RANGE	

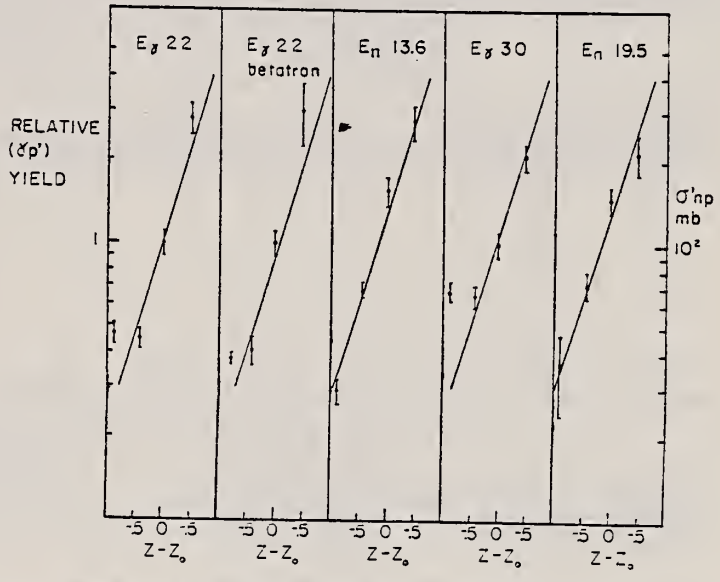

FIG. 1. The relative yields of the first-proton photoreactions in four Ti isotopes plotted as a function of $Z - Z_0$, where $Z = 22$ and Z_0 is the value of Z which minimizes $M(A, Z)$. For ^{50}Ti, $Z - Z_0 = -0.88$, and for ^{49}Ti, ^{48}Ti, and ^{47}Ti the values of $Z - Z_0$ are -0.44, $+0.01$, and $+0.46$ respectively. Three plots are shown, one obtained at 22 MeV using the linac, one at 30 MeV with the linac, and one at 22 MeV with the betatron. Also shown are cross sections of the first-proton reactions induced by fast neutrons, of energies 13.6 and 19.5 MeV, in Ti isotopes (Pai 1966).

REF.

Y. Oka, T. Kato, K. Nomura, T. Saito, Hui-Tuh Tsai
Bull. Chem. Soc. Japan 41, 380 (1968)

ELEM. SYM.	A	Z
Ti	47	22

METHOD

REF. NO.	
68 Ok 3	egf

REACTION	RESULT	EXCITATION ENERGY	SOURCE		DETECTOR		ANGLE
			TYPE	RANGE	TYPE	RANGE	
G,P	ABY	THR-20	C	20	ACT-I		4PI

TABLE 1. SUMMARY OF DATA ON (γ, p) REACTIONS WITH 20 MeV BREMSSTRAHLUNG

Nuclide: Parent (Natural abundance, %)	Nuclide: Residual (Half-life)	S_p (MeV)	Observed γ-ray: Energy (MeV)	Observed γ-ray: Branching ratio (%)	Observed γ-ray: Type of multipole transition	Yield determined: μCi/mg[a]	Yield determined: Yield/mol·R
^{25}Mg (10.11)	^{24}Na (15 hr)	12.06	1.37	100	$E2$	1.48×10^{-1}	1.7×10^{5}
^{29}Si (4.71)	^{28}Al (2.27 min)	12.33	1.78	100	$E2$	1.91	2.8×10^{5}
^{30}Si (3.12)	^{29}Al (6.56 min)	13.59	1.28	93.8	$E2+M1$	6.51×10^{-1}	1.5×10^{5}
^{44}Ca (2.06)	^{43}K (22.4 hr)	12.17	0.374	85	$E2+M1$	7.86×10^{-3}	1.3×10^{5}
^{47}Ti (7.32)	^{46}Sc (84.1 d)	10.47	0.887	100	$E2$	7.11×10^{-4}	3.1×10^{5}
^{48}Ti (73.99)	^{47}Sc (3.4 d)	11.44	0.160	100	$E2+M1$	6.83×10^{-3}	1.2×10^{5}
^{49}Ti (5.46)	^{48}Sc (1.8 d)	11.35	1.31	100	$E2$	4.40×10^{-3}	5.8×10^{4}
^{53}Cr (9.55)	^{52}V (3.8 min)	11.15	1.43	100	$E2$	5.01×10^{-1}	6.6×10^{4}
^{57}Fe (2.17)	^{56}Mn (2.58 hr)	10.57	1.81	23.5	$E2+M1$	8.10×10^{-3}	2.1×10^{5}
^{74}Ge (36.74)	^{73}Ga (4.8 hr)	10.92	0.295	97	($E2$)	3.70×10^{-1}	1.3×10^{5}
^{77}Se (7.58)	^{76}As (26.5 hr)	9.61	0.559	41	$E2$	1.48×10^{-3}	1.3×10^{5}
^{87}Sr (7.02)	^{86}Rb (19 d)	9.41	1.08	9	$E2$	5.15×10^{-4}	9.9×10^{4}
^{111}Cd (12.26)	^{112}Ag (3.2 hr)	9.74	1.39	35	$E2$	1.91×10^{-2}	2.1×10^{4}
^{117}Sn (7.57)	^{116m}In (54 min)	9.58	1.27	84	$E2$	9.80×10^{-3}	6.9×10^{5}
^{137}Ba (11.32)	^{136}Cs (13 d)	8.67	0.830	100	$E2$	1.68×10^{-4}	2.2×10^{4}
^{199}Hg (16.84)	^{198}Au (2.7 d)	7.27	0.412	100	$E2$	8.43×10^{-4}	2.2×10^{4}

a) The value corrected at the end of 1 hr irradiation (9.4×10^{6} R/min).

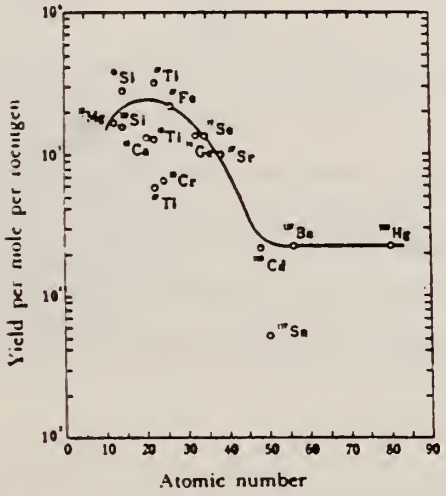

Fig. 2. The yield curve for the (γ, p) reaction with 20 MeV bremsstrahlung.

Y. Oka, T. Kato and N. Sato
Bull. Chem. Soc. Japan 42, 387 (1969)

Ti	47	22

METHOD

REF. NO. 69 Ok 1 hmg

REACTION	RESULT	EXCITATION ENERGY	SOURCE		DETECTOR		ANGLE
			TYPE	RANGE	TYPE	RANGE	
G,P	RLY	THR-60	C	30-60	NAI-D		4PI

YLD REL 12C(G,N)

TABLE 6. THE RELATIVE YIELDS FOR (γ, p) REACTIONS ON TITANIUM NUCLEI EXPRESSED AS THOSE PER MOLE

Reaction	Yield per mole relative to $^{12}C(\gamma, n)^{11}C$			
	30 MeV	45 MeV	55 MeV	60 MeV
$^{47}Ti(\gamma, p)^{46}Sc$	5.4×10^{-1}	5.8×10^{-1}	5.4×10^{-1}	6.3×10^{-1}
$^{48}Ti(\gamma, p)^{47}Sc$	2.0×10^{-1}	2.4×10^{-1}	2.8×10^{-1}	2.8×10^{-1}
$^{49}Ti(\gamma, p)^{48}Sc$	1.2×10^{-1}	2.1×10^{-1}	2.2×10^{-1}	2.1×10^{-1}

REF. V. K. Rasmussen
Phys. Rev. C13, 631 (1976)

ELEM. SYM.	A	Z
Ti	47	22

METHOD

REF. NO. 76 Ra 1 hmg

REACTION	RESULT	EXCITATION ENERGY	SOURCE TYPE	SOURCE RANGE	DETECTOR TYPE	DETECTOR RANGE	ANGLE
G,G	LFT	2, 2	C	1- 5	SCD-D		DST
		(2.162,2.297)		(1.3-4.7)			

2162,2297,2548 KEV

TABLE II. Mean lives of some levels in the titanium isotopes.

Mass no., ground state, spin, & abund.	Level energy (keV)	Level spin	Γ_0 (meV)	τ (pres. meas.) (fs)	τ (other) (fs)
46, 0^+	3168	1^-	7.3 ± 2.0	41 ± 12	71 ± 12 [a]
7.95%	4316	1	(172 ± 26) Γ/Γ_0	0.96 ± 0.14 [b]	<44 [a]
47, $\frac{5}{2}^-$	2162	$\frac{3}{2}^-$	18 ± 5	38 ± 10	31 ± 8 [c]
7.75%	2297	$(\frac{5}{2}^-, \frac{1}{2}^-)$	104 ± 10 or [d] 78 ± 8	4.7 ± 0.5 or [d] 6.3 ± 0.7	11 ± 7 [c]
	2548	$\frac{3}{2}^-$	72 ± 8	9 ± 1	
48, 0^+ 73.45%	2421	2_2^+	0.74 ± 0.18	44 ± 12	35 ± 7 [e] Γ_0 = 0.66 ± 0.11 meV and 0.77 ± 0.14 [f]
	3371	2_3^+	5.5 ± 0.6	16.1 ± 2.1	18 ± 7 [e]
	3700	$1^{(+)}$	20.4 ± 2.3	15.1 ± 1.6	35 ± 3 [g]
	3739	1^+	101 ± 10	4.2 ± 0.4	16 ± 3 [g]
49, $\frac{7}{2}^-$	1623	$(\frac{3}{2}^-, \frac{5}{2}^-, \frac{7}{2}^-)$	11.4 ± 1.5 [h]	55 ± 7	
5.51%	1763	$\frac{5}{2}^-$	18.3 ± 2.2	36 ± 4.3	
50, 0^+	1554	2_1^+	0.52 ± 0.15	1300 ± 400	Γ = 0.48 ± 0.04 meV [i]
5.34%	(4311)	2^+	85 ± 60	1 < τ < 6	<80 [j]
(47, 49)	3917		(90 ± 20) $\Gamma/g\Gamma_0$ [k]		
	2810		(29 ± 4) $\Gamma/g\Gamma_0$ [k]		

[a] Reference 11.
[b] Assuming Γ_0/Γ = 0.50.
[c] Reference 18.
[d] The larger width and shorter lifetime correspond to spin $\frac{5}{2}$.
[e] Reference 23.
[f] Coulomb excitation and (e, e'), J. Heisenberg, J. S. McCarthy, and I. Sick, Nucl. Phys. A164, 353 (1971).
[g] C. D. Kavaloski and W. J. Kossler, Phys. Rev. 180, 971 (1969).
[h] Assuming spin $\frac{7}{2}$.
[i] From Coulomb excitation results of C. W. Towsley, D. Cline, and R. Horoshko, Nucl. Phys. A250, 381 (1975).
[j] Reference 12.
[k] Calculated as if ^{49}Ti, g is the statistical factor.

[11] P.A. Assimakopoulos, et al., Nucl. Phys. A180, 131 (1972).
[12] J. G. Pronko et al., Phys. Rev. C10, 1345 (1974).
[18] J.J. Weaver et al., Nucl. Phys. A196, 269 (1972).
[23] T.T. Bardin et al., Phys. Rev. C7, 190 (1973).

Tl
A=48

Tl
A=48

Ref. P.C. Stein, A.C. Odian, A. Wattenberg, R. Weinstein
Phys. Rev. 119, 348 (1960)

Elem. Sym.	A	Z
Ti	48	22

Method: 320 MeV synchrotron; proton telescope; neutron counter

Ref. No.: 60 St 1. JHH

Reaction	E or ΔE	E_o	Γ	$\int \sigma dE$	Jπ	Notes
$Ti^{48}(\gamma,np)$	Bremss. 320					$(\sigma/\sigma_{H^2}) = 5.6 \pm 0.8$ $[\sigma_{H^2} = 63\ \mu b]$ Mean photon energy - 262 MeV Proton counter at 76°

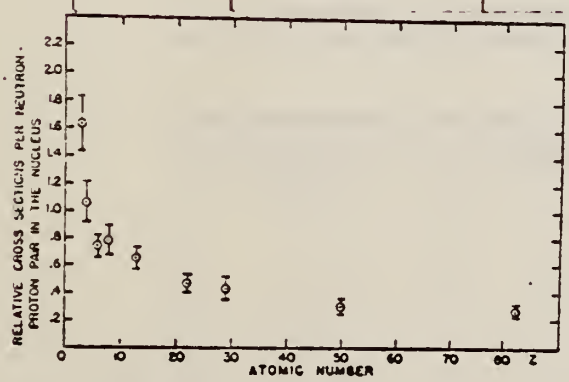

FIG. 2. Relative cross sections per neutron-proton pair in the nucleus versus atomic number. The cross section of the element of interest is divided by the cross section for deuterium and by the factor NZ/A.

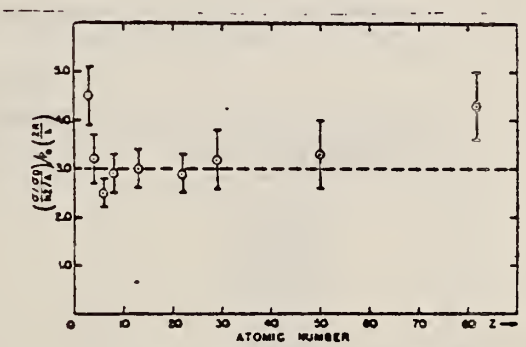

FIG. 3. The relative cross sections per neutron-proton pair corrected for the probability of escape is plotted against atomic number. The probability of escape factor is calculated using $r_0 = 1.30 \times 10^{-13}$ cm and $\lambda = 3.6 \times 10^{-13}$ cm. The probability of escape factor is given in expression (1). The data shown are those of Fig. 2 divided by $P(2R/\lambda)$.

Ref. T.R. Sherwood, W.E. Turchinetz
Nuclear Phys. 29, 292 (1962)

Elem. Sym.	A	Z
Ti	48	22

Method
Bremss.; Canberra electron synchrotron; activity

Ref. No.
62 Sh 5

EGF

Reaction	E or ΔE
$Ti^{48}(\gamma, np)$	Bremss.
$Ti^{48}(\gamma, p)$	14-31

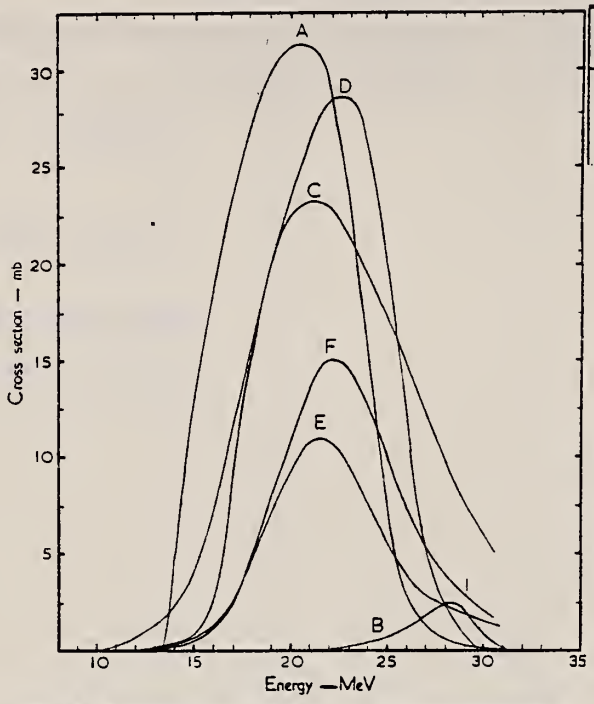

Fig. 2. Excitation function for the photo-disintegration of titanium. A: $^{46}Ti(\gamma, n) + 1.09\ ^{47}Ti(\gamma, 2n)$; B: $^{49}Ti(\gamma, np)$; C: $^{47}Ti(\gamma, p) + 10.1\ ^{48}Ti(\gamma, np)$; D: $^{48}Ti(\gamma, p) + 0.07\ ^{49}Ti(\gamma, np)$; E: $^{49}Ti(\gamma, p) + 0.96$ Ti (γ, np); F: $^{50}Ti(\gamma, p)$.

TABLE 3

Integrated (to 31 MeV) cross sections

Reactions	Relative weights	Integrated cross section (MeV · mb)
$^{46}Ti(\gamma, n) : {}^{47}Ti(\gamma, 2n)$	1 : 1.09	260±34
$^{48}Ti(\gamma, np)$		8.8±1.4 [a]
$^{47}Ti(\gamma, p) : {}^{48}Ti(\gamma, np)$	1 : 10.1	246±38
$^{49}Ti(\gamma, p) : {}^{49}Ti(\gamma, np)$	1 : 0.07	217±32
$^{49}Ti(\gamma, p) : {}^{50}Ti(\gamma, np)$	1 : 0.96	86±13
$^{50}Ti(\gamma, p)$		113±32

[a]) Upper limit. The partial cross section from the ^{44}Sc formed in the ground state is 4.4 MeV · mb.

TABLE 4

Comparison of experimental results with statistical theory predictions for gamma rays of 22 MeV

Ratio of cross sections	Experimental	Theoretical
$\frac{^{47}Ti(\gamma, p)}{^{48}Ti(\gamma, p)}$	0.81	1.40
$\frac{^{49}Ti(\gamma, p)}{^{48}Ti(\gamma, p)}$	0.39	0.63
$\frac{^{50}Ti(\gamma, p)}{^{48}Ti(\gamma, p)}$	0.45	0.56
$\frac{^{48}Ti(\gamma, p)}{^{46}Ti(\gamma, n)}$	0.98	0.34

Notes

Table 3: $Cu^{63}(\gamma, n)$ by Berman and Brown [Phys. Rev. 96, 83 (1954)] used as standard.

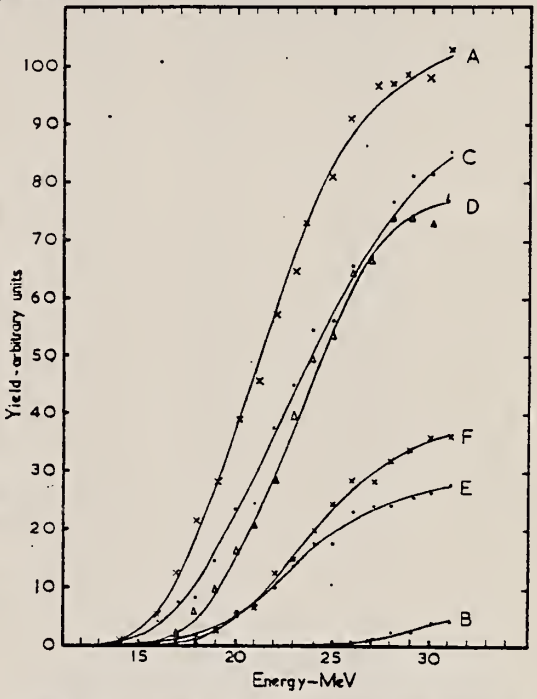

Fig. 1. Activation curves for the photo-disintegration of titanium. A: ^{45}Ti; B: ^{44}Sc (ground state decay); C: ^{46}Sc; D: ^{47}Sc; E: ^{48}Sc; F: ^{49}Sc.

FORM NBS-418
(8-1-63)
USCOMM-DC 16556-P63

REF.

A. F. Akkerman, V.L. Kochetkov, V.N. Chekanov, V.V. Suvorov, A.K. Shtol'ts
Zhur. Eksp. i Teoret. Fiz. 45, 1778 (1963); Soviet Phys. JETP 18, 1218 (1964)

ELEM. SYM.	A	Z
Ti	48	22

METHOD

Radioactive source; gaseous $V^{48}Cl_4$

REF. NO. 63 Ak 1 | NVB

REACTION	RESULT	EXCITATION ENERGY	SOURCE TYPE	SOURCE RANGE	DETECTOR TYPE	DETECTOR RANGE	ANGLE
G,G	LFT	2	D	2	NAI-D		150
		(2.310)		(2.310)			

Lifetime of 2.310 MeV level $(4^+) = 2^{+0.9}_{-0.7} \times 10^{-12}$ sec.

REF. E. C. Booth, B. Chasan and K. A. Wright
Nucl. Phys. 57, 403-420 (1964)

ELEM. SYM.	A	Z
Ti	48	22

METHOD

REF. NO. 64 Bo 1 NVB

REACTION	RESULT	EXCITATION ENERGY	SOURCE TYPE	SOURCE RANGE	DETECTOR TYPE	DETECTOR RANGE	ANGLE
G,G	LFT	1-3	C	1 - 3	NAI-D		100
		(0.5 - 3.0)		(0.5 - 3.0)			

ABI

TABLE 1
Cases of observed resonance fluorescence

Nucleus multipol.	State (MeV)	Spin	Γ_0/Γ	$T(g w \Gamma_0^2/\Gamma^2)^{-1}$ (sec).	Mean lifetime T BCW (sec)	Mean lifetime T other (sec)	Ref.	Γ_0/Γ_W BCW
Ti^{48}	0.00	0^+						
E2[a])	0.99	2^+	1	$11 \pm 4 \times 10^{-13}$	$3.6 \pm 1.5 \times 10^{-13}$	6×10^{-13}, 14×10^{-13}	6, 17)	18
[E2][a])	2.30[b])	4^+[2^+]	?	$6.7^{+3}_{-3} \times 10^{-14}$	$21^{+9}_{-9}(\Gamma_0/\Gamma)^2 \times 10^{-14}$			$5.6\Gamma/\Gamma_0$

REF. H. L. Pai and K. G. McNeill
Can. J. Phys. 45, 3235 (1967)

ELEM. SYM.	A	Z
Ti	48	22

METHOD

REF. NO. 67 Pa 2

EGF

REACTION	RESULT	EXCITATION ENERGY	SOURCE		DETECTOR		ANGLE
			TYPE	RANGE	TYPE	RANGE	
G,P	RLY	THR- 30	C	22,30	ACT-I		4PI
G,NP	RLY	THR- 30	C	22,30	ACT-I		4PI

TABLE I

Yields, Y, and cross sections, σ, of the proton reactions in Ti isotopes excited by photons or neutrons. (The yields and cross sections with primes are "first proton" yields and cross sections)

		1	2	3	4	5	6	7
		E_γ = 22 MeV				E_n = 13 MeV		
Compound nucleus	Target nucleus	$Y_{\gamma p}$	$Y_{\gamma pn}$	$Y_{\gamma np}$	$Y_{\gamma p}'$ (cols. 1 + 2)	σ_{np}	$\sigma_{n,pn}$	σ_{np}' (cols. 5 + 6)
^{47}Ti*	^{47}Ti ^{49}Ti	57	(<1)[a]	(<1)	~57	277	(<10)	~280
^{48}Ti*	^{48}Ti ^{47}Ti	20	E.I.[b]	E.I.	20	121	34	155
^{49}Ti*	^{49}Ti ^{48}Ti	9.2	<0.1	<0.1	9.2	69	<1	~70
^{50}Ti*	^{50}Ti ^{48}Ti	9.6	E.I.	E.I.	9.6	29	<1	~30

		1	2	3	4	5	6	7
		E_γ = 30 MeV				E_n = 19 MeV		
Compound nucleus	Target nucleus	$Y_{\gamma p}$	$Y_{\gamma pn}$	$Y_{\gamma np}$	$Y_{\gamma p}'$	σ_{np}	σ_{npn}	σ_{np}'
^{47}Ti*	^{47}Ti ^{46}Ti	5.5	(0.03)	(0.04)	5.5	167	47	214
^{48}Ti*	^{48}Ti ^{47}Ti	2.5	0.24	0.41	2.7	77	70	147
^{49}Ti*	^{49}Ti ^{48}Ti	1.5	0.29	0.57	1.8	42	31	73
^{50}Ti*	^{50}Ti ^{49}Ti	1.6	0.17	0.37	1.8	28	9	37

[a] Bracketed values are calculated from yields for production of ^{43}Ti, as ^{43}Sc is stable.
[b] E.I. = energetically impossible.

REF. H. L. Pai and K. G. McNeill
Can. J. Phys. 45, 3235 (1967)

ELEM. SYM.	A	Z
Ti	48	22

METHOD

REF. NO.	
67 Pa 2	EGF

REACTION	RESULT	EXCITATION ENERGY	SOURCE		DETECTOR		ANGLE
			TYPE	RANGE	TYPE	RANGE	

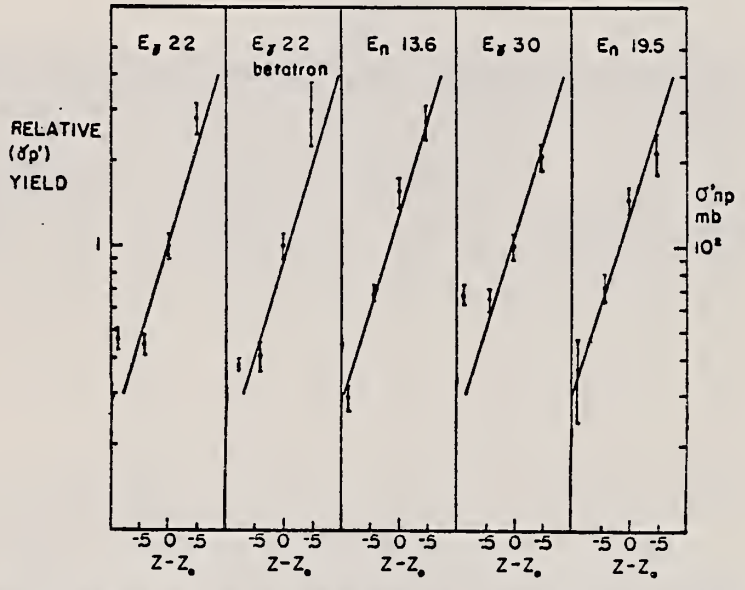

FIG. 1. The relative yields of the first-proton photoreactions in four Ti isotopes plotted as a function of $Z - Z_0$, where $Z = 22$ and Z_0 is the value of Z which minimizes $M(A, Z)$. For ^{46}Ti, $Z - Z_0 = -0.88$, and for ^{48}Ti, ^{49}Ti, and ^{47}Ti the values of $Z - Z_0$ are -0.44, $+0.01$, and $+0.46$ respectively. Three plots are shown, one obtained at 22 MeV using the linac, one at 30 MeV with the linac, and one at 22 MeV with the betatron. Also shown are cross sections of the first-proton reactions induced by fast neutrons, of energies 13.6 and 19.5 MeV, in Ti isotopes (Pai 1966).

REF. Y. Oka, T. Kato, K. Nomura, T. Saito, Hui-Tuh Tsai
Bull. Chem. Soc. Japan 41, 380 (1968)

ELEM. SYM.	A	Z
Ti	48	22

METHOD

REF. NO. 68 Ok 3 egf

REACTION	RESULT	EXCITATION ENERGY	SOURCE TYPE	SOURCE RANGE	DETECTOR TYPE	DETECTOR RANGE	ANGLE
G,P	ABY	THR-20	C	20	ACT-I		4PI

TABLE 1. SUMMARY OF DATA ON (γ, p) REACTIONS WITH 20 MeV BREMSSTRAHLUNG

Nuclide: Parent (Natural abundance, %)	Nuclide: Residual (Half-life)	S_p (MeV)	Observed γ-ray: Energy (MeV)	Observed γ-ray: Branching ratio (%)	Observed γ-ray: Type of multipole transition	Yield determined: μCi/mg[a]	Yield determined: Yield/mol·R
^{25}Mg (10.11)	^{24}Na (15 hr)	12.06	1.37	100	$E2$	1.48×10^{-1}	1.7×10^{5}
^{29}Si (4.71)	^{28}Al (2.27 min)	12.33	1.78	100	$E2$	1.91	2.8×10^{5}
^{30}Si (3.12)	^{29}Al (6.56 min)	13.59	1.28	93.8	$E2+M1$	6.51×10^{-1}	1.5×10^{5}
^{44}Ca (2.06)	^{43}K (22.4 hr)	12.17	0.374	85	$E2+M1$	7.86×10^{-1}	1.3×10^{5}
^{47}Ti (7.32)	^{46}Sc (84.1 d)	10.47	0.887	100	$E2$	7.11×10^{-4}	3.1×10^{5}
^{48}Ti (73.99)	^{47}Sc (3.4 d)	11.44	0.160	100	$E2+M1$	6.83×10^{-2}	1.2×10^{6}
^{49}Ti (5.46)	^{48}Sc (1.8 d)	11.35	1.31	100	$E2$	4.40×10^{-3}	5.8×10^{4}
^{53}Cr (9.55)	^{52}V (3.8 min)	11.15	1.43	100	$E2$	5.01×10^{-1}	6.6×10^{4}
^{57}Fe (2.17)	^{56}Mn (2.58 hr)	10.57	1.81	23.5	$E2+M1$	8.10×10^{-2}	2.1×10^{5}
^{74}Ge (36.74)	^{73}Ga (4.8 hr)	10.92	0.295	97	($E2$)	3.70×10^{-1}	1.3×10^{5}
^{77}Se (7.58)	^{76}As (26.5 hr)	9.61	0.559	41	$E2$	1.48×10^{-2}	1.3×10^{5}
^{87}Sr (7.02)	^{86}Rb (19 d)	9.41	1.08	9	$E2$	5.15×10^{-4}	9.9×10^{4}
^{113}Cd (12.26)	^{112}Ag (3.2 hr)	9.74	1.39	35	$E2$	1.91×10^{-2}	2.1×10^{5}
^{117}Sn (7.57)	^{116m}In (54 min)	9.58	1.27	84	$E2$	9.80×10^{-3}	6.9×10^{5}
^{137}Ba (11.32)	^{136}Cs (13 d)	8.67	0.830	100	$E2$	1.68×10^{-4}	2.2×10^{4}
^{199}Hg (16.84)	^{198}Au (2.7 d)	7.27	0.412	100	$E2$	8.43×10^{-4}	2.2×10^{4}

a) The value corrected at the end of 1 hr irradiation (9.4×10^{6} R/min).

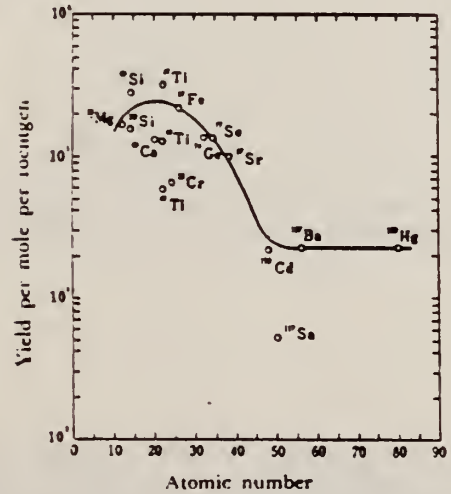

Fig. 2. The yield curve for the (γ, p) reaction with 20 MeV bremsstrahlung.

Y. Oka, T. Kato and N. Sato
Bull. Chem. Soc. Japan 42, 387 (1969)

Ti	48	22

METHOD

REF. NO. 69 Ok 1 hmg

REACTION	RESULT	EXCITATION ENERGY	SOURCE TYPE	SOURCE RANGE	DETECTOR TYPE	DETECTOR RANGE	ANGLE
G,P	RLY	THR-60	C	30-60	NAI-D		4PI

YLD REL 12C(G,N)

TABLE 6. THE RELATIVE YIELDS FOR (γ, p) REACTIONS ON TITANIUM NUCLEI EXPRESSED AS THOSE PER MOLE

Reaction	Yield per mole relative to $^{12}C(\gamma, n)^{11}C$			
	30 MeV	45 MeV	55 MeV	60 MeV
$^{47}Ti(\gamma, p)^{46}Sc$	5.4×10^{-1}	5.8×10^{-1}	5.4×10^{-1}	6.3×10^{-1}
$^{48}Ti(\gamma, p)^{47}Sc$	2.0×10^{-1}	2.4×10^{-1}	2.8×10^{-1}	2.8×10^{-1}
$^{49}Ti(\gamma, p)^{48}Sc$	1.2×10^{-1}	2.1×10^{-1}	2.2×10^{-1}	2.1×10^{-1}

REF. J. Heisenberg, J. S. McCarthy and I. Sick
Nucl. Phys. A164, 353 (1971)

ELEM. SYM.	A	Z
Ti	48	22

METHOD

REF. NO. 71 He 1 egf

REACTION	RESULT	EXCITATION ENERGY	SOURCE TYPE	SOURCE RANGE	DETECTOR TYPE	DETECTOR RANGE	ANGLE
E,E/	FMF	1-3	D	198-300	MAG-D		DST

3 LEVELS

TABLE 3

Inelastic parameters

Isotope	E^a (MeV)	L	Shape	c_{tr} [a]) (fm)	z_{tr} [a]) (fm)	G [b]) (s.p.u.)	R_{tr} [a]) (fm)	G(s.p.u.) heavy-particle scattering [19])
^{40}Ca	3.740	3	2	3.536±0.030	1.483±0.020	24.9 ±1.0	4.835±0.030	23.6±3.5
	4.480	5	2	3.538±0.050	1.260±0.035	9.7 ±0.6	4.810	17.7±2.7
			3			17.7 ±1.5	5.467±0.060	11.3±1.7
^{42}Ca	3.440	3	2	3.565±0.018	1.383±0.014	12.4 ±0.5	4.719±0.023	12.0±1.8
	4.100	5	2	3.231±0.030	1.404±0.025	3.4 ±0.3	4.816±0.044	9.0±1.4
^{44}Ca	3.30	3	2	3.555±0.018	1.313±0.013	6.95±0.28	4.618±0.023	8.0±1.2
	2.28	4	2	4.091±0.030	1.268±0.016	2.66±0.15	5.135±0.030	1.3±0.3
	3.91	5	2	3.268±0.030	1.397±0.024	2.30±0.20	4.832±0.045	4.4±0.7
^{46}Ti	2.00	4	2	4.264±0.021	1.229±0.013	7.61±0.30	5.226±0.026	
^{48}Ti	2.286	4	2	4.330±0.021	1.196±0.013	3.37±0.15	5.237±0.026	
^{50}Ti	4.42	3	2	3.645±0.017	1.244±0.012	3.76±0.15	4.600±0.023	5.4±0.8 5.9 [20])
	2.50	4	2	3.865±0.017	1.347±0.012	4.7 ±0.15	5.064±0.026	3.3±0.7 2.7 [20])
	3.20	5	2	3.254±0.032	1.345±0.026	0.83±0.08	4.724±0.045	

Present experiment

[a]) Errors do not reflect any model dependence.
[b]) Given errors do not include the 6 % error of normalization.

[19] A. M. Bernstein, Adv. in Nucl. Phys. 3 (1969) 325.

13) J. Simpson, J. Cookson, D. Eccleshall and M. Yates, Nucl. Phys. 62 (1965) 385
14) G. M. Temmer and N. P. Heydenburg, Phys. Rev. 104 (1956) 967
15) D. S. Andreyev, A. P. Grinberg, K. I. Erokhina and I. Kh. Lemberg, Nucl. Phys. 19 (1960) 400
16) F. R. Metzger, Nucl. Phys. 27 (1961) 612
17) W. H. Kelly and G. B. Beard, Nucl. Phys. 27 (1961) 188
18) R. B. Begzhanov, A. A. Islamov, D. K. Kaipov and Yu. K. Shubnyi, JETP (Sov. Phys.) 17 (1963) 94

[over]

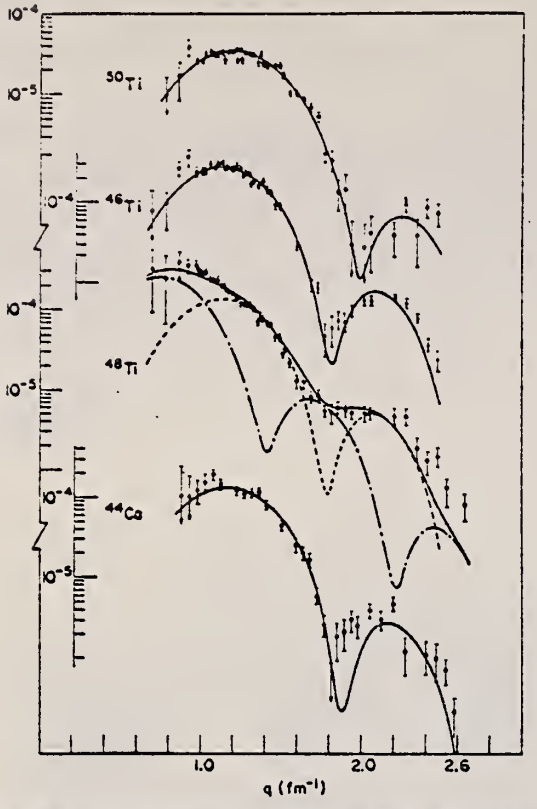

Fig. 6. Fits to ^{50}Ti, ^{46}Ti, ^{48}Ti and ^{44}Ca 4$^+$ levels. For ^{48}Ti we show the decomposition into contributions of the 2.42 MeV 2$^+$ level (dash-dot curve) and the 2.286 MeV 4$^+$ level (dashed curve).

TABLE 2

Inelastic parameters for 2$^+$ levels

Isotope	E^* (MeV)	B(E2) Coulomb Excit. ($e^2 \cdot fm^4$)	Shape	c_{tr} [a]) (fm)	z_{tr} [a]) (fm)	Fitted B(E2) ($e^2 \cdot fm^4$) [b])	R_{tr} [a]) (fm)	B(E2)($e^2 \cdot fm^4$) heavy-particle scattering
^{42}Ca	1.520	364± 82 [9])	2	3.541±0.025	1.459±0.020	320±20	4.619±0.030	476± 74 [19])
^{44}Ca	1.160	350± 70 [10])	2	3.691±0.027	1.428±0.020	480±30	4.704±0.030	507±100 [19])
			1	3.454±0.025	0.690±0.010	1270±85	5.553±0.030	
	3.259		2			54±10		
^{46}Ti	0.885	830±170 [14])	2	3.807±0.014	1.397±0.010	740±20	4.763±0.017	867 [20])
		560±100 [13])	1	3.562±0.014	0.669±0.005	1680±50	5.510±0.020	738 [11])
^{48}Ti	0.984	700±140 [14])	2	3.777±0.014	1.340±0.010	537±15	4.671±0.017	788±120 [19])
		310± 70 [13])	1	3.539±0.014	0.633±0.005	1110±30	5.321±0.020	673 [11])
								659 [20])
	2.420		2			49± 8		57± 10 [19])
^{50}Ti	1.580	240± 20 [12])	2	3.768±0.014	1.255±0.010	307±10	4.567±0.017	349 [20])
			1	3.535±0.014	0.576±0.005	515±17	5.047±0.020	260 [21])
								431 [24])
	4.320		2			51± 8		72 [24])
^{56}Fe	0.880	877± 70 [c])	2	4.048±0.024	1.357±0.014	945±45	4.919±0.025	
			1	3.878±0.024	0.651±0.006	1570±70	5.454±0.030	
				Present experiment				

[a]) Errors do not reflect any model dependence.
[b]) Given errors do not include the 6 % error of normalization.
[c]) Average for B(E2) formed from values of refs. [12–18]).

J. W. Lightbody Jr.
Phys. Letters 38B, 475 (1972)

ELEM. SYM.	A	Z
Ti	48	22

METHOD

REF. NO.: 72 Li 1 egf

REACTION	RESULT	EXCITATION ENERGY	SOURCE TYPE	SOURCE RANGE	DETECTOR TYPE	DETECTOR RANGE	ANGLE
E,E/	FMF	0-3	D	60-120	MAG-D		DST

.99, 2.44 MEV

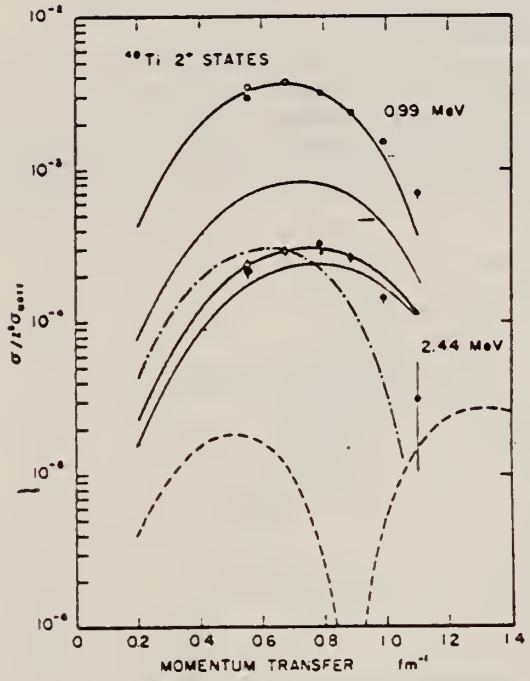

Fig. 2. Electron scattering form factors for the lowest two 2^+ states in ^{48}Ti. Solid lines were calculated using a best fit admixture and phase. The dashed line represents the harmonic two-phonon form factor. The dot-dashed line represents a best fit attempt for the 2^+_2 state with $\Phi = 0$. The shaded area was determined using an admixture which fit the measured BR for $\Phi = \pi$. For clarity the $\Phi = 0$ BR fit region is not shown.

REF. V. K. Rasmussen
Phys. Rev. C13, 631 (1976)

ELEM. SYM.	A	Z
Ti	48	22

METHOD

REF. NO. 76 Ra 1 hmg

REACTION	RESULT	EXCITATION ENERGY	SOURCE TYPE	SOURCE RANGE	DETECTOR TYPE	DETECTOR RANGE	ANGLE
G,G	LFT	2- 4	C	1- 5	SCD-D		DST
		(3.371-3.739)		(1.3-4.7)			

4 LEV,2421-3739 KEV

TABLE II. Mean lives of some levels in the titanium isotopes.

Mass no., ground state, spin, & abund.	Level energy (keV)	Level spin	Γ_0 (meV)	τ (pres. meas.) (fs)	τ (other) (fs)
46, 0^+	3168	1^-	7.3 ± 2.0	41 ± 12	71 ± 12 [a]
7.95%	4316	1	$(172 \pm 26)\Gamma/\Gamma_0$	0.96 ± 0.14 [b]	<44 [a]
47, $\frac{5}{2}^-$	2162	$\frac{3}{2}^-$	18 ± 5	38 ± 10	31 ± 8 [c]
7.75%	2297	$(\frac{5}{2}^-, \frac{7}{2}^-)$	104 ± 10 or [d] 78 ± 8	4.7 ± 0.5 or [d] 6.3 ± 0.7	11 ± 7 [c]
	2548	$\frac{3}{2}^-$	72 ± 8	9 ± 1	
48, 0^+	2421	2_2^+	0.74 ± 0.18	44 ± 12	35 ± 7 [e]
73.45%					$\Gamma_0 = 0.66 \pm 0.11$ meV and 0.77 ± 0.14 [f]
	3371	2_3^+	5.5 ± 0.6	16.1 ± 2.1	18 ± 7 [e]
	3700	$1^{(+)}$	20.4 ± 2.3	15.1 ± 1.6	35 ± 3 [g]
	3739	1^+	101 ± 10	4.2 ± 0.4	16 ± 3 [g]
49, $\frac{7}{2}^-$	1623	$(\frac{3}{2}^-, \frac{5}{2}^-, \frac{7}{2}^-)$	11.4 ± 1.5 [h]	55 ± 7	
5.51%	1763	$\frac{5}{2}^-$	18.3 ± 2.2	36 ± 4.3	
50, 0^+	1554	2_1^+	0.52 ± 0.15	1300 ± 400	$\Gamma = 0.48 \pm 0.04$ meV [i]
5.34%	(4311)	2^+	85 ± 60	$1 < \tau < 6$	<80 [j]
(47, 49)	3917		$(90 \pm 20)\Gamma/g\Gamma_0$ [k]		
	2810		$(29 \pm 4)\Gamma/g\Gamma_0$ [k]		

[a] Reference 11.
[b] Assuming $\Gamma_0/\Gamma = 0.50$.
[c] Reference 18.
[d] The larger width and shorter lifetime correspond to spin $\frac{5}{2}$.
[e] Reference 23.
[f] Coulomb excitation and (e, e'), J. Heisenberg, J. S. McCarthy, and I. Sick, Nucl. Phys. A164, 353 (1971).
[g] C. D. Kavaloski and W. J. Kossler, Phys. Rev. 180, 971 (1969).
[h] Assuming spin $\frac{9}{2}$.
[i] From Coulomb excitation results of C. W. Towsley, D. Cline, and R. Horoshko, Nucl. Phys. A250, 381 (1975).
[j] Reference 12.
[k] Calculated as if ^{49}Ti, g is the statistical factor.

[11] P.A. Assimakopoulos, et al., Nucl. Phys. A180, 131 (1972).
[12] J.G. Pronko et al., Phys. Rev. C10, 1345 (1974).
[18] J.J. Weaver et al., Nucl. Phys. A196, 269 (1972).
[23] T.T. Bardin et al., Phys. Rev. C7, 190 (1973).

REF. K. Masumoto, T. Kato, N. Suzuki
Nucl. Inst. Meth. 157, 567 (1978)

ELEM. SYM.	A	Z
Ti	48	22

METHOD

REF. NO.	
78 Ma 10	hg

REACTION	RESULT	EXCITATION ENERGY	SOURCE		DETECTOR		ANGLE
			TYPE	RANGE	TYPE	RANGE	
G,P	ABY	11-68	C	30-68	ACT		4PI

Analysis is made of reactions interfering with photon activation analysis procedures.

The activation yield curves have been presented for a number of photonuclear reactions in the energy range from 30 to 68 MeV, in order to evaluate quantitatively the interferences due to competing reactions in multielement photon activation analysis. The general features of the yields as functions of both target mass number and excitation energy were elucidated from the data obtained, discussion being given on the results in terms of the reaction mechanism.

Simultaneous neutron activation due to appreciable neutron production from the converter and surrounding materials has also been studied, and, finally, the magnitudes of interferences in real multielement analysis were given in the form of their energy dependences.

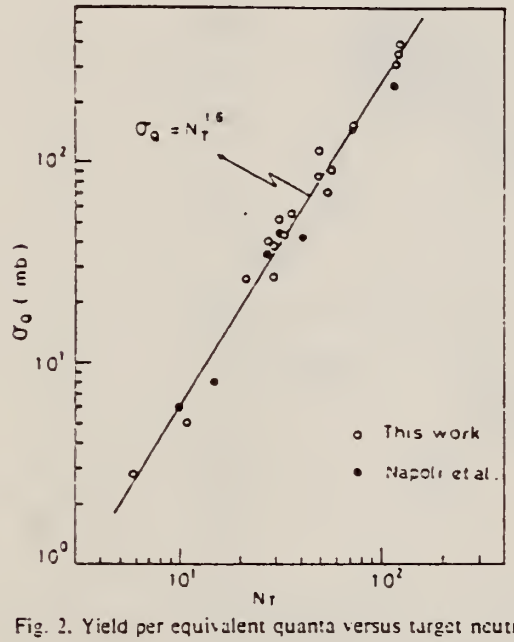

Fig. 2. Yield per equivalent quanta versus target neutron number.

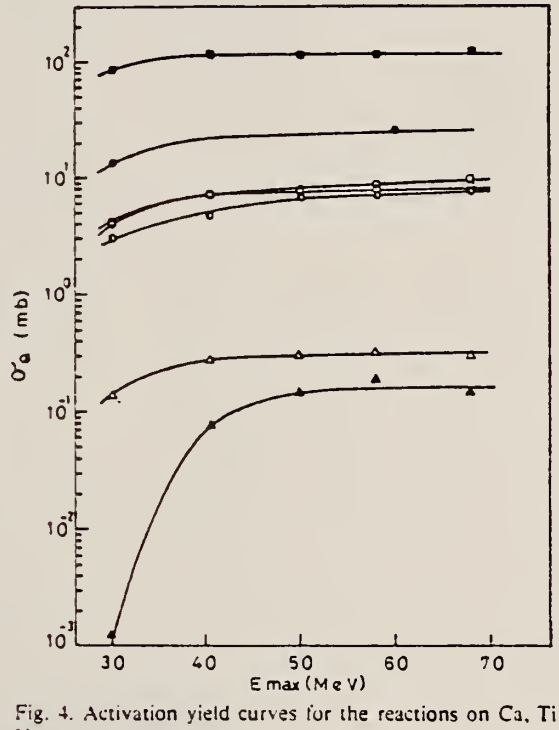

Fig. 4. Activation yield curves for the reactions on Ca, Ti and V.
■ $^{48}Ca(\gamma, n)^{47}Ca$, □ $^{44}Ca(\gamma, p)^{43}K$, ● $^{46}Ti(\gamma, n)^{45}Ti$,
○ $^{48}Ti(\gamma, p)^{47}Sc$, ◐ $^{49}Ti(\gamma, p)^{48}Sc$, △ $^{51}V(\gamma, \alpha)^{47}Sc$,
▲ $^{51}V(\gamma, zn)^{46}Sc$.

(over)

FORM N3S-41d
U.S. DEPARTMENT OF COMMERCE

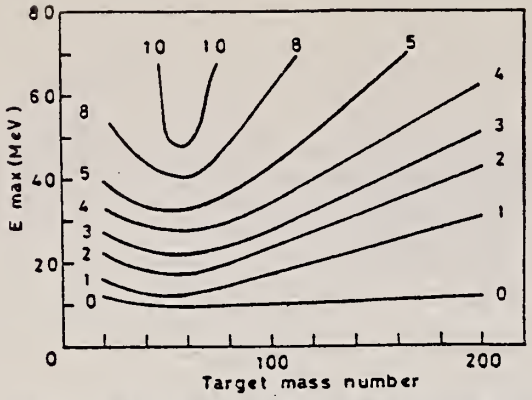

Fig. 10. Yields of the (γ, p) reactions as a function of bremsstrahlung maximum energy and target mass number. The numerical values in the figure are yields per equivalent quanta in mb.

REF. R. Sutton, M.N. Thompson, M. Sugawara, K. Shoda, T. Saito, H. Tsubota
Nucl. Phys. A339, 125 (1980)

ELEM. SYM.	A	Z
Ti	48	22

METHOD

REF. NO. 80 Su 6 hg

REACTION	RESULT	EXCITATION ENERGY	SOURCE		DETECTOR		ANGLE
			TYPE	RANGE	TYPE	RANGE	
G,XN	ABX	11-28	C	11-28	BF3=I		4PI

Abstract: A high resolution measurement of the ^{48}Ti(γ, n) cross section is reported. Evidence for isospin splitting of the giant dipole resonance is found to be consistent with the prediction. In addition the deformation splitting of the GDR is consistent with predictions of the dynamic collective model.

E NUCLEAR REACTIONS ^{48}Ti(γ, n), $E \approx 15$–27.5 MeV; measured $\sigma(E, \theta)$; ^{48}Ti deduced GDR splitting. Dynamic collective model.

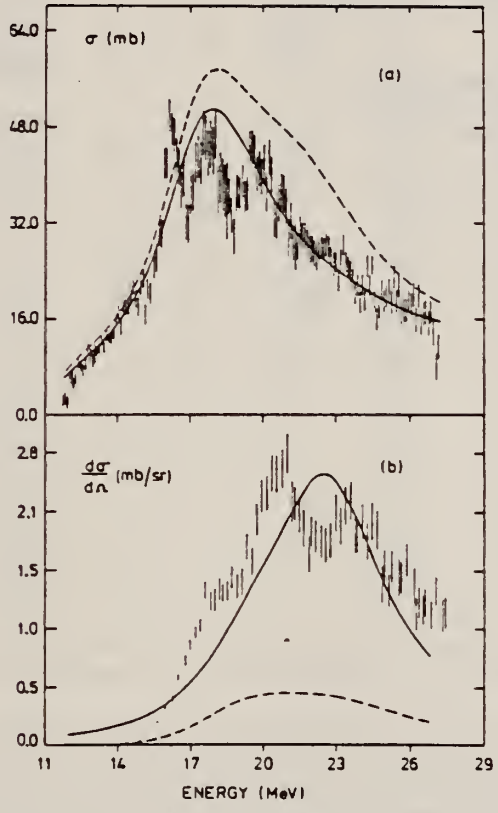

Fig. 1. (a) The ^{48}Ti photoneutron cross section. Vertical bars show statistical errors only. (b) The ^{48}Ti photoproton differential cross section, measured at $\theta = 90°$, from ref. [10]). Curves show a statistical model calculation of the shape of the photonuclear cross sections of ^{48}Ti. Solid lines show the calculation if isospin effects are included, compared to the ^{48}Ti(γ, n) (a) and ^{48}Ti(γ, p) (b) cross sections. The broken line results if the calculation ignores isospin.

Y. Cauchois, H. Ben Abdelaziz, R. Kherout, C. Schloesing-Moller
J. Phys. G7, 1539 (1981)

Ti	48	22

METHOD

REF. NO. 81 Ca 2 hg

REACTION	RESULT	EXCITATION ENERGY	SOURCE TYPE	SOURCE RANGE	DETECTOR TYPE	DETECTOR RANGE	ANGLE
G,G	LFT	1	C	0 - 2	SCD-D		
		(.984)					

.984 MeV

Abstract. Lifetimes of 49 excited states below 1.65 MeV have been measured in ^{24}Mg, ^{27}Al, ^{48}Ti, ^{58}Ni, ^{59}Co, ^{61,62}Ni, ^{63,65}Cu, ^{64,66,68}Zn, ^{75}As, ^{103}Rh, ^{113,115}In, ^{116,118,120}Sn and ^{121,123}Sb by means of nuclear resonance fluorescence experiments. The levels are excited by bremsstrahlung x-ray photons. The self-absorption technique applied to suitable cases provides nuclear absorption cross sections, widths and lifetimes from which the x-ray spectral distributions are also obtained. Scattering experiments are performed for all other cases in order to obtain widths and lifetimes from these x-ray photon curves. The Compton effect in the sample is taken into account. Self-absorption provides $g\Gamma_0$ from which Γ is deduced using adopted J^π and Γ_0/Γ values; scattering provides $u = g(\Gamma_0^2/\Gamma)W(\theta)$ from which Γ is also deduced with J, Γ_0/Γ and mixing ratios taken from the literature. Thanks to simultaneous determination of the x-ray spectra all the lifetimes as given by our programs with their statistical errors form an unusually coherent set of values.

NUCLEAR REACTIONS (γ, γ'), bremsstrahlung excitation; natural isotopes; ^{24}Mg, ^{27}Al, ^{48}Ti, ^{58}Ni, ^{59}Co, ^{61,62}Ni, ^{63,65}Cu, ^{64,66,68}Zn, ^{75}As, ^{103}Rh, ^{113,115}In, ^{116,118,120}Sn and ^{121,123}Sb; $E \simeq 0.5$–1.65 MeV; measured $g\Gamma_0$ or $g(\Gamma_0^2/\Gamma)W(\theta)$; deduced $T_{1/2}$.

(OVER)

Tableau 3. Résultats des mesures des niveaux étudiés par diffusion.

Table 3. Results obtained using the diffusion method.

Isotope	Energie (keV)	J^π	J^π_δ	Γ_0/Γ	δ	$u=g(\Gamma_0^2/\Gamma)W(\theta)$ (meV)	τ (ps) ce travail	τ_{ref} (ps)	Références †
^{24}Mg	1368.59(4)	2^+	0^+	1	E2	1,08(13)	1,76(21)	1,98(4)	Endt et van der Leun (1978)
^{27}Al	1014.45(3)	$\frac{1}{2}^-$	$\frac{1}{2}^+$	0,971	+ 0,351(12)	0,186(13)	2,20(16)	2,12(8)	Endt et van der Leun (1978)
^{48}Ti	983.512(3)	2^+	0^+	1	E2	0.282(23)	6,74(55)	6,1(13)	Been (1978)
^{58}Ni	1454.45(15)	2^+	0^+	1	E2	2,11(26)	0,90(11)	0,92(3)	Kocher et Auble (1976)
^{59}Co	1099,224(25)	$\frac{7}{2}^-$	$\frac{7}{2}^-$	1	(E2)	0.069(8)	4,79(55)	3,17(58)	Kim (1976)
^{59}Co	1458.8(3)	$\frac{9}{2}^-$	$\frac{7}{2}^-$	0,91	(E2)	0,68(8)	1,17(14)	1,52(16)	Kim (1976)
^{59}Co	1480.9(3)	$\frac{5}{2}^-$	$\frac{7}{2}^-$	0.8	$< 0.35^a$	1,23(15)	0.254(31)	0.31(3)	Kim (1976)
^{61}Ni	1185,7(6)	$\frac{1}{2}^-$	$\frac{1}{2}^-$	$0.77(8)^i$	$\lvert 0{,}14 \rvert$	1,88(49)	0.21(5)	0.16(3)	Andreev *et al* (1974)
^{62}Ni	1172,91(9)	2^+	0^+	1	E2	0,88(17)	2,15(42)	2,09(3)	Halbert (1979a)
^{63}Cu	1327.00(7)	$\frac{7}{2}^-$	$\frac{3}{2}^-$	0.84	(E2)	1,04(14)	0.84(11)	0,88(4)	Auble (1979b)
^{63}Cu	1412.05(4)	$\frac{5}{2}^-$	$\frac{3}{2}^-$	0.72	$+0.61\{^{+9}_{-8}\}$	0,260(38)	1,90(28)	1,61(3)	Auble (1979b)
^{64}Zn	991.54(7)	2^+	0^+	1	E2	0,640(54)	2,97(25)	2,60(13)	Halbert (1979b)
^{65}Cu	1481,83(5)	$\frac{7}{2}^-$	$\frac{3}{2}^-$	0,85	(E2)	1,13(19)	0,79(13)	0,49(5)	Auble (1975a)
^{66}Zn	1039,37(6)	2^+	0^+	1	E2	0,70(6)	2,71(23)	2,25(15)	Auble (1975b)
^{68}Zn	1077,38(5)	2^+	0^+	1	E2	0,70(6)	2,71(23)	2,34(23)	Lewis (1975)
^{73}As	572,5(10)	$\frac{5}{2}^-$	$\frac{3}{2}^-$	1^d	$0{,}39^b$	0,236(26)	4,14(46)	3,5(9)	Horen et Lewis (1975)
^{73}As	823,0(10)	$\frac{7}{2}^-$	$\frac{3}{2}^-$	0.86^d	(E2)	0,214(22)	4,27(43)	3,5(3)	Robinson *et al* (1967)
^{75}As	865,5(10)	$\frac{5}{2}^+$	$\frac{3}{2}^-$	0.83^d	—[c]	0,78(6)	0,863(68)	0,60(12)	Celliers *et al* (1977)
^{75}As	1076,0(10)	$\frac{3}{2}^-$	$\frac{3}{2}^-$	$0{,}94^d$	$0{,}38^d$	1,97(13)	0,287(19)	0,32(7)	Celliers *et al* (1977)
^{75}As	1128,5(10)	$\frac{1}{2}^+$	$\frac{3}{2}^-$	1	$E1^d$	0,224(24)	1,47(16)	—	
^{75}As	1349,0(10)	$\frac{3}{2}^-$	$\frac{3}{2}^-$	0.67^d	$0{,}20^d$	1,61(29)	0,180(32)	0,12(3)	Wilson (1970)
^{75}As	1370,0(10)	$\frac{3}{2}^-$	$\frac{3}{2}^-$	$0{,}47^d$	$0{,}47^d$	0,64(13)	0,218(44)	—	
^{103}Rh	803.1(2)	$\frac{1}{2}^-$	$\frac{1}{2}^-$	0.70	M1	1,85(16)	0,174(15)	—	Harmatz (1979)
^{103}Rh	1277.0(2)	$\frac{3}{2}^-$	$\frac{1}{2}^-$	0,75	$-0.62(30)^c$	0,81(9)	0,87(10)	1,3(9)	Harmatz (1979)
^{113}In	1177(1)	$\frac{9}{2}^+$	$\frac{9}{2}^+$	1	+ 0,5(2)	9,1(8)	0.086(8)	0,10(6)	Tuttle *et al* (1976)
^{113}In	1510(1)	$\frac{7}{2}^+$	$\frac{9}{2}^+$	0,935	$-0.5\{^{+1}_{-2}\}$	6,4(9)	0.071(10)	$0{,}11\{^{+4}_{-2}\}$	Tuttle *et al* (1976)
^{115}In	1077,7(10)	$\frac{5}{2}^+$	$\frac{9}{2}^+$	0.81^j	(E2)	0,159(24)	1,61(24)	1,23(7)	Tuttle *et al* (1976)
^{115}In	1290.59(3)	$\frac{9}{2}^+$	$\frac{9}{2}^+$	0.98^j	(E2)	1,31(11)	0.66(6)	0.55(4)	Tuttle *et al* (1976)
^{115}In	1448,78(3)	$\frac{7}{2}^+$	$\frac{9}{2}^+$	0.86	-8^f	0,90(11)	0,50(6)	0,52(20)	Tuttle *et al* (1976)
^{115}In	1486.1(1)	$\frac{9}{2}^+$	$\frac{9}{2}^+$	0.787	-0.8^f	0,63(9)	0,63(9)	0,4(3)	Tuttle *et al* (1976)
^{115}In	1497.2(4)	$(\frac{5}{2}^+)$	$\frac{9}{2}^+$	< 1	(E2)	1,33(16)	< 0,30(4)	—	
^{115}In	1607.8(15)	$(\frac{5}{2}^+)$	$\frac{9}{2}^+$	⩽ 1	(E2)	1,54(24)	⩽ 0,26(4)	—	
^{116}Sn	1293.54(2)	2^+	0^+	1	E2	3,58(37)	0,53(6)	0,522(14)	Carlson *et al* (1975)
^{118}Sn	1229.64(4)	2^+	0^+	1	E2	2,75(28)	0,69(7)	0,67(2)	Carlson *et al* (1976)
^{120}Sn	1171,6(2)	2^+	0^+	1	E2	1,83(16)	1,04(9)	0,91(2)	Kocher (1976)
^{121}Sb	1023.5(10)	$\frac{7}{2}^+$	$\frac{5}{2}^+$	1	$\lvert 0{.}57 \rvert^g$	3,69(34)	0.228(21)	$0.20(7)^h$	Tamura *et al* (1979)
^{121}Sb	1105.5(10)	$\frac{9}{2}^+$	$\frac{7}{2}^+$	0.4	—	0.47(4)	0.42(4)	—	
^{121}Sb	1142.5(10)	$\frac{9}{2}^+$	$\frac{5}{2}^+$	0.6	(E2)	0,85(8)	0.449(40)	$0.41(8)^h$	Booth *et al* (1973)
^{121}Sb	1384.0(10)	$\frac{5}{2}^+$	$\frac{5}{2}^+$	1	$\lvert 0{.}45 \rvert^g$	4,7(5)	0.092(10)	$0.088(14)^h$	Booth *et al* (1973)
^{123}Sb	1029.5(10)	$\frac{9}{2}^+$	$\frac{7}{2}^+$	1	$\lvert 0{.}57 \rvert^g$	2,96(27)	0,272(25)	$0.26(4)^h$	Booth *et al* (1973)
^{123}Sb	1086.5(10)	$\frac{7}{2}^+$	$\frac{5}{2}^+$	1	$\lvert \delta \rvert > 1.26^g$	1,06(9)	0,67(6)	$0.72(15)^h$	Booth *et al* (1973)

† Références pour les colonnes 3, 4, 5, 6 et 9 de chaque ligne, sauf indication appelée au bas de ce tableau. Pour les autres données se reporter au texte.

Remarque. Pour calculer δ^2 quand nous ne disposons que de $B(E2)$, pour un mélange (E2) + (M1), nous déduisons $g\Gamma_0(E2) \propto B(E2)E_\gamma^5$; en admettant $W(\theta)=1$ et connaissant Γ_0/Γ, notre détermination de u donne une première approximation de $g\Gamma_0$ d'où une valeur de $\delta^2=(g\Gamma_0(E2))/(g\Gamma_0-g\Gamma_0(E2))$ qui permet d'améliorer $W(\theta)$ et $g\Gamma_0$ de proche en proche.

[a] Swann (1971); [b] Robinson *et al* (1967); [c] $W(\theta)=0.99$ calculé d'après la formule de Celliers *et al* (1977); [d] Abbondanno *et al* (1978); [e] Sayer *et al* (1972); [f] Tuttle *et al* (1976); [g] d'après $B(E2)$ de Barnes *et al* (1966); [h] calculé d'après Booth *et al* (1973); [i] Williams *et al* (1975); [j] Dietrich *et al* (1970).

TI
A=49

TI
A=49

Ref. T.R. Sherwood, W.E. Turchinetz
Nuclear Phys. 29, 292 (1962)

Elem. Sym.	A	Z
Ti	49	22

Method
Bremss.; Canberra electron synchrotron; activity

Ref. No.
62 Sh 5

EGF

Reaction	E or ΔE
$Ti^{49}(\gamma,np)$	Bremss.
$Ti^{49}(\gamma,p)$	14-31

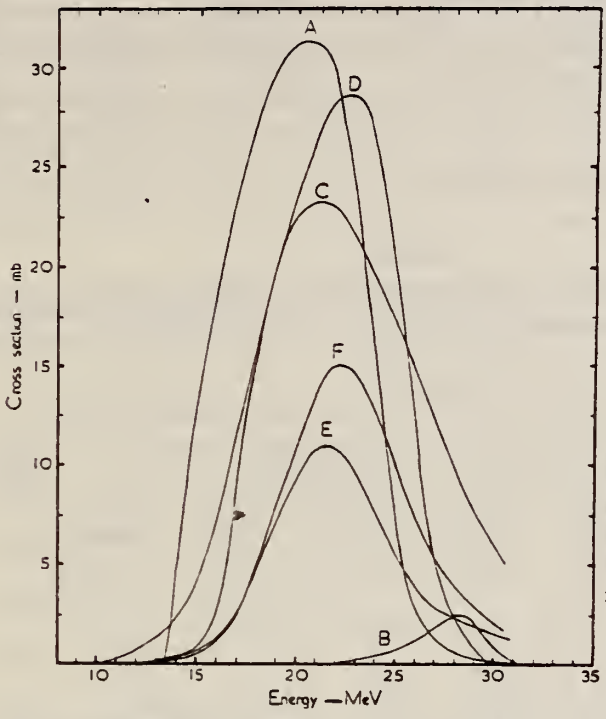

Fig. 2. Excitation function for the photo-disintegration of titanium. A: $^{46}Ti(\gamma, n) + 1.09\ ^{47}Ti(\gamma, 2n)$; B: $^{46}Ti(\gamma, np)$; C: $^{47}Ti(\gamma, p) + 10.1\ ^{46}Ti(\gamma, np)$; D: $^{48}Ti(\gamma, p) + 0.07\ ^{46}Ti(\gamma, np)$; E: $^{48}Ti(\gamma, p) + 0.96$ Ti (γ, np); F: $^{50}Ti(\gamma, p)$.

TABLE 3

Integrated (to 31 MeV) cross sections

Reactions	Relative weights	Integrated cross section (MeV · mb)
$^{46}Ti(\gamma, n) : {}^{47}Ti(\gamma, 2n)$	1 : 1.09	260±34
$^{46}Ti(\gamma, np)$		8.8±1.4 [a]
$^{47}Ti(\gamma, p) : {}^{46}Ti(\gamma, np)$	1 : 10.1	246±38
$^{48}Ti(\gamma, p) : {}^{46}Ti(\gamma, np)$	1 : 0.07	217±32
$^{49}Ti(\gamma, p) : {}^{50}Ti(\gamma, np)$	1 : 0.96	86±13
$^{50}Ti(\gamma, p)$		113±32

[a]) Upper limit. The partial cross section from the ^{44}Sc formed in the ground state is 4.4 MeV · mb.

TABLE 4

Comparison of experimental results with statistical theory predictions for gamma rays of 22 MeV

Ratio of cross sections	Experimental	Theoretical
$\frac{^{47}Ti(\gamma, p)}{^{48}Ti(\gamma, p)}$	0.81	1.40
$\frac{^{46}Ti(\gamma, p)}{^{48}Ti(\gamma, p)}$	0.39	0.63
$\frac{^{50}Ti(\gamma, p)}{^{48}Ti(\gamma, p)}$	0.45	0.56
$\frac{^{49}Ti(\gamma, p)}{^{46}Ti(\gamma, n)}$	0.98	0.34

Notes

Table 3: $Cu^{63}(\gamma,n)$ by Berman and Brown [Phys. Rev. 96, 83 (1954)] used as standard.

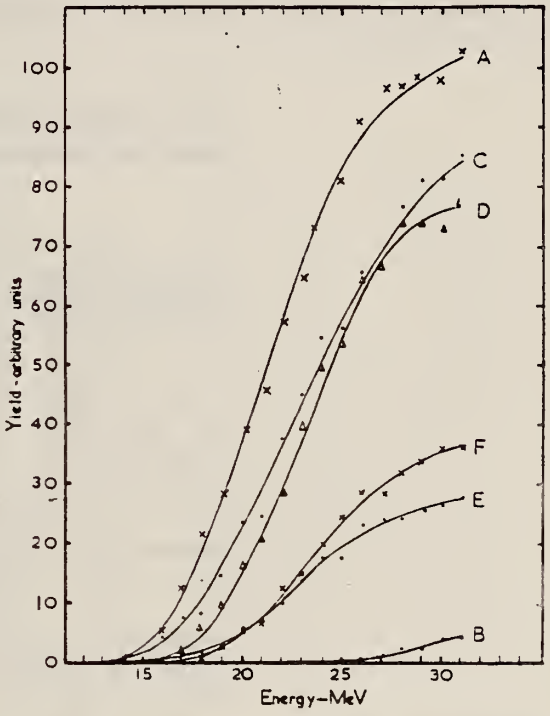

Fig. 1. Activation curves for the photo-disintegration of titanium. A: ^{46}Ti; B: ^{44}Sc (ground state decay); C: ^{46}Sc; D: ^{47}Sc; E: ^{48}Sc; F: ^{49}Sc.

FORM NBS-418
(8-1-63)
USCOMM-OC 18556-P63

REF. H. L. Pai and K. G. McNeill
Can. J. Phys. 45, 3235 (1967)

ELEM. SYM.	A	Z
Ti	49	22

METHOD

[Page 1 of 2]

REF. NO. 67 Pa 2

EGF

REACTION	RESULT	EXCITATION ENERGY	SOURCE		DETECTOR		ANGLE
			TYPE	RANGE	TYPE	RANGE	
G,P	RLY	THR- 30	C	22,30	ACT-I		4PI
G,NP	RLY	THR- 30	C	22,30	ACT-I		4PI

TABLE I

Yields, Y, and cross sections, σ, of the proton reactions in Ti isotopes excited by photons or neutrons. (The yields and cross sections with primes are "first proton" yields and cross sections)

		1	2	3	4	5	6	7
		E_γ = 22 MeV				E_n = 13 MeV		
Compound nucleus	Target nucleus	$Y_{\gamma p}$	$Y_{\gamma pn}$	$Y_{\gamma np}$	$Y_{\gamma p}'$ (cols. 1 + 2)	σ_{np}	$\sigma_{n,pn}$	σ_{np}' (cols. 5 + 6)
$^{47}Ti^*$	^{47}Ti ^{46}Ti	57	(<1)[a]	(<1)	~57	277	(<10)	~280
$^{48}Ti^*$	^{48}Ti ^{47}Ti	20	E.I.[b]	E.I.	20	121	34	155
$^{49}Ti^*$	^{49}Ti ^{48}Ti	9.2	<0.1	<0.1	9.2	69	<1	~70
$^{50}Ti^*$	^{50}Ti ^{49}Ti	9.6	E.I.	E.I.	9.6	29	<1	~30

		1	2	3	4	5	6	7
		E_γ = 30 MeV				E_n = 19 MeV		
Compound nucleus	Target nucleus	$Y_{\gamma p}$	$Y_{\gamma pn}$	$Y_{\gamma np}$	$Y_{\gamma p}'$	σ_{np}	σ_{npn}	σ_{np}'
$^{47}Ti^*$	^{47}Ti ^{46}Ti	5.5	(0.03)	(0.04)	5.5	167	47	214
$^{48}Ti^*$	^{48}Ti ^{47}Ti	2.5	0.24	0.41	2.7	77	70	147
$^{49}Ti^*$	^{49}Ti ^{48}Ti	1.5	0.29	0.57	1.8	42	31	73
$^{50}Ti^*$	^{50}Ti ^{49}Ti	1.6	0.17	0.37	1.8	28	9	37

[a] Bracketed values are calculated from yields for production of ^{45}Ti, as ^{45}Sc is stable.
[b] E.I. = energetically impossible.

REF. H. L. Pai and K. G. McNeill
Can. J. Phys. 45, 3235 (1967)

ELEM. SYM.	A	Z
Ti	49	22

METHOD

REF. NO. 67 Pa 2

EGF

REACTION	RESULT	EXCITATION ENERGY	SOURCE		DETECTOR		ANGLE
			TYPE	RANGE	TYPE	RANGE	

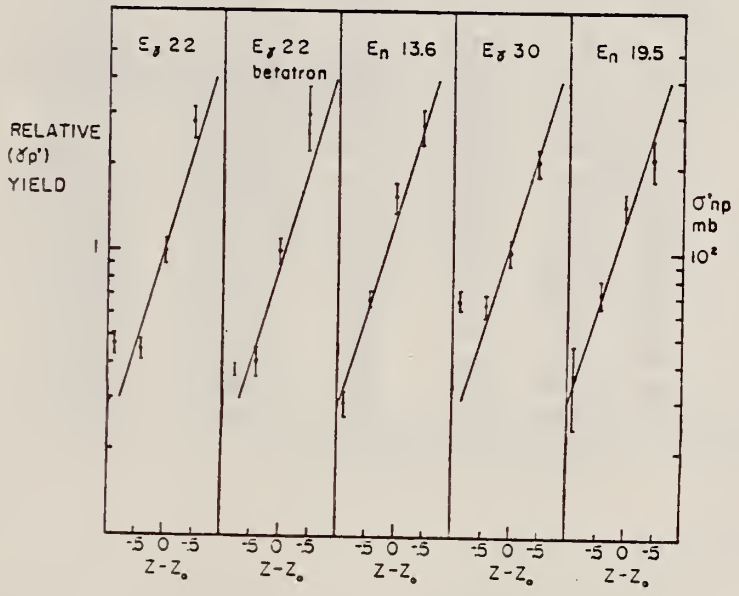

FIG. 1. The relative yields of the first-proton photoreactions in four Ti isotopes plotted as a function of $Z - Z_0$, where $Z = 22$ and Z_0 is the value of Z which minimizes $M(A, Z)$. For ^{50}Ti, $Z - Z_0 = -0.88$, and for ^{49}Ti, ^{48}Ti, and ^{47}Ti the values of $Z - Z_0$ are -0.44, $+0.01$, and $+0.46$ respectively. Three plots are shown, one obtained at 22 MeV using the linac, one at 30 MeV with the linac, and one at 22 MeV with the betatron. Also shown are cross sections of the first-proton reactions induced by fast neutrons, of energies 13.6 and 19.5 MeV, in Ti isotopes (Pai 1968).

REF. Y. Oka, T. Kato, K. Nomura, T. Saito, Hui-Tuh Tsai
Bull. Chem. Soc. Japan 41, 380 (1968)

ELEM. SYM.	A	Z
Ti	49	22

METHOD

REF. NO. 68 Ok 3 egf

REACTION	RESULT	EXCITATION ENERGY	SOURCE		DETECTOR		ANGLE
			TYPE	RANGE	TYPE	RANGE	
G,P	ABY	THR-20	C	20	ACT-I		4PI

TABLE I. SUMMARY OF DATA ON (γ, p) REACTIONS WITH 20 MeV BREMSSTRAHLUNG

Nuclide: Parent (Natural abundance, %)	Nuclide: Residual (Half-life)	S_p (MeV)	Observed γ-ray: Energy (MeV)	Observed γ-ray: Branching ratio (%)	Observed γ-ray: Type of multipole transition	Yield determined: μCi/mg[a]	Yield determined: Yield/mol·R
^{25}Mg (10.11)	^{24}Na (15 hr)	12.06	1.37	100	$E2$	1.48×10^{-1}	1.7×10^{5}
^{29}Si (4.71)	^{28}Al (2.27 min)	12.33	1.78	100	$E2$	1.91	2.8×10^{5}
^{30}Si (3.12)	^{29}Al (6.56 min)	13.59	1.28	93.8	$E2+M1$	6.51×10^{-1}	1.5×10^{5}
^{44}Ca (2.06)	^{43}K (22.4 hr)	12.17	0.374	85	$E2+M1$	7.86×10^{-3}	1.3×10^{5}
^{47}Ti (7.32)	^{46}Sc (84.1 d)	10.47	0.887	100	$E2$	7.11×10^{-4}	3.1×10^{5}
^{48}Ti (73.99)	^{47}Sc (3.4 d)	11.44	0.160	100	$E2+M1$	6.83×10^{-2}	1.2×10^{5}
^{49}Ti (5.46)	^{48}Sc (1.8 d)	11.35	1.31	100	$E2$	4.40×10^{-3}	5.8×10^{4}
^{53}Cr (9.55)	^{52}V (3.8 min)	11.15	1.43	100	$E2$	5.01×10^{-1}	6.6×10^{4}
^{57}Fe (2.17)	^{56}Mn (2.58 hr)	10.57	1.81	23.5	$E2+M1$	8.10×10^{-2}	2.1×10^{5}
^{74}Ge (36.74)	^{73}Ga (4.8 hr)	10.92	0.295	97	$(E2)$	3.70×10^{-1}	1.3×10^{5}
^{77}Se (7.58)	^{76}As (26.5 hr)	9.61	0.559	41	$E2$	1.48×10^{-2}	1.3×10^{5}
^{87}Sr (7.02)	^{86}Rb (19 d)	9.41	1.08	9	$E2$	5.15×10^{-4}	9.9×10^{4}
^{110}Cd (12.26)	^{109}Ag (3.2 hr)	9.74	1.39	35	$E2$	1.91×10^{-2}	2.1×10^{4}
^{117}Sn (7.57)	^{116m}In (54 min)	9.58	1.27	84	$E2$	9.80×10^{-3}	6.9×10^{5}
^{137}Ba (11.32)	^{136}Cs (13 d)	8.67	0.830	100	$E2$	1.68×10^{-4}	2.2×10^{4}
^{199}Hg (16.84)	^{198}Au (2.7 d)	7.27	0.412	100	$E2$	8.43×10^{-4}	2.2×10^{4}

a) The value corrected at the end of 1 hr irradiation (9.4×10^{6} R/min).

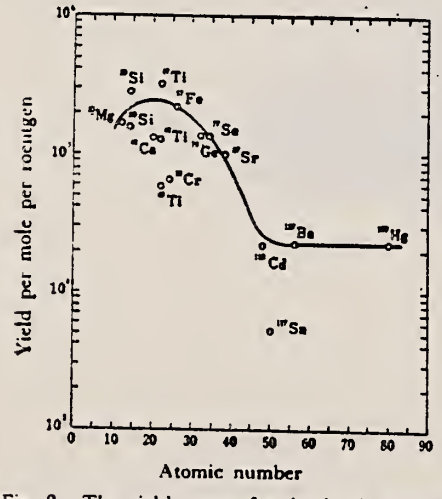

Fig. 2. The yield curve for the (γ, p) reaction with 20 MeV bremsstrahlung.

Y. Oka, T. Kato and N. Sato
Bull. Chem. Soc. Japan 42, 387 (1969)

Ti	49	22

METHOD

REF. NO. 69 Ok 1 hmg

REACTION	RESULT	EXCITATION ENERGY	SOURCE TYPE	SOURCE RANGE	DETECTOR TYPE	DETECTOR RANGE	ANGLE
G.P	RLY	THR-60	C	30-60	NAI-D		4PI

YLD REL 12C(γ,N)

TABLE 6. THE RELATIVE YIELDS FOR (γ, p) REACTIONS ON TITANIUM NUCLEI EXPRESSED AS THOSE PER MOLE

Reaction	Yield per mole relative to $^{12}C(\gamma, n)^{11}C$			
	30 MeV	45 MeV	55 MeV	60 MeV
$^{47}Ti(\gamma, p)^{46}Sc$	5.4×10^{-1}	5.8×10^{-1}	5.4×10^{-1}	6.3×10^{-1}
$^{46}Ti(\gamma, p)^{47}Sc$	2.0×10^{-1}	2.4×10^{-1}	2.8×10^{-1}	2.8×10^{-1}
$^{48}Ti(\gamma, p)^{47}Sc$	1.2×10^{-1}	2.1×10^{-1}	2.2×10^{-1}	2.1×10^{-1}

REF.

V. K. Rasmussen
Phys. Rev. C13, 631 (1976)

ELEM. SYM.	A	Z
Ti	49	22

METHOD

REF. NO.	
76 Ra 1	hmg

REACTION	RESULT	EXCITATION ENERGY	SOURCE		DETECTOR		ANGLE
			TYPE	RANGE	TYPE	RANGE	
G,G	LFT	1, 1	C	1- 5	SCD-D		DST
		(1.623,1.763)		(1.3-4.7)			

1623,1763 KEV

TABLE II. Mean lives of some levels in the titanium isotopes.

Mass no., ground state, spin, & abund.	Level energy (keV)	Level spin	Γ_0 (meV)	τ (pres. meas.) (fs)	τ (other) (fs)
46, 0^+	3168	1^-	7.3 ± 2.0	41 ± 12	71 ± 12 [a]
7.95%	4316	1	$(172 \pm 26)\Gamma/\Gamma_0$	0.96 ± 0.14 [b]	<44 [a]
47, $\frac{5}{2}^-$	2162	$\frac{3}{2}^-$	18 ± 5	38 ± 10	31 ± 8 [c]
7.75%	2297	$(\frac{5}{2}^-, \frac{7}{2}^-)$	104 ± 10 or [d] 78 ± 8	4.7 ± 0.5 or [d] 6.3 ± 0.7	11 ± 7 [c]
	2548	$\frac{3}{2}^-$	72 ± 8	9 ± 1	
48, 0^+	2421	2_2^+	0.74 ± 0.18	44 ± 12	35 ± 7 [e]
73.45%					$\Gamma_0 = 0.66 \pm 0.11$ meV and 0.77 ± 0.14 [f]
	3371	2_3^+	5.5 ± 0.6	16.1 ± 2.1	18 ± 7 [e]
	3700	$1^{(+)}$	20.4 ± 2.3	15.1 ± 1.6	35 ± 3 [g]
	3739	1^+	101 ± 10	4.2 ± 0.4	16 ± 3 [g]
49, $\frac{7}{2}^-$	1623	$(\frac{3}{2}^-, \frac{5}{2}^-, \frac{7}{2}^-)$	11.4 ± 1.5 [h]	55 ± 7	
5.51%	1763	$\frac{5}{2}^-$	18.3 ± 2.2	36 ± 4.3	
50, 0^+	1554	2_1^+	0.52 ± 0.15	1300 ± 400	$\Gamma = 0.48 \pm 0.04$ meV [i]
5.34%	(4311)	2^+	85 ± 60	$1 < \tau < 6$	<80 [j]
(47, 49)	3917		$(90 \pm 20)\Gamma/g\Gamma_0$ [k]		
	2810		$(29 \pm 4)\Gamma/g\Gamma_0$ [k]		

[a] Reference 11.
[b] Assuming $\Gamma_0/\Gamma = 0.50$.
[c] Reference 18.
[d] The larger width and shorter lifetime correspond to spin $\frac{5}{2}$.
[e] Reference 23.
[f] Coulomb excitation and (e, e'), J. Heisenberg, J. S. McCarthy, and I. Sick, Nucl. Phys. A164, 353 (1971).
[g] C. D. Kavaloski and W. J. Kossler, Phys. Rev. 180, 971 (1969).
[h] Assuming spin $\frac{9}{2}$.
[i] From Coulomb excitation results of C. W. Towsley, D. Cline, and R. Horoshko, Nucl. Phys. A250, 381 (1975).
[j] Reference 12.
[k] Calculated as if ^{49}Ti, g is the statistical factor.

[11] P.A. Assimakopoulos, et al., Nucl. Phys. A180, 131 (1972).
[12] J.G. Pronko et al,, Phys. Rev. C10, 1345 (1974).
[18] J.J. Weaver et al., Nucl. Phys. A196, 269 (1972).
[23] T.T. Bardin et al., Phys. REv. C7, 190 (1973).

REF. K. Masumoto, T. Kato, N. Suzuki
Nucl. Inst. Meth. 157, 567 (1978)

ELEM. SYM.	A	Z
Ti	49	22

METHOD

REF. NO. 78 Ma 10 hg

REACTION	RESULT	EXCITATION ENERGY	SOURCE		DETECTOR		ANGLE
			TYPE	RANGE	TYPE	RANGE	
G,P	ABY	11-68	C	30-68	ACT		4PI

Analysis is made of reactions interfering with photon activation analysis procedures.

The activation yield curves have been presented for a number of photonuclear reactions in the energy range from 30 to 68 MeV, in order to evaluate quantitatively the interferences due to competing reactions in multielement photon activation analysis. The general features of the yields as functions of both target mass number and excitation energy were elucidated from the data obtained, discussion being given on the results in terms of the reaction mechanism.

Simultaneous neutron activation due to appreciable neutron production from the converter and surrounding materials has also been studied, and, finally, the magnitudes of interferences in real multielement analysis were given in the form of their energy dependences.

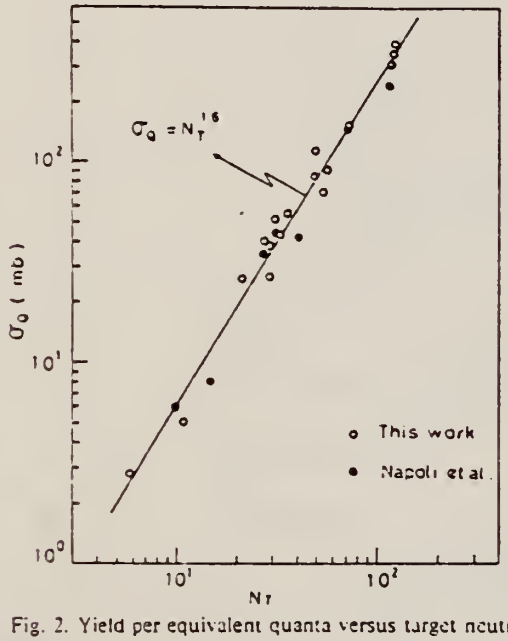

Fig. 2. Yield per equivalent quanta versus target neutron number.

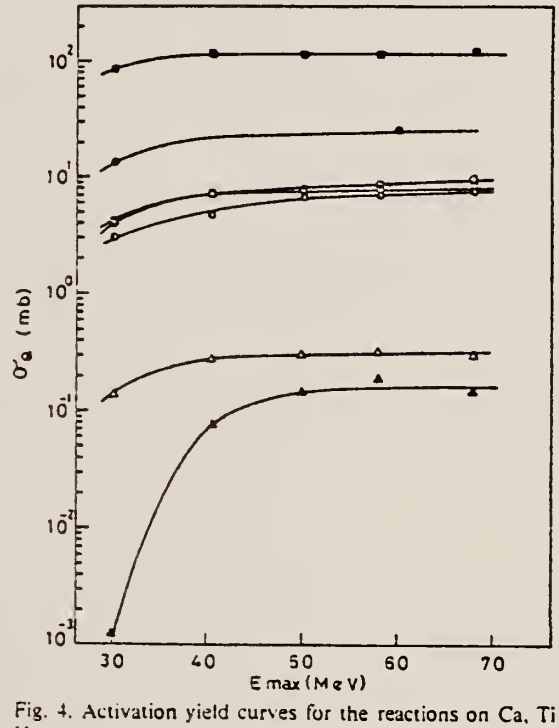

Fig. 4. Activation yield curves for the reactions on Ca, Ti and V.

■ $^{48}Ca(\gamma, n)^{47}Ca$, □ $^{44}Ca(\gamma, p)^{43}K$, ● $^{46}Ti(\gamma, n)^{45}Ti$,
○ $^{48}Ti(\gamma, p)^{47}Sc$, ◐ $^{49}Ti(\gamma, p)^{48}Sc$, △ $^{51}V(\gamma, \alpha)^{47}Sc$,
▲ $^{51}V(\gamma, xn)^{46}Sc$.

(over)

FORM NBS-418
U.S. DEPARTMENT OF COMMERCE

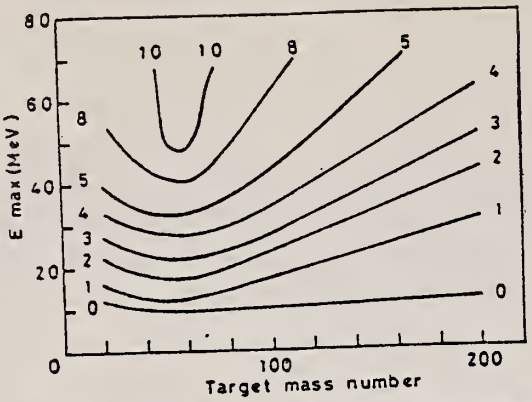

Fig. 10. Yields of the (γ, p) reactions as a function of bremsstrahlung maximum energy and target mass number. The numerical values in the figure are yields per equivalent quanta in mb.

REF. Z. Berant, Y. Birenbaum, R. Moreh, O. Shahal
Nucl. Phys. A368, 201 (1981)

ELEM. SYM.	A	Z
Ti	49	22

METHOD

REF. NO. 81 Be 10 hg

REACTION	RESULT	EXCITATION ENERGY	SOURCE TYPE	SOURCE RANGE	DETECTOR TYPE	DETECTOR RANGE	ANGLE
G,G	NOX	9 (8.884)	D	9 (8.884)	SCD-D		DST
G,N	SPC	9 (8.884)	D	9 (8.884)	MOD-D		DST

Abstract: An unbound level in ^{49}Ti at 8884 keV was photoexcited using a γ-beam obtained from the Cr(n, γ) reaction. The γ-decay and n-decay properties of this level were studied using angular distributions and polarization measurements. Thus spin and parity assignments of some levels in ^{49}Ti were made. The neutron width and the total radiative widths of the 8884 keV level were determined to be: $\Gamma_n = 0.25 \pm 0.05$ eV. $\Gamma_\gamma = 2.55 \pm 0.80$ eV.

G,G 8.884 MEV, J-PI=7/2+
G,N DECAY,8.884MEV,LEV

E NUCLEAR REACTIONS ^{49}Ti(γ, γ'): measured E_γ, $I_\gamma(0)$. ^{49}Ti deduced levels. J, π, EI, Γ_γ, Γ_n.

Z. Berant et al. ^{49}*Ti*

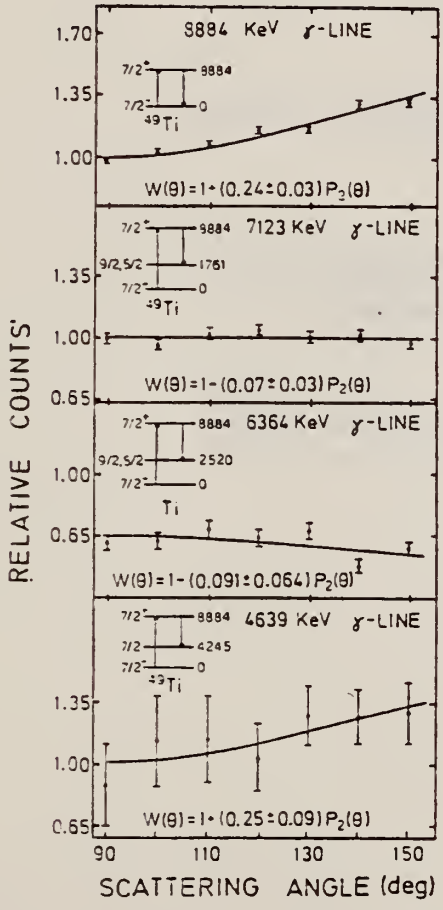

Fig. 2. Angular distribution of the elastic and inelastically scattered γ-lines from ^{49}Ti. The solid lines are least-square fits to the experimental distributions and have the form $W(\theta) = 1 + AP_2(\cos\theta)$.

(OVER)

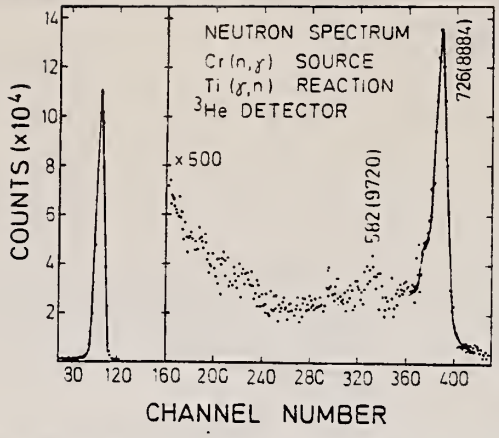

Fig. 3. Photoneutron spectrum of the ^{49}Ti(γ, n) reaction showing the strong n-group at 726 keV arising from the n-emission from the 8884 keV resonance level to the ^{48}Ti ground state. The weak n-group at 582 keV is produced by the 9720 keV γ-line proceeding to the 983 keV level in ^{48}Ti.

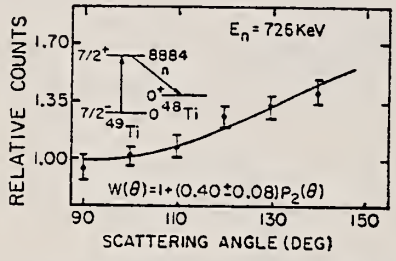

Fig. 4. Angular distribution of the 826 keV n-group as measured using a ^{3}He n-spectrometer. The generation process of this n-group through the ^{49}Ti(γ, n) reaction is shown.

TABLE 2

Measured values of $\Gamma_0 \cdot \Gamma_\gamma$, the elastic scattering cross sections σ_γ, the neutron emission cross section σ_n, the energy separation δ (between the incident γ-line and resonance level), the deduced value of the radiative widths Γ_0, Γ_γ and the neutron width Γ_n for the ^{49}Ti level at 8884 keV

E_x (keV)	$\Gamma_0 \cdot \Gamma_\gamma$	σ_n (mb)	σ_γ (mb)	δ (eV)	Γ_0 (eV)	Γ_n (eV)	Γ_γ (eV)
8884	0.13 ± 0.05	33 ± 4	43 ± 4	9.0 ± 0.8	0.33 ± 0.040	0.25 ± 0.05	2.54 ± 0.80

TI
A=50

TI
A=50

TI
A=50

E. Silva, J. Goldemberg
An. Acad. Brasil. Cienc. 30, 51 (1958)

Ti	50	22

METHOD: Betatron

REF. NO.: 58 Si 4 | NVB

REACTION	RESULT	EXCITATION ENERGY	SOURCE		DETECTOR		ANGLE
			TYPE	RANGE	TYPE	RANGE	
G,P	RLX	12 - 22	C	THR-22	ACT-I		4PI

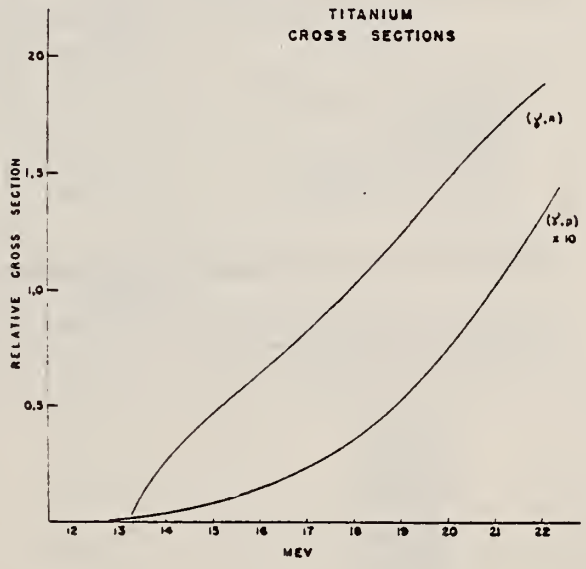

Fig. 4

Ref. T.R. Sherwood, W.E. Turchinetz
Nuclear Phys. 29, 292 (1962)

Elem. Sym.	A	Z
Ti	50	22

Method
Bremss.; Canberra electron synchrotron; activity

Ref. No.
62 Sh 5

EGF

Reaction	E or ΔE	E_0	Γ	$\int \sigma dE$	Jπ
$Ti^{50}(\gamma,p)$	Bremss.				
$Ti^{50}(\gamma,pn)$	14-31				

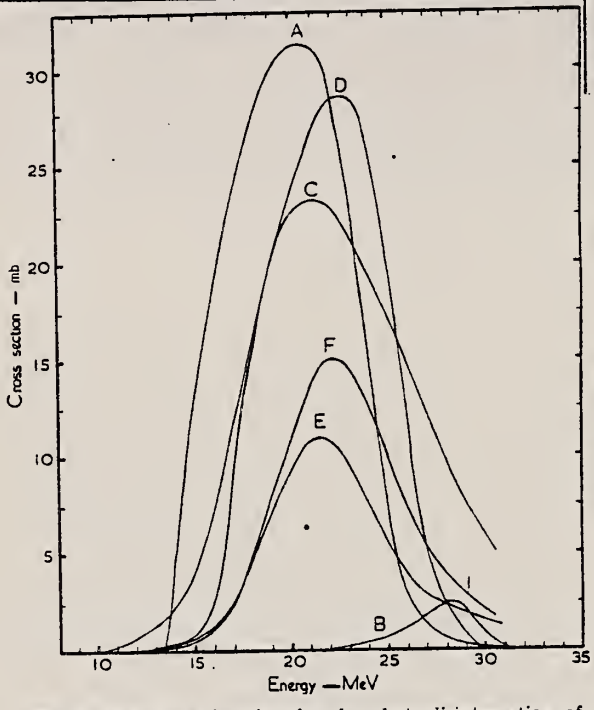

Fig. 2. Excitation function for the photo-disintegration of titanium. A: $^{46}Ti(\gamma, n) + 1.09\ ^{47}Ti(\gamma, 2n)$; B: $^{46}Ti(\gamma, np)$; C: $^{47}Ti(\gamma, p) + 10.1\ ^{46}Ti(\gamma, np)$; D: $^{48}Ti(\gamma, p) + 0.07\ ^{49}Ti(\gamma, np)$; E: $^{49}Ti(\gamma, p) + 0.96$ Ti (γ, np); F: $^{50}Ti(\gamma, p)$.

TABLE 3

Integrated (to 31 MeV) cross sections

Reactions	Relative weights	Integrated cross section (MeV · mb)
$^{46}Ti(\gamma, n) : {}^{47}Ti(\gamma, 2n)$	1 : 1.09	260±34
$^{46}Ti(\gamma, np)$		8.8±1.4 [a])
$^{47}Ti(\gamma, p) : {}^{46}Ti(\gamma, np)$	1 : 10.1	246±38
$^{48}Ti(\gamma, p) : {}^{46}Ti(\gamma, np)$	1 : 0.07	217±32
$^{49}Ti(\gamma, p) : {}^{50}Ti(\gamma, np)$	1 : 0.96	86±13
$^{50}Ti(\gamma, p)$		113±32

[a]) Upper limit. The partial cross section from the ^{44}Sc formed in the ground state is 4.4 MeV · mb.

TABLE 4

Comparison of experimental results with statistical theory predictions for gamma rays of 22 MeV

Ratio of cross sections	Experimental	Theoretical
$\frac{^{47}Ti(\gamma, p)}{^{48}Ti(\gamma, p)}$	0.81	1.40
$\frac{^{49}Ti(\gamma, p)}{^{48}Ti(\gamma, p)}$	0.39	0.63
$\frac{^{50}Ti(\gamma, p)}{^{48}Ti(\gamma, p)}$	0.45	0.56
$\frac{^{46}Ti(\gamma, p)}{^{46}Ti(\gamma, n)}$	0.98	0.34

Notes

Table 3: $Cu^{63}(\gamma,n)$ by Berman and Brown [Phys. Rev. 96, 83 (1954)] used as standard.

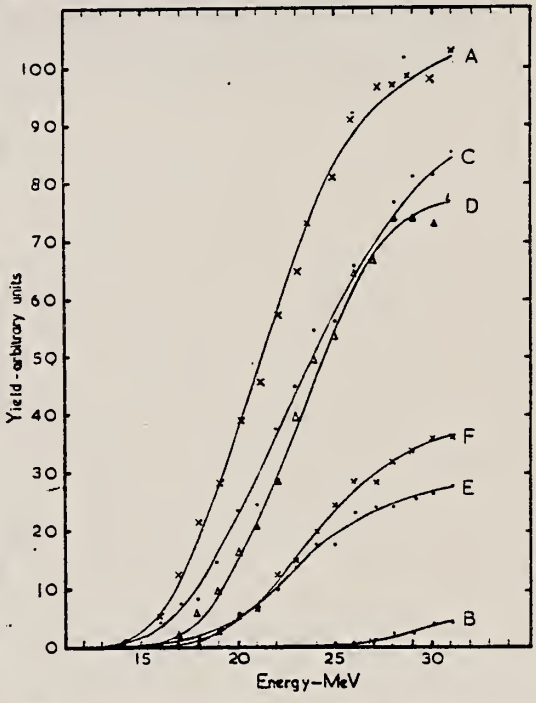

Fig. 1. Activation curves for the photo-disintegration of titanium. A: ^{46}Ti; B: ^{44}Sc (ground state decay); C: ^{46}Sc; D: ^{47}Sc; E: ^{48}Sc; F: ^{49}Sc.

REF. H. L. Pai and K. G. McNeill
Can. J. Phys. 45, 3235 (1967)

ELEM. SYM.	A	Z
Ti	50	22

METHOD

REF. NO. 67 Pa 2

EGF

REACTION	RESULT	EXCITATION ENERGY	SOURCE		DETECTOR		ANGLE
			TYPE	RANGE	TYPE	RANGE	
G,P	RLY	THR- 30	C	22,30	ACT-I		4PI
G,NP	RLY	THR- 30	C	22,30	ACT-I		4PI

TABLE I

Yields, Y, and cross sections, σ, of the proton reactions in Ti isotopes excited by photons or neutrons. (The yields and cross sections with primes are "first proton" yields and cross sections)

		1	2	3	4	5	6	7
		E_γ = 22 MeV				E_n = 13 MeV		
Compound nucleus	Target nucleus	$Y_{\gamma p}$	$Y_{\gamma pn}$	$Y_{\gamma np}$	$Y_{\gamma p}'$ (cols. 1 + 2)	σ_{np}	$\sigma_{n,pn}$	σ_{np}' (cols. 5 + 6)
^{47}Ti*	^{47}Ti / ^{46}Ti	57	(<1)[a]	(<1)	~57	277	(<10)	~280
^{48}Ti*	^{48}Ti / ^{47}Ti	20	E.I.[b]	E.I.	20	121	34	155
^{49}Ti*	^{49}Ti / ^{48}Ti	9.2	<0.1	<0.1	9.2	69	<1	~70
^{50}Ti*	^{50}Ti / ^{49}Ti	9.6	E.I.	E.I.	9.6	29	<1	~30

		1	2	3	4	5	6	7
		E_γ = 30 MeV				E_n = 19 MeV		
Compound nucleus	Target nucleus	$Y_{\gamma p}$	$Y_{\gamma pn}$	$Y_{\gamma np}$	$Y_{\gamma p}'$	σ_{np}	σ_{npn}	σ_{np}'
^{47}Ti*	^{47}Ti / ^{46}Ti	5.5	(0.03)	(0.04)	5.5	167	47	214
^{48}Ti*	^{48}Ti / ^{47}Ti	2.5	0.24	0.41	2.7	77	70	147
^{49}Ti*	^{49}Ti / ^{48}Ti	1.5	0.29	0.57	1.8	42	31	73
^{50}Ti*	^{50}Ti / ^{49}Ti	1.6	0.17	0.37	1.8	28	9	37

[a] Bracketed values are calculated from yields for production of ^{49}Ti, as ^{49}Sc is stable.
[b] E.I. = energetically impossible.

REACTION	RESULT	EXCITATION ENERGY	SOURCE		DETECTOR		ANGLE
			TYPE	RANGE	TYPE	RANGE	

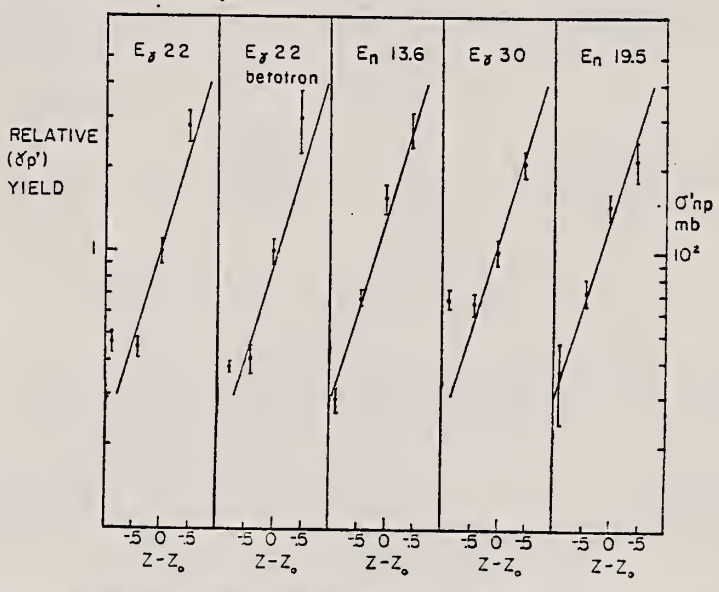

FIG. 1. The relative yields of the first-proton photoreactions in four Ti isotopes plotted as a function of $Z - Z_0$, where $Z = 22$ and Z_0 is the value of Z which minimizes $M(A, Z)$. For ^{50}Ti, $Z - Z_0 = -0.88$, and for ^{49}Ti, ^{48}Ti, and ^{47}Ti the values of $Z - Z_0$ are -0.44, $+0.01$, and $+0.46$ respectively. Three plots are shown, one obtained at 22 MeV using the linac, one at 30 MeV with the linac, and one at 22 MeV with the betatron. Also shown are cross sections of the first-proton reactions induced by fast neutrons, of energies 13.6 and 19.5 MeV, in Ti isotopes (Pai 1966).

REF. J. Heisenberg, J. S. McCarthy and I. Sick
Nucl. Phys. A164, 353 (1971)

ELEM. SYM.	A	Z
Ti	50	22

METHOD

REF. NO. 71 He 1 egf

REACTION	RESULT	EXCITATION ENERGY	SOURCE TYPE	SOURCE RANGE	DETECTOR TYPE	DETECTOR RANGE	ANGLE
E,E/	FMF	1-5	D	198-300	MAG-D		DST

5 LEVELS

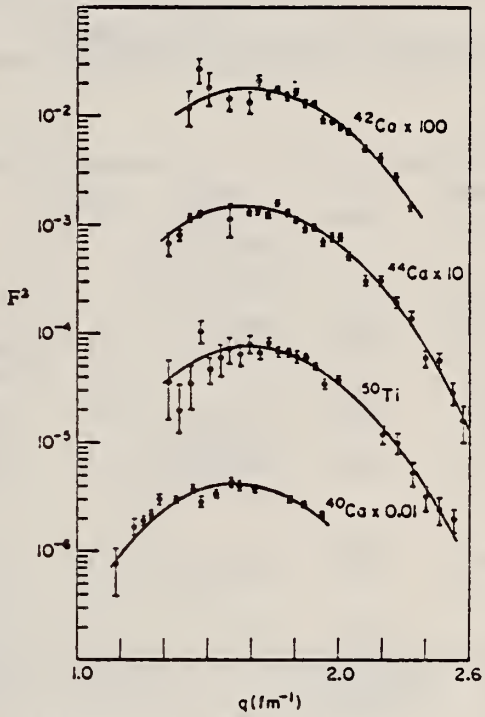

Fig. 7. Fits to ^{42}Ca, ^{40}Ca, ^{44}Ca and ^{50}Ti 5$^-$ levels.

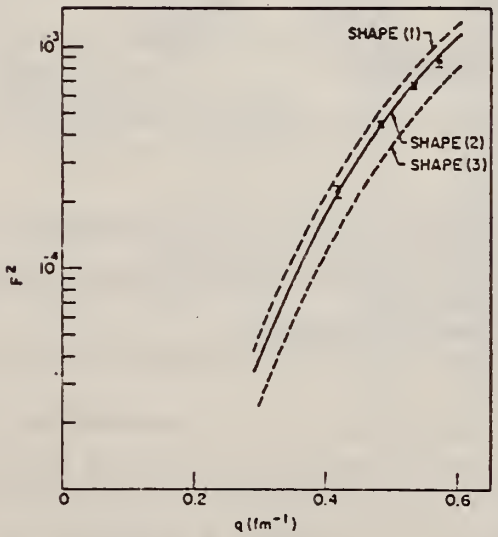

Fig. 5. Low-energy data for ^{40}Ca 3$^-$ level from ref. [8]. The curves represent the best fits to our high-energy data using shapes (1), (2) and (3) as explained in the text.

[over]

TABLE 3

Inelastic parameters

Isotope	E^* (MeV)	L	Shape	c_{tr} [a]) (fm)	z_{tr} [a]) (fm)	G [b]) (s.p.u.)	R_{tr} [a]) (fm)	G(s.p.u.) heavy-particle scattering [19])
^{40}Ca	3.740	3	2	3.536±0.030	1.483±0.020	24.9 ±1.0	4.835±0.030	23.6±3.5
	4.480	5	2	3.538±0.050	1.260±0.035	9.7 ±0.6	4.810	17.7±2.7
			3			17.7 ±1.5	5.467±0.060	11.3±1.7
^{42}Ca	3.440	3	2	3.565±0.018	1.383±0.014	12.4 ±0.5	4.719±0.023	12.0±1.8
	4.100	5	2	3.231±0.030	1.404±0.025	3.4 ±0.3	4.816±0.044	9.0±1.4
^{44}Ca	3.30	3	2	3.555±0.018	1.313±0.013	6.95±0.28	4.618±0.023	8.0±1.2
	2.28	4	2	4.091±0.030	1.268±0.016	2.66±0.15	5.135±0.030	1.3±0.3
	3.91	5	2	3.268±0.030	1.397±0.024	2.30±0.20	4.832±0.045	4.4±0.7
^{46}Ti	2.00	4	2	4.264±0.021	1.229±0.013	7.61±0.30	5.226±0.026	
^{48}Ti	2.286	4	2	4.330±0.021	1.196±0.013	3.37±0.15	5.237±0.026	
^{50}Ti	4.42	3	2	3.645±0.017	1.244±0.012	3.76±0.15	4.600±0.023	5.4±0.8
								5.9 [20])
	2.50	4	2	3.865±0.017	1.347±0.012	4.7 ±0.15	5.064±0.026	3.3±0.7
								2.7 [20])
	3.20	5	2	3.254±0.032	1.345±0.026	0.83±0.08	4.724±0.045	
					Present experiment			

[a]) Errors do not reflect any model dependence.
[b]) Given errors do not include the 6 % error of normalization.

[19] A. M. Bernstein, Adv. in Nucl. Phys. 3 (1969) 325.

TABLE 2

Inelastic parameters for 2⁺ levels

Isotope	E^* (MeV)	B(E2) Coulomb Excit. ($e^2 \cdot fm^4$)	Shape	c_{tr} [a]) (fm)	z_{tr} [a]) (fm)	Fitted B(E2) ($e^2 \cdot fm^4$) [b])	R_{tr} [a]) (fm)	B(E2)($e^2 \cdot fm^4$) heavy-particle scattering
^{42}Ca	1.520	364± 82 [9])	2	3.541±0.025	1.459±0.020	320±20	4.619±0.030	476± 74 [19])
^{44}Ca	1.160	350± 70 [10])	2	3.691±0.027	1.428±0.020	480±30	4.704±0.030	507±100 [19])
			1	3.454±0.025	0.690±0.010	1270±85	5.553±0.030	
	3.259		2			54±10		
^{46}Ti	0.885	830±170 [14])	2	3.807±0.014	1.397±0.010	740±20	4.763±0.017	867 [20])
		560±100 [13])	1	3.562±0.014	0.669±0.005	1680±50	5.510±0.020	738 [11])
^{48}Ti	0.984	700±140 [14])	2	3.777±0.014	1.340±0.010	537±15	4.671±0.017	788±120 [19])
		310± 70 [13])	1	3.539±0.014	0.633±0.005	1110±30	5.321±0.020	673 [11])
								659 [20])
	2.420		2			49± 8		57± 10 [19])
^{50}Ti	1.580	240± 20 [12])	2	3.768±0.014	1.255±0.010	307±10	4.567±0.017	349 [20])
			1	3.535±0.014	0.576±0.005	515±17	5.047±0.020	260 [21])
								431 [24])
	4.320		2			51± 8		72 [24])
^{56}Fe	0.880	877± 70 [c])	2	4.048±0.024	1.357±0.014	945±45	4.919±0.025	
			1	3.878±0.024	0.651±0.006	1570±70	5.454±0.030	
					Present experiment			

[a]) Errors do not reflect any model dependence.
[b]) Given errors do not include the 6 % error of normalization.
[c]) Average for B(E2) formed from values of refs. [12–18]).

13) J. Simpson, J. Cookson, D. Eccleshall and M. Yates, Nucl. Phys. 62 (1965) 385
14) G. M. Temmer and N. P. Heydenburg, Phys. Rev. 104 (1956) 967
15) D. S. Andreyev, A. P. Grinberg, K. I. Erokhina and I. Kh. Lemberg, Nucl. Phys. 19 (1960) 400
16) F. R. Metzger, Nucl. Phys. 27 (1961) 612
17) W. H. Kelly and G. B. Beard, Nucl. Phys. 27 (1961) 188
18) R. B. Begzhanov, A. A. Islamov, D. K. Kaipov and Yu. K. Shubnyi, JETP (Sov. Phys.) 17 (1963) 94

REF. Phan Xuan Ho, J. Bellicard, Ph. Leconte, I. Sick
Nucl. Phys. A210, 189 (1973)

ELEM. SYM.	A	Z
Ti	50	22

METHOD

REF. NO. 73 Ho 4 egf

REACTION	RESULT	EXCITATION ENERGY	SOURCE TYPE	SOURCE RANGE	DETECTOR TYPE	DETECTOR RANGE	ANGLE
E,E/	FMF	1- 5	D	209	MAG-D		DST

1.55, 2.68, 4.40

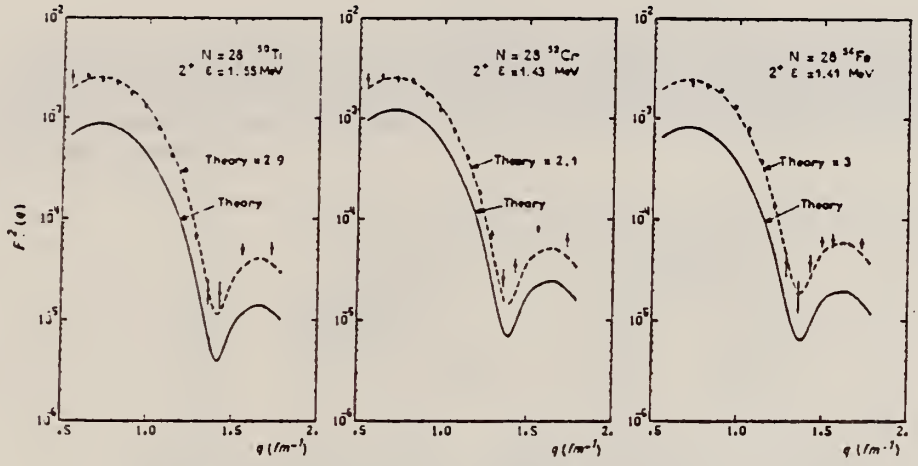

Fig. 5a. Squared inelastic form factor for 2^+ states of the $N = 28$ isotones.

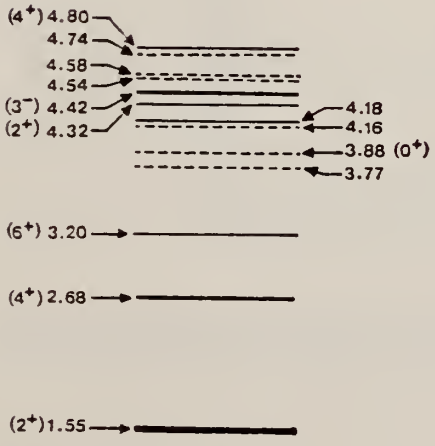

TABLE 2
Inelastic cross sections for $E_e = 209$ MeV on ^{50}Ti

θ (deg.)	$(2^+)\varepsilon = 1.55$ MeV $d\sigma/d\Omega$ (mb/sr)	$(3^-)\varepsilon = 4.40$ MeV $d\sigma/d\Omega$ (mb/sr)	$(4^+)\varepsilon = 2.68$ MeV $d\sigma/d\Omega$ (mb/sr)
30	0.308 E−1±0.510 E−2		
35	0.167 E−1±0.130 E−2	0.376 E−2±0.124 E−2	0.419 E−3±0.282 E−3
40	0.904 E−2±0.540 E−3	0.330 E−2±0.440 E−3	0.703 E−3±0.364 E−3
45	0.502 E−2±0.360 E−3	0.225 E−2±0.160 E−3	0.451 E−3±0.112 E−3
50	0.264 E−2±0.160 E−3	0.163 E−2±0.800 E−4	0.394 E−3±0.440 E−4
55	0.131 E−2±0.770 E−3	0.112 E−2±0.600 E−4	0.309 E−3±0.250 E−4
60	0.550 E−3±0.330 E−4	0.793 E−3±0.410 E−4	0.231 E−3±0.170 E−4
65	0.212 E−3±0.110 E−4	0.468 E−3±0.230 E−4	0.184 E−3±0.130 E−4
70	0.710 E−4±0.340 E−5	0.282 E−3±0.160 E−4	0.143 E−3±0.100 E−4
75	0.182 E−4±0.170 E−5	0.140 E−3±0.700 E−5	0.925 E−4±0.630 E−5
80	0.393 E−5±0.108 E−5	0.805 E−4±0.490 E−5	0.596 E−4±0.340 E−5
85	0.277 E−5±0.810 E−6	0.370 E−4±0.220 E−5	0.386 E−4±0.270 E−5
95	0.449 E−5±0.540 E−6	0.647 E−5±0.111 E−5	0.130 E−4±0.800 E−6
110	0.214 E−5±0.310 E−6	0.881 E−6±0.299 E−6	0.164 E−5±0.260 E−6

Energy level diagram given by ref. [24]). Levels excited in our experiment are shown with solid lines, dashed lines correspond to other levels. The experimental values are normalized on our elastic cross sections considered as reference values.

24 Nuclear Data Sheets B (1970).

(over)

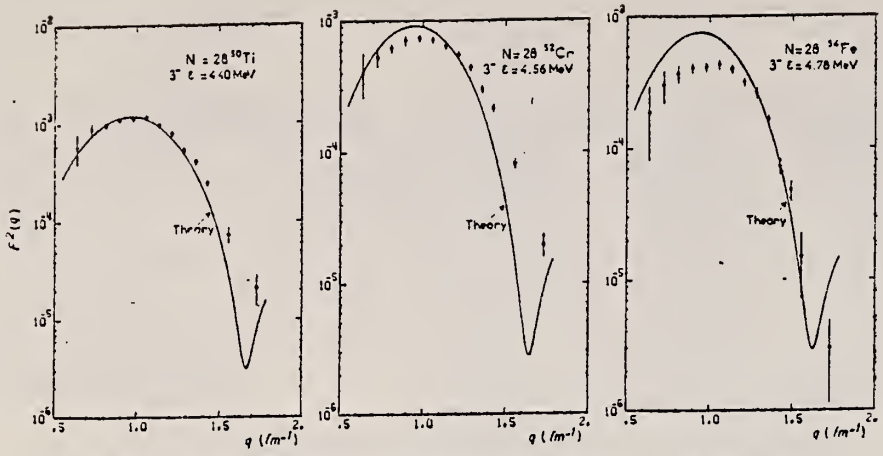

Fig. 6a. Squared inelastic form factor for 3^- states of the $N = 28$ isotones.

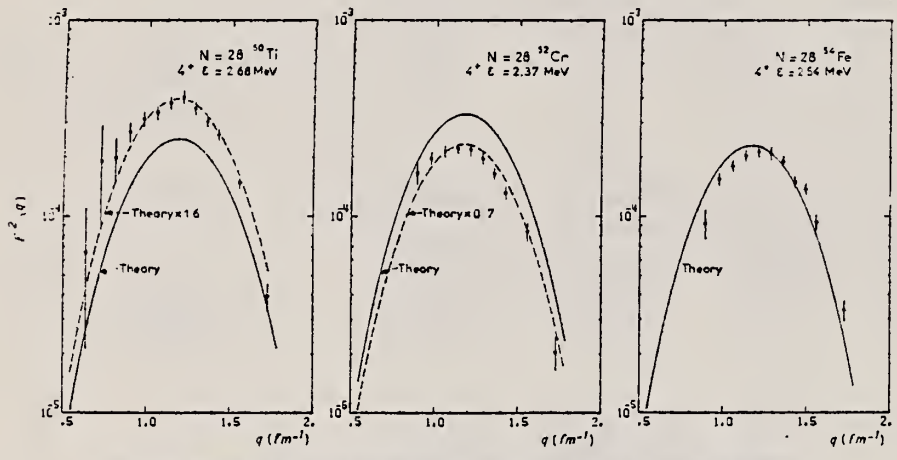

Fig. 7a. Squared inelastic form factor for 4^+ states of the $N = 28$ isotones.

REF. G. Eulenberg, D.I. Sober, W. Steffen, H.-D. Gräf, G. Küchler, A. Richter, E. Spamer, B.C. Metsch, W. Knüpfer
Phys. Lett. 116B, 113 (1982)

ELEM. SYM.	A	Z
Ti	50	22

METHOD

REF. NO. 82 Eu 1 egf

REACTION	RESULT	EXCITATION ENERGY	SOURCE		DETECTOR		ANGLE
			TYPE	RANGE	TYPE	RANGE	
E,E/	ABX	8-12	D	30-58	MAG-D		DST

M1 STRENGTH

Following the recent discovery of a very strong magnetic dipole transition in ^{48}Ca to a state at 10.23 MeV in high-resolution inelastic electron scattering, results of a detailed search for M1 strength in the other $N = 28$ isotones ^{50}Ti, ^{52}Cr and ^{54}Fe are described. The M1 strength found in the investigated region of excitation energy $E_x \approx 7$–12 MeV is very fragmented and considerably quenched in comparison to predictions of shell model calculations in a model space that includes up to 2p–2h excitations.

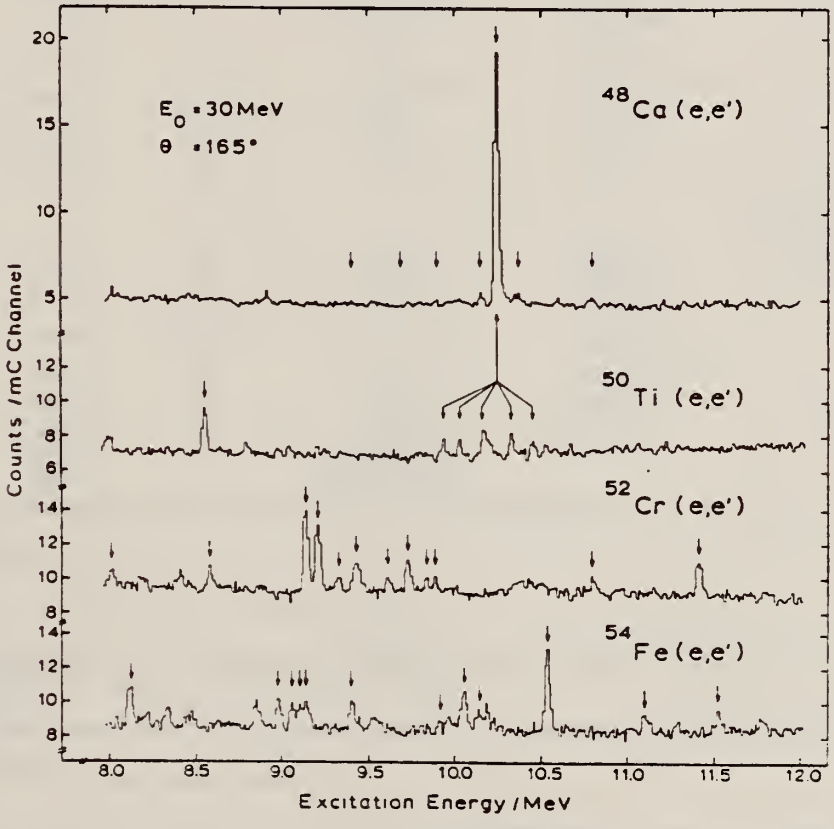

Fig. 1. High-resolution inelastic electron scattering spectra of the $N = 28$ isotones all measured at $E_0 = 30$ MeV and at $\theta = 165°$. The strongest magnetic dipole transitions are indicated by arrows.

(OVER)

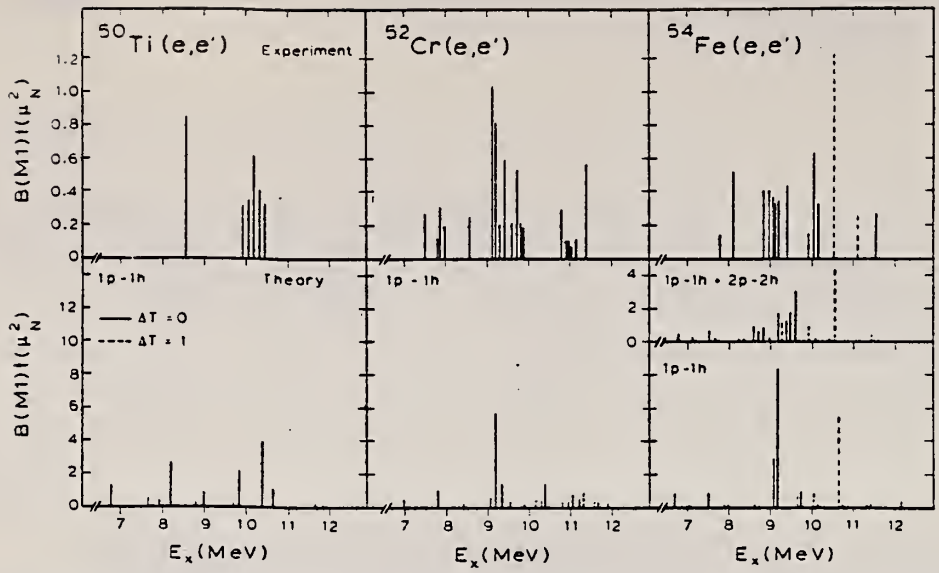

Fig. 3. Comparison of experimental and calculated M1 strength distributions for ^{50}Ti, ^{52}Cr and ^{54}Fe. Note the scale difference. For details, see the main text.

REF.	ELEM. SYM.	A	Z
V. K. Rasmussen Phys. Rev. C13, 631 (1976)	Ti	50	22

METHOD	REF. NO.
	76 Ra 1 egf

REACTION	RESULT	EXCITATION ENERGY	SOURCE		DETECTOR		ANGLE
			TYPE	RANGE	TYPE	RANGE	
G,G	LFT	1, 5	C	1- 5	SCD-D		DST
		(1.554-4.311)		(1.3-4.7)			

1554,4311 KEV

TABLE II. Mean lives of some levels in the titanium isotopes.

Mass no., ground state, spin, & abund.	Level energy (keV)	Level spin	Γ_0 (meV)	τ (pres. meas.) (fs)	τ (other) (fs)
46, 0^+	3168	1^-	7.3 ± 2.0	41 ± 12	71 ± 12 [a]
7.95%	4316	1	$(172 \pm 26)\Gamma/\Gamma_0$	0.96 ± 0.14 [b]	<44 [a]
47, $\frac{5}{2}^-$	2162	$\frac{3}{2}^-$	18 ± 5	38 ± 10	31 ± 8 [c]
7.75%	2297	$(\frac{5}{2}^-, \frac{1}{2}^-)$	104 ± 10 or [d] 78 ± 8	4.7 ± 0.5 or [d] 6.3 ± 0.7	11 ± 7 [c]
	2548	$\frac{3}{2}^-$	72 ± 8	9 ± 1	
48, 0^+	2421	2_2^+	0.74 ± 0.18	44 ± 12	35 ± 7 [e]
73.45%					$\Gamma_0 = 0.66 \pm 0.11$ meV and 0.77 ± 0.14 [f]
	3371	2_3^+	5.5 ± 0.6	16.1 ± 2.1	18 ± 7 [e]
	3700	$1^{(+)}$	20.4 ± 2.3	15.1 ± 1.6	35 ± 3 [g]
	3739	1^+	101 ± 10	4.2 ± 0.4	16 ± 3 [g]
49, $\frac{7}{2}^-$	1623	$(\frac{9}{2}^-, \frac{5}{2}^-, \frac{7}{2}^-)$	11.4 ± 1.5 [h]	55 ± 7	
5.51%	1763	$\frac{5}{2}^-$	18.3 ± 2.2	36 ± 4.3	
50, 0^+	1554	2_1^+	0.52 ± 0.15	1300 ± 400	$\Gamma = 0.48 \pm 0.04$ meV [i]
5.34%	(4311)	2^+	85 ± 60	$1 < \tau < 6$	<80 [j]
(47, 49)	3917		$(90 \pm 20)\Gamma/g\Gamma_0$ [k]		
	2810		$(29 \pm 4)\Gamma/g\Gamma_0$ [k]		

[a] Reference 11.
[b] Assuming $\Gamma_0/\Gamma = 0.50$.
[c] Reference 18.
[d] The larger width and shorter lifetime correspond to spin $\frac{5}{2}$.
[e] Reference 23.
[f] Coulomb excitation and (e, e'), J. Heisenberg, J. S. McCarthy, and I. Sick, Nucl. Phys. A164, 353 (1971).
[g] C. D. Kavaloski and W. J. Kossler, Phys. Rev. 180, 971 (1969).
[h] Assuming spin $\frac{9}{2}$.
[i] From Coulomb excitation results of C. W. Towsley, D. Cline, and R. Horoshko, Nucl. Phys. A250, 381 (1975).
[j] Reference 12.
[k] Calculated as if ^{49}Ti, g is the statistical factor.

[11] P.A. Assimakopoulos, et al., Nucl. Phys. A180, 131 (1972).
[12] J.G. Pronko et al., Phys. Rev. C10, 1345 (1974).
[18] J.J. Weaver et al., Nucl. Phys. A196, 269 (1972).
[23] T.T. Bardin et al., Phys. Rev. C7, 190 (1973).

REF. R.E. Pywell, M.N. Thompson and R.A. Hicks
Nucl. Phys. A325, 116 (1979)

ELEM. SYM.	A	Z
Ti	50	22

METHOD

REF. NO. 79 Py 6 hg

REACTION	RESULT	EXCITATION ENERGY	SOURCE		DETECTOR		ANGLE
			TYPE	RANGE	TYPE	RANGE	
G,XN	ABX	10-27	C	10-27	BF3-I		4PI
(G,NO)	RLX	10-26	C	15-26	SCI-D		90

Abstract: Measurements of the $^{50}Ti(\gamma, n)$ and $^{50}Ti(\gamma, n_0)$ cross sections have been made in the energy range of the giant dipole resonance (GDR). Assuming the GDR is split into two isospin components, approximated as Lorentzians, a calculation based on statistical decay of the GDR states is consistent with the experimental results.

E NUCLEAR REACTIONS $^{50}Ti(\gamma, n)$, bremsstrahlung, E = th–28 MeV; measured yield curves, deduced σ. $B^{10}F_3$ detector. Enriched target. $^{50}Ti(\gamma, n_0)$, bremsstrahlung, E = 15.5–26 MeV; measured neutron spectra, deduced σ. Stilbene detector. Enriched target.

COMMENT: Blatt & Weisskopf statistical model used to obtain $\sigma(\gamma,sn)$ from measured $\sigma(\gamma,xn)$. Sample used was 68.1% ^{50}Ti and about 31.9% ^{48}Ti. Yield curve was corrected using data from second sample enriched in ^{48}Ti.

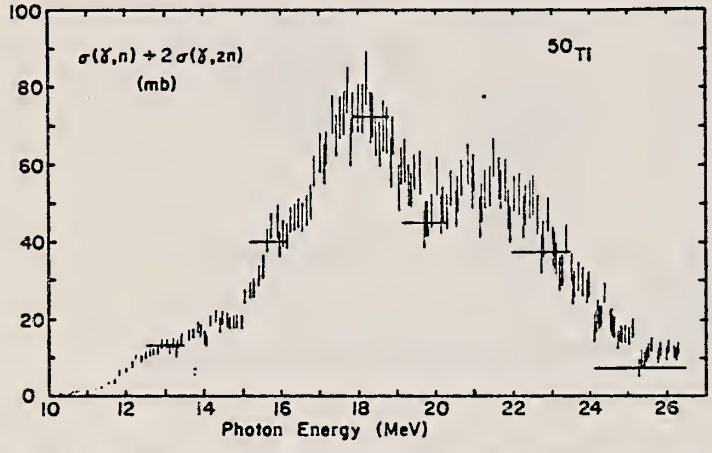

Fig. 2. The $^{50}Ti[\sigma(\gamma, n)+2\sigma(\gamma, 2n)]$ cross section derived using the VBPL technique. Vertical error bars are statistical only. There is a 10% uncertainty in the absolute cross section scale. Horizontal bars show the analysis bin width used.

(OVER)

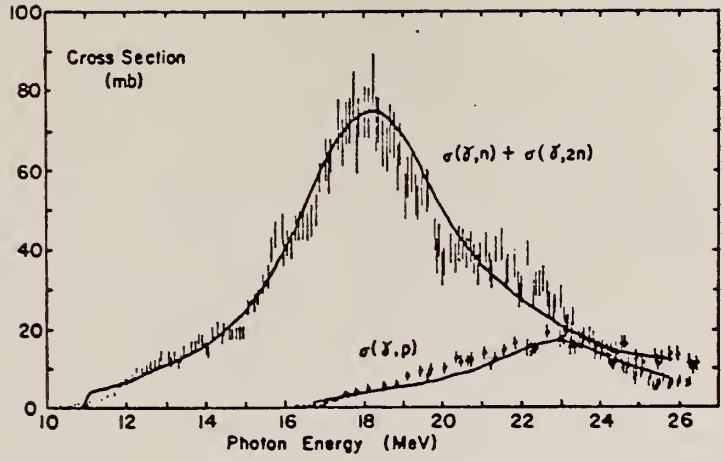

Fig. 3. Error bars only show the ^{50}Ti[$\sigma(\gamma, n)+\sigma(\gamma, 2n)$] cross section after correction for the double counting of the $(\gamma, 2n)$ cross section using a statistical model. Solid dots with error bars show the ^{50}Ti(γ, p) cross section from ref. [13]). Solid lines are the calculated (γ, n) and (γ, p) cross sections as described in the text.

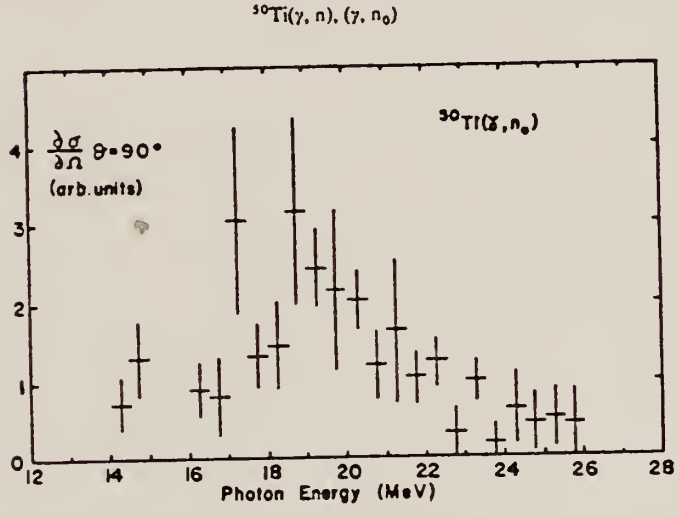

Fig. 5. The derived ^{50}Ti(γ, n_0) differential cross section at $\theta = 90°$. Cross section scale is arbitrary.

TI
A=52

TI
A=52

R.E. Peschel, J.M. Long, H.D. Shay, and D.A. Bromley

REF. Nucl. Phys. A232, 269 (1974)

ELEM. SYM.	A	Z
Ti	52	22

METHOD

REF. NO. 74 Pe 3 egf

REACTION	RESULT	EXCITATION ENERGY	SOURCE TYPE	SOURCE RANGE	DETECTOR TYPE	DETECTOR RANGE	ANGLE
A,G	ABX	13- 20	D	6- 14	NAI-D		90

$d\sigma/d\Omega(90^\circ)$ measured

The isospin allowed reaction $^{48}Ca(\alpha,\gamma)^{52}Ti$ was investigated in the α-particle energy range from 6.0–14.0 MeV, corresponding to 12.7–20.4 MeV excitation energy in ^{52}Ti (taking into account the target thickness). The intense low energy background made possible only the study of the $^{48}Ca(\alpha,\gamma_0)^{52}Ti$ reaction. Fig. 8 shows the γ-radiation spectrum obtained at the maximum of the 90° differential cross section in the region studied. The differential cross section extracted from this spectrum gives

$$d\sigma/d\Omega(90^\circ) = 45\pm8 \text{ nb/sr}, \qquad E_\alpha^{lab} = 7.00 \text{ MeV}.$$

For the remainder of the energy region studied, only an upper limit on the 90° differential cross section was obtained,

$$d\sigma/d\Omega(90^\circ) < 30 \text{ nb/sr}.$$

The $^{12}C(\alpha,\gamma_0)^{16}O$ reaction was used to check both the energy calibration and the γ-spectrometer immediately following the $^{48}Ca(\alpha,\gamma)^{52}Ti$ investigation. Because of the extremely low cross section of the $^{48}Ca(\alpha,\gamma)^{52}Ti$ reaction, no angular distribution measurements were attempted.

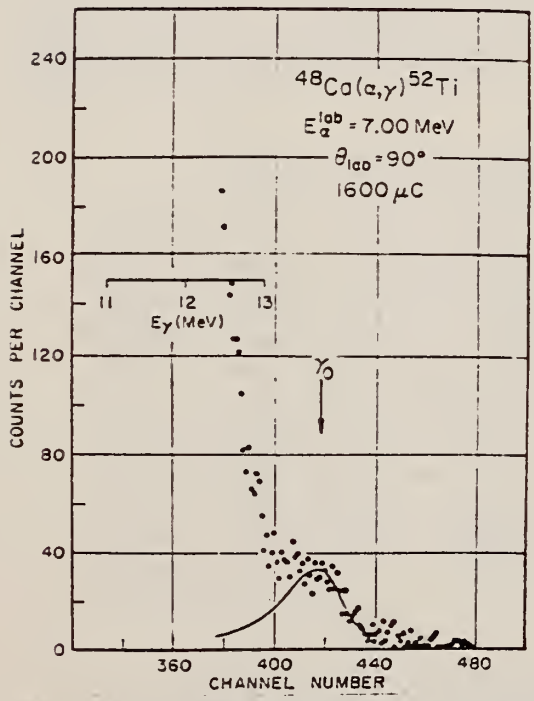

Fig. 8. The γ-radiation spectrum for the reaction $^{48}Ca(\alpha,\gamma)^{52}Ti$ at $E_\alpha^{lab} = 7.0$ MeV. A background subtraction for the residual cosmic radiation has been performed. Only the ground state transition was observed. From the systematics of the first excited state in doubly even Ti nuclei, the γ_1 transition would appear below channel 400.

# VANADIUM
Z=23

Andres Manuel del Río in 1801, discovered a new element in vanadinite from Zimapán, Mexico. A few years later he decided he was mistaken and that the brown ore was merely a basic lead chromate. In 1805 Collet-Descotils confirmed del Río's analysis and for twenty-five years no more was heard of the new element.

In 1830, N. G. Sefstrom discovered a new element in iron from the Taberg mine in Smaland. He named it vanadium, from Vanadis, the Scandinavian goddess of beauty and youth — a name suggested by the beautiful colors of its compounds in solution. Just before this, F. Wöhler had reexamined the vanadinite ore from Zimapán and found that the new element surmised and abandoned by Del Río was identical with the vanadium of Sefstrom. Wöhler failed to report his findings because of an illness due to poisoning by hydrogen fluoride vapor. In a charming letter to Wöhler, Berzelius wrote:

V
A=49

> In regard to the sample which I am sending with this, I want to tell the following anecdote: In the far north there lived in olden times the goddess Vanadis, beautiful and lovable. One day some one knocked at her door. The goddess remained comfortably seated and thought: let the person knock again; but there was no more knocking, and the one who had knocked went down the steps. The goddess was curious to see who it might be that was so indifferent to being admitted, sprang to the window, and looked at the one who was going away. Alas! she said to herself, that's that fellow Wöhler. Well, he surely deserved it; if he had been a little more concerned about it, he would have been admitted. The fellow does not look up to the window once in passing by....
>
> After a few days some one knocked again at the door; but this time the knocking continued. The goddess finally came herself and opened the door. Sefstrom entered, and from this union vanadium was born.

V
A=49

REF. I. Fodor, I. Demeter, L. Keszthelyi, I. Szentpetery, Z. Szokefalvi-Nagy, J. Szucs, L. Varga and J. Zimanyi
Nucl. Phys. A116, 167 (1968)

ELEM. SYM.	A	Z
V	49	23

METHOD

REF. NO.	
68 Fo 1	egf

REACTION	RESULT	EXCITATION ENERGY	SOURCE		DETECTOR		ANGLE
			TYPE	RANGE	TYPE	RANGE	
P,G	LFT	8	D	1	SCD-D	0-8	DST

ANALOG STATE

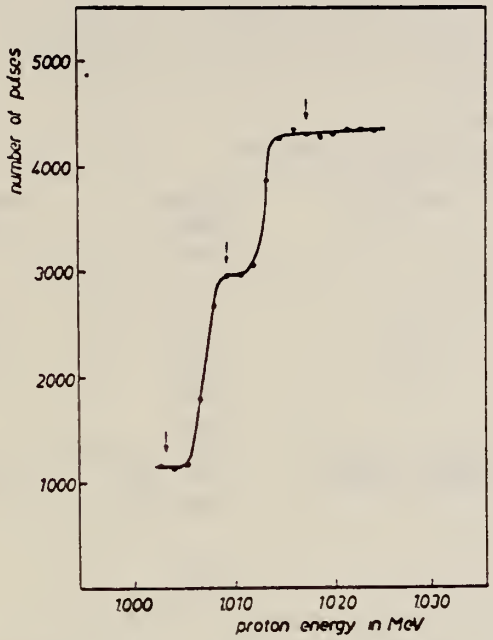

Fig. 5. Excitation function of the 1.007 and 1.013 MeV resonances in the $^{49}Ti(p,\gamma)^{50}V$ reaction on the "quasi-thick" target.

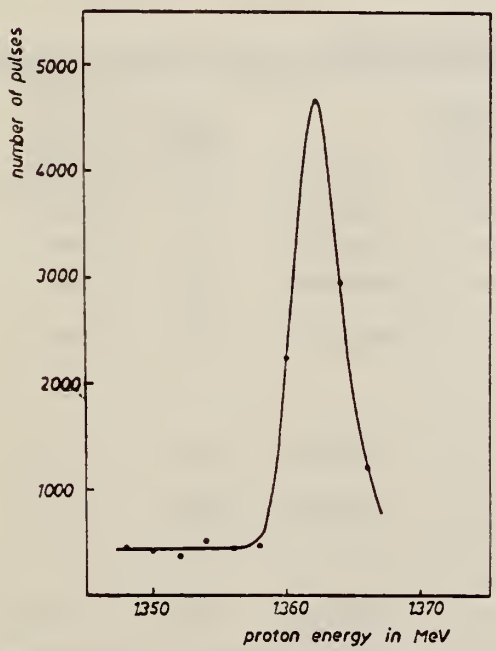

Fig. 6. Excitation function of the 1.362 MeV resonance in the $^{49}Ti(p,\gamma)^{50}V$ reaction.

[over]

TABLE 2

γ-transitions, relative intensities and absolute widths in ^{49}V

Energy of resonant level(MeV)	Spin and parity	Transitions into states		Relative intensity	Multipolarity	Measured widths (eV)	Weisskopf estimate (eV)
		E(keV)	J, π				
7.735	$\frac{3}{2}^-$	0	$\frac{7}{2}^-$	<6			
		90.6	$\frac{5}{2}^-$	113	M1	0.15	9.56
		153	$\frac{3}{2}^-$	100	M1	0.13	9.25
		1633		30		0.04	
		1648		20		0.03	
7.741	$\frac{3}{2}^-$	0	$\frac{7}{2}^-$	<9	0.998M1+0.002E2	0.22 M1	9.6
		90.6	$\frac{5}{2}^-$	100		0.0004 E2	0.23
		153	$\frac{3}{2}^-$	<9			
		1633		30		0.07	
		1648		7		0.02	
8.088	$\frac{1}{2}^-$	0	$\frac{7}{2}^-$	<5			
		90.6	$\frac{5}{2}^-$	<7			
		153	$\frac{3}{2}^-$	100	M1	1.7	10.6
		1633		3			
		1648		4			

REF. J.C. Legg, D.G. Megli, D.R. Abraham, L.D. Ellsworth, and S. Hechtl
Phys. Rev. 186, 1138 (1969)

ELEM. SYM.	A	Z
V	49	23

METHOD

REF. NO. 69 Le 1 egf

REACTION	RESULT	EXCITATION ENERGY	SOURCE		DETECTOR		ANGLE
			TYPE	RANGE	TYPE	RANGE	
P,G	LFT	7-8	D	1-2	SCD-D		DST

4 LEVELS

TABLE I (*Continued*)

Proton resonance energy (keV)	Primary γ-ray energy (keV)	Final-state energy (keV)	A_2/A_0	Radiative width (eV)	Radiative width in Weisskopf units[a]	J_i^π/I	J_f^π/I	Mixing ratio δ
1387	8022	89	−0.27±0.17	0.009	0.0005	$\frac{1}{2}^-$	$\frac{3}{2}^-$	−0.11±0.15
	7962	152	0.00±0.05	0.05	0.025	$\frac{1}{2}^-$	$\frac{3}{2}^-$	0.26±0.03
	7366	747	0.375±0.079	0.03	0.0004	$\frac{1}{2}^-$	$\frac{1}{2}^+$	0.01±0.05 −4.07±0.80
	6977	1138	0.028±0.085	0.03	0.002	$\frac{1}{2}^-$	$\frac{1}{2}^-$	0.11±0.08 3.0±0.7
					0.2	$\frac{1}{2}^-$	$\frac{3}{2}^-$	−0.12±0.08 1.9±0.4
	6472	1639	−0.15±0.11	0.02	0.00008	$\frac{1}{2}^-$	$\frac{1}{2}^+$	−0.19±0.06 2.9±0.5
	6454	1658	−0.04±0.12	0.02	0.004	$\frac{1}{2}^-$	$\frac{3}{2}^-$	−0.25±0.06 3.5±0.6
					0.020	$\frac{1}{2}^-$	$\frac{3}{2}^-$	0.28±0.09 41±31
	6125	1990	−0.17±0.06	0.05	0.0002	$\frac{1}{2}^-$	$\frac{1}{2}^+$	−0.18±0.03 2.9±0.3

[a] V. F. Weisskopf, Phys. Rev. 83, 1073 (1951).

[over]

TABLE I. γ decay of resonances.

Proton resonance energy (keV)	Primary γ-ray energy (keV)	Final-state energy (keV)	A_2/A_0	Radiative width (eV)	Radiative width in Weisskopf units[a]	J_i^π	J_f^π	Mixing ratio δ
1007	7653	89	0.043±0.035	0.11	0.007	$\frac{3}{2}^-$	$\frac{1}{2}^-$	0.13±0.03 2.84±0.29
	7591	152	0.469±0.028	0.15	0.08	$\frac{3}{2}^-$	$\frac{1}{2}^-$	−0.05±0.02 −3.25±0.23
	6101	1639	−0.426±0.064	0.05	0.0002	$\frac{3}{2}^-$	$\frac{1}{2}^+$	−0.038±0.035 1.91±0.17
	6086	1658	0.04±0.06	0.05	0.01	$\frac{3}{2}^-$	$\frac{1}{2}^-$	−0.29±0.03 4.04±0.54
					0.05	$\frac{3}{2}^-$	$\frac{3}{2}^-$	0.23±0.04 −33.7±19.4
	5504	2237	−0.68±0.28	0.01		$\frac{3}{2}^-$	$\frac{1}{2}$	0.11±0.23 1.37±0.60
							$\frac{3}{2}$	No solution
							$\frac{5}{2}$	−0.28±0.33 −3.08±1.9
	5438	2303	0.403±0.103	0.03	0.01	$\frac{3}{2}^-$	$\frac{1}{2}^-$	−0.51±0.07 19.1±9.6
					0.05	$\frac{3}{2}^-$	$\frac{3}{2}^-$	0.00±0.07 −3.87±0.95
1013	7748	0	0.17±0.27	0.007	0.01	$\frac{3}{2}^-$	$\frac{1}{2}^-$	0.03±0.38 1.35±0.90
	7658	89	−0.030±0.20	0.17	0.01	$\frac{3}{2}^-$	$\frac{1}{2}^-$	0.058±0.019 3.61±0.28
	7597	152	0.58±0.23	0.009	0.005	$\frac{3}{2}^-$	$\frac{1}{2}^-$	−0.13±0.15 −2.51±0.95
	7002	747	0.4±0.4	0.005	0.0001	$\frac{3}{2}^-$	$\frac{1}{2}^+$	−0.07±0.27 −3.02±1.45
	6238	1510	−0.03±0.20	0.01		$\frac{3}{2}^-$	$\frac{1}{2}$	−0.25±0.11 3.5±1.0
							$\frac{3}{2}$	0.28±0.15 40±35
							$\frac{5}{2}$	0.06±0.18 3.6±1.6
	6110	1639	−0.469±0.043	0.06	0.0003	$\frac{3}{2}^-$	$\frac{1}{2}^+$	−0.02±0.03 1.80±0.10
	6093	1658	−0.089±0.093	0.02	0.004	$\frac{3}{2}^-$	$\frac{1}{2}^-$	−0.22±0.05 3.19±0.44
					0.02	$\frac{3}{2}^-$	$\frac{3}{2}^-$	0.32±0.07 16.4±8.3
	5445	2303	0.25±0.10	0.03	0.009	$\frac{3}{2}^-$	$\frac{1}{2}^-$	−0.41±0.06 7.1±2.0
					0.045	$\frac{3}{2}^-$	$\frac{3}{2}^-$	0.09±0.06 −6.2±1.8
1361	7935	152	−0.008±0.010	1.4	0.065	$\frac{3}{2}^-$	$\frac{1}{2}^-$	
	6451	1639	−0.08±0.06	0.17	0.0007	$\frac{3}{2}^-$	$\frac{1}{2}^+$	
	6432	1658	...	<0.02		$\frac{3}{2}^-$	$\frac{1}{2}^-, \frac{3}{2}^-$	

V
A=51

V
A=51

V
A=51

REF.

F. Heinrich, H. Wäffler, and M. Walter .
Helv. Phys. Acta 29, 3 (1956)

ELEM. SYM.	A	Z
V	51	23

METHOD

REF. NO.: 56 He 2 | EGF

REACTION	RESULT	EXCITATION ENERGY	SOURCE		DETECTOR		ANGLE
			TYPE	RANGE	TYPE	RANGE	
G,A	RLY	THR - 31	C	31	ACT-I		
G,2P	RLY	THR - 31	C	31	ACT-I		

Yield measured relative to (γ,n) yield in ^{63}Cu.

31 MeV bremsstrahlung yields

$$\frac{^{51}V(\gamma,a)}{^{63}Cu(\gamma,n)} = (7\pm2) \times 10^{-3}$$

$$\frac{^{51}V(\gamma,2p)}{^{51}V(\gamma,a)} = 1.9 \times 10^{-2}$$

Ref. P. Erdos, P. Scherrer, P. Stoll
Helva. Phys. Acta 30, 639 (1957)

Elem. Sym.	A	Z
V	51	23

Method: Betatron; α yield; radioacitivity; $Cu^{65}(\gamma,n)$ reaction

Ref. No.: 57 Er 1 | EGF

Reaction	E or ΔE	E_o	Γ	$\int \sigma dE$	Jπ	Notes
$V^{51}(\gamma,\alpha)$	Bremss. 32			5.5±2 MeV-mb		Based on yield measurement.

S.G. Chidley, L. Katz, S. Kowalski
Can. J. Phys. 36, 407 (1958)

ELEM. SYM.	A	Z
V	51	23

Betatron

REF. NO.	
58 Ch 2	NVB

REACTION	RESULT	EXCITATION ENERGY	SOURCE		DETECTOR		ANGLE
			TYPE	RANGE	TYPE	RANGE	
G,N	RLY	THR	C	THR	BF3-I		4PI

See 58 Ka 1 for cross sections

THRESHOLD

TABLE I

MEASURED PHOTONEUTRON THRESHOLDS

Reaction	Measured Q value, Mev.	Other Q values, Mev.	Method	Reference
$V^{51}(\gamma, n)V^{50}$	11.16±0.05			
		11.15 ±0.20	Threshold	Sher *et al.* (1951)
		11.24 ±0.23	Mass data	Wapstra (1955)
		11.05 ±0.12	Mass data	Duckworth (unpublished)

REF.

A. Halsteinslid, K. Nybo and R. B. Mollerud
Univ. Bergen Arb. Naturv. R. Nr. 15, 1 (1958)

ELEM. SYM.	A	Z
V	51	23

METHOD

[Page 1 of 2]

REF. NO.	
58 Ha 1	EGF

REACTION	RESULT	EXCITATION ENERGY	SOURCE		DETECTOR		ANGLE
			TYPE	RANGE	TYPE	RANGE	
G,XP	SPC	THR - 30	C	30	EMU-D	2 - 20	DST

$$I(\theta) = a + b \sin^2\theta \, (1 + p \cos^2\theta)^2$$

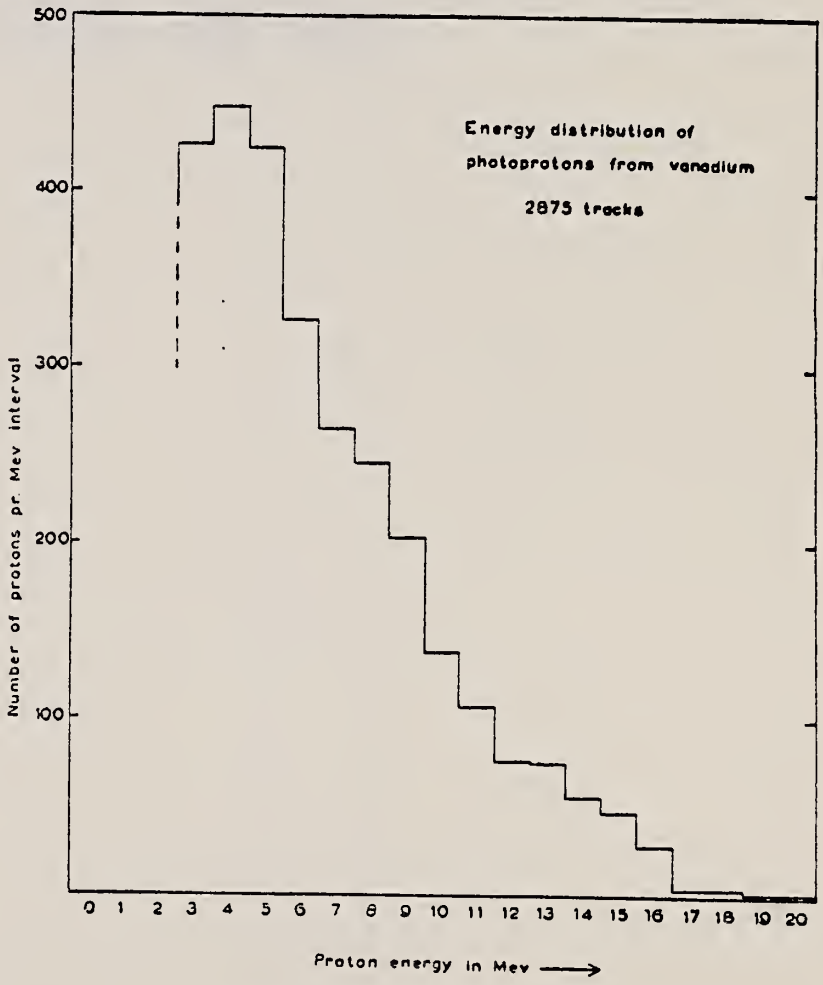

Fig. 3. Energy distribution of photoprotons per Mev-interval, corrected for energy loss in the target.

REACTION	RESULT	EXCITATION ENERGY	SOURCE		DETECTOR		ANGLE
			TYPE	RANGE	TYPE	RANGE	

Table

Proton energy E_p	b/a	p	$\sigma q/\sigma d$
$0 < E_p \leq 10$ Mev	0,5 ±0,1	0,6 ±0,2	0,07 ±0,03
10 Mev $< E_p$	1,5 ±1,3	0,25 ±0,2	$0{,}01 \pm^{0{,}03}_{0{,}01}$

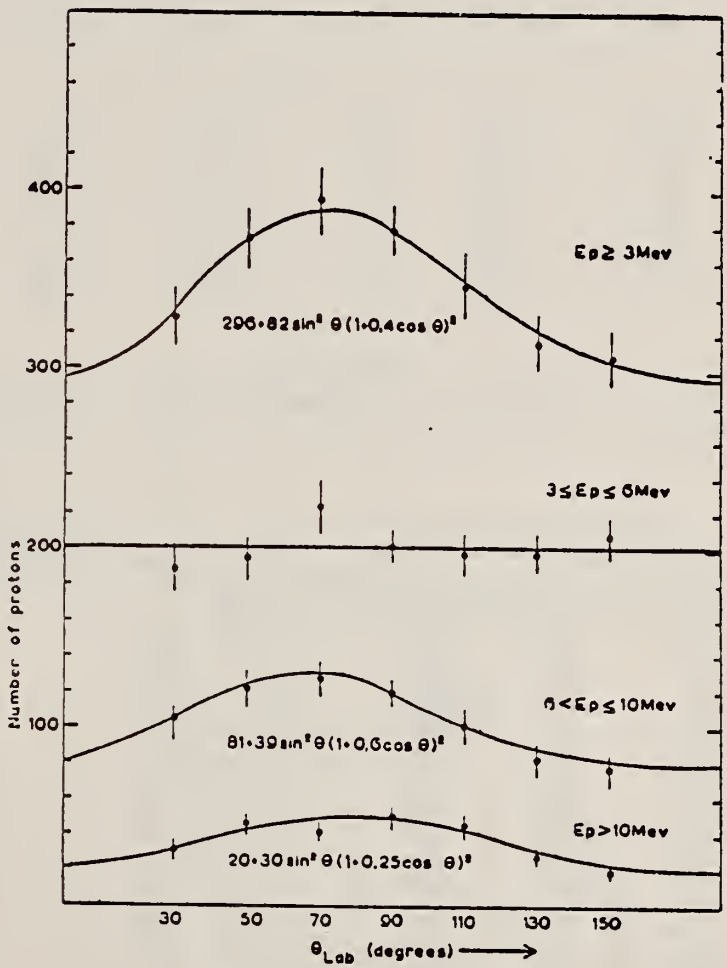

Fig. 4. Angular distribution of photoprotons of various energies, corrected for energy loss in the target.

REF.		ELEM. SYM.	A	Z
	L. Katz, G.B. Chidley Nuclear Reactions at Low and Medium Energies (Academy of Science, USSR: 1958) 371	V	51	23
METHOD	Betatron; neutron cross section; BF_3 counters; ion chamber monitor	REF. NO. 58 Ka 1		NVB

REACTION	RESULT	EXCITATION ENERGY	SOURCE		DETECTOR		ANGLE
			TYPE	RANGE	TYPE	RANGE	
G,XN	ABX	12-22	C	12-22	BF3-I		4PI

Таблица 2

Пороги испускания фотонейтронов

Изотоп	B_n, *Мэв*	B_{2n}, *Мэв*	Изотоп	B_n, *Мэв*	B_{2n}, *Мэв*
V^{51}	11,16	20,5	L^{139}	8,81	16,1
Mn^{55}	10,14	19,2	Pr^{141}	9,46	17,6
Co^{59}	10,44	18,6	Tb^{159}	8,16	14,8
As^{75}	10,24	18,1	Ho^{165}	8,10	14,6
Y^{89}	11,82	20,7	Tm^{169}	8,00	14,7
Nb^{93}	8,86	17,1	Lu^{175}	7,77	14,2
Rh^{103}	9,46	16,8	Ta^{181}	7,66	13,8
J^{127}	9,14	16,2	Au^{197}	7,96	13,3
Cs^{133}	9,11	16,5	Bi^{209}	7,43	14,5

THRESHOLDS

не приведены, поскольку они превышают 22 *Мэв* во всех случаях, кроме золота, для которого B_{2n}=21 *Мэв*. Свойства сечений $\sigma_C(\gamma)$ сведены в табл. 3.

Таблица 1

Изотоп	$E_{макс}$, *Мэв*	$\sigma_n(E_\gamma)$, барн	Γ, *Мэв*	Γ^{12}, *Мэв·барн*	Y(22), 10^8 нейтрон/100 р·*моль*
V^{51}	18,4	0,062	5,2	0,33	1,62
Mn^{55}	20,2	0,060	7,0	0,39	2,01
Co^{59}	18,3	0,068	6,3	0,44	2,30
As^{75}	16,4	0,090	9,5	0,74	4,25
Y^{89}	17,1	0,172	5,2	0,93	5,33
Nb^{93}	18,0	0,156	7,5	1,17	6,80
Rh^{103}	17,5	0,160	9,4	1,40	8,28
J^{127}	15,2	0,273	6,8	1,76	11,9
Cs^{133}	16,5	0,238	7,7	1,59	10,7
La^{139}	15,5	0,325	3,8	1,55	11,2
Pr^{141}	15,0	0,320	4,9	1,93	13,1
Tb^{159}	15,6	0,274	9,8	2,49	18,1
Ho^{165}	13,5	0,305	8,9	2,52	18,7
Tm^{169}	16,4	0,250	8,4	1,91	14,9
Lu^{175}	16,0	0,225	8,4	1,90	23,0
Ta^{181}	14,5	0,380	8,5	3,15	22,0
Au^{197}	13,8	0,475	4,7	3,04	22,6
Bi^{209}	13,2	0,455	5,9	2,89	23,2

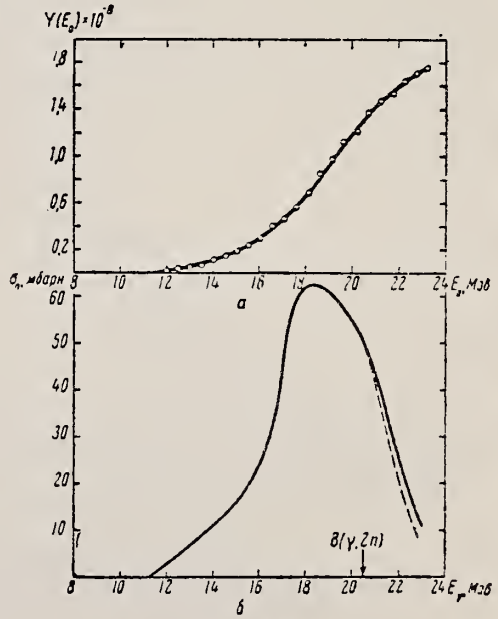

Рис. 1.

а — Выход фотонейтронов для V;
б — $\sigma_n(E_\gamma)$ и $\sigma_C(\gamma)$ для V

Ref. M.E. Toms, J. McElhinney
Phys. Rev. 111, 561 (1958)

Elem. Sym.	A	Z
V	51	23

Method: Betatron; alpha yield; nuclear emulsion

Ref. No.: 58 To 2 | NVB

Reaction	E or ΔE	E_o	Γ	$\int \sigma dE$	Jπ	Notes
V(γ,α)	Bremss. 22					Yield = 0.4×10^{-4} alpha/mole/roentgen

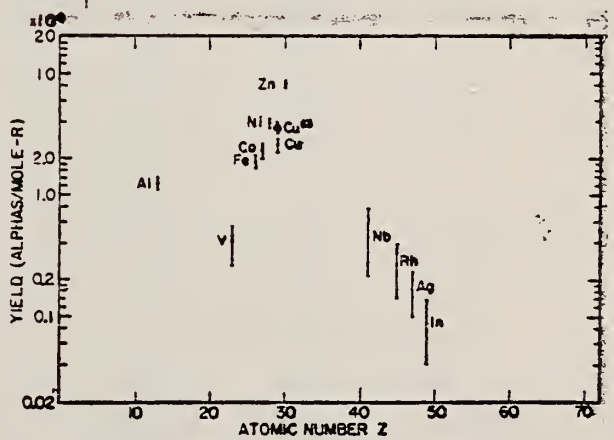

FIG. 8. Photo-alpha yields plotted against atomic numbers for the exposures of the survey.

Ref. P. Dyal, J.P. Hummel
Phys. Rev. 115, 1264 (1959)

Elem. Sym.	A	Z
V	51	23

Method
Betatron; activation, Victoreen r-thimble monitor

Ref. No. 59 Dy 1 | JHH

Reaction	E or ΔE	E_0	Γ	$\int \sigma dE$	Jπ	Notes
$V^{51}(\gamma,\alpha)$	Bremss. 10.5-25	23		$\int_0^{24.5} = 4.3\pm0.4$ MeV-mb		σ_{max}(E = 23 MeV) = 0.81 mb.

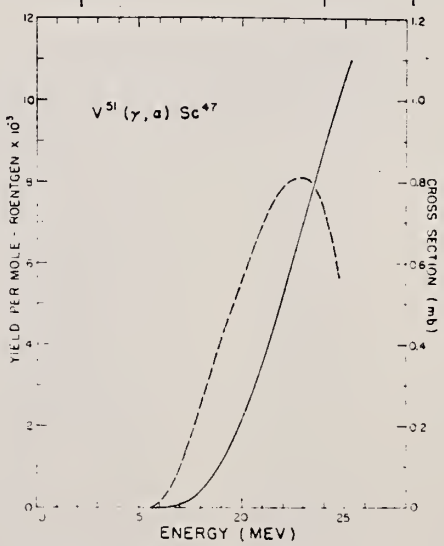

FIG. 1. Solid line—yield curve for the $V^{51}(\gamma,\alpha)Sc^{47}$ reaction, use scale on left; abscissa is the betatron operating energy. Dashed line—cross sections for the $V^{51}(\gamma,\alpha)Sc^{47}$ reaction, use scale on right; abscissa is the gamma-ray energy.

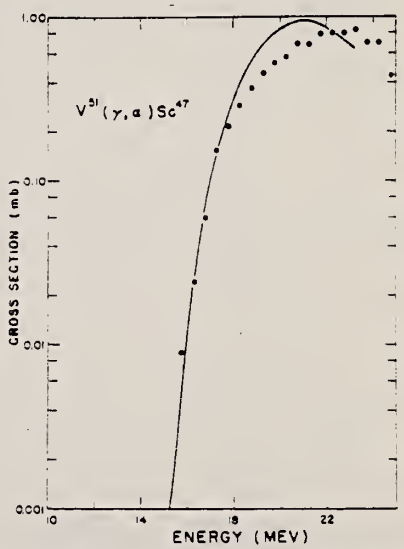

FIG. 2. Comparison of observed and theoretical cross sections for the $V^{51}(\gamma,\alpha)Sc^{47}$ reaction. The solid line represents the theoretical excitation function, and the points are the experimental cross sections derived from the yield curve by the photon difference method.

K. N. Geller, J. Halpern, and E. G. Muirhead
Phys. Rev. 118, 1302-12 (1960)

ELEM. SYM.	A	
V	51	23

METHOD

Betatron; neutron threshold; ion chamber

REF. NO.	
60 Ge 3	NVB

REACTION	RESULT	EXCITATION ENERGY	SOURCE		DETECTOR		ANGLE
			TYPE	RANGE	TYPE	RANGE	
G,N	NØX	THR	C THR		BF3-I		4 PI

THRESHØLD

TABLE I. Summary and comparison of neutron separation energies inferred from present threshold measurements with values predicted from mass data and reaction energies. All energies are expressed in the center-of-mass system in Mev.

Reaction	No. runs	Present results	Other results	Method	Reference
$V^{51}(\gamma,n)V^{50}$	1	11.04 ±0.06	11.040±0.004	mass data	g
			11.16 ±0.05	threshold	f

f See reference 4.
g C. F. Giese and J. L. Benson, Phys. Rev. 110, 712 (1958).

Ref. K. Reibel, A.K. [illegible]
Phys. Rev. 118, 701 (1960)

Elem. Sym.	A	Z
V	51	23

Method: γ's from $F^{19}(p,\alpha\gamma)$ reaction; protons from VandeGraaff; NaI.

Ref. No.: 60 Re 1 JHH

Reaction	E or ΔE	E_o	Γ	$\int \sigma dE$	Jπ	Notes
(γ,γ)	$E_\gamma \sim$ 7MeV					$\langle\sigma\rangle$ (E_p=2.05MeV) = 0.65 ± .10 mb

R.G. Baker, K.G. McNeill
Can. J. Phys. 39, 1158 (1961)

V	51	23

METHOD: Betatron; fast neutron yield, angular distribution; Si threshold detector; ion chamber

REF. NO.: 61 Ba 2 | NVB

REACTION	RESULT	EXCITATION ENERGY	SOURCE		DETECTOR		ANGLE
			TYPE	RANGE	TYPE	RANGE	
G,XN	ABY	THR-22	C	22	THR-I	5-+	DST

In Table 4:

$\bar{\sigma}$ = average cross section of detector weighted with neutron spectrum

$\bar{\Phi}$ = neutrons/100 roentgen/mole

$$W(\theta) = a_o \sum_{n=1}^{\infty} [1 + A_n P_n (\cos \theta)]$$

TABLE IV

I Element	II a_0	III a_1	IV a_2	V $(\bar{\sigma}\Phi)\times 10^{24}$	VI Φ_{total} (22 Mev)$\times 10^{5}$	VII Φ_{fast}/Φ_{total}
Vanadium	245(1±0.06)	0.01±0.08	−0.00±0.10	6.05	0.21	0.12
Chromium	164(1±0.03)	0.04±0.04	−0.05±0.05	4.05	0.17	0.10
Manganese	308(1±0.02)	0.07±0.03	−0.09±0.04	7.61	0.25	0.12
Iron	200(1±0.03)	0.05±0.04	−0.17±0.05	4.94	0.18	0.11
Cobalt	390(1±0.02)	0.08±0.03	−0.22±0.04	9.63	0.26	0.15
Nickel	145(1±0.05)	0.07±0.07	−0.23±0.09	3.58	0.12	0.12
Copper	347(1±0.02)	0.05±0.03	−0.29±0.04	8.57	0.30	0.12
Arsenic	482(1±0.03)	0.11±0.04	−0.24±0.05	11.91	0.33	0.15
Rubidium	638(1±0.05)	0.13±0.06	−0.14±0.08	15.76		
Strontium	409(1±0.05)	0.10±0.06	−0.17±0.08	10.10		
Yttrium	290(1±0.10)	0.08±0.12	−0.12±0.15	7.16		
Silver	590(1±0.04)	0.10±0.06	−0.22±0.08	14.57	0.87	0.07
Cadmium	905(1±0.02)	0.02±0.02	−0.26±0.03	22.35		
Iodine	1133(1±0.03)	0.04±0.04	−0.29±0.05	27.99	1.42	0.08
Barium	1048(1±0.04)	0.10±0.06	−0.38±0.08	25.89		
Lanthanum	1595(1±0.02)	0.02±0.03	−0.42±0.04	39.40	1.04	0.15
Cerium	1316(1±0.05)	0.05±0.06	−0.39±0.08	32.50		
Dysprosium	1652(1±0.08)	0.04±0.10	−0.34±0.13	40.80		
Tantalum	1558(1±0.02)	0.04±0.03	−0.22±0.04	38.48	2.50	0.06
Tungsten	1365(1±0.02)	−0.07±0.03	−0.24±0.04	33.71		
Mercury	1345(1±0.02)	0.04±0.03	−0.31±0.04	33.22		
Lead	2274(1±0.01)	0.02±0.02	−0.42±0.03	56.17	2.72	0.08
Bismuth	2162(1±0.02)	0.05±0.03	−0.45±0.04	53.40	3.36	0.06
Thorium	3031(1±0.04)	0.06±0.05	−0.32±0.07	74.87		
Uranium	4630(1±0.02)	0.05±0.03	−0.17±0.04	114.36		

*$(\bar{\sigma}\Phi) = 2.47\times 10^{7}\, a_0$ millibarn-neutron. Errors are standard errors due to counting statistics only.

J.H. Carver
Proc. Phys. Soc. 77, 417 (1961)

V	51	23

METHOD: Synchrotron; alpha cross section; Radioactivity

REF. NO.: 61 Ca 2 | NVB

REACTION	RESULT	EXCITATION ENERGY	SOURCE TYPE	SOURCE RANGE	DETECTOR TYPE	DETECTOR RANGE	ANGLE
G,A	ABX	THR-32	C	THR-32	ACT- I		4PI

742

σ_{peak} = 0.95 mb

E_{peak} = 22 MeV

$\int_0^{32} \sigma dE$ = 12±2 MeV-mb

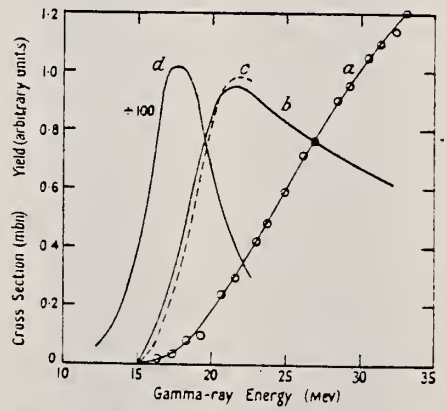

Fig. 3. *a*, activation curve for the $^{51}V(\gamma, \alpha)^{47}Sc$ reaction; *b*, the derived $^{51}V(\gamma, \alpha)$ cross section; *c*, the $^{51}V(\gamma, \alpha)$ cross section calculated by means of the statistical theory; *d*, the $^{51}V(\gamma, n)$ cross section of Goldemberg and Katz (1954) used in the calculation of curve *c*. (Note difference in cross section scale for curve *d*.)

Ref. S.C.Fultz,R.L.Bramblett, J.T.Caldwell, N.E.Hansen, C.P.Jupiter

Phys.Rev. 128, 2345 (1962)

Elem. Sym.	A	Z
V	51	23

Method

e^+ annihilation - ion chamber, BF_3

Ref. No. 62Ful

BG

Reaction	E or ΔE	E_o	Γ	$\int \sigma dE$	Jπ	Notes 433+
(γ,n)	8.5 - 28	18.25	6	$.451\pm.045)^{28}_{o}$		(γ,2n) threshold = 20.25±0.3 MeV
(γ,2n)	(443)	23.75		$.106\pm.011)^{28}_{0}$		It is estimated (γ,p) reaction would contribute 22% to formation cross section, i.e.
(γ,n)+(γ,2n) +(γ,np)				$.557\pm.056)^{28}_{0}$		$\int[\sigma(\gamma,n) + \sigma(\gamma,2n) + \sigma(\gamma,np) + \sigma(\gamma,p)]dE = .68$ MeVb

$$\sigma_{-2} = \int_0^{.28} \sigma(E)E^{-2}dE = 1.56 \text{ mb-MeV}^{-1}$$

$$Q_o = .66\pm0.09\text{b}$$

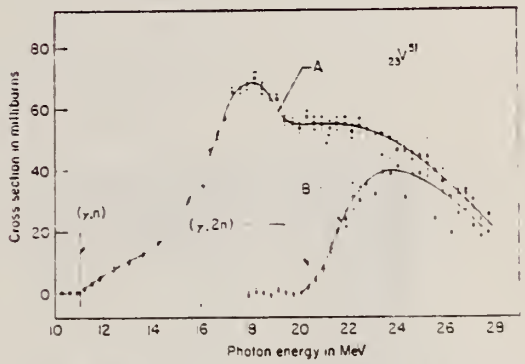

FIG. 4. Cross sections for V from neutron yield data. Curve A consists of $\sigma(\gamma,n)+2\sigma(\gamma,2n)+\sigma(\gamma,np)+3\sigma(\gamma,3n)$ and was obtained from single-neutron counting data. Curve B consists of $2\sigma(\gamma,2n)+6\sigma(\gamma,3n)$ and was obtained from double-neutron counting data.

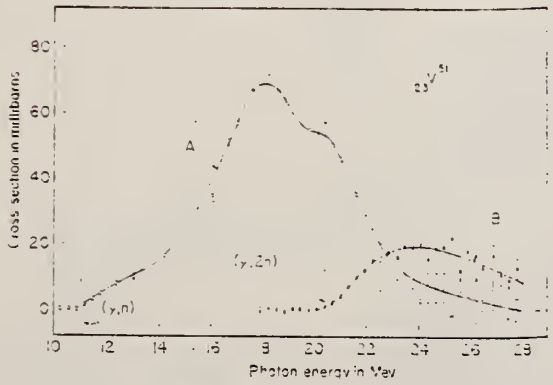

FIG. 5. Partial cross-section curves for V. Curve A consists of $\sigma(\gamma,n)+\sigma(\gamma,np)$. Curve B consists of $\sigma(\gamma,2n)+3\sigma(\gamma,3n)$.

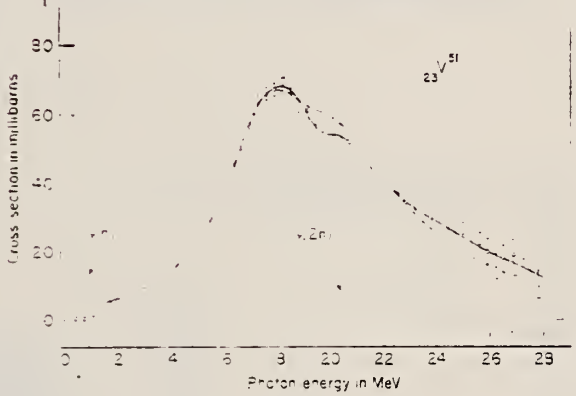

FIG. 6. The formation cross section $\sigma(\gamma,n)+\sigma(\gamma,2n)+\sigma(\gamma,np)$ for the compound nucleus V^{51}. The solid curve represents an average line through the data points. The dashed curve is the sum of two Lorentz lines with parameters given in Table I.

TABLE I. Lorentz line and nuclear shape parameters for Co and V.

Element	σ_1 (mb)	Γ_1 (MeV)	E_1 (MeV)	σ_2 (mb)	Γ_2 (MeV)	E_2 (MeV)	Q_o (b)	a (10^{-24} cm)	δ (10^{-24} cm)	ϵ
Co^{59}	40	3.75	16.5	43.4	7.0	19.25	0.94	5.33	4.68	0.353
V^{51}	41	3.60	17.5	46	6.5	20.25	0.66	4.40	5.15	0.336

TABLE II. Integrated cross sections and nuclear level density parameters. a_{np} includes estimated contributions for (γ,p) reactions.

Element	σ_{-1} (mb/MeV)	$0.00225A^{4/3}$ mb/MeV	a MeV^{-1}	$\int_0^{B_n} \sigma dE$ (MeV-b)	$\int_0^{B_n} \sigma_{np} dE + \Pi'$ (MeV-b)	$0.06\pi^2 Z/A$ (MeV-b)
Co^{59}	1.42	2.014	5.49	0.336	0.67	0.879
V^{51}	1.56	1.964	6.18	0.337	0.84	0.758

FORM NBS-418
(8-1-63)
USCOMM-DC 18556-P63

U.S. DEPARTMENT OF COMMERCE
NATIONAL BUREAU OF STANDARDS

Ref. H.W.Kendall, I.Talmi

Phys.Rev. 128, 792 (1962)

Elem. Sym.	A	Z
V	51	23

Method

Stanford MKIII accelerator - counter telescope

Ref. No. 62Kel

B G

Reaction	E or ΔE	E_o	Γ	$\int \sigma dE$	Jπ	Notes
(e,e')	183,300 600	0.930 1.609,1.813 also see Fig. 1			see Fig. 1	1.609 and 1.813 MeV levels were not completely resolved in any of the runs. Levels calculated from pure shell model $f_{7/2}^3$ configuration and effective two-body forces taken from $f_{7/2}^3$ configurations agree well with measured low-lying energy levels. E2 transition rates between good shell-model $f_{7/2}^3$ states are strongly enhanced. B(E2) proportional to E2 transition rate. $_2$ are strength parameters. $_m$ = measured transition rates to ground states.

tions. It is possible that although we can calculate energies using shell-model wave functions by replacing the free nucleon interaction by effective interactions,

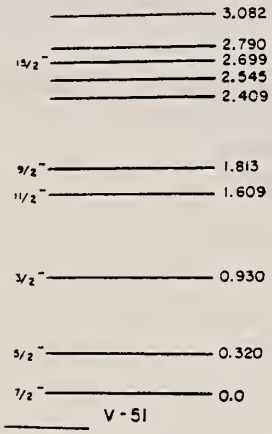

FIG. 1. The energy levels of V^{51}. (See reference 3.) The present experiment is concerned with the levels at 0.930, 1.609, and 1.813 MeV, all members of the $f_{7/2}^3$ proton configurations. The spins of other members of the configuration are indicated.

[3] See J. E. Schwager, Phys. Rev. 121, 569 (1961) for the most recent experimental results and for a number of references on shell-model calculations.

792

TABLE II. Experimental Values of δ_0, Γ_m, $B(E2)$, and G. The table gives the electron scattering results for transitions in V^{51}. The ϵ are the transition energies. The uncertainties in the δ_0 are standard deviations from counting statistics and from uncertainties in the radius parameter required in the predicted F^2. These uncertainties are reflected in Γ_m, the gamma-ray decay rates, in the reduced transition rates $B_m(E2)$ for the upward transitions, and in the values of G, the enhancements of the $B_m(E2)$. Additional uncertainties in these latter quantities are written last and are discussed in the text. The $B_m(E2)$ are given in terms of the single-particle values $A\times0.02\times10^{-48}$ cm^4. The G are found using the single-particle predictions from Table I.

ϵ (MeV)	j	δ_0	Γ_m (sec^{-1})	$B_m(E2)$	G
0.930	5/2	$7.2\pm1.1)\times10^{-4}$	$1.6\pm0.24\pm0.48)\times10^{11}$	$0.467\pm0.068\pm0.14$	$11.0\pm1.7\pm3.3$
1.609		$1.6\pm0.25)\times10^{-4}$		$1.03\pm0.16\pm0.3$	$4.84\pm0.76\pm1.4$
1.813[f]					
1.609	11/2	$8.0\pm3.0)\times10^{-4}$	$9.23\pm3.5\pm2.8)\times10^{10}$	$0.516\pm0.19\pm0.15$	$3.12\pm1.2\pm0.9$
1.813	9/2	$8.0\pm3.0)\times10^{-4}$	$2.00\pm0.84\pm0.67)\times10^{11}$	$0.516\pm0.19\pm0.15$	$10.1\pm3.7\pm3.3$

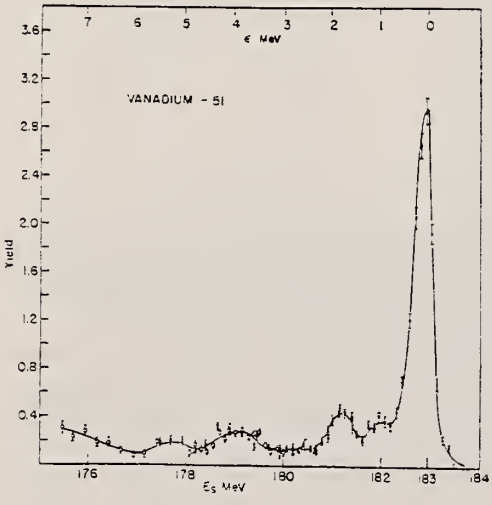

FIG. 2. In this and succeeding figures through Fig. 7 we show raw and corrected spectra of electrons scattered elastically and inelastically from V^{51} and from carbon and polystyrene. E_s is the scattered electron energy, and ϵ is the nuclear excitation energy after the scattering. Three overlapping runs with the 27-channel detector are indicated by different symbols. The smooth curve is a visual fit to the data. The present figure refers to scattering of 183-MeV electrons from V^{51} at a laboratory angle of 60°.

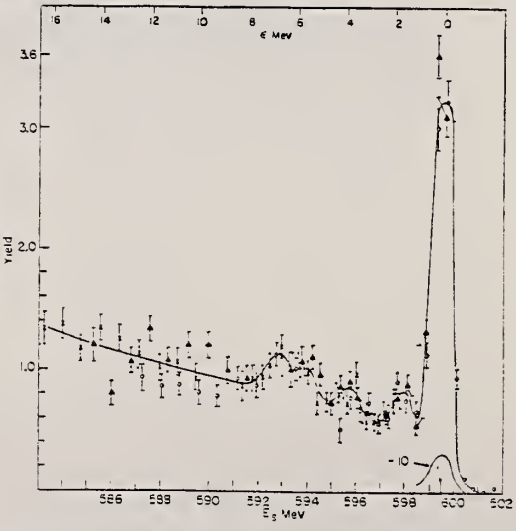

FIG. 4. Scattering of 600-MeV electrons from V^{51} at a laboratory angle of 31°. Cf. caption to Fig. 2.

Ref. M. Kregar, B. Povh
Phys. Letters 2, 103 (1962)

Elem. Sym.	A	Z
V	51	23

Method
Betatron; solid state detector

Ref. No. 62 Kr 1 JHH

Reaction	E or ΔE	E_o	Γ	$\int \sigma dE$	Jπ	Notes
$V^{51}(\gamma,\alpha)$	Bremss. 21 30			$\int_0^{21}$ = 2.4±0.72 MeV-mb $\int_0^{30}$ = 6.0±1.8 MeV-mb		Data were taken at $\theta_\alpha = 90^\circ$, and isotropy was assumed to get the $\int \sigma dE$ values given here.

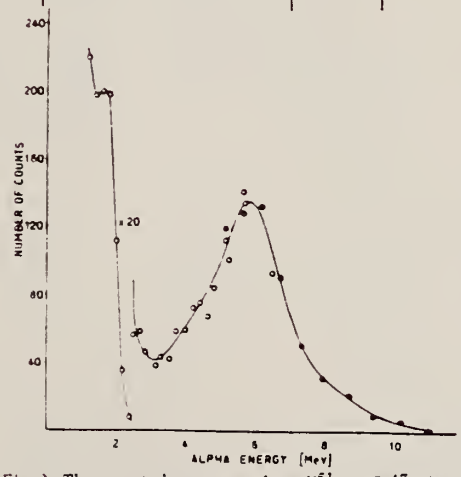

Fig. 2. The α-particle spectrum from $V^{51}(\gamma,\alpha)Sc^{47}$ taken at 90° and 21 MeV end point betatron energy. The lower part was measured with a 300 μm counter (open circles), while the higher part with a 5000 μm counter (black points). The stopping of alphas in the target shifts the peak for about 1 3 MeV. The pulses at the lower part of the spectrum are mostly due to the protons that are effectively cut off at 3.5 MeV α-energy.

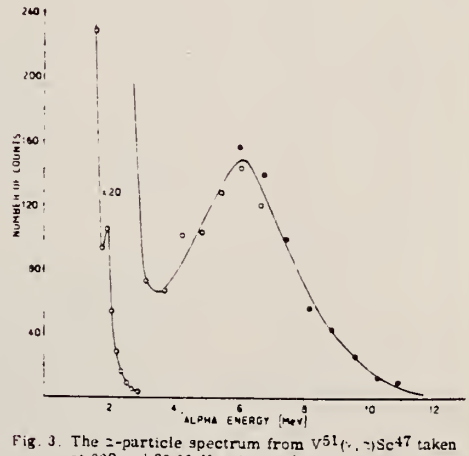

Fig. 3. The α-particle spectrum from $V^{51}(\gamma,\alpha)Sc^{47}$ taken at 90° and 30 MeV end point betatron energy. For explanation see fig. 2.

Ref. H.W.Kendall, I.Talmi

Ref. Kregar, B. Povh
Nuclear Phys. 43, 170 (1963)
Erratum in Nuclear Phys. 47, 528 (1963)

Elem. Sym.	A	Z
V	51	23

Method
Betatron; α yields; solid state detectors; NBS chamber monitor

Ref. No.: 63 Kr 1 | JHH

Reaction	E or ΔE	E_o	Γ	$\int \sigma dE$	$J\pi$	Notes
V (γ,α)	Bremss.					
	21					
	30					

TABLE I
Relative yields

Element	21 MeV		30 MeV	
	Number of alphas	Relative yield at 90	Number of alphas	Relative yield at 90
Ni	1209	40	536	13
Cu	1124	13	590	"
Fe	1108	4.5	653	1.7
V	372	1	363	1
Cd	136	0.7		

Ref. O.M.M. Mitchell, K.G. McNeill
Can. J. Phys. 41, 871 (1963)

Elem. Sym.	A	Z
V	51	23

Method: Betatron; proton yield; angular distribution; scintillator; ion chamber.

Ref. No.: 63 Mi 5 | NVB

Reaction	E or ΔE	E_o	Γ	$\int \sigma dE$	Jπ	Notes
V(γ,xp)	Bremss. 22					Angular distribution: $Y(\theta) = a + b \sin^2\theta (1 + p \cos\theta)^2$ where a = 100±10, b = 0±1 and b/a = 0.0±0.2. Yield (E_p > 8 MeV): (1.1±0.1) 10^5 protons/mole-r Yield (3.7 < E_p < 14): (6.6±0.7) 10^5

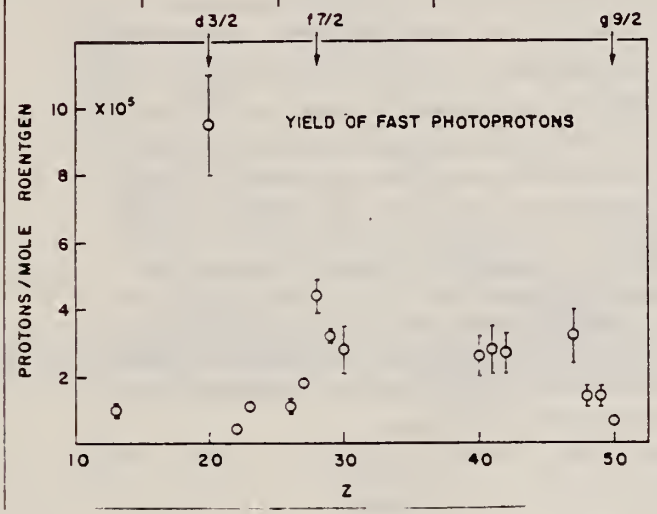

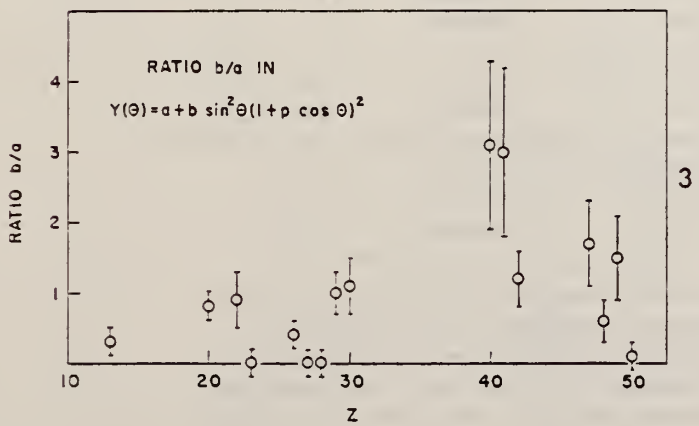

FIG. 2. The yields of fast photoprotons (E_p > 8 Mev) obtained from targets of various elements when irradiated with 22-Mev bremsstrahlung. The target thicknesses range from 551 to 572 mg/cm² (about 8 Mev for protons). The errors noted are statistical.

FIG. 3. The anisotropy coefficient b/a for fast photoprotons (E_p > 8 Mev) from 16 elements. The errors noted are statistical.

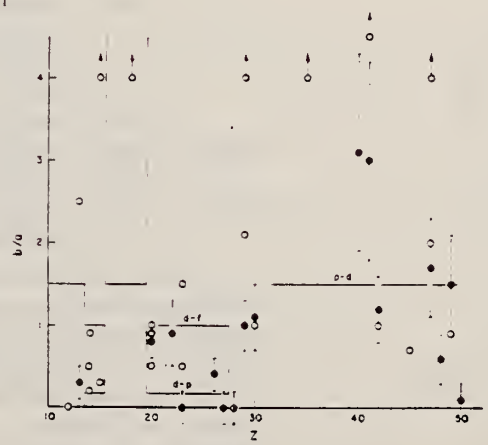

FIG. 4. The values of the fast photoproton anisotropy coefficient b/a obtained in the present experiment (●) and other workers (○) in the region of the periodic table 10 ≤ Z ≤ 50. Vertical lines indicate uncertainties. The references to the results of other workers are given in the text. The designations are explained in the text.

FORM NBS-418
(8-1-63)
USCOMM-DC 18556-P63

U.S. DEPARTMENT OF COMMERCE
NATIONAL BUREAU OF STANDARDS

Ref. H.W.Kendall, I.Talmi
H. Bernatowicz and H. A. Medicus
PICNS-67 Contributions, International Conference on Nuclear Structure, Tokyo, Japan 1967 (Institute for Nuclear Study, University of Tokyo, Tanashi-shi, Tokyo, Japan) 10.20, p.384

V | 51 | 23

METHOD

REF. NO. 67 Be 8 | EGF

REACTION	RESULT	EXCITATION ENERGY	SOURCE TYPE	SOURCE RANGE	DETECTOR TYPE	DETECTOR RANGE	ANGLE
G,2N	ABY	20-37	C	25-37	ACT-I		4PI
G,2P	ABY	20-37	C	25-37	ACT-I		4PI
G,A	ABY	10-37	C	25-37	ACT-I		4PI
G,NA	ABY	21-37	C	25-37	ACT-I		4PI
G,3N	ABY	30-37	C	37	ACT-I		4PI

Photonuclear Reactions with Emission of Several Nucleons

H. Bernatowicz and H. A. Medicus
Rensselaer Polytechnic Institute, Troy, N.Y., U.S.A.

Photonuclear reactions were induced on scandium and vanadium by bremsstrahlung at the Rensselaer Electron Linac. The activity of the residual nuclei was measured. The approximate energy dependence of the photonuclear reactions was either estimated by rough application of the photon difference method or calculated. This permitted determination of integrated cross sections by comparison with the activity of a beam monitor with known cross section.

Competing reactions, especially those involving emission of more than one particle, are a sensitive test of evaporation theory. Detailed calculations were therefore performed using various level density formulas. The Fermi gas formula, $\rho \sim e^{2\sqrt{aU}}/U^{5/4}$, (where $a = A/8$ Mev^{-1} and U is the excitation energy minus pairing energy), Weisskopf's formula, $\rho \sim e^{2\sqrt{aU}}$, and the constant temperature formula $\rho \sim e^{(E - E_0)/T}$ were tried. Corrections to the Fermi gas formula for shell effects have been made by Newton[1] and by Gilbert and Cameron[2]. Gilbert and Cameron also proposed a composite formula which joins the Fermi gas expression smoothly to a constant temperature formula below 8 Mev. The calculated integrated cross sections using these formulas were found to differ by as much as several orders of magnitude. The composite formula with Gilbert and Cameron's parameters gave the best overall agreement with our experimental data. The composite formula results with optical model inverse cross sections[3] and giant resonance data from Fultz, et al.,[4] are given in the table. Results using the constant temperature, Fermi gas, and Fermi gas formula with shell corrections by Newton have been included in one case. Integrated cross sections are in Mev-mb.

Target	End Point	Results	(γ,n)	(γ,2n)	(γ,3n)	(γ,2p)	(γ,α)	(γ,Ca)
^{45}Sc	48 MeV	Composite	310	78		2.0×10^{-1}		
		Experiment	430 ± 70	68 ± 12		3.0 ± 0.8		
^{51}V	37 MeV	Composite		140	1.4	6.3×10^{-1}	3.1	1.6
		Constant T		99	2.0	3.8	1.3	0.37
		Fermi Gas		97	1.3	3.5×10^{-2}	1.0	30
		Newton		101	2.1	3.2×10^{-3}	0.44	8.6
		Experiment		124 ± 35	2.5 ± 0.5	$(2.4 \pm 0.5) \times 10^{-1}$	7.1 ± 1.5	5.0 ± 2.
^{51}V	29 MeV	Composite		106		4.2 ± 10^{-2}	2.9	
		Experiment		115 ± 30		$(1.7 \pm 0.3) \times 10^{-2}$	6.8 ± 1.4	
^{51}V	25 MeV	Composite		60		3.0 ± 10^{-4}	2.4	
		Experiment		62 ± 12		$(2.6 \pm 0.3) \times 10^{-4}$	4.9 ± 1.2	

When the parameters of Newton were used in a composite level density formula agreement improved but remained significantly poorer than obtained with Gilbert and Cameron's parameters. The large disparity found in the ^{45}Sc(γ,2p) result would be eliminated by a 15 percent increase in the level density parameter of ^{44}Ca which has a closed proton shell. Our work indicates that this type of experiment can be of significant value in the study of nuclear level densities.

References: 1. Newton, T. D. Can. J. Phys. 34, 804 (1956).
2. Gilbert, A. and Cameron, A. G. W. Can. J. Phys. 43, 1449 (1965).
3. Maldner, H. and Lindner, A. Z. Physik 180, 362 (1964).
4. Fultz, S. C., Bramblett, R. L., Caldwell, J. T., Hansen, N. E., and Jupiter, C. P. Phys. Rev. 128, 2345 (1962).

REF. R. Garfagnini and G. Piragino
Nucl. Phys. A122, 49 (1968)

ELEM. SYM.	A	Z
V	51	23

METHOD

REF. NO. 68 Ga 1 egf

REACTION	RESULT	EXCITATION ENERGY	SOURCE		DETECTOR		ANGLE
			TYPE	RANGE	TYPE	RANGE	
$G,XN	SPC	THR-85	C	85	CCH	1-15	135

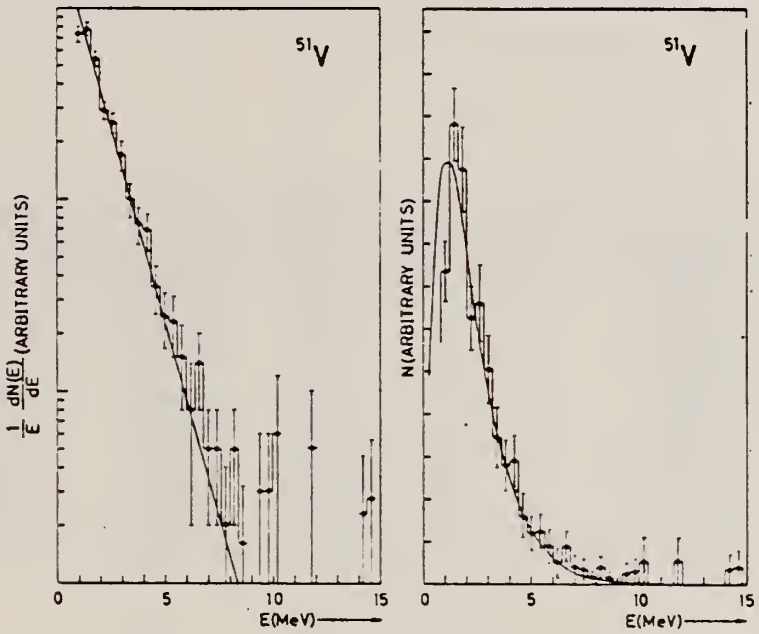

Fig. 2. Energy spectrum of photoneutrons from ^{51}V (at the right) and semi-logarithmic plot of the spectrum after dividing by the neutron energy (at the left). The full line is the typical evaporation spectrum normalized as described in the text.

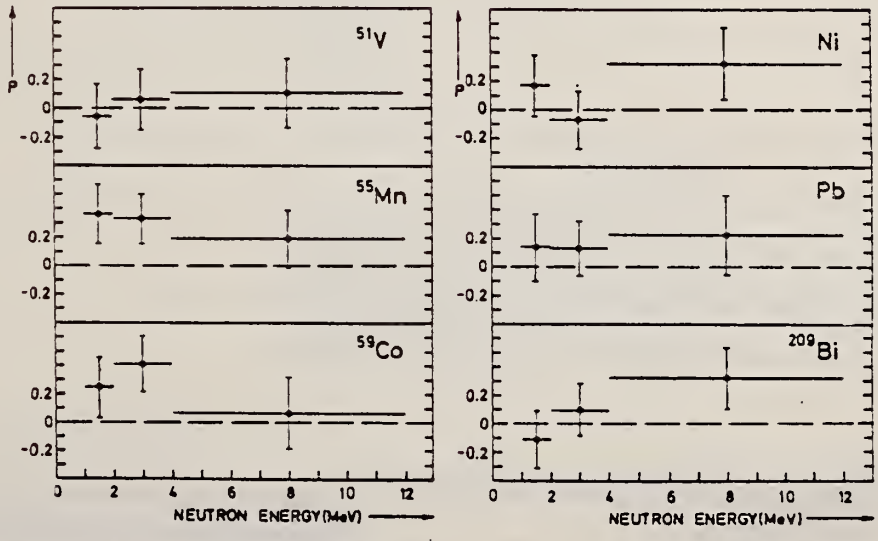

Fig. 7. Polarization of photoneutrons from ^{51}V, ^{55}Mn, ^{59}Co, natural Ni, natural Pb and ^{209}Bi.

FORM NBS-418
(REV. 7-1-64)
USCOMM-DC 28010-P64

REF.

J. W. Jury, J. S. Hewitt, and K. G. McNeill
Can. J. Phys. 46, 1823 (1968)

ELEM. SYM.	A	Z
V	51	23

METHOD

REF. NO.	
68 Ju 1	EGF

REACTION	RESULT	EXCITATION ENERGY	SOURCE		DETECTOR		ANGLE
			TYPE	RANGE	TYPE	RANGE	
G,N	NOX	THR-32	C	32	THR	5-	DST

$W(\theta) = a_o + a_1 P_1 + a_2 P_2$

TABLE I

Target element	Z	Energy	a_0*	a_1/a_0	a_2/a_0
Vanadium	23	32	640±50	0.11±0.10	−0.09±0.11
Chromium	24	22	365±39	0.02±0.08	0.00±0.10
Manganese	25	22	450±33	0.07±0.05	−0.11±0.06
Bromine	35	27	874±54	0.05±0.06	−0.15±0.08
Molybdenum	42	22	610±60	0.09±0.05	−0.35±0.06
Ruthenium	44	27	1100±25	0.12±0.02	−0.29±0.03
Rhodium	45	27	1270±47	0.06±0.03	−0.14±0.03
Palladium	46	27	1350±29	0.26±0.02	−0.12±0.02
Antimony	51	27	2140±62	0.04±0.08	−0.25±0.11
Lanthanum	57	27	1940±70	0.12±0.10	−0.52±0.14
Praseodymium	59	30	1800±58	0.20±0.08	−0.40±0.09
Platinum	78	27	2600±52	0.17±0.02	−0.15±0.03
Lead	82	22	2274±59	0.08±0.08	−0.46±0.09

*The yield per mole per 100 r was normalized to a yield of 2274 for the lead sample at the same energy.

REACTION	RESULT	EXCITATION ENERGY	SOURCE		DETECTOR		ANGLE
			TYPE	RANGE	TYPE	RANGE	
G,A	ABX	THR-300	C	20-300	ACT-I		4PI
G,A3N	ABX	THR-300	C	20-300	ACT-I		4PI

TABLE 1

Summary of integrated cross sections $\int_0^{E_{max}} \sigma dE$(MeV · mb) for the reactions studied

Reaction/E_{max}(MeV)	65	105	145	215	295
$^{16}O(\gamma, 2n)^{14}O$	0.42±0.02	0.57±0.04	0.56±0.05	0.63±0.09	1.29±0.16
$^{19}F(\gamma, 2pn)^{16}N$	3.7 ±0.2	5.0 ±0.3	6.1 ±0.5	8.4 ±1.0	13.6 ±1.5
$^{27}Al(\gamma, 2pn)^{24}Na$	8.3 ±0.3	13.3 ±0.7	17.1 ±1.2	24.1 ±2.3	31.2 ±3.3 [a]
$^{51}V(\gamma, \alpha)^{47}Sc$	12.3 ±1.7	20.2 ±3.5	32.5 ±2.6	68.4 ±3.8	112 ±14
$^{51}V(\gamma, \alpha 3n)^{44}Sc$	0.7 ±0.2	6.0 ±0.9	12.2 ±1.3	34.1 ±4.1	91 ±11

[a]) E_{max} = 275 MeV.

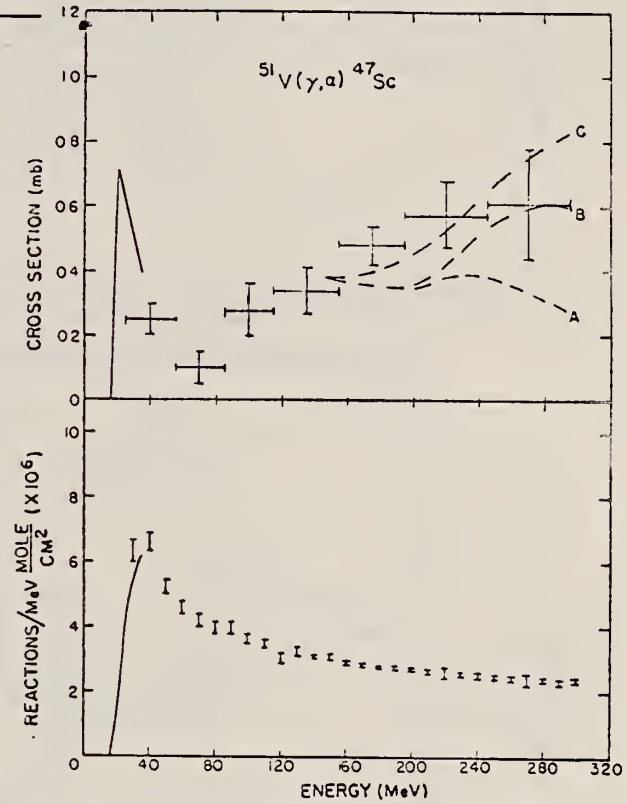

Fig. 4. Yields and cross sections for the $^{51}V(\gamma, \alpha)^{47}Sc$ reaction. The solid lines show the normalised low-energy yield and cross section results obtained by Carver [8]). The dashed line labelled A gives the expected cross sections for quasi-deuteron processes. Dashed line B gives the sum of the cross sections for quasi-deuteron and pion emission processes, and dashed line C gives the cross section sum for all three mechanisms considered (quasi-deuteron, pion emission and pion re-absorption).

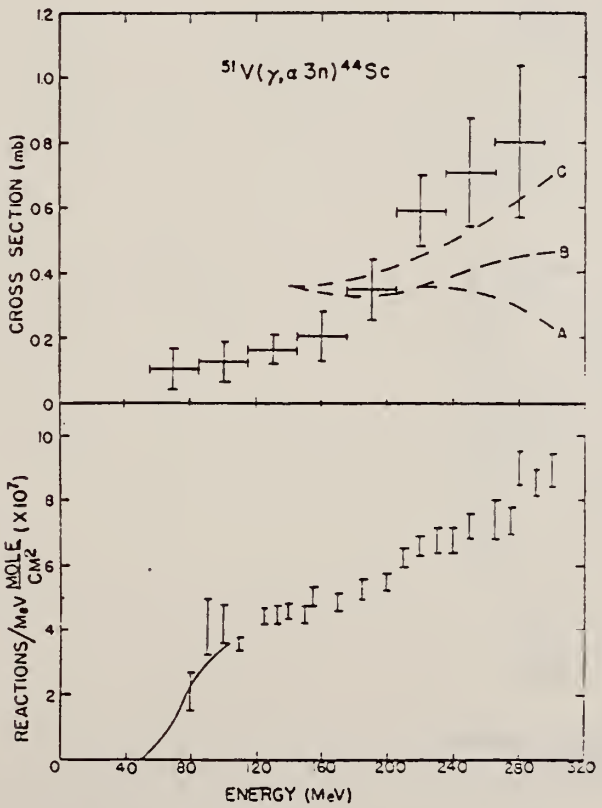

Fig. 5. Yields and cross sections for the $^{51}V(\gamma, \alpha 3n)^{44}Sc$ reaction. The solid line shows the assumed extrapolated yield curve behavior near the reaction threshold. The dashed lines have the same significance as in fig. 4.

REF.

G. Nydahl and B. Forkman
Nucl. Phys. B7, 97 (1968)

ELEM. SYM.	A	Z
V	51	23

METHOD

REF. NO.	
68 Ny 1	egf

REACTION	RESULT	EXCITATION ENERGY	SOURCE		DETECTOR		ANGLE
			TYPE	RANGE	TYPE	RANGE	
* G,PI+	ABX	140-700	C	140-700	ACT-I		4PI
** G,PI2N	ABX	140-700	C	140-700	ACT-I		4PI

* TI-51 ACT
** CR-49 ACT

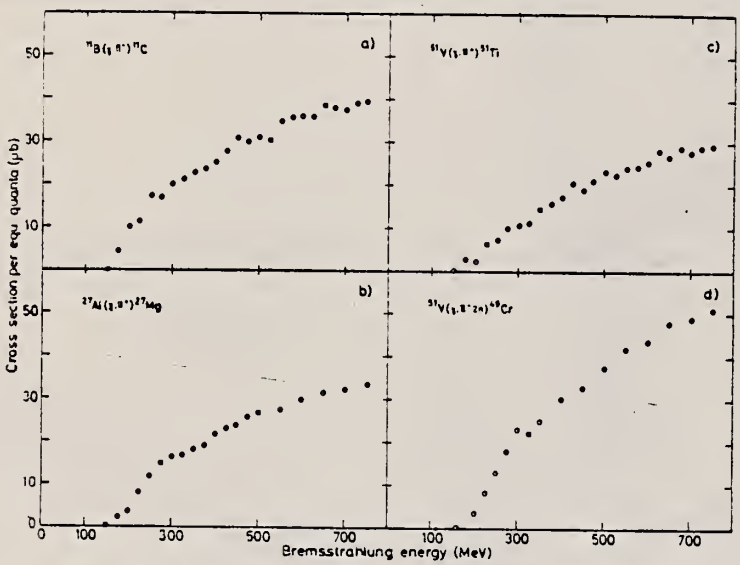

Fig. 3. Absolute yields for the measured reactions.

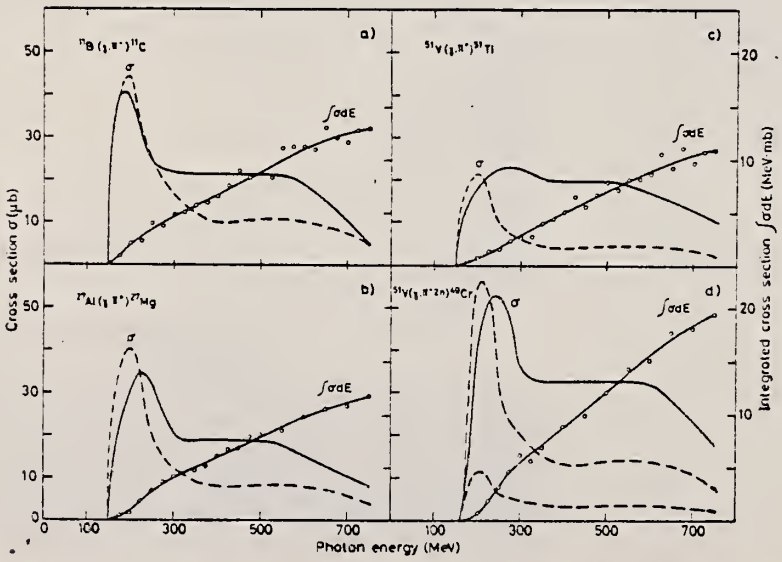

Fig. 4. Experimentally determined true and integrated cross sections. Theoretical calculations of the cross sections are marked with dashed lines.

REF. Y. Oka, T. Kato, K. Nomura, T. Saito and H. T. Tsai
Bull. Chem. Soc. Japan 41, 2660 (1968)

ELEM. SYM.	A	Z
V	51	23

METHOD

REF. NO. 68 Ok 1 egf

REACTION	RESULT	EXCITATION ENERGY	SOURCE		DETECTOR		ANGLE
			TYPE	RANGE	TYPE	RANGE	
G.A	ABY	THR-20	C	20	ACT-I		4PI

TABLE 1. SUMMARY OF DATA ON (γ, α) REACTIONS WITH 20 MeV BREMSSTRAHLUNG

Nuclide		E_{th}	Observed gamma-ray			Results obtained	
Parent (Natural abundance, %)	Product (Half-life)	$(-Q, MeV)$	Energy (MeV)	Branching ratio (%)	Type of multipole transition	$\mu Ci/mg^{a)}$	Yield $(mol^{-1} \cdot R^{-1})$
$^{51}V(99.75)$	$^{47}Sc(3.4\,d)$	10.27	0.160	100	$M1+E2$	1.99×10^{-3}	2.8×10^{3}
$^{63}Cu(30.9)$	$^{61}Co(99\,min)$	6.75	0.068	99	$M1+E2$	7.23×10^{-3}	9.7×10^{3}
$^{71}Ga(39.6)$	$^{67}Cu(61\,hr)$	5.15	0.184	41	$M1$	2.70×10^{-3}	9.6×10^{3}
$^{73}Ge(7.67)$	$^{69m}Zn(14\,hr)$	5.89	0.435	100	$M4$	1.11×10^{-2}	5.0×10^{3}
$^{81}Br(49.48)$	$^{77}As(39\,hr)$	6.46	0.246	2.81	$M1+E2$	1.97×10^{-4}	4.3×10^{2}
$^{109}Ag(48.65)$	$^{105}Rh(36\,hr)$	3.28	0.319+0.306	24.8	$M1+E2$	8.29×10^{-4}	3.7×10^{1}
$^{115}In(95.77)$	$^{111}Ag(7.6\,d)$	3.78	0.340	6	$M1+E2$	5.70×10^{-5}	4.3×10^{1}

a) The value corrected at the end of 1 hr irradiation (9.4×10^{6} R/min).

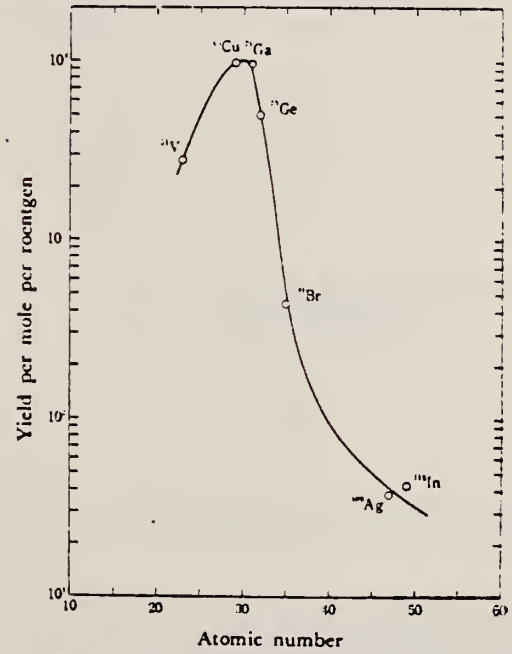

Fig. 1. The yield curve for (γ, α) reaction with 20 MeV bremsstrahlung.

K. Abe, N. Kawamura, H. Nihei, T. Osawa, N. Mutsuro
J. Phys. Soc. Japan 26, 577 (1969)

V	51	23

METHOD

REF. NO.	
69 Ab 2	egf

REACTION	RESULT	EXCITATION ENERGY	SOURCE		DETECTOR		ANGLE
			TYPE	RANGE	TYPE	RANGE	
G,XP	SPC	8-27	C	27	SCD-D	3-15	90
		(26.6)		(26.6)			

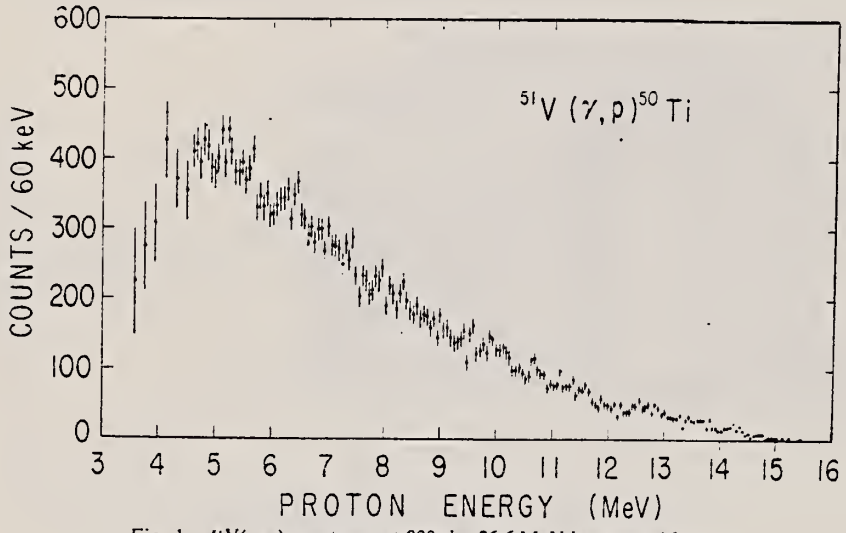

Fig. 1. $^{51}V(\gamma, p)$ spectrum at 90°, by 26.6 MeV bremsstrahlung.

REF.

R. Garfagnini, G. Piragino & A. Zanini
Atti Accad. Naz. Lincei, Rend.
Cl. Sci. Fis. Mat. Natur. 47, 33 (1969)

ELEM. SYM.	A	Z
V	51	23

METHOD

REF. NO.	
69 Ga 3	egf

REACTION	RESULT	EXCITATION ENERGY	SOURCE		DETECTOR		ANGLE
			TYPE	RANGE	TYPE	RANGE	
G,XN	SPC	12-85	C	85	CCH-D		135

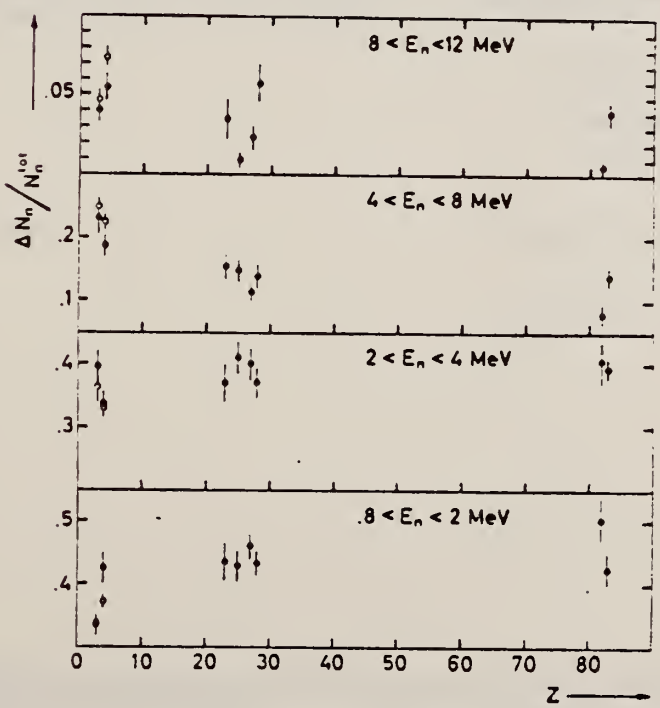

Fig. 1. – Percentage of the photoneutrons emitted at 135°, in the respective energy interval as a function of Z, by a γ-ray bremsstrahlung beam with $E_{\gamma\,max}$ = = 85 MeV. The open circles represent the values obtained at 60° for ^{7}Li and ^{9}Be.

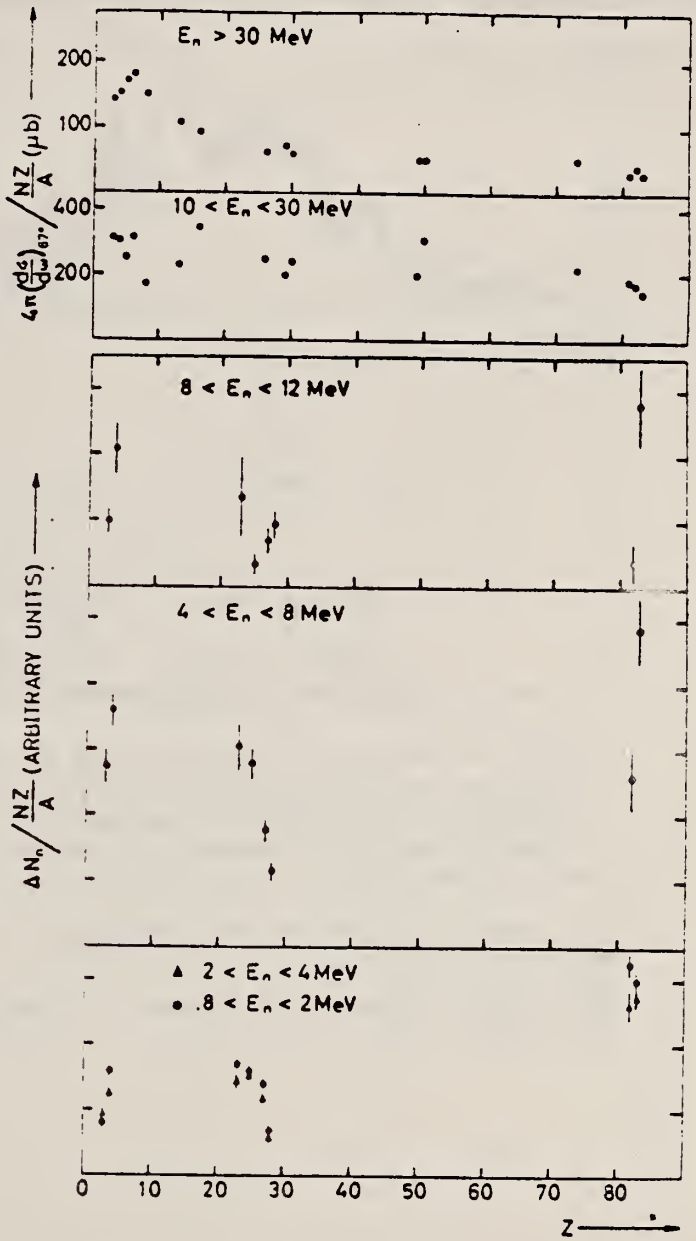

Fig. 2. – Number of photoneutrons emitted at 135°, normalized to the sum rule factor NZ/A, as a function of Z. In the upper part is reported the effective cross section divided by NZ/A for photoproduction of fast neutrons by 55-85 MeV bremsstrahlung photons as deduced by Kaushal *et al.* [1].

[1] N. N. Kaushal et al., Phys. Rev. 175, 1330 (1968).

IMERCE
IDAROS

Ref. H.W. Kendall, [illegible]

B.I. Goryachev, B.S. Ishkhanov, I.M. Kapitonov, I.M. Piskarev, V.G. Shevchenko & O.P. Shevchenko
Izv. Akad. Nauk. Fiz. 33, 1736 (1969)
Bull. Acad. Sci. USSR-Phys. 33, 1588 (1969)

V	51	23

METHOD

REF. NO. 69 Go 3 hmg

REACTION	RESULT	EXCITATION ENERGY	SOURCE TYPE	SOURCE RANGE	DETECTOR TYPE	DETECTOR RANGE	ANGLE
G,XN	ABX	11-30	C	11-30	BF3-I		4PI

448

448

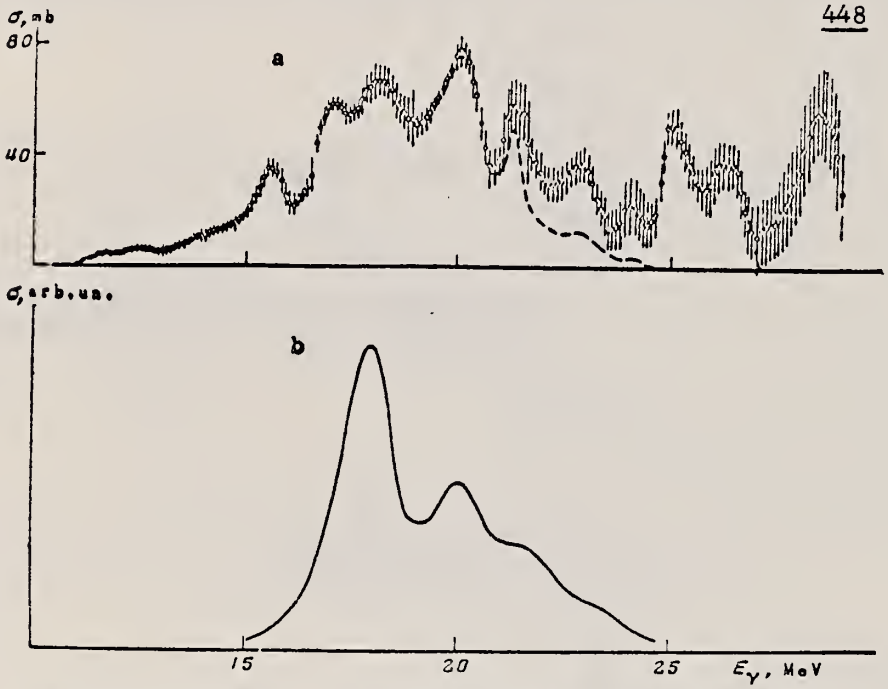

Fig.1. a - The $(\gamma,n) + (\gamma,2n)$ cross section for ^{51}V; the broken curve represents $\sigma(\gamma,n)$ near the $(\gamma,2n)$ threshold, as deduced from our results via the statistical theory[5]; b - theoretical absorption cross-section from Ref. 6.

[5] J.M. Blatt & V.F. Weisskopf, Theoretical Nuclear Physics, New York, 1952.

[6] M.G. Huber, M. Danos, H.J. Weber & W. Greiner, Phys. Rev. 155, 1073 (1967).

(over)

Characteristics of the Photoneutron Cross Sections (in MeV-mb)

Nucleus	Integral cross sections*				Center of gravity $\sigma(\gamma n)+\sigma(\gamma, 2n)$, MeV	Refs.	Dipole sum rule $60NZ/A$, MeV·mb
	$\sigma(\gamma n)+2\sigma(\gamma, 2n)$	$\sigma(\gamma n)+\sigma(\gamma, 2n)$	$\sigma(\gamma n)$	$\sigma(\gamma, 2n)$			
^{51}V	820 (30)	600 (30)	380 (30)	220 (30)	21,3	Our work	760
	670 (28)	560 28)	450 (28)	110 (28)		[9]	
	590 (24)					[10]	
	560 (25)					[11]	
^{52}Cr	950 (30)	740	530 (30)	210 (30)	20,4	Our work	775
	600 (24)					[10]	
^{59}Co	1030 (30)	740 (30)	450 (30)	290 (30)	20,2	Our work	880
	730 (28)	590 (28)	450 (28)	140 (28)		[9]	
	870 (29)					[12]	
	840 (25)					[13]	
	660 (28)					[14]	
	630 (25)					[11]	

*The upper integration limits are given in parentheses.

9. S.C.Fultz, R.L.Bramblett, I.T.Caldwell, N.E.Hansen & C.P.Jupiter, Phys. Rev. 128, 2345 (1962).

10. J.Goldemberg & L.Katz, Canadian J. Phys. 32, 49 (1954).

11. B.Nathans & J.Halpern, Phys. Rev. 93, 437 (1954).

12. E.B.Bazhanov, A.P.Komar & A.V.Kulikov, Zh. Eksperim. i teor. fiz. 46, 1497 (1964). (Trans. Soviet Physics - JETP.)

13. P.A.Flournoy, R.S.Tickle & W.D.Whitehead, Phys. Rev. 120, 1424 (1960).

14. G.Baciu, G.C.Bonazzola, B.Minetti, C.Molino, L.Pasqualini & G.Piragino, Nuclear Phys. 68, 178 (1965).

Ref. H.W. Kendall, J. Tolmie

Y. Oka, T. Kato and N. Sato Bull. Chem. Soc. Japan 42, 387 (1969)	V	51	23

METHOD	REF. NO.	
	69 Ok 1	hmg

REACTION	RESULT	EXCITATION ENERGY	SOURCE		DETECTOR		ANGLE
			TYPE	RANGE	TYPE	RANGE	
G,3N	RLY	THR-60	C	30-60	NAI-D		4PI
G,SC46	RLY	THR-60	C	30-60	NAI-D		4PI
G,SC47	RLY	THR-60	C	30-60	NAI-D		4PI
G,SC48	RLY	THR-60	C	30-60	NAI-D		4PI

YLD REL 12C(G,N)

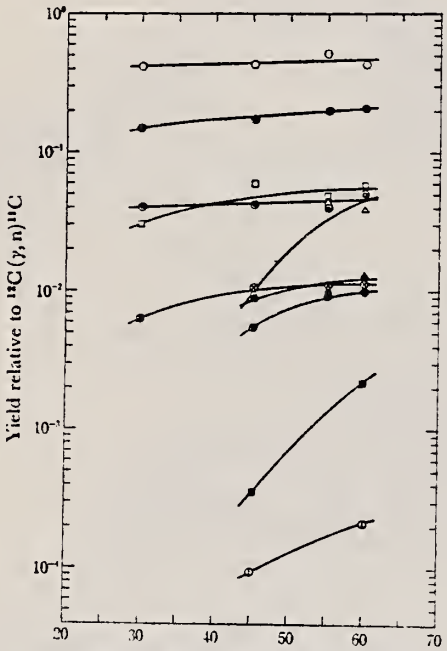

Fig. 6. The yield relative to $^{12}C(\gamma,n)^{11}C$ as a function of bremsstrahlung maximum energy.

○ : ^{45}Ti from titanium
● : ^{44}Sc from titanium
◎ : ^{46}Sc from titanium
⊙ : ^{47}Sc from titanium
⊗ : ^{48}Sc from titanium
△ : ^{48}V from vanadium
▲ : ^{46}Sc from vanadium
□ : ^{47}Sc from vanadium
■ : ^{48}Sc from vanadium
⊕ : ^{47}Ca from titanium

REF. H. Arenhovel, J. M. Maison
Nucl. Phys. A147, 305 (1970)

ELEM. SYM.	A	Z
V	51	23

METHOD

REF. NO. 70 Ar 1 egf

REACTION	RESULT	EXCITATION ENERGY	SOURCE		DETECTOR		ANGLE
			TYPE	RANGE	TYPE	RANGE	
G,G	ABX	12-30	C	32	NAI	12-30	DST

GETS G,G/ TO 2+

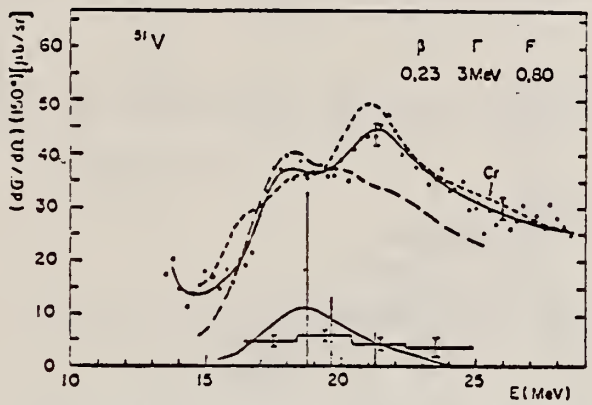

Fig. 5. Differential total scattering cross section at 150° for ^{51}V. See caption for fig. 4. To compare with ^{51}V the scattering cross section for Cr is shown.

Fig. 4. Differential total scattering cross section at 150° for natural Ti. The full curve through experimental points is only a guide for the eyes. The vertical bars represent the relative strength of dipole levels calculated by the D.C.M. with parameters of table 1. Theoretical elastic plus inelastic scattering is computed from these levels with a common width Γ (dashed curve). Experimental inelastic scattering (histogram) and theoretical inelastic scattering to the first 2^- (full curve) are shown in the lower part of the figure. Open circles give the cross section after background subtraction.

TABLE 4

Integrated inelastic scattering cross section

Nucleus	Limits of integration (in MeV)	Experimental [a] $\int \sigma_i(E)dE$ (MeV · μb)	Theoretical [a] 2^+	Theoretical [a] 2^- (MeV · μb)	Total
Ti(^{48}Ti)	16 −24	250 ± 50	425	109	534
^{51}V(^{52}Cr)	16.4−24.9	492 ± 50	509	116	579
Cr	16.4−23.4	431 ± 60	509	116	579
^{75}As(^{76}Se)	14.1−23.6	1254 ± 120	1373	414	1787
Se(^{80}Se)	14.1−24.6	1035 ± 100	1066	353	1419
^{89}Y					364
Cd(^{112}Cd)	13.6−23.3	3264 ± 240	1894	370	2264
In(^{114}Cd)	13.6−23.6	2840 ± 220	2173	388	2561
Sn(^{110}Sn)	14.2−24.2	2363 ± 220			643

[a]) We assume an angular distribution of the form $1 + \frac{1}{13}\cos^2\theta$.

REF. G. J. Kumbartzki, Ung Kim and Ch. K. Kwan
Nucl. Phys. A160, 237 (1971)

ELEM. SYM.	A	Z
V	51	23

METHOD

REF. NO. 71 Ku 2 egf

REACTION	RESULT	EXCITATION ENERGY	SOURCE TYPE	SOURCE RANGE	DETECTOR TYPE	DETECTOR RANGE	ANGLE
G,SPL	ABY	THR-999	C	800-999	ACT-I		4PI

$\sigma_q(A,Z) = K\exp\left[PA - R(A - SZ + TZ^2)^2\right]$, cross section for equivalent quantum. 999 = 2.1 GEV

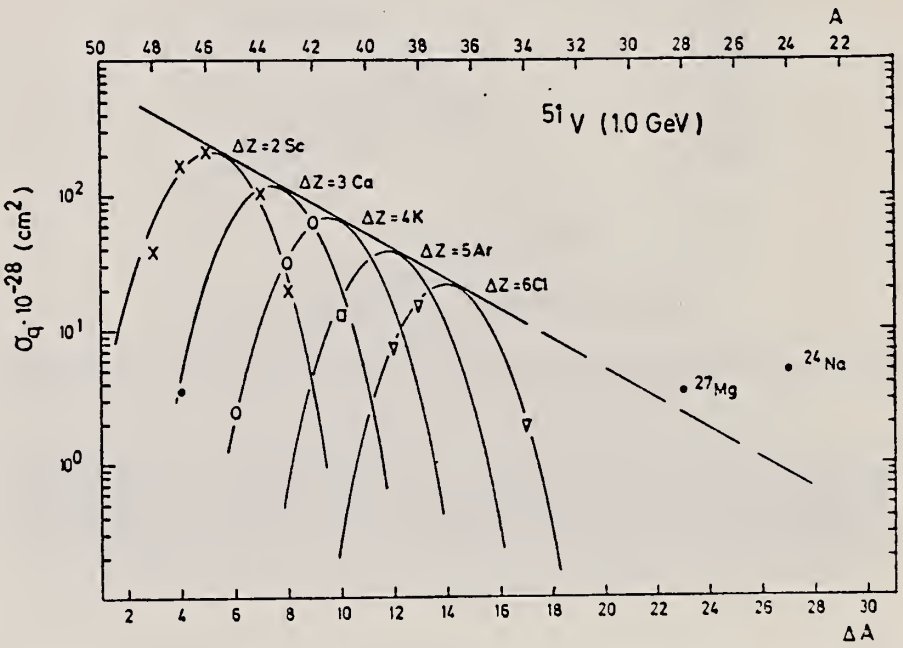

Fig. 3. Photonuclear yields obtained from vanadium after irradiation with 1.0 GeV bremsstrahlung as a function of the number of emitted nucleons.

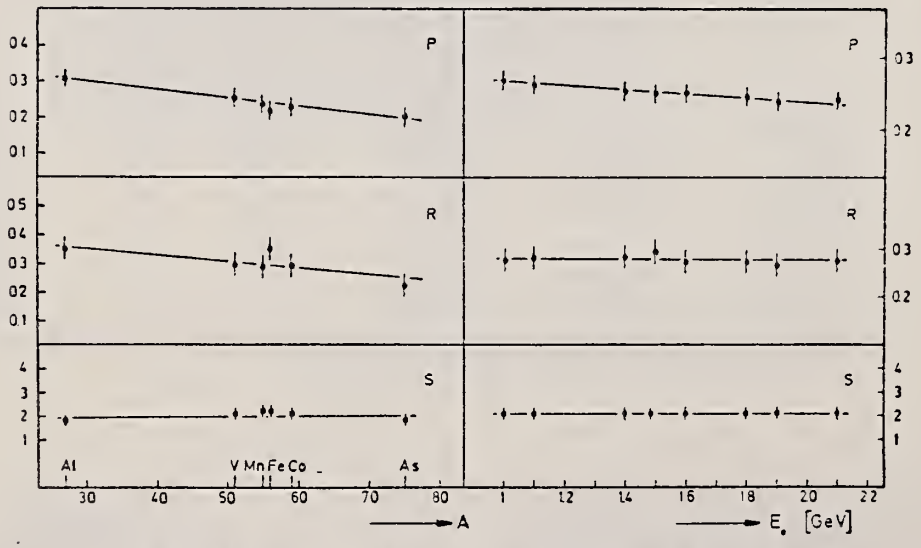

Fig. 6. Behaviour of the parameters P, R and S as functions of A and E_0.

over

U.S. DEPARTMENT OF COMMERCE
NATIONAL BUREAU OF STANDARDS

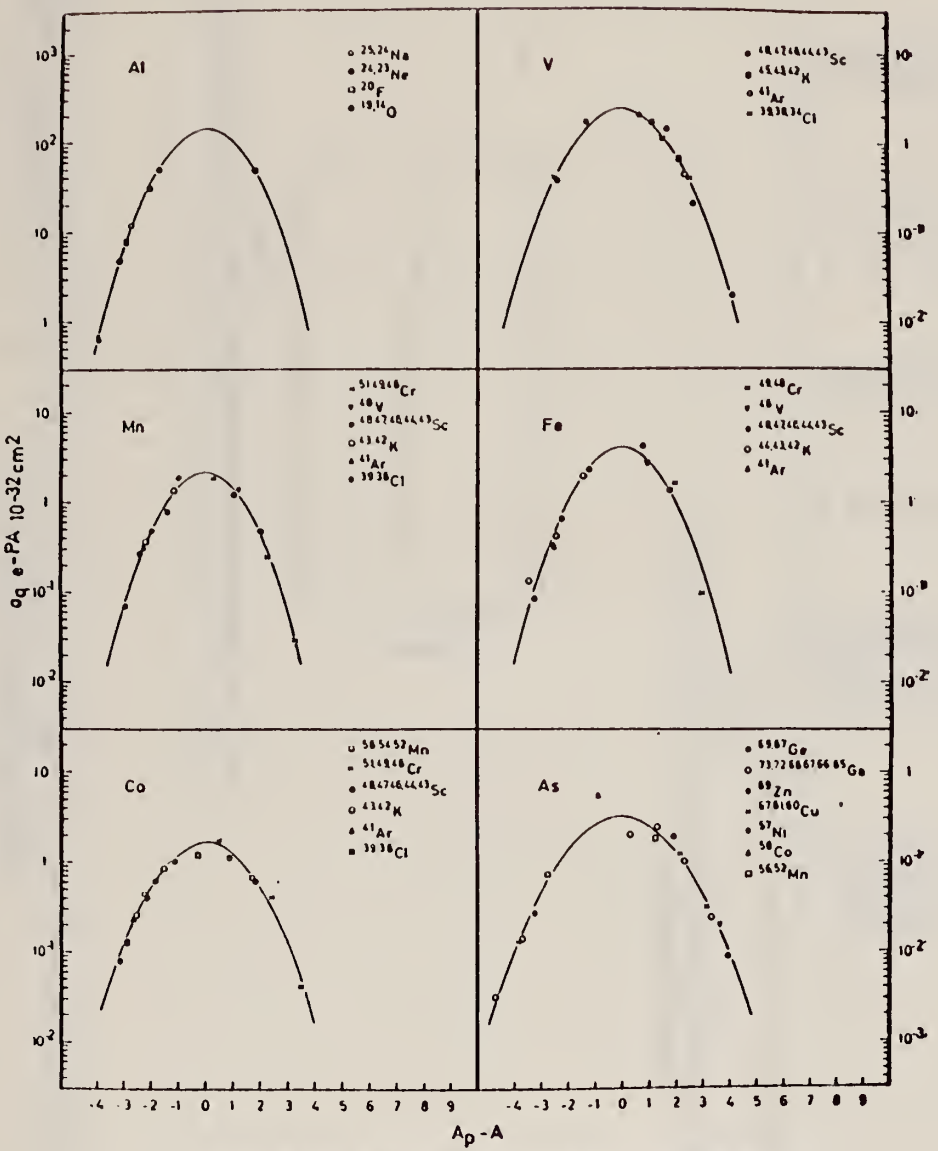

Fig. 4. Yield distributions from various targets with bremsstrahlung of 1.5 GeV.

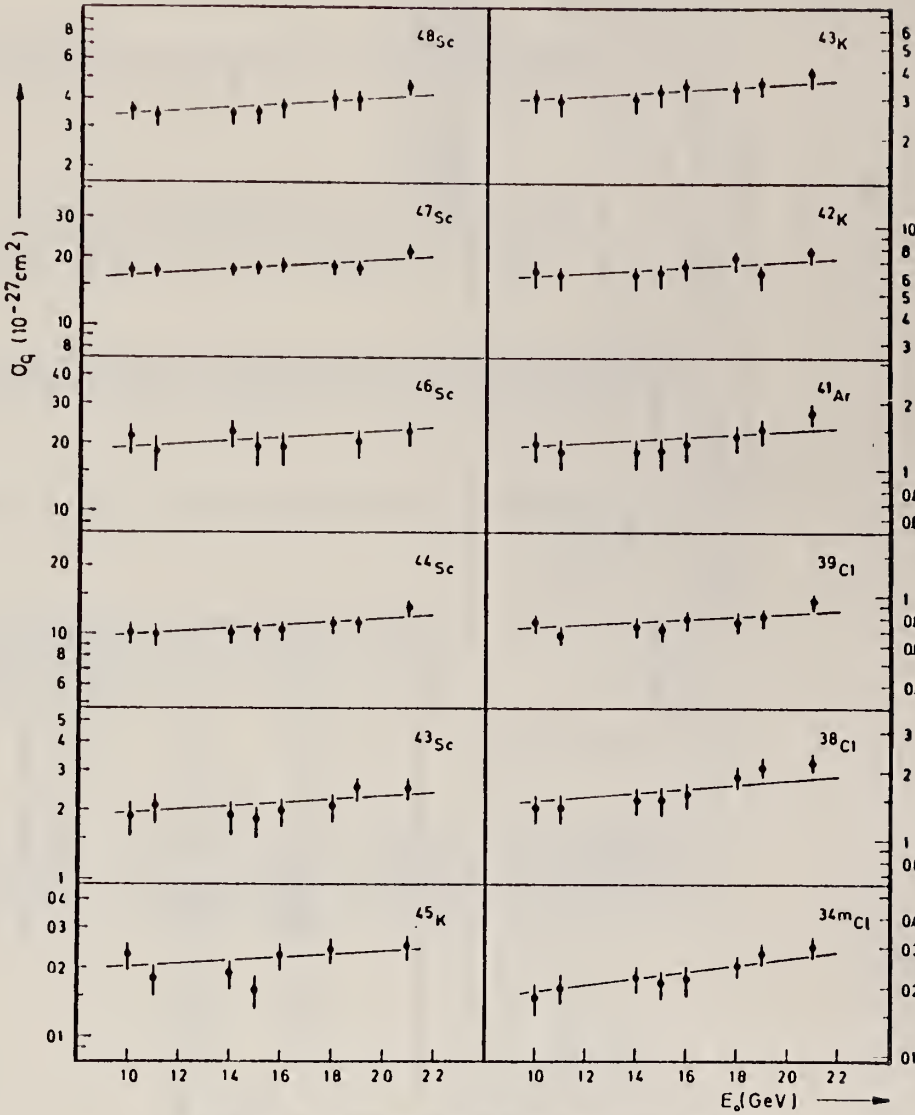

Fig. 5. Yields of spallation products using vanadium targets.

G. Kumbartzki and U. Kim
Nucl. Phys. A176, 23 (1971)

ELEM. SYM.	A	Z
V	51	23

METHOD

REF. NO. 71 Ku 5 egf

REACTION	RESULT	EXCITATION ENERGY	SOURCE TYPE	SOURCE RANGE	DETECTOR TYPE	DETECTOR RANGE	ANGLE
* G,SPL	ABY	THR-999	C	999	ACT-I		4PI
** G,PI+	ABY	THR-999	C	200-999	ACT-I		4PI

* 999 = 1.5 GEV
**999 = 2.2 GEV

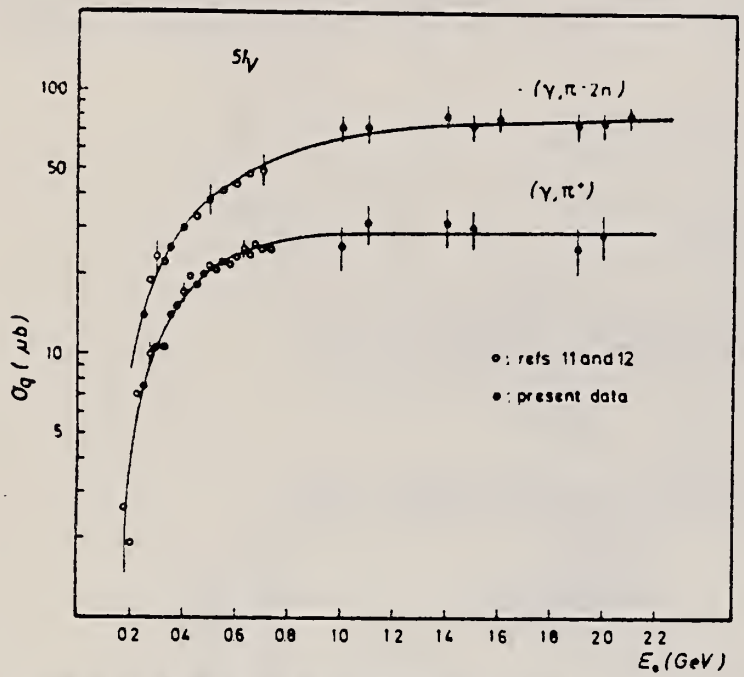

Fig. 2. Yields for the reactions $^{51}V(\gamma,\pi^+)^{51}Ti$ and $^{51}V(\gamma,\pi^-2n)^{59}Cr$ as a function of the maximum energy of bremsstrahlung.

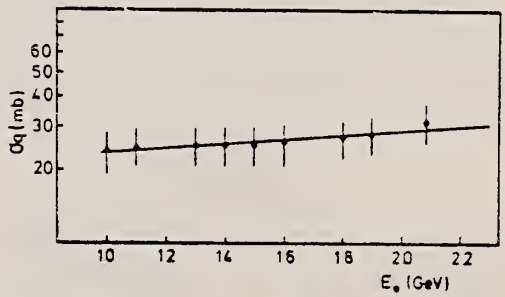

Fig. 4. Total spallation yields of vanadium target as a function of bremsstrahlung energy.

(over)

TABLE I

Decay data and yields of radioactive nucleides in vanadium and iron at 1.5 GeV bremsstrahlung energy

Nuclide	Half-life	Gamma-energy (keV)	Intensity	σ_e (10^{-28} cm^2) (vanadium)	σ_e (10^{-28} cm^2) (iron)
^{53}Fe	8.6 min	380.0	32		12.6 ±1.6
^{52}Fe	8.2 h	168.1	100		0.40±0.05
^{56}Mn	2.57 h	846.7	100		3.5 ±0.4
^{54}Mn	312 d	834.8	100		72.0 ±9.0
^{52m}Mn	21 min	1434.4	98		9.1 ±1.0
^{52}Mn	5.7 d	1434.4	100		7.9 ±0.9
^{51}Cr	27.8 d	320.1	9		39 ±4
^{49}Cr	42 min	153.6	13	0.77±0.09	5.9 ±0.6
^{48}Cr	23 h	307.8	99		0.46±0.6
^{48}V	16 d	983.7	100	10.2 ±1.3	12.8 ±1.4
^{52}V	3.8 min	1434.4	100		1.6 ±0.3
^{51}Ti	5.8 min	320.1	95	0.31±0.07	
^{48}Sc	1.83 d	1038.5	100	3.49±0.43	0.34±0.06
^{47}Sc	3.4 d	159.4	70	18.2 ±2.7	1.63±0.20
^{46}Sc	83.9 d	1120.0	100	19.4 ±3.3	4.8 ±0.7
^{44m}Sc	2.44 d	270.8	86	5.2 ±0.7	3.8 ±0.4
^{44}Sc	3.92 h	1156.9	100	5.2 ±0.8	4.1 ±0.5
^{43}Sc	3.92 h	372.8	22	1.8 ±0.2	1.9 ±0.3
^{43}K	22.4 h	617.2	81	3.1 ±0.4	0.51±0.08
^{42}K	12.4 h	1524.7	18	6.2 ±0.9	2.4 ±0.5
^{44}K	22 min	1156.9	61	1.7 ±0.3	
^{45}K	20 min	175	80	0.20±0.05	
^{41}Ar	1.83 h	1293.0	99	1.24±0.23	0.26±0.04
^{39}Cl	55.5 min	1266.4	50	0.71±0.12	0.16±0.04
^{38}Cl	37.3 min	1642.2	33	1.47±0.21	0.48±0.09
^{34m}Cl	32 min	147.2	45	0.21±0.04	
^{29}Al	6.6 min	1273.1	94	0.41±0.09	0.28±0.08
^{28}Al	2.3 min	1778.7	100	0.86±0.15	0.78±0.12
^{28}Mg	21 h	1342.0	70	0.09±0.03	0.03±0.01
^{27}Mg	9.5 min	843.2	70	0.42±0.07	0.18±0.04
^{24}Na	15 h	1368.5	100	0.51±0.08	0.29±0.04
^{24}Ne	3.4 min	472.0	100	0.04±0.01	

REF. P.K.A. de Witt Huberts, J.E.P. de Bie
PICNS-72, 421 (1972) Sendai

ELEM. SYM.	A	Z
V	51	23

METHOD

REF. NO. 72 De 9 hvm

REACTION	RESULT	EXCITATION ENERGY	SOURCE		DETECTOR		ANGLE
			TYPE	RANGE	TYPE	RANGE	
E,E/	FMF	1, 2	D	25- 85	MAG-D		DST

1=1.61; 2=2.41 MEV

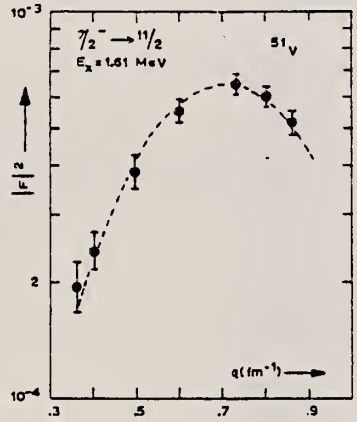

Fig. 8. Experimental form factor for the 1.61 MeV transition in ^{51}V. The dashed curve is the best fit result obtained with a $(1f_{7/2} \rightarrow 1f_{7/2})$ transition density in a harmonic oscillator basis.

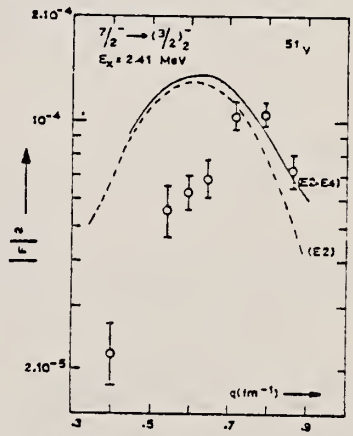

Fig. 9. Experimental form factor for the 2.41 MeV transition in ^{51}V. The two curves shown are the DWBA predictions for E2 and (E2+E4) strength obtained with a $(1f_{7/2} \rightarrow 2p_{3/2})$ transition density in a harmonic oscillator basis.

REF. D. Hiramatsu, T. Kamae, H. Muramatsu, K. Nakamura, N. Izutsu, and Y. Watase
PICNS-72, p.429 Sendai (see 73H15)

ELEM. SYM.	A	Z
V	51	23

METHOD

REF. NO. 72 Hi 8 hvm

REACTION	RESULT	EXCITATION ENERGY	SOURCE TYPE	SOURCE RANGE	DETECTOR TYPE	DETECTOR RANGE	ANGLE
E,E/P	NOX	0* 60	D	700	MAG-D		DST

*SEP ENERGY RANGE

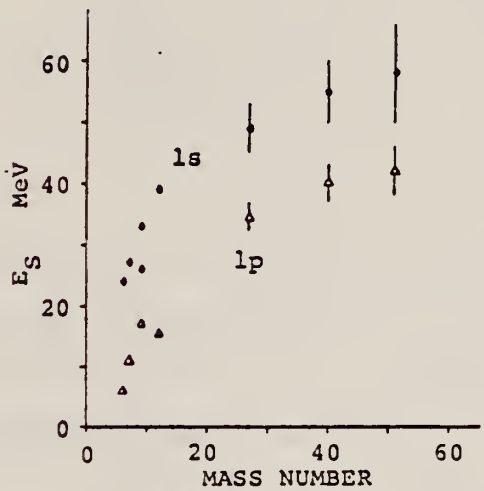

Fig. 6. The separation energy of 1s and 1p states as a function of the mass number.

N. A. Keller and D. B. McConnell
Can. J. Phys. 50, 1554 (1972)

V	51	23

METHOD

REF. NO. 72 Ke 4 hmg

REACTION	RESULT	EXCITATION ENERGY	SOURCE		DETECTOR		ANGLE
			TYPE	RANGE	TYPE	RANGE	
G,A	RLY	10-32	C	32	SCD-D		DST

TABLE 3. Observed angular distribution parameters for 32 MeV electron energy

Element	A_0	A_1/A_0	A_2/A_0
Ti	7.03 ± 0.15	0.073 ± 0.052	−0.286 ± 0.073
V	2.58 ± 0.06	0.037 ± 0.042	−0.126 ± 0.069
Fe	10.22 ± 0.30	0.006 ± 0.043	−0.333 ± 0.072
Co	6.80 ± 0.20	0.022 ± 0.048	−0.016 ± 0.077
Ni	15.95 ± 0.49	0.051 ± 0.048	−0.213 ± 0.074
Cu	8.37 ± 0.28	0.076 ± 0.056	−0.035 ± 0.081
Zn	17.87 ± 0.61	0.004 ± 0.045	−0.270 ± 0.073
Ag	0.39 ± 0.01	0.115 ± 0.049	+0.093 ± 0.074

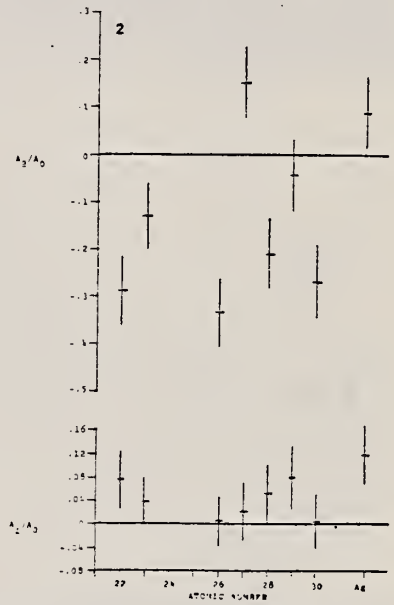

FIG. 2. Angular distributions for 32 MeV electron energy.

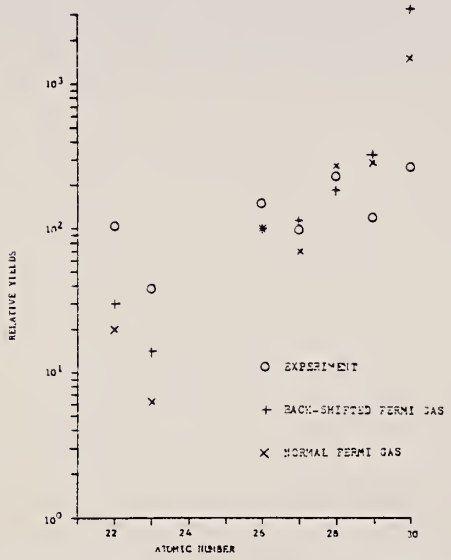

FIG. 13. Experimental and theoretical relative photo-alpha yields for 32 MeV electron beam energy.

REF. G.A. Peterson, K. Hosoyama, M. Nagao, A. Nakada, Y. Torizuka
PICNS-72, 399 (1972) Sendai
(See 73 Pe 1)

ELEM. SYM.	A	Z
V	51	23

METHOD

REF. NO.	
72 Pe 3	hvm

REACTION	RESULT	EXCITATION ENERGY	SOURCE TYPE	SOURCE RANGE	DETECTOR TYPE	DETECTOR RANGE	ANGLE
E,E/	FMF	0- 4	D	183,250	MAG-D		DST

7 LEVELS

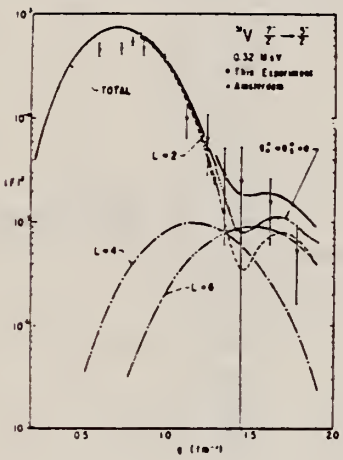

Fig.1. Form factors for the 0.32 MeV($5/2^-$) state.

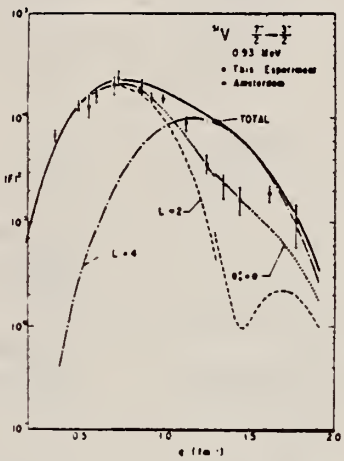

Fig.2. Form factors for the 0.93 MeV($3/2^-$)$_1$ state

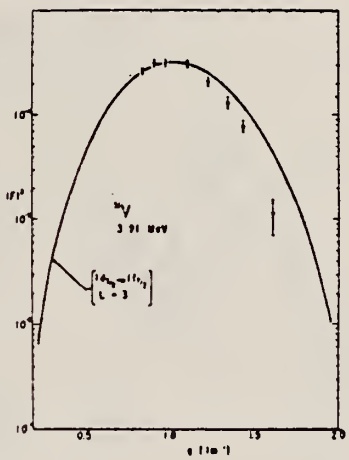

Fig.7. Form factors for the 3.91 MeV state.

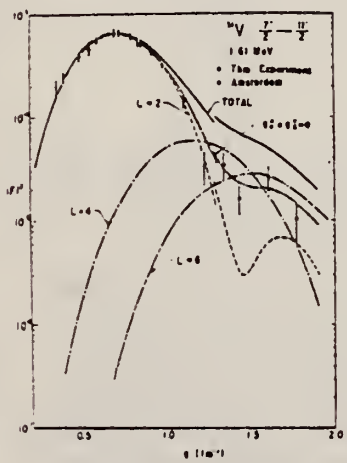

Fig.3. Form factors for the 1.61 MeV($11/2^-$) state.

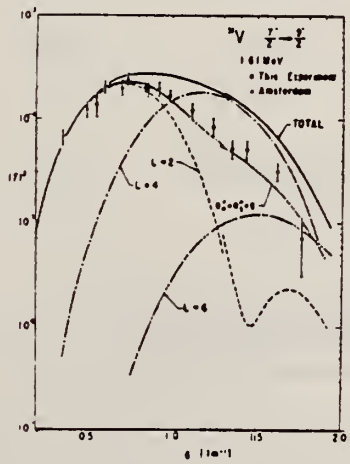

Fig.4. Form factors for the 1.81 MeV($9/2^-$) state.

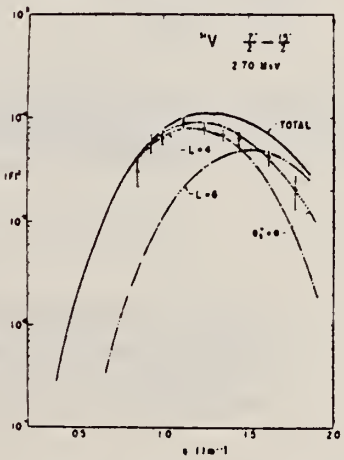

Fig.5. Form factors for the 2.70 MeV($15/2^-$) state.

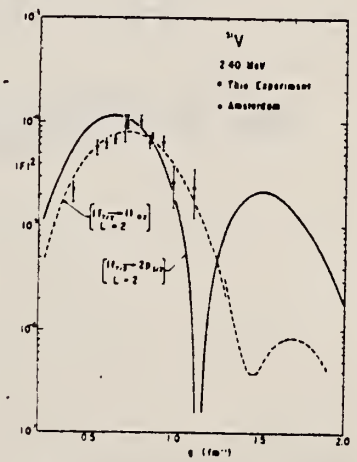

Fig.6. Form factors for the 2.40 MeV($3/2^-$)$_2$ state.

Ref. H.W. Kendall, J. Talm...

R.F. Barrett, J.R. Birkelund, B.J. Thomas, K.S. Lam, and H.H. Thies
Nucl. Phys. A210, 355 (1973)

V	51	23

METHOD

REF. NO. 73 Ba 20 egf

REACTION	RESULT	EXCITATION ENERGY	SOURCE TYPE	SOURCE RANGE	DETECTOR TYPE	DETECTOR RANGE	ANGLE
G,N	NOX	THR- 27	C	10- 27	BF3-I		4PI

MEAN NEUT ENERGY

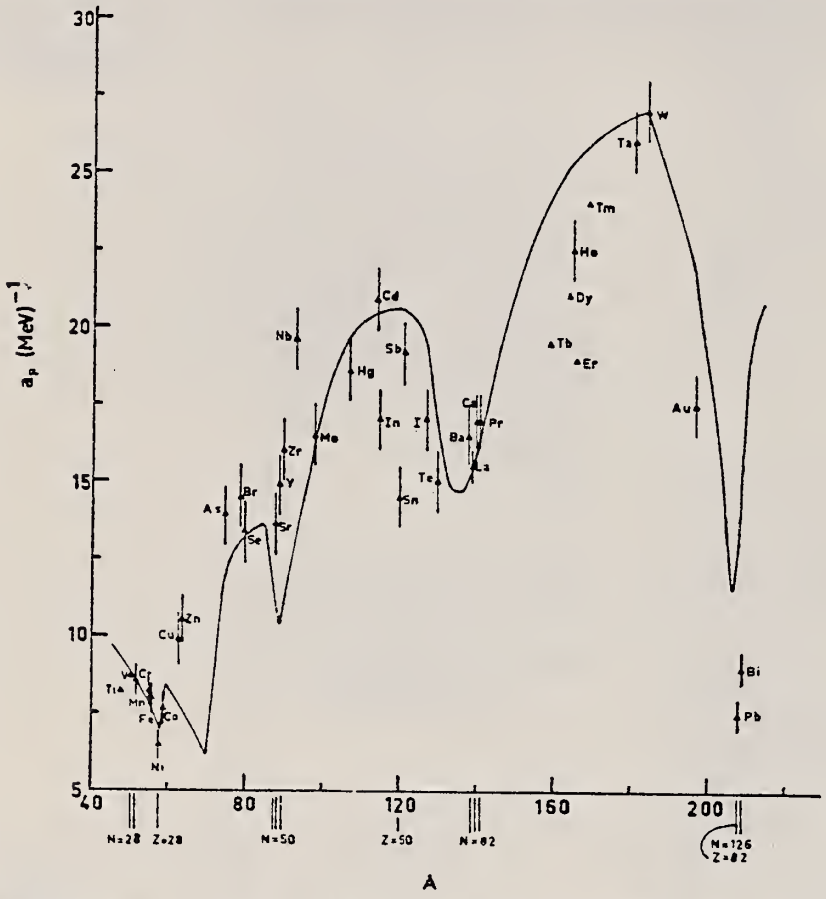

Fig. 12. Experimental values of the level density parametcr a_p (Fermi gas formula plus pairing correction) versus atomic number A. The continuous curve is a least-squares fit to the data of a theoretical calculation from Newton [15].

1
H. Baba and S. Baba, Japan Atomic Energy Research Institute report JAERI-1183 (1969).
2
H. Baba, Nucl. Phys. A159, 625 (1970).
15
T.D. Newton, Can. J. Phys. 34, 804 (1956).

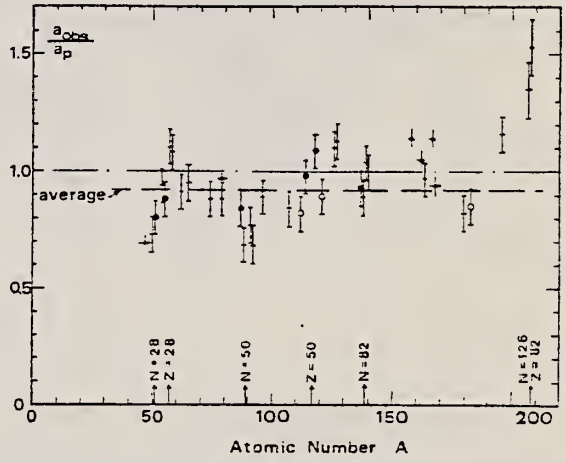

Fig. 15. Ratio a_{obs}/a_p versus atomic number A. Here a_{obs} is the level density parameter taken from the neutron resonance work of refs. [1,2]), and a_p is the level density parameter derived from the present (γ, n) work. Filled circles represent points where nuclei in the neutron resonance and in the (γ, n) experiment were the same. Open circles represent points where the respective nuclei were approximately matched. Triangles represent points which are based on measurement of neutron mean energies at two bremsstrahlung energies only.

(over)

TABLE 3

Comparison of experimental and theoretical data on nuclear level densities with Fermi gas formulae, and comparison of nuclear level density parameters from (γ, n) and n-resonance absorption experiments

Target	N (residual nucleus) [a]		Goodness of fit [b]		$\hat{E}_n(24)$ (MeV) [c]	T (MeV) [d]	a_p (MeV^{-1}) [e]	a_{obs} (MeV^{-1}) [f]	a_{obs}/a_p
			no p.c.	with p.c.					
Ti [g]	23	8%			1.93		8.1–^{47}Ti	6.41–^{47}Ti	0.79
	24	8%							
	25	73%							
	26	5%							
	27	5%							
V [g]	27	100%			1.96		8.7–^{50}V	6.35–^{51}V	0.73
Cr	25	4%	P	G	1.89		8.6–^{51}Cr	6.9 –^{51}Cr	0.80
	27	84%							
	28	10%							
	29	2%							
Mn	29	100%	V.P.	G	2.1		8.2–^{54}Mn	7.82–^{56}Mn	0.94
Fe	27	6%	F	G	1.96		8.0–^{55}Fe	7.06–^{55}Fe	0.88
	29	92%							
	30	2%							
Co	31	100%	P	F	2.12		7.7–^{58}Co	8.35–^{60}Co	1.08
Ni	29	68%	V.P.	P	2.04	1.4	6.5–$^{57.7}$Ni	7.19–^{59}Ni	1.10
($Z = 28$)	31	26%							
	32	1%							
	33	4%							
	35	1%							
Cu	33	69%	V.P.	P	1.78	1.0	9.8–^{62}Cu	8.90–^{64}Cu	0.91
	35	31%							
Zn	33	49%	F	F	1.61		10.5–$^{64.4}$Zn	10.0–^{65}Zn	0.95
	35	28%							
	36	4%							
	37	19%							
As	41	100%	V.P.	F	1.44		14.5–^{74}As	12.81–^{76}As	0.88
Se [g]	41	9%			1.39		13.3–^{78}Se	12.8 –^{78}Se	0.97
	42	8%							
	43	24%							
	45	50%							
	47	9%							
Br	43	45%	V.P.	V.P.	1.41		14.5–^{79}Br	12.69–^{80}Br	0.88
	45	49%							
Sr	47	10%	F	G	1.31		13.6–^{87}Sr	11.4 –^{87}Sr	0.84
	48	7%							
	49	83%							

[a]) Neutron numbers and abundances of respective residual nuclei in (γ, n) experiments.

[b]) These give an assessment of the goodness of fit of a calculated $\hat{E}_n$ versus E_0 curve to the observed data, using the Fermi gas level density formula both without and with pairing corrections.

[c]) Bremsstrahlung photoneutron mean energies $\hat{E}_n$ for peak bremsstrahlung energy $E_0 = 24$ MeV.

[d]) Nuclear temperature from fit with constant-temperature formula.

[e]) Level density parameter a_p derived from the present (γ, n) experiment, using a Fermi gas formula plus pairing correction, and corresponding residual nucleus (the atomic weight shown is the weighted average of atomic weights of the respective isotopes present).

[f]) As column 7, but using data on n-resonance absorption from refs. [1,2]).

[g]) Measurements of $\hat{E}_n(E_0)$ for these nuclei were made only for $E_0 = 21$, 23 and 24 MeV.

REF. R. Bergere, H. Beil, P. Carlos, A. Lepretre, A. Veyssiere
PICNS-73, Vol.I, p.525 Asilomar

ELEM. SYM.	A	Z
V	51	23

METHOD

REF. NO. 73 Be 10 hmg

REACTION	RESULT	EXCITATION ENERGY	SOURCE		DETECTOR		ANGLE
			TYPE	RANGE	TYPE	RANGE	
G,N	ABX	13- 28	D	13- 28	BF3-I		4PI
G,2N	ABX	20- 28	D	20- 28	BF3-I		4PI

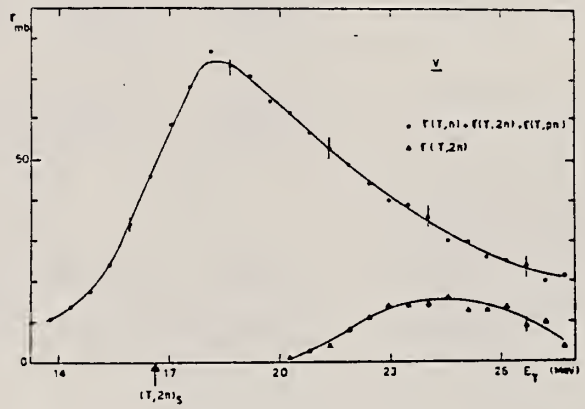

Fig. 12 Partial photoneutron $\sigma(\gamma,n)+\sigma(\gamma,pn)$ and $\sigma(\gamma,2n)$ cross sections of ^{51}V.

REF. A. Järund, B. Fríberg, and B. Forkman
Z. Physik 262, 15 (1973)

ELEM. SYM.	A	Z
V	51	23

METHOD

REF. NO. 73 Ja 3 egf

REACTION	RESULT	EXCITATION ENERGY	SOURCE		DETECTOR		ANGLE
			TYPE	RANGE	TYPE	RANGE	
G,NA24	ABY	THR-999	C	100-999	ACT-I		4PI

999=1 GEV

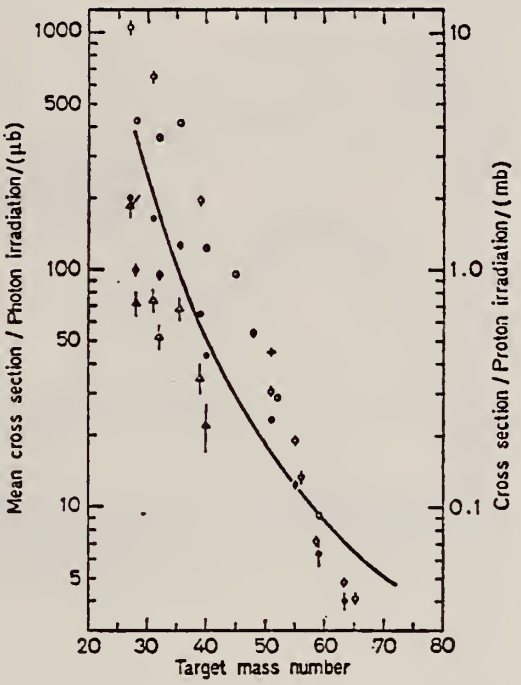

Fig. 7. Mean cross sections for ^{24}Na production as a function of target mass number. Present work filled circles. Noga *et al.* [3] open triangles, Kumbartzki *et al.* [13] cross and Korteling *et al.* [1] 400 MeV protons open circles. The solid line gives the mean cross sections calculated by Jonsson *et al.* [17]

[1] Korteling, R.G. et al., J. Inorg. Nucl. Chem. 29, 2863 (1967).

[3] Noga, V.I. et al., Sov. J. Nucl. Phys. 9, 637 (1969).

[13] Kumbartzki, G. et al., Nucl. Phys. A176, 23 (1971).

[17] Jonsson, G.G. et al., LUNP7212, Oct. 1972, to be published in Physica Scripta.

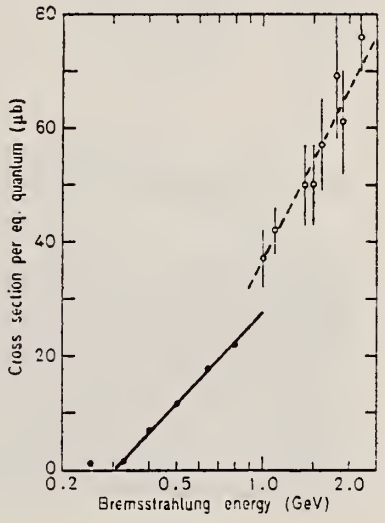

Fig. 5

Fig. 5. The determined yield for the reaction $^{51}V \rightarrow {}^{24}Na$. Present work filled circles, Kumbartzki *et al.* [13] open circles

REACTION	RESULT	EXCITATION ENERGY	SOURCE TYPE	SOURCE RANGE	DETECTOR TYPE	DETECTOR RANGE	ANGLE
E,E/	FMF	0- 4	D	183,250	MAG-D		DST

7 LEVELS

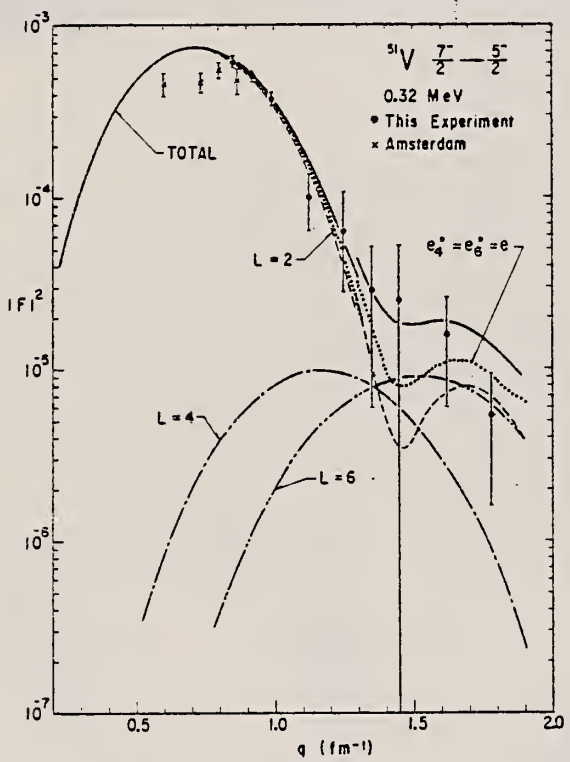

FIG. 6. The square of the form factor for the excitation of the 0.32-MeV level of ^{51}V by inelastic electron scattering versus momentum transfer. The calculated form factors are for a $(1f_{7/2})^3$ configuration of protons in a harmonic-oscillator potential. The curves for the $L=2$, $L=4$, and $L=6$ multipoles and their total were calculated for an effective charge of $1.84e$. The curve labeled $e_4^*=e_6^*=e$ is the sum of the form factors assuming the effective charge is $1.84e$, e, and e for the $L=2$, 4, and 6 multipoles, respectively.

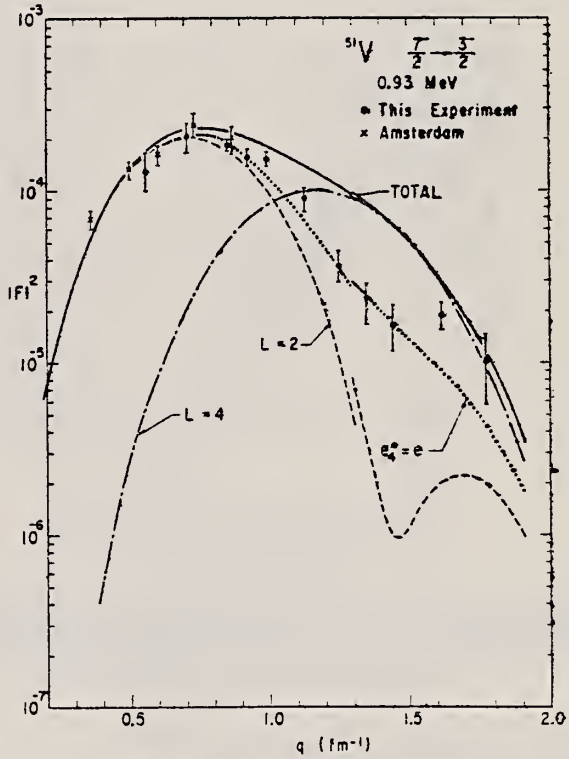

FIG. 7. Form factors for the 0.93-MeV excitation. See the caption to Fig. 6. The total curve was calculated assuming an effective charge of $2.01e$.

(over)

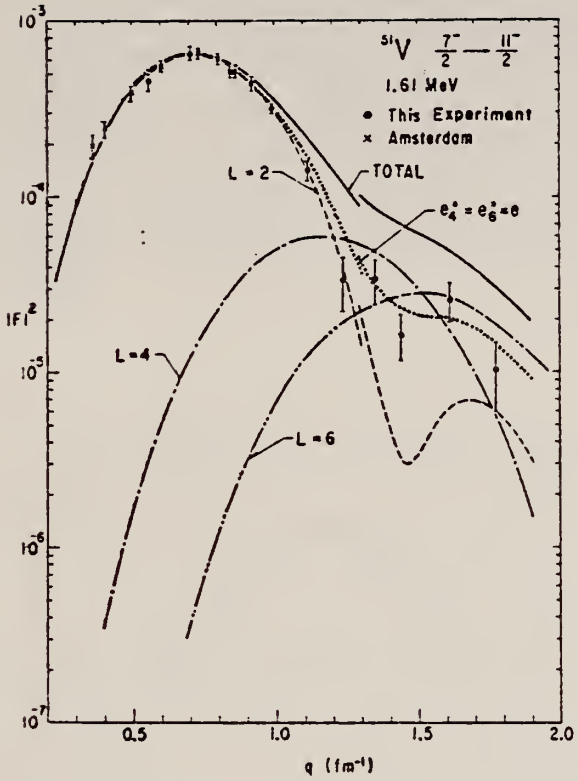

FIG. 8. Form factors for the 1.61-MeV excitation. See the caption to Fig. 6. The total curve was calculated for an effective charge of 1.79e.

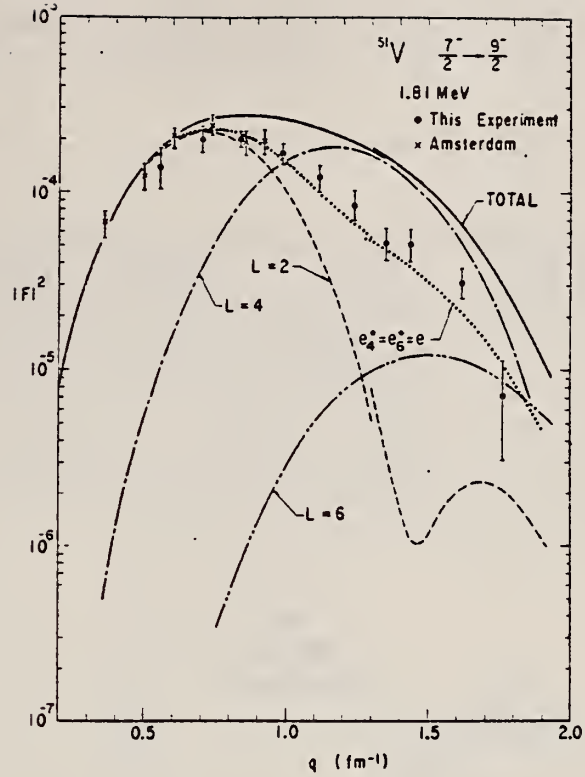

FIG. 9. Form factors for the 1.81-MeV excitation. See the caption to Fig. 6. The total curve was calculated for an effective charge of 1.88e.

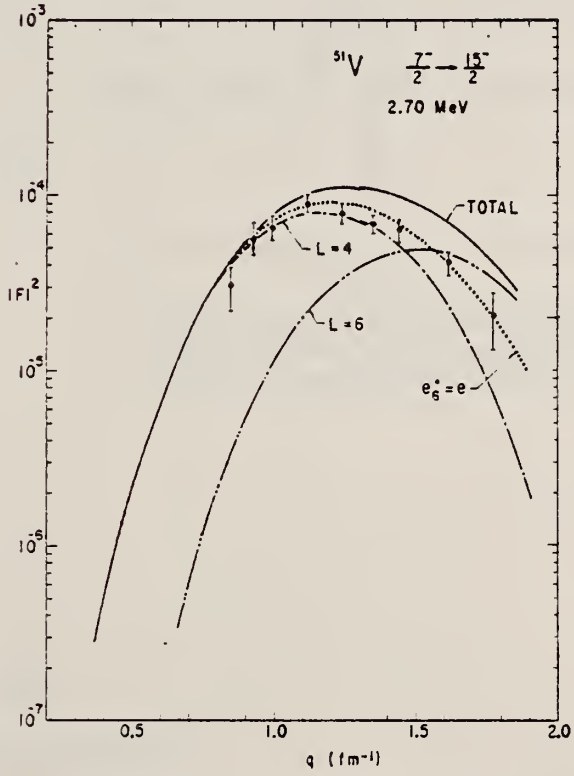

FIG. 10. Form factors for the 2.70-MeV excitation. See the caption to Fig. 6. The total curve was calculated for an effective charge of 1.69e.

REACTION	RESULT	EXCITATION ENERGY	SOURCE		DETECTOR		ANGLE
			TYPE	RANGE	TYPE	RANGE	

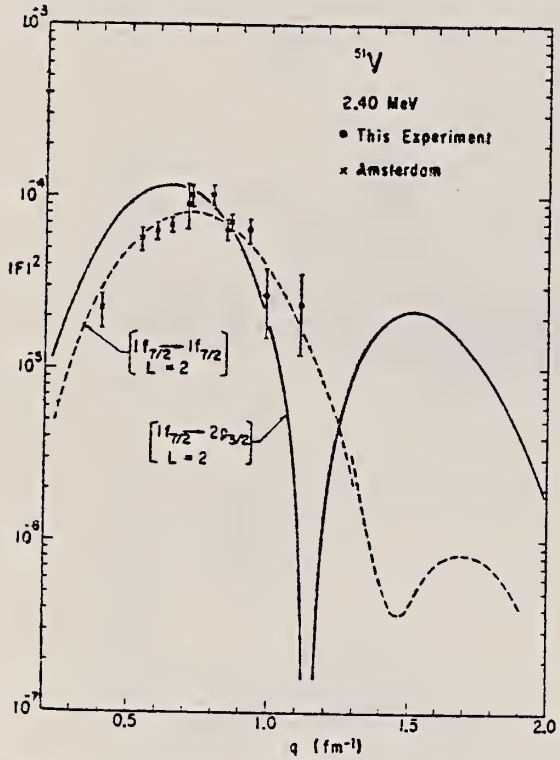

FIG. 12. $E2$ form factors for the 2.40-MeV excitation calculated for a proton transition from a $1f_{7/2}$ to a $2p_{3/2}$ configuration and for a transition within the $1f_{7/2}$ shell.

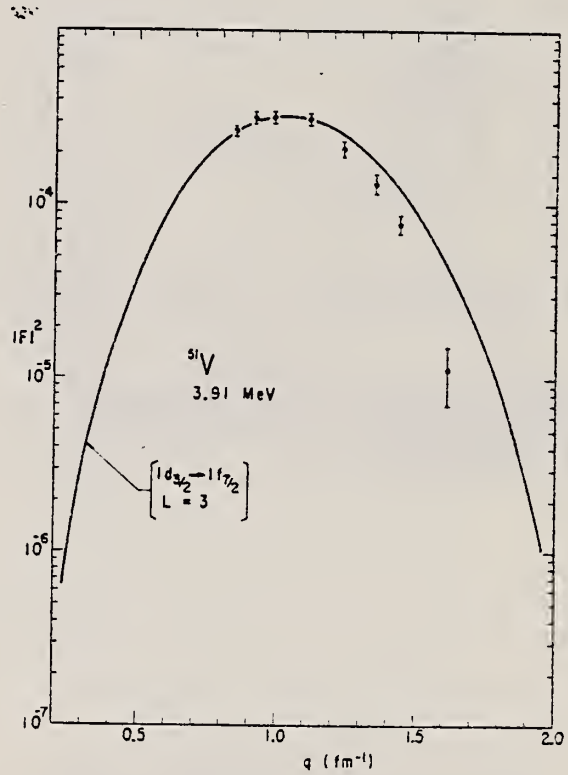

FIG. 13. $E3$ form factor for the 3.91-MeV excitation calculated for a $1d_{3/2}$ to $1f_{7/2}$ transition.

REF.

A. Veyssiere, H. Beil, R. Bergere, P. Carlos, A. Lepretre, and A. De Miniac
Nucl. Phys. A227, 513 (1974)

ELEM. SYM.	A	Z
V	51	23

METHOD

REF. NO. 74 Ve 1 egf

REACTION	RESULT	EXCITATION ENERGY	SOURCE TYPE	SOURCE RANGE	DETECTOR TYPE	DETECTOR RANGE	ANGLE
* G,N	ABX	13- 29	D	13- 29	BF3-I		4PI
** G,2N	ABX	20- 29	D	20- 29	BF3-I		4PI

* 909
** 910

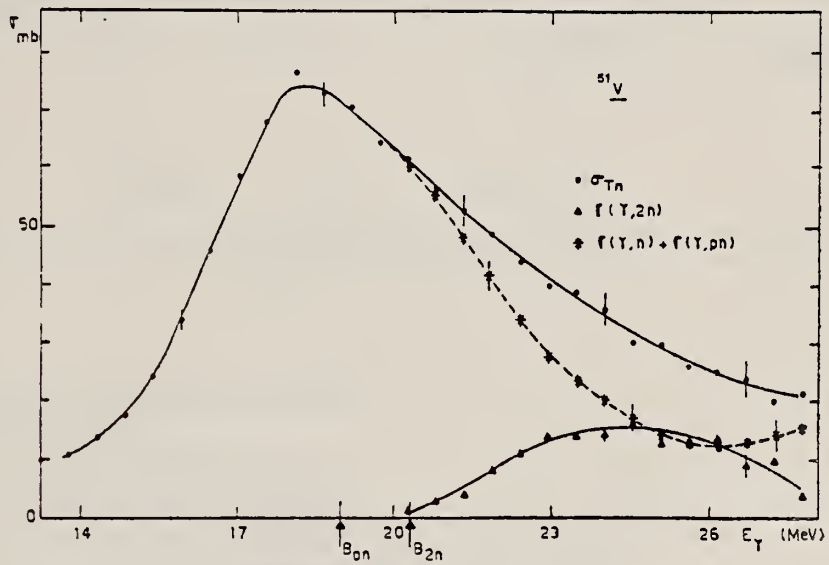

Fig. 14. Photoneutron cross sections σ_{Tn}, $[\sigma(\gamma, n)+\sigma(\gamma, 2n)]$ and $\sigma(\gamma, 2n)$ of ^{51}V.

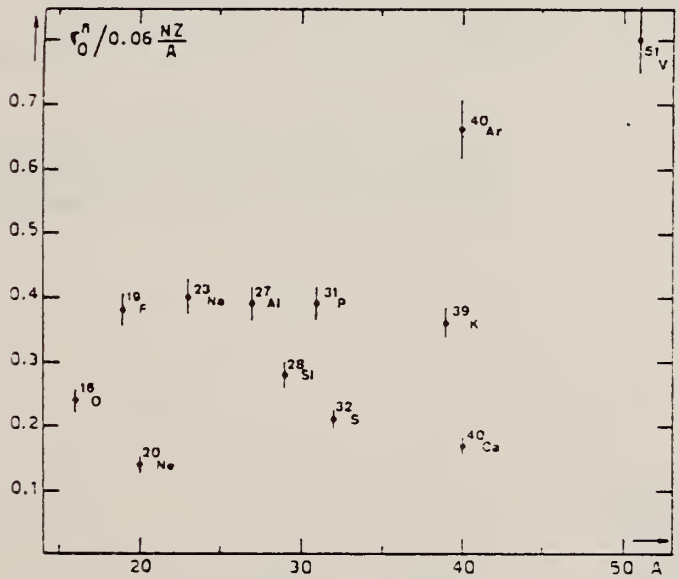

Fig. 22. Ratio of experimental integrated photoneutron cross section σ_0^n over the Thomas, Reiche and Kuhn sum rule $[0.06\,NZ/A]$. Numerical values and upper integration limits E_M are taken from table 3. Also $\Delta\sigma_0^n = \pm 7\%$ for all nuclei.

(over)

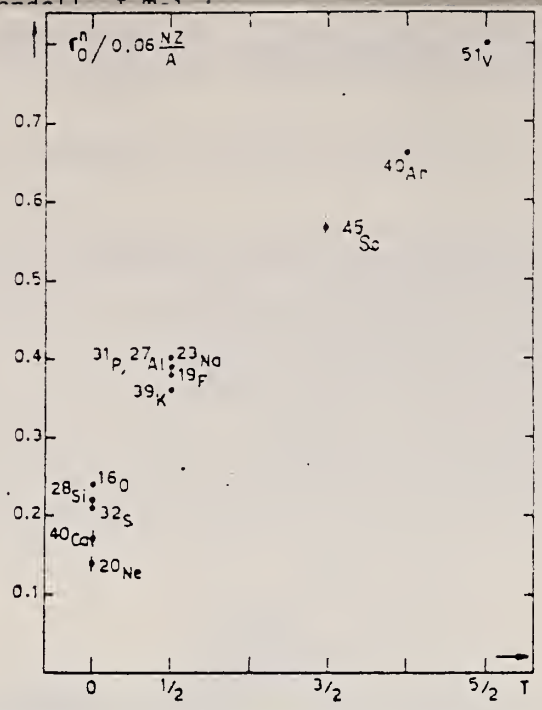

Fig. 24. The $[\sigma_0^n/(0.06\,NZ/A)]$ ratio as a function of isospin T. Possible overall errors of $\pm 7\%$ are to be applied to all nuclei shown.

TABLE 3

Experimental integrated photoneutron cross sections $\sigma_0^n = \int_0^{E_M} \sigma_{T_n}(E)\mathrm{d}E$ compared with the classical sum rule $[0.06\,NZ/A]$ of Thomas, Reich and Kuhn

	$T=0$					$T=\frac{1}{2}$					$T=\frac{3}{2}$	$T=2$	$T=\frac{5}{2}$
Nucleus	^{16}O	^{20}Ne	^{28}Si	^{32}S	^{40}Ca	^{19}F	^{23}Na	^{27}Al	^{31}P	^{39}K	^{45}Sc	^{40}Ar	^{51}V
σ_0^n (MeV · mb)	58 ±4	42 ±3	94 ±7	98 ±7	100 ±7	108 ±7	137 ±9	158 ±10	182 ±12	210 ±14	383 ±25	393 ±28	602 ±42
$\sigma_0^n/(0.06NZ/A)$	0.24	0.14	0.22	0.21	0.17	0.38	0.40	0.39	0.39	0.36	0.57	0.66	0.6
E_M (MeV)	30	26.7	30	30	29.5	29	30	30	29	30	28.1	26.7	28

REF.

C. O. Wene
Z. Phys. A272, 77 (1975)

ELEM. SYM.	A	Z
V	51	23

METHOD

REF. NO. 75 We 4 egf

REACTION	RESULT	EXCITATION ENERGY	SOURCE		DETECTOR		ANGLE
			TYPE	RANGE	TYPE	RANGE	
G,P	ABX	18	D	18	SCD-D		90

18 = 17.6 MEV

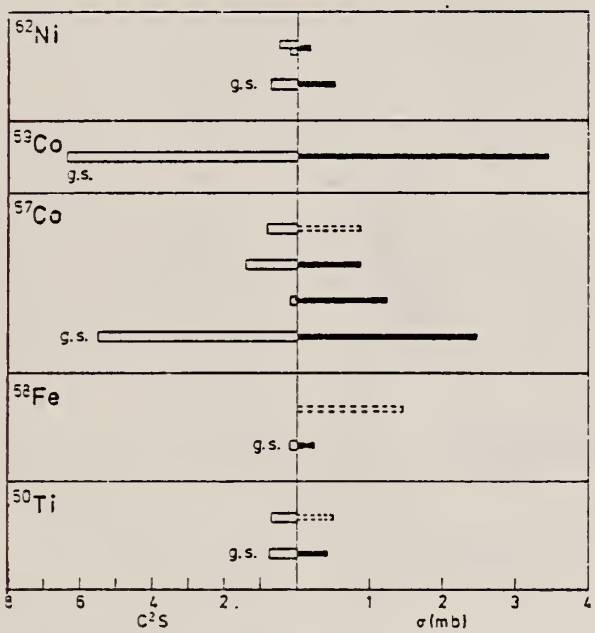

Fig. 5. Correlation between the spectroscopic factors and the cross-sections measured in this work. Open staples indicate $\ell_p = 3$ pick-up and cross hatched staples $\ell_p = 1$ pick-up. Dashed staples indicate that the cross section is uncertain due to the subtraction of a large back-ground

Table 2

Daughter nucleus	Level (MeV)	J^π	σ^a (mb)
^{44}Ca	0	0^+	$\leqq 0.2^b$
	1.16	2^+	$\leqq 0.5^b$
^{50}Ti	0	0^+	0.41 ± 0.05
	2.68	4^+	$(0.5)^c$
^{55}Fe	0	0^+	0.23 ± 0.08
	3.24?	0^+?	$(1.5)^c$
^{57}Co	0	$7/2^-$	2.5 ± 0.2^d
	1.76	$3/2^-$	1.2 ± 0.3
	1.90	$7/2^-$	0.9 ± 0.2
	2.31	$7/2^-$	$(0.9)^c$
^{59}Co	0	$7/2^-$	3.5 ± 0.8
^{62}Ni	0	0^+	0.51 ± 0.09
	1.18	2^+	0.2 ± 0.1

[a] The quoted errors are only those due to counting statistics.
[b] Confidence level 95%.
[c] Uncertain because of large background.
[d] $\sigma = 2.4$ mb from [43].

43. Miyase, H., Oikawa, S., Suzuki, A., Uegaki, J., Saito, T., Sugawara, M., Shoda, K.: The photoproton reactions of Ni-isotopes. In: Proc. Int. Conf. Photonuclear Reactions and Applications, Vol. I, p. 553. Livermore, USA 1973 (see Ref. 15)

REF.

I. Blomqvist, P. Janecek, G.G. Jonsson R. Petersson,
H. Dinter and K. Tesch
Z. Physik A278, 83 (1976)

ELEM. SYM.	A	Z
V	51	23

METHOD

REF. NO.	
76 B1 12	egf

REACTION	RESULT	EXCITATION ENERGY	SOURCE		DETECTOR		ANGLE
			TYPE	RANGE	TYPE	RANGE	
G,SPL	ABY	THR - 580	C	130-580	ACT-I		4PI
E,SPL	ABY	THR - 580	C	130-580	ACT-I		4PI

Cross-sections for some electro- and photoinduced spallation reactions on ^{27}Al and ^{51}V have been measured in the energy region 130-580 MeV with the activation method. The cross sections per photon are compared to Monte-Carlo calculations based on a cascade-evaporation model. The electrodisintegration cross sections are compared to calculations based on the Dalitz formalism for virtual photon spectra.

GIVES YLD RATIO G/E

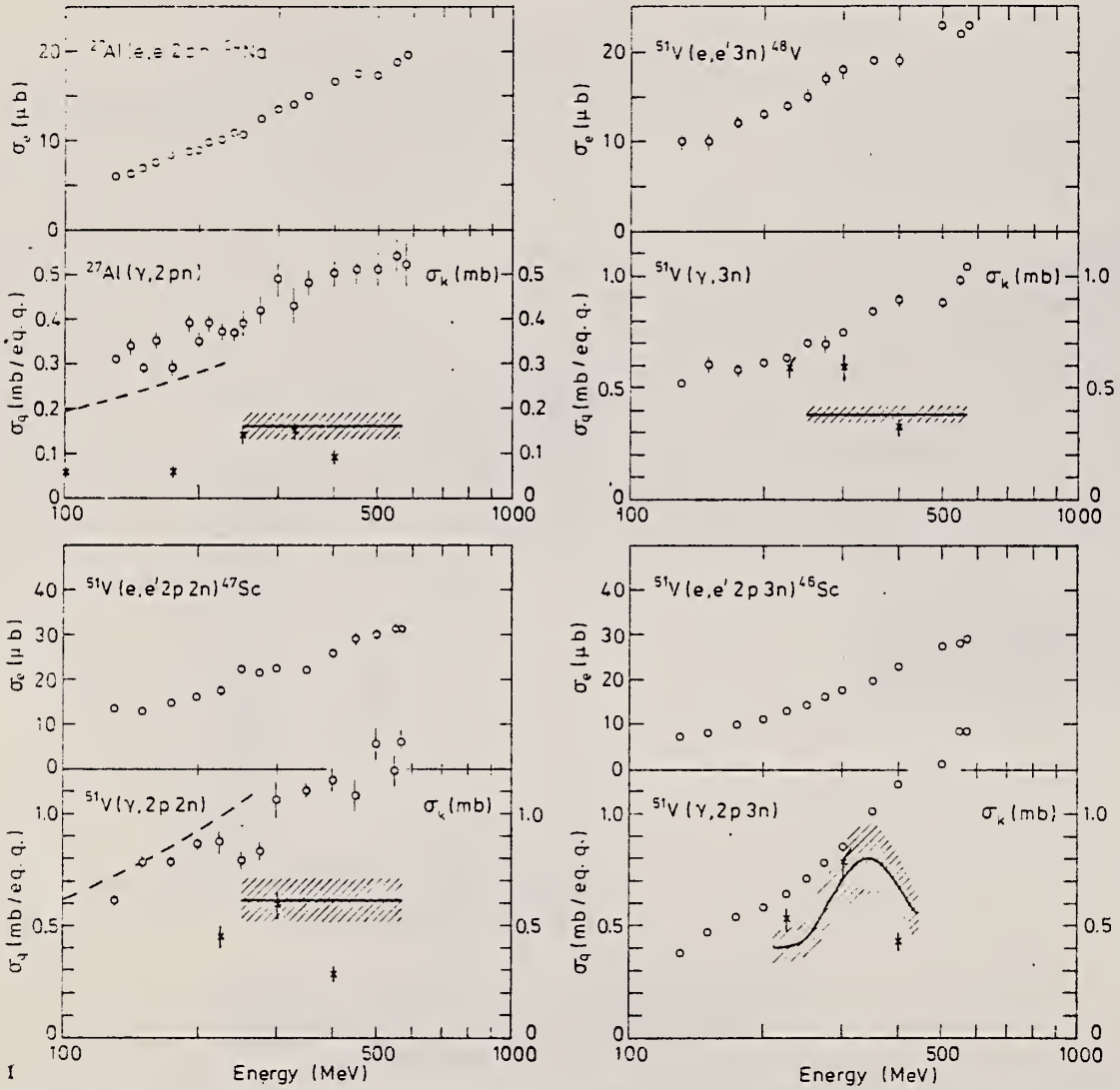

Figs. 1 and 2. Experimental cross sections σ_q and σ_e versus energy for different reactions on ^{27}Al and ^{51}V. The cross sections σ_k deduced from σ_q are given by the solid drawn curves, the hatched areas showing the uncertainty. Dashed curves show σ_q calculated from the low-energy data in Reference 11. Crosses give σ_k calculated with Monte-Carlo method

11 Meyer,R.A., Walters,W.B., Hummel,J.P.: Nucl. Phys. A122, 606 (1968)

(over)

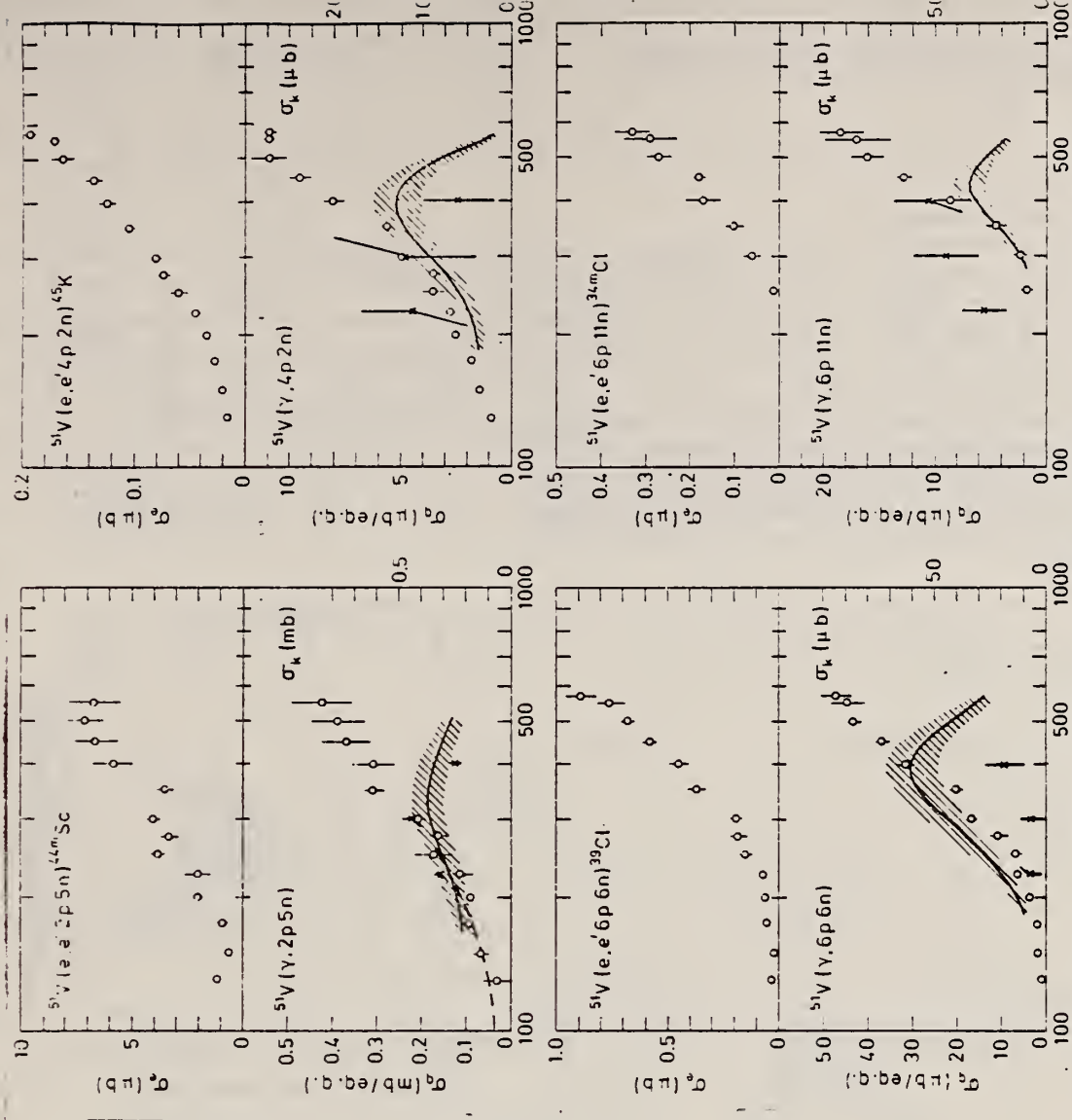

Figs. 1 and 2. Experimental cross sections σ_e and σ_γ versus energy for different reactions on ^{27}Al and ^{51}V. The cross sections σ_γ deduced from σ_e are given by the solid drawn curves, the hatched areas showing the uncertainty. Dashed curves show σ_γ calculated from the low-energy data in Reference 11. Crosses give σ_γ calculated with Monte-Carlo method

11 Meyer,R.A., Walters,W.B., Hummel,J.P.: Nucl. Phys. A122, 606 (1968)

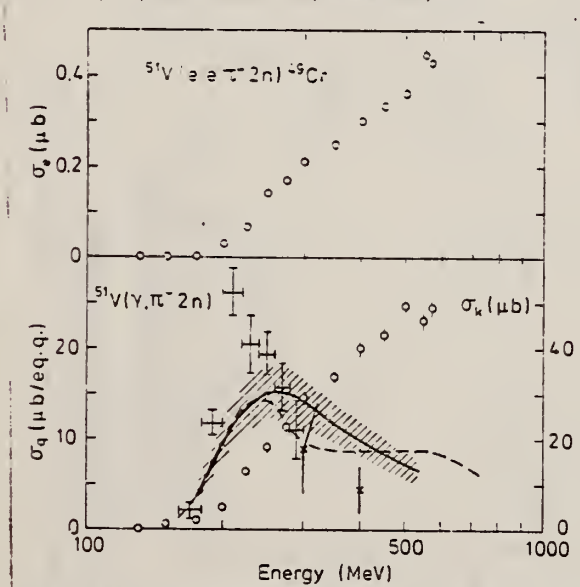

Fig. 3. Experimental and calculated cross sections for the reaction $^{51}V\left(\begin{matrix}\gamma\\ e'e'\end{matrix},\pi^-2n\right)^{49}Cr$; se caption to Figures 1–2. + show the corrected σ_k by Meyer and Hummel [16], the dashed curve the corrected σ_k by Nydahl and Forkman [17]

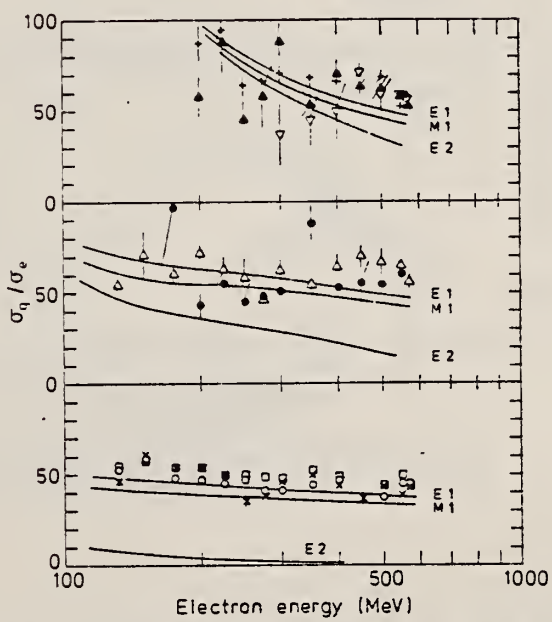

Fig. 5. The ratio σ_q/σ_e versus electron energy for different reactions on ^{51}V. ○ $3n$ emitted, × $2p\,2n$, □ $2p\,3n$, ● $2p\,5n$, △ $4p\,2n$, + π^-2n, ▲ $6p\,6n$, ▽ $6p\,11n$. The curves show calculated cross-section ratios for π^-2n (top), $2p\,5n$ (middle), $2p\,2n$ (bottom)

16 Meyer,R.A., Hummel,J.P., Phys. Rev. 140, B48 (1965)

17 Nydahl,G., Forkman,B: Nucl. Phys. B7, 97 (1968)

REF.

B. Bülow, B. Johnsson, M. Nilsson and B. Forkman
Z. Physik A278, 89 (1976)

ELEM. SYM.	A	Z
V	51	23

REF. NO.	
76 Bu 11	egf

Comment: Table of cross section results

REACTION	RESULT	EXCITATION ENERGY	SOURCE		DETECTOR		ANGLE
			TYPE	RANGE	TYPE	RANGE	
G,JPKN	ABX	THR - 800	C	75-800	ACI-I		4PI

The yields of $^{51}V(\gamma, xpyn)$ reactions have been measured at maximum bremsstrahlung energies from 75 to 800 MeV. Mean cross sections have been deduced, compared to Monte-Carlo calculations and analysed with a semiempirical Rudstam formula. Total isobaric mean cross sections and an N/Z dispersion curve in the mass region $A = 42$–48 have been obtained. The results are in agreement with cascade-evaporation theory and with earlier data obtained with photons and protons.

J=2-11,K-2-16

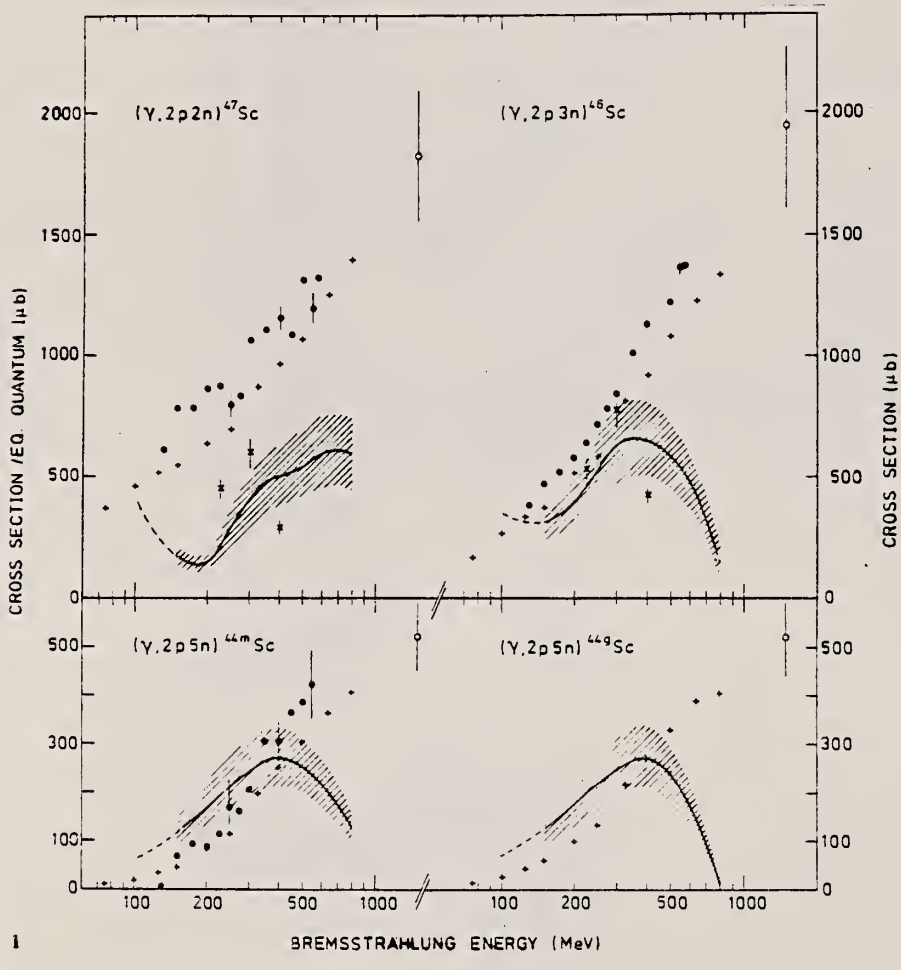

1

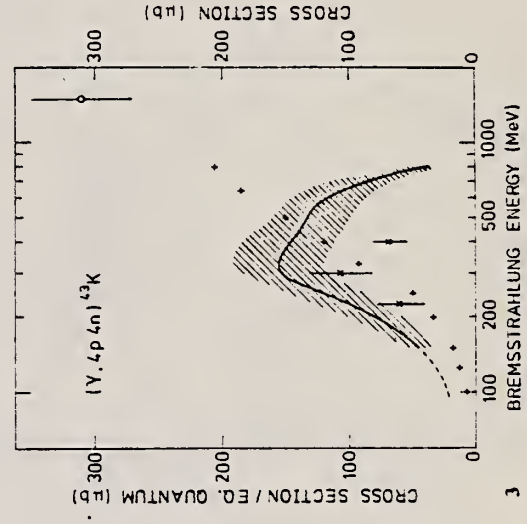

3

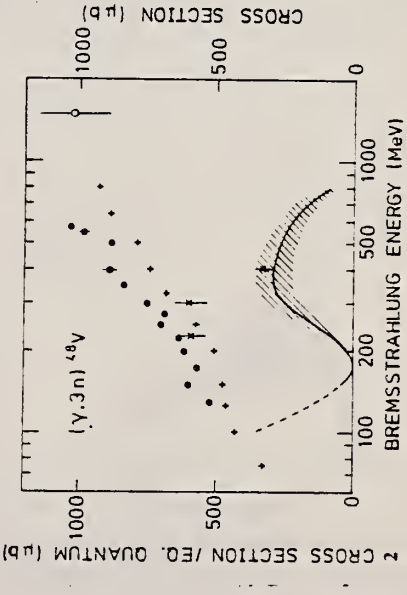

2

Figs. 1–3. Yields for $^{51}V(\gamma, xpyn)$ reactions. + Present work; ● Reference 12; ○ Reference 8, 1.5 GeV; × Monte-Carlo. The solid curves show the cross-sections and the hatched areas indicate the errors

(OVER)

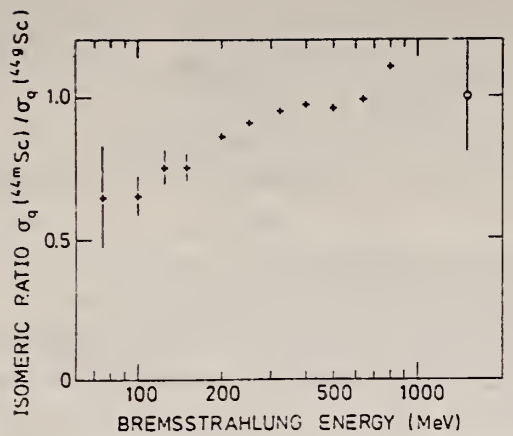

Fig. 4. Isomeric ratios vs. bremsstrahlung energy. + present work, ○ Reference 8

[8] Kumbartzki, G., Kim, U.: Nucl. Phys. A176, 23 (1971)

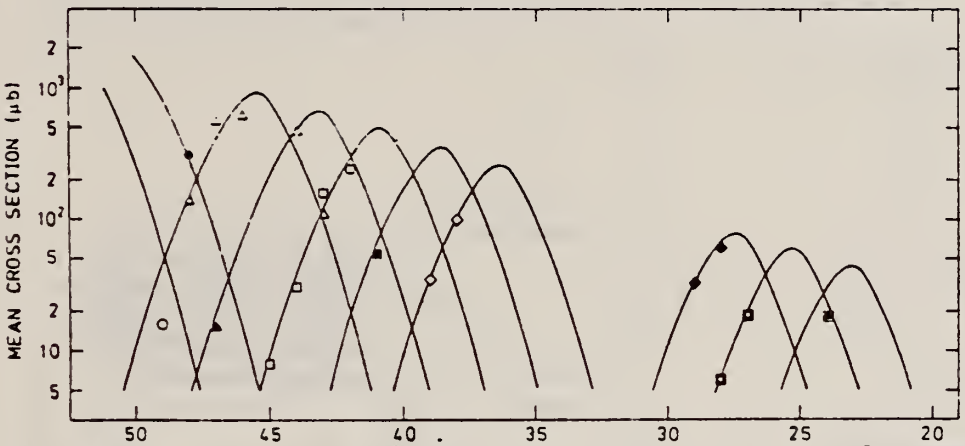

Fig. 5. Mean cross-section distributions for different elements. ○ Cr, ● V, △ Sc, ▲ Ca, □ K, ■ Ar, ◇ Cl, ◆ Al, □ Mg, ■ Na

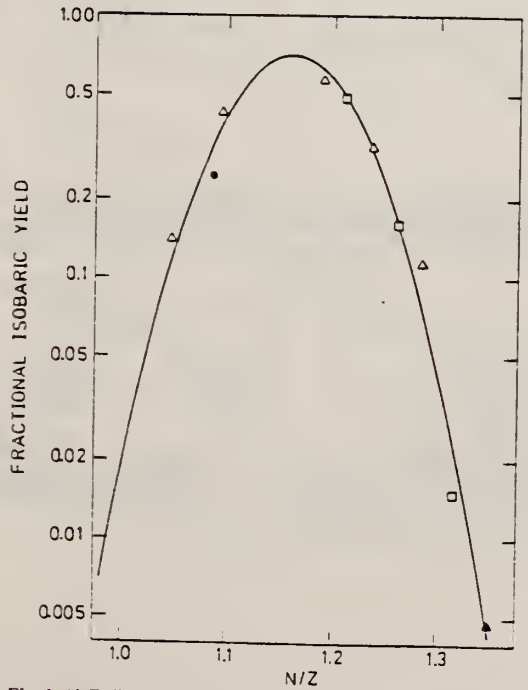

Fig. 6. N/Z dispersion of products in the mass region 42–48 calculated from mean cross-sections in the energy range 250–400 MeV. The solid line shows the Gaussian curve giving a best fit to the data. The symbols used are: ● V, △ Sc, ▲ Ca, □ K

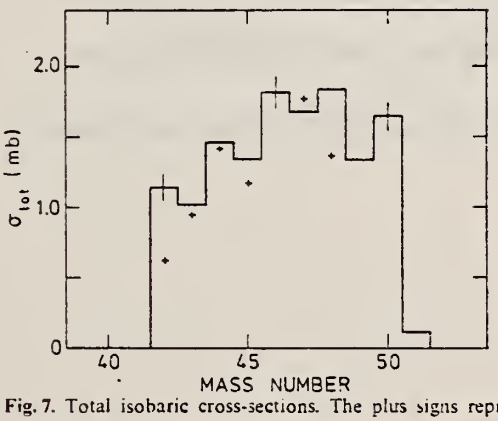

Fig. 7. Total isobaric cross-sections. The plus signs represent the experimental results and the histogram displays arithmetic mean values from Monte-Carlo calculations

REF.	ELEM. SYM.	A	Z
A. S. Danagulyan, N. A. Demekhina Yad. Fiz. 24, 681 (1976) Sov. J. Nucl. Phys. 24, 355 (1976)	V	51	23

METHOD	REF. NO.	
	76 Da 4	hmg

REACTION	RESULT	EXCITATION ENERGY	SOURCE		DETECTOR		ANGLE
			TYPE	RANGE	TYPE	RANGE	
G,NA24	ABX	THR* 5	C	2* 5	ACT-I		4PI

*ENERGY,GEV

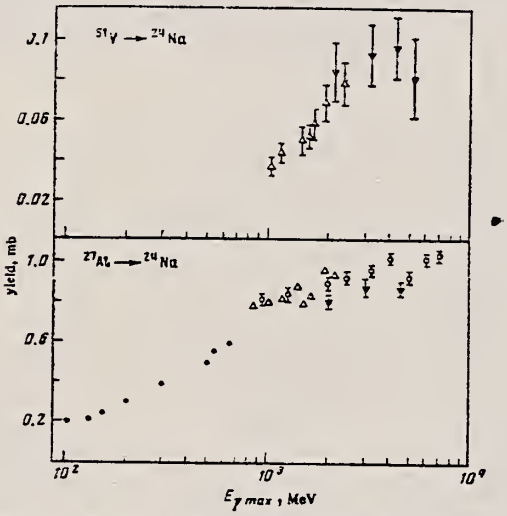

FIG. 1. Yields of the reactions. Points: ▼—present work, ●—Ref. 10, △—Ref. 3, ○—Ref. 9.

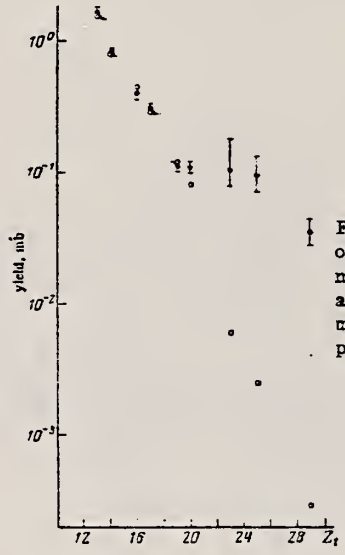

FIG. 2. Yield values and theoretical values according to the modified Rudstam formula as a function of the target charge number Z_t. Points: ●—experiment, ○—theory.

[3] G. Kumbartzki et al., Nucl. Phys. A176, 23 (1971).

[9] G. Andersson et al., Nucl. Phys. A197, 44 (1972).

[10] I. Blomqvist et al., Nucl. Phys. A162, 193 (1971).

TABLE I. Experimental yields and reaction cross sections obtained in the measurements at the Erevan electron accelerator.

Target nucleus	Reaction yield, mb, $E_{\gamma\,max}$ GeV					Reaction cross section, mb
	2	3	4	4.5	5	
^{27}Al	0.81±0.08	0.87		0.87		0.07213±0.0345
^{28}Si	0.27±0.02	0.28		0.29		0.0267±0.013
^{32}S	0.24±0.02	0.22		0.27		0.0323±0.0155
Cl	0.28±0.03	0.30		0.29		—
^{39}K	0.1±0.01	0.125		0.15		0.06±0.0288
^{40}Ca	0.086±0.01	0.09		0.115		0.035±0.0168
^{51}V	0.085±0.02	0.094±0.02	0.095±0.02		0.082±0.025	0.019
^{55}Mn	0.079±0.02	0.075±0.02	0.087±0.017		0.088±0.015	0.01076±0.0036
Cu	0.029±0.006	0.037±0.007	0.036±0.007		0.034±0.007	0.00547±0.0025

Note. The reaction cross sections have been calculated in the $1/E$ approximation of the bremsstrahlung spectrum.

REF.

K. Nakamura, S. Hiramatsu, T. Kamae, H. Muramatsu, N. Izutsu, Y. Watase
Nucl. Phys. A271, 221 (1976)

ELEM. SYM.	A	Z
V	51	23

METHOD

REF. NO. 76 Na 3 egf

REACTION	RESULT	EXCITATION ENERGY	SOURCE		DETECTOR		ANGLE
			TYPE	RANGE	TYPE	RANGE	
E,E/P	SPC	0*130	D	700	MAG-D		DST

Abstract: Information on proton hole states has been obtained for ^{27}Al, ^{40}Ca and ^{51}V through the (e, e'p) reaction. Lower-lying hole states have been identified. For ^{40}Ca an extensive analysis has been performed to study the structure of the 1s hole state. For ^{27}Al and ^{51}V, the properties of the 1s hole states have also been determined. The separation energies of the 1p and 1s states seem to be constant (40 and 60 MeV, respectively) for $A > 30$.

*SEPARATION ENERGY

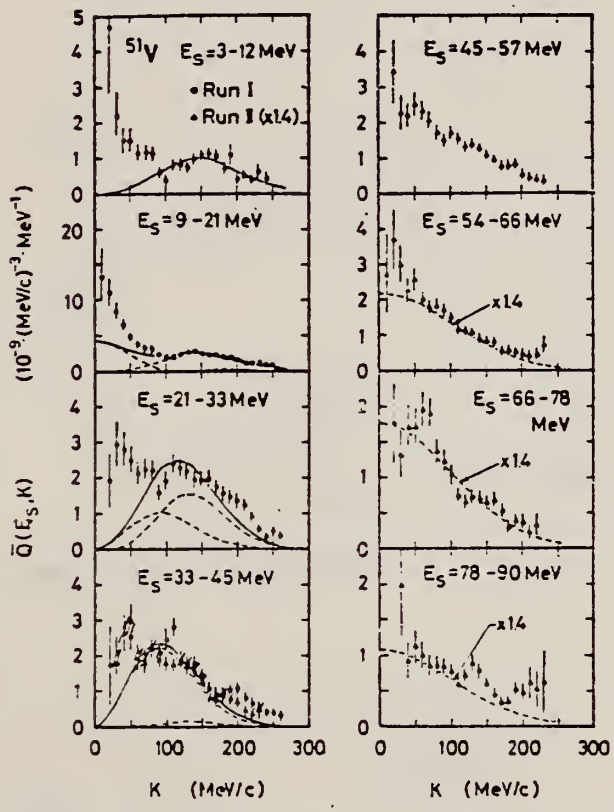

Fig. 5b. Recoil momentum distributions for ^{51}V. The curves are as in fig. 4a.

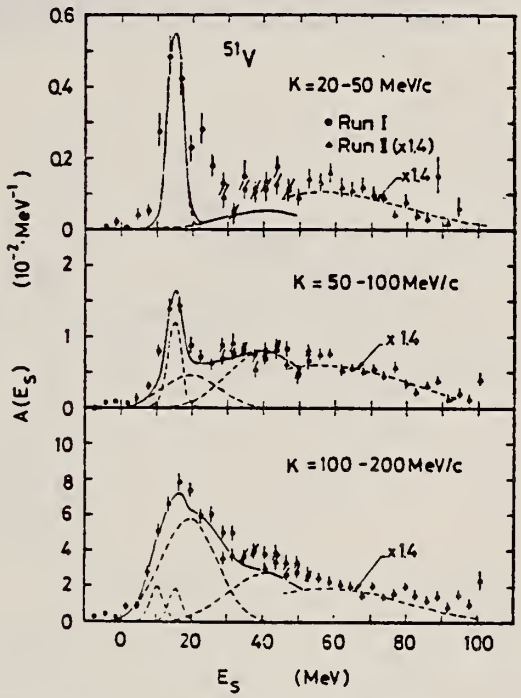

Fig. 5a. Proton separation energy spectra for ^{51}V. The curves are as in fig. 4a.

(over)

TABLE 6

Results of the PWIA analysis

Nucleus	α	Z'_α	Peak energy (MeV)	Width (FWHM) [a] (MeV)	Oscillator const (MeV/c)
^{27}Al	2s	0.12±0.01	14.3±0.2	4± 3	82±4
	1d	1.6 ±0.1	14.0±0.6	12± 2	91±1
	1p	2.4 ±0.2	34 ±1	31± 3	100±1
	1s [b]		57 ±3	31± 9	148±4
^{40}Ca	$1d_{3/2}$	1.1 ±0.3	10.9±0.7	9± 1	76±4
	2s	0.9 ±0.1	14.4±0.3	13± 1	83±3
	$1d_{5/2}$	1.5 ±0.3	19.0±1.1	10± 1	93±4
	1p	1.8 ±0.4	35 ±1	21± 3	85±3
	1s [b]		59 ±3	34±10	144±6
^{51}V	1f	0.4 ±0.1	10.3±1.1	5± 3	115±8
	2s	0.3 ±0.1	15.1±0.2	5± 2	99±5
	1d	1.7 ±0.3	19.5±0.5	19± 2	94±6
	1p	1.1 ±0.1	40 ±1	25± 4	91±4
	1s [b]		60 ±3	36±11	143±4

The errors are statistical only except for those assigned to the peak energies and widths for the 1s states.

[a] The experimental energy resolution (≈ 7 MeV) is not unfolded.

[b] Parameters were determined from the fit to the data of run II.

REF.

I. Blomqvist, P. Janecek, G. G. Jonsson, H. Dinter, K. Tesch, N. Freed, P. Ostrander
Phys. Rev. C15, 988 (1977)

ELEM. SYM.	A	Z
V	51	23

METHOD

REF. NO. 77 B1 2 hmg

REACTION	RESULT	EXCITATION ENERGY	SOURCE		DETECTOR		ANGLE
			TYPE	RANGE	TYPE	RANGE	
E,PI+	ABX	150-577	D	131-577	ACT-I		4PI
G,PI+	ABY	150-577	D	131-577	ACT-I		4PI
E,PI-	ABY	150-577	D	131-577	ACT-I		4PI
G,PI-	ABY	150-577	D	131-577	ACT-I		4PI

Cross sections for electroproduction and photoproduction of charged pions on ^{27}Al and ^{51}V have been measured in the energy region 130–580 MeV by use of the activation method. Special care has been taken to subtract out background yields. Photoproduction cross sections have been calculated from the region just above threshold to the tail of the (3,3) resonance. π-nucleus final state interactions are taken into account through optical potentials. Calculated photoproduction cross sections are decomposed into multipoles which are used to derive relative bremsstrahlung-induced to electron-induced yields. The pronounced effect of final state interactions is pointed out and discussed.

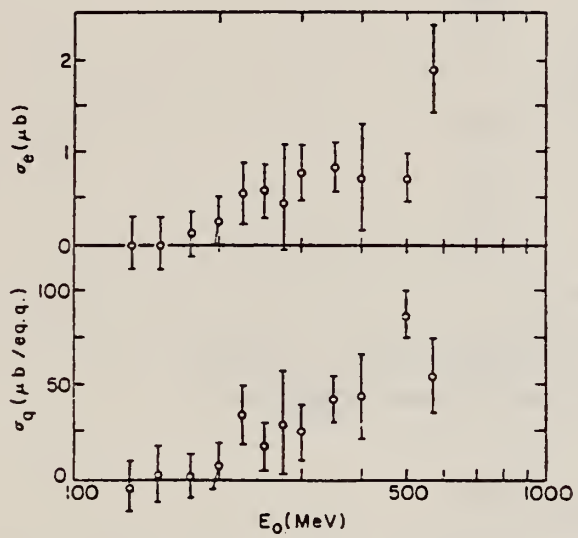

FIG. 5. σ_q and σ_e for the reactions $^{51}V(\gamma,\pi^-)^{51}Cr$ and $^{51}V(e,e'\pi^-)^{51}Cr$. See Fig. 3.

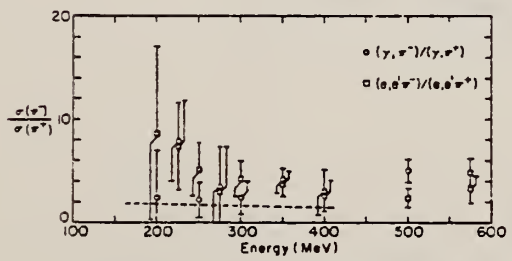

FIG. 11. Ratio of negative to positive pion electroproduction and photoproduction cross sections on ^{51}V. The dashed line is the calculated ratio with fsi absent.

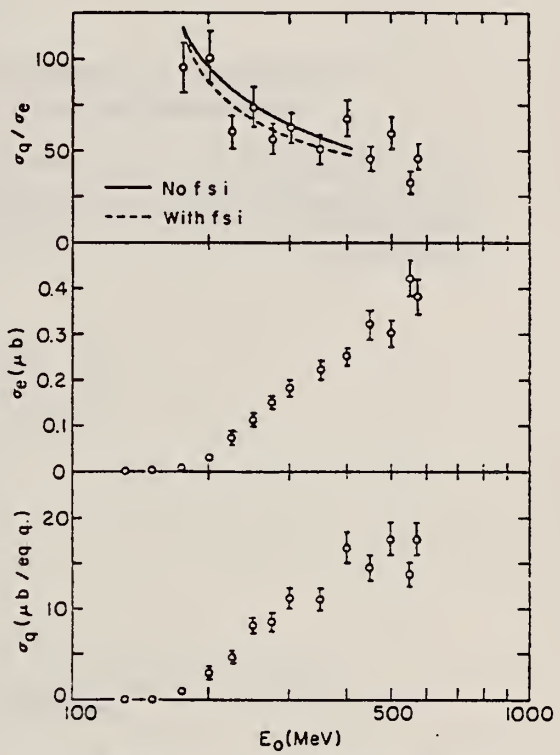

FIG. 4. Same as Fig. 3 for the reactions $^{51}V(\gamma,\pi^+)^{51}Ti$ and $^{51}V(e,e'\pi^+)^{51}Ti$.

(over)

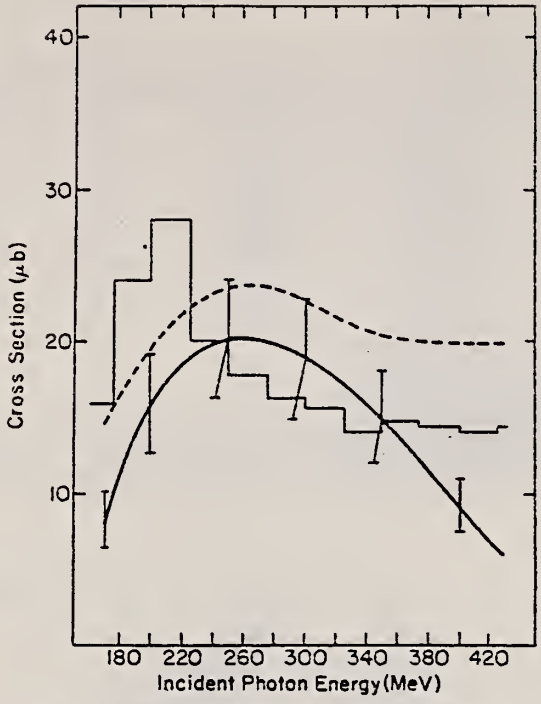

FIG. 7. Experimental cross sections per photon for the reaction $^{51}V(\gamma, \pi^+)^{51}Ti$. The solid curve with error bars is the result of the present work. The dashed curve is the work of Ref. 13. The histogram represents the data of Ref. 14.

[13] G. Nydahl et al., Nucl. Phys. B7, 97 (1968).
[14] I. Blomqvist et al., Nucl. Phys. A162, 193 (1971).

REF.

A.S. Danagulyan, N.A. Demekhina and G.A. Vartapetyan
Nucl. Phys. A285, 482 (1977)

ELEV. SYM.	A	Z
V	51	23

METHOD

REF. NO.	
77 Da 3	egf

REACTION	RESULT	EXCITATION ENERGY	SOURCE		DETECTOR		ANGLE
			TYPE	RANGE	TYPE	RANGE	
G,SPL	ABY	THR * 5	C	2*5	ACT-I		4PI

*ENERGY,GEV

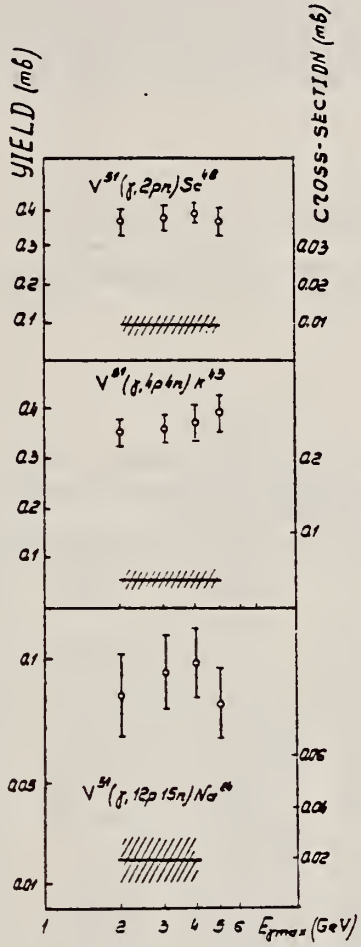

Fig. 2. Yields of some spallation reactions in ^{51}V, ^{55}Mn and Cu targets. The cross section estimates are obtained in the $1/E$ approximation for bremsstrahlung.

(over)

U.S. DEPARTMENT OF COMMERCE
NATIONAL BUREAU OF STANDARDS

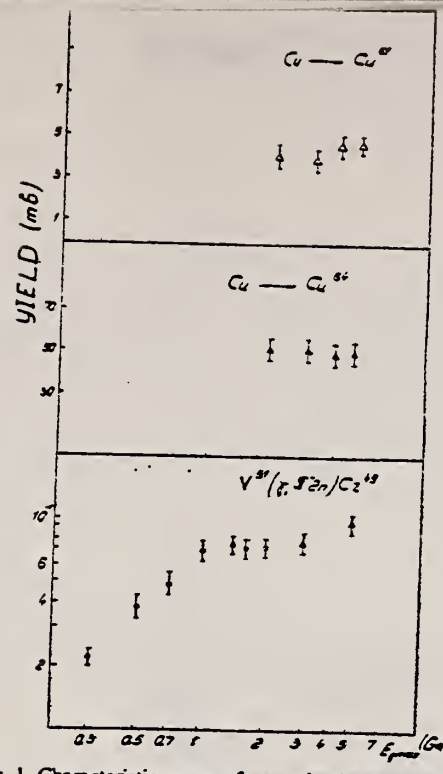

Fig. 1. Characteristic curves of some simple reaction yields.

TABLE 2

Photospallation reaction yields (mb per eq. quantum)

Residual nuclei	Reaction yields (mb)					Reaction cross sections (mb)
	$E_{\gamma max}$ = 2 GeV (exp)	3 GeV (exp)	4 GeV (exp)	5 GeV (exp)	5 GeV (cal)	
			^{51}V target			
^{49}Cr		0.081 ±0.008		0.1 ±0.01		
^{48}V	1.15 ±0.13	1.19 ±0.13	1.25 ±0.15	1.2 ±0.2	1.13	0.0798 ±0.038
^{48}Sc	0.37 ±0.04	0.38 ±0.04	0.39 ±0.03	0.37 ±0.04	0.464	0.0092 ±0.0044
^{47}Sc	1.68 ±0.1	1.65 ±0.08	1.74 ±0.1	1.6 ±0.2	1.44	
^{46}Sc	2.05 ±0.3	2.14 ±0.3	2.03 ±0.2	2.0 ±0.3	2.95	
^{44}Sc	0.55 ±0.06	0.45 ±0.06	0.57 ±0.07	0.56 ±0.07	1.03	
^{44m}Sc	0.47 ±0.03	0.47 ±0.03	0.44 ±0.04	0.46 ±0.04		
^{43}Sc	0.2 ±0.025	0.191 ±0.025	0.217 ±0.02	0.185 ±0.02	0.25	
^{44}K			≦ 0.029		0.093	
^{43}K	0.34 ±0.03	0.351 ±0.03	0.36 ±0.04	0.38 ±0.04	0.335	0.0345 ±0.0166
^{42}K	0.6 ±0.06	0.54 ±0.06	0.55 ±0.06	0.53 ±0.08	0.88	
^{39}Cl	0.06 ±0.009	0.068 ±0.009	0.061 ±0.009	0.074 ±0.01	0.077	0.0086 ±0.004
^{38}Cl		0.14 ±0.02	0.19 ±0.04	0.17 ±0.02	0.24	
^{24}Na	0.085 ±0.2	0.094 ±0.02	0.098 ±0.02	0.082 ±0.015	0.04	0.019 ±0.009

Calculated values are obtained using Rudstam's formula. Cross section estimates are made in the $1/E$ approximation.

REF.

V. di Napoli, M.L. Terranova, H.G. de Carvalho, J.B. Martins
J.D. Pinheiro Filo and O.A.P. Tavares
J. Inorg. Nucl. Chem. 39, 1727 (1977)

ELEM. SYM.	A	Z
V	51	23

METHOD

REF. NO. 77 Di 6 egf

REACTION	RESULT	EXCITATION ENERGY	SOURCE		DETECTOR		ANGLE
			TYPE	RANGE	TYPE	RANGE	
G,3N	ABY	THR-999	C	300-999	ACT-I		4PI

Abstract—Cross sections per equivalent quantum, in the energy range 0.3–1.0 GeV, have been measured for $^{209}Bi(\gamma, 2n)$, $^{209}Bi(\gamma, 3n)$, $^{209}Bi(\gamma, 4n)$, $^{59}Co(\gamma, 2n)$, $^{59}Co(\gamma, 3n)$, $^{59}Co(\gamma, 4n)$ and $^{51}V(\gamma, 3n)$ reactions. From the calculated mean absolute cross sections and the data already available in literature for (γ, xn) reactions $(x \geq 1)$, a cross section formula has been deduced which reproduces, within a factor of two, most of the experimental cross sections for target nuclei ranging between ^{9}Be and ^{238}U.

999=1 GeV

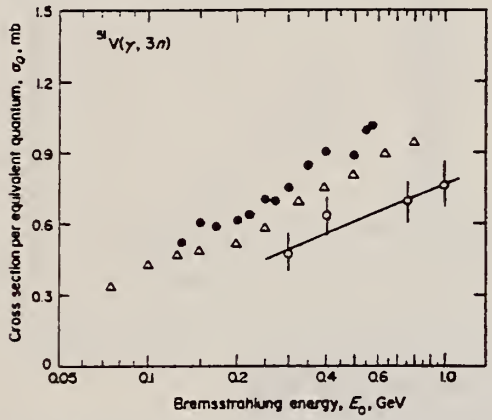

Fig. 1. Yields for the $^{51}V(\gamma, 3n)$ reaction. Open circles present experiment; filled circles from Ref. [17]; open triangles from Ref. [18]. The straight line is a least-squares fit of the present work experimental points.

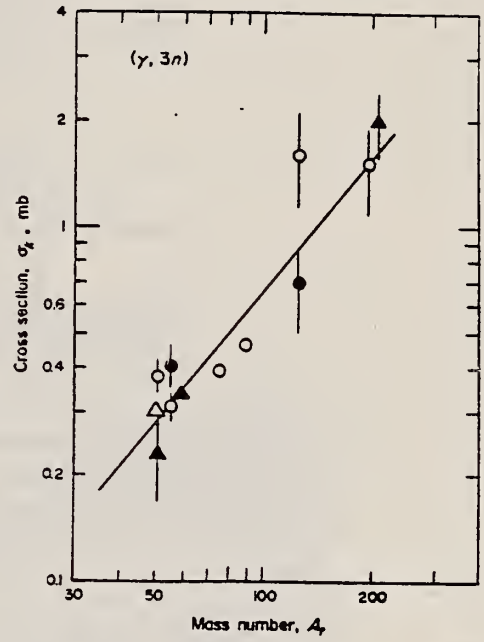

Fig. 5. The same as in Fig. 4 for the $(\gamma, 3n)$ reactions. Filled circles are taken from our earlier experiments: ^{55}Mn, Ref. [7]; ^{127}I, Ref. [3]. Open circles: ^{51}V, Ref. [17]; ^{55}Mn, Ref. [11]; ^{75}As, Ref. [12]; ^{89}Y, Ref. [14]; ^{127}I, Ref. [9, 10, 13]; ^{197}Au, Ref. [15]. Open triangle: ^{51}V, Ref. [18]. Filled triangles are the results of the present work for ^{51}V, ^{59}Co and ^{209}Bi. The straight line is a least-squares fit of the experimental points.

over

Table 2. Mean absolute cross sections for the (γ, xn) reactions with $1 < x < 5$, in complex nuclei at intermediate energies.

Target nucleus	Reaction	Energy-range (GeV)	Ref.	Cross section, $\bar{\sigma}_k$(mb) (Experimental)	(Calc.†)
^{9}Be	$(\gamma, 2n)$	0.3–1.0	8	0.021 ± 0.002	0.007
^{12}C	$(\gamma, 2n)$	0.2–0.8	16	0.0277 ± 0.0004	0.025
^{16}O	$(\gamma, 2n)$	0.2–0.8	16	0.0113 ± 0.0003	0.072
^{51}V	$(\gamma, 3n)$	0.3–1.0	This work	0.23 ± 0.06	0.268
		0.25–0.60	17	0.38 ± 0.04	0.268
		0.25–0 80	18	0.307 ± 0.012	0.268
^{55}Mn	$(\gamma, 3n)$	0.3–1.0	7	0.41 ± 0.05	0.33
		0.3–0.8	11	0.311 ± 0.016	0.33
	$(\gamma, 4n)$	0.3–1.0	7	0.053 ± 0.004	0.079
^{59}Co	$(\gamma, 2n)$	0.4–1.0	This work	1 ± 1	1.3
	$(\gamma, 3n)$	0.3–1.0	This work	0.337 ± 0.007	0.4
	$(\gamma, 4n)$	0.3–1.0	This work	0.06 ± 0.01	0.1
^{75}As	$(\gamma, 3n)$	0.2–0.9	12	0.39	0.7
	$(\gamma, 4n)$	0.2–0.9	12	0.24	0.24
^{89}Y	$(\gamma, 3n)$	0.25–1.0	14	0.47	1.0
^{103}Rh	$(\gamma, 2n)$	0.4–0.9	4, 6	5.1 ± 2.4	2.7
^{127}I	$(\gamma, 2n)$	0.1–0.8	9	7.4‡	3.4
		0.3–1.0	3	20 ± 7	3.4
	$(\gamma, 3n)$	0.3–1.0	3	0.7 ± 0.2	1.9
		0.25–0.9	9, 10, 13	1.6 ± 0.5	1.9
	$(\gamma, 4n)$	0.25–0.9	9, 10, 13	1.4 ± 0.4	1.0
^{197}Au	$(\gamma, 2n)$	0.3–0.9	15	2 ± 2	5.2
		0.3–1.0	5	7 ± 5	5.2
	$(\gamma, 3n)$	0.3–0.9	15	1.5 ± 0.4	3.6
^{209}Bi	$(\gamma, 2n)$	0.3–1.0	This work	6 ± 1	5.5
	$(\gamma, 3n)$	0.3–1.0	This work	2.0 ± 0.4	3.8
	$(\gamma, 4n)$	0.3–1.0	This work	1.3 ± 0.2	2.5

†Calculated values according to eqn (12)
‡Deduced value from the interpolated σ_Q curve as indicated in Ref. [9].

3. V. di Napoli, F. Dobici, F. Salvetti and H. G. de Carvalho, *Nuovo Cimento* 43B, 1 (1967).
4. V. di Napoli, D. Margadonna, F. Salvetti, H. G. de Carvalho and J. B. Martins, *Lett. Nuovo Cimento* 1, 308 (1969).
5. V. di Napoli, A. M. Lacerenza, D. Margadonna, F. Salvetti, H. G. de Carvalho and J. B. Martins, *Lett. Nuovo Cimento* 1, 65 (1971).
6. C. Aurisicchio, V. di Napoli, F. Salvetti and M. L. Terranova, *Gazz. Chim. Ital.* 102, 378 (1972).
7. H. G. de Carvalho, J. B. Martins, O. A. P. Tavares, V. di Napoli, F. Salvetti, *Proceedings of the International Conference on Photonuclear Reactions and Applications*, Pacific Grove, Cal., Sect 8C5-1 (1973); V. di Napoli, J. B. Martins, G. Persichelli and M. L. Terranova, *Lett. Nuovo Cimento* 11, 179 (1974).
8. V. di Napoli, M. L. Terranova, H. G. de Carvalho and J. B. Martins, *Gazz. Chim. Ital.* 104, 463 (1974).
9. G. G. Jonsson and B. Forkman, *Nucl. Phys.* A107, 52 (1968).
10. G. G. Jonsson, B. Forkman and K. Lindgren, *Phys. Lett.* 26B, 508 (1968).
11. G. Andersson, B. Forkman and B. Friberg, Report LUNP 6901, Lund Institute of Technology, Lund University, p. 4, Sect. 8, 1969 (unpublished).
12. G. Andersson and B. Forkman, Annual Report, University of Lund, Lund Institute of Technology, p. 48, (1970) (unpublished).
13. G. G. Jonsson and B. Persson, *Nucl. Phys.* A153, 32 (1970).
14. J. Sternby, Report LUNP 7011, Lund Institute of Technology, Lund University, September 1970 (unpublished). Also quoted in G. G. Jonsson and K. Lindgren, *Phys. Scr.* 7, 49 (1973).
15. K. Lindgren and G. G. Jonsson, *Nucl. Phys.* A166, 643, (1971).
16. B. Johnsson, M. Nilsson and K. Lindgren, University of Lund Report LUNFD6/NFFR-3005/1-18/, LUTFD 6/(TFKF-3003/1-18/, October (1976).
17. L. Blomqvist, P. Janeček, G. G. Jonsson, R. Petersson, H. Dinter and K. Tesch, *Z. Physik* A278, 83 (1976).
18. B. Bülow, B. Johnsson, M. Nilsson and B. Forkman, *Z. Physik* A278, 89 (1976).
19. G. G. Jonsson and K. Lindgren, *Phys. Scr.* 7, 49 (1973).
20. G. G. Jonsson and K. Lindgren, *Nucl. Phys.* A141, 355 (1970).
21. T. A. Gabriel and R. G. Alsmiller, Jr., *Phys. Rev.* 182, 1035 (1969).
22. V. S. Barashenkov, F. G. Gereghi, A. S. Iljinov, G. G. Jonsson, and V. D. Toneev, *Nucl. Phys.* A231, 462 (1974).
23. V. di Napoli, D. Margadonna, F. Salvetti, H. G. de Carvalho, and J. B. Martins, *Nucl. Instr. Methods* 93, 77 (1971).
24. C. M. Lederer, J. B. Hollander and I. Perlman, *Table of Isotopes*. Wiley, New York (1967).
25. V. di Napoli, F. Salvetti, M. L. Terranova, H. G. de Carvalho and J. B. Martins, *Phys. Rev.* C8, 206 (1973); V. di Napoli, A. M. Lacerenza, F. Salvetti, S. M. Terenzi, H. G. de Carvalho and J. B. Martins, *J. Inorg. Nucl. Chem.* 35, 1419 (1973).

REF. V.S. Kuz'menko, A.V. Mitrofanova, V.I. Noga, Yu.N. Ranyuk, P.V. Sorokin, Yu.N. Telegin, I. Blomqvist, G.G. Jonsson, and N. Freed
Phys. Rev. C 16, 1513 (1977)

ELEM. SYM.	A	Z
V	51	23

METHOD

REF. NO. 77 Ku 3 hmg

REACTION	RESULT	EXCITATION ENERGY	SOURCE		DETECTOR		ANGLE
			TYPE	RANGE	TYPE	RANGE	
E,PI+	RLX	150-999	C	600-999	ACT-I		4PI

Cross sections for photoproduction and electroproduction of π^+ on ^{27}Al and ^{51}V leading to bound states in the daughter nuclei have been measured at Kharkov in the energy range 600–1200 MeV by use of the activation method. Careful comparison is made to other recent results obtained at intermediate and high energies. Agreement is found between the present data and results of earlier work carried out at Lund and DESY. Discrepancies between photoproduction data taken at different laboratories are attributed to differences between methods of background subtraction. Relative bremsstrahlung-induced to electron-induced yield ratios are compared with predictions based on the Dalitz-Yennie formalism for virtual-photon spectra.

999=1.2 GeV,Ratio σ/E

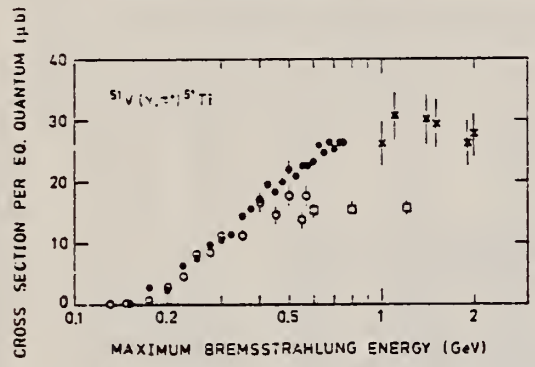

FIG. 3. Same as Fig. 2 for the reaction $^{51}V(\gamma,\pi^+)^{51}Ti$. □, present work; ○, Ref. 2; ●, Ref. 10; ×, Ref. 15.

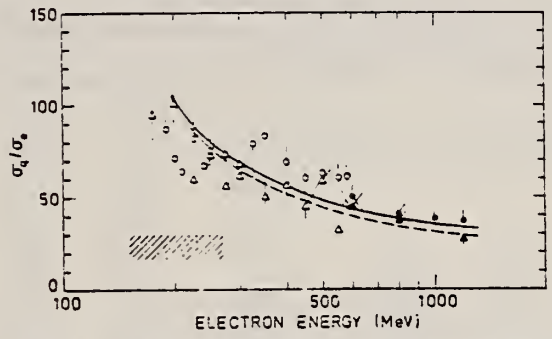

FIG. 6. The cross section ratio σ_q/σ_e versus electron energy. ^{27}Al—^{27}Mg: ●, present work; ○, Ref. 2; hatched region, Ref. 11. ^{51}V—^{51}Ti: ▲, present work; △, Ref. 2. The solid and dashed curves are calculated results assuming $E1$ and $M1$ transitions, respectively.

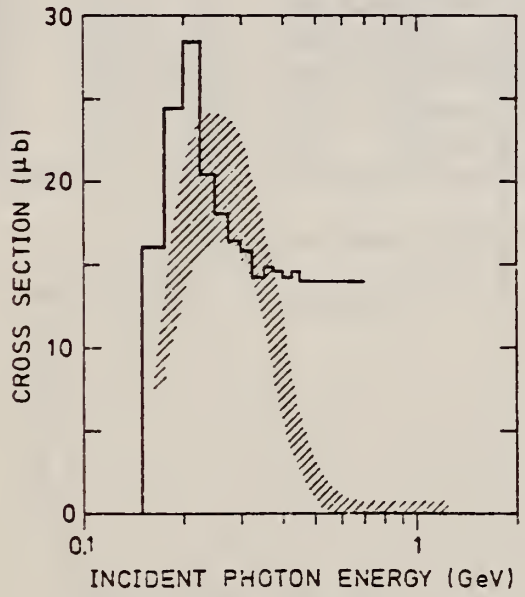

FIG. 5. Same as Fig. 4 for the reaction $^{51}V(\gamma,\pi^+)^{51}Ti$. The hatched area represents the present work with uncertainties indicated. The histogram is from Ref. 10.

[2] I. Blomqvist, P. Janecek, G.G. Jonsson, H. Dinter K. Tesch, n. Freed, and P. Ostrander, Phys.Rev. C15, 988 (1977); DESY Report No. 76/51 (umpublished)

[10] I. Blomqvist, G. Nydahl, and B. Forkman, Nucl. Phys. A162, 193 (1971)

[11] V.I. Noga, Yu. Ranyuk, P.V. Sorokin, and V.A. Tkachenko, Yad. Fiz. 14, 904 (1971) [Sov. J. Nucl. Phys. 14, 506 (1972)]

[15] G. Kumbartzki and U. Kim, Nucl. Phys. A176, 23 (1971)

REF. A.S. Danagulyan, N.A. Demekhina
Yad. Fiz. 27, 877 (1978)
Sov. J. Nucl. Phys. 27, 466 (1978)

ELEM. SYM.	A	Z
V	51	23

METHOD

REF. NO.	
78 Da 13	hg

REACTION	RESULT	EXCITATION ENERGY	SOURCE		DETECTOR		ANGLE
			TYPE	RANGE	TYPE	RANGE	
G,2P5N	ABX	THR*5	C	2*5	ACT-D		4PI

*GEV, ISOMER YLD

We discuss data concerning the ratios of the yields of different isomeric states in the elements ^{44}Sc and ^{52}Mn. Experimental results are presented for measurement of the yields of ^{44g,m}Sc and ^{52g,m}Mn in disintegration of targets of ^{51}V, ^{55}Mn, and Cu by photons with energies from 2 to 5 GeV; theoretical values of yields for these elements were obtained by means of the five-parameter Rudstam formula. The pattern of formation of high-spin states in photodisintegration reactions is discussed in terms of the cascade-evaporative model.

PACS numbers: 25.20. + y, 27.40. + z

TABLE I.

Type of target	Isomeric states	Yield, mb				
		Experiment				Theory
		$E_{\gamma max}$ = 2 GeV	3 GeV	4 GeV	5 GeV	5 GeV
^{51}V	^{44m}Sc	0.47±0.03	0.47±0.03	0.44±0.04	0.46±0.04	1.03
	^{44g}Sc	0.55±0.06	0.45±0.06	0.57±0.07	0.56±0.07	
^{55}Mn	^{44m}Sc	0.45±0.04	0.47±0.04	0.42±0.05	0.55±0.05	1.3
	^{44g}Sc	0.42±0.04	0.42±0.04	0.55±0.1	0.45±0.05	
^{55}Mn	^{52m}Mn	0.48±0.05	0.43±0.04	0.6±0.06	0.48±0.05	1.34
	^{52g}Mn	0.55	0.55	0.55	0.55	
Cu	^{44m}Sc	0.25±0.03	0.27±0.03	0.26±0.026	0.24±0.03	0.35
	^{44g}Sc	–	0.13±0.01	0.15±0.02	0.14±0.05	
Cu	^{52m}Mn	–	–	0.128±0.01		0.55
	^{52g}Mn	0.55±0.05	0.47±0.05	0.525±0.05	0.473±0.05	

TABLE II.

Type of target	Photon energy, MeV	Isomeric yield ratio	Remarks
		^{44m}Sc/^{44g}Sc	
^{51}V	65–300	0.75±0.03	[11]
	100–800	0.88	[10]
	2000–5000	0.87±0.04	Present work
^{54,56}Fe	250	0.61±0.02	[7]
	250–300	1.03±0.05	[8]
^{55}Mn	225	0.72	[7]
	300	0.64	[7]
	250–800	1.09±0.04	[8]
	2000–5000	1.02±0.02	Present work
^{59}Co	250–800	1.24±0.06	[8]
Cu	2000–5000	1.84±0.16	Present work
^{75}As	250–800	1.9±0.3	[8]
		^{52g}Mn/^{52m}Mn	
^{54,56}Fe	70	0.47	[7]
	100–250	0.56	[7]
^{55}Mn	100–300	0.88	[7]
	2000–5000	1.12±0.1	Present work
^{59}Co	150	1.62	[7]
Cu	4000	4.1±0.4	Present work

REF. V. di Napoli, F. Salvetti, M. L. Terranova, H. G. de Carvalho, J. B. Martins, O. A. P. Tavares
J. Inorg. Nucl. Chem. 40, 175 (1978)

ELEM. SYM.	A	Z
V	51	23

METHOD

REF. NO. 78Di12 hg

REACTION	RESULT	EXCITATION ENERGY	SOURCE TYPE	SOURCE RANGE	DETECTOR TYPE	DETECTOR RANGE	ANGLE
G,SPL	ABY	THR-999	C	300-999	ACT-I		4PI

Abstract—Cross sections per equivalent quantum, in the energy range 0.3–1.0 GeV, have been measured for spallation residuals from ^{51}V, ^{55}Mn, natural Fe, and ^{59}Co targets. Mean cross sections per photon have been deduced in this energy range and the data analysed in terms of charge-dispersion curves and mass-yield distributions. The mean cross sections per photon have also been compared with a semiempirical Rudstam's formula. A satisfactorily good agreement has been found with the calculated yields within a factor of two.

YLDS 24NE TO 49CR

Table 2. Yields of radionuclides in units of μb per equivalent quantum. Vanadium target

Nuclide	E_0(GeV) 0.30	0.40	0.50	0.60	0.75	0.90	1.00
^{24}Ne	1.4 ± 0.3	2.0 ± 0.4	2.5 ± 0.4	2.6 ± 0.4	3.4 ± 0.4	3.5 ± 0.4	3.8 ± 0.4
^{24}Na	10 ± 3	20 ± 4	25 ± 4	25 ± 4	28 ± 4	32 ± 4	30 ± 4
^{24}Na	2.0 ± 0.4	8.0 ± 1.2	15.0 ± 1.8	20 ± 2	25 ± 2	32 ± 2	34 ± 2
^{27}Mg	3.0 ± 0.6	10 ± 1	15 ± 2	20 ± 2	25 ± 2	28 ± 2	30 ± 2
^{28}Mg	1.5 ± 0.5	2.5 ± 0.8	3.8 ± 0.8	5.0 ± 0.8	6.5 ± 0.9	7.5 ± 0.9	8 ± 1
^{28}Al	12 ± 4	25 ± 5	35 ± 5	50 ± 6	60 ± 7	75 ± 9	80 ± 10
^{29}Al	10 ± 3	17 ± 4	20 ± 5	25 ± 3	34 ± 4	37 ± 4	40 ± 5
^{34}Cl^m	1.0 ± 0.3	5.2 ± 1.3	9.0 ± 1.8	12.0 ± 1.4	15.0 ± 1.8	18 ± 2	20 ± 3
^{38}Cl	40 ± 10	60 ± 9	80 ± 12	90 ± 13	110 ± 13	120 ± 14	130 ± 16
^{39}Cl	15 ± 5	25 ± 7	35 ± 6	40 ± 6	50 ± 6	55 ± 6	60 ± 6
^{41}Ar	20 ± 4	40 ± 6	50 ± 6	65 ± 6	80 ± 8	90 ± 8	100 ± 10
^{42}K	200 ± 30	250 ± 40	350 ± 42	420 ± 50	417 ± 40	500 ± 50	540 ± 55
^{43}K	50 ± 7	83 ± 12	120 ± 18	150 ± 18	176 ± 20	200 ± 30	190 ± 30
^{44}K	35 ± 10	45 ± 14	50 ± 15	60 ± 15	65 ± 15	72 ± 12	75 ± 12
^{45}K	1.0 ± 0.3	4 ± 1	7 ± 2	9 ± 2	11 ± 2	13 ± 3	15 ± 3
^{47}Ca	10 ± 3	13 ± 4	15 ± 5	18 ± 4	19 ± 4	25 ± 5	23 ± 5
^{43}Sc	20 ± 3	44 ± 7	80 ± 10	100 ± 12	107 ± 10	130 ± 10	150 ± 10
^{44}Sc^m	214 ± 20	300 ± 30	350 ± 40	400 ± 40	475 ± 40	500 ± 40	525 ± 40
^{44}Sc^g	250 ± 20	320 ± 30	350 ± 40	410 ± 40	470 ± 40	490 ± 40	530 ± 40
^{46}Sc	714 ± 70	950 ± 76	1000 ± 100	1100 ± 100	1200 ± 100	1400 ± 100	1430 ± 100
^{47}Sc	1100 ± 100	1300 ± 100	1300 ± 100	1400 ± 110	1500 ± 110	1600 ± 100	1700 ± 100
^{48}Sc	120 ± 10	200 ± 16	200 ± 16	250 ± 15	260 ± 15	300 ± 15	346 ± 15
^{48}V	470 ± 40	630 ± 50	630 ± 50	650 ± 50	690 ± 50	740 ± 50	760 ± 50
^{48}Cr	56 ± 10	63 ± 12	65 ± 13	70 ± 10	75 ± 10	77 ± 10	80 ± 10
^{49}Cr	15 ± 3	20 ± 4	23 ± 4	25 ± 5	28 ± 5	30 ± 5	31 ± 5

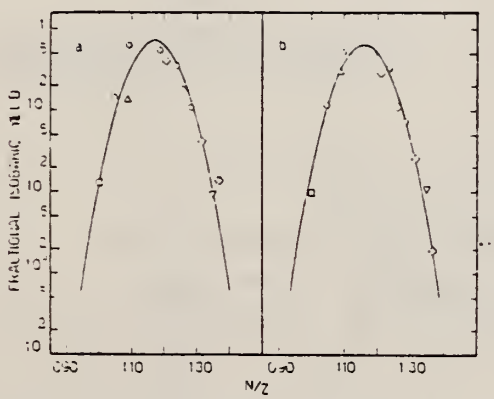

Fig. 1. Fractional isobaric yield vs the N/Z ratio for $42 \le A \le 48$. Mean cross sections per photon in the energy range 0.3–1 GeV. Graph (a): ^{51}V target; (b): ^{55}Mn target. The symbols are: □, for Cr; ○, for Sc; △, for V; ◇, for K; ▽, for Ca isotopes.

Table 6. Mean cross sections in the energy range 0.3–1 GeV in units of μb

Produced radionuclide	Target nucleus: Vanadium Present work	Vanadium Bülow *et al.*[26]	Manganese	Iron	Cobalt
^{24}Ne	2.0 ± 0.4				
^{24}Na	16 ± 4				
^{24}Na	30 ± 2	18 ± 2	10 ± 1	10 ± 1	7 ± 1
^{27}Mg	22 ± 2	18 ± 3	9 ± 1	10 ± 1	8 ± 1
^{28}Mg	6 ± 1	6 ± 1	2.7 ± 0.5	2.7 ± 0.5	2.2 ± 0.3
^{28}Al	58 ± 7	59 ± 4	29 ± 4	35 ± 4	25 ± 3
^{29}Al	25 ± 4	32 ± 2	11 ± 2	15 ± 2	16 ± 3
^{34}Cl^m	16 ± 2	14 ± 2	30 ± 4	30 ± 4	19 ± 3
^{38}Cl	75 ± 13	96 ± 5	45 ± 8	50 ± 8	37 ± 7
^{39}Cl	37 ± 7	35 ± 1	12 ± 2	19 ± 3	13 ± 2
^{41}Ar	65 ± 6	54 ± 2	35 ± 4	28 ± 3	12 ± 2
^{42}K	280 ± 50	243 ± 11	94 ± 17	80 ± 15	66 ± 12
^{43}K	128 ± 20	128 ± 4	43 ± 7	30 ± 5	28 ± 5
^{44}K	33 ± 12	30 ± 3	11 ± 4	10 ± 4	9.5 ± 4
^{45}K	12 ± 2	8 ± 1	1.0 ± 0.5	1.2 ± 0.5	1.0 ± 0.5
^{47}Ca	12 ± 4	15 ± 1	6.5 ± 2.4	6 ± 2	2.2 ± 0.8
^{43}Sc	104 ± 10	109 ± 6	72 ± 7	77 ± 8	52 ± 6
^{44}Sc^m	260 ± 30	243 ± 14	115 ± 15	100 ± 12	84 ± 10
^{44}Sc^g	230 ± 40	218 ± 13	116 ± 20	90 ± 16	71 ± 13
^{46}Sc	575 ± 100	605 ± 18	260 ± 45	214 ± 35	220 ± 40
^{47}Sc	457 ± 100	540 ± 33	200 ± 45	160 ± 30	127 ± 30
^{48}Sc	165 ± 15	138 ± 8	50 ± 5	30 ± 3	25 ± 3
^{48}V	210 ± 50	307 ± 12	200 ± 50	184 ± 45	100 ± 25
^{48}Cr	20 ± 10		7 ± 3	8 ± 4	5.0 ± 2.5
^{49}Cr	13 ± 5	16 ± 2	40 ± 15	64 ± 25	20 ± 8
^{51}Cr			480 ± 150	570 ± 150	330 ± 150
^{52}Mn				25 ± 5	
^{52}Mn^m				75 ± 40	49 ± 25
^{54}Mn				96 ± 40	84 ± 25
^{55}Mn				944 ± 300	584 ± 100
^{52}Fe					1.6 ± 0.8

Table 7. N/Z dispersion parameters of the mean cross sections per photon†

Target nucleus	Mass region	A_m	N/Z_p	Z_p	FWHM	ΔZ	Ref.
^{51}V	42–48	45	1.16	20.8	0.143	1.36	Present work
			1.16	20.8	0.142	1.37	[26]
			1.16	20.9	0.168	1.63	[35]
^{55}Mn	42–48	45	1.16	20.8	0.142	1.37	Present work
^{nat}Fe	42–48	45	1.16	20.8	0.140	1.35	Present work
	48–54	51	1.16	23.6	0.126	1.38	Present work
^{59}Co	42–48	45	1.16	20.8	0.141	1.36	Present work
	48–54	51	1.16	23.6	0.124	1.36	Present work

†A_m is the median mass of the mass region under consideration. N/Z_p is the neutron/proton ratio for the most probable nuclear charge Z_p of A_m. FWHM is the full width at half-maximum of the CD curves. ΔZ is the spread in Z as calculated from the FWHM for the two abscissas N/Z_1 and N/Z_2 (see also Refs. [26] and [35]).

REF. K. Masumoto, T. Kato, N. Suzuki
Nucl. Inst. Meth. 157, 567 (1978)

ELEM. SYM.	A	Z
V	51	23

METHOD

REF. NO. 78 Ma 10 hg

REACTION	RESULT	EXCITATION ENERGY	SOURCE		DETECTOR		ANGLE
			TYPE	RANGE	TYPE	RANGE	
G,A	ABY	10-68	C	30-68	ACT - I		4PI
G,AN	ABY	18-68	C	30-68	ACT - I		4PI

Analysis is made of reactions interfering with photon activation analysis procedures.

The activation yield curves have been presented for a number of photonuclear reactions in the energy range from 30 to 68 MeV, in order to evaluate quantitatively the interferences due to competing reactions in multielement photon activation analysis. The general features of the yields as functions of both target mass number and excitation energy were elucidated from the data obtained, discussion being given on the results in terms of the reaction mechanism.

Simultaneous neutron activation due to appreciable neutron production from the converter and surrounding materials has also been studied, and, finally, the magnitudes of interferences in real multielement analysis were given in the form of their energy dependences.

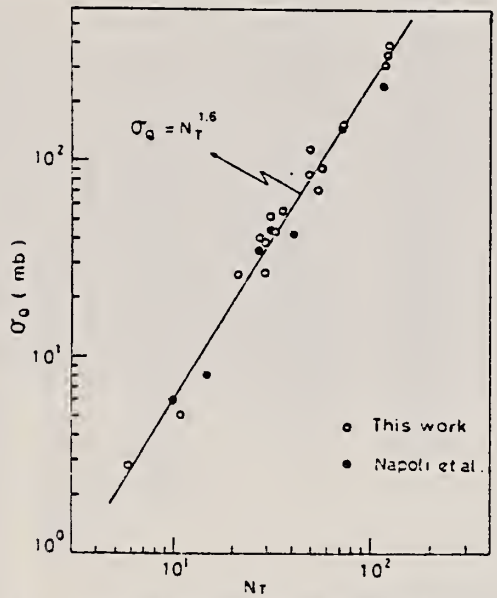

Fig. 2. Yield per equivalent quanta versus target neutron number.

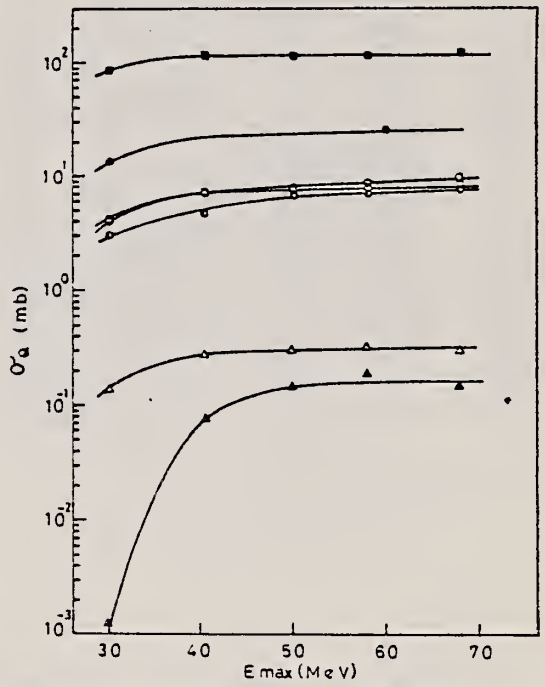

Fig. 4. Activation yield curves for the reactions on Ca, Ti and V.
■ $^{48}Ca(\gamma, n)^{47}Ca$, □ $^{44}Ca(\gamma, p)^{43}K$, ● $^{46}Ti(\gamma, n)^{45}Ti$,
○ $^{48}Ti(\gamma, p)^{47}Sc$, ◐ $^{49}Ti(\gamma, p)^{48}Sc$, △ $^{51}V(\gamma, \alpha)^{47}Sc$,
▲ $^{51}V(\gamma, zn)^{46}Sc$.

REF. H. Tsubota, S. Oikawa, J. Uegaki and T. Tamae
Nucl. Phys. A303, 333 (1978)

ELEM. SYM.	A	Z
V	51	23

METHOD

REF. NO. 78 Ts 1

REACTION	RESULT	EXCITATION ENERGY	SOURCE		DETECTOR		ANGLE
			TYPE	RANGE	TYPE	RANGE	
E,XP	ABX	15- 29	D	15- 29	MAG-D		90

Abstract: The differential cross sections of the (e, e'p) reactions for ^{51}V and ^{59}Co have been measured at 90° over the region of excitation corresponding to the electric giant dipole resonance. The (γ, p) cross sections of these nuclei were deduced from differential cross sections assuming isotropic angular distributions of protons. The results are compared with the (γ, n) cross sections, and are used to obtain strengths of the $T_<$ and $T_>$ giant dipole states separately by using the statistical theory. For each nucleus the ratio of the separated strengths and the splitting energy are consistent with those expected by the isospin formalism.

G,XP E1-VIRTUAL PHOT

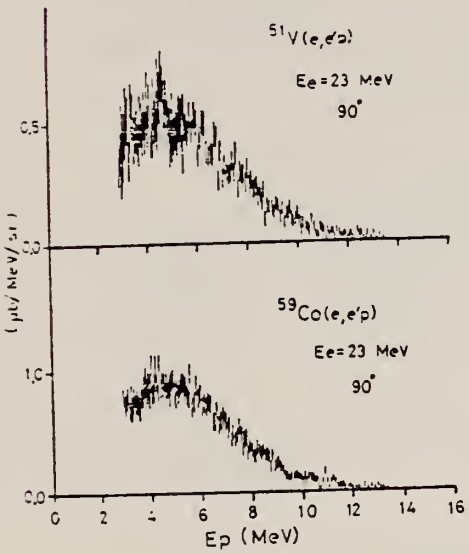

Fig. 2. Typical proton energy spectra of the (e, e'p) reactions of ^{51}V and ^{59}Co nuclei at 23.0 MeV of the incident electron energy.

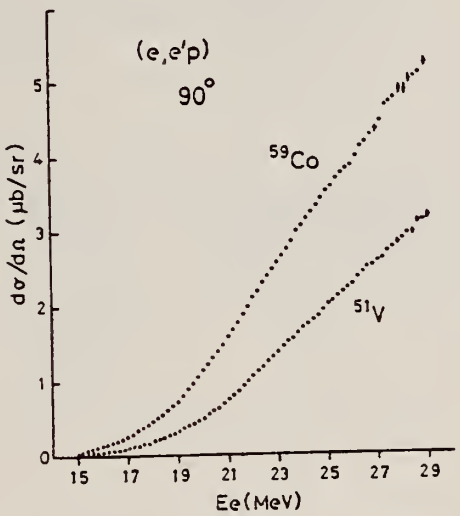

Fig. 3. Proton yield curves of the (e, e'p) reactions of ^{51}V and ^{59}Co nuclei at 90°.

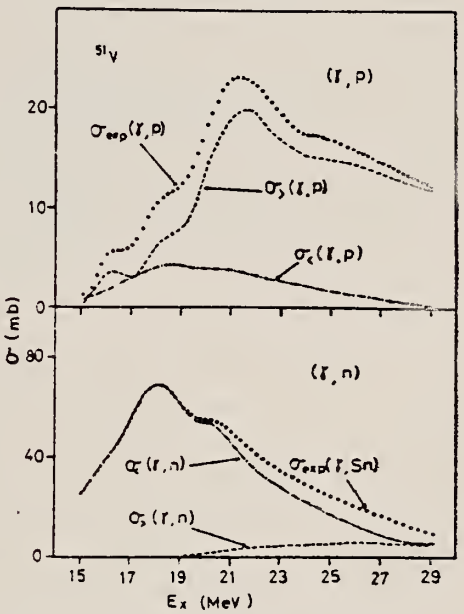

Fig. 8. Comparison between the experimental cross sections and separated isospin components of ^{51}V for (γ, p) and (γ, n) reactions. Notations are explained in the text.

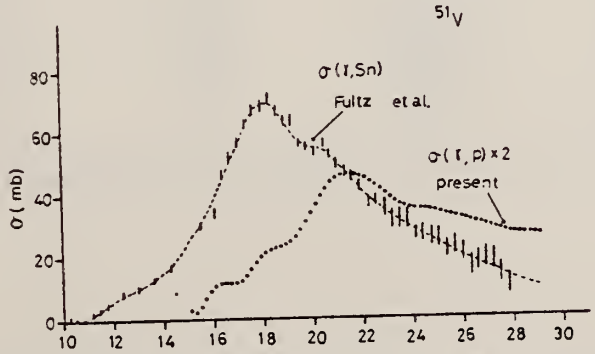

Fig. 5. Comparison between (γ, p) and (γ, Sn) cross sections [$\sigma(\gamma, \mathrm{Sn}) = \sigma(\gamma, \mathrm{n}) + \sigma(\gamma, \mathrm{np}) + \sigma(\gamma, 2\mathrm{n})$] of ^{51}V. The dashed curve is the (γ, Sn) cross section used in the present analysis.

over

TABLE 2

Summary of the parameters obtained from the differential cross sections at 90° for ^{51}V and ^{59}Co

	Range of measurement (MeV)	$\int \frac{d\sigma(\gamma, p)}{d\Omega} dE$ (MeV · mb/sr)	$4\pi \int \frac{d\sigma(\gamma, p)}{d\Omega} dE$ (MeV · mb)
^{51}V	15.0–29.0	16.32 ± 1.39	205 ± 17
^{59}Co	15.0–29.0	28.10 ± 2.00	353 ± 25

REF. H. Tsubota, S. Oikawa, J. Uegaki, T. Tamae
Nucl. Phys. A321, 157 (1979)

ELEM. SYM.	A	Z
V	51	23

METHOD

REF. NO. 79Ts2 hg

REACTION	RESULT	EXCITATION ENERGY	SOURCE		DETECTOR		ANGLE
			TYPE	RANGE	TYPE	RANGE	
G,PØ	ABX	14-26	C	15-26	MAG-D		DST

Abstract: The differential cross sections at 90° for the $^{51}V(e, p_0)^{50}Ti$ and $^{52}Cr(e, p_0+p_1)^{51}V$ reactions have been measured over the giant dipole resonance region. These cross sections were used to obtain the differential cross sections of the $^{51}V(\gamma, p_0)^{50}Ti$ and $^{52}Cr(\gamma, p_0+p_1)^{51}V$ reactions. The results show two peaks that appear at the same energies as the main peaks of the (γ, n) and (γ, p) cross section for both nuclei. The angular distributions of protons from the (e, p) reaction have also been measured at several points of the incident electron energy. The coefficients A_2 obtained by fitting with a series of Legendre polynomials, $W(\theta) = 1 + A_1 P_1(\cos\theta) + A_2 P_2(\cos\theta)$, varies with excitation energy. These results are discussed in terms of the direct-semidirect process considering isospin effects in the giant dipole resonance.

VIRTUAL PHOTON ANAL.

E NUCLEAR REACTIONS ^{51}V, $^{52}Cr(e, p_0)$, (γ, p_0), E = 15.0–26.0 MeV; measured $\sigma(E, \theta)$ at θ = 90°, measured $\sigma(E, \theta)$ at several E-values for ^{51}V and at E = 21.4 MeV for ^{52}Cr. Deduced $\sigma(E, 0)$ for $^{51}V(\gamma, p_0)$ and for $^{52}Cr(\gamma, p_0+p_1)$ at θ = 90°; natural target (^{51}V), enriched target (^{52}Cr).

TABLE 2

Experimental results of the (γ, p_0) reactions

	$\frac{d\sigma(\gamma, p_0)dE}{d\Omega}(90°)$ (MeV · mb sr)	$4\pi \frac{d\sigma(\gamma, p_0)dE}{d\Omega}$ (MeV · mb)	$\frac{d\sigma(\gamma, p)dE}{d\Omega}$ (MeV mb sr)	$\frac{d\sigma(\gamma, p_0)dE}{d\Omega} \cdot \frac{d\sigma(\gamma, p)dE}{d\Omega}$
^{51}V	0.46 ± 0.07	5.78 ± 0.88	(15–29 MeV) [b] 16.32	0.03
^{52}Cr	1.70 ± 0.22 [a]	21.36 ± 2.76 [a]	(15–29 MeV) [c] 19	0.09

[a] The (γ, p_0+p_1) cross section.
[b] Ref. [1]. [c] Ref. [24]).

TABLE 3

Coefficients obtained by fitting a series of Legendre polynomials $W(\theta) = 1 + A_1 P_1(\cos\theta) + A_2 P_2(\cos\theta)$

	E_x (MeV)	E_x (MeV)	A_1	A_2
^{51}V	17.0	15.4–16.5	0.21 ± 0.05	0.33 ± 0.09
	18.0	16.4–17.5	0.33 ± 0.04	0.33 ± 0.06
	19.0	17.4–18.5	0.28 ± 0.06	0.25 ± 0.11
	21.0	19.4–20.5	0.21 ± 0.07	0.21 ± 0.13
	22.0	20.4–21.5	0.51 ± 0.08	−0.11 ± 0.13
^{52}Cr	21.4	20.5–21.0	0.06 ± 0.07	0.05 ± 0.11

The range of the excitation energy E_x is also indicated.

(over)

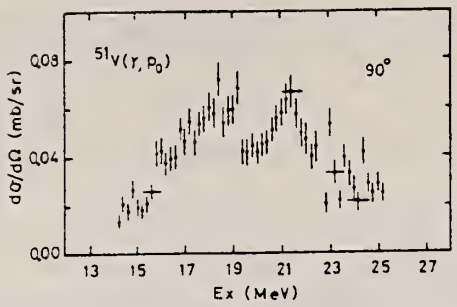

Fig. 2. The differential cross section at 90° for the $^{51}V(\gamma, p_0)^{50}Ti$ reaction.

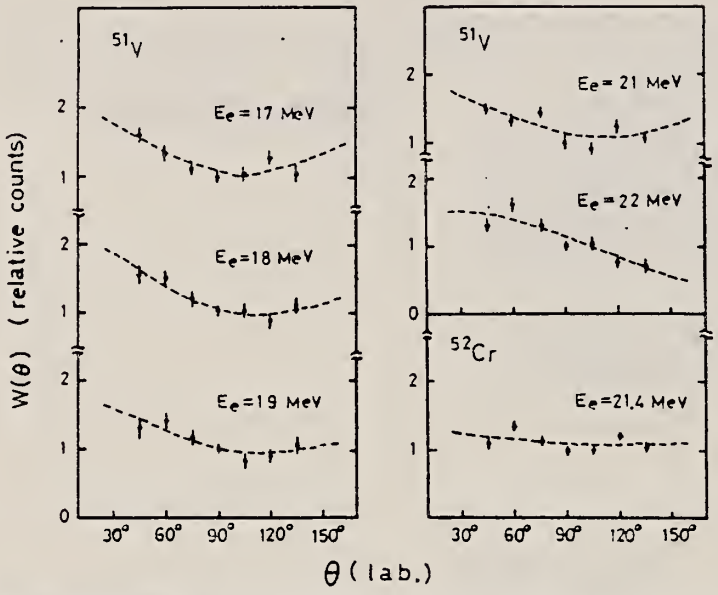

Fig. 6. The angular distributions of protons from the $^{51}V(e, p_{\cdot})^{50}Ti$ and $^{52}Cr(e, p_0 + p_1)^{51}V$ reactions. The dashed curves are the results fitted with the sum of Legendre polynomials, $W(\theta) = 1 + A_1 P_1(\cos\theta) + A_2 P_2(\cos\theta)$.

CHROMIUM
Z=24

L. N. Vauquelin first isolated chromium in 1797 from the mineral crocoite or Sibinan red lead. The name comes from the Greek word "chromos", meaning color, due to the variety of hues in its compounds. The red color of the ruby is caused by the presence of chromic oxide, which distinguishes this costly gem from common crystalline corundum.

Cr

Cr

Ref. F. Ferrero, R. Malvano, C. Tribuno
Nuovo Cimento 6, 385 (1957)

Elem. Sym.	A	Z
Cr		24

Method: Betatron; neutron yield; threshold detector

Ref. No.: 57 Fe 2 | NVB

Reaction	E or ΔE	E_o	Γ	$\int \sigma dE$	Jπ	Notes
Cr(γ,n!)	Bremss. 14-30					R = ratio between area of second maximum in cross section and first maximum. R = 0.7±0.14 Detector at 90°.

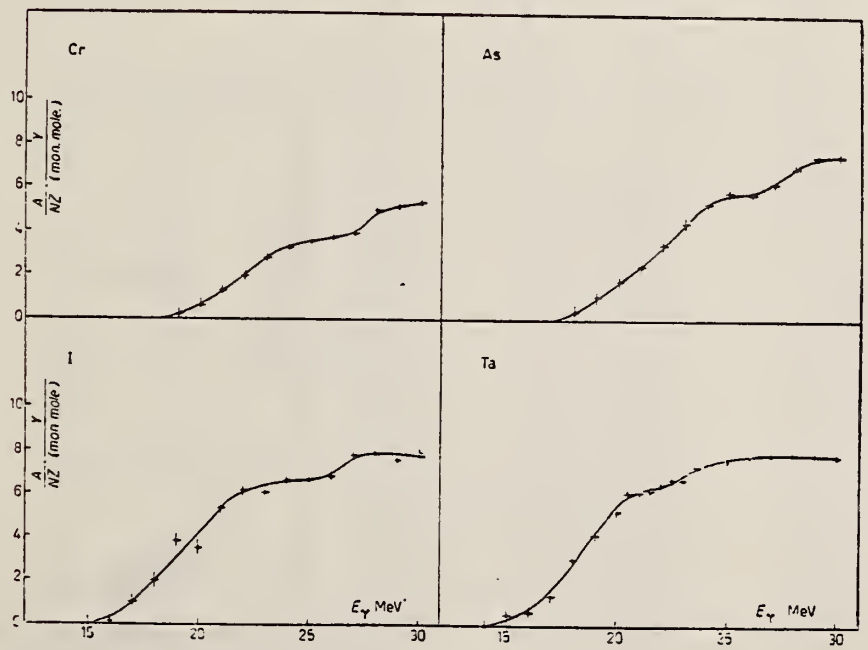

Fig. 1.

Ref. G. Cortini, C. Milone, A. Rubbino, F. Ferrero
Nuovo Cimento 9, 85 (1958)

Elem. Sym.	A	Z
Cr		24

Method: Emulsions; Betatron; ionization chamber

Ref. No.: 58 Co 1 | EH

Reaction	E or ΔE	E_o	Γ	$\int \sigma dE$	Jπ	Notes
Cr(γ,n)	Bremss 20 30					E_{th} = 11.54 MeV; 90° spectrum. Solid curve from level density formula: $\omega(E_R) = C \exp [2\sqrt{\alpha E_R}]$; $\alpha = \frac{\pi^2 A}{160}$

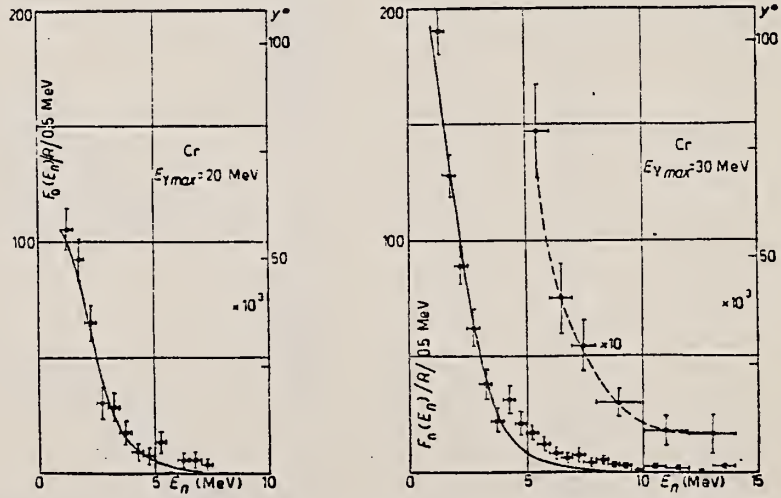

Fig. 2. – Energy spectrum of the photoneutrons from Cr. Experimental figures for the high energy tail are multiplied × 10. The continuous curve is the calculated evaporation spectrum (see text). Y* = neutrons /R/0.5 MeV/mole/ΔΩ.

Ref. E. Bellotti, A.M. Bruno
Phys. Rev. 118, 701 (1960)

Elem. Sym.	A	Z
Cr		24

Method γ's from $F^{19}(p,\alpha\gamma)$ reaction; protons from VandeGraaff; NaI.

Ref. No. 60 Re 1 JHH

Reaction	E or ΔE	E_o	Γ	$\int \sigma dE$	$J\pi$	Notes
(γ,γ)	E_γ~ 7MeV					$\langle\sigma\rangle$ (E_p=2.05MeV) = 0.30 ± .05 mb

E.G. Baker, K.G. McNeill
Can. J. Phys. 39, 1158 (1961)

ELEM. SYM.	
Cr	24

METHOD: Betatron; fast neutron yield, angular distribution; Si threshold detector; ion chamber

REF. NO.: 61 Ba 2 | NVB

REACTION	RESULT	EXCITATION ENERGY	SOURCE		DETECTOR		ANGLE
			TYPE	RANGE	TYPE	RANGE	
G,XN	ABY	THR-22	C	22	THR-I	5-+	DST

In Table 4:

$\bar{\sigma}$ = average cross section of detector weighted with neutron spectrum

$\bar{\Phi}$ = neutrons/100 roentgen/mole

$$W(\vartheta) = a_o \sum_{n=1}^{\infty} [1 + A_n P_n (\cos\theta)]$$

TABLE IV

I Element	II a_0	III a_1	IV a_2	V $(\bar{\sigma}\Phi)\times10^{9}$*	VI Φ_{total} (22 Mev)$\times10^{9}$	VII Φ_{fast}/Φ_{total}
Vanadium	245 (1±0.06)	0.01±0.08	−0.00±0.10	6.05	0.21	0.12
Chromium	164 (1±0.03)	0.04±0.04	−0.05±0.05	4.05	0.17	0.10
Manganese	308 (1±0.02)	0.07±0.03	−0.09±0.04	7.61	0.25	0.12
Iron	200 (1±0.03)	0.05±0.04	−0.17±0.05	4.94	0.18	0.11
Cobalt	390 (1±0.02)	0.08±0.03	−0.22±0.04	9.63	0.26	0.15
Nickel	145 (1±0.05)	0.07±0.07	−0.23±0.09	3.58	0.12	0.12
Copper	347 (1±0.02)	0.05±0.03	−0.29±0.01	8.57	0.30	0.12
Arsenic	482 (1±0.03)	0.11±0.04	−0.24±0.05	11.91	0.33	0.15
Rubidium	638 (1±0.05)	0.13±0.06	−0.14±0.08	15.76		
Strontium	409 (1±0.05)	0.10±0.06	−0.17±0.08	10.10		
Yttrium	290 (1±0.10)	0.08±0.12	−0.12±0.15	7.16		
Silver	590 (1±0.01)	0.10±0.06	−0.22±0.08	14.57	0.87	0.07
Cadmium	905 (1±0.02)	0.02±0.02	−0.26±0.03	22.35		
Iodine	1133 (1±0.03)	0.04±0.04	−0.29±0.05	27.99	1.42	0.08
Barium	1048 (1±0.04)	0.10±0.06	−0.38±0.08	25.89		
Lanthanum	1595 (1±0.02)	0.02±0.03	−0.12±0.04	39.40	1.04	0.15
Cerium	1316 (1±0.05)	0.05±0.06	−0.39±0.08	32.50		
Dysprosium	1652 (1±0.08)	0.04±0.10	−0.34±0.13	40.80		
Tantalum	1558 (1±0.02)	0.01±0.03	−0.22±0.04	38.48	2.50	0.06
Tungsten	1365 (1±0.02)	−0.07±0.03	−0.24±0.01	33.71		
Mercury	1345 (1±0.02)	0.04±0.03	−0.31±0.04	33.22		
Lead	2274 (1±0.01)	0.02±0.02	−0.42±0.03	56.17	2.72	0.08
Bismuth	2162 (1±0.02)	0.05±0.03	−0.45±0.04	53.40	3.36	0.06
Thorium	3031 (1±0.01)	0.06±0.05	−0.32±0.07	74.87		
Uranium	4630 (1±0.02)	0.05±0.03	−0.17±0.04	114.36		

*$(\bar{\sigma}\Phi)$ = 2.47×10⁹ as millibarn-neutron. Errors are standard errors due to counting statistics only.

REF.

F.R. Allum, T.W. Quirk, and B.M. Spicer
Nucl. Phys. 53, 545 (1964)

ELEM. SYM.	A	Z
Cr		24

METHOD

REF. NO.: 64 A1 5 JOC

REACTION	RESULT	EXCITATION ENERGY	SOURCE		DETECTOR		ANGLE
			TYPE	RANGE	TYPE	RANGE	
G,XN	NØX	THR-34	C	34	THR-I	6-	DST

TABLE 1

Summary of present experimental data at 34 MeV bremsstrahlung

Element		$-\frac{a_2}{a_0}$	$\frac{a_1}{a_0}$
$_{4}$Be		0.43±0.02	0.05±0.01
$_{6}$C		0.61±0.04	0.09±0.02
$_{13}$Al		0.39±0.03	0.05±0.01
$_{22}$Ti		0.34±0.02	0.06±0.01
$_{24}$Cr	34 MeV	0.33±0.02	0.02±0.01
	22 MeV	0.13±0.07	−0.02±0.03
$_{29}$Cu		0.36±0.02	0.10±0.01
$_{50}$Sn		0.38±0.02	0.11±0.01
$_{56}$Ba		0.39±0.03	0.11±0.02
$_{73}$Ta	Before installation of iron shielding	0.26±0.04	0.13±0.02
	After installation of iron shielding	0.27±0.02	0.12±0.01
$_{82}$Pb	target diameter 3.0 cm	0.39±0.03	0.15±0.02
	target diameter 1.5 cm	0.40±0.03	0.19±0.02
$_{83}$Bi		0.42±0.03	0.17±0.02

$$Y = a_0 + a_1 \cos\theta + a_2 \cos^2\theta$$

Synchrotron; $C^{12}(\gamma,n)$ monitor

REACTION	RESULT	EXCITATION ENERGY	SOURCE TYPE	SOURCE RANGE	DETECTOR TYPE	DETECTOR RANGE	ANGLE
C.XN	ABY	THR - 80	C	80	BF3-I		4 PI

Table 1

Element	Yield (36) eV cm^2 mol MeV	60 NZ/A (mb MeV)	20 Σ_0	80 Σ_0	30 80 Σ/Σ 0 0	E_m (MeV)	σ_m (mb)
$_{24}Cr$	83 x10^{-5}	777	1.21	2.1	0.58	18.5	97
$_{25}Mn$	108 x10^{-5}	818	1.52	2.33	0.65	18.5	114
$_{26}Fe$	68 x10^{-5}	832	0.88	1.46	0.60	17.5	75
$_{27}Co$	89 x10^{-5}	878	1.08	1.82	0.59	17.5	92
$_{28}Ni$	44 x10^{-5}	879	0.55	1.07	0.51	18.5	56
$_{29}Cu$	95 x10^{-5}	947	1.06	1.99	0.53	17.5	98
$_{30}Zn$	98 x10^{-5}	975	0.94	1.68	0.56	17.5	86
$_{31}Ga$	130 x10^{-5}	1034	1.29	2.18	0.59	17.5	151
$_{32}Ge$	139 x10^{-5}	1064	1.35	2.29	0.59	17.5	158
$_{33}As$	137 x10^{-5}	1109	1.22	2.18	0.56	17.5	127

$$\Sigma_0^{30} = \frac{\int_0^{30} \sigma(\gamma,xn)dE}{60\ NZ/A}$$

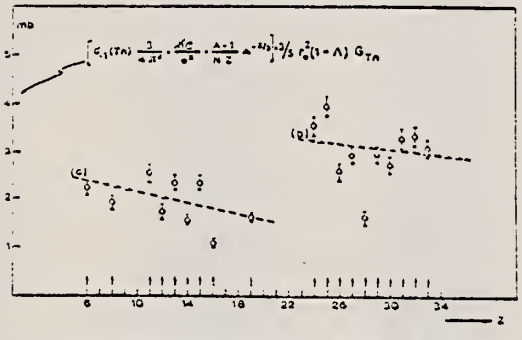

Fig. 2. Bremsstrahlung weighted cross sections, $\sigma_{-1}(Tn)$, conveniently normalized, versus Z.

Table 2

Element	maximum yield (x 10^{-5})	$\sigma_{-1}(Tn)$	$\sigma_{-1}(Tn) \times \left[\frac{3}{4\pi^2}\frac{\hbar c}{e^2}\left(\frac{A-1}{NZ}\right)A^{-\frac{2}{3}}\right]$
$_6C$	4.0	3.54	2.18
$_8O$	5.2	4.95	1.92
$_{11}Na$	12.6	11.60	2.49
$_{12}Mg$	10.0	9.81	1.73
$_{13}Al$	15.9	13.92	2.30
$_{14}Si$	11.6	9.96	1.55
$_{15}P$	19.8	17.56	2.32
$_{16}S$	9.5	8.55	1.07
$_{19}K$	19.6	17.90	1.61
$_{20}Ca$	12.1	11.68	1.02
$_{24}Cr$	86	61.6	3.56
$_{25}Mn$	115	76.1	3.96
$_{26}Fe$	71	50.5	2.55
$_{27}Co$	94	62.5	2.94
$_{28}Ni$	46	34.2	1.59
$_{29}Cu$	102	72.3	2.96
$_{30}Zn$	93	65.7	2.68
$_{31}Ga$	140	93.6	3.31
$_{32}Ge$	150	101.5	3.36
$_{33}As$	151	99.8	3.12

REF. J. W. Jury, J. S. Hewitt, and K. G. McNeill
Can. J. Phys. 46, 1823 (1968)

ELEM. SYM.	A	Z
Cr		24

METHOD

REF. NO. 68 Ju 1 EGF

REACTION	RESULT	EXCITATION ENERGY	SOURCE		DETECTOR		ANGLE
			TYPE	RANGE	TYPE	RANGE	
G,N	NOX	THR-22	C	22	THR	5-	DST

$$W(\theta) = a_o + a_1 P_1 + a_2 P_2$$

TABLE I

Target element	Z	Energy	a_0*	a_1/a_0	a_2/a_0
Vanadium	23	32	640±50	0.11±0.10	−0.09±0.11
Chromium	24	22	365±39	0.02±0.08	0.00±0.10
Manganese	25	22	450±33	0.07±0.05	−0.11±0.06
Bromine	35	27	874±54	0.05±0.06	−0.15±0.08
Molybdenum	42	22	610±60	0.09±0.05	−0.35±0.06
Ruthenium	44	27	1100±25	0.12±0.02	−0.29±0.03
Rhodium	45	27	1270±47	0.06±0.03	−0.14±0.03
Palladium	46	27	1350±29	0.26±0.02	−0.12±0.02
Antimony	51	27	2140±62	0.04±0.08	−0.25±0.11
Lanthanum	57	27	1940±70	0.12±0.10	−0.52±0.14
Praseodymium	59	30	1800±58	0.20±0.08	−0.40±0.09
Platinum	78	27	2600±52	0.17±0.02	−0.15±0.03
Lead	82	22	2274±59	0.08±0.08	−0.46±0.09

*The yield per mole per 100 r was normalized to a yield of 2274 for the lead sample at the same energy.

REF. K. G. McNeill, J. S. Hewitt, and J.W. Jury
Can. J. Phys. 46, 1974 (1968)

ELEM. SYM.	A	Z
Cr		24

METHOD

REF. NO. 68 Mc 1 egf

REACTION	RESULT	EXCITATION ENERGY	SOURCE		DETECTOR		ANGLE
			TYPE	RANGE	TYPE	RANGE	
G,XN	SPC	THR-32	C	22-32	THR-I	5-	DST

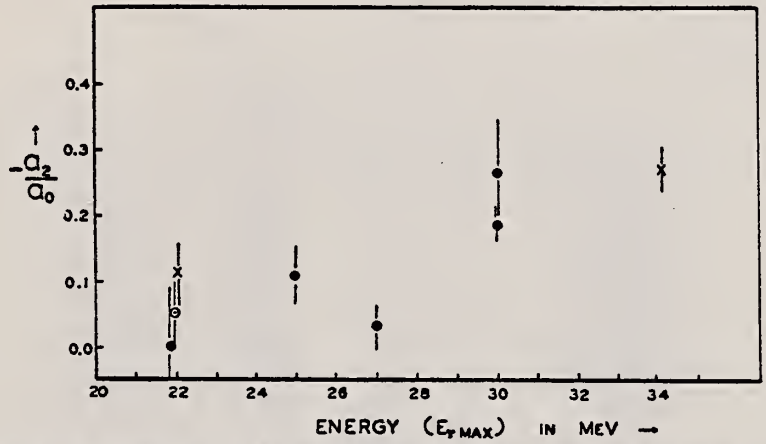

FIG. 2. The variation of anisotropy of fast photoneutrons from chromium with maximum X-ray energy. ⊙, present work; ⊙, Baker and McNeill (1961); ×, Allum *et al.* (1964).

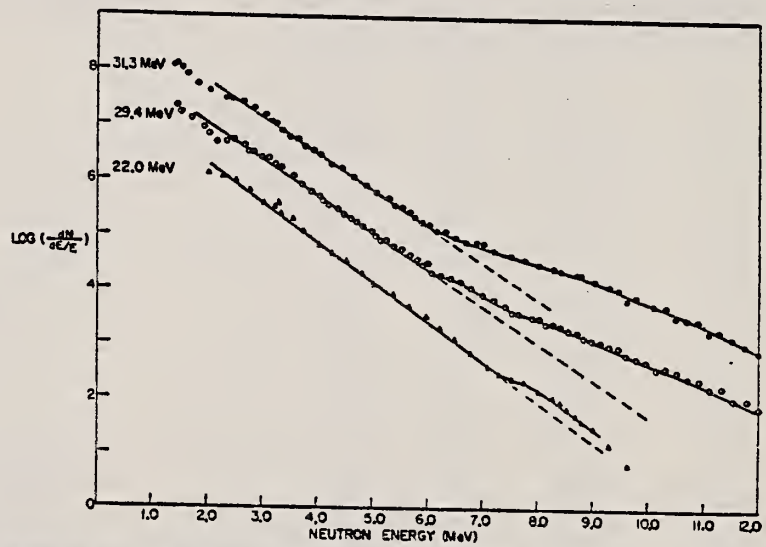

FIG. 3. The energy spectra of neutrons from chromium, measured by neutron time-of-flight techniques with resolution of 0.2 ns/m at three different maximum X-ray energies. The axes are such that a Maxwellian distribution gives a straight line. The experimental errors are approximately the sizes of the plotted points. The ordinate scale for each curve is arbitrary.

REF. H. Arenhovel, J. M. Maison
Nucl. Phys. A147, 305 (1970)

ELEM. SYM.	A	Z
Cr		24

METHOD

REF. NO. 70 Ar 1 egf

REACTION	RESULT	EXCITATION ENERGY	SOURCE		DETECTOR		ANGLE
			TYPE	RANGE	TYPE	RANGE	
G,G	ABX	12-30	C	32	NAI	12-30	DST

GETS G,G/ TO 2+

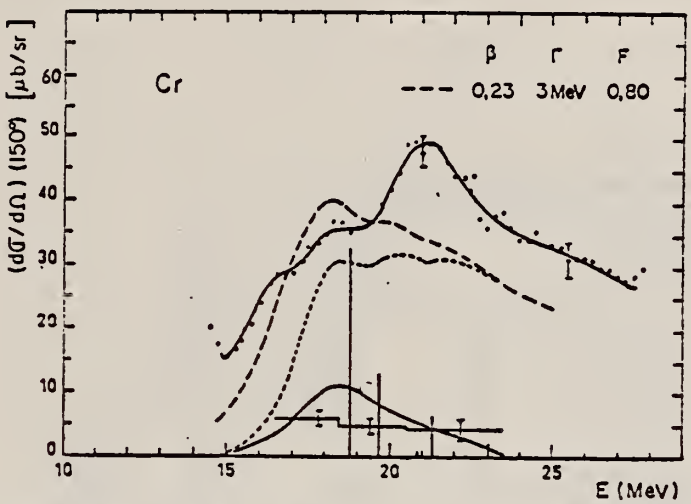

Fig. 6. Differential total scattering cross section at 150° for natural Cr. See caption for fig. 4. The upper dashed curve is the theoretical total scattering cross section and the lower one the theoretical elastic scattering cross section only.

Fig. 4. Differential total scattering cross section at 150° for natural Ti. The full curve through experimental points is only a guide for the eyes. The vertical bars represent the relative strength of dipole levels calculated by the D.C.M. with parameters of table 1. Theoretical elastic plus inelastic scattering is computed from these levels with a common width Γ (dashed curve). Experimental inelastic scattering (histogram) and theoretical inelastic scattering to the first 2^+ (full curve) are shown in the lower part of the figure. Open circles give the cross section after background subtraction.

TABLE 4

Integrated inelastic scattering cross section

Nucleus	Limits of integration (in MeV)	Experimental [a] $\int \sigma_i(E)dE$ (MeV · μb)	Theoretical [a] 2^+	$2^{+\prime}$ (MeV · μb)	Total
Ti(^{48}Ti)	16 −24	250 ± 50	425	109	534
^{51}V(^{52}Cr)	16.4−24.9	492 ± 50	509	116	579
Cr	16.4−23.4	431 ± 60	509	116	579
^{75}As(^{76}Se)	14.1−23.6	1254 ± 120	1373	414	1787
Se(^{80}Se)	14.1−24.6	1035 ± 100	1066	353	1419
^{89}Y					364
Cd(^{112}Cd)	13.6−23.3	3264 ± 240	1894	370	2264
In(^{114}Cd)	13.6−23.6	2840 ± 220	2173	388	2561
Sn(^{110}Sn)	14.2−24.2	2363 ± 220			643

[a]) We assume an angular distribution of the form $1 + \frac{1}{13}\cos^2\theta$.

REF.

R.F. Barrett, J.R. Birkelund, B.J. Thomas, K.S. Lam, and H.H. Thies
Nucl. Phys. A210, 355 (1973)

ELEM. SYM.	A	Z
Cr		24

METHOD

REF. NO. 73 Ba 20 egf

REACTION	RESULT	EXCITATION ENERGY	SOURCE TYPE	SOURCE RANGE	DETECTOR TYPE	DETECTOR RANGE	ANGLE
G,N	NOX	THR- 27	C	10- 27	BF3-I		4PI

MEAN NEUT ENERGY

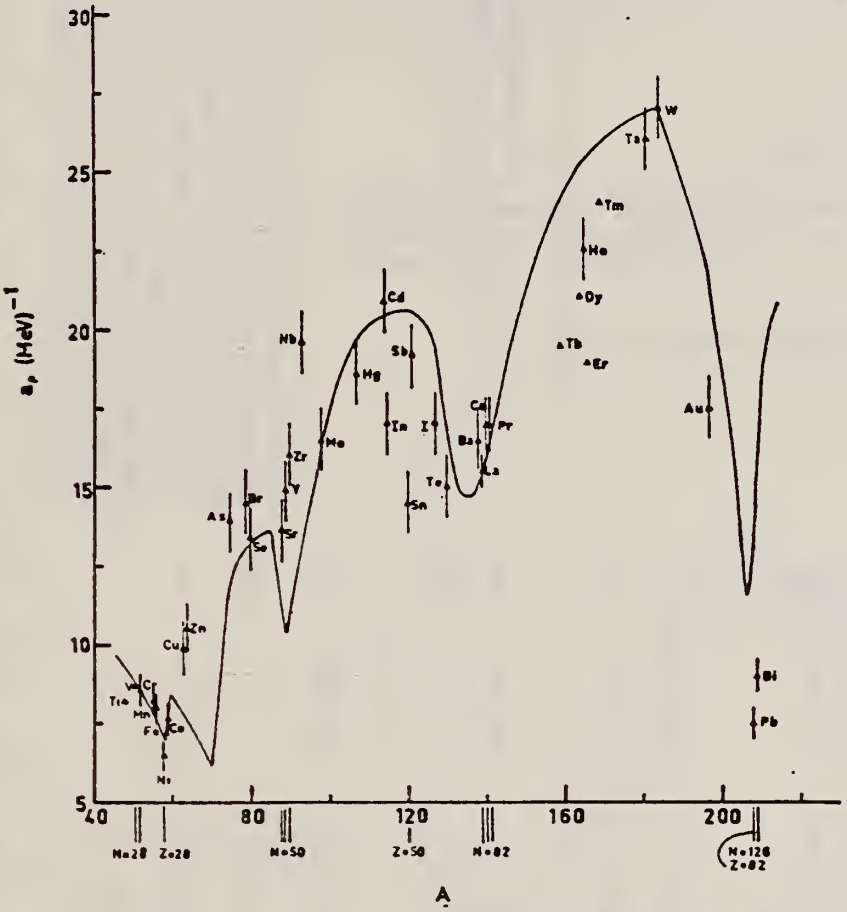

Fig. 12. Experimental values of the level density parameter a_p (Fermi gas formula plus pairing correction) versus atomic number A. The continuous curve is a least-squares fit to the data of a theoretical calculation from Newton [15]).

1
H. Baba and S. Baba, Japan Atomic Energy Research Institute report JAERI-1183 (1969).
2
H. Baba, Nucl. Phys. A159, 625 (1970).
15
T.D. Newton, Can. J. Phys. 34, 804 (1956).

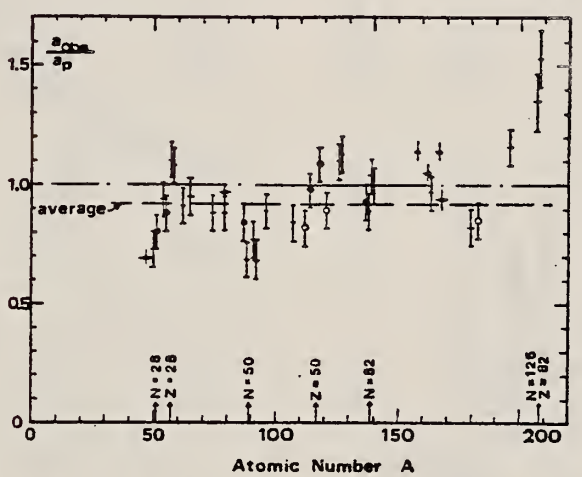

Fig. 15. Ratio a_{obs}/a_p versus atomic number A. Here a_{obs} is the level density parameter taken from the neutron resonance work of refs. [1,2]), and a_p is the level density parameter derived from the present (γ, n) work. Filled circles represent points where nuclei in the neutron resonance and in the (γ, n) experiment were the same. Open circles represent points where the respective nuclei were approximately matched. Triangles represent points which are based on measurement of neutron mean energies at two bremsstrahlung energies only.

(over)

TABLE 3

Comparison of experimental and theoretical data on nuclear level densities with Fermi gas formulae, and comparison of nuclear level density parameters from (γ, n) and n-resonance absorption experiments

Target	N (residual nucleus) [a]		Goodness of fit [b]		$\hat{E}_0(24)$ (MeV) [c]	T (MeV) [d]	a_p (MeV^{-1}) [e]	a_{obs} (MeV^{-1}) [f]	a_{obs}/a_p
			no p.c.	with p.c.					
Ti [g]	23	8%			1.93		8.1–^{47}Ti	6.41–^{47}Ti	0.79
	24	8%							
	25	73%							
	26	5%							
	27	5%							
V [g]	27	100%			1.96		8.7–^{50}V	6.35–^{51}V	0.73
Cr	25	4%	P	G	1.89		8.6–^{51}Cr	6.9 –^{51}Cr	0.80
	27	84%							
	28	10%							
	29	2%							
Mn	29	100%	V.P.	G	2.1		8.2–^{54}Mn	7.82–^{56}Mn	0.94
Fe	27	6%	F	G	1.96		8.0–^{55}Fe	7.06–^{55}Fe	0.88
	29	92%							
	30	2%							
Co	31	100%	P	F	2.12		7.7–^{58}Co	8.35–^{60}Co	1.08
Ni	29	68%	V.P.	P	2.04	1.4	6.5–$^{57.7}$Ni	7.19–^{59}Ni	1.10
($Z = 28$)	31	26%							
	32	1%							
	33	4%							
	35	1%							
Cu	33	69%	V.P.	P	1.78	1.0	9.8–^{62}Cu	8.90–^{64}Cu	0.91
	35	31%							
Zn	33	49%	F	F	1.61		10.5–$^{64.4}$Zn	10.0–^{65}Zn	0.95
	35	28%							
	36	4%							
	37	19%							
As	41	100%	V.P.	F	1.44		14.5–^{74}As	12.81–^{76}As	0.88
Se [g]	41	9%			1.39		13.3–^{78}Se	12.8 –^{78}Se	0.97
	42	8%							
	43	24%							
	45	50%							
	47	9%							
Br	43	45%	V.P.	V.P.	1.41		14.5–^{79}Br	12.69–^{80}Br	0.88
	45	49%							
Sr	47	10%	F	G	1.31		13.6–^{87}Sr	11.4 –^{87}Sr	0.84
	48	7%							
	49	83%							

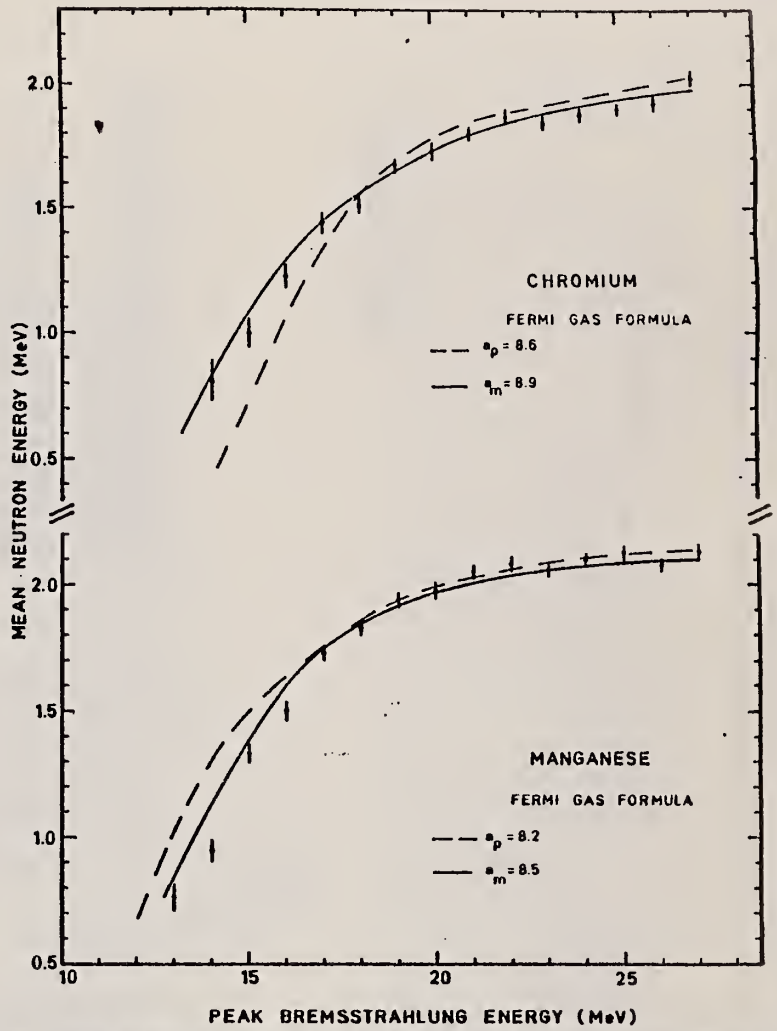

Fig. 5. Variation of photoneutron mean energy with peak bremsstrahlung energy, for chromium and manganese: experimental and calculated results.

[a]) Neutron numbers and abundances of respective residual nuclei in (γ, n) experiments.

[b]) These give an assessment of the goodness of fit of a calculated $\hat{E}_n$ versus E_0 curve to the observed data, using the Fermi gas level density formula both without and with pairing corrections.

[c]) Bremsstrahlung photoneutron mean energies $\hat{E}_0$ for peak bremsstrahlung energy $E_0 = 24$ MeV.

[d]) Nuclear temperature from fit with constant-temperature formula.

[e]) Level density parameter a_p derived from the present (γ, n) experiment, using a Fermi gas formula plus pairing correction, and corresponding residual nucleus (the atomic weight shown is the weighted average of atomic weights of the respective isotopes present).

[f]) As column 7, but using data on n-resonance absorption from refs. [1,2]).

[g]) Measurements of $\hat{E}_n(E_0)$ for these nuclei were made only for $E_0 = 21$, 23 and 24 MeV.

REF. J. Weise, M.N. Thompson, K. Shoda and H. Tsubota
Aust. J. Phys. 30, 401 (1977)

ELEM. SYM.	A	Z
Cr		24

METHOD

REF. NO. 77 We 2 egf

REACTION	RESULT	EXCITATION ENERGY	SOURCE		DETECTOR		ANGLE
			TYPE	RANGE	TYPE	RANGE	
G,XN	ABX	12- 26	C	8- 27	BF3-I		4PI

Abstract

A high resolution measurement of the total photoneutron cross section of chromium from threshold to 27 MeV has been obtained. The result is compared with an earlier measurement and an interpretation in terms of isospin effects is made.

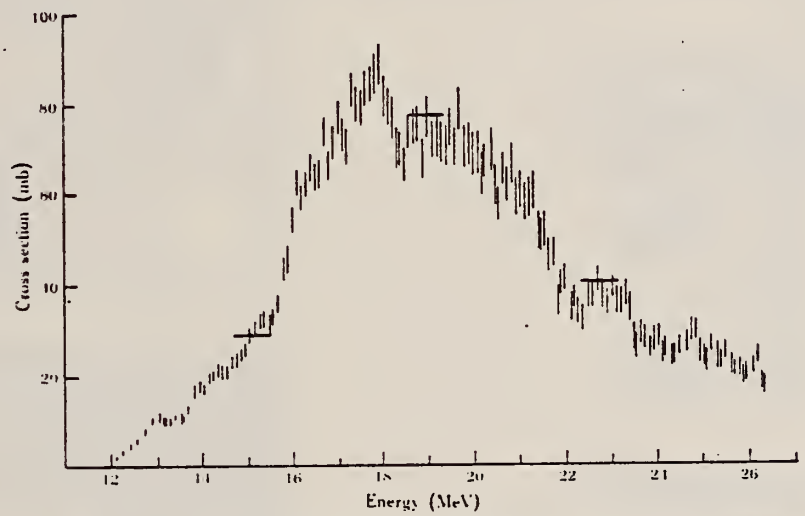

Fig. 1. Photoneutron cross section for natural chromium. The bold horizontal bars represent the analysis bin widths used.

REF. B.S. Ishkhanov, Yu.A. Novikov, E.S. Omarov, I.M. Piskarev
Sov. J. Nucl. Phys. 32, 757 (1980)
Yad. Fiz. 32, 1465 (1980)

ELEM. SYM.	A	Z
Cr		24

METHOD

REF. NO. 80 Is 6 hg

REACTION	RESULT	EXCITATION ENERGY	SOURCE		DETECTOR		ANGLE
			TYPE	RANGE	TYPE	RANGE	
G,G	ABX	14 - 31	C	13 - 31	NAI-D		90

Natural isotopic composition target

B. S. Ishkhanov, Yu. A. Novikov, E. S. Omarov, and I. M. Piskarev

Institute of Nuclear Physics, Moscow State University
(Submitted 21 February 1980)
Yad. Fiz. 32, 1465–1475 (December 1980)

The energy spectra of photons scattered at 90° by ^{28}Si and ^{52}Cr targets have been measured in the betatron bremsstrahlung beam at 16 values of the maximum bremsstrahlung energy from 13.1 to 31 MeV. The photon elastic scattering cross sections in the vicinity of the giant resonance, as well as the cross sections for photon inelastic scattering with excitation of the 1.75 and 4.98 MeV levels of ^{28}Si and the 1.43 and 2.98 MeV levels of ^{52}Cr, were calculated from the spectra. A dispersion-theory analysis of the results enabled us to identify the peaks in the cross sections for which $E1$ photoabsorption is dominant. The experimental data are compared with the results of shell-model and simple-rotator-model calculations. The nature of the peaks observed in the scattering cross sections is discussed.

PACS numbers: 25.20. + y, 27.30. + t, 27.40. + z

TABLE I. Integrated characteristics of scattering process for ^{28}Si and ^{52}Cr targets.

Target nucleus	Process	Integrated cross section (MeV · mb) out to 32 MeV: The present work	Other studies
^{28}Si, mass, 159 g	Elastic scattering	2.2±0.4	2.8±0.4 [3] 2.0±0.5 [4]
	NRE (1.78 MeV, $J^\pi = 2^+$)	0.8±0.3	Not observed [4]
	Inelastic scattering to the 4.98 MeV 0^+ level	0.7±0.4	–
	Inelastic scattering to the 15.3 MeV 2^+ level	0.24±0.02	–
^{52}Cr, mass, 150 g	Elastic scattering	6.0±0.5	5.5±0.5 [3]
	NRE (1.43 MeV $J^\pi = 2^+$)	3.0±0.5	3.8±0.7 [4] 0.6±0.2 [3]
	Inelastic scattering to the 2.96 MeV 2^+ level	1.2±0.5	

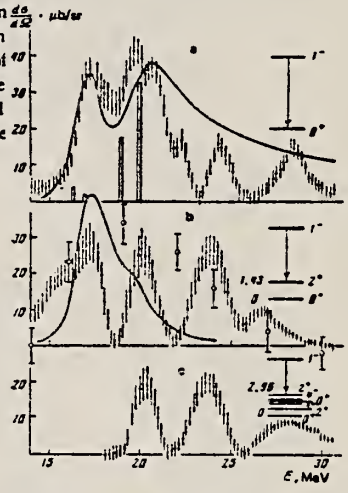

FIG. 4. a) Photon elastic scattering differential cross section for ^{52}Cr. The full curve was calculated using the simple rotator model. The vertical bars were calculated using the theory of finite Fermi systems.[43] b) Differential cross section for the nuclear Raman effect obtained in the present work (black points) and in Ref. 4 (open circles). The full curve was calculated using the simple rotator model. c) Photon inelastic scattering differential cross section for excitation of the 2.96 MeV $J^\pi = 2^+$ level.

[3]H. Arenhövel and J. M. Maison, Nucl. Phys. A147, 305 (1970).
[4]B. S. Ishkhanov *et al.*, Yad. Fiz. 30, 1177 (1979) [Sov. J. Nucl. Phys. 30, 610 (1979)].

TABLE III. Characteristics of levels observed in photon scattering from ^{52}Cr.

Total absorption [4,44]		Elastic scattering (the present work)		Inelastic scattering to the indicated levels of ^{52}Cr (the present work)				$\frac{\sigma^{tot}}{\sigma_{el}}$, b	$\delta\pi R^2$, b
				1.43 MeV (NRE)		2.96 MeV			
E_γ, MeV	σ, mb	E_γ, MeV	σ, μb	E_γ, MeV	σ, μb	E_γ, MeV	σ, μb		
17.5	≤70	17.2±0.5	380±30	17.0±0.5	350±40			13±3	24.5
20.5	90	20.0±0.5	430±50	20.0±0.5	340±40	20.2±0.5	240±30	19±4	18.4
24.5	20	24.2±0.5	210±20	24.0±0.5	340±40	23.5±0.5	240±30	2±0.5	12.0
28.0*	–	28.0±0.5	200±20	27.0±0.5	120±20	28.0±0.5	120±20		

*Observed in the (γ, n) cross section.[21]

C_R
A=50

C_R
A=50

C_R
A=50

Ref. W.E. Del Bianco, W.E. Stephens
Phys. Rev. 126, 709 (1962)

Elem. Sym.	A	Z
Cr	50	24

Method Electrostatic generator, $H^2(p,\gamma)He^4$ reaction; activation of positron emitter; 2 NaI in coincidence.

Ref. No. 62 De 1 JHH

Reaction	E or ΔE	E_o	Γ	$\int \sigma dE$	Jπ	Notes
(γ,n)	20.48					σ(γ,n) = 29.1±6.0 mb

REF. R. Moreh, S. Shlomo, and A. Wolf
Phys. Rev. C2, 1144 (1970)

ELEM. SYM.	A	Z
Cr	50	24

METHOD

REF. NO. 70 Mo 2 hmg

REACTION	RESULT	EXCITATION ENERGY	SOURCE TYPE	SOURCE RANGE	DETECTOR TYPE	DETECTOR RANGE	ANGLE
G,G	ABX	9	D	9	SCD-D		DST
		(8.888)		(8.888)			

9 = 8.888, LFT

TABLE III. Summary of the results of spins, parities, and total widths of resonance levels excited by γ rays obtained from neutron capture in iron. Parities in parantheses are uncertain.

Isotope	Energy (MeV)	$\delta=\lvert E_\gamma - E_a\rvert$ (eV)	J^π_0	J^π_γ	Transition	Γ_0/Γ_γ (±8%)	Γ_γ (10^{-3} eV)
^{50}Cr	8.888	18 ±1	0^+	1	···	0.90	750±200
^{62}Ni	7.646	14 ±1	0^+	1^-	$E1$	0.64	480± 50
^{74}Ge	6.018	4.5±0.5	0^+	1^-	$E1$	0.19	120± 15
^{75}As	7.646	7.4±0.3	$3/2^-$	$1/2^{(+)}$	···	0.11	360±100
^{109}Ag	7.632	9 ±1	$1/2^-$	3/2	···	0.7	2± 1
^{112}Cd	7.632	4.8±0.4	0^+	1^-	$E1$	0.55	86± 15
^{139}La	6.018	8.2±0.6	$7/2^+$	$7/2^-$	$E1$	0.50	51^{+14}_{-8}
^{141}Pr	7.632	$11.4^{+0.3}_{-0.9}$	$5/2^+$	$5/2^+$	$M1$	0.46	72^{+24}_{-8}
^{205}Tl	7.646	9.3±0.3	$1/2^+$	$1/2^{(-)}$	···	0.58	980± 90
^{208}Pb	7.279	7.1±0.3	0^+	1^+	$M1$	1.00	780± 60

TABLE IV. Effective elastic scattering cross section $\langle\sigma_\gamma\rangle=\sigma_0^\pi(\Gamma_0/\Gamma_\gamma)\Psi(x_0,t_0)$, where δ, J, Γ_0, Γ_γ were taken from Table III. The temperature of the scatterer was 300°K, while that of the iron γ source was 640°K.

Target	Resonance energy (MeV)	$\langle\sigma_\gamma\rangle$ (mb)
^{50}Cr	8.888	905
^{62}Ni	7.646	569
^{74}Ge	6.018	61
^{75}As	7.646	4.4
^{109}Ag	7.632	3.5
^{112}Cd	7.632	198
^{139}La	6.018	39
^{141}Pr	7.632	20
^{205}Tl	7.646	574
^{208}Pb	7.279	5560

REF. W. Del Bianco, S. Kundu and P. Boucher
Nucl. Phys. A209, 181 (1973)

ELEM. SYM.	A	Z
Cr	50	24

METHOD

REF. NO. 73 De 5 egf

REACTION	RESULT	EXCITATION ENERGY	SOURCE		DETECTOR		ANGLE
			TYPE	RANGE	TYPE	RANGE	
G,N	ABX	20- 23	D	20- 23	ACT-I		4PI

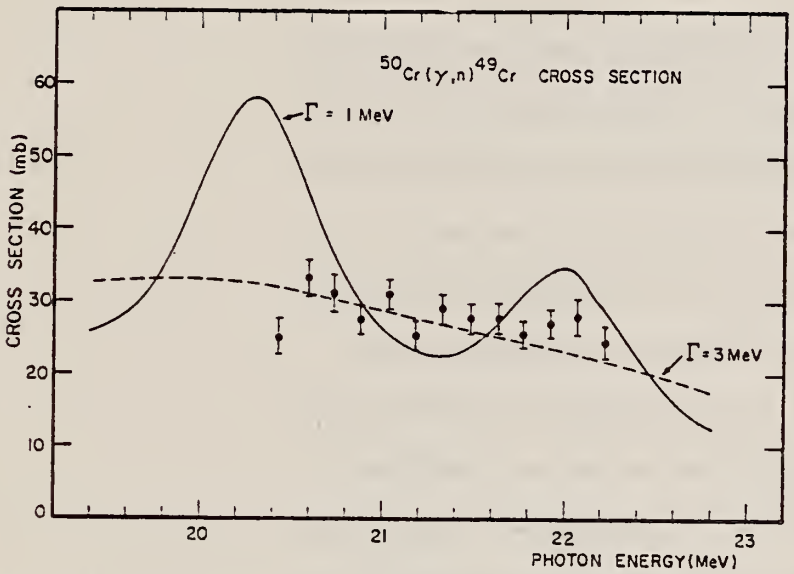

Fig. 4. The $^{50}Cr(\gamma, n)^{49}Cr$ cross section. The points are the results of this experiment. The curves represent the normalized theoretical absorption cross section of ref. [2]): the solid curve corresponds to $\Gamma = 1$ MeV and the dashed curve to $\Gamma = 3$ MeV, the other parameters being the same as in fig. 1.

[2] M.G. Huber, M. Danos, H.J. Weber and W. Greiner, Phys.Rev. 155, 1073 (1967).

TABLE 1
Total cross section of the $^{50}Cr(\gamma, n)^{49}Cr$ reaction

E_γ (MeV)	σ (mb)
20.43	25.2±2.5
20.58	33.4±2.6
20.73	31.3±2.3
20.88	27.6±2.0
21.03	30.9±2.0
21.18	25.3±1.8
21.33	29.0±1.9
21.48	27.7±1.7
21.63	27.9±1.7
21.78	25.6±1.6
21.92	27.1±1.6
22.07	27.8±2.6
22.22	24.6±2.1

† New England Nuclear Corporation, Boston, USA.

REF. W. Del Bianco, S. Kundu, and P. Boucher
PICNS-73, Vol.I, p.557 Asilomar

ELEM. SYM.	A	Z
Cr	50	24

METHOD

REF. NO. 73 De 8 hmg

REACTION	RESULT	EXCITATION ENERGY	SOURCE		DETECTOR		ANGLE
			TYPE	RANGE	TYPE	RANGE	
G,N	ABX	20- 22	D	20 -22	ACT-I		4PI

The measurement of (γ, n) cross sections in spherical medium weight nuclei is of great interest for determining the coupling of low energy surface vibrations and high energy dipole oscillations. The coupling has been theoretically investigated by Huber et al.[1] and found to result in a considerable splitting of the photonuclear resonance. Experimentally bremsstrahlung measurements have indicated a pronounced structure in (γ, n) cross sections [2,3] which is not present in measurements with γ-rays from positron annihilation in flight[4,5]. In this experiment a photoactivation method and monochromatic γ-rays from the $^{3}H(p,\gamma)^{4}He$ reaction were employed to measure the (γ, n) cross section for ^{50}Cr and ^{64}Zn. The γ-rays were monitored by a NaI(Tℓ) crystal enclosed in a lead and paraffin shield to reduce background radiation. The positron activity was determined by a coincidence detector consisting of two NaI(Tℓ) crystals set on the annihilation radiation photopeaks. The γ-ray energy was varied in steps of 150 keV from 20.43 to ≈ 22.2 MeV and the energy resolution was less than 110 keV over the entire energy range. The experimental cross sections of the two reactions were found to vary smoothly as a function of energy. The results for the $^{64}Zn(\gamma, n)$ process do not agree with those of Owen et al.[2], who observed two resonances ≈ 0.5 to 1 MeV wide in the same energy range. The shape of the ^{50}Cr (γ, n) cross section is in fair agreement with the calculation of Huber et al.[1] for widths of the dipole states of the order of 3 MeV.

(over)

1) M.G. Huber, M. Danos, H. Weber and W. Greiner, Phys. Rev. 155, 1073(1967).

2) D.G. Owen, E.G. Muirhead and B.M. Spicer, Nucl. Phys. A122, 177(1968).

3) P.H. Cannington, R.J. Stewart and B.M. Spicer, Nucl. Phys. A109, 385(1968).

4) R.L. Bramblett, J.T. Caldwell, B.L. Berman, R.R. Harvey and S.C. Fultz, Phys. Rev. 148, 1198 (1966).

5) R.E. Sund, V.V. Verbinki, H. Weber and L.A. Kull, Phys. Rev. C2, 1129 (1970).

REF. K. Masumoto, T. Kato, N. Suzuki
Nucl. Inst. Meth. 157, 567 (1978)

ELEM. SYM.	A	Z
Cr	50	24

METHOD

REF. NO.	
78 Ma 10	hg

REACTION	RESULT	EXCITATION ENERGY	SOURCE		DETECTOR		ANGLE
			TYPE	RANGE	TYPE	RANGE	
G,PN	ABY	23-68	C	30-68	ACT - I		4PI
G,2N	ABY	24-68	C	30-68	ACT - I		4PI

Analysis is made of reactions interfering with photon activation analysis procedures.

The activation yield curves have been presented for a number of photonuclear reactions in the energy range from 30 to 68 MeV, in order to evaluate quantitatively the interferences due to competing reactions in multielement photon activation analysis. The general features of the yields as functions of both target mass number and excitation energy were elucidated from the data obtained, discussion being given on the results in terms of the reaction mechanism.

Simultaneous neutron activation due to appreciable neutron production from the converter and surrounding materials has also been studied, and, finally, the magnitudes of interferences in real multielement analysis were given in the form of their energy dependences.

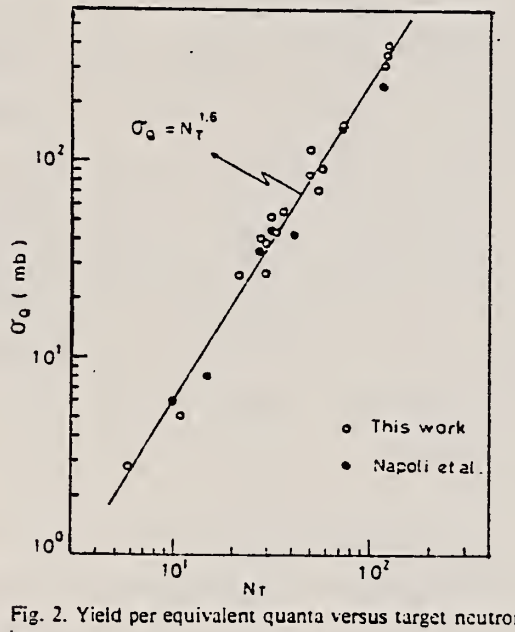

Fig. 2. Yield per equivalent quanta versus target neutron number.

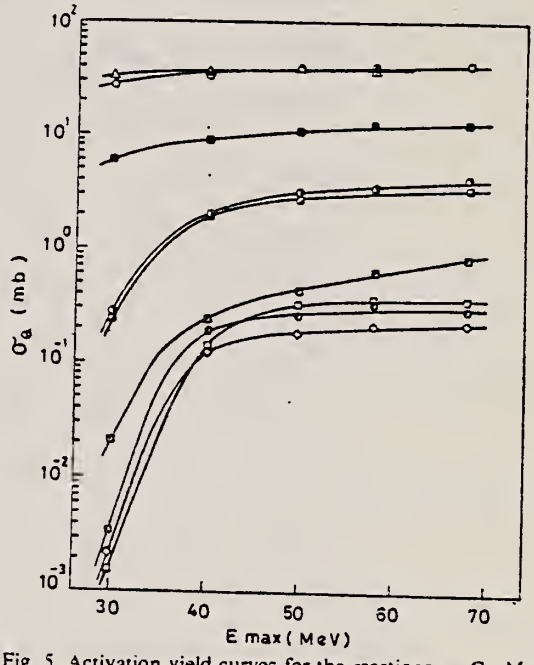

Fig. 5. Activation yield curves for the reactions on Cr, Mn and Fe.
○ $^{52}Cr(\gamma, n)^{51}Cr$, ◑ $^{50}Cr(\gamma, pn)^{48}V$, ◐ $^{50}Cr(\gamma, 2n)^{48}Cr$,
△ $^{55}Mn(\gamma, n)^{54}Mn$, ◪ $^{57}Fe(\gamma, p)^{56}Mn$, ◩ $^{54}Fe(\gamma, pn)^{52g}Mn$,
◪ $^{56}Fe(\gamma, pn)^{54}Mn$, □ $^{56}Fe(\gamma, 2n)^{51}Cr$, ◇ $^{54}Fe(\gamma, 2n)^{52}Fe$.

(over)

FORM N3S-418
REV. 7-14-71

U.S. DEPARTMENT OF COMMERCE

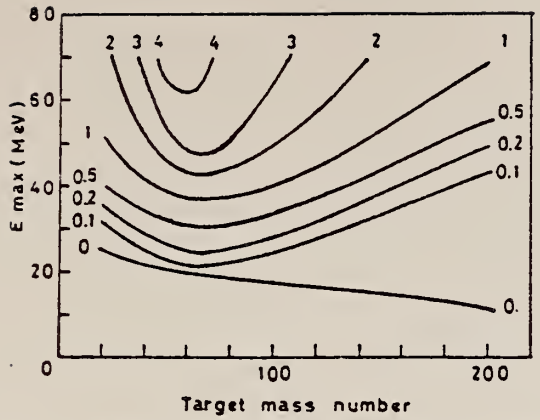

Fig. 11. Yields of the (γ, pn) reactions as a function of bremsstrahlung maximum energy and target mass number. The numerical values in the figure are yields per equivalent quanta in mb.

Cr
A=52

Cr
A=52

K. N. Geller, J. Halpern, and E. G. Muirhead
Phys. Rev. 118, 1302-12 (1960)

ELEM. SYM.	A	
Cr	52	24

METHOD
Betatron; neutron threshold; ion chamber

REF. NO.
60 Ge 3 NVB

REACTION	RESULT	EXCITATION ENERGY	SOURCE		DETECTOR		ANGLE
			TYPE	RANGE	TYPE	RANGE	
G,N	NØX	THR	C THR		BF3-I		4 PI

THRESHØLD

TABLE I. Summary and comparison of neutron separation energies inferred from present threshold measurements with values predicted from mass data and reaction energies. All energies are expressed in the center-of-mass system in Mev.

Reaction	No. runs	Present results	Other results	Method	Reference
$Cr^{52}(\gamma,n)Cr^{51}$	1	$\leqslant 12.18 \pm 0.14$	12.053 ± 0.004	mass data	g

[g] C. F. Giese and J. L. Benson, Phys. Rev. 110, 712 (1958).

TABLE II. Comparison of measured threshold energies with neutron binding energies predicted by mass data for transitions with $\Delta I \geq 7/2$. All energies in Mev.

Reaction	ΔI[a]	Observed threshold	Mass data Q value	$E_{th}-Q$	Excited state energy
$Cr^{52}(\gamma,n)Cr^{51}$	7/2	12.18 ± 0.14	12.053 ± 0.004[b]	0.13 ± 0.14	...
$Y^{89}(\gamma,n)Y^{88}$	7/2	11.59 ± 0.08	11.53 ± 0.40[c]	0.06 ± 0.41	0.387[d]
$In^{115}(\gamma,n)In^{114}$	7/2	9.22 ± 0.03	9.35 ± 0.43[e]	-0.13 ± 0.43	0.191[a]
$Ce^{142}(\gamma,n)Ce^{141}$	(7/2)[e]	7.24 ± 0.07	6.97 ± 0.07[f]	0.27 ± 0.10	...
$Nd^{146}(\gamma,n)Nd^{145}$	7/2	6.38 ± 0.16	5.97 ± 0.19[f]	0.41 ± 0.25	0.690[a]
$Sm^{149}(\gamma,n)Sm^{148}$	7/2	6.45 ± 0.16	5.87 ± 0.28[f]	0.58 ± 0.33	0.562[a]
$Er^{167}(\gamma,n)Er^{166}$	7/2	6.65 ± 0.08	6.45 ± 0.06[g]	0.20 ± 0.10	0.081[a]
$Hf^{177}(\gamma,n)Hf^{176}$	7/2	6.69 ± 0.03	6.28 ± 0.06[g]	0.64 ± 0.07	0.088[a]
$Hf^{179}(\gamma,n)Hf^{178}$	9/2	6.31 ± 0.07	6.17 ± 0.06[g]	0.14 ± 0.09	0.093[a]
$Hf^{180}(\gamma,n)Hf^{179}$	9/2	7.85 ± 0.11	7.32 ± 0.06[g]	0.53 ± 0.13	0.375[a]

[a] D. Strominger, J. M. Hollander, and G. T. Seaborg, Revs. Modern Phys. 30, 585 (1958).
[b] C. F. Giese and J. L. Benson, Phys. Rev. 110, 712 (1958).
[c] Henry E. Duckworth, *Mass Spectroscopy* (Cambridge University Press, New York, 1958), p. 177.
[d] S. Dzelepov and L. K. Peker, Atomic Energy of Canada Limited Report Tr. AECL-457 (unpublished).
[e] The discrepancy in the case of Ce^{142} predicts a ground-state spin for Ce^{142} of 0, since the spin of Ce^{141} is known to be 7/2.
[f] W. H. Johnson, Jr., and A. O. Nier, Phys. Rev. 105, 1014 (1957).
[g] W. H. Johnson, Jr., and V. B. Bhanot, Phys. Rev. 107, 6 (1957).

REF.

J. Bellicard and P. Barreau and D. Blum
Nucl. Phys. 60, 319-336 (1964)

ELEM. SYM.	A	Z
Cr	52	24

METHOD

Linac; Faraday cup/SEM monitor

REF. NO.	
64 Be 3	JOC

REACTION	RESULT	EXCITATION ENERGY	SOURCE		DETECTOR		ANGLE
			TYPE	RANGE	TYPE	RANGE	
E,E/	FMF	0 - 9	D	150,180	MAG-D		DST

TABLE 1

Values of the fitting parameters β_L with the Born approximation inelastic form factors for transitions of angular momentum change L.

ε (MeV)	$J\pi$	β	Γ (eV)	$B\frac{(L\to 0)}{e^2}$	$B^{sp}\frac{(L\to 0)}{e^2}$	G
1.43	2+	0.0390	0.50×10^{-3}	103 fm^4	11.1 fm^4	9.25
		30	4	8		75
2.37	4+	0.0177	2.00×10^{-12}	7500 fm^8	2200 fm^8	3.4
		30	34	1300		6
2.97	4+	0.0132	11.2×10^{-12}	5580 fm^8	2200 fm^8	2.52
		18	1.5	760		35

Values of the reduced transition probabilities $B_{exp}(L\to 0)$ are compared with the single-particle estimate of Moszkowski [22] $B_{sp}(L\to 0)$. Their ratio $G = B_{exp}(L\to 0)/B_{sp}(L\to 0)$ is also indicated. Values of γ-ray widths $\Gamma_{exp}(L\to 0)$ are calculated from the corresponding value of $B_{exp}(L\to 0)$.

J-PI

TABLE 2

Values of the fitting parameters β_{exp} with the Born approximation inelastic form factors given by Walecka theory for one and two-surfon quadrupole transitions are compared with the theoretical estimates β_{th} given in this theory.

ε (MeV)	Transition	β_{th} ($\times 10^3$)	β_{exp} ($\times 10^3$)
1.43	$0^+ \xrightarrow{2} 2^+$	3.9	3.9
2.65	$0^+ \xrightarrow{2^2} 0^+$	0.0168	0.05
3.16	$0^+ \xrightarrow{2^2} 2^+$	0.385	2.9

TABLE 3

Values of the fitting parameters β_3 with the Born approximation inelastic form factors for transitions of angular momentum change 3

ε (MeV)	$J\pi$	β	Γ (eV)	$\frac{B(L\to 0)}{e^2}$	$\frac{B_{sp}(L\to 0)}{e^2}$	G
4.60	3−	0.0290	15.6×10^{-6}	932 fm^6	152 fm^6	6.1
		15		48		3
5.50	3−	0.0053	10.7×10^{-6}	186 fm^6		1.2
		12		40		24
6.60	3−	0.0096	65.2×10^{-6}	316 fm^6		2.00
		12		40		24
7.10	3−	0.0120	138×10^{-6}	400 fm^6		2.40
		12		40		24
7.90	3−	0.0120	292×10^{-6}	400 fm^6		2.40
		12		40		24
8.60	3−	0.0096	422×10^{-6}	316 fm^6		2.00
		12		40		24

Values of the reduced transition probabilities $B_{exp}(3\to 0)$ compared with the single-particle estimate of Moszkowski [22] $B_{sp}(3\to 0)$. Their ratio $G = B_{exp}(3\to 0)/B_{sp}(3\to 0)$ is also indicated. Values of γ-ray widths $\Gamma_{exp}(3\to 0)$ are calculated from the corresponding values of $B_{exp}(3\to 0)$.

U.S. DEPARTMENT OF COMMERCE
NATIONAL BUREAU OF STANDARDS

USCOMM-DC 26010-P64

PHOTONUCLEAR DATA SHEET

REF. E. C. Booth, B. Chasan and K. A. Wright
Nucl. Phys. 57, 403-420 (1964)

ELEM. SYM.	A	Z
Cr	52	24

METHOD
Van de Graaff; resonance fluorescence

REF. NO. 64 Bo 1 NVB

REACTION	RESULT	EXCITATION ENERGY	SOURCE TYPE	SOURCE RANGE	DETECTOR TYPE	DETECTOR RANGE	ANGLE
G,G	LFT	1-3	C	1 - 3	NAI-D		100
		(0.5 - 3.0)		(0.5 - 3.0)			

ABI

TABLE 1
Cases of observed resonance fluorescence

Nucleus multipol.	State (MeV)	Spin	Γ_0/Γ	$T(g w \Gamma_0^2/\Gamma^2)^{-1}$ (sec).	Mean lifetime T BCW (sec)	Mean lifetime T other (sec)	Ref.	Γ_0/Γ_W BCW
Cr^{52}	0.00	0^+						
E2[a])	1.43	2^+	1	$3.4\pm1\times10^{-13}$	$11\pm3\times10^{-13}$	$10.2\pm1.3\times10^{-13}$	c)	15

REF. S. Costa, F. Ferrero, S. Ferroni and R. Malvano
Proc. Paris Conference 1034 (1964)

ELEM. SYM.	A	Z
Cr	52	24

METHOD: 100 MeV synchrotron

REF. NO.: 64 Co 3 JDM

REACTION	RESULT	EXCITATION ENERGY	SOURCE		DETECTOR		ANGLE
			TYPE	RANGE	TYPE	RANGE	
G,N	ABS	THR-80	C	10-80	BF3-I		4PI

TABLE

ELEMENT	Yield (36 MeV) $\left(\frac{\text{n. cm}^2}{\text{mol. MeV}} \times 10^5\right)$	Σ_0^{30}	Σ_0^{80}	$\Sigma_0^{30}/\Sigma_0^{80}$	σ_{-1} (mb)
$_{24}$Cr	83	1.21	2.1	0.58	62
$_{25}$Mn	108	1.52	2.33	0.65	76
$_{26}$Fe	68	0.88	1.46	0.60	50
$_{27}$Co	89	1.08	1.82	0.59	64
$_{28}$Ni	44	0.55	1.07	0.51	34
$_{29}$Cu	95	1.06	1.99	0.53	72
$_{30}$Zn	88	0.94	1.68	0.56	66
$_{31}$Ga	130	1.29	2.18	0.59	94
$_{32}$Ge	139	1.35	2.29	0.59	101
$_{33}$As	137	1.22	2.18	0.56	100

$\sum_a^b = \frac{A}{60\,NZ}\int_a^b \sigma(E)\,dE$ is the integrated cross section measured in units of the classical dipole $60\,NZ/A$ mb. MeV.

REF. B.I. Goryachev, B.S. Ishkhanov, I.M. Kapitonov, I.M. Piskarev, V.G. Shevchenko & O.P. Shevchenko
Izv. Akad. Nauk. Fiz. 33, 1736 (1969)
Bull. Acad. Sci. USSR-Phys. 33, 1588 (1969)

ELEM. SYM.	A	Z
Cr	52	24

METHOD

REF. NO. 69 Go 3 hmg

REACTION	RESULT	EXCITATION ENERGY	SOURCE		DETECTOR		ANGLE
			TYPE	RANGE	TYPE	RANGE	
G,XN	ABX	12-30	C	12-30	BF3-I		4PI

449→

449

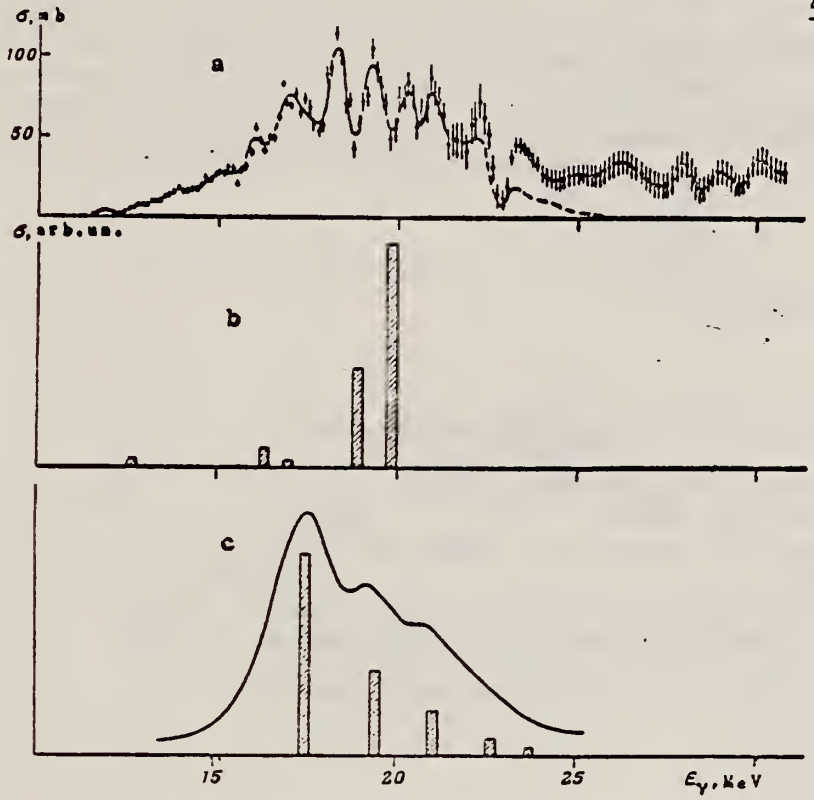

Fig.2. a - The (γ,n) + (γ,2n) cross section for ^{52}Cr; b & c - theoretical absorption cross sections calculated via: b - the theory of finite Fermi systems[7], c - the collective dynamic model[8].

[7] G.G. Bunatyan, Yadernaya fizika 4, 920 (1966). (Trans. Soviet Journal of Nuclear Physics.)

[8] D. Drechsel & C. Toepffer, Nucl. Phys. A100, 161 (1967).

(over)

Characteristics of the Photoneutron Cross Sections (in MeV-mb)

Nucleus	Integral cross sections*				Center of gravity σ(γn)+σ(γ, 2n), MeV	Refs.	Dipole sum rule 60NZ/A, MeV·mb
	σ(γn)+2σ(γ, 2n)	σ(γn)+σ(γ, 2n)	σ(γn)	σ(γ, 2n)			
^{51}V	820 (30)	600 (30)	380 (30)	220 (30)	21,3	Our work	760
	670 (28)	560 28)	450 (28)	110 (28)		[9]	
	590 (24)					[10]	
	560 (25)					[11]	
^{52}Cr	950 (30)	740	530 (30)	210 (30)	20,4	Our work	775
	600 (24)					[10]	
^{59}Co	1030 (30)	740 (30)	450 (30)	290 (30)	20,2	Our work	880
	730 (28)	590 (28)	450 (28)	140 (28)		[9]	
	870 (29)					[12]	
	840 (25)					[13]	
	660 (28)					[14]	
	630 (25)					[11]	

*The upper integration limits are given in parentheses.

9. S.C.Fultz, R.L.Bramblett, I.T.Caldwell, N.E.Hansen & C.P.Jupiter, Phys. Rev. 128, 2345 (1962).

10. J.Goldemberg & L.Katz, Canadian J. Phys. 32, 49 (1954).

11. B.Nathans & J.Halpern, Phys. Rev. 93, 437 (1954).

12. E.B.Bazhanov, A.P.Komar & A.V.Kulikov, Zh. Eksperim. i teor. fiz. 46, 1497 (1964). (Trans. Soviet Physics - JETP.)

13. P.A.Flournoy, R.S.Tickle & W.D.Whitehead, Phys. Rev. 120, 1424 (1960).

14. G.Baciu, G.C.Bonazzola, B.Minetti, C.Molino, L.Pasqualini & G.Piragino, Nuclear Phys. 68, 178 (1965).

REF. B.S. Ishkhanov, I.M. Kapitonov, I.M. Piskarev, V.G. Shevchenko, and O.P. Shevchenko
Yad. Fiz. 11, 485 (1970)
Sov. J. Nucl. Phys. 11, 272 (1970)

ELEM. SYM.	A	Z
Cr	52	24

METHOD

REF. NO. 70 Is 4 hmg

REACTION	RESULT	EXCITATION ENERGY	SOURCE TYPE	SOURCE RANGE	DETECTOR TYPE	DETECTOR RANGE	ANGLE
G,P	ABX	10-30	C	10-30	SCD-D	1-	XXX
		(9.6 - 30)		(9.6 - 30)			

XXX PROB 90

We measured the photoproton cross sections for the nuclei Cr^{52}, Ni^{58}, and Ni^{60} from the threshold to 30 MeV. We registered protons with energy larger than 1 MeV. A number of maxima were obtained in the cross sections. The values of the integral cross sections for Cr^{52}, Ni^{58}, and Ni^{60} are equal respectively to 240, 570, and 320 MeV-mb. The anomalously large cross section for the production of photoprotons for Ni^{58}, and also the shift of the centers of gravity of the photoproton cross sections towards higher excitation energies relative to the photoneutron cross sections in the case of Cr^{52} and Ni^{60}, can be attributed to the influence of analog states.

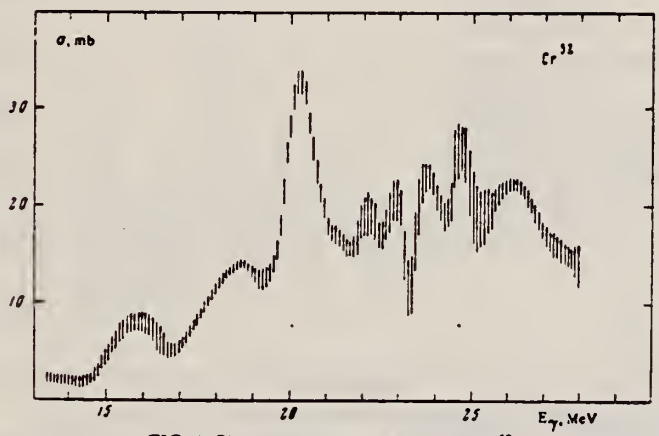

FIG. 1. Photoproton cross section for Cr^{52}.

Integral characteristics of the photoproton cross sections σ_p, of the photoneutron cross sections σ_n, and of the total absorption cross sections $\sigma_\gamma = \sigma_n + \sigma_p$

Nuclei	$\int_0^{30}\sigma_n dE$, MeV-mb	$\int_0^{30}\sigma_p dE$, MeV-mb	$\int_0^{30}\sigma_\gamma dE$, MeV-mb	$60(NZ/A)$, MeV-mb	$\int_0^{30}\sigma_p dE \Big/ \int_0^{30}\sigma_\gamma E$	$\bar{E}(\sigma) = \int_0^{30} E\sigma dE \Big/ \int_0^{30}\sigma dE$	
						$\bar{E}(\sigma_n)$, MeV	$\bar{E}(\sigma_p)$, MeV
Cr^{52}	730±60	240±50	970±110	775	0.25	20.4±0.3	23.0±0.4
Ni^{58}	310±30	570±60 (100±20)	880±90	870	0.65	21.9±0.3	21.4±0.3
Ni^{60}	620±50	320±50 (60±20)	940±100	895	0.34	20.7±0.3	22.6±0.3

Note. The parentheses contain the integral cross sections of the photoproton reactions for protons with energy $E_p \geq 8$ MeV.

REF. W. B. Walters, J. R. Van Hise, W. L. Switzer, J. P. Hummel
Nucl. Phys. A157, 73 (1970)

ELEM. SYM.	A	Z
Cr	52	24

METHOD

REF. NO.	
70 Wa 3	egf

REACTION	RESULT	EXCITATION ENERGY	SOURCE		DETECTOR		ANGLE
			TYPE	RANGE	TYPE	RANGE	
G,2N	RLY	THR-305	C	150-305	ACT-I		4PI
G,PN	RLY	THR-305	C	150-305	ACT-I		4PI

TABLE 1
Summary of measured yield ratios

Target	Bremsstrahlung energy (MeV)	Measured yield ratio
natural Cr	150	$^{48}Cr/^{48}V = 0.043 \pm 0.002$
	250	0.047 ± 0.009
	305	0.042 ± 0.002
enriched ^{52}Cr	250	0.025 ± 0.005
natural Fe	250	$^{52}Fe/^{52}Mn = 0.037 \pm 0.003$
enriched ^{56}Fe	250	0.024 ± 0.005
		$^{52g}Mn/(^{52m}Mn + ^{52g}Mn) = 0.47 \pm 0.02$
natural Y	150	$^{87}Y/^{87m}Sr = 12.9 \pm 1.6$
natural Mo	150	$^{90}Mo/^{90}Nb = 0.41 \pm 0.05$
	280	0.49 ± 0.05

TABLE 2
Summary of experimental and theoretical ratios of $(\gamma, 2n)$ to (γ, pn) yields

Target isotope	Bremsstrahlung energy (MeV)	Experimental $(\gamma, 2n)/(\gamma, pn)$ yield ratio	Calculated $(\gamma, 2n)/(\gamma, pn)$ yield ratio
^{50}Cr	250	0.095 ± 0.025	0.14
^{54}Fe	250	0.10 ± 0.03	0.07
^{89}Y	150	7.4 ± 1.0	6.7
^{92}Mo	150	0.41 ± 0.05	0.15
	280	0.49 ± 0.05	0.16

REF. R. J. Baglan, C. D. Bowman and B. L. Berman
Phys. Rev. C3, 672 (1971)

ELEM. SYM.	A	Z
Cr	52	24

METHOD

REF. NO. 71 Ba 2 hmg

REACTION	RESULT	EXCITATION ENERGY	SOURCE		DETECTOR		ANGLE
			TYPE	RANGE	TYPE	RANGE	
G,N	ABX	12-14	C	12,14	TOF-D		135
		(12.3-13.7)					

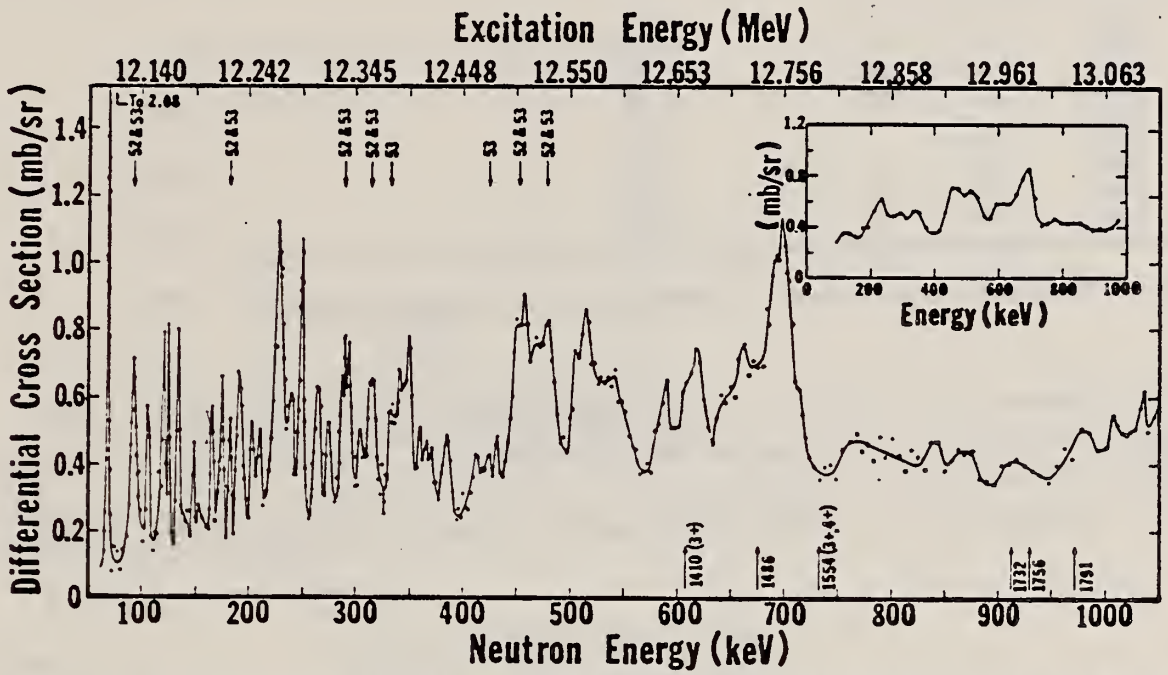

FIG. 14. The 135° differential threshold photoneutron cross section for ^{52}Cr (see caption to Fig. 4). The arrows below the data indicate the positions of isobaric analogs of low-lying states of ^{52}V. Next to the arrows are the values of J^{π} and the energy in keV of these low-lying states.

Also see:
R. J. Baglan et al.
Phys. Rev. C3, 2475
(1971)

[over]

TABLE VI *(Continued)*

Nucleus	E_L (keV)	E_{ex} (MeV)	$g_\gamma\Gamma_{\gamma 0}\Gamma_n/\Gamma$ (eV)	GS or ES	J^π	$\Gamma_{\gamma 0}$ (eV)	E_n (keV) (This work)	E_n (keV) from neutron-induced reactions (Ref. a)	(Ref. b)	(Ref. c)
^{52}Cr	68.2	12.107	0.69	GS			73.0			
	105	12.145	0.40	GS			112			
	121	12.161	0.71	GS			129			
	125	12.165	0.35	GS			133			
	133	12.173	0.60	GS			141			
	147	12.188	0.31				156			
	166	12.208	0.50	GS			176			
	175	12.217	0.62	GS			185			
	191	12.233	0.95	GS			202			
	203	12.245	0.49	GS			215			
	210	12.253	0.43	GS			222			
	229	12.272	2.47	GS			242			
	238	12.282	0.71	GS			251			
	249	12.293	1.22	GS			263			
	264	12.308	0.95	GS			279			
	274	12.319	0.61	GS			289			
	286	12.331	0.55				301			
	293	12.338	0.59				309			
	341	12.388	0.78	GS			359			
	349	12.396	1.04	GS			368			
	385	12.432	0.66	GS			405			

[a]See Ref. 17.
[b]See R. W. Hockenbury, Z. M. Bartolome, J. R. Tatarczuk, W. R. Moyer, and R. C. Block, Phys. Rev. 178, 1746 (1969).
[c]See Ref. 19.

[17]C.D. Bowman, E.G. Bilpuch, and H.W. Newson, Ann. Phys. (N.Y.) 17, 319 (1962).

[b]See R.W. Hockenbury, Z.M. Bartolome, J.R. Tatarczuk, W.R. Moyer, and R.C. Block, Phys. Rev. 178, 1746 (1969).

[19]R.G. Steiglitz, Ph.D. thesis, Rensselaer Polytechnic Institute, 1970 (unpub.)

REF. J. E. P. de Bie, P. K. A. de Witt Huberts
PICNS-72, 423 (1972) Sendai

ELEM. SYM.	A	Z
Cr	52	24

METHOD

REF. NO. 72 De 8 hvm

REACTION	RESULT	EXCITATION ENERGY	SOURCE		DETECTOR		ANGLE
			TYPE	RANGE	TYPE	RANGE	
E,E/	FMF	1, 3	D	80	MAG-D		DST

1=1.43, 3=3.6 MEV

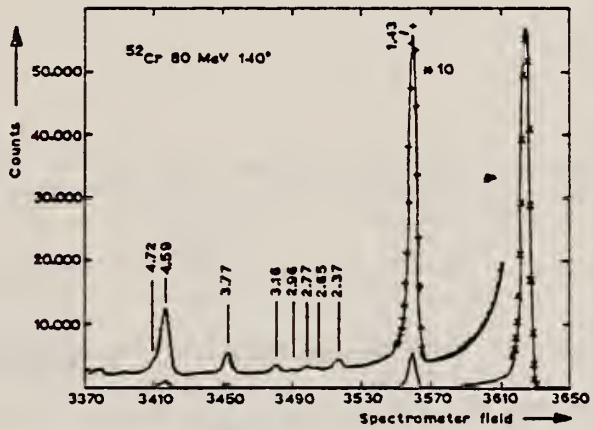

Fig. 10. A typical spectrum of elastic and inelastic scattered electrons from ^{52}Cr. The drawn curve is the peak fitted spectrum.

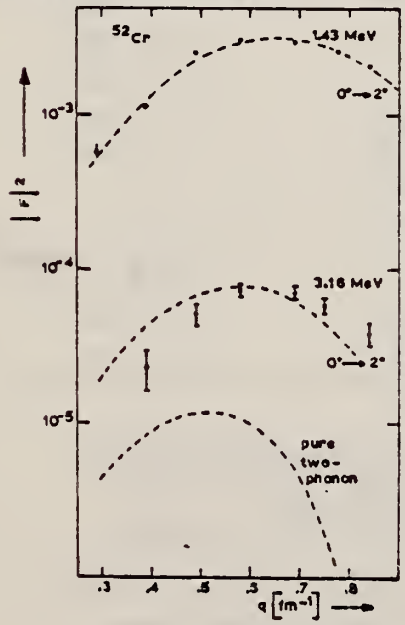

Fig. 11. Experimental form factor curves for the 1.43 and 3.16 MeV level in ^{52}Cr. The dashed curves represent the best fit results in Born approximation of the mixed one- and two phonon form factors. Also drawn is the two phonon prediction for the 3.16 MeV level with the radius and collective parameters fixed by the one phonon fit to the 1.43 MeV level.

REF. S. Penner, J.W. Lightbody,Jr., S.P. Fivozinsky, H. Crannell, P.L. Hallowell, and M. Finn
PICNS-72, 49 (1972) Sendai

ELEM. SYM.	A	Z
Cr	52	24

METHOD

REF. NO. 72 Pe 2 hvm

REACTION	RESULT	EXCITATION ENERGY	SOURCE TYPE	SOURCE RANGE	DETECTOR TYPE	DETECTOR RANGE	ANGLE
E,E/	FMF	1, 3	D	40-110	MAG-D		128

1=1.434, 3=3.16 MEV

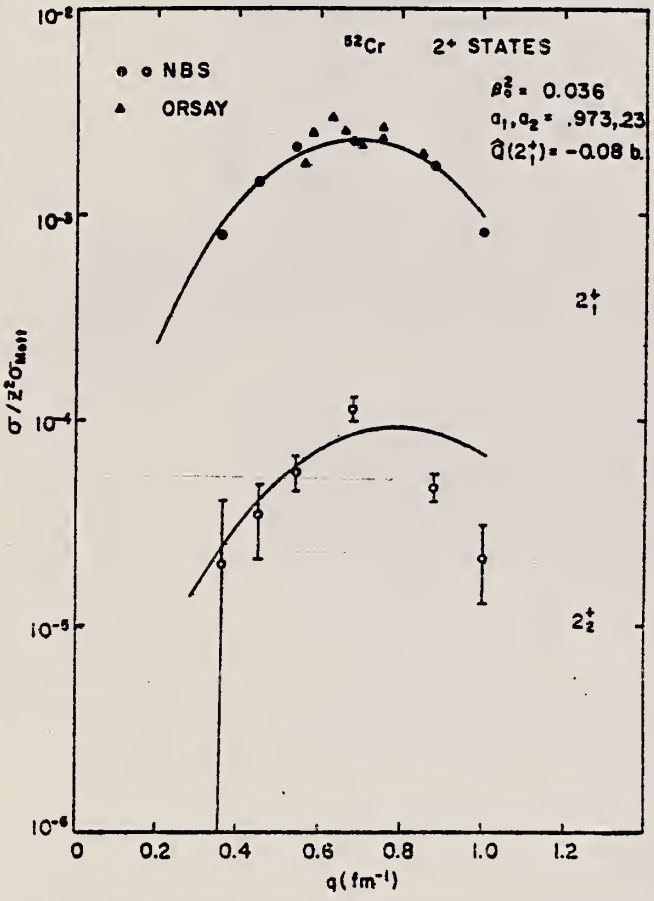

Fig. 1. Form factors for excitation of the first and second 2^+ states in ^{52}Cr. The smooth curves are the best fits of the anharmonic vibrator model.

Table 2. First Excited State Static Quadrupole Moments

Nucleus	Q, barns electron scattering	Q, barns reorientation effect
^{48}Ti	-.177 ± .008[b]	-.22 ± .08 [c]
		-.135± .082[d]
		-.38 ± .13 [e]
^{52}Cr	-.082 ± .016[a]	-.07 ± .13 [f]
^{60}Ni	-.104 ± .018[b]	0 ± .13 [g]
^{64}Zn	-.135 ± .016[b]	-
^{70}Zn	-.21 ± .03 [b]	-
^{110}Pd	-.28 ± .03 [a]	(-.27 OR -.48)±.05[h] (-.45 OR -.72)±.12[i]
^{114}Cd	-.29 ± .03 [a]	-.32 ± .08 [j]
^{116}Sn	-.14 ± .03 [a]	+.09 ± .13 [k]

a) New preliminary values
b) From Ref. (1)
c) O. Hausser, et al., Nucl. Phys. A150, 417 (1970)
d) P.M.S. Lesser, et al., University of Rochester Annual Report, 1970 (unpublished)
e) N.V. deCastro-Faria, et al., Nucl. Phys. A174, 37 (1971)
f) D. Cline, University of Rochester Report UR-NSRL-40, 1971 (unpublished)
g) D. Cline, et al., Nucl. Phys. A133, 445 (1969)
h) R. Beyer, et al., Phys. Rev. C2, 1469 (1970)
i) R.P. Harper, et al., Nucl. Phys. A162, 161 (1971)
j) Z. Berant, et al., Phys. Rev. Letters 27, 110 (1971)
k) A.M. Kleinfeld, et al., Nucl. Phys. A154, 499 (1970)

REF. D. Branford, G.S. Foote, R.A.I. Bell, D.C. Weisser, F.C.P. Huang and R.B. Watson
PICNS-73, Vol.II, p.943 (1973) Asilomar

ELEM. SYM.	A	Z
Cr	52	24

METHOD

REF. NO.	
73 Br 7	egf

REACTION	RESULT	EXCITATION ENERGY	SOURCE		DETECTOR		ANGLE
			TYPE	RANGE	TYPE	RANGE	
G,A	ABX	- 25	D	16	NAI-D		DST

NO ANG DST DATA

Table 1. Preliminary Results with Relative Errors; Absolute Errors ≈ 30%

Reaction	$\int\sigma(\gamma_0,\alpha_0)dE$ mb. MeV	$\int\sigma(\gamma_1,\alpha_0)dE$ mb. MeV	Excitation Energy (MeV)
$^{40}Ar(\alpha,\gamma)^{44}Ca$	1.4 ± 0.3	0.42 ± 0.08	15.5
$^{48}Ti(\alpha,\gamma)^{52}Cr$	3.0 ± 0.6	0.48 ± 0.10	17.0
$^{56}Fe(\alpha,\gamma)^{60}Ni$	7.8 ± 1.5	1.52 ± 0.30	16.0

REF. Phan Xuan Ho, J. Bellicard, Ph. Leconte, I. Sick
Nucl. Phys. A210, 189 (1973)

ELEM. SYM.	A	Z
Cr	52	24

METHOD

REF. NO. 73 Ho 4 egf

REACTION	RESULT	EXCITATION ENERGY	SOURCE TYPE	SOURCE RANGE	DETECTOR TYPE	DETECTOR RANGE	ANGLE
E,E/	FMF	1- 5	D	209	MAG-D		DST

1.43, 2.37, 4.56

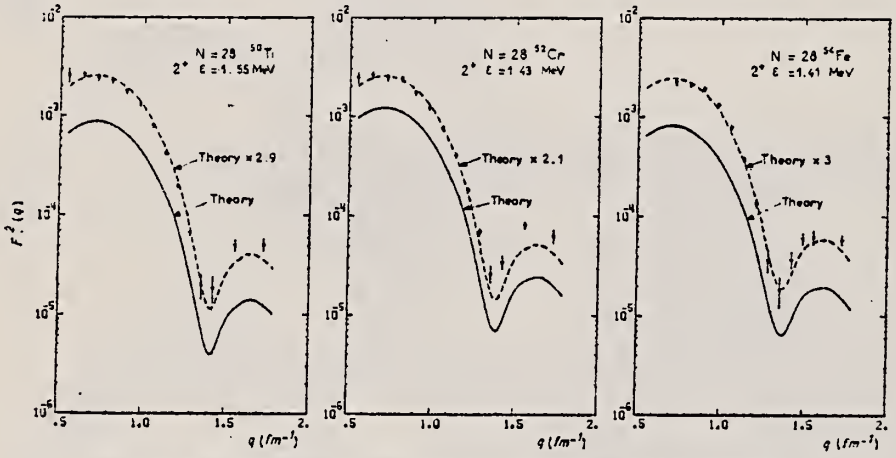

Fig. 5a. Squared inelastic form factor for 2^+ states of the $N = 28$ isotones.

TABLE 3

Inelastic cross sections for $E_e = 209$ MeV on ^{52}Cr

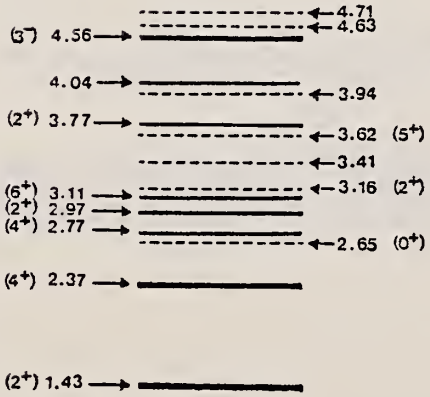

θ (deg.)	$(2^+)\varepsilon = 1.43$ MeV $d\sigma/d\Omega$ (mb/sr)	$(3^-)\varepsilon = 4.56$ MeV $d\sigma/d\Omega$ (mb/sr)	$(4^+)\varepsilon = 2.37$ MeV $d\sigma/d\Omega$ (mb/sr)
30	0.353 E−1±0.460 E−2		
35	0.201 E−1±0.140 E−2	0.313 E−2±0.115 E−2	
40	0.110 E−1±0.800 E−3	0.235 E−2±0.360 E−3	
45	0.653 E−2±0.420 E−3	0.169 E−2±0.110 E−3	
50	0.312 E−2±0.210 E−3	0.125 E−2±0.900 E−4	0.292 E−3±0.400 E−4
55	0.146 E−2±0.900 E−4	0.873 E−3±0.430 E−4	0.233 E−3±0.160 E−4
60	0.633 E−3±0.390 E−4	0.585 E−3±0.310 E−4	0.176 E−3±0.120 E−4
65	0.241 E−3±0.150 E−4	0.373 E−3±0.170 E−4	0.129 E−3±0.700 E−5
70	0.780 E−4±0.540 E−5	0.231 E−3±0.130 E−4	0.925 E−4±0.590 E−5
75	0.220 E−4±0.200 E−5	0.136 E−3±0.800 E−5	0.615 E−4±0.380 E−5
80	0.625 E−5±0.120 E−5	0.697 E−4±0.440 E−5	0.387 E−4±0.250 E−5
85	0.622 E−5±0.900 E−6	0.380 E−4±0.230 E−5	0.235 E−4±0.180 E−5
95	0.854 E−5±0.670 E−6	0.856 E−5±0.690 E−6	0.879 E−5±0.890 E−6
110	0.312 E−5±0.460 E−6	0.980 E−6±0.184 E−6	0.102 E−5±0.190 E−6

Energy level diagram given by ref. [24]). Levels excited in our experiment are shown with solid lines, dashed lines correspond to other levels. The experimental values are normalized on our elastic cross sections considered as reference values.

24 Nuclear Data Sheets B (1970).

(OVER)

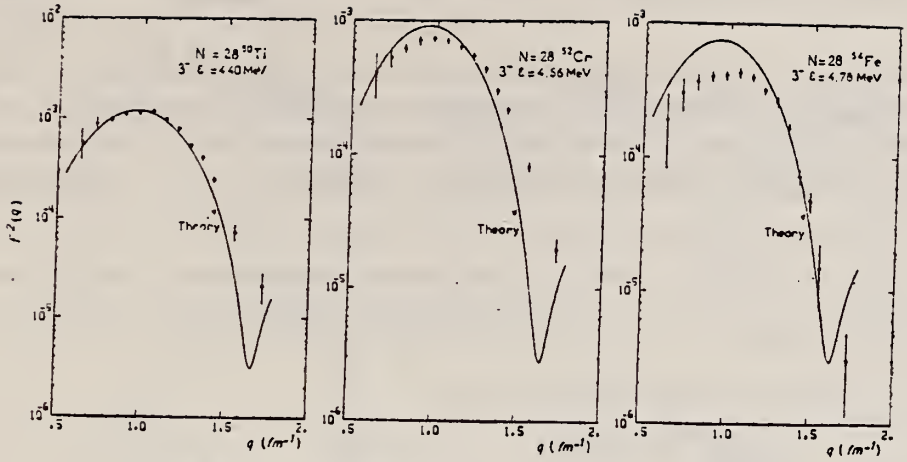

Fig. 6a. Squared inelastic form factor for 3^- states of the $N = 28$ isotones.

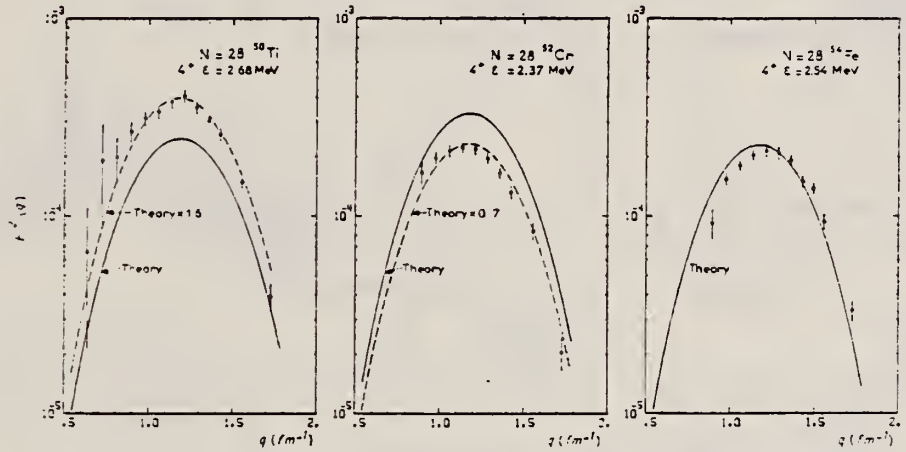

Fig. 7a. Squared inelastic form factor for 4^+ states of the $N = 28$ isotones.

REF. G.S. Foote, D. Branford, D.C. Weisser, N. Shikazono, and F.C.P. Huang
J. Phys. A: Math., Nucl. Gen., 7, L4 (1974)

ELEM. SYM.	A	Z
Cr	52	24

METHOD

REF. NO. 74 Fo 4 egf

REACTION	RESULT	EXCITATION ENERGY	SOURCE TYPE	SOURCE RANGE	DETECTOR TYPE	DETECTOR RANGE	ANGLE
G,A	ABX	15- 20	D	6- 11	NAI-D		90

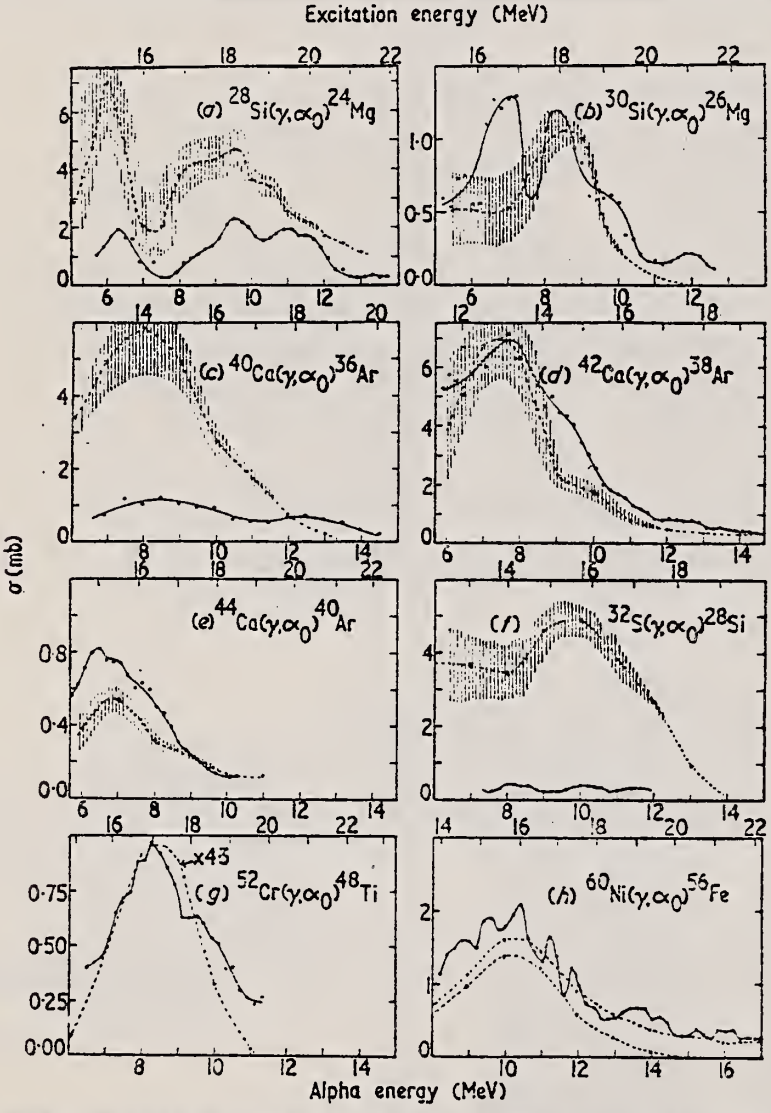

Figure 1. Excitation functions for the (γ, α_0) reaction obtained from α capture data using the principle of detailed balance. The data shown in (*a*) and (*f*) are from Meyer-Shutzmeister *et al* (1968). Those in (*b*) are from Watson *et al* (1973). The relative experimental errors are approximately ± 10%. The absolute errors are ± 25%. The broken curves are the results of calculations (see text). The vertical lines indicate the relative errors due to uncertainties in the total photonuclear cross sections where they are greater than ± 10%. The crosses indicate the energies at which transmission coefficients were calculated.

REF.		ELEM. SYM.	A	Z
	G. S. Foote, D. Branford, D. C. Weisser, N. Shikazono, R.A.I. Bell, F.C.P. Huang Nucl. Phys. A263, 349 (1976)	Cr	52	24
METHOD		REF. NO.		
		76 Fo 2		egf

REACTION	RESULT	EXCITATION ENERGY	SOURCE		DETECTOR		ANGLE
			TYPE	RANGE	TYPE	RANGE	
A,G	ABX	15- 21	D	6- 12	NAI-D		DST

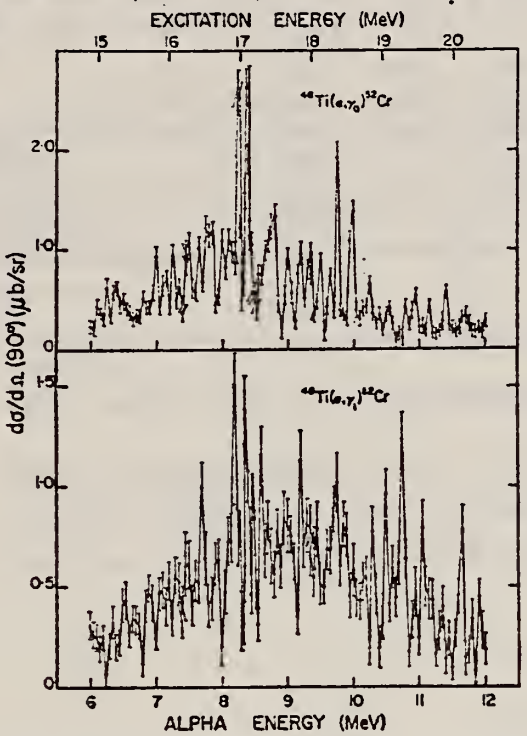

Fig. 4. Absolute differential cross sections for the $^{48}Ti(\alpha,\gamma_0)^{42}Cr$ and $^{48}Ti(\alpha,\gamma_1)^{52}Cr$ reactions measured at 90° to the beam direction versus bombarding energy. The absolute error is 30 %. The continuous line is a guide to the eye.

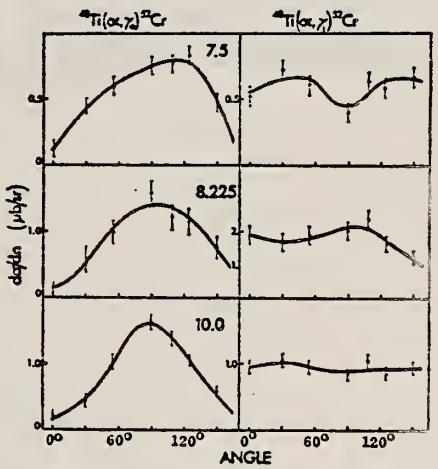

Fig. 7. Angular distribution measurements for the $^{48}Ti(\alpha,\gamma_0)^{52}Cr$ reaction and the $^{48}Ti(\alpha,\gamma_1)$ reaction at the bombarding energies (MeV) indicated. Only relative statistical errors are shown. The continuous lines represent Legendre polynomial fits to the data.

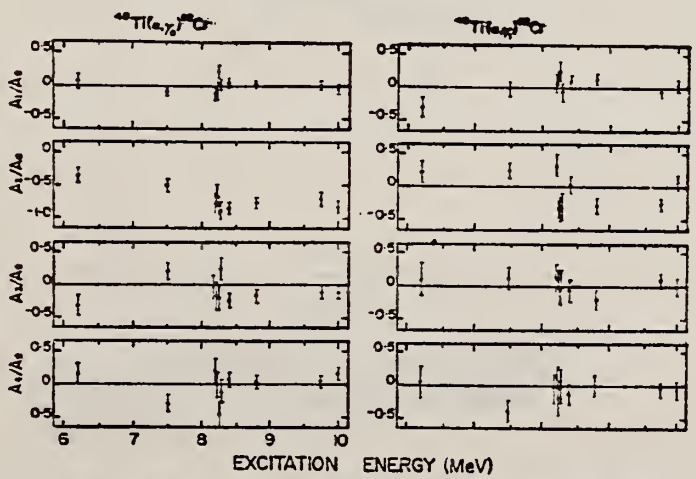

Fig. 10. Normalised Legendre polynomial coefficients determined by linear least squares fitting of the γ-ray distributions measured for the $^{48}Ti(\alpha,\gamma_0)^{52}Cr$ and $^{48}Ti(\alpha,\gamma_1)^{44}Ca$ reaction.

(over)

TABLE 3

Comparisons of energy integrated (γ, α) cross sections, peak energies of the broad structures in the (γ, α) excitation functions and the particle threshold energies

Final [a] nucleus	Range of integration (MeV)	$\int\sigma(\gamma,\alpha)dE$ [b] (mb · MeV)	$\int\sigma(\gamma,\alpha)dE$ [b] cds (%)	Particle threshold energies α (MeV)	n (MeV)	p (MeV)	E [c] (MeV)	Exp. peak energy (MeV)	GDR energy (MeV)	Refs.
^{28}Si	14.5–22.5	9.6	2.3	9.99	17.18	11.59	15.2	18.0	20	[1]
^{30}Si	14.0–22.0	5.3	1.2	10.65	10.62	13.51	15.7	16.5	18	[1]
^{32}Si	13.1–22.7	2.7	0.57	6.95	15.09	8.87	13.0	16	20	[1]
^{40}Ca	12.5–22.2	4.8	0.8	7.04	15.62	8.33	14.2	14.0	20	[6]
^{42}Ca	11.0–20.5	30.2	4.8	6.25	11.49	10.28	13.3	13.0	17.4	this work
^{44}Ca	13.5–18.8	2.6	3.09	8.84	11.13	12.16	15.9	15.3	17	this work
^{44}Ca*	13.5–18.8	0.76	0.12				15.9		18.5	this work
^{44}Ti	10.5–20.6	6.1	0.9	5.18	5.18	8.66	13.9	14.0		[15]
^{52}Ti	12.7–20.4	≈0.3	≈0.04	7.67	7.80	13.53	16.1			[15]
^{52}Cr	15.0–20.5	2.9	0.38	9.35	12.05	10.52	17.6	17.0	18	this work
^{52}Cr*	15.0–20.5	0.51	0.07				17.6			this work
^{60}Ni	13.9–22.8	9.6	1.07	6.29	11.39	9.53	15.7	15.8	16.6	[3]
^{60}Ni*	13.9–22.8	1.7	0.18	4.96			15.7		17.9	[3]

[a] The asterisk denotes first excited state.
[b] The errors are approximately ±30 %.
[c] E is the α-particle threshold energy plus Coulomb barrier height (see text).

[1] L. Meyer-Schutzmeister et al., Nucl. Phys. A108, 180 (1968).
[3] G. S. Foote et al., Nucl. Phys. A220, 505 (1974).
[6] R. B. Watson et al., Nucl. Phys. A203, 209 (1973).
[15] R. E. Peshel et al., Nucl. Phys. A232, 269 (1974).

REF.	ELEM. SYM.	A	Z
J.W. Lightbody, Jr., S. Penner, S.P. Fivozinsky, P.W. Hallowell and Hall Crannell Phys. Rev. C14, 952 (1976)	Cr	52	24

METHOD	REF. NO.
	76 Li 5 hmg

REACTION	RESULT	EXCITATION ENERGY	SOURCE		DETECTOR		ANGLE
			TYPE	RANGE	TYPE	RANGE	
E,E/	FMF	1, 3	D	39-111	MAG-D		127
		(1.43,3.16)					

LEVEL 1.43,3.16

TABLE V. ^{52}Cr Tassie model transition charge distribution parameters.

Excited state		c_{tr}/c	z_{tr}/z	$B(E2)\ e^2\text{fm}^4$	$\chi^2/(N-P)$	$N-P$
1.43 MeV	Present data	0.956± 0.040	0.905± 0.115	634± 39	2.2	3
2$^+$ State	de Bie (Ref. 19)	0.933± 0.010	0.991	761± 30	1.6	8
	Towsley *et al.* (Ref. 20)			666± 29		
3.16 MeV	Present data	0.901± 0.041	0.991[a]	12.4± 2.3	2.5	4
2$^+$ State	de Bie	0.931± 0.040	0.991[a]	15.5± 2.0	1.0	5

[a] By assumption, from de Bie.

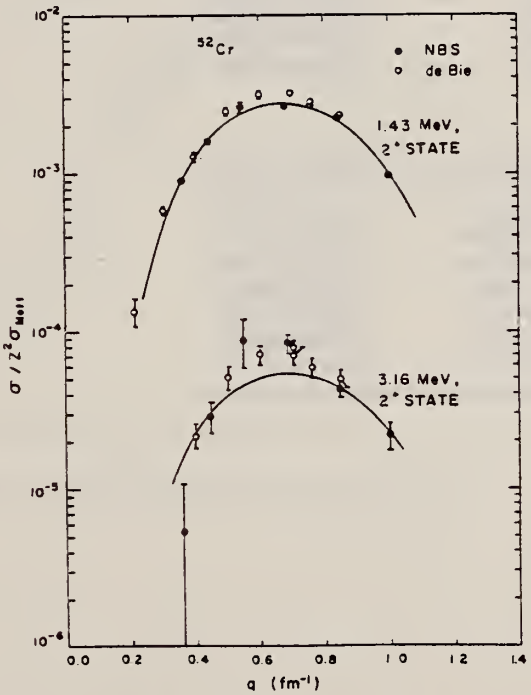

FIG. 4. Cross section for ^{52}Cr in units of $Z^2\,\sigma_{Mott}$ for the 1.43 and 3.16 MeV, σ_{Mott} 2$^+$ states. Also shown are the data of de Bie. Tassie model fits to the NBS data alone are given by the solid curves.

(over)

TABLE III. Ratios of inelastic scattering cross sections to $Z^2\sigma_{Mott}$.

E_i (MeV)	θ (deg)	1.43 MeV, 2^+ state	3.16 MeV, 2^+ state
		^{52}Cr	
39.38	127.74	(0.90 ± 0.04)-03	(0.55 ± 0.55)-05
49.44	127.74	(0.159± 0.006)-02	(0.29 ± 0.07)-04
59.84	127.71	(0.26 ± 0.02)-02	(0.89 ± 0.30)-04
75.22	127.71	(0.265± 0.007)-02	(0.842± 0.012)-04
92.73	127.74	(0.222± 0.005)-02	(0.428± 0.052)-04
110.20	127.69	(0.97 ± 0.02)-03	(0.222± 0.044)-04

E_i (MeV)	θ (deg)	0.374 MeV, 2_1^+ state	0.81 MeV, 2_2^+ state
		^{110}Pd	
39.38	127.74	(0.35 ± 0.03)-02	(0.45± 0.14)-04
49.44	127.74	(0.40 ± 0.02)-02	(0.10± 0.01)-03
59.84	127.71	(0.40 ± 0.02)-02	(0.10± 0.01)-03
75.22	127.71	(0.233± 0.003)-02	(0.86± 0.07)-04
92.73	127.74	(0.40 ± 0.05)-03	(0.48± 0.06)-04
110.20	127.69	(0.23± 0.01)-03	(0.17± 0.17)-05

E_i (MeV)	θ (deg)	0.558 MeV, 2_1^+ state	1.208 MeV, 2_2^+ state
		^{114}Cd	
39.38	127.74	(0.20 ± 0.02)-02	(0.46± 0.07)-04
49.44	127.74	(0.28 ± 0.02)-02	(0.40± 0.06)-04
59.84	127.71	(0.220± 0.014)-02	(0.58± 0.11)-04
75.22	127.71	(0.118± 0.005)-02	(0.34± 0.04)-04
92.73	127.74	(0.204± 0.007)-03	(0.11± 0.04)-04
110.20	127.69	(0.155± 0.007)-03	(0.61± 0.35)-05

E_i (MeV)	θ (deg)	1.294 MeV, 2_1^+ state	2.112 MeV, 2_2^+ state	2.266 MeV, 3^- state
		^{116}Sn		
39.38	127.74	(0.65± 0.04)-03	(0.68± 1.05)-05	(0.18± 0.02)-03
49.44	127.74	(0.88± 0.04)-03	(0.26± 0.69)-05	(0.40± 0.01)-03
59.84	127.71	(0.84± 0.03)-03	(0.21± 0.06)-04	(0.63± 0.02)-03
75.22	127.71	(0.36± 0.02)-03	(0.5 ± 7.4)-06	(0.84± 0.02)-03
75.02	127.81	(0.34± 0.02)-03	(0.47± 0.39)-05	(0.82± 0.01)-03
92.73	127.74	(0.50± 0.09)-04	(0± 0.19)-04	(0.60± 0.01)-03
110.20	127.69	(0.85± 0.10)-04	(0± 0.8)-05	(0.14± 0.01)-03

REF. K. Masumoto, T. Kato, N. Suzuki
Nucl. Inst. Meth. 157, 567 (1978)

ELEM. SYM.	A	Z
Cr	52	24

METHOD

REF. NO.	
78 Ma 10	hg

REACTION	RESULT	EXCITATION ENERGY	SOURCE		DETECTOR		ANGLE
			TYPE	RANGE	TYPE	RANGE	
G,N	ABY	12-68	C	30-68	ACT - I		4PI

Analysis is made of reactions interfering with photon activation analysis procedures.

The activation yield curves have been presented for a number of photonuclear reactions in the energy range from 30 to 68 MeV, in order to evaluate quantitatively the interferences due to competing reactions in multielement photon activation analysis. The general features of the yields as functions of both target mass number and excitation energy were elucidated from the data obtained, discussion being given on the results in terms of the reaction mechanism.

Simultaneous neutron activation due to appreciable neutron production from the converter and surrounding materials has also been studied, and, finally, the magnitudes of interferences in real multielement analysis were given in the form of their energy dependences.

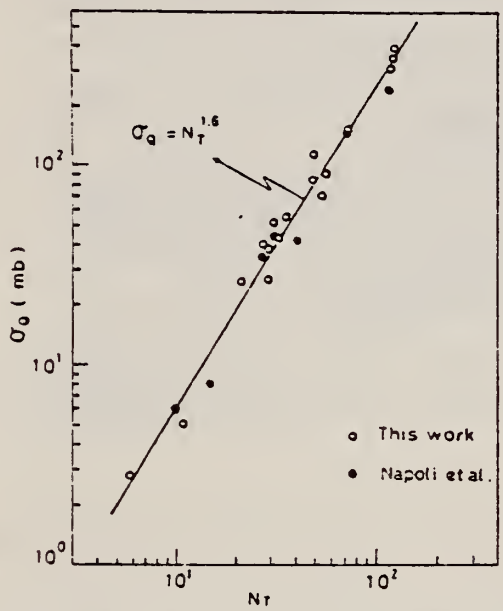

Fig. 2. Yield per equivalent quanta versus target neutron number.

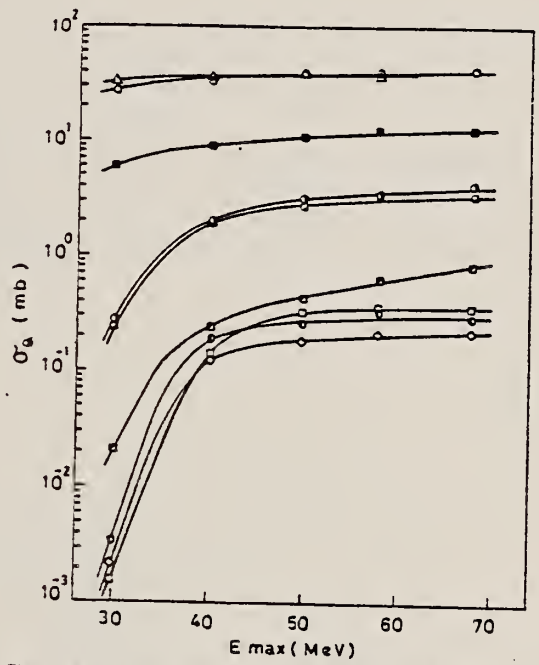

Fig. 5. Activation yield curves for the reactions on Cr, Mn and Fe.
○ $^{52}Cr(\gamma, n)^{51}Cr$, ◑ $^{50}Cr(\gamma, pn)^{48}V$, ◐ $^{50}Cr(\gamma, 2n)^{48}Cr$,
△ $^{55}Mn(\gamma, n)^{54}Mn$, ◪ $^{57}Fe(\gamma, p)^{56}Mn$, ◩ $^{54}Fe(\gamma, pn)^{52g}Mn$,
◪ $^{56}Fe(\gamma, pn)^{54}Mn$, □ $^{56}Fe(\gamma, 2n)^{51}Cr$, ◇ $^{54}Fe(\gamma, 2n)^{52}Fe$.

(over)

FORM NBS-418
REV. 7-73
U.S. DEPARTMENT OF COMMERCE

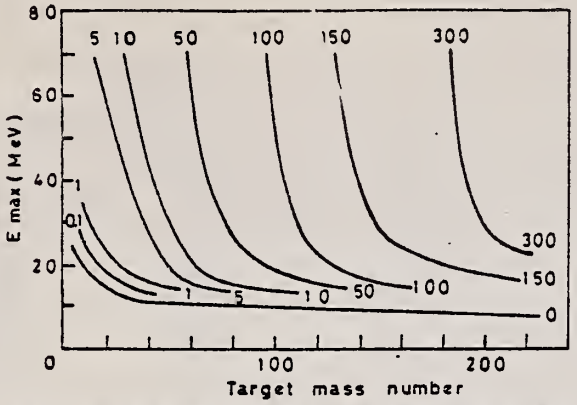

Fig. 9. Yields of the (γ, n) reactions as a function of bremsstrahlung maximum energy and target mass number. The numerical values in the figure are yields per equivalent quanta in mb.

REF. V.N. Polishchuk, n.G. Shevchenko, N.G. Afanas'ev, A.A. Khomich, A.Yu. Buki, B.V. Mazan'ko
Yad. Fiz. 27, 1145 (1978)
Sov. J. Nucl. Phys. 27, 607 (1978)

ELEM. SYM.	A	Z
Cr	52	24

METHOD

REF. NO. 78 Po 3 hg

REACTION	RESULT	EXCITATION ENERGY	SOURCE TYPE	SOURCE RANGE	DETECTOR TYPE	DETECTOR RANGE	ANGLE
E,E/	BEL	1	D	120, 227	MAG-D		DST

1 LEVEL 1.43 MEV

Inelastic electron scattering has been used to measure the form factors of the 1.43-MeV level in ^{52}Cr and the 0.56-, 1.01-, 1.29-, and 1.97-MeV levels in ^{53}Cr. The measurements were made with an initial electron energy $E_0 = 90$, 120, and 226 MeV in the momentum-transfer region 0.85–1.7 F^{-1} and 0.74–1.15 F^{-1} respectively for ^{52}Cr and ^{53}Cr. For these states reduced transition probabilities $B(E2)\uparrow$ were obtained, respectively 800 ± 80, 100 ± 20, 170 ± 18, 335 ± 30, and 190 ± 15 $e^2 \cdot F^4$. The results obtained are discussed in terms of the excited-core model.

PACS numbers: 25.30.Cg, 27.40. + z, 23.20.Ck

TABLE I. Reduced probabilities for transition from the ground state of the nucleus to excited states for the isotopes ^{52,53}Cr.

Nucleus	Transition $J_i \to J_f$	ω, MeV	λ	Value of $B(E\lambda)\uparrow$, $e^2 \cdot F^{2\lambda}$: Experiment: Our data	[7]	[14]	[15]	Theory [1]: Generalized model $\varepsilon_n = \varepsilon$	Generalized model $\varepsilon_n = 0$	Shell model	[14]	[15]	[16] ν	[16] ∞
^{53}Cr	$^3/_2^- \to {}^1/_2^-$	0.56	2	100±20	115±12	110±20	89	98	50	218	73	59	62.5	66.5
	$^3/_2^- \to {}^3/_2^-$	1.01	2	170±18	72±8	20±4	53	113	64	33	53	162	20.3	64.5
	$^5/_2^- \to {}^3/_2^-$	1.29	2	335±34	301±40	240±60	138	220	135	236	192		98	244
	$^3/_2^- \to {}^5/_2^-$	1.97	2	190±15				54	55	132	93			
	$^5/_2^- \to {}^5/_2^-$	2.32	2					33	50				149	160

Nucleus	Transition $J_i \to J_f$	ω, MeV	λ	Our data	[7]	[14]	[15]	[17] $\varepsilon_n = 0.6$	[17] $\varepsilon_n = 0.7$	[18]				
^{52}Cr	$0 \to 2^+$	1.43	2	800±80	720±80	720	761±30	610	720	940				

[1] Calculation carried out for $M_{22} = 25\ e \cdot F^2$ and $\xi = -0.169$ MeV, $\eta = -0.0002$ MeV $\cdot e^{-2} \cdot F^{-4}$.
[2] Calculation carried out for $M_{22} = 25\ e \cdot F^2$ and $\xi = -0.125$ MeV, $\eta = -0.00055$ MeV $\cdot e^{-2} \cdot F^{-4}$.

REF. N. Kumagai, T. Ishimatsu, E. Tanaka, K. Kageyama, G. Isoyama
Nucl. Phys. A329, 205 (1979)

ELEM. SYM.	A	Z
Cr	52	24

METHOD

REF. NO. 79Ku4 hg

REACTION	RESULT	EXCITATION ENERGY	SOURCE TYPE	SOURCE RANGE	DETECTOR TYPE	DETECTOR RANGE	ANGLE
G,G	LFT	7-10	C	14	SCD-D		DST

Abstract: The resonance scattering of electron bremsstrahlung from natural chromium and iron targets has been studied for photon energies up to 12 MeV. Seven γ-transitions of energies higher than 7 MeV were observed for each of the targets, which suggests seven resonant levels in each of ^{52}Cr and ^{56}Fe at excitation energies above 7 MeV. The spins of these levels were all assigned to be 1 from the relative yields at scattering angles of 125° and 150°. Radiative widths of these levels were obtained. A discussion is made about the possibility that these levels are $T_<$ components of the M1 giant resonance in ^{52}Cr and ^{56}Fe.

7 LEVELS

E NUCLEAR REACTIONS ^{52}Cr, ^{56}Fe(γ, γ) bremsstrahlung E_e = 14 MeV; measured E_γ, $I_\gamma(\theta$ = 125°, 150°); ^{52}Cr, ^{56}Fe deduced levels, J, Γ_γ. Natural targets.

TABLE 2

Electromagnetic transitions in ^{11}B used for calibration of $N\varepsilon\Omega$ [a])

Initial state	J^π	Γ (eV)	Branching ratios (%) to final states [b]) g.s.	2.125	4.445	5.021
4.445	$\frac{1}{2}^-$	0.610 ± 0.030	100 [c])			
5.021	$\frac{1}{2}^-$	1.80 ± 0.13 [d])	84 ± 2 [e])	16 ± 2 [f])		
7.286	$\frac{1}{2}^+$	1.17 ± 0.26 [d])	87 ± 2		5.5 ± 1	7.5 ± 1
8.920 [g])	$\frac{1}{2}^-$	4.20 ± 0.52 [d])	95 ± 1		5 ± 0.5	

[a]) Ref. [9]) except where shown.
[b]) Ref. [8]).
[c]) $\delta = -0.19 \pm 0.15$ [ref. [9])].
[d]) Ref. [7]).
[e]) $\delta = 0.03 \pm 0.05$ [ref. [9])].
[f]) $\delta = -0.05 \pm 0.20$ [ref. [9])].
[g]) $\delta = -0.11 \pm 0.04$ [ref. [10])].

TABLE 3

Electromagnetic transtions in ^{24}Mg used for calibration of $N\varepsilon\Omega$ [a])

Initial state	J^π	Γ (eV)	Branching ratios (%) to final states g.s.	1.369
9.966	1^-	8.8 ± 2.3	65 ± 2	35 ± 2
10.712	1^+	19.9 ± 1.8	78 ± 4	22 ± 4

[a]) Ref. [11]).

TABLE 5

Summary of the experimental results of ^{56}Fe

Level energy (MeV)	$I(150°)/I(125°)$	J	Γ [a]) (eV)	B(M1, $1^+ \rightarrow 0^+$) [b]) (μ_N^2)
6.927	1.27 ± 0.37	1	1.10 ± 0.29	0.29
7.212	1.29 ± 0.44	1	0.77 ± 0.22	0.18
8.131	1.30 ± 0.27	1	3.55 ± 0.74	0.57
8.243	1.37 ± 0.19	1	5.75 ± 0.92	0.89
8.538	1.35 ± 0.27	1	4.92 ± 0.95	0.68
10.479	1.32 ± 0.27	1	3.44 ± 0.64	0.26
11.133	1.17 ± 0.28	1	2.08 ± 0.52	0.13

[a]) Deduced on the assumption of 100 % ground-state transition.
[b]) Deduced on the assumption of even parity.

REF. H. Tsubota, S. Oikawa, J. Uegaki, T. Tamae
Nucl. Phys. A321, 157 (1979)

ELEM. SYM.	A	Z
Cr	52	24

METHOD

REF. NO. 79Ts2 hg

REACTION	RESULT	EXCITATION ENERGY	SOURCE TYPE	SOURCE RANGE	DETECTOR TYPE	DETECTOR RANGE	ANGLE
G,P	ABX	15-26	C	15-26	MAG-D		DST
				(15.8-26)			

Abstract: The differential cross sections at 90° for the $^{51}V(e, p_0)^{50}Ti$ and $^{52}Cr(e, p_0+p_1)^{51}V$ reactions have been measured over the giant dipole resonance region. These cross sections were used to obtain the differential cross sections of the $^{51}V(\gamma, p_0)^{50}Ti$ and $^{52}Cr(\gamma, p_0+p_1)^{51}V$ reactions. The results show two peaks that appear at the same energies as the main peaks of the (γ, n) and (γ, p) cross section for both nuclei. The angular distributions of protons from the (e, p) reaction have also been measured at several points of the incident electron energy. The coefficients A_2 obtained by fitting with a series of Legendre polynomials, $W(\theta) = 1 + A_1P_1(\cos\theta) + A_2P_2(\cos\theta)$, varies with excitation energy. These results are discussed in terms of the direct-semidirect process considering isospin effects in the giant dipole resonance.

V-PHOTON ANL, P=PØ+P1

E NUCLEAR REACTIONS ^{51}V, $^{52}Cr(e, p_0)$, (γ, p_0), E = 15.0–26.0 MeV; measured $\sigma(E, \theta)$ at θ = 90°, measured $\sigma(E, \theta)$ at several E-values for ^{51}V and at E = 21.4 MeV for ^{52}Cr. Deduced $\sigma(E, \theta)$ for $^{51}V(\gamma, p_0)$ and for $^{52}Cr(\gamma, p_0+p_1)$ at θ = 90°; natural target (^{51}V), enriched target (^{52}Cr).

TABLE 2

Experimental results of the (γ, p_0) reactions

	$\frac{d\sigma(\gamma, p_0)dE}{d\Omega}(90°)$ (MeV · mb/sr)	$4\pi\frac{d\sigma(\gamma, p_0)dE}{d\Omega}$ (MeV · mb)	$\frac{d\sigma(\gamma, p)dE}{d\Omega}$ (MeV · mb/sr)	$\frac{d\sigma(\gamma, p_0)dE}{d\Omega} / \frac{d\sigma(\gamma, p)dE}{d\Omega}$
^{51}V	0.46 ± 0.07	5.78 ± 0.88	(15–29 MeV) [b] 16.32	0.03
^{52}Cr	1.70 ± 0.22 [a]	21.36 ± 2.76 [a]	(15–29 MeV) [c] 19	0.09

[a] The (γ, p_0+p_1) cross section.
[b] Ref. [1]. [c] Ref. [24].

TABLE 3

Coefficients obtained by fitting a series of Legendre polynomials $W(\theta) = 1 + A_1P_1(\cos\theta) + A_2P_2(\cos\theta)$

	E_γ (MeV)	E_x (MeV)	A_1	A_2
^{51}V	17.0	15.4–16.5	0.21 ± 0.05	0.33 ± 0.09
	18.0	16.4–17.5	0.33 ± 0.04	0.33 ± 0.06
	19.0	17.4–18.5	0.28 ± 0.06	0.25 ± 0.11
	21.0	19.4–20.5	0.21 ± 0.07	0.21 ± 0.13
	22.0	20.4–21.5	0.51 ± 0.08	−0.11 ± 0.13
^{52}Cr	21.4	20.5–21.0	0.06 ± 0.07	0.05 ± 0.11

The range of the excitation energy E_x is also indicated.

(over)

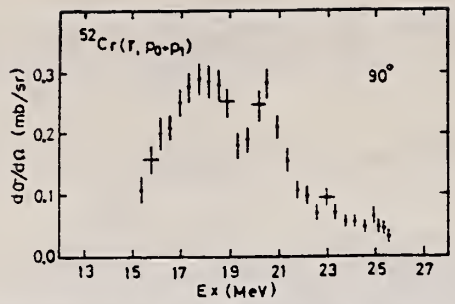

Fig. 3. The differential cross section at 90° for the ^{52}Cr(γ, p_0+p_1)^{51}V reaction.

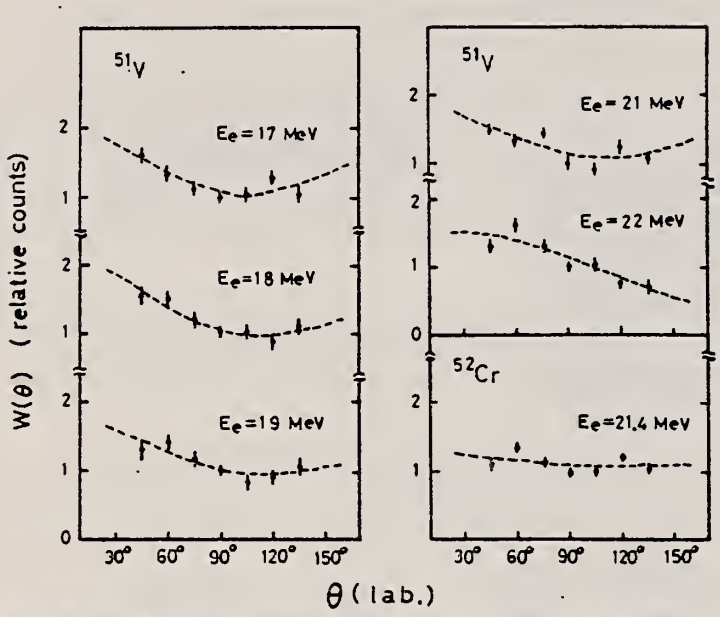

Fig. 6. The angular distributions of protons from the ^{51}V(e, p_0)^{50}Ti and ^{52}Cr(e, p_0+p_1)^{51}V reactions. The dashed curves are the results fitted with the sum of Legendre polynomials, $W(\theta) = 1 + A_1 P_1(\cos\theta) + A_2 P_2(\cos\theta)$.

REF. J. Ahlert M. Schumacher
Z. Phys. A301, 75 (1981)

ELEM. SYM.	A	Z
Cr	52	24

METHOD

REF. NO. 81 Ah 6 hg

REACTION	RESULT	EXCITATION ENERGY	SOURCE TYPE	SOURCE RANGE	DETECTOR TYPE	DETECTOR RANGE	ANGLE
G,G	LFT	1	D	1	NAI-D		100
		(1.434)		(1.434)			

B(EL), LEVEL 1.434 MEV

A resonance fluorescence self-absorption experiment has been carried out for the 1,434 MeV first excited state in ^{52}Cr, using gaseous $^{52}MnI_2$ as source for the exciting gamma radiation. The $B(E2, 0_1^+ \rightarrow 2_1^+) = (687 \pm 13)\, e^2\,fm^4$ is in agreement with the most recent Coulomb excitation and inelastic electron scattering experiments yielding $(660 \pm 30)\, e^2\,fm^4$ and $(634 \pm 39)\, e^2\,fm^4$, respectively, and disagrees with former electron scattering experiments.

Table 1. Experimental results of self-absorption experiment

$\dot{N}_{Cr}, \dot{N}_{Ie}$	0.7594 ± 0.0041
β	1.0142 ± 0.0007
$\mu(\Gamma_0)$	0.7488 ± 0.0041
Γ_0	(673 ± 13) μeV
τ	(0.979 ± 0.019) ps
$B(E2)$	(687 ± 13) $e^2\,fm^4$

Table 2. Comparison of present and prevois $B(E2)$ for the 1.4341 MeV level in ^{52}Cr

Experiment		Ref.	$B(E2, 0_1^+ \rightarrow 2_1^+)$ $e^2\,fm^4$
Coul. excitation			
Ad	1960	7	620 ± 150
Mc Gow	1962	8	720 ± 90
Sim	1965	9	480 ± 20
Tow	1975	10	660 ± 30
electron scatt.			
Bel	1964	11	520 ± 4
Pet	1971	12	430 ± 70[a]
			710 ± 90[b]
Lig	1976	13	634 ± 39
DSAM			
Spr	1971	14	680 ± 200
nucl. res. fluor.			
Of	1959	15	841 ± 210
Bo	1964	16	610 ± 170
present work			687 ± 13

Ref. 64 Be 3

Ref. 76 Li 5

Ref. 64 Bol

[a] Microscopic model [b] Macroscopic model

REF. U.E.P. Berg, D. Ruck, K. Ackermann, K. Bangert, C. Blasing, K. Kobras, W. Naatz, R.K.M. Schneider, R. Stock, K. Wienhard
Phys. Lett. 103B, 301 (1981)

ELEM. SYM.	A	Z
Cr	52	24

METHOD

REF. NO. 81 Be 9 hg

REACTION	RESULT	EXCITATION ENERGY	SOURCE		DETECTOR		ANGLE
			TYPE	RANGE	TYPE	RANGE	
$ G,G	SPC	7 - 10	C	20	SCD-D		90

Nuclear resonance fluorescence experiments with polarized bremsstrahlung were performed to search for magnetic dipole strength. Previous interpretations that states at 7730, 7896 and 9787 keV in ^{52}Cr are due to M1 excitations can not be confirmed. These transitions are unexpectedly strong E1 excitations, exceeding 1 m Weisskopf unit in strength. The remaining identified M1 strength of $\Sigma B(M1)\uparrow = 2.5 \pm 0.7\ \mu_k^2$ is in agreement with the observation of missing M1 strength in heavy nuclei.

COH BREM

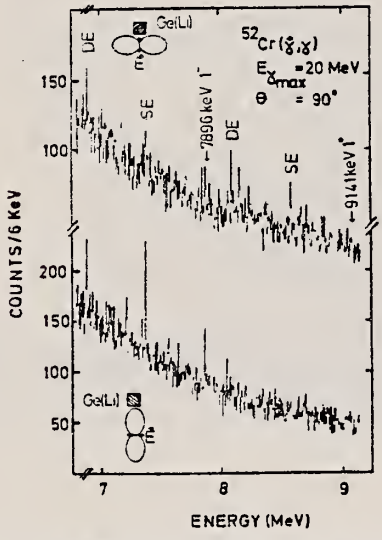

Fig. 1. Parts of the ^{52}Cr($\vec{\gamma}$, γ) spectra from photon scattering of linearly polarized bremsstrahlung. In the upper part the electric field vector E of the incoming photon was parallel and in the lower part perpendicular to the scattering plane as shown in the insert.

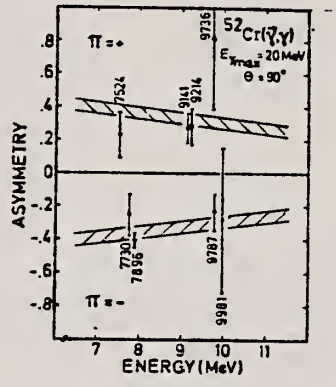

Fig. 2. Asymmetries for different ground-state dipole transitions in ^{52}Cr. The numbers at the error bars are the corresponding excitation energies in keV. The hatched bands were determined with help of the ^{2}H($\vec{\gamma}$, p) reaction and show the expected asymmetries for even parity (upper part) and odd parity (lower part) excitation.

REF. T.J. Bowles, R.J. Holt, H.E. Jackson, R.M. Laszewski, R.D. McKeown, A.M. Nathan, J.R. Specht
Phys. Rev. C24, 1940 (1981)

ELEM. SYM.	A	Z
Cr	52	24

METHOD

REF. NO.: 81 Bo 5 hg

REACTION	RESULT	EXCITATION ENERGY	SOURCE		DETECTOR		ANGLE
			TYPE	RANGE	TYPE	RANGE	
G,G	ABX	15-23	D	15-23	NAI-D		90

Quasimonochromatic photons have been used to measure elastic and inelastic photon scattering cross sections in the giant dipole resonance region of ^{52}Cr, Fe, ^{60}Ni, ^{92}Mo, and ^{96}Mo in an experiment in which the elastic and inelastic scattering are resolved. The elastic scattering cross sections show clear evidence for isospin splitting of the giant dipole resonance. The inelastic scattering to low-lying vibrational levels, which is a measure of the coupling between the giant dipole resonance and collective surface vibrations, is in qualitative agreement with the predictions of the dynamic collective model. However, when examined in detail, this model does not provide an adequate description of the scattering data.

[NUCLEAR REACTIONS ^{52}Cr, Fe, ^{60}Ni, ^{92,96}Mo (γ,γ'), $14 \leq E_\gamma \leq 22$ MeV; measured E_γ, $E_{\gamma'}$, $d\sigma/d\Omega$ for γ_0,γ_1. Compared to DCM predictions. Tagged photons.]

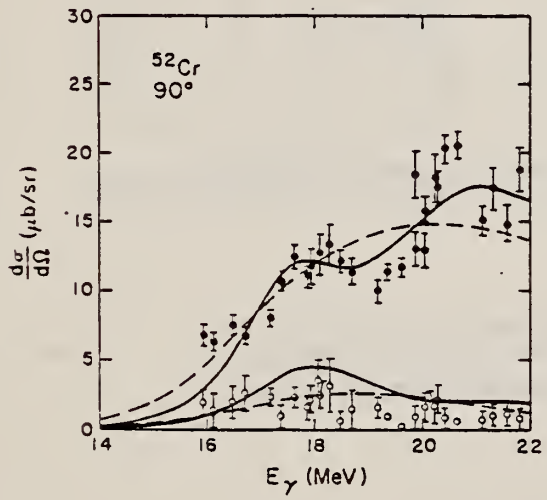

FIG. 8. Elastic (closed circles) and inelastic (open circles) scattering cross sections at $\theta = 90°$ for ^{52}Cr. The error bars represent statistical uncertainties only. The solid (dashed) lines are DCM calculations for the elastic and inelastic cross sections including (not including) the effect of isospin splitting.

REF. B.S. Ishkhanov, Yu.A. Novikov, E.S. Omarov, I.M. Piskarev
Izv. Akad. Nauk SSSR 45, 147 (1981)
Bull. Acad. Sci. 45, 129 (1981)

ELEM. SYM.	A	Z
Cr	52	24

METHOD

REF. NO. 81 Is 5 hg

REACTION	RESULT	EXCITATION ENERGY	SOURCE		DETECTOR		ANGLE
			TYPE	RANGE	TYPE	RANGE	
G,G	ABX	5-17	C	6-17	NAI-D		90

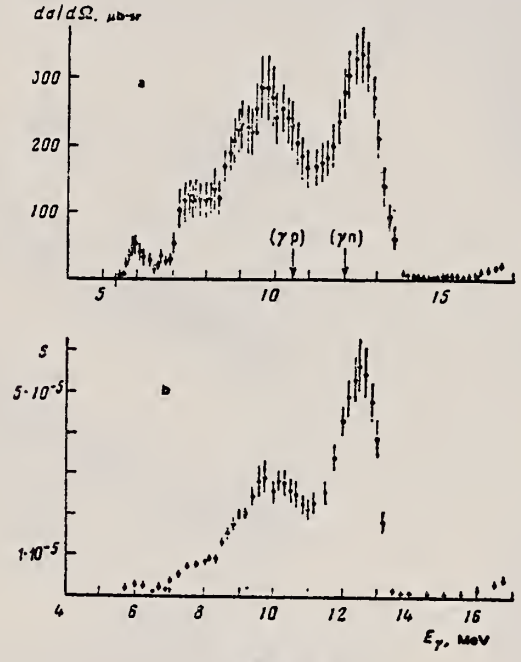

Fig. 2

Table 2

Integral Cross Sections for Scattering of Protons by an ^{52}Cr Nucleus

Position of maximum, MeV	Integral cross section, MeV·mb
6,0±0.1	0.50±0,15
7.4±0.2	0,9±0,2
9,7±0.2	5,0±0,5
12.5±0.2	5,0±0,5

Fig. 2. a) Cross section for the elastic scattering of protons by a ^{52}Cr nucleus. The arrows denote the thresholds of the (γn)- and (γp)-reactions; b) photon strength function for the ^{52}Cr nucleus, as calculated from the elastic-scattering cross section.

REF. B.S. Ishkhanov, Yu.A. Novikov, E.S. Omarov, I.M. Piskarev
Sov. J. Nucl. Phys. 33, 296 (1981)
Yad. Fiz. 33, 570 (1981)

ELEM. SYM.	A	Z
Cr	52	24

METHOD

REF. NO.	
81 Is 6	hg

REACTION	RESULT	EXCITATION ENERGY	SOURCE		DETECTOR		ANGLE
			TYPE	RANGE	TYPE	RANGE	
G,NG	ABX	12-32	C	10-32	SCD-D		135
G,PG	ABX	10-32	C	10-32	SCD-D		135

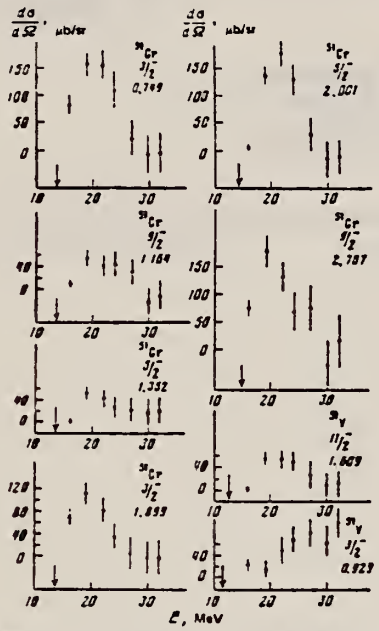

FIG. 1. Differential cross sections for excitation of ^{51}Cr and ^{51}V levels in the $^{52}Cr(\gamma,X\gamma)$ reaction.

TABLE I. Levels populated in the $^{52}Cr(\gamma, X\gamma)$ reaction.

Excitation energy, MeV (Ref. 1)	J^π (Ref. 1)	Integrated cross section, MeV · mb	Final nucleus
0.749	$3/2^-$	19±2	
0.777	$1/2^-$		
1.184	$5/2^-$	6±2	
1.352	$3/2^-$	6±2	
1.557	$7/2^-$	6±2	^{51}Cr
1.899	$5/2^-$	10±2	
2.001	$5/2^-$	17±2	
2.767	$5/2^-$	20±3	
3.282	–	16±2	
0.320	$3/2^-$	13±3	
0.929	$5/2^-$	12±2	^{51}V
1.608	$11/2^-$	7±2	

REF. G. Eulenberg, D.I. Sober, W. Steffen, H.-D. Gräf, G. Küchler, A. Richter, E. Spamer, B.C. Metsch, W. Knüpfer
Phys. Lett. 116B, 113 (1982)

ELEM. SYM.	A	Z
Cr	52	24

METHOD

REF. NO.: 82 Eu 1 egf

REACTION	RESULT	EXCITATION ENERGY	SOURCE TYPE	SOURCE RANGE	DETECTOR TYPE	DETECTOR RANGE	ANGLE
E,E/	ABX	8-12	D	30-58	MAG-D		DST

M1 STRENGTH

Following the recent discovery of a very strong magnetic dipole transition in ^{48}Ca to a state at 10.23 MeV in high-resolution inelastic electron scattering, results of a detailed search for M1 strength in the other $N = 28$ isotones ^{50}Ti, ^{52}Cr and ^{54}Fe are described. The M1 strength found in the investigated region of excitation energy $E_x \approx 7-12$ MeV is very fragmented and considerably quenched in comparison to predictions of shell model calculations in a model space that includes up to 2p–2h excitations.

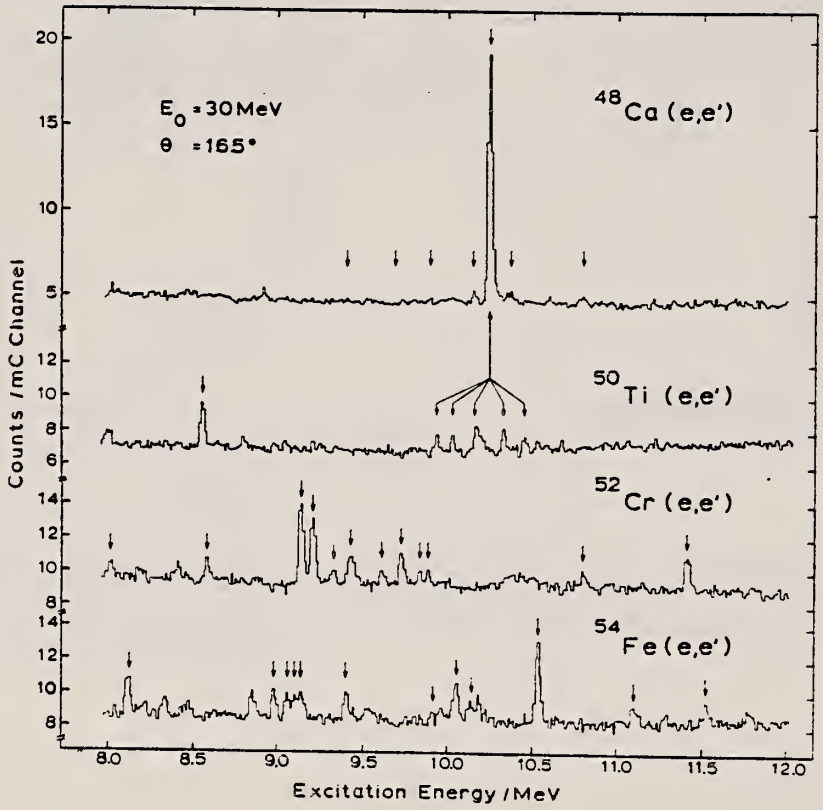

Fig. 1. High-resolution inelastic electron scattering spectra of the $N = 28$ isotones all measured at $E_0 = 30$ MeV and at $\theta = 165°$. The strongest magnetic dipole transitions are indicated by arrows.

(OVER)

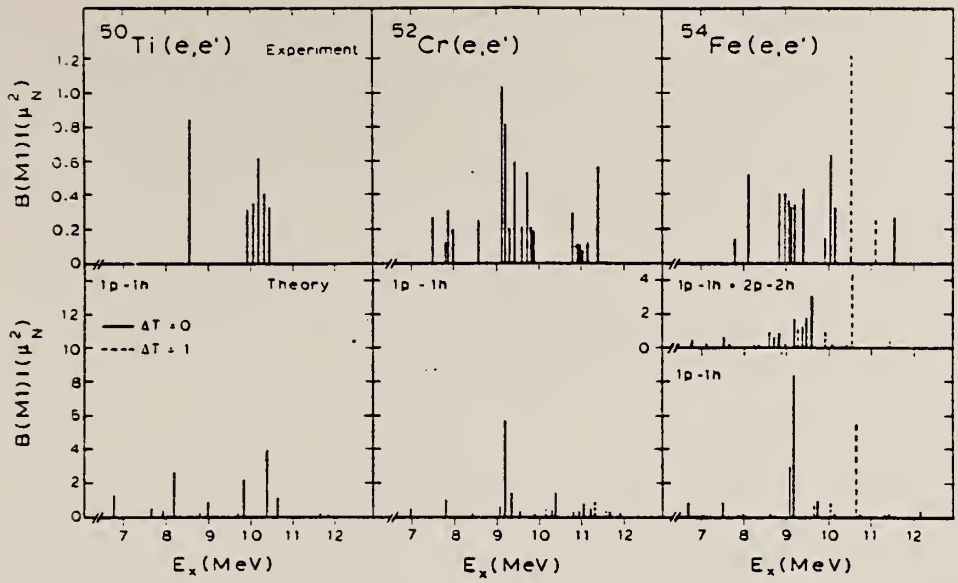

Fig. 3. Comparison of experimental and calculated M1 strength distributions for ^{50}Ti, ^{52}Cr and ^{54}Fe. Note the scale difference. For details, see the main text.

CR
A=53

CR
A=53

CR
A=53

K. N. Geller, J. Halpern, and E. G. Muirhead
Phys. Rev. 118, 1302-12 (1960)

Cr	53	24

METHOD: Betatron; neutron threshold; ion chamber

REF. NO.: 60 Ge 3 | NVB

REACTION	RESULT	EXCITATION ENERGY	SOURCE		DETECTOR		ANGLE
			TYPE	RANGE	TYPE	RANGE	
G,N	NØX	THR	C THR		BF3-I		4 PI

THRESHØLD

TABLE I. Summary and comparison of neutron separation energies inferred from present threshold measurements with values predicted from mass data and reaction energies. All energies are expressed in the center-of-mass system in Mev.

Reaction	No. runs	Present results	Other results	Method	Reference
$Cr^{53}(\gamma,n)Cr^{52}$	1	7.92 ±0.06	7.946±0.007	$Cr^{53}(d,p)Cr^{54}$	i
			7.943±0.004	mass data	g

[g] C. F. Giese and J. L. Benson, Phys. Rev. 110, 712 (1958).
[h] P. M. Endt et al., Phys. Rev. 105, 1002 (1957).
[i] M. Mazari, W. W. Buechner, and A. Sperduto, Phys. Rev. 112, 1691 (1958).

REF. E. C. Booth, B. Chasan and K. A. Wright
Nucl. Phys. 57, 403-420 (1964)

ELEM. SYM.	A	Z
Cr	53	24

METHOD

REF. NO. 64 Bo 1 NVB

REACTION	RESULT	EXCITATION ENERGY	SOURCE TYPE	SOURCE RANGE	DETECTOR TYPE	DETECTOR RANGE	ANGLE
G,G	LFT	1-3	C	1 - 3	NAI-D		100
		(0.5 - 3.0)		(0.5 - 3.0)			

ABI

TABLE 1
Cases of observed resonance fluorescence

Nucleus multipol.	State (MeV)	Spin	Γ_0/Γ	$T(g w \Gamma_0^2/\Gamma^2)^{-1}$ (sec).	Mean lifetime T BCW (sec)	Mean lifetime T other (sec)	Ref.	Γ_0/Γ_W BCW
Cr^{53}	0.00	$\frac{3}{2}^-$						
M1[a])	2.32	$\frac{1}{2}^-$	(1)	$6.2\pm2\times10^{-15}$	$3.1\pm1\times10^{-15}$			0.9
Mn^{55}	0.00	$\frac{5}{2}^-$						
M1[a])	1.53	$\frac{3}{2}$	0.9	$27\pm8\times10^{-14}$	$15\pm4\times10^{-14}$			5×10^{-3}
[M1][a])	1.88	$[\frac{3}{2}^-]$	0.82	$23\pm7\times10^{-15}$	$15\pm5\times10^{-15} g W$			0.4
[M1][a])	2.20	$[\frac{3}{2}^-]$	?	$28^{+15}_{-11}\times10^{-15}$				$0.16\Gamma/\Gamma_0$
[M1][a])	2.56	$[\frac{3}{2}^-]$	?	$17^{+15}_{-7}\times10^{-15}$				$0.18\Gamma/\Gamma_0$

REF.

Y. Oka, T. Kato, K. Nomura, T. Saito, Hui-Tuh Tsai
Bull. Chem. Soc. Japan 41, 380 (1968)

ELEM. SYM.	A	Z
Cr	53	24

METHOD

REF. NO.	
68 Ok 3	egf

REACTION	RESULT	EXCITATION ENERGY	SOURCE		DETECTOR		ANGLE
			TYPE	RANGE	TYPE	RANGE	
G,P	ABY	THR-20	C	20	ACT-I		4PI

TABLE 1. SUMMARY OF DATA ON (γ, p) REACTIONS WITH 20 MeV BREMSSTRAHLUNG

Nuclide: Parent (Natural abundance, %)	Nuclide: Residual (Half-life)	S_p (MeV)	Observed γ-ray: Energy (MeV)	Observed γ-ray: Branching ratio (%)	Observed γ-ray: Type of multipole transition	Yield determined: μCi/mg[a]	Yield determined: Yield/mol·R
^{25}Mg (10.11)	^{24}Na (15 hr)	12.06	1.37	100	$E2$	1.48×10^{-1}	1.7×10^{6}
^{29}Si (4.71)	^{28}Al (2.27 min)	12.33	1.78	100	$E2$	1.91	2.8×10^{6}
^{30}Si (3.12)	^{29}Al (6.56 min)	13.59	1.28	93.8	$E2+M1$	6.51×10^{-1}	1.5×10^{6}
^{44}Ca (2.06)	^{43}K (22.4 hr)	12.17	0.374	85	$E2+M1$	7.86×10^{-3}	1.3×10^{5}
^{47}Ti (7.32)	^{46}Sc (84.1 d)	10.47	0.887	100	$E2$	7.11×10^{-4}	3.1×10^{5}
^{48}Ti (73.99)	^{47}Sc (3.4 d)	11.44	0.160	100	$E2+M1$	6.83×10^{-3}	1.2×10^{5}
^{49}Ti (5.46)	^{48}Sc (1.8 d)	11.35	1.31	100	$E2$	4.40×10^{-3}	5.8×10^{4}
^{53}Cr (9.55)	^{52}V (3.8 min)	11.15	1.43	100	$E2$	5.01×10^{-1}	6.6×10^{4}
^{57}Fe (2.17)	^{56}Mn (2.58 hr)	10.57	1.81	23.5	$E2+M1$	8.10×10^{-2}	2.1×10^{5}
^{74}Ge (36.74)	^{73}Ga (4.8 hr)	10.92	0.295	97	($E2$)	3.70×10^{-1}	1.3×10^{5}
^{77}Se (7.58)	^{76}As (26.5 hr)	9.61	0.559	41	$E2$	1.48×10^{-3}	1.3×10^{6}
^{87}Sr (7.02)	^{86}Rb (19 d)	9.41	1.08	9	$E2$	5.15×10^{-4}	9.9×10^{4}
^{113}Cd (12.26)	^{112}Ag (3.2 hr)	9.74	1.39	35	$E2$	1.91×10^{-2}	2.1×10^{6}
^{117}Sn (7.57)	^{116m}In (54 min)	9.58	1.27	84	$E2$	9.80×10^{-3}	6.9×10^{5}
^{137}Ba (11.32)	^{136}Cs (13 d)	8.67	0.830	100	$E2$	1.68×10^{-4}	2.2×10^{6}
^{199}Hg (16.84)	^{198}Au (2.7 d)	7.27	0.412	100	$E2$	8.43×10^{-4}	2.2×10^{6}

a) The value corrected at the end of 1 hr irradiation (9.4×10^{6} R/min).

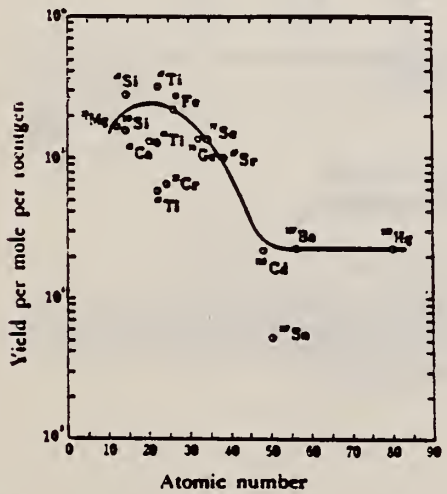

Fig. 2. The yield curve for the (γ, p) reaction with 20 MeV bremsstrahlung.

REF. R. J. Baglan, C. D. Bowman and B. L. Berman
Phys. Rev. C3, 672 (1971)

ELEM. SYM.	A	Z
Cr	53	24

METHOD

REF. NO. 71 Ba 2

hmg

REACTION	RESULT	EXCITATION ENERGY	SOURCE		DETECTOR		ANGLE
			TYPE	RANGE	TYPE	RANGE	
G,N	ABX	9-12	C	9,12	TOF-D		135
		(9.2-11.5)					

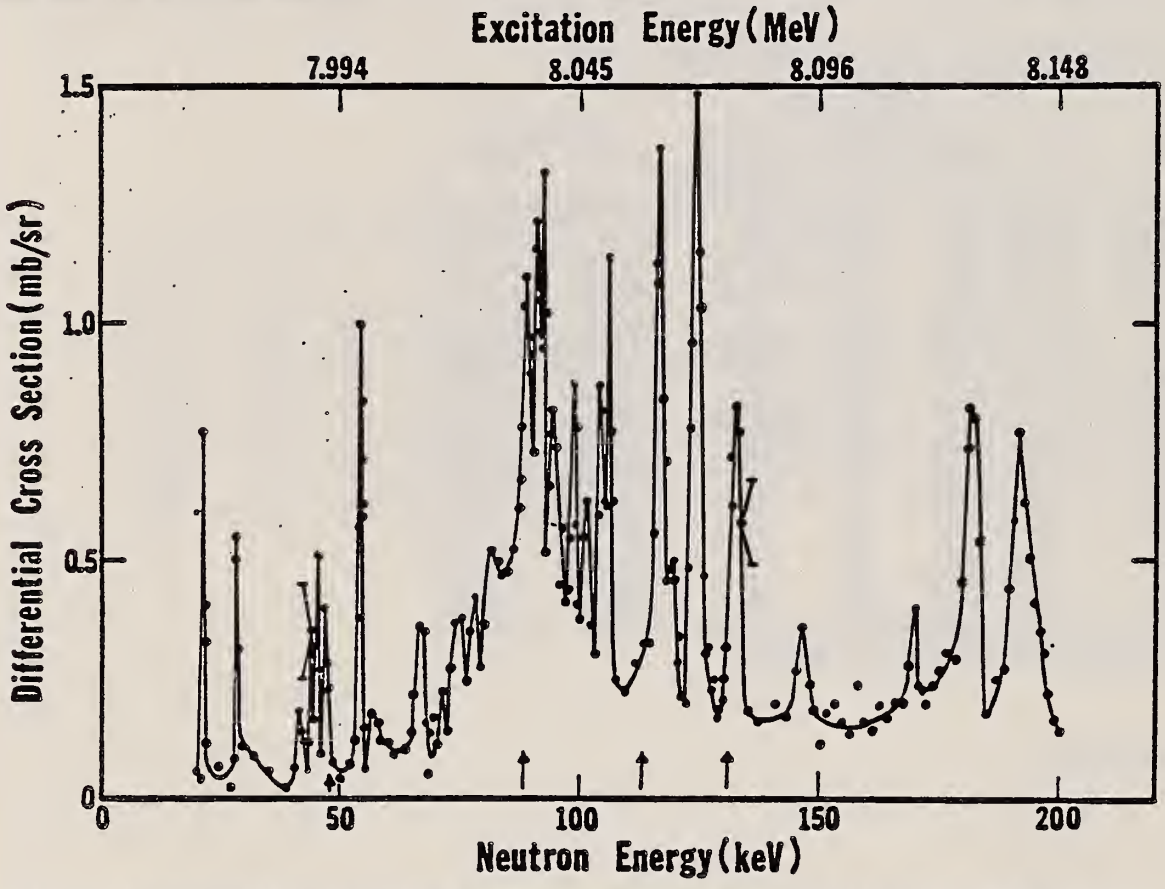

FIG. 12. The 135° differential threshold photoneutron cross section for ^{53}Cr, at low energies (see caption to Fig. 4). The arrows below the data indicate the positions of $J^{\pi} = \frac{1}{2}^{+}$ states obtained from neutron total cross-section measurements on ^{52}Cr.

FIG. 4. The 135° differential threshold photoneutron cross section for ^{207}Pb at low energies versus the energy of the emitted neutron (lower scale) and the excitation energy (upper scale). The arrows indicate peaks which decay to excited states of the residual nucleus (ES), or peaks owing to contaminating isotopes in the photoneutron sample. The inset shows the ^{207}Pb(γ, n) cross section averaged with a square 40-keV wide smoothing function.

Also see:
R. J. Baglan et al.
Phys. Rev. C3, 2475
(1971)

[over]

TABLE VI *(Continued)*

Nucleus	E_L (keV)	E_{ex} (MeV)	$g_\gamma\Gamma_{\gamma 0}\Gamma_n/\Gamma$ (eV)	GS or ES	J^π	$\Gamma_{\gamma 0}$ (eV)	E_n (keV) (This work)	E_n (keV) from neutron-induced reactions (Ref. a)	(Ref. b)	(Ref. c)
	543	11.761	0.97	GS			568			
	576	11.795	0.34				602			
	594	11.813	1.89	GS			621			
	627	11.847	2.30	GS			656			
	705	11.927	0.37				737			
^{53}Cr	21.4	7.964	0.013				23.0			22.9
	28.3	7.971	0.031				30.3			
	44.4	7.988	0.022				47.2			
	45.5	7.989	0.034				48.4			48.3
	47.1	7.991	0.042		$\frac{1}{2}^+$ [a,c]	0.17	50.1	51		50.2
	54.5	7.998	0.084	GS			57.8			57.8
	67.2	8.011	0.049				71.1			
	89.0	8.034	0.38				94.0			
	91.0	8.036	0.17				96.1			
	92.7	8.037	0.057				97.9			
	94.4	8.039	0.25				99.6			
	98.6	8.044	0.15				104			
	102	8.047	0.11				108			107
	104	8.049	0.13				110			111
	106	8.051	0.10				112			113
	117	8.062	0.31	GS			123			123.2
	124	8.070	0.34	GS			131	130		132
	132	8.078	0.20	GS			139			
	147	8.093	0.065				155			155
	170	8.117	0.054				179			
	182	8.129	0.31	GS			191			
	191	8.138	0.35	GS			201	199		
	212	8.160	0.084				223	224		
	224	8.172	0.40	GS	$\frac{1}{2}^+$ [a]	1.6	235	235		
	234	8.182	0.07				246	246		
	272	8.221	0.18	GS	$\frac{1}{2}^+$ [a,c]	0.72	285	281		285.4
	292	8.242	0.58	GS			306			
	315	8.266	0.74	GS	$\frac{1}{2}^+$ [a,c]	3.0	330	326		331.1
	333	8.284	0.60	GS			349	349		
	347	8.298	0.32		$\frac{1}{2}^+$ [a]	1.3	364	364		
	371	8.323	0.20				389			
	389	8.341	0.09		$\frac{1}{2}^+$ [a]	0.36	408	401		
	404	8.357	0.06		$\frac{1}{2}^+$ [a]	0.24	423	418		
	422	8.375	0.24				443	442		
	440	8.394	0.11				461			
	454	8.408	0.54	GS			475			
	480	8.434	0.68	GS			502			
	510	8.465	0.19	GS	$\frac{1}{2}^+$ [a]	0.76	533	530		
	519	8.474	0.20	GS			543			

[a] See Ref. 17.
[b] See R. W. Hockenbury, Z. M. Bartolome, J. R. Tatarczuk, W. R. Moyer, and R. C. Block, Phys. Rev. 178, 1746 (1969).
[c] See Ref. 19.

[17] C.D. Bowman, E.G. Bilpuch, and H.W. Newson, Ann. Phys. (N.Y.) 17, 319 (1962).

[b] See R.W. Hockenbury, Z.M. Bartolome, J.R. Tatarczuk, W.R. Moyer, and R.C. Block, Phys. Rev. 178, 1746 (1969).

[19] R.G. Steiglitz, Ph.D. thesis, Rensselaer Polytechnic Institute, 1970 (unpub.)

REF. R. J. Baglan, C. D. Bowman and B. L. Berman
Phys. Rev. C3, 672 (1971)

ELEM. SYM.	A	Z
Cr	53	24

METHOD

REF. NO. 71 Ba 2

hmg

REACTION	RESULT	EXCITATION ENERGY	SOURCE		DETECTOR		ANGLE
			TYPE	RANGE	TYPE	RANGE	

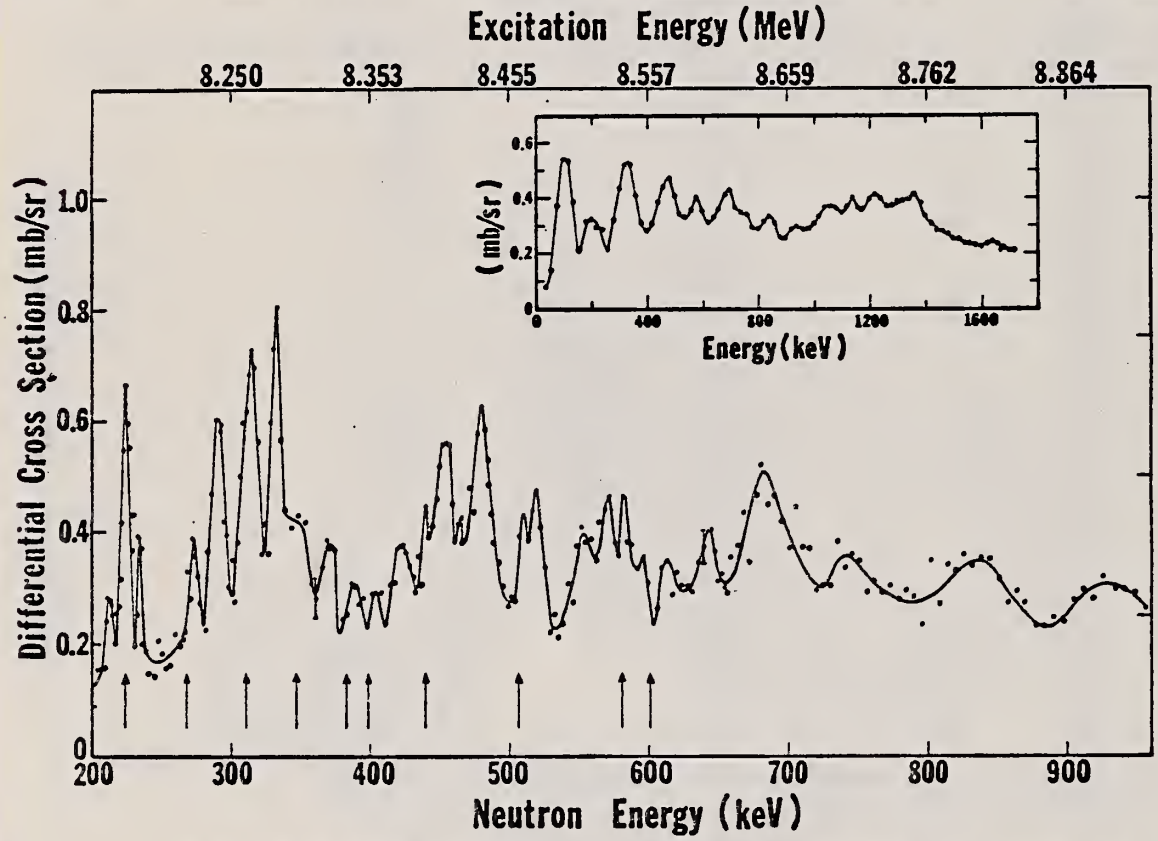

FIG. 13. The 135° differential threshold photoneutron cross section for ^{53}Cr, at high energies (see caption to Fig. 4). The arrows below the data indicate the positions of $J^{\pi} = \frac{1}{2}^{+}$ states obtained from neutron total cross-section measurements on ^{52}Cr.

REF. H. E. Jackson and E. N. Strait
Phys. Rev. C4, 1314 (1971)

ELEM. SYM.	A	Z
Cr	53	24

METHOD

REF. NO. 71 Ja 1 hmg

REACTION	RESULT	EXCITATION ENERGY	SOURCE		DETECTOR		ANGLE
			TYPE	RANGE	TYPE	RANGE	
G,N	RLX	7-9	C	7-9	TOF-D		DST
		(7.9 - 9.1)		(7.9-9.1)			

No evidence found near threshold for doorway states.

TABLE I. Angular momentum assignments for resonances in the reaction $^{53}Cr(\gamma, n)$. Excitation of levels is assumed to take place only by absorption of dipole radiation.

$E_n(\gamma, n)$ (keV)	$\frac{d\sigma(90°)/d\Omega}{d\sigma(135°)/d\Omega}$	J^π	$E_n(\gamma, n)$ (keV)	$\frac{d\sigma(90°)/d\Omega}{d\sigma(135°)/d\Omega}$	J^π
47.7	*s* wave	$\frac{1}{2}^+$	196	0.78 ± 0.08	$\frac{1}{2}^-$
92	*s* wave	$\frac{1}{2}^+$	226	*s* wave	$\frac{1}{2}^+$
101	0.54 ± 0.06	$\frac{1}{2}^-$	233	1.10 ± 0.06	$\frac{1}{2}^-$
105	0.69 ± 0.06	$\frac{1}{2}^-$	241	0.72 ± 0.08	$\frac{1}{2}^-$
107	0.70 ± 0.06	$\frac{1}{2}^-$	274	0.66 ± 0.07	$\frac{1}{2}^-$
117	*s* wave	$\frac{1}{2}^+$	294	1.09 ± 0.04	$\frac{1}{2}^-$
125	0.53 ± 0.03	$\frac{1}{2}^-$	315	*s* wave	$\frac{1}{2}^+$
133	0.66 ± 0.04	$\frac{1}{2}^-$	317	0.71 ± 0.03	$\frac{1}{2}^-$
146	1.01 ± 0.10	$\frac{1}{2}^-$	333	1.01 ± 0.04	$\frac{1}{2}^-$
182	1.15 ± 0.03	$\frac{1}{2}^-$	350	0.68 ± 0.06	$\frac{1}{2}^-$
193	1.10 ± 0.03	$\frac{1}{2}^-$	373	1.06 ± 0.11	$\frac{1}{2}^-$

TABLE II. Energies and parameters for resonances in the reaction $^{53}Cr(\gamma, n)$. The ±20% error in the quantity $\Gamma_{\gamma 0}\Gamma_n/\Gamma$ for all resonances is due mainly to the uncertainty in the absolute normalization of the data. The energies given in column 2 are calculated from those of column 1 by applying a correction for recoil effects. For unassigned levels, column 4 gives $g\Gamma_{\gamma 0}\Gamma_n/\Gamma$.

$E_n(\gamma, n)$ References 18, 19 (keV)	$E_n(\gamma, n)$ at $\theta = 135°$ Calc. (keV)	Obs. (keV)	$\Gamma_{\gamma 0}\Gamma_n/\Gamma$ (eV)
	$J = \frac{1}{2}^+$		
50.2 ± 0.3	47.3	47.7	0.179
97.1 ± 0.8	92.0	92.0	1.275
123.2 ± 1.0	117	117	0.930
141.4 ± 1.2	134	...	...
239.4 ± 2.2	228	226	1.315
285.4 ± 2.8	272	...	...
331.1 ± 3.5	316	315	0.184
			Total 3.884
	$J = \frac{1}{2}^-$		
155 ± 1.2	147	146	0.234
...	...	182	1.210
...	...	193	1.137
...	...	233	0.409
...	...	294	0.748
...	...	333	1.324
			Total 5.062
	$J = \frac{1}{2}^-$		
107 ± 0.8	101	101	0.075
111 ± 0.9	105	105	0.102
113 ± 0.9	107	107	0.143
132 ± 0.9	125	125	0.256
...	...	133	0.193
...	...	196	0.151
...	...	241	0.069
...	...	274	0.077
...	...	317	0.395
...	...	350	0.249
			Total 1.710
	Unassigned levels		
22.9 ± 1.0	21.3	21.4	0.026
48.3 ± 0.21	45.4	45.5	0.009
57.8 ± 0.28	54.5	54.6	0.046
...	...	175	0.046
			Total 0.127

(over)

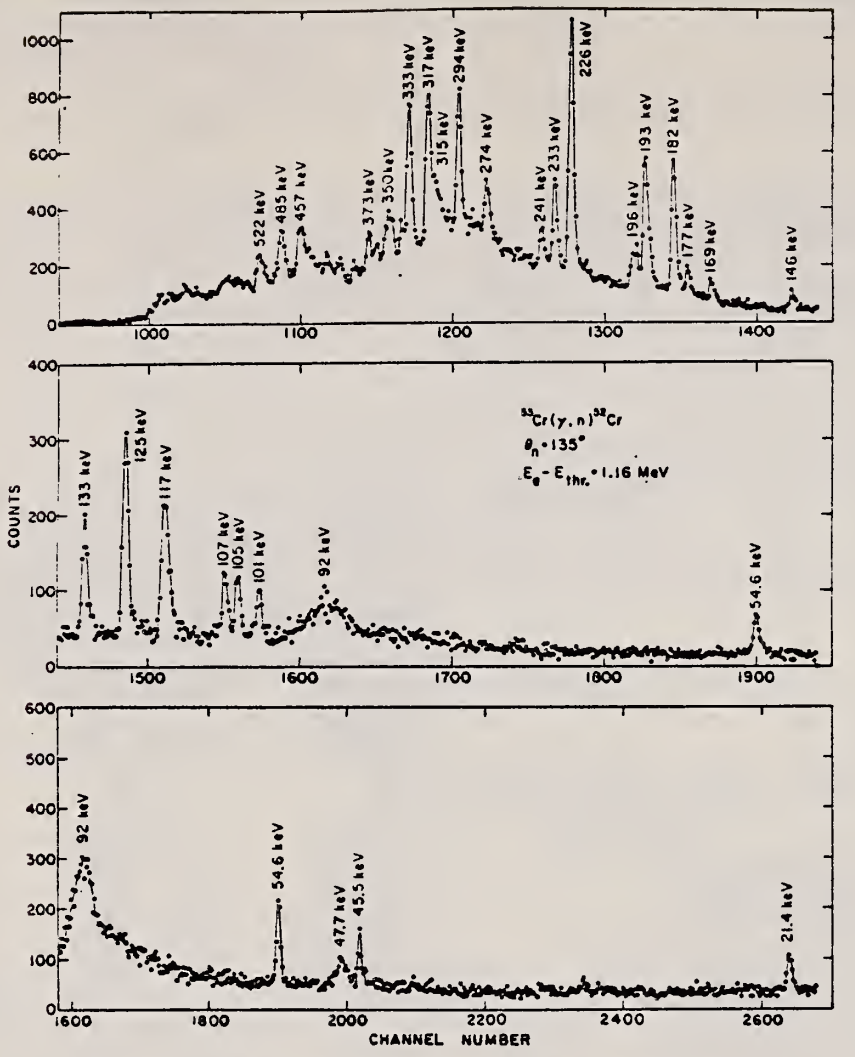

FIG. 4. Photoneutron time-of-flight spectrum for $^{53}Cr(\gamma,n)$. The flight path was 9 m. In the section for channels 1600 to 2700, each point represents the sum of two adjacent channels.

TABLE VII. Integrated yields and reduced widths for electric and magnetic dipole radiation. Integrated yields are given for all resonances observed, but reduced widths for magnetic dipole transitions are calculated only from yields for p-wave levels above 100-keV neutron energy (see discussion in Sec. IV). The number of resonance widths used to obtain each $\bar{k}$ is given by n. The errors given were calculated by assuming that the individual $\Gamma_{\gamma 0}$'s follow a Porter-Thomas distribution.

Target	J^π	$\sum g\Gamma_{\gamma 0}\Gamma_n/\Gamma$ (eV)	$\sum \Gamma_{\gamma 0}\Gamma_n/\Gamma$ (eV)	n	$10^3\times$ reduced width Individual average	
^{53}Cr	$\frac{1}{2}^+$	0.97	3.88	7	$\bar{k}_{E1} = 1.7^{+1.7}_{-0.5}$	
	$\frac{1}{2}^-$	1.27	5.06	6	$\bar{k}_{M1} = 41$	$\bar{k}_{M1} = 28^{+15}_{-9}$
	$\frac{3}{2}^-$	0.86	1.71	10	$\bar{k}_{M1} = 16$	
^{57}Fe	$\frac{1}{2}^+$	0.83	1.66	8	$\bar{k}_{E1} = 0.86^{+0.8}_{-0.3}$	
	$\frac{1}{2}^-$	0.37	0.74	4	$\bar{k}_{M1} = 9$	$\bar{k}_{M1} = 10^{+10}_{-3}$
	$\frac{3}{2}^+$	0.84	0.84	3	$\bar{k}_{M1} = 10$	
^{61}Ni	$\frac{1}{2}^+$	0.37	1.48	11	$\bar{k}_{E1} = 0.96^{+0.47}_{-0.19}$	
	$\frac{1}{2}^-$	0.41	1.65	5	$\bar{k}_{M1} = 27$	$\bar{k}_{M1} = 20^{+18}_{-7}$
	$\frac{3}{2}^-$	0.54	1.07	3	$\bar{k}_{M1} = 12$	

REF.

B. S. Ratner
ZhETF Pis. Red. 13, 628 (1971)
JETP Letters 13, 447 (1971)

ELEM. SYM.	A	Z
Cr	53	24

METHOD

REF. NO.	
71 Ra 1	hmg

REACTION	RESULT	EXCITATION ENERGY	SOURCE		DETECTOR		ANGLE
			TYPE	RANGE	TYPE	RANGE	
G,P	RLY	11-14	C	11-14	ACT-I		4PI

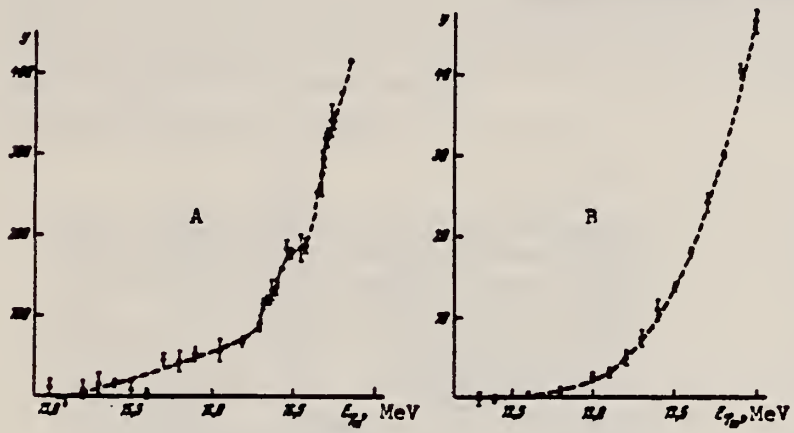

Fig. 1. Yield of reactions $Ni^{64}(\gamma, p)Co^{63}$ (A) and $Cr^{53}(\gamma, p)U^{52}$ (B) near the threshold, averaged over $E_{\gamma m}$ in the interval 10 - 100 keV

REF. B. S. Ratner
Yad. Fiz. 21, 1147 (1975)
Sov. J. Nucl. Phys. 21, 590 (1976)

ELEM. SYM.	A	Z
Cr	53	24

METHOD

REF. NO. 75 Ra 2 hmg

REACTION	RESULT	EXCITATION ENERGY	SOURCE		DETECTOR		ANGLE
			TYPE	RANGE	TYPE	RANGE	
G,P	RLY	11- 14	C	12- 14	ACT-I		4PI

The yields of (γ, p) reactions on ^{62}Ni, ^{64}Ni, and ^{53}Cr are studied in ranges of $E_{\gamma max}$ near the respective thresholds. Considerable differences are found between the curve shapes, yields, and observed thresholds for the Ni isotopes and ^{53}Cr.

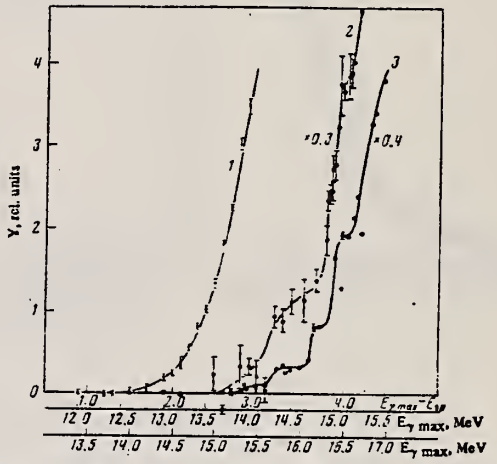

FIG. 3. Yields of the reactions ^{53}Cr(γ, p)^{52}V (curve 1), ^{64}Ni(γ, p)^{63}Co (curve 2), and ^{62}Ni(γ, p)^{61}Co (curve 3) as functions of $E_{\gamma\ max}$. Lowest scale for ^{64}Ni(γ, p); middle scale for ^{62}Ni(γ, p) and ^{53}Cr(γ, p).

REF. V.N. Polishchuk, N.G. Shevchenko, N.G. Afanas'ev, A.A. Khomich, A.Yu. Buki, B.V. Mazan'ko
Yad. Fiz. 27, 1145 (1978)
Sov. J. Nucl. Phys. 27, 607 (1978)

ELEM. SYM.	A	Z
Cr	53	24

METHOD

REF. NO. 78 Po 3 hg

REACTION	RESULT	EXCITATION ENERGY	SOURCE TYPE	SOURCE RANGE	DETECTOR TYPE	DETECTOR RANGE	ANGLE
E,E/	FMF	0-2	D	90, 120	MAG-D		DST

LEV .56, 1.01, 1.29, 1.97

Inelastic electron scattering has been used to measure the form factors of the 1.43-MeV level in ^{52}Cr and the 0.56-, 1.01-, 1.29-, and 1.97-MeV levels in ^{53}Cr. The measurements were made with an initial electron energy $E_0 = 90$, 120, and 226 MeV in the momentum-transfer region 0.85–1.7 F^{-1} and 0.74–1.15 F^{-1} respectively for ^{52}Cr and ^{53}Cr. For these states reduced transition probabilities $B(E2)\uparrow$ were obtained, respectively 800 ± 80, 100 ± 20, 170 ± 18, 335 ± 30, and 190 ± 15 $e^2 \cdot F^4$. The results obtained are discussed in terms of the excited-core model.

PACS numbers: 25.30.Cg, 27.40. + z, 23.20.Ck

TABLE I. Reduced probabilities for transition from the ground state of the nucleus to excited states for the isotopes ^{52,53}Cr.

Nucleus	Transition $J_i \to J_f$	ω, MeV	λ	Value of $B(E\lambda)\uparrow$, $e^2 \cdot F^{2\lambda}$: Experiment — Our data	[*]	[*]	[*]	Theory [*] Generalized model $\varepsilon_n = \varepsilon$	Generalized model $\varepsilon_n = 0$	Shell model	[*]	[*]	[*]	
^{53}Cr	$^3/_2^- \to {}^1/_2^-$	0.56	2	100±20	115±12	110±20	89	98	50	20	73	59	62.5	66.5
	$^3/_2^- \to {}^3/_2^-$	1.01	2	170±18	72±14	20±6	52	113	~1	33	53	162	20.3	54.5
	$^3/_2^- \to {}^5/_2^-$	1.29	2	335±30	300±60	260±60	138	240	≈0	230	135		99	244
	$^3/_2^- \to {}^5/_2^-$	1.97	2	190±15				64	56	132	93			
	$^3/_2^- \to {}^7/_2^-$	2.32	2					33	50				149	140
				Our data	[*]	[**]	[**]	[**] $\varepsilon_n = 0.6$	[**] $\varepsilon_n = 0.7$	[**]				
^{52}Cr	$0 \to 2^+$	1.43	2	800±80	720±90	720	761±30	610	720	940				

[1] Calculation carried out for $M_{22} = 25\ e \cdot F^2$ and $\xi = -0.169$ MeV, $\eta = -0.0002$ MeV $\cdot e^{-2} \cdot F^{-4}$.
[2] Calculation carried out for $M_{22} = 25\ e \cdot F^2$ and $\xi = -0.125$ MeV, $\eta = -0.00055$ MeV $\cdot e^{-2} \cdot F^{-4}$.

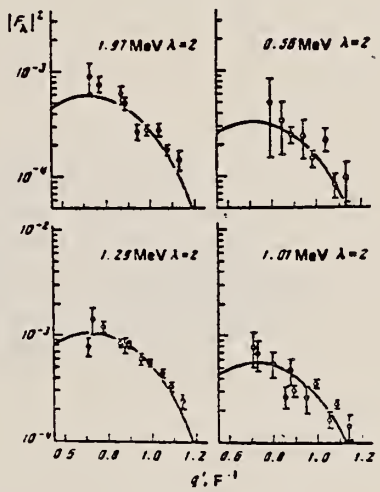

FIG. 1. Form factors of the levels 1/2⁻ (0.56 MeV), 5/2⁻ (1.01 MeV), 7/2⁻ (1.29 MeV), and 5/2⁻ (1.97 MeV) in the nucleus ^{53}Cr. The points are experimental, and the curves are calculated by a phase-shift analysis.

# MANGANESE
Z=25

Manganese was first recognized as an element by the Swedish chemist Scheele in 1774 while working with the MnO_2 ore pyrolysite. The metal is frequently found in conjunction with iron ores and was named for the magnetic properties exhibited by pyrolusite from the Latin "magnes" or magnet; the German equivalent is "mangan" and the French, "manganese".

Mn
A=51

Mn
A=51

REF.

B. Erlandsson
Arkiv Fysik 34, 285 (1967)

ELEM. SYM.	A	Z
Mn	51	25

METHOD

REF. NO.	
67 Er 1	egf

REACTION	RESULT	EXCITATION ENERGY	SOURCE		DETECTOR		ANGLE
			TYPE	RANGE	TYPE	RANGE	
P,G	NOX	6-7	P	1-2	SCD-D	1-7	DST

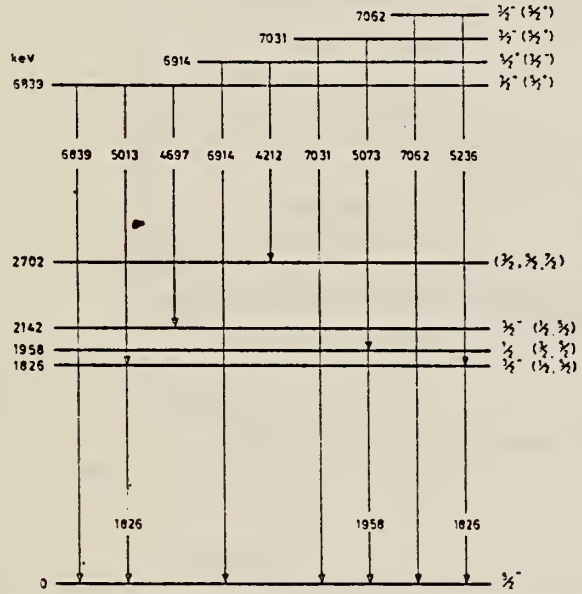

Fig. 1. The level and decay scheme of Mn^{51} from this investigation.

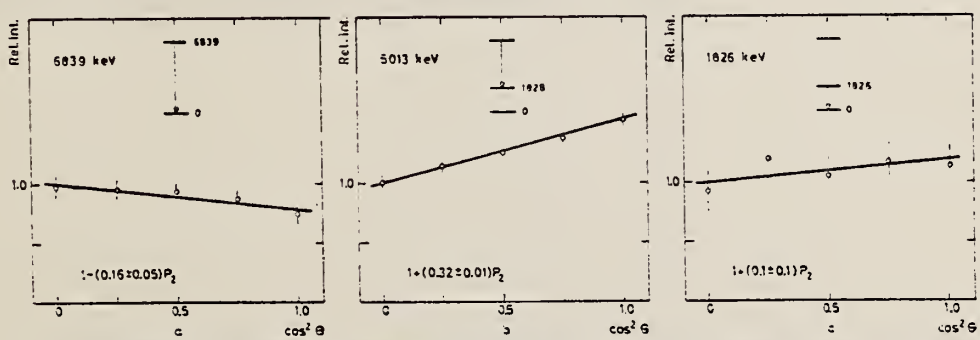

Fig. 2. Angular distributions of the 6839, 5013 and 1826 keV gamma lines as measured at the 1602 keV resonance.

[over]

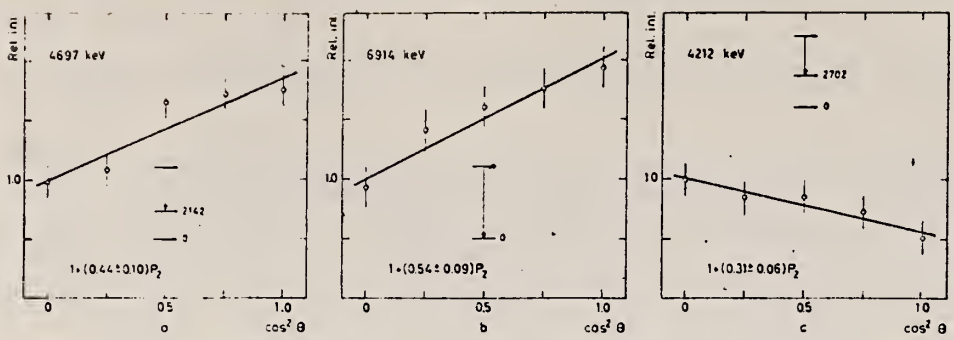

Fig. 3. Angular distributions of the 4697 keV gamma line as measured at the 1602 keV resonance and the 6914 and 4212 keV gamma lines as measured at the 1679 keV resonance.

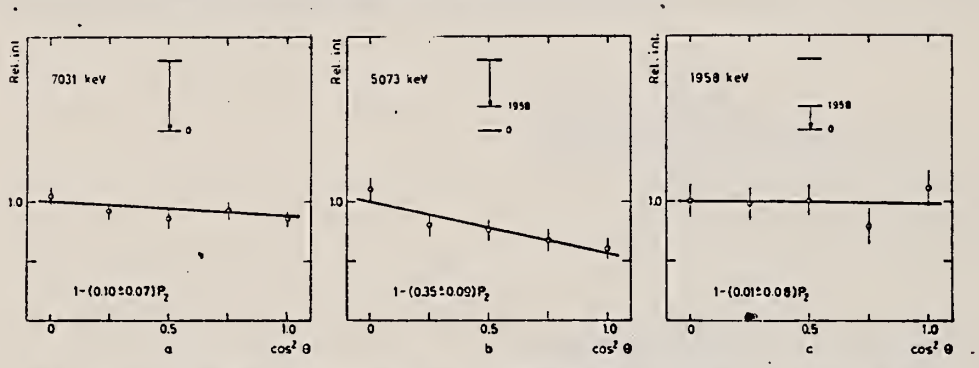

Fig. 4. Angular distributions of the 7031, 5073 and 1958 keV gamma lines as measured at the 1798 keV resonance.

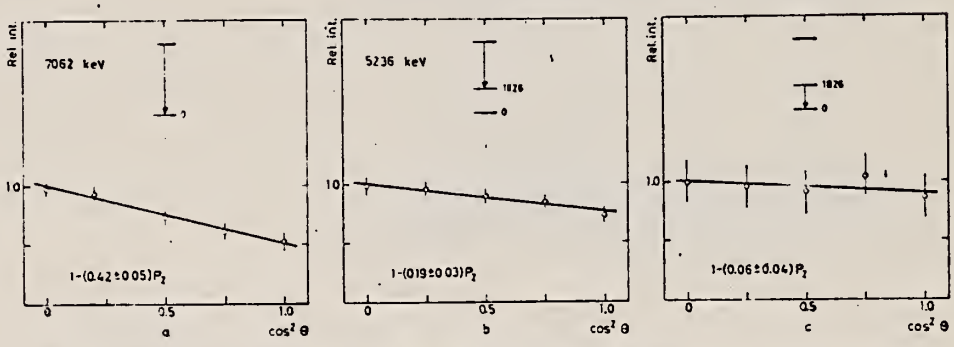

Fig. 5. Angular distributions of the 7062, 5236 and 1826 keV gamma lines as measured at the 1830 keV resonance.

MN
A=53

MN
A=53

REF. P. H. Vuister
Nuclear Phys. 83, 593 (1966)

ELEM. SYM.	A	Z
Mn	53	25

METHOD
3 MeV Van de Graaff

[Page 1 of 2]

REF. NO. 66 Vu 1 JDM

REACTION	RESULT	EXCITATION ENERGY	SOURCE		DETECTOR		ANGLE
			TYPE	RANGE	TYPE	RANGE	
P,G	RLY	7-9	D	1-2	NAI-D	4-9	90

TABLE 1
Resonances in the $^{52}Cr(p, \gamma)^{53}Mn$ reaction [a, b]

No. res.	E_p [c] (keV)	E_x [d] (MeV)	$(2J+1)\gamma$ [e] (eV)	Γ_p(ref. [a]) (keV)	No. res.	E_p (keV)	E_x (MeV)	$(2J+1)\gamma$ (eV)	Remarks
1	1367.5	7.903	0.43	1366	48	1657.2	8.187	0.04	
2	1374.4	7.909	0.03		49	1661.0	8.191	0.06	
3	1382.2	7.917	0.07	1381	50	1662.3	8.192	0.34	
4	1387.5	7.922	1.2	1387	51	1664.0	8.194	0.7	
5	1394.8	7.929	0.8	1394	52	1666.1	8.196	0.5	
6	1405.2	7.940	0.32	1405	53	1667.8	8.197	0.29	
7	1431.5	7.965	0.28	1433	54	1672.8	8.202	0.11	
8	1442.9	7.977	0.7	1444	55	1689.5	8.219	0.6	
9	1444.9	7.979	0.03		56	1695.1	8.224	0.43	
10	1448.4	7.982	0.04		57	1705.1	8.234	0.06	
11	1460.9	7.994	0.09		58	1706.9	8.236	0.05	
12	1472.7	8.006	0.09		59	1717.7	8.246	0.30	
13	1473.5	8.007	0.7		60	1723.6	8.252	2.2	
14	1479.0	8.012	0.12		61	1726.9	8.255	0.14	
15	1483.5	8.017	0.10	Remarks	62	1729.5	8.258	0.40	
16	1493.2	8.026	0.26		63	1735.7	8.264	0.6	
17	1493.9	8.027	0.20		64	1743.9	8.272	0.6	
18	1496.8	8.030	0.30		65	1747.9	8.276	(0.38)	double?
19	1498.5	8.031	0.10		66	1749.4	8.277	0.22	
20	1506.1	8.039	(0.24)	double?	67	1755.2	8.283	0.05	
21	1508.6	8.041	0.03		68	1761.5	8.289	0.09	
22	1514.5	8.047	0.12		69	1767.2	8.295	1.0	
23	1521.2	8.053	0.6		70	1769.1	8.297	0.48	
24	1525.0	8.057	0.42		71	1770.2	8.298	0.08	
25	1528.2	8.060	0.02		72	1771.8	8.299	0.06	
26	1532.9	8.065	0.04		73	1778.6	8.306	1.1	
27	1539.5	8.071	0.29		74	1780.6	8.308	0.49	
28	1544.1	8.076	0.21		75	1784.9	8.312	0.05	
29	1550.0	8.082	0.38		76	1788.2	8.315	0.7	
30	1554.3	8.086	0.13		77	1796.4	8.323	0.14	
31	1555.9	8.088	0.6		78	1797.6	8.325	0.26	
32	1563.3	8.095	0.7		79	1803.1	8.330	1.2	
33	1568.0	8.099	0.12		80	1806.3	8.333	0.05	
34	1569.8	8.101	0.06		81	1811.3	8.338	0.29	
35	1577.3	8.109	0.12		82	1813.0	8.340	0.6	
36	1587.4	8.118	0.15		83	1824.5	8.351	0.5	
37	1590.1	8.121	0.32		84	1825.7	8.352	0.10	
38	1600.5	8.131	0.29		85	1827.8	8.354	0.17	
39	1602.2	8.133	0.23		86	1829.2	8.356	0.8	
40	1603.6	8.134	0.6		87	1833.3	8.360	0.30	
41	1608.5	8.139	1.2		88	1834.3	8.361	0.03	
42	1626.7	8.157	0.7		89	1836.1	8.362	0.33	
43	1632.8	8.163	0.04		90	1841.9	8.368	0.03	
44	1643.5	8.174	0.05		91	1846.8	8.373	0.02	
45	1646.6	8.177	0.7		92	1851.9	8.378	(0.27)	double?
46	1650.7	8.181	0.03		93	1853.5	8.379	0.41	
47	1653.4	8.183	0.14		94	1857.4	8.383	0.07	

[a]) Not reported are about 30 resonances of which the assignment to the $^{52}Cr(p, \gamma)^{53}Mn$ reaction is uncertain; their strength is less than 0.05 eV if they belong to this reaction.
[b]) For all resonances the natural width is smaller than the experimental resolution of 400 eV.
[c]) The error in E_p increases from 1.4 keV at E_p = 1350 keV to 2.0 keV at E_p = 2250 keV.
[d]) All ±7 keV.
[e]) The values of $(2J+1)\Gamma_p\Gamma_\gamma/\Gamma \equiv (2J+1)\gamma$ are considered to be correct within a factor of 2.

REF.

P. H. Vuister
Nuclear Phys. 83, 593 (1966)

ELEM. SYM.	A	Z
Mn	53	25

METHOD

3 MeV Van de Graaff

[Page 2 of 2]

REF. NO.

66 Vu 1

JDM

REACTION	RESULT	EXCITATION ENERGY	SOURCE		DETECTOR		ANGLE
			TYPE	RANGE	TYPE	RANGE	

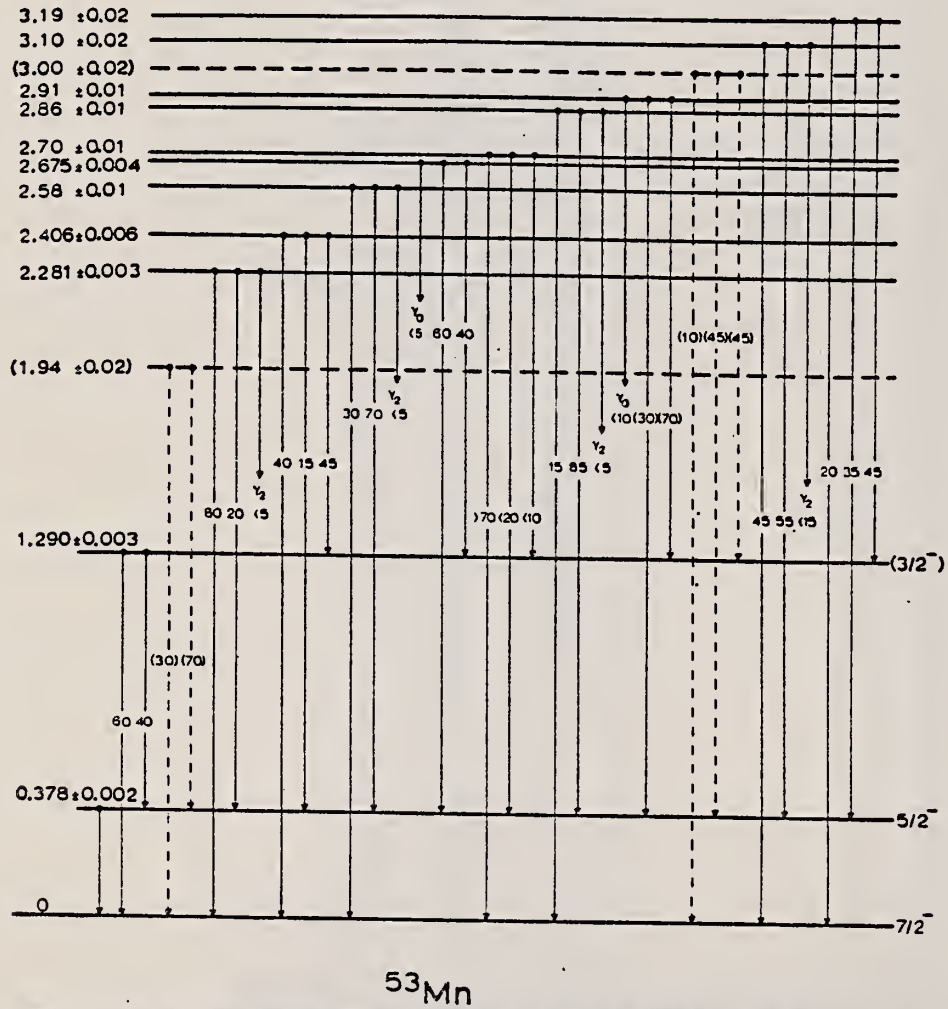

^{53}Mn

Fig. 15. Level and decay scheme of ^{53}Mn. Transitions between levels with $E_x > 1.30$ MeV were not investigated.

REF.

K. Beckert, H.W. Hersch, D. Grambole, F. Herrmann, P. Kleinvechter, C. Schneiderait, H. Schobbert, H.J. Thomas
Izv. Akad. Nauk SSSR. Ser. Fiz. 38, 2087 (1974)
Bull. Acad. Sci. USSR Phys. Ser. 38, 63 (1974)

ELEM. SYM.	A	Z
Mn	53	25

METHOD

REF. NO.: 74 Be 13 hmg

REACTION	RESULT	EXCITATION ENERGY	SOURCE TYPE	SOURCE RANGE	DETECTOR TYPE	DETECTOR RANGE	ANGLE
P,G	SPC	6- 11	D	3- 5	SCD-D		DST

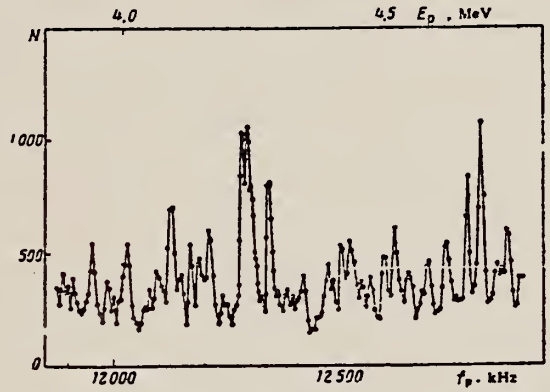

Fig. 1. Excitation function for $^{52}Cr(p,\gamma)^{53}Mn$ (measured at 90° to the beam) for E_γ > 7 MeV (N is the number of counts for 60 μCi).

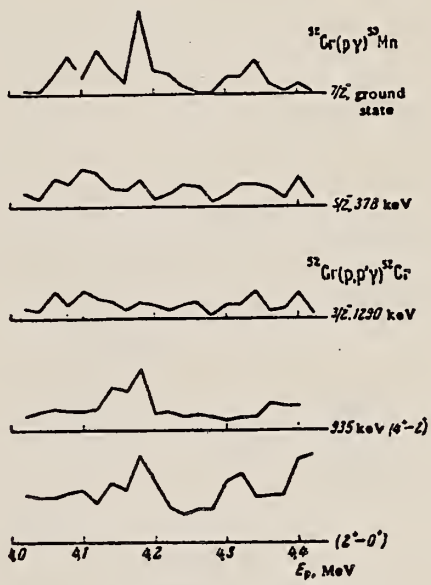

Fig. 2. Differential excitation functions for transitions from the capture level to the first bound states of ^{53}Mn and for transitions accompanying inelastic proton scattering $^{52}Cr(p,p'\gamma)$.

TABLE 1

Main γ Transitions Observed in the Decay of the Resonance at E_p = 4183 keV at 55° to the Beam

Final state E_x, keV	Branching ratio, %*	I^π [10]	Final state E_x, keV	Branching ratio, %*	I^π [10]
0	42,4	$^7/_2^-$	2672,0 (2,5)	} 4,5	$^7/_2$
378,3 (0,5)	13,5	$^5/_2^-$	2685,9 (1,0)		
1289,9 (0,7)	6,4	$^3/_2^-$	2876,9 (1,0)	2,4	$^3/_2$
1435 (4)	4,3	$^{11}/_2^-$	2942,2 (2,0)	1,7	$^9/_2$
1620,3 (0,4)	1,8	$^9/_2^-$	3004,1 (1,0)	0,9	
2274,2 (0,4)	4,5	$^7/_2$, $^5/_2$	3093,3 (1,0)	2,2	$^3/_2$, $^5/_2$
2407,0 (1,0)	1,5	$^5/_2$	3198,3 (1,5)	4,3	$^5/_2$, $^9/_2$
2573,7 (1,0)	5,0	$^7/_2$	3467,5 (2,0)	2,9	

*The relative error in the intensity of the transition to the ground state is about 10%. The corresponding errors for the other transitions are 20-25%.

MN
A=55

MN
A=55

MN
A=55

Ref. E.G. Fuller, E. Hayward
Phys. Rev. 101, 692 (1956)

Elem. Sym.	A	Z
Mn	55	25

Method
Betatron; photon scattering; NaI spectrometer

Ref. No. 56 Fu 1 | EH

Reaction	E or ΔE	E_o	Γ	$\int \sigma dE$	Jπ	Notes
$Mn^{55}(\gamma,\gamma)$	Bremss. 4-40					Detector at 120°. Cross sections given here are 13% too high due to erroneous cos θ factor in denominator of Eq. 5. [See footnote 8 in Phys. Rev. 106, 993 (1957)].

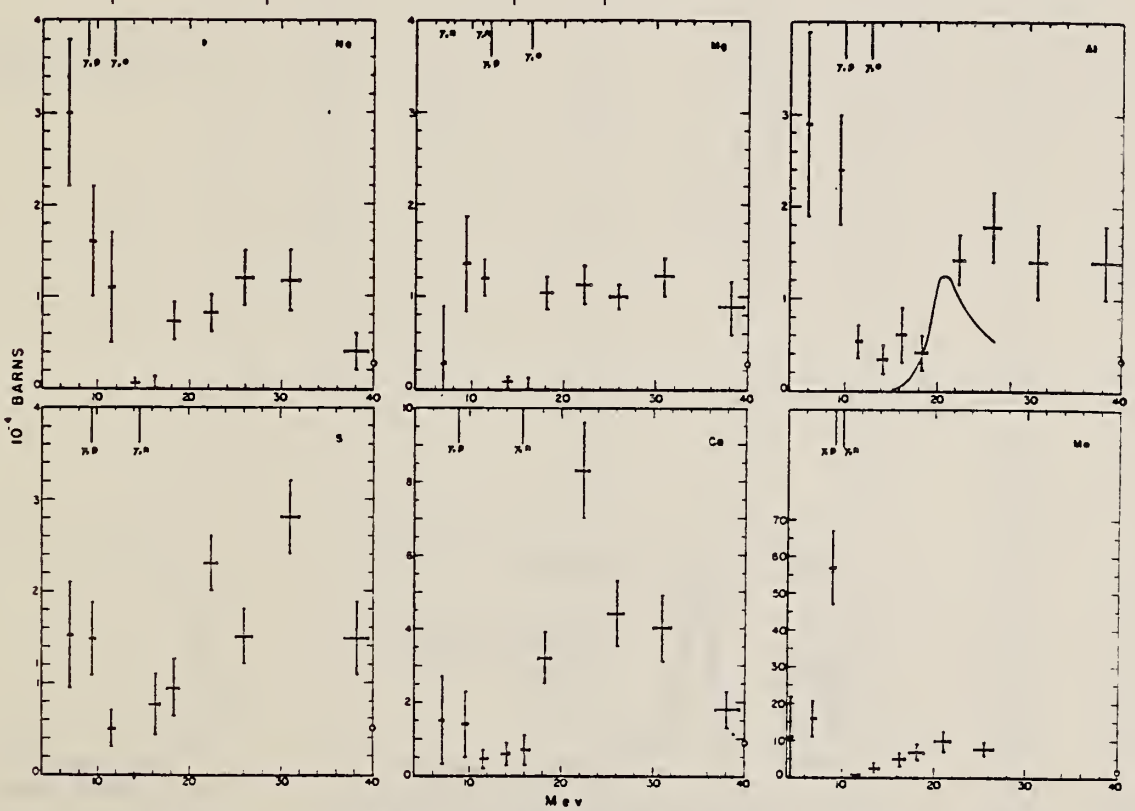

FIG. 4. The elastic scattering cross sections for Na, Mg, Al, S, Ca, and Mn. The indicated spread in energy is the width of the differential discriminator channel, and the standard deviations are based only on the number of counts. The vertical lines at the top represent the particle thresholds for the most important isotopes. The open circles at the extreme right indicate the magnitude of the Thomson cross section for Z free protons scattering coherently. The solid curve superimposed on the Al data is the scattering cross section calculated from the dispersion relation by substituting for $\sigma_s(E)$ in Eq. (6) the sum of the neutron and proton yield[1,15] cross sections.

Ref. R.L. Hines
Phys. Rev. 105, 1534 (1957)

Elem. Sym.	A	Z
Mn	55	25

Method Michigan University synchrotron; Victoreen counter; Betatron 21 min.

Ref. No. 57 Hi 1 | EGF

Reaction	E or ΔE	E_o	Γ	$\int \sigma dE$	Jπ	Notes
(e,e'3n)	63.5 81.5	42				No corrections made for finite ~~signs~~ sizes of nucleus. $Mn^{55}(\gamma,3n)Mn^{52^x}$ cross section from Hines [Pnys. Rev. 91, 474(A),(1953)].

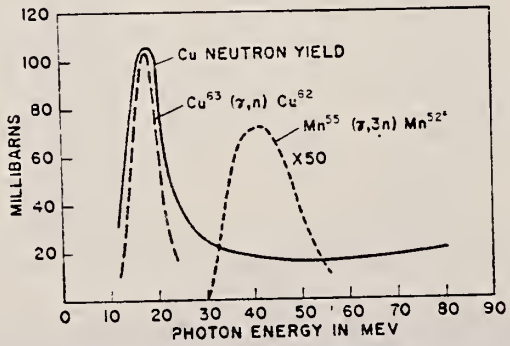

FIG. I. Photoneutron yield cross section for Cu shown in comparison with $Cu^{63}(\gamma,n)Cu^{62}$ and $Mn^{55}(\gamma,3n)Mn^{52*}$ cross sections

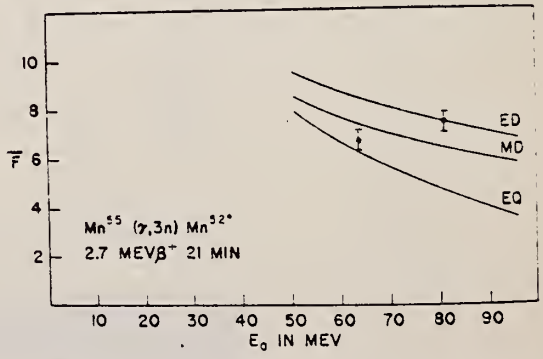

5. Experimental and theoretical values of $\bar{F}$ for manganese.

B.G. Chidley, L. Katz, S. Kowalski
Can. J. Phys. 36, 407 (1958)

ELEM. SYM.	A	Z
Mn	55	25

ACC
Betatron

REF. NO.
58 Ch 2
NVB

REACTION	RESULT	EXCITATION ENERGY	SOURCE		DETECTOR		ANGLE
			TYPE	RANGE	TYPE	RANGE	
G,N	RLY	THR	C	THR	BF3-I		4PI

THRESHOLD

TABLE I

MEASURED PHOTONEUTRON THRESHOLDS

Reaction	Measured Q value, Mev.	Other Q values, Mev.	Method	Reference
$Mn^{55}(\gamma, n)Mn^{54}$	10.14±0.05			
		10.15 ±0.20	Threshold	Hanson *et al.* (1949)
		10.00 ±0.20	Threshold	Sher *et al.* (1951)
		10.14 ±0.26	Mass data	Wapstra (1955)
		10.28 ±0.07	Mass data	Duckworth (unpublished)
			Q^+ value	Jung and Pool (1956)
		10.09 ±0.10	Mass data	Duckworth (unpublished)
			Q^- value	Way *et al.* (1955)

See 58 Ka 1 for cross sections

L. Katz, G.B. Chidley Nuclear Reactions at Low and Medium Energies (Academy of Science, USSR: 1958) 371	Mn	55	25
METHOD: Betatron; neutron cross section; BF_3 counters; ion chamber monitor	REF. NO. 58 Ka 1		NVB

REACTION	RESULT	EXCITATION ENERGY	SOURCE		DETECTOR		ANGLE
			TYPE	RANGE	TYPE	RANGE	
G,XN	ABX	11-22	C	11-22	BF3-I		4PI

Таблица 2

Пороги испускания фотонейтронов

Изотоп	B_n, *Мэв*	B_{2n}, *Мэв*	Изотоп	B_n, *Мэв*	B_{2n}, *Мэв*
V^{51}	11,16	20,5	L^{139}	8,81	16,1
Mn^{55}	10,14	19,2	Pr^{141}	9,46	17,6
Co^{59}	10.44	18,6	Tb^{159}	8,16	14,8
As^{75}	10.24	18,1	Ho^{165}	8,10	14,6
Y^{89}	11,82	20,7	Tm^{169}	8,00	14,7
Nb^{93}	8,86	17,1	Lu^{175}	7,77	14,2
Rh^{103}	9,46	16,8	Ta^{181}	7,66	13,8
J^{127}	9,14	16,2	Au^{197}	7,96	13,3
Cs^{133}	9,11	16,5	Bi^{209}	7,43	14,5

THRESHOLDS

не приведены, поскольку они превышают 22 *Мэв* во всех случаях, кроме золота, для которого B_{2n}=21 *Мэв*. Свойства сечений $\sigma_C(\gamma)$ сведены в табл. 3.

Таблица 1

Изотоп	$E_{макс}$, *Мэв*	$\sigma_n(E_\gamma)$, *барн*	Γ, *Мэв*	Γ^{22}, *Мэв·барн*	Y(22), 10^6 *нейтрон/100 р·моль*
V^{51}	18,4	0,062	5,2	0,33	1,62
Mn^{55}	20,2	0,060	7,0	0,39	2,01
Co^{59}	18,3	0,068	6,3	0,44	2,30
As^{75}	16,4	0,090	9,5	0,74	4,25
Y^{89}	17,1	0,172	5,2	0,93	5,33
Nb^{93}	18,0	0,156	7,5	1,17	6,80
Rh^{103}	17,5	0,160	9,4	1,40	8,28
J^{127}	15,2	0,273	6,8	1,76	11,9
Cs^{133}	16,5	0,238	7,7	1,59	10,7
La^{139}	15,5	0,325	3,8	1,55	11,2
Pr^{141}	15,0	0,320	4,9	1,93	13,1
Tb^{159}	15,6	0,274	9,8	2,49	18,1
Ho^{165}	13,5	0,305	8,9	2,52	18,7
Tm^{169}	16,4	0,250	8,4	1,91	14,9
Lu^{175}	16,0	0,225	8,4	1,90	23,0
Ta^{181}	14,5	0,380	8,5	3,15	22,0
Au^{197}	13,8	0,475	4,7	3,04	22,6
Bi^{209}	13,2	0,455	5,9	2,89	23,2

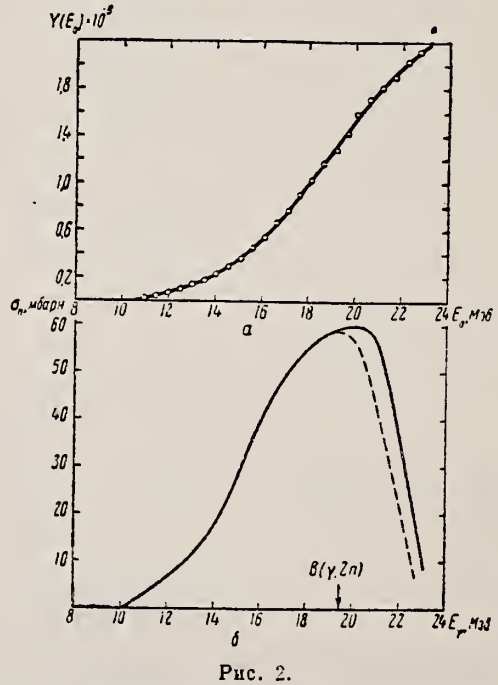

Рис. 2.

а — Выход фотонейтронов для Mn; б — $\sigma_n(E_\gamma)$ и $\sigma_C(\gamma)$ для Mn

Ref. R.W. Parsons
Can. J. Phys. 37, 1344 (1959)

Elem. Sym.	A	Z
Mn	55	25

Method 24 MeV betatron; neutron yield; BF_3 chamber, Lucite ionization chamber

Ref. No. 59 Pa 2 | EH

Reaction	E or ΔE	E_o	Γ	$\int \sigma dE$	Jπ	Notes
$Mn^{55}(\gamma,n)$	Bremss. 24	19.5 ±0.25	4.5 MeV			σ_b = 62.7 mb.
		16.75 ±0.25	3.0 MeV			σ_a = 45.9 mb
						Q_o = 0.73±0.14 b compared to 1.26 from Coulomb excitation experiments of Mark et al [Phys. Rev. 98, 1245 (1955)].
						Data cannot be fitted with two resonances.

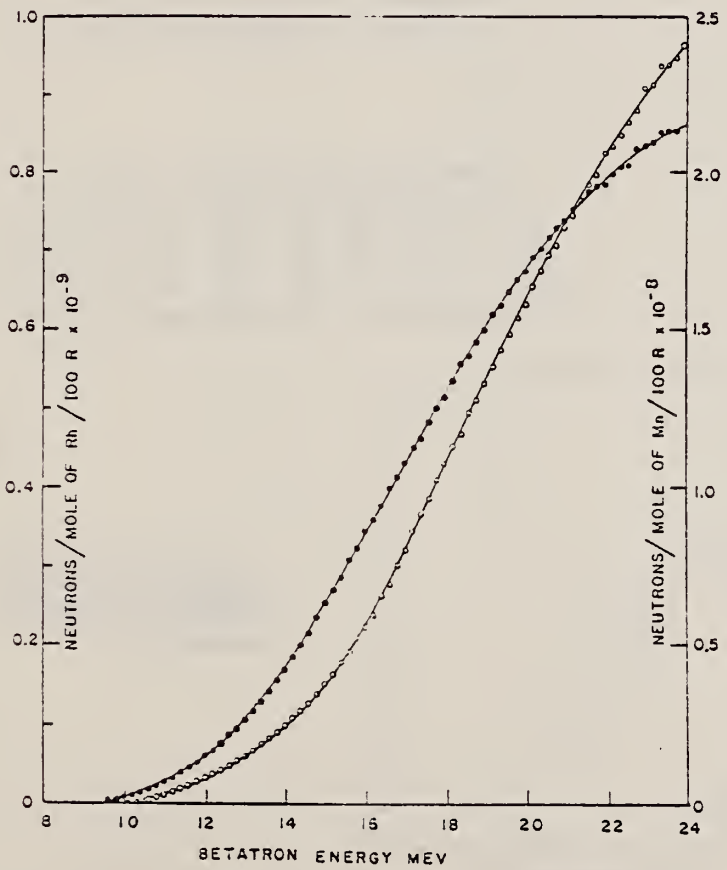

FIG. 1. Photoneutron yield versus betatron energy. ○ manganese; ● rhodium.

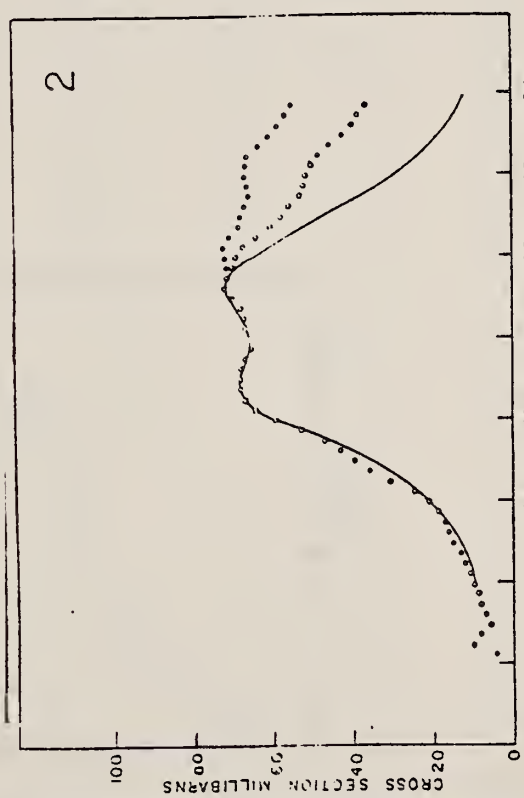

FIG. 2. $\sigma_1+\sigma_2$ (○) and $\sigma_1+2\sigma_2$ (●) for manganese versus photon energy. The full curve is compounded of two resonance curves whose parameters are given in the text.

Ref. P.A. Flournoy, R.S. Tickle, W.D. Whitehead
Phys. Rev. 120, 1424 (1960)

Elem. Sym.	A	Z
Mn	55	25

Method: Synchrotron; BF_3 counters in 4π geom.

Ref. No.: 60 F1 1 JHH

Reaction	E or ΔE	E_o	Γ	$\int \sigma dE$	Jπ	Notes
(γ,xn)	12-30	16.8±.25	2.7	25 MeV 627 MeV-mb 12		σ_{max} (16.8 MeV) = 90 mb
		19.75±.25	4.0 (From Brent-Wigner fit: see Table I)			σ_{max} (19.75 MeV) = 77 mb
						Intrinsic quadrupole moment Q_o = +0.78±0.10 barn if $\sigma_{total} \cong \sigma(\gamma,n) + \sigma(\gamma,2n)$ in this region, using $R_o = 1.2 \times 10^{-13}$ cm.
						In Figure 3, open circles are uncorrected for neutron multiplicity; closed circles are corrected.
						Integrated cross section is $\sigma(\gamma,n) + \sigma(\gamma,pn) + \sigma(\gamma,2n) + \ldots$

TABLE I. Parameters of Breit-Wigner fit to data.

Element	E_a (Mev)	Γ_a (Mev)	σ_a (mb)	E_b (Mev)	Γ_b (Mev)	σ_b (mb)	$\Gamma_{\sigma_b}/\Gamma_{\sigma_a}$
Manganese	16.8	2.7	70	19.75	4.0	64	1.35
Cobalt	16.5	2.0	78	19.0	4.0	78	2.00

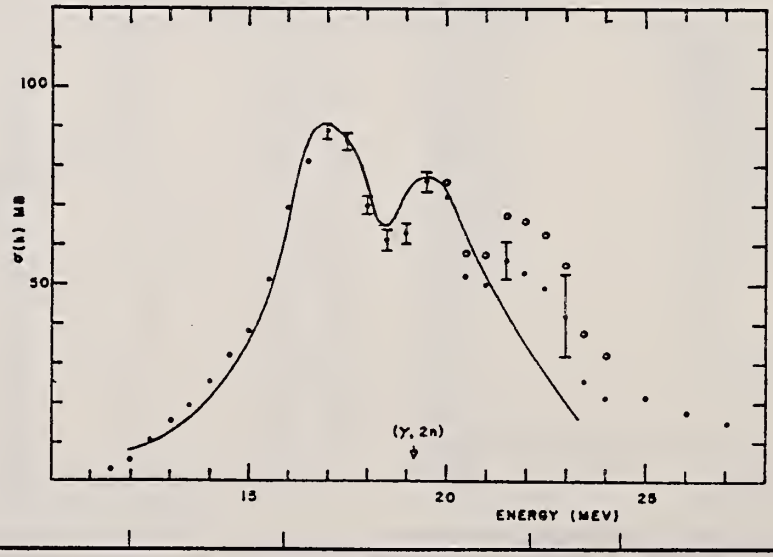

FIG. 3. Neutron cross section of manganese. Open circles represent uncorrected data. Closed circles represent data corrected for neutron multiplicity.

K. N. Geller, J. Halpern, and E. G. Muirhead
Phys. Rev. 118, 1302-12 (1960)

ELEM. SYM.	A	
Mn	55	25

METHOD

Betatron; neutron threshold; ion chamber

REF. NO.	
60 Ge 3	NVB

REACTION	RESULT	EXCITATION ENERGY	SOURCE		DETECTOR		ANGLE
			TYPE	RANGE	TYPE	RANGE	
G,N	NØX	THR	C THR		BF3-I		4 PI

THRESHØLD

TABLE I. Summary and comparison of neutron separation energies inferred from present threshold measurements with values predicted from mass data and reaction energies. All energies are expressed in the center-of-mass system in Mev.

Reaction	No. runs	Present results	Other results	Method	Reference
$Mn^{55}(\gamma,n)Mn^{54}$	13	10.192±0.020	10.209±0.007	mass data	g
			10.14±0.05	threshold	f

[f] See reference 4.
[g] C. F. Giese and J. L. Benson, Phys. Rev. 110, 712 (1958).

K. Reibel, A.K. Mann
Phys. Rev. 118, 701 (1960)

Elem. Sym.	A	Z
Mn	55	25

Method: γ's from $F^{19}(\gamma,\alpha\gamma)$ reaction; protons from Van de Graaff; NaI

Ref. No. 60 Re 1

JHH

Reaction	E or ΔE	E_o	Γ	$\int \sigma dE$	$J\pi$	Notes
$Mn^{55}(\gamma,\gamma)$	~ 7					$\langle \bar{\sigma} \rangle$ (E_p = 2.05 MeV) = 0.31±0.05 mb

REF. R. G. Baker and K. G. McNeill
Can. J. Phys. 39, 1158 (1961)

ELEM. SYM.	A	Z
Mn	55	25

METHOD Betatron; fast neutron yield; angular distribution; Si threshold detector; ion chamber.

REF. NO. 61 Ba 2 NVB

REACTION	RESULT	EXCITATION ENERGY	SOURCE		DETECTOR		ANGLE
			TYPE	RANGE	TYPE	RANGE	
G,XN	ABY	THR- 22	C	22	THR-I		DST

In Table IV: $\bar{\sigma}$ = average cross section of detector weighted with neutron spectrum;

Φ = neutrons/100 roentgen/mole

$$W(\Theta) = a_0 \sum_{n=1}^{\infty} (1+a_n P_n(\cos\Theta))$$

TABLE IV

I Element	II a_0	III a_1	IV a_2	V $(\bar{\sigma}\Phi)\times 10^{9*}$	VI Φ_{total}(22 Mev)$\times 10^9$	VII Φ_{fast}/Φ_{total}
Vanadium	215 (1±0.06)	0.01±0.08	−0.00±0.10	6.05	0.21	0.12
Chromium	161 (1±0.03)	0.01±0.04	−0.05±0.05	4.05	0.17	0.10
Manganese	308 (1±0.02)	0.07±0.03	−0.09±0.04	7.61	0.25	0.12
Iron	200 (1±0.03)	0.05±0.04	−0.17±0.05	4.94	0.18	0.11
Cobalt	390 (1±0.02)	0.08±0.03	−0.22±0.04	9.63	0.26	0.15
Nickel	145 (1±0.05)	0.07±0.07	−0.23±0.09	3.58	0.12	0.12
Copper	347 (1±0.02)	0.05±0.03	−0.29±0.04	8.57	0.30	0.12
Arsenic	482 (1±0.03)	0.11±0.04	−0.21±0.05	11.91	0.33	0.15
Rubidium	638 (1±0.05)	0.13±0.06	−0.14±0.08	15.76		
Strontium	409 (1±0.05)	0.10±0.06	−0.17±0.08	10.10		
Yttrium	290 (1±0.10)	0.08±0.12	−0.12±0.15	7.16		
Silver	590 (1±0.01)	0.10±0.06	−0.22±0.08	14.57	0.87	0.07
Cadmium	905 (1±0.02)	0.02±0.02	−0.26±0.03	22.35		
Iodine	1133 (1±0.03)	0.04±0.04	−0.29±0.05	27.99	1.42	0.08
Barium	1018 (1±0.01)	0.10±0.06	−0.38±0.08	25.89		
Lanthanum	1595 (1±0.02)	0.02±0.03	−0.42±0.04	39.40	1.01	0.15
Cerium	1316 (1±0.05)	0.05±0.06	−0.39±0.08	32.50		
Dysprosium	1652 (1±0.08)	0.01±0.10	−0.31±0.13	40.80		
Tantalum	1558 (1±0.02)	0.04±0.03	−0.22±0.04	38.48	2.50	0.06
Tungsten	1365 (1±0.02)	−0.07±0.03	−0.24±0.04	33.71		
Mercury	1345 (1±0.02)	0.04±0.03	−0.31±0.04	33.22		
Lead	2274 (1±0.01)	0.02±0.02	−0.42±0.03	56.17	2.72	0.08
Bismuth	2162 (1±0.02)	0.05±0.03	−0.45±0.04	53.40	3.36	0.06
Thorium	3031 (1±0.04)	0.06±0.05	−0.32±0.07	74.87		
Uranium	4630 (1±0.02)	0.05±0.03	−0.17±0.04	114.36		

*$(\bar{\sigma}\Phi) = 2.47\times 10^7\, a_0$ millibarn-neutron. Errors are standard errors due to counting statistics only.

Ref. F. Tagliabue, J. Goldemberg
Nuclear Phys. 23, 144 (1961)

Elem. Sym.	A	Z
Mn	55	25

Method: 22 MeV betatron; $Si^{28}(n,p)Al^{28}$ threshold detector.

Ref. No.: 61 Ta 1 JHH

Reaction	E or ΔE	E_0	Γ	$\int \sigma dE$	Jπ	Notes
(γ,n)	Bremss. 22					$E_n > 6$ MeV. $W(\theta_n) = A + B \sin^2\theta$ where $B/A = \simeq 0$

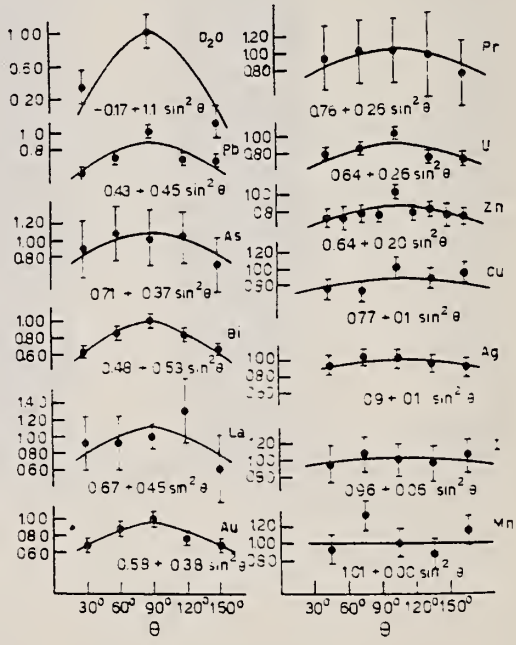

Figure 4: Angular distributions of fast photoneutrons as observed with the $Si^{28}(n,p)Al^{28}$ detector. Data normalized at 90° in each case.

REF. E. C. Booth, B. Chasan and K. A. Wright
Nucl. Phys. 57, 403-420 (1964)

ELEM. SYM.	A	Z
Mn	55	25

METHOD
Van de Graaff; resonance fluorescence

REF. NO.	
64 Bo 1	NVB

REACTION	RESULT	EXCITATION ENERGY	SOURCE		DETECTOR		ANGLE
			TYPE	RANGE	TYPE	RANGE	
G,G	LFT	1-3	C	1 - 3	NAI-D		100
		(0.5 - 3.0)		(0.5 - 3.0)			

ABI

TABLE 1
Cases of observed resonance fluorescence

Nucleus multipol.	State (MeV)	Spin	Γ_0/Γ	$T(gw\Gamma_0^2/\Gamma^2)^{-1}$ (sec).	Mean lifetime T BCW (sec)	Mean lifetime T other (sec)	Ref.	Γ_0/Γ_W BCW
Mn^{55}	0.00	$\frac{5}{2}^-$						
M1[a])	1.53	$\frac{3}{2}$	0.9	$27\pm8\times10^{-14}$	$15\pm4\times10^{-14}$			5×10^{-2}
[M1][a])	1.88	$[\frac{3}{2}^-]$	0.82	$23\pm7\times10^{-15}$	$15\pm5\times10^{-15}gW$			0.4
[M1][a])	2.20	$[\frac{3}{2}^-]$	?	$28^{+15}_{-11}\times10^{-15}$				$0.16\Gamma/\Gamma_0$
[M1][a])	2.56	$[\frac{3}{2}^-]$	?	$17^{+18}_{-7}\times10^{-15}$				$0.18\Gamma/\Gamma_0$

synchrotron; $C^{12}(\gamma,n)$ monitor

REACTION	RESULT	EXCITATION ENERGY	SOURCE		DETECTOR		ANGLE
			TYPE	RANGE	TYPE	RANGE	
C,AA	ABY	THR - 80	C	80	BF3-I		4 PI

Table 1

Element	Yield (28) eV cm^2 mol MeV	60 NZ/A (mb MeV)	Σ_0^{30}	Σ_0^{60}	$\Sigma_0^{30} / \Sigma_0^{60}$	E_m (MeV)	σ_m (mb)
$_{24}$Cr	83 x10^{-5}	777	1.21	2.1	0.58	18.5	97
$_{25}$Mn	108 x10^{-5}	818	1.52	2.33	0.65	18.5	114
$_{26}$Fe	68 x10^{-5}	832	0.68	1.46	0.80	17.5	75
$_{27}$Co	89x10^{-5}	878	1.08	1.82	0.59	17.5	92
$_{28}$Ni	44x10^{-5}	879	0.55	1.07	0.51	18.5	56
$_{29}$Cu	95x10^{-5}	947	1.06	1.99	0.53	17.5	98
$_{30}$Zn	88x10^{-5}	975	0.94	1.68	0.56	17.5	86
$_{31}$Ga	130x10^{-5}	1034	1.29	2.18	0.59	17.5	151
$_{32}$Ge	139x10^{-5}	1034	1.35	2.29	0.59	17.5	158
$_{33}$As	137x10^{-5}	1109	1.22	2.18	0.56	17.5	127

$$\Sigma_0^{30} = \frac{\int_0^{30} \sigma(\gamma,xn)dE}{60\ NZ/A}$$

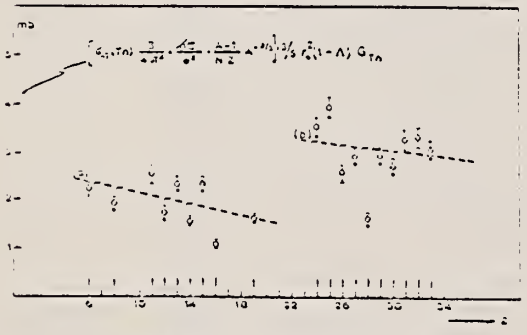

Fig. 2. Bremsstrahlung weighted cross sections, $\sigma_{-1}(Zn)$, conveniently normalized, versus Z.

Table 2

Element	maximum yield (x 10^{-5})	$\sigma_{-1}(Zn)$	$\sigma_{-1}(Zn) \times \left[\frac{3}{4\pi^2}\frac{\hbar c}{e^2}\left(\frac{A-1}{NZ}\right)A^{-\frac{2}{3}}\right]$
$_6$C	4.0	3.54	2.16
$_8$O	5.2	4.65	1.92
$_{11}$Na	13.6	11.60	2.49
$_{12}$Mg	10.0	8.81	1.78
$_{13}$Al	15.9	13.92	2.80
$_{14}$Si	11.6	9.96	1.55
$_{15}$P	19.8	17.56	2.82
$_{16}$S	8.5	8.55	1.37
$_{19}$K	19.6	17.90	1.91
$_{20}$Ca	12.1	11.65	1.02
$_{24}$Cr	86	81.6	3.56
$_{25}$Mn	118	78.1	3.06
$_{26}$Fe	71	50.5	2.85
$_{27}$Co	84	68.5	2.04
$_{28}$Ni	48	34.2	1.50
$_{29}$Cu	102	72.3	2.06
$_{30}$Zn	92	65.7	2.05
$_{31}$Ga	140	98.6	3.01
$_{32}$Ge	150	101.5	3.06
$_{33}$As	131	90.3	3.12

REF.

S. Costa, F. Ferrero, S. Ferroni and R. Malvano
Proc. Paris Conference 1034 (1964)

ELEM. SYM.	A	Z
Mn	55	25

METHOD

·100 MeV synchrotron

REF. NO. 64 Co 3 JDM

REACTION	RESULT	EXCITATION ENERGY	SOURCE		DETECTOR		ANGLE
			TYPE	RANGE	TYPE	RANGE	
G,N	ABΣ	THR-80	C	10-80	BF3-I		4PI

TABLE

ELEMENT	Yield (36 MeV) $\left(\frac{\text{n. cm}^2}{\text{mol. MeV}} \times 10^5\right)$	Σ_0^{30}	Σ_0^{60}	$\Sigma_0^{30}/\Sigma_0^{60}$	σ_{-1} (mb)
$_{24}$Cr	83	1.21	2.1	0.58	62
$_{25}$Mn	108	1.52	2.33	0.65	76
$_{26}$Fe	68	0.88	1.46	0.60	50
$_{27}$Co	89	1.08	1.82	0.59	64
$_{28}$Ni	44	0.55	1.07	0.51	34
$_{29}$Cu	95	1.06	1.99	0.53	72
$_{30}$Zn	88	0.94	1.68	0.56	66
$_{31}$Ga	130	1.29	2.18	0.59	94
$_{32}$Ge	139	1.35	2.29	0.59	101
$_{33}$As	137	1.22	2.18	0.56	100

$\sum_a^b = \frac{A}{60\,NZ}\int_a^b \sigma(E)\,dE$ is the integrated cross section measured in units of the classical dipole $60\,NZ/A$ mb. MeV.

REF.
W. B. Walters and J. P. Hummel
Phys. Rev. 150, 867 (1966)

ELEM. SYM.	A	Z
Mn	55	25

METHOD
Betatron

REF. NO.
66 Wa 1
JDM

REACTION	RESULT	EXCITATION ENERGY	SOURCE		DETECTOR		ANGLE
			TYPE	RANGE	TYPE	RANGE	
G,3N	RLY	THR-300	C	100-300	ACT-I		4PI
G,4P7N	RLY	THR-300	C	100-300	ACT-I		4PI

Measured isomeric yield ratios.

TABLE III. Summary of the results for the photoproduction of the Mn^{52} isomers (spins 2 and 6).

Target isotope and spin	Bremsstrahlung energy (MeV)	Fraction of yield to high-spin isomer
$Fe^{54,56}$ ($I=0$)[a]	100	0.39±0.03
	150	0.36±0.02
	200	0.35±0.02
	250	0.37±0.02
Mn^{55} ($I=\frac{5}{2}$)	100	0.44±0.04
	150	0.48±0.02
	225	0.47±0.02
	300	0.47±0.02
Co^{59} ($I=\frac{7}{2}$)	150	0.62±0.02

[a] It is assumed that most of the yield is due to reactions involving the two lightest isotopes present in natural iron (Fe^{54} and Fe^{56}).

TABLE II. Summary of the results for the photoproduction of the Sc^{44} isomers (spins 2 and 6).

Target isotope and spin	Bremsstrahlung energy (MeV)	Fraction of yield to high-spin isomer
Sc^{45} ($I=\frac{7}{2}$)	50	0.21±0.04
	75	0.21±0.03
	175	0.20±0.02
	223	0.18±0.01
	264	0.17±0.02
	300	0.21±0.02
$Fe^{54,56}$ ($I=0$)[a]	250	0.38±0.02
Mn^{55} ($I=\frac{5}{2}$)	225	0.42±0.04
	300	0.39±0.02

[a] It is assumed that most of the yield is due to reactions involving the two lightest isotopes present in natural iron (Fe^{54} and Fe^{56}).

REF. J. M. Loiseaux, J. M. Maison, and M. Langevin
J. de Physique 28, 11 (1967)

ELEM. SYM.	A	Z
Mn	55	25

METHOD

REF. NO. 67 Lo 1 JOC

REACTION	RESULT	EXCITATION ENERGY	SOURCE		DETECTOR		ANGLE
			TYPE	RANGE	TYPE	RANGE	
G,G/	ABX	14-32	C	34	NAI-D		DST

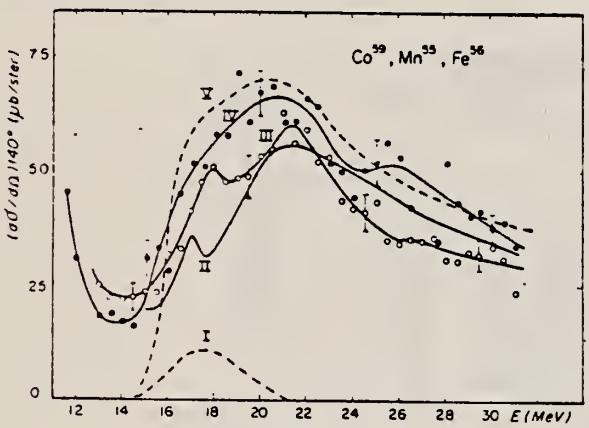

FIG. 10.

Sections efficaces différentielles de diffusion à 140° pour ^{55}Mn (courbe II), ^{56}Fe (courbe III), ^{59}Co (courbe IV). Section efficace de diffusion tenseur (courbe I) et section efficace de diffusion scalaire – tenseur (courbe V) calculées avec les paramètres de Fultz et al. [16] pour ^{59}Co.

REF. W. J. Alston III, H. H. Wilson and E. C. Booth
Nucl. Phys. A116, 281 (1968)

ELEM. SYM.	A	Z
Mn	55	25

METHOD

REF. NO. 68 A1 1 egf

REACTION	RESULT	EXCITATION ENERGY	SOURCE		DETECTOR		ANGLE
			TYPE	RANGE	TYPE	RANGE	
G,G	LFT	0 - 3	C	4	SCD-D	0-3	130
		(2.75)					

Angle greater than 90° for all measurements.

SELF-ABSORPTION

TABLE 1

Direct and absorption measurements of resonance fluorescence

Nucleus	E_r (MeV)	J_r	Γ_0/Γ	$gW\Gamma_0\Gamma_0/\Gamma$ (meV)	Error (%)	This work Γ_0 (meV)	Other work Γ_0
^{55}Mn	0.000	$\frac{5}{2}^-$					
	1.527	$(\frac{3}{2}^-)$	0.9	5.2	25	8–12	
				abs [a]	40	8.0	
	1.884	?	0.82 [b]	41	25	$50/gW$	
				abs [a]	10	$55/g$	
	2.197	?	(0.8) [c]	17	25	$21/gW$	
				abs	20	$17/g$	
	2.252	?	(0.9) [c]	17	25	$19/gW$	
				abs	20	$13/g$	
	2.365	?	?	3.5	36	$(2–6)\Gamma/\Gamma_0$	
	2.564	?	(1.0)	50	25	$50/gW$	
				abs [a]	20	$61/g$	
	2.751	?	?	6.7	42	$6.7(\Gamma/\Gamma_0)/gW$	
^{59}Co	0.000	$\frac{7}{2}^-$					
	1.187	$(\frac{5}{2}^-)$	(1.0)	6.8	25	7.5	0.33(E2) [d]
				abs	25 [a]	12	
		$(\frac{3}{2}^-)$	(1.0)	6.8	25	(5.4–6.5)	0.27(E2)
				abs	25 [a]	9.6	
^{63}Cu	0.000	$\frac{3}{2}^-$					
	1.414	$\frac{5}{2}^-$	?	1.6	30	$(1.1–1.7)\Gamma/\Gamma_0$	
	1.551	$\frac{3}{2}^-$	?	1.7	37	$(1.7–2.5)\Gamma/\Gamma_0$	0.1(E2) [e]
^{69}Ga	0.000	$\frac{3}{2}^-$					
	0.872	$(\frac{1}{2}^-)$	0.95	1.1	35	$0.8/W$	
	1.107	$(\frac{5}{2}^-)$	0.95	8.0	20	$8.4/W$	
^{75}As	0.000	$\frac{3}{2}^-$					
	0.86	?	?	1.7	20	$1.7\,\Gamma/gW\Gamma_0$	
	1.07	?	?	2.6	30	$2.6\,\Gamma/gW\Gamma_0$	
	1.35	?	?	3.6	20	$3.6\,\Gamma/gW\Gamma_0$	
^{89}Y	0.000	$\frac{1}{2}^-$					
	1.51	$\frac{3}{2}^-$	(1.0)	52 [a]	30	28	0.37(E2) [f]
				abs [a]	15	22	

[a]) Measured with NaI.
[b]) Ref. [24]).
[c]) Measured with a Ge(Li) detector to ±10 %.
[d]) Ref. [13]). [e]) Ref. [14]). [f]) Ref. [23]).

[13] D.G. Alkhazov, K.I. Erokhina and I.K. Lemberg, Izv.Akad.Nauk. SSSR(ser.fiz.) 28 (1964) 1667.
[14] B.G. Harvey, J.R. Meriwether and A. Bussiere, Nucl. Phys. 70 (1965) 305.
[23] G.A. Peterson and J. Alster, Phys. Rev. 166 (1968) 136.
[24] N. Nath, M.A. Rothman, D.M. Van Patter and C.E. Mandeville, Nucl.Phys. 13 (1959) 74.

[over]

TABLE 2

Transition strengths for ^{44}Mn levels

Energy (MeV)	Transition	Multipolarity	$\Gamma_{s.p.}$(M1) ×1/10 (meV)	Γ_0(E2) calc. [a] (meV)	Γ_0(M1) calc. [a] (meV)	Γ_0(M1+E2) present work (meV)
0.983	$\frac{6}{2}^- \rightarrow \frac{4}{2}^-$	E2				< 1 [b]
1.527	$\frac{3}{2}^- \rightarrow \frac{4}{2}^-$	(M1+E2)	7	0.5	1.9	8 ± 3
1.884	$\frac{7}{2}^- \rightarrow \frac{4}{2}^-$	(M1+E2)	15		43	41 ± 6
2.197	$\frac{5}{2}^- \rightarrow \frac{4}{2}^-$	(M1+E2)	22		111	25 ± 5
2.252	$\frac{1}{2}^- \rightarrow \frac{4}{2}^-$	(M1+E2)	24			13 ± 3 [c]
2.564	$\frac{3}{2}^- \rightarrow \frac{4}{2}^-$	(M1+E2)	36		2.7	91 ± 18
	$\frac{5}{2}^- \rightarrow \frac{4}{2}^-$	(M1+E2)	36		1.0	61 ± 12
	$\frac{7}{2}^- \rightarrow \frac{4}{2}^-$	(M1+E2)	36		16	45 ± 9

[a]) Ref. [10]).

[b]) Assuming $\Gamma_0/\Gamma = 0.07$ from ref. [24]).

[c]) Strength from the 2.365 → 0.127 transition may be contributing to this partial width.

[10] J. Vervier, Nucl. Phys. 78 (1966) 497.

[24] N. Nath, M.A. Rothman, D.M. Van Patter and C.E. Mandeville, Nucl. Phys. 13 (1959) 74.

REF.

R. Garfagnini and G. Piragino
Nucl. Phys. A122, 49 (1968)

ELEM. SYM.	A	Z
Mn	55	25

METHOD

REF. NO.	
68 Ga 1	egf

REACTION	RESULT	EXCITATION ENERGY	SOURCE		DETECTOR		ANGLE
			TYPE	RANGE	TYPE	RANGE	
$G,XN	SPC	THR-85	C	85	CCH	1-15	135

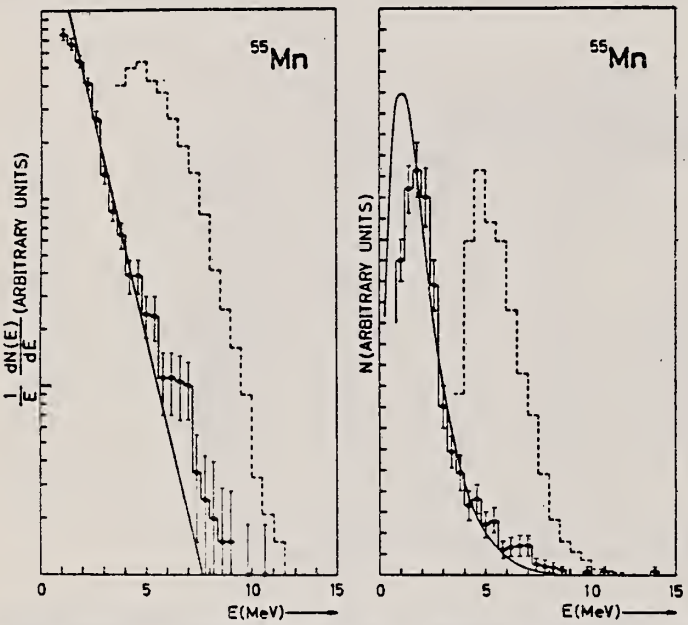

Fig. 4. Energy spectrum of photoneutrons from ^{55}Mn compared with the spectrum of photoprotons ($E_{\gamma\,max}$ = 20.5 MeV) deduced from ref. [27]) (dashed histogram). The spectra are normalized to maximum value of N. The full line has the same meaning as in fig. 2.

[27] K. Shoda, Nucl. Phys. 72, 305 (1965).

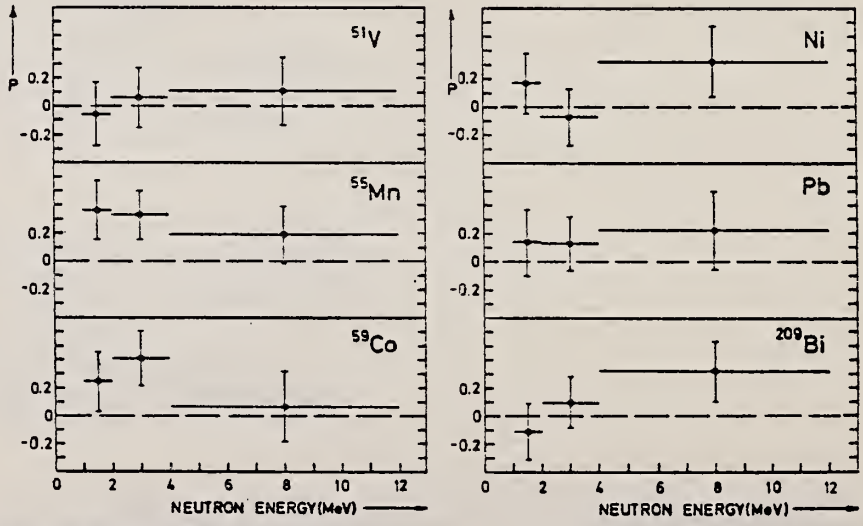

Fig. 7. Polarization of photoneutrons from ^{51}V, ^{55}Mn, ^{59}Co, natural Ni, natural Pb and ^{209}Bi.

FORM NBS-418
(REV. 7-14-64)
USCOMM-DC 26010-P64

REF.

J. W. Jury, J. S. Hewitt, and K. G. McNeill
Can. J. Phys. 46, 1823 (1968)

ELEM. SYM.	A	Z
Mn	55	25

METHOD

REF. NO.	
68 Ju 1	EGF

REACTION	RESULT	EXCITATION ENERGY	SOURCE		DETECTOR		ANGLE
			TYPE	RANGE	TYPE	RANGE	
G,N	NOX	THR - 22	C	22	THR	5-	DST

$$W(\theta) = a_o + a_1 P_1 + a_2 P_2$$

TABLE I

Target element	Z	Energy	a_0*	a_1/a_0	a_2/a_0
Vanadium	23	32	640±50	0.11±0.10	−0.09±0.11
Chromium	24	22	365±39	0.02±0.08	0.00±0.10
Manganese	25	22	450±33	0.07±0.05	−0.11±0.06
Bromine	35	27	874±54	0.05±0.06	−0.15±0.08
Molybdenum	42	22	610±60	0.09±0.05	−0.35±0.06
Ruthenium	44	27	1100±25	0.12±0.02	−0.29±0.03
Rhodium	45	27	1270±47	0.06±0.03	−0.14±0.03
Palladium	46	27	1350±29	0.26±0.02	−0.12±0.02
Antimony	51	27	2140±62	0.04±0.08	−0.25±0.11
Lanthanum	57	27	1940±70	0.12±0.10	−0.52±0.14
Praseodymium	59	30	1800±58	0.20±0.08	−0.40±0.09
Platinum	78	27	2600±52	0.17±0.02	−0.15±0.03
Lead	82	22	2274±59	0.08±0.08	−0.46±0.09

*The yield per mole per 100 r was normalized to a yield of 2274 for the lead sample at the same energy.

REF. K. Shoda, K. Abe, T. Ishizuka, N. Kawamura, M. Oyamada, and Baik-Nung Sung
J. Phys. Soc. Japan 25, 664 (1968)

ELEM. SYM.	A	Z
Mn	55	25

METHOD

REF. NO. 68 Sh 3 egf

REACTION	RESULT	EXCITATION ENERGY	SOURCE TYPE	SOURCE RANGE	DETECTOR TYPE	DETECTOR RANGE	ANGLE
G,XP	ABX	THR-23	C	13-23	SCI-I		DST

SPECTRA ALSO GIVEN

Table II. Anisotropic factor B/A of angular distributions determined by least-squares fits with $A+B\sin^2\theta$.

^{55}Mn	
$E_{\gamma\,max}$=20.5 MeV)	
E_p(MeV)	B/A
2.8–5.2	0.1±0.2
5.2–6.1	1.3±0.3
6.1≦	2.4±0.6
2.8≦	0.6±0.1

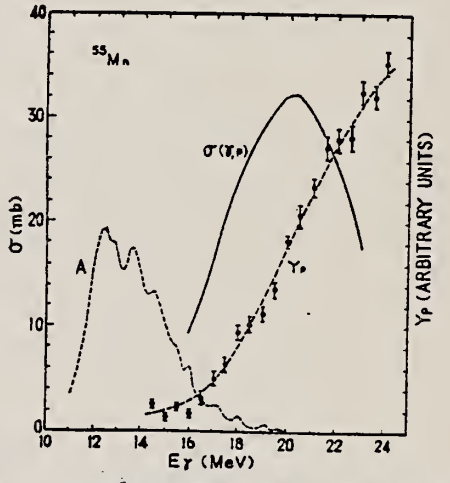

Fig. 14. Comparison among the photoproton cross sections on ^{55}Mn. Curve A is the cross section calculated from the present energy distribution under the assumption that the residual nucleus is completely left in the ground state. Photoproton yield curve using ZnS(Ag) scintillation counters and the cross section calculated from it are indicated by Y_p and $\sigma(\gamma, p)$ respectively.

REF. H. G. De Carvalho, V. Di Napoli, D. Margadonna, F. Salvetti and K. Tesch
Nucl. Phys. A126, 505 (1969)

ELEM. SYM.	A	Z
Mn	55	25

METHOD

REF. NO. 69 De 1 egf

REACTION	RESULT	EXCITATION ENERGY	SOURCE		DETECTOR		ANGLE
			TYPE	RANGE	TYPE	RANGE	
G,N	ABY	THR-999	C	2-6	ACT-I		4PI
G,3N	ABY	THR-999	C	2-6	ACT-I		4PI
				(2.0-5.5)			

Yield per equivalent quantum.

999 = 5.5 GEV

In addition to the reactions mentioned above, we measured in the energy range 2-5.5 GeV, the following reactions: $^{55}Mn(\gamma, n)$, $^{55}Mn(\gamma, 3n)$, $^{103}Rh(\gamma, 2n)$ and $^{127}I(\gamma, 3n)$. The resulting cross sections per equivalent quantum are 43 mb, 0.55 mb, 21 mb and 9.5 mb, respectively. Within the experimental error of 20 %, we found no variation of these cross sections with the maximum bremsstrahlung energy.

B. S. Dolbilkin, A. I. Isakov, V. I. Korin, and L. E. Lazareva
ZhETF Pis. Red. 10, 365 (1969)
JETP Letters 10, 231 (1969)

ELEM. SYM.	A	Z
Mn	55	25

METHOD

REF. NO.	
69 Do 1	hmg

REACTION	RESULT	EXCITATION ENERGY	SOURCE		DETECTOR		ANGLE
			TYPE	RANGE	TYPE	RANGE	
G,MU-T	ABX	10-30	C	10-260	MAG-D	10-28	4PI

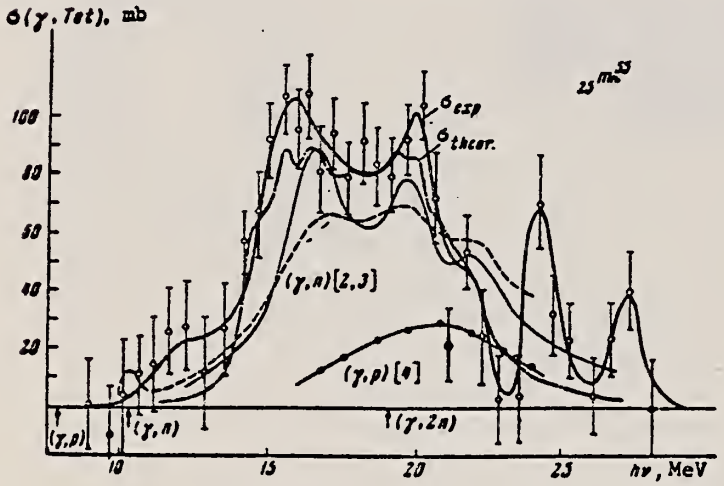

Cross section for the photo-absorption by Mn^{55} nuclei in the giant-resonance region.

REF.

R. Garfagnini, G. Piragino & A. Zanini
Atti Accad. Naz. Lincei, Rend.
Cl. Sci. Fis. Mat. Natur. 47, 33 (1969)

ELEM. SYM.	A	Z
Mn	55	25

METHOD

REF. NO.	
69 Ga 3	egf

REACTION	RESULT	EXCITATION ENERGY	SOURCE		DETECTOR		ANGLE
			TYPE	RANGE	TYPE	RANGE	
G,XN	SPC	11-85	C	85	CCH-D		135

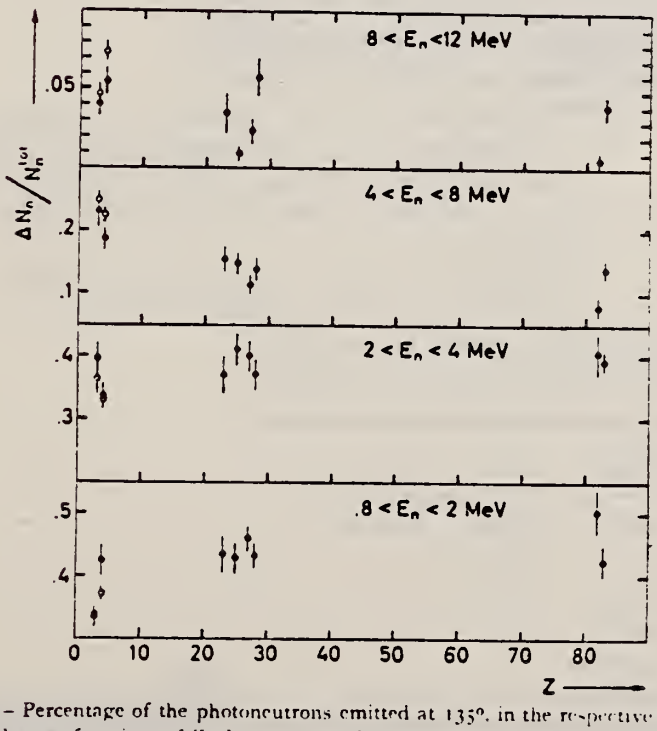

Fig. 1. – Percentage of the photoneutrons emitted at 135°, in the respective energy interval as a function of Z, by a γ-ray bremsstrahlung beam with $E_{\gamma max}$ = 85 MeV. The open circles represent the values obtained at 60° for ^{7}Li and ^{9}Be.

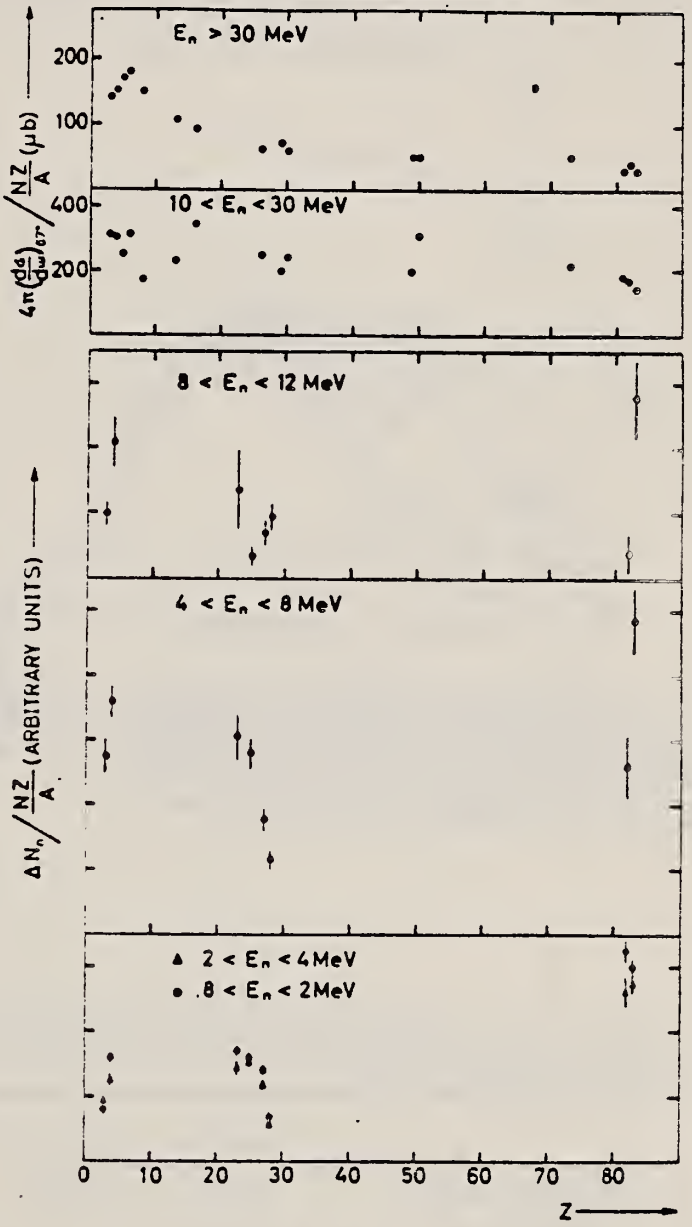

Fig. 2. – Number of photoneutrons emitted at 135°, normalized to the sum rule factor NZ/A, as a function of Z. In the upper part is reported the effective cross section divided by NZ/A for photoproduction of fast neutrons by 55-85 MeV bremsstrahlung photons as deduced by Kaushal *et al.* [1].

[1] N.N. Kaushal et al., Phys. Rev. 175, 1330 (1968).

H. Theissen, R. J. Peterson, W. J. Alston,III, and J. R. Stewart
Phys. Rev. 186, 1119 (1969)

ELEM. SYM.	A	Z
Mn	55	25

METHOD

REF. NO. 69 Th 1 hmg

REACTION	RESULT	EXCITATION ENERGY	SOURCE TYPE	SOURCE RANGE	DETECTOR TYPE	DETECTOR RANGE	ANGLE
E,E/	ABX	0-4	D	51-61	MAG-D		DST
		(.98 - 3.05)		(50.2-60.2)			

$E_0 = 60.2$ MeV

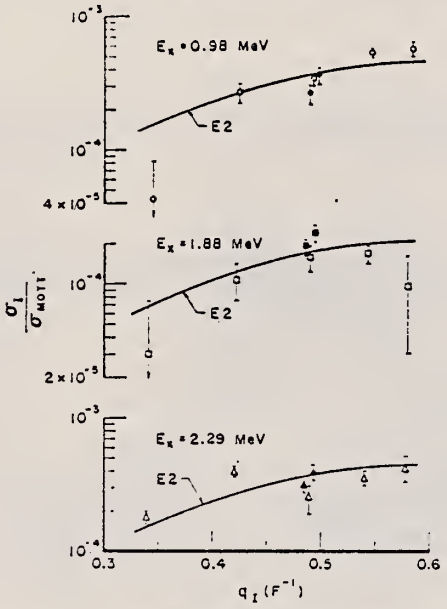

FIG. 3. Differential inelastic cross section σ_I in units of the Mott cross section σ_{Mott} as a function of the inelastic momentum transfer q_I for the 0.98-, 1.88-, and 2.29-MeV transitions in Mn^{55}. Open symbols represent points taken at $E_0 = 60.2$ MeV. Closed symbols refer to additional points taken at $q_I = 0.49$ F^{-1}, but different electron energies (see text). The best theoretical fits assuming pure $E2$ transitions are given by the solid lines.

$q_I = 0.49$ F^{-1}

B(EL)

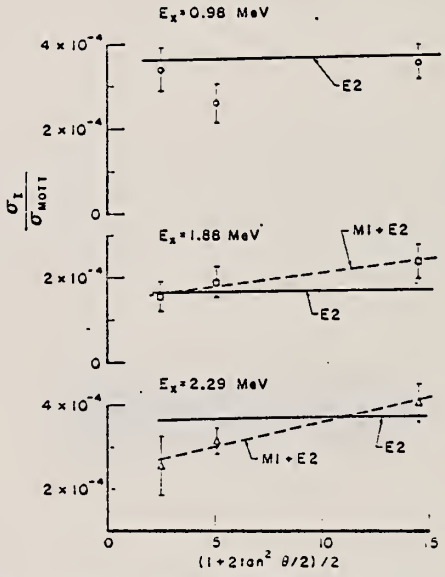

FIG. 4. Differential inelastic cross section σ_I divided by the Mott cross section σ_{Mott}, taken at constant inelastic momentum transfer, as a function of $\frac{1}{2}(1+2\tan^2\frac{1}{2}\theta)$, i.e., points at $q_I = 0.49$ F^{-1} of Fig. 3 replotted. The solid lines represent the best theoretical fits from Fig. 3 for pure $E2$ transitions. The dashed lines are obtained under the assumption of an $E2$-$M1$ mixture (see text).

[1] I. Gabrielli, B. G. Harvey, D. L. Hendrie, J. Mahoney, J. R. Meriwether, and T. Valentine, Nuovo Cimento (to be published).
[2] R. J. Peterson, Ann. Phys. (N.Y.) 53, 40 (1969).
[4] W. J. Alston,III, H. H. Wilson, and E. C. Booth, Nucl. Phys. A116, 281 (1968).

TABLE III. Results for inelastic scattering. E_x is the excitation energy, J^π is the spin and parity of corresponding level, $B(E2\uparrow)$ is the reduced transition probability, and Γ_γ^0 is the ground-state radiation width. The $B(E2)$'s quoted as the results of this work have been obtained assuming the strict hydrodynamical model. The model dependence was taken into account by adding a ±15% uncertainty to the statistical error (see text).

	E_x(MeV), J^π: 0.98 ($\frac{3}{2}^-$)	1.53 ($\frac{5}{2}^-$)	1.88 ($\frac{7}{2}^-$)	(2.29)	(3.05)
$B(E2\uparrow)$(F^4), this work	147±30	(28±16)	68±15	154±30	(34±10)
$B(E2\uparrow)$(F^4), (α,α')[a]	167.0	···	119.0	89.4[d]	
$B(E2\uparrow)$(F^4), (p,p')[b]	201	···	125	125[d]	
$\Gamma_\gamma^0(E2)$ (10^{-3} eV), this work	0.066±0.014	(0.28±0.16)	0.96±0.21	···	···
$\Gamma_\gamma^0(M1+E2)$ (10^{-3} eV), (RF)[c]	···	8±3	41±6	···	···
$\delta^2=\Gamma_\gamma^0(E2)/\Gamma_\gamma^0(M1)$	···	(0.04±0.04)	0.024±0.009	···	···

[a] Reference 1.
[b] Reference 2.
[c] Reference 4.
[d] Strengths of the 2.25- and 2.37-MeV transitions were added.

DEPARTMENT OF COMMERCE
ONAL BUREAU OF STANDARDS

REF. B. S. Ishkhanov, I. M. Kapitonov, E. V. Lazutin, I. M. Piskarev, and O. P. Shevchenko
Izv. Akad. Nauk Fiz. 34, 2228 (1970)
Bull. Acad. Sci. USSR Phys. 34, 1988 (1970)

ELEM. SYM.	A	Z
Mn	55	25

METHOD

REF. NO. 70 Is 7 hmg

REACTION	RESULT	EXCITATION ENERGY	SOURCE TYPE	SOURCE RANGE	DETECTOR TYPE	DETECTOR RANGE	ANGLE
G,XN	ABX	10- 30	C	7- 30	BF3-I		4PI

$$\int_{10}^{29.5} \sigma(\gamma,xn)dE = 780\pm80 \text{ MeV mb}$$

$$\int_{o}^{29.5} \sigma(\gamma,SN)dE = 620\pm60 \text{ MeV mb}$$

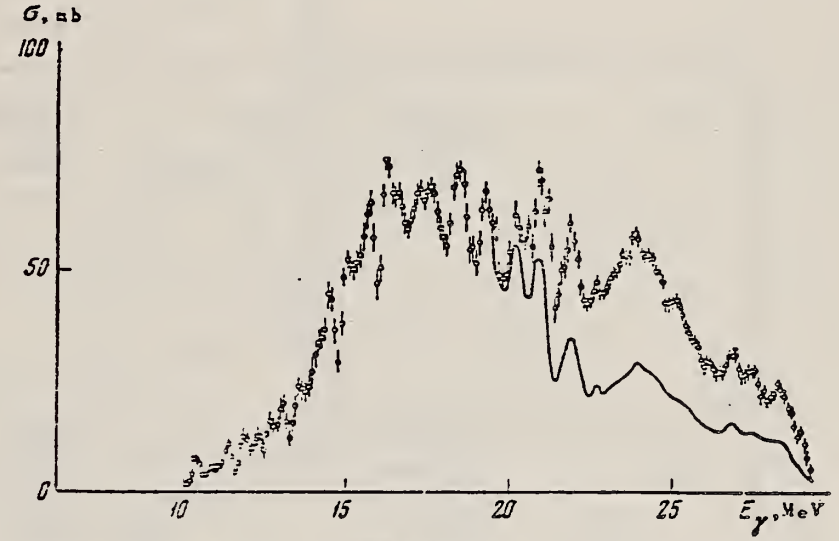

Fig.1. Photoneutron cross section $\sigma(\gamma,Tn) = \sigma(\gamma,n) + \sigma(\gamma,np) + 2\sigma(\gamma,2n)$ for ^{55}Mn. The full curve shows the cross section $\sigma(\gamma,n) + \sigma(\gamma,np)\ \sigma(\gamma,2n)$ above the $(\gamma,2n)$ threshold.

REF. G. J. Kumbartzki, Ung Kim and Ch. K. Kwan
Nucl. Phys. A160, 237 (1971)

ELEM. SYM.	A	Z
Mn	55	25

METHOD

REF. NO.: 71 Ku 2 | egf

REACTION	RESULT	EXCITATION ENERGY	SOURCE		DETECTOR		ANGLE
			TYPE	RANGE	TYPE	RANGE	
G,SPL	ABY	THR-999	C	999	ACT-I		4PI

$\sigma_q(A,Z) = K\exp[PA-R(A-SZ+TZ^2)^2]$, cross section per equivalent quantum. 999 = 1.5 GEV

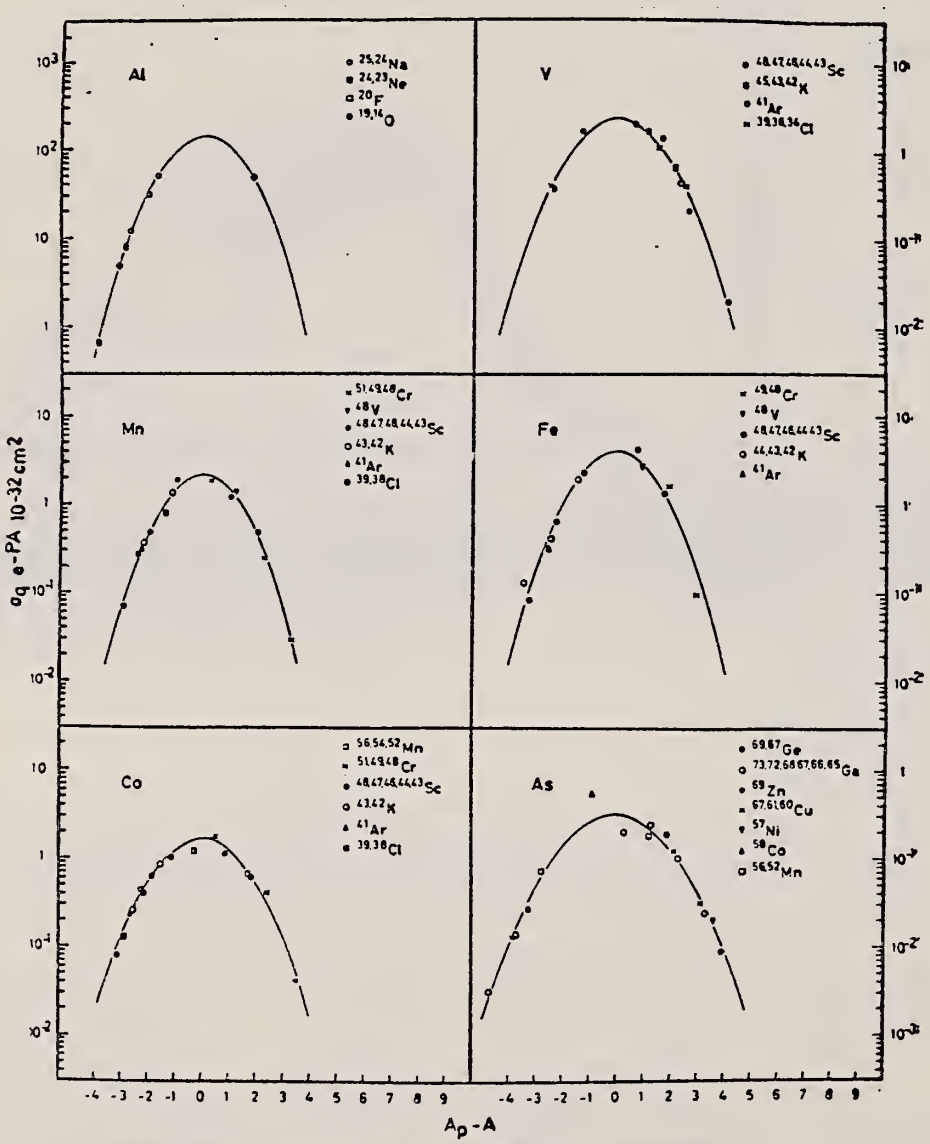

Fig. 4. Yield distributions from various targets with bremsstrahlung of 1.5 GeV.

[over]

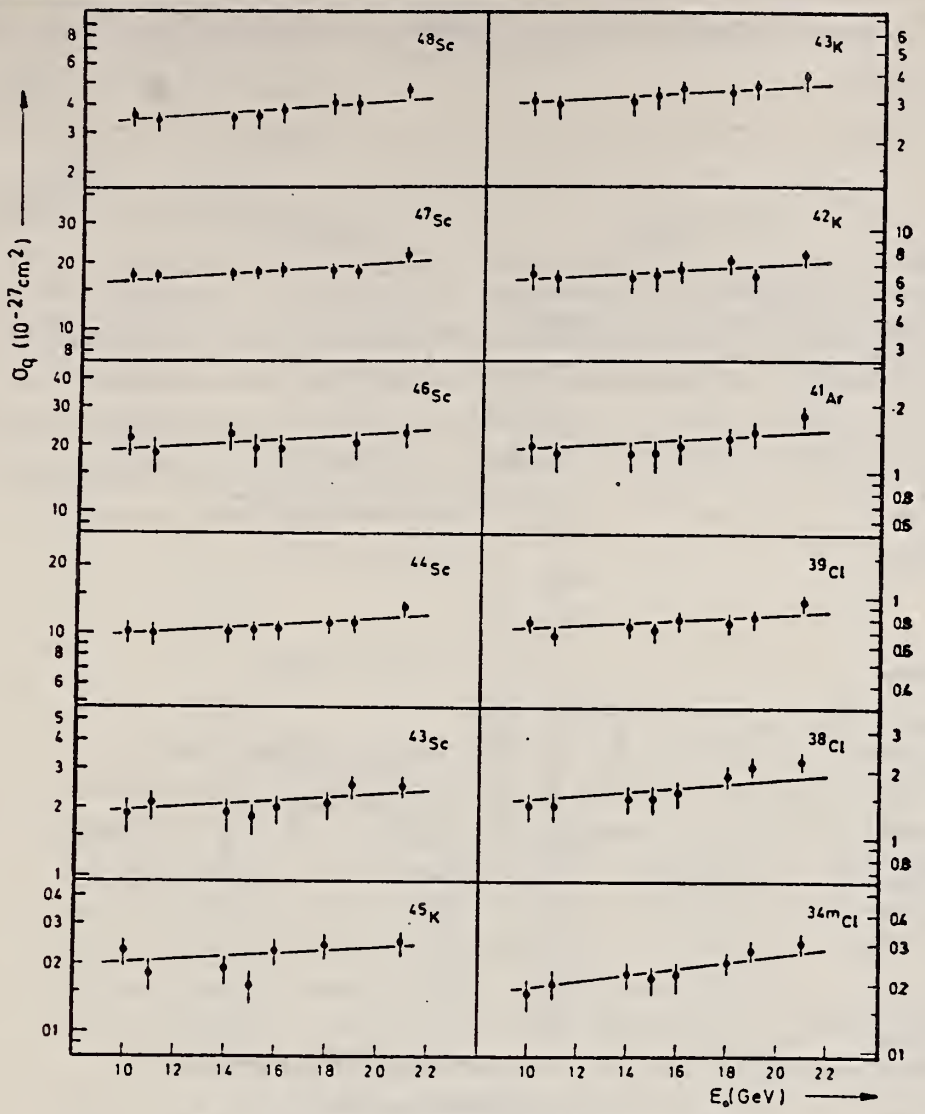

Fig. 5. Yields of spallation products using vanadium targets.

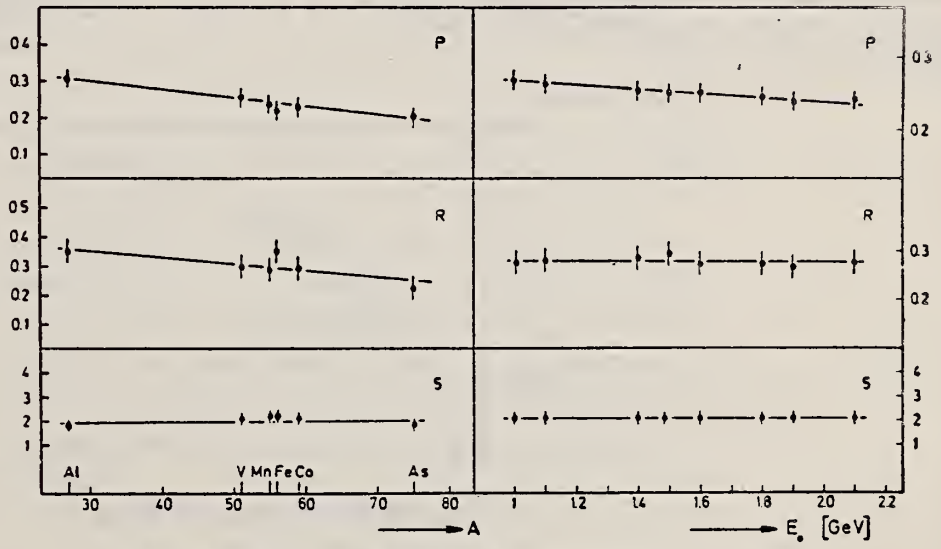

Fig. 6. Behaviour of the parameters P, R and S as functions of A and E_o.

REF.

Tatsuya Saito
Nippon Kagaku Zasshi 92, 164 (1971)

ELEM. SYM.	A	Z
Mn	55	25

METHOD

REF. NO.: 71 Sa 1 egf

REACTION	RESULT	EXCITATION ENERGY	SOURCE TYPE	SOURCE RANGE	DETECTOR TYPE	DETECTOR RANGE	ANGLE
G,N	ABY	10-68	C	10-68	ACT-I		4PI

Nippon Kagaku Zasshi, 92, 164~168(1971)

The Yields of Radioactivities Induced by (γ, n) Reactions with Bremsstrahlung up to 68 MeV

by Tatsuya SAITO

The (γ, n) yields of 12 target nuclides have been measured at 10, 13, 16, 30, 45 and 68 MeV bremsstrahlung by observing the induced activities.

The energy dependence of the yields has been investigated extensively in the same way as in the previous work at 20 MeV bremsstrahlung.

In the case of heavy nuclides, the yields rise greatly as a function of maximum bombarding energy up to 20 MeV, and rise gradually from 20 MeV up to 68 MeV. However, in the case of light nuclides, the yields rise greatly up to 30 MeV, because the neutron separation energies of light ones are larger than those of heavy ones, and the bremsstrahlung spectrum covers the giant resonance and so the yields rise gradually from 30 MeV up to 68 MeV.

The yields have approximately been estimated from the parameter of the giant resonance, that is the peak cross section and the half width, in order to compare with the experimental data. As a result, the experimental data of light nuclides and heavy ones are nearly in agreement with the estimated data of Nathans et al., Johns et al. and Montalbetti et al., but those of medium weight ones are relatively lower values.

Department of Chemistry, Faculty of Science, Tohoku University; Katahira-cho, Sendai-shi, Japan

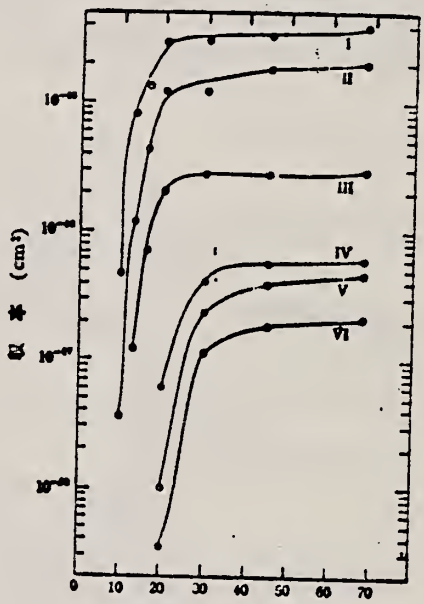

誘導輻射最大エネルギー

I: $^{197}Au(\gamma, n)^{196}Au$, II: $^{127}I(\gamma, n)^{126}I$
III: $^{55}Mn(\gamma, n)^{54}Mn$, IV: $^{23}Na(\gamma, n)^{22}Na$
V: $^{16}O(\gamma, n)^{15}O$, VI: $^{12}C(\gamma, n)^{11}C$

図 3 (γ, n)反応の収率

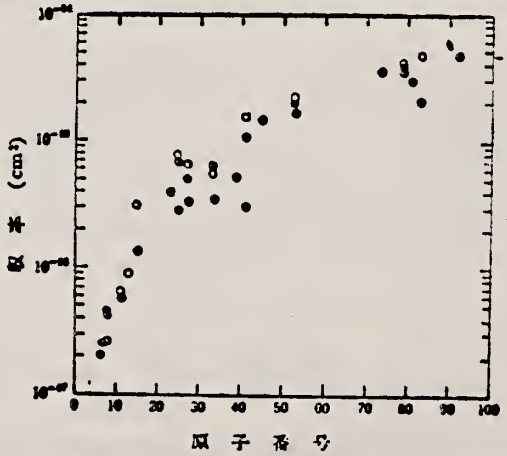

原子番号

●: 実験値, ⊕: Johns ら,
◑: Nathans ら, ○: Monialbetti ら

図 4 (γ, n)反応の収率の比較

REF. R.A. Alvarez, B.L. Berman, F.H. Lewis, and P. Meyer
PICNS-73, Vol.I, p.545 Asilomar

ELEM. SYM.	A	Z
Mn	55	25

METHOD

REF. NO. 73 A1 6 hmg

REACTION	RESULT	EXCITATION ENERGY	SOURCE		DETECTOR		ANGLE
			TYPE	RANGE	TYPE	RANGE	
G,N	ABX	10- 37	D	10- 37	BF3-I		4PI
G,2N	ABX	17- 37	D	17- 37	BF3-I		4PI
G,3N	ABX	29- 37	D	29- 37	BF3-I		4PI

518+

We have measured the photoneutron cross sections for ^{55}Mn with nearly monoenergetic photons from in-flight annihilation of positrons from the new Livermore electron-positron linac. The technique and apparatus used were nearly identical to those used in the experiments on the nickel isotopes.[1] Measurements at each energy were also made of the ^{59}Co cross sections without changing the accelerator or beam-transport system tuning. This provides added confidence that fine structure observed in one isotope but not the other is indeed an effect of the nuclear dynamics and not a fluctuation caused by the apparatus. The ^{59}Co results are reported in a separate paper.[2]

Our results are shown in Fig. 1. The photon energy resolution is approximately 100 keV. The error bars shown are statistical only. Systematic errors are approximately the same as for the nickel isotopes.[1]

The giant resonance in ^{55}Mn is unusually broad, and is divided into three main groups of sub-structures, the first two of which have nearly equal peak cross sections of about 65-70 mb and central energies of about 17 and 19.5 MeV. The third large cluster of strength lies near 23 MeV with a peak cross section a bit greater than 50 mb; this cluster is located near the maximum in the (γ,2n) cross section. The (γ,2n) cross section has a peak value of just over 20 mb and an integrated cross section (to 36.5 MeV) of 166 MeV-mb. This is to be compared with a total photoneutron integrated cross section of 805 MeV-mb. The statistical accuracy of the (γ,3n) cross section measurement is very poor, but one can conclude that the cross section is quite small up to 37 MeV.

Superimposed on the gross structure in the giant-resonance region, a rather rich fine structure can be observed. We note particularly the structure on the low-energy edge of the giant resonance, including the sharp peak right at the (γ,n) threshold, a behavior similar to that observed in ^{58}Ni.[1]

(over)

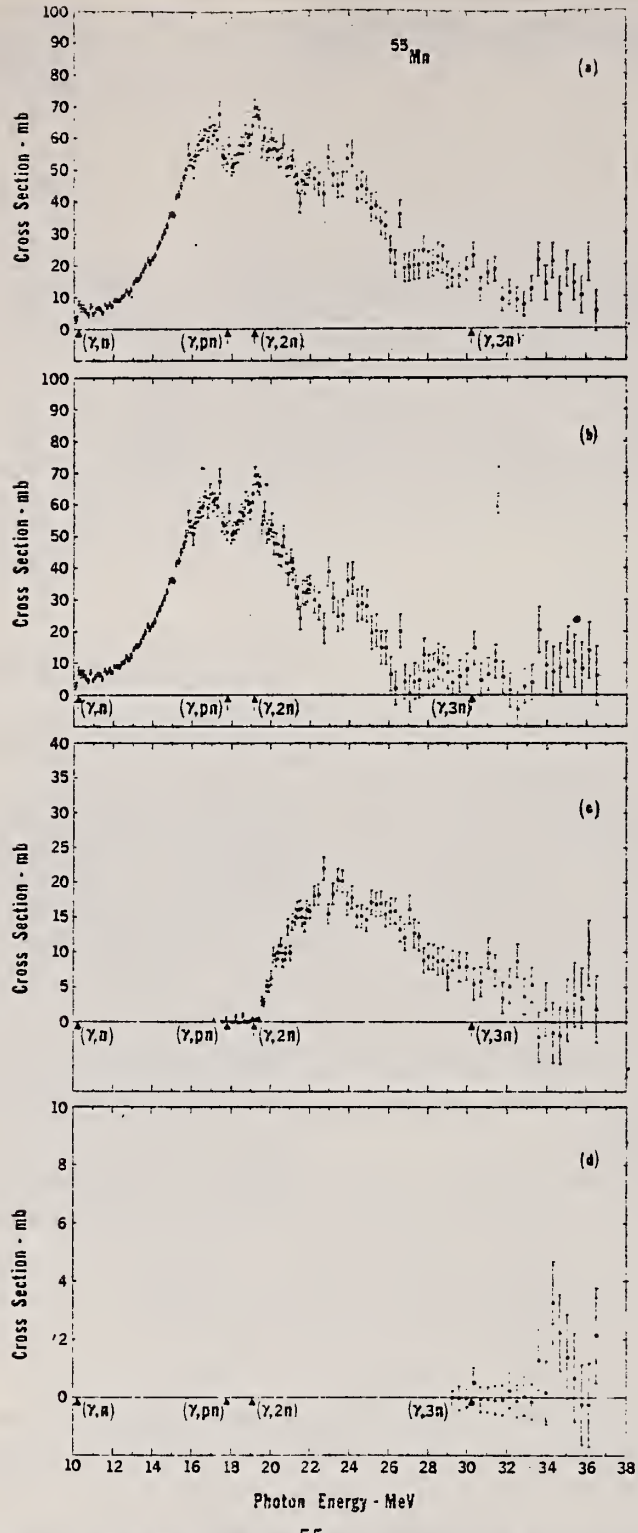

Figure 1. Photoneutron cross sections of ^{55}Mn. Thresholds are indicated by arrows. (a) Total photoneutron cross section: $\sigma[(\gamma,n) + (\gamma,pn) + (\gamma,2n) + (\gamma,3n)]$; (b) $\sigma[(\gamma,n) + (\gamma,pn)]$; (c) $\sigma(\gamma,2n)$; (d) $\sigma(\gamma,3n)$.

REF.

R.F. Barrett, J.R. Birkelund, B.J. Thomas, K.S. Lam, and H.H. Thies
Nucl. Phys. A210, 355 (1973)

ELEM. SYM.	A	Z
Mn	55	25

METHOD

REF. NO. 73 Ba 20 egf

REACTION	RESULT	EXCITATION ENERGY	SOURCE		DETECTOR		ANGLE
			TYPE	RANGE	TYPE	RANGE	
G,N	NOX	THR- 27	C	10- 27	BF3-I		4PI

MEAN NEUT ENERGY

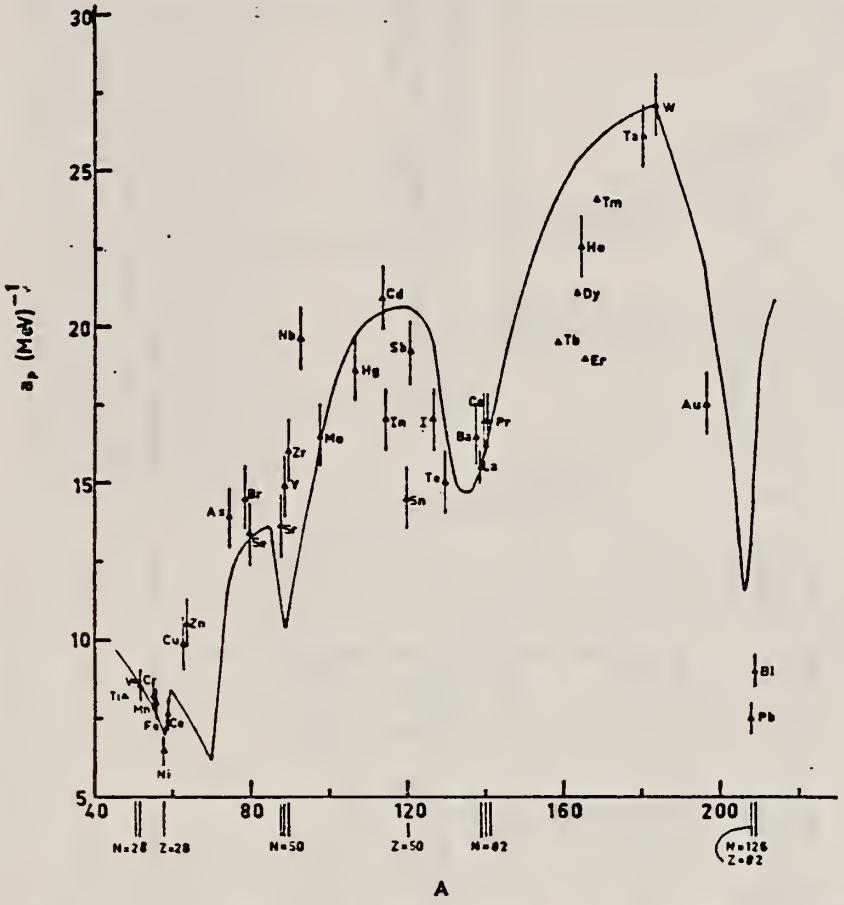

Fig. 12. Experimental values of the level density parameter a_p (Fermi gas formula plus pairing correction) versus atomic number A. The continuous curve is a least-squares fit to the data of a theoretical calculation from Newton [15]).

1
H. Baba and S. Baba, Japan Atomic Energy Research Institute report JAERI-1183 (1969).
2
H. Baba, Nucl. Phys. A159, 625 (1970).
15
T.D. Newton, Can. J. Phys. 34, 804 (1956).

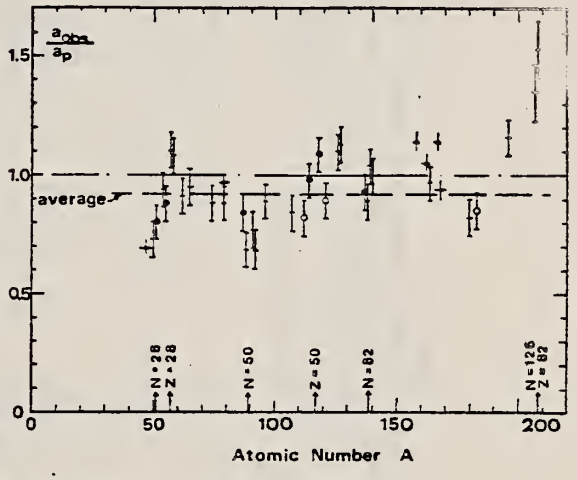

Fig. 15. Ratio a_{obs}/a_p versus atomic number A. Here a_{obs} is the level density parameter taken from the neutron resonance work of refs. [1,2]), and a_p is the level density parameter derived from the present (γ, n) work. Filled circles represent points where nuclei in the neutron resonance and in the (γ, n) experiment were the same. Open circles represent points where the respective nuclei were approximately matched. Triangles represent points which are based on measurement of neutron mean energies at two bremsstrahlung energies only.

(over)

TABLE 3

Comparison of experimental and theoretical data on nuclear level densities with Fermi gas formulae, and comparison of nuclear level density parameters from (γ, n) and n-resonance absorption experiments

Target	N (residual nucleus) [a]		Goodness of fit [b]		$\hat{E}_0(24)$ (MeV) [c]	T (MeV) [d]	a_p (MeV^{-1}) [e]	a_{obs} (MeV^{-1}) [f]	a_{obs}/a_p
			no p.c.	with p.c.					
Ti [g]	23	8%			1.93		8.1–^{47}Ti	6.41–^{47}Ti	0.79
	24	8%							
	25	73%							
	26	5%							
	27	5%							
V [g]	27	100%			1.96		8.7–^{50}V	6.35–^{51}V	0.73
Cr	25	4%	P	G	1.89		8.6–^{51}Cr	6.9 –^{51}Cr	0.80
	27	84%							
	28	10%							
	29	2%							
Mn	29	100%	V.P.	G	2.1		8.2–^{54}Mn	7.82–^{56}Mn	0.94
Fe	27	6%	F	G	1.96		8.0–^{55}Fe	7.06–^{55}Fe	0.88
	29	92%							
	30	2%							
Co	31	100%	P	F	2.12		7.7–^{58}Co	8.35–^{60}Co	1.08
Ni	29	68%	V.P.	P	2.04	1.4	6.5–$^{57.7}$Ni	7.19–^{59}Ni	1.10
($Z = 28$)	31	26%							
	32	1%							
	33	4%							
	35	1%							
Cu	33	69%	V.P.	P	1.78	1.0	9.8–^{62}Cu	8.90–^{64}Cu	0.91
	35	31%							
Zn	33	49%	F	F	1.61		10.5–$^{64.4}$Zn	10.0–^{65}Zn	0.95
	35	28%							
	36	4%							
	37	19%							
As	41	100%	V.P.	F	1.44		14.5–^{74}As	12.81–^{76}As	0.88
Se [g]	41	9%			1.39		13.3–^{78}Se	12.8 –^{78}Se	0.97
	42	8%							
	43	24%							
	45	50%							
	47	9%							
Br	43	45%	V.P.	V.P.	1.41		14.5–^{79}Br	12.69–^{80}Br	0.88
	45	49%							
Sr	47	10%	F	G	1.31		13.6–^{87}Sr	11.4 –^{87}Sr	0.84
	48	7%							
	49	83%							

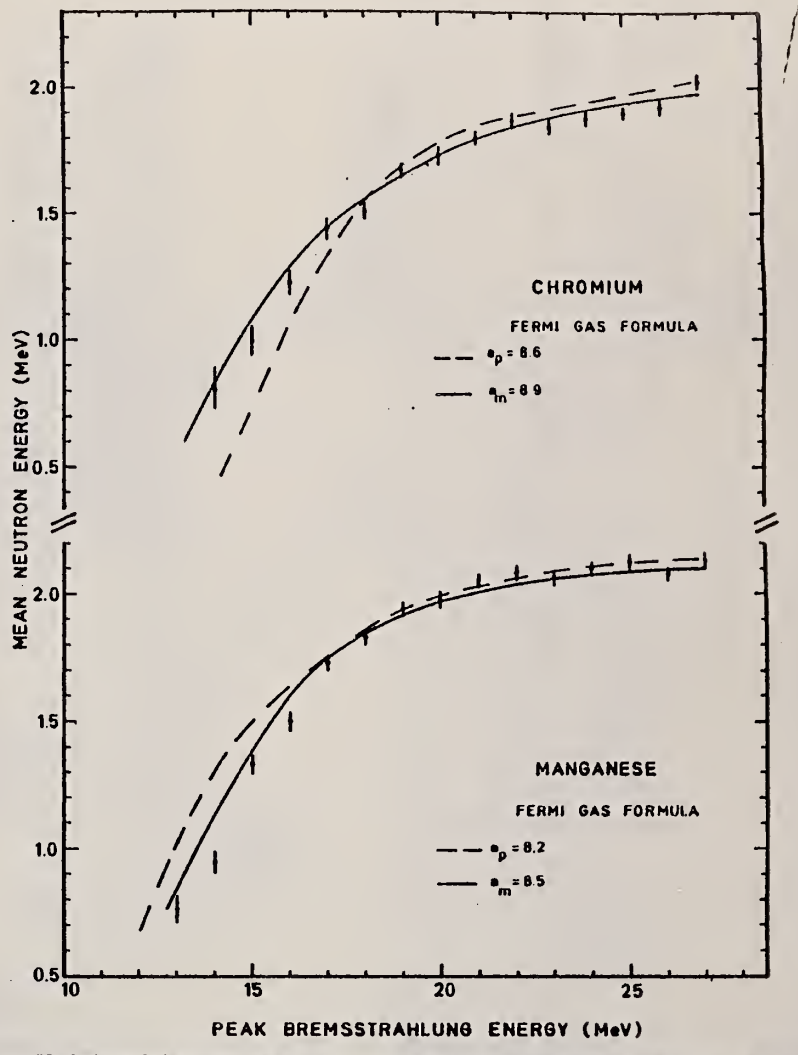

Fig. 5. Variation of photoneutron mean energy with peak bremsstrahlung energy, for chromium and manganese: experimental and calculated results.

[a]) Neutron numbers and abundances of respective residual nuclei in (γ, n) experiments.

[b]) These give an assessment of the goodness of fit of a calculated $\hat{E}_n$ versus E_0 curve to the observed data, using the Fermi gas level density formula both without and with pairing corrections.

[c]) Bremsstrahlung photoneutron mean energies $\hat{E}_n$ for peak bremsstrahlung energy $E_0 = 24$ MeV.

[d]) Nuclear temperature from fit with constant-temperature formula.

[e]) Level density parameter a_p derived from the present (γ, n) experiment, using a Fermi gas formula plus pairing correction, and corresponding residual nucleus (the atomic weight shown is the weighted average of atomic weights of the respective isotopes present).

[f]) As column 7, but using data on n-resonance absorption from refs. [1,2]).

[g]) Measurements of $\hat{E}_0(E_0)$ for these nuclei were made only for $E_0 = 21$, 23 and 24 MeV.

REF. H.G. De Carvalho, J.B. Martins, O.A.P. Tavares, V. Di Napoli, F. Salvetti
PICNS-73, 983 (1973)

ELEM. SYM.	A	Z
Mn	55	25

METHOD

REF. NO. 73 Ca 8 hg

REACTION	RESULT	EXCITATION ENERGY	SOURCE		DETECTOR		ANGLE
			TYPE	RANGE	TYPE	RANGE	
G,N	ABY	10-999	C	300-999	ACT-I		4PI
G,3N	ABY	31-999	C	300-999	ACT-I		4PI
G,4N	ABY	33-999	C	300-999	ACT-I		4PI

(G,3N) ISO YLD, ANAL 79DI1

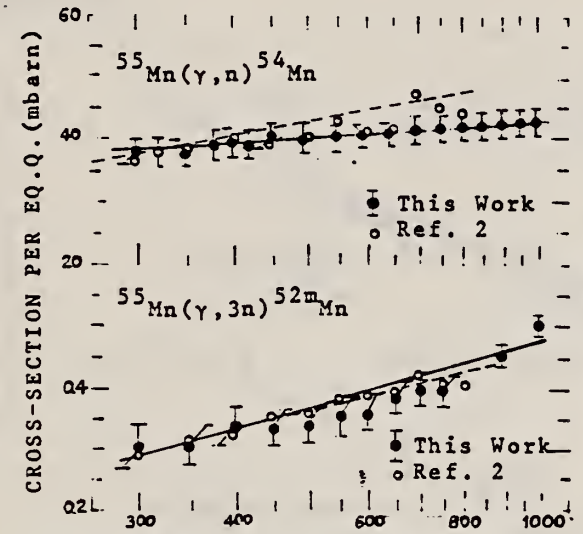

FIG. 1

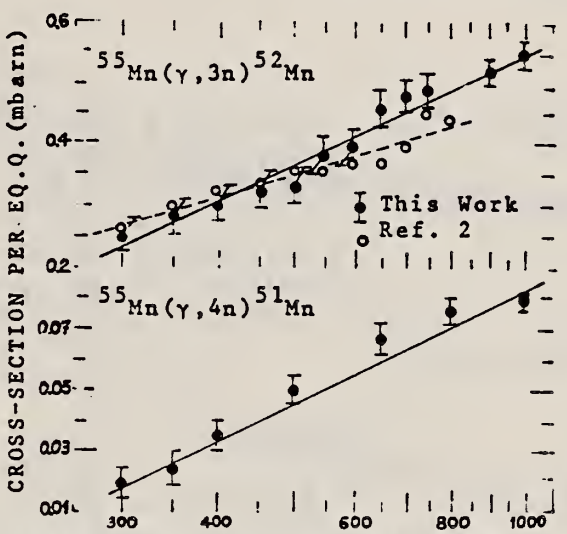

FIG. 2

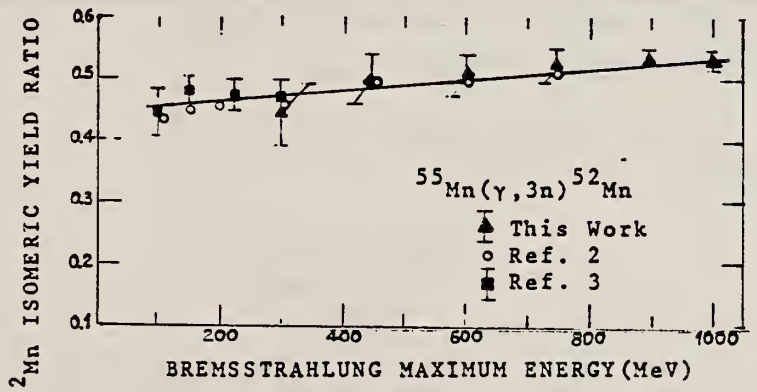

FIG. 3

[2] G. Anderson, B. Forkman, B. Friberg; Annual Report 1968,Lund Institute of Technology, Lund University, NP 6901, Sect. 4b (1969).

[3] W.B. Walters and J. P. Hummel, Phys. Rev. 150, 867 (1966).

REF.

H. G. de Carvalho, J. B. Martins, O. A. P. Tavares,
V. di Napoli, F. Salvetti
PICNS-73, Vol. II, 983 (1973)

ELEM. SYM.	A	Z
Mn	55	25

METHOD

REF. NO.	
73 De 7	egf

REACTION	RESULT	EXCITATION ENERGY	SOURCE		DETECTOR		ANGLE
			TYPE	RANGE	TYPE	RANGE	
G,N *	ABY	THR*	C	*	ACT-I		4PI
G,3N **	ABY	THR*	C	*	ACT-I		4PI
G,4N *	ABY	THR*	C	*	ACT-I		4PI

* E IN GEV
** 1 GEV ISOMER RATIO

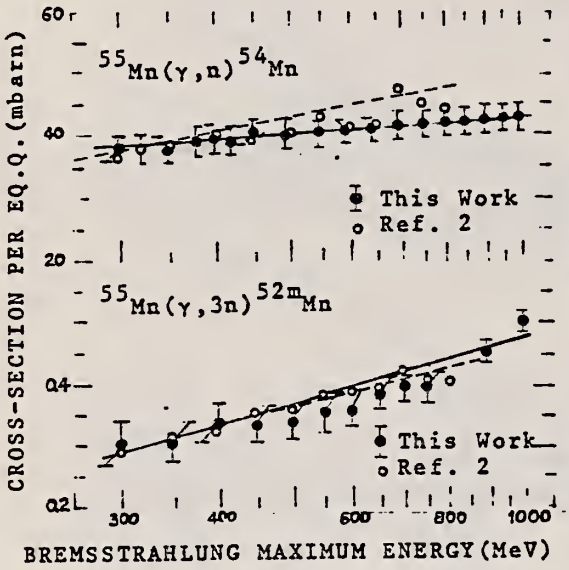

FIG. 1

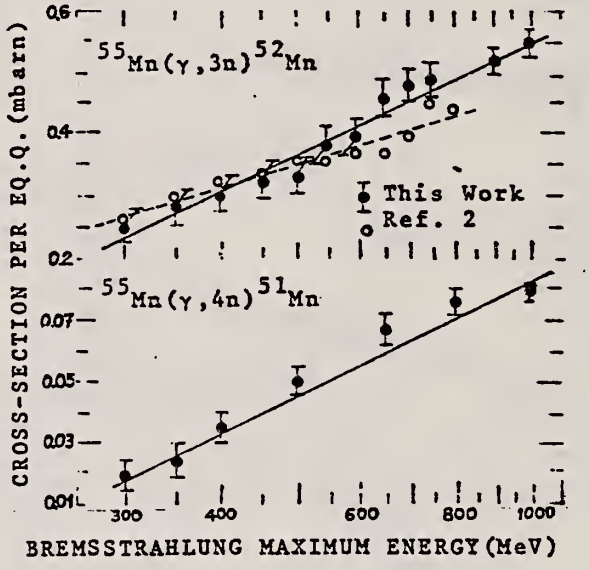

FIG. 2

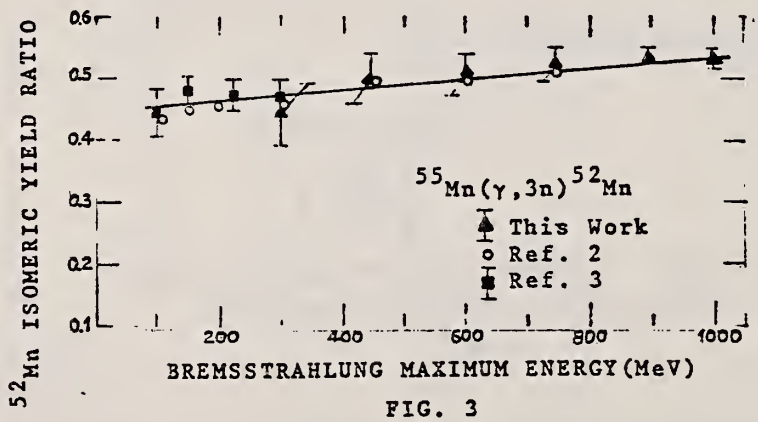

FIG. 3

REF. M. Eriksson and G. G. Jonsson
PICNS-73, Vol.II, p.995 (1973) Asilomar

ELEM. SYM.	A	Z
Mn	55	25

METHOD

REF. NO. 73 Er 1 egf

REACTION	RESULT	EXCITATION ENERGY	SOURCE		DETECTOR		ANGLE
			TYPE	RANGE	TYPE	RANGE	
G,SPL	NGX	0-800	C	100-800	ACT-I		4PI

SC-44 ISOMER RATIO

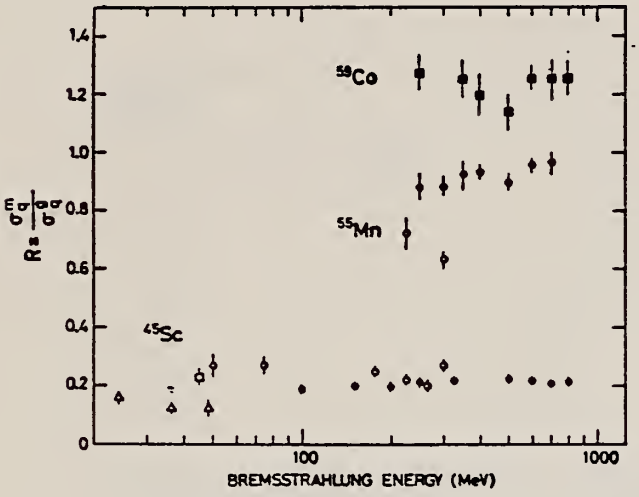

Isomeric yield ratio, $^{44}Sc^{m}(6+)/^{44}Sc^{g}(2+)$, versus bremsstrahlung end point energy.
●, ■ this work, Δ ref 1, O ref 2, □ ref 3.

[1] J.R. Tatarczuk and H.A. Medicus, Phys. Rev. 143 (1966) 818.
[2] W.B. Walters and J.P. Hummel, Phys. Rev. 150 (1966) 867.
[3] R. Völpel, Nucl. Phys. A182 (1972) 311.

REF. A. Järund, B. Friberg, and B. Forkman
Z. Physik 262, 15 (1973)

ELEM. SYM.	A	Z
Mn	55	25

METHOD

REF. NO. 73 Ja 3 egf

REACTION	RESULT	EXCITATION ENERGY	SOURCE TYPE	SOURCE RANGE	DETECTOR TYPE	DETECTOR RANGE	ANGLE
G,NA24	ABY	THR-999	G	100-999	AGT-I		4PI

999=1 GEV

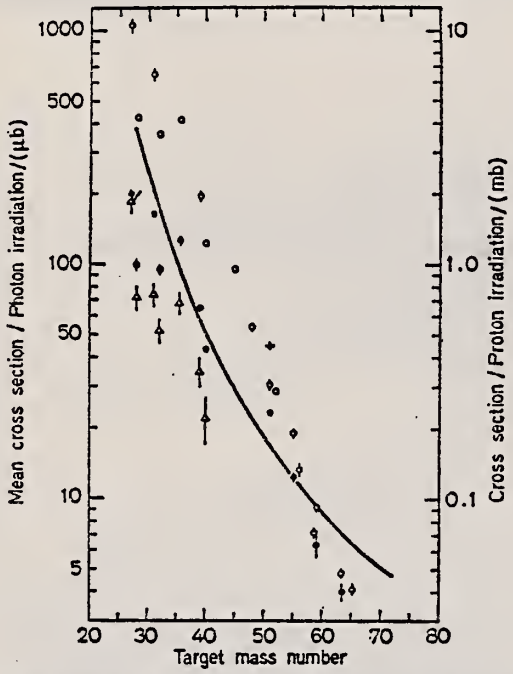

Fig. 7. Mean cross sections for ^{24}Na production as a function of target mass number. Present work filled circles. Noga *et al.* [3] open triangles, Kumbartzki *et al.* [13] cross and Korteling *et al.* [1] 400 MeV protons open circles. The solid line gives the mean cross sections calculated by Jonsson *et al.* [17]

[1] Korteling, R.G. et al., J. Inorg. Nucl. Chem. 29, 2863 (1967).

[3] Noga, V.I. et al., Sov. J. Nucl. Phys. 9, 637 (1969).

[13] Kumbartzki, G. et al., Nucl. Phys. A176, 23 (1971).

[17] Jonsson, G.G. et al., LUNP7212, Oct. 1972, to be published in Physica Scripta.

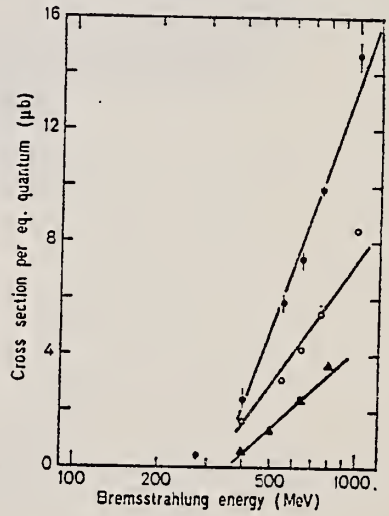

Fig. 6

Fig. 6. The determined yields for the reactions ^{55}Mn → ^{24}Na (filled circles), ^{59}Co → ^{24}Na (open circles) and ^{63,65}Cu → ^{24}Na (filled triangles)

REF. R. E. Van de Vyver, R. Carchon, J. Devos, C. Van Deynse and H. Ferdinande
PICNS-73, Vol.I, p. 543 Asilomar

ELEM. SYM.	A	Z
Mn	55	25

METHOD

REF. NO. 73 Va 5 hmg

REACTION	RESULT	EXCITATION ENERGY	SOURCE		DETECTOR		ANGLE
			TYPE	RANGE	TYPE	RANGE	
G,XN	ABX	10- 23	C	10- 23	BF3-I		4PI

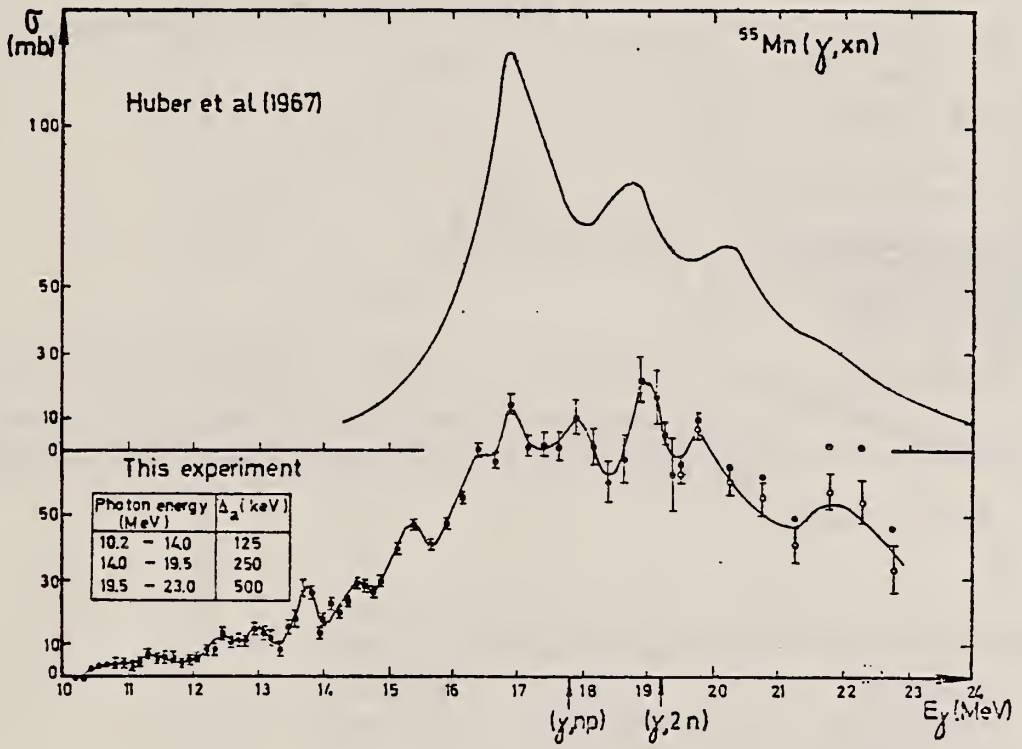

References :

1) M.G. Huber, M. Danos, H.J. Weber and W. Greiner, Phys.Rev. 155 (1967) 1073

REF.

R. Carchon, J. Devos, R. Van De Vyver, C. Van Deynse, and H. Ferdinande
Nucl. Phys. A223, 416 (1974)

ELEM. SYM.	A	Z
Mn	55	25

METHOD

REF. NO. 74 Ca 6 egf

REACTION	RESULT	EXCITATION ENERGY	SOURCE TYPE	SOURCE RANGE	DETECTOR TYPE	DETECTOR RANGE	ANGLE
G,XN	ABX	10- 23	C	10- 23	BF3-I		4PI

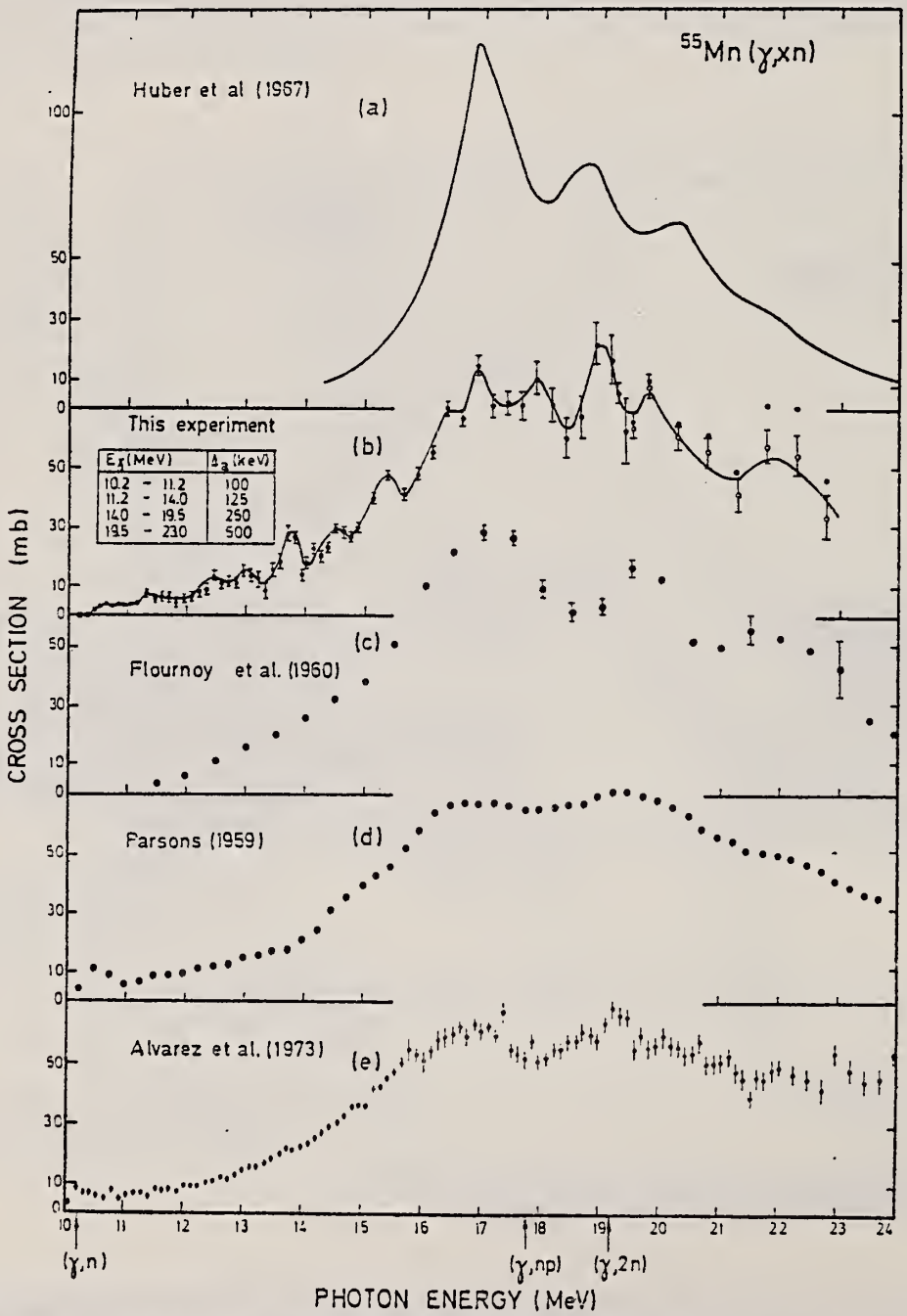

Fig. 1. Comparison of the present total photoneutron cross section for ^{55}Mn with previous measurements and with the DCM theory. In part (b) the open circles are the cross section values corrected for multiplicity.

FORM NBS-418
(REV. 7-14-64)
USCOMM-DC 26010-P64

DEPARTMENT OF COMMERCE
NAL BUREAU OF STANDARDS

REF.

V. Di Napoli, J.B. Martins, G. Persichelli, and M.L. Terranova
Nuovo Cimento Lett. 11, 179 (1974)

ELEM. SYM.	A	Z
Mn	55	25

METHOD

REF. NO.: 74 Di 8 egf

REACTION	RESULT	EXCITATION ENERGY	SOURCE TYPE	SOURCE RANGE	DETECTOR TYPE	DETECTOR RANGE	ANGLE
G,3N	ABY	THR* 1	C	100* 1	ACT-I		4PI

*1=1 GEV,ISOMER YLD

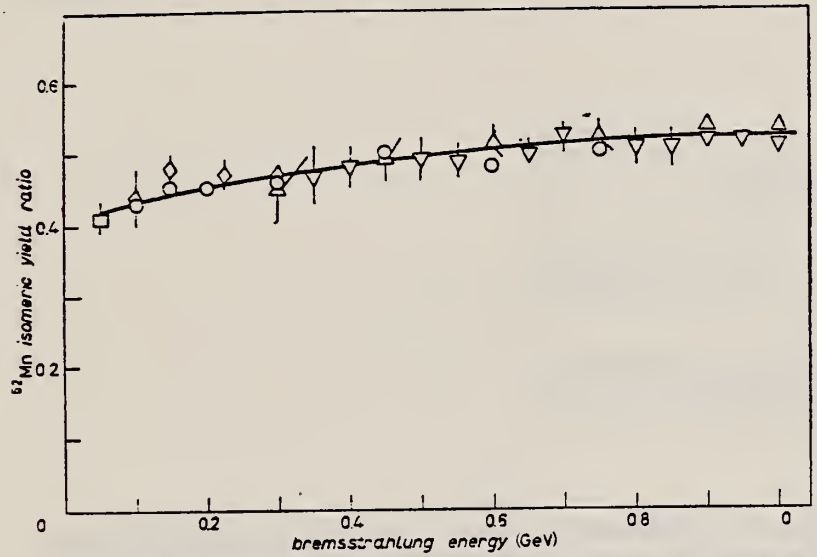

Fig. 1. – Experimental values of the isomeric-yield ratio for ^{55}Mn *vs.* the bremsstrahlung maximum energy. Square: ref. (4), rhombs: ref. (3), circles: ref. (5), triangles: ref. (6), reversed triangles: present work. The smoothed curve is a best fit to the experimental points in the energy range from 40 MeV up to 1 GeV.

[3] W.B. Walters et al., Phys. Rev. 150, 867 (1966).

[4] R. Volpel: Nucl.Phys. 182A, 411 (1972).

[5] G. Andersson: U.of Lund Report No.LUNP 6901 (1969),p.11 unpublished.

[6] H.G.DeCarvalho et al.: Proc. Intnat'l Conf.Photo.Reac.&Applic. Pacific Grove, Cal.Sect.8C5-1(73).

TABLE II. – *Cross-sections per equivalent quantum and isomeric-yield ratio for the photoproduction of* ^{52}Mn^{g} *and* ^{52}Mn^{m} *from* ^{55}Mn.

Bremsstrahlung energy (GeV)	σ_Q (mb) ^{55}Mn(γ, 3n)^{52}Mn^{g}	^{55}Mn(γ, 3n)^{52}Mn^{m}	Isomeric-yield ratio
0.35	0.28 ± 0.03	0.32 ± 0.03	0.47 ± 0.03
0.40	0.30 ± 0.03	0.33 ± 0.03	0.48 ± 0.03
0.50	0.33 ± 0.03	0.34 ± 0.03	0.49 ± 0.03
0.55	0.38 ± 0.02	0.39 ± 0.02	0.49 ± 0.02
0.65	0.46 ± 0.02	0.46 ± 0.02	0.50 ± 0.02
0.70	0.48 ± 0.02	0.44 ± 0.02	0.52 ± 0.02
0.80	0.49 ± 0.02	0.47 ± 0.02	0.51 ± 0.02
0.85	0.50 ± 0.01	0.48 ± 0.02	0.51 ± 0.02
0.90	0.52 ± 0.01	0.48 ± 0.01	0.52 ± 0.01
0.95	0.54 ± 0.01	0.50 ± 0.01	0.52 ± 0.01
1.00	0.55 ± 0.01	0.53 ± 0.01	0.51 ± 0.01

REF.

J. Tenenbaum, R. Moreh, and A. Nof
Nucl. Phys. A218, 95 (1974)

ELEM. SYM.	A	Z
Mn	55	25

METHOD

REF. NO. 74 Te 1 egf

REACTION	RESULT	EXCITATION ENERGY	SOURCE TYPE	SOURCE RANGE	DETECTOR TYPE	DETECTOR RANGE	ANGLE
G,G	LFT	7	D	4- 8	SCD-D		DST

7=7.491

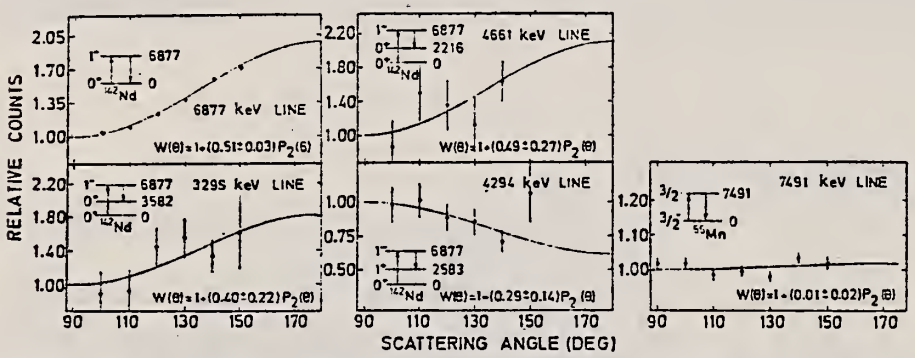

Fig. 5. Angular distributions of elastically scattered γ-lines from ^{55}Mn and ^{142}Nd. The distributions of three inelastic γ-lines from ^{142}Nd are also shown. The solid lines have the form $W(\theta) = 1 + A_2 P_2$ (cos θ) and are least squares fits to the experimental distribution. In each case the corresponding γ-γ cascade is indicated.

TABLE 2

Measured angular distribution coefficients A_2, the ratios $N_{||}/N_{\perp}$, the spins and parities of the ground and the resonance levels, J_0^{π} and J_r^{π}, and the character of the ground state transition

Scatterer	E_γ (keV)	A_2	$N_{\|\|}/N_{\perp}$	J_0^{π}	J_r^{π}	Transition
^{55}Mn	7491	0.01±0.02	1.00±0.02	$\frac{5}{2}^-$	$\frac{3}{2}$	
^{140}Ce	5660	0.51±0.02	1.14±0.04	0^+	1^-	E1
^{141}Pr	6877	0.11±0.02	0.95±0.03	$\frac{5}{2}^+$	$\frac{7}{2}^+$	M1
^{142}Nd	6877	0.51±0.03	1.10±0.04	0^+	1^-	E1
^{202}Hg	4922	0.51±0.02	1.18±0.03	0^+	1^-	E1
^{209}Bi	5603	0.06±0.02	0.97±0.02	$\frac{9}{2}^-$	$\frac{11}{2}^-$	M1

TABLE 4

Values of Γ, Γ_0 and the energy separation δ (between the incident γ-line and the resonance level) as obtained from the analysis of the various experiments

Scatterer	E_γ (keV)	Γ (meV)	Γ_0 (meV)	δ (eV)	D (eV)	K_{E1} (10^{-9} MeV^{-3})	K_{M1} (10^{-9} MeV^{-3})
^{55}Mn	7491	450±250	80± 40	17 ±1			
^{140}Ce [a])	5660	13± 3	12± 2	4.7±0.3	6800	0.33	
^{141}Pr [a])	6877	85± 35	17± 9	6.7±1.5	450		116
^{142}Nd [a])	6877	340± 40	270± 20	12.4±0.3	1200	26	
^{202}Hg	4922	300± 50	260± 20	4.2±0.5	19000	3.4	
^{209}Bi [a])	5603	950±200	950±200	13 ±1	34000		160

The radiative strengths K_{E1} and K_{M1} are also given. The level spacing D refers to the excitation energy of the resonance level E_γ.

[a]) These values are slightly different from those of ref. [8]) and were obtained from a renewed analysis of the experimental results.

[8] A. Wolf, R. Moreh, A. Nof, O. Shahal, J. Tenenbaum, Phys. Rev. C6, 2276 (1972).

U.S. DEPARTMENT OF COMMERCE
NATIONAL BUREAU OF STANDARDS

REF. M. Eriksson and G. G. Jonsson
Nucl. Phys. A242, 507 (1975)

ELEM. SYM.	A	Z
Mn	55	25

METHOD

REF. NO. 75 Er 2 egf

REACTION	RESULT	EXCITATION ENERGY	SOURCE		DETECTOR		ANGLE
			TYPE	RANGE	TYPE	RANGE	
G,SC44	ABY	THR-800	C	250-800	ACT-I		4PI

ISOMER RATIO

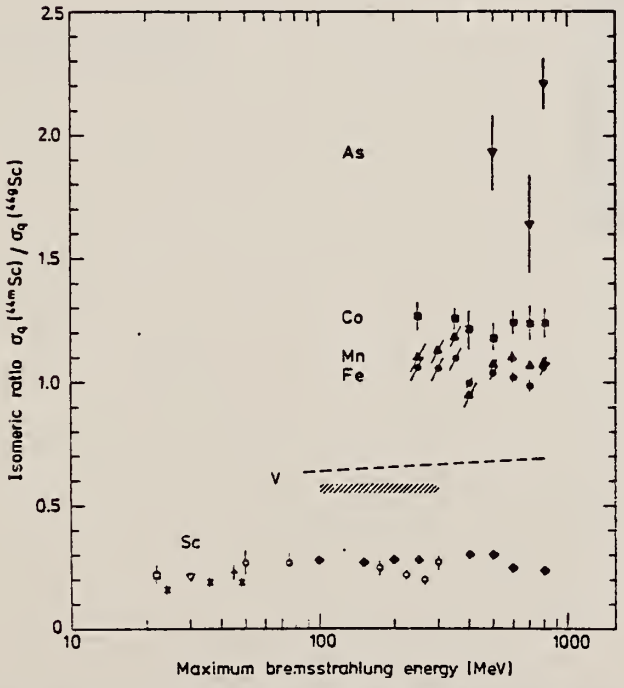

Fig. 6. Isomeric ratio $\sigma_q(^{44m}Sc)/\sigma_q(^{44g}Sc)$ versus bremsstrahlung end-point energy for the different targets. Sc target: ◆ – this work, □ – ref. [15]), × – ref. [16]), ▽ – ref. [17]), + – ref. [18]), ○ – ref. [19]); V target: dashed curve – ref. [20]), dashed area – ref. [21]); Fe target: ⊖ – this work; Mn target: ▲ – this work; Co target: ■ – this work; As target: ▼ – this work.

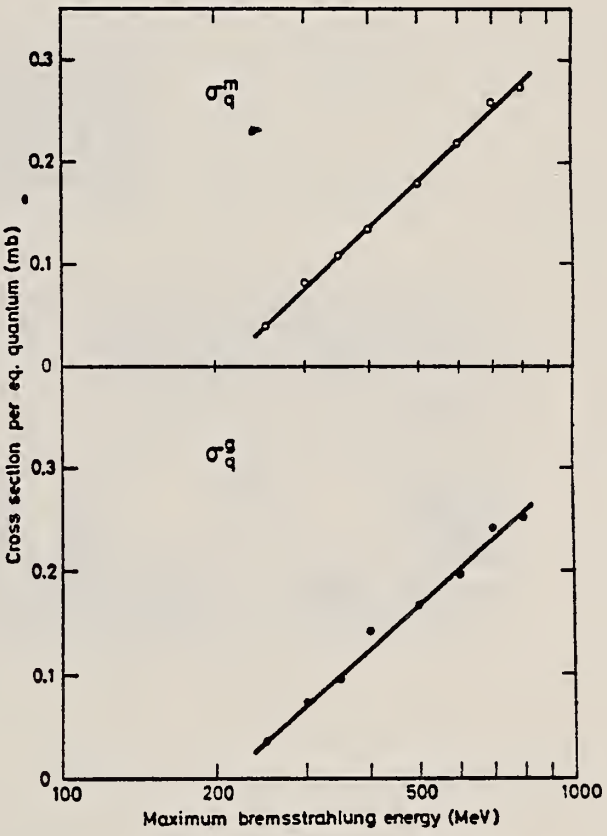

Fig. 3. Yield curves for the reaction $^{55}Mn(\gamma, 4p7n)^{44}Sc$.

(over)

TABLE 2

Comparison between experimental and calculated cross sections and isomeric ratios

Target	$\bar{\sigma}_{exp}$ (mb) 250–800 MeV	σ_{MC} (mb) 400 MeV	$\bar{\sigma}_{SE}$ (mb) 250–800 MeV	$\sigma(m)/\sigma(g)_{exp}$ 250–800 MeV	$\sigma(m)/\sigma(g)_{calc}$ 400 MeV
^{45}Sc	≈ 0.5	0.58 ± 0.05		≈ 0	0.05
^{51}V	≈ 0.5	0.48 ± 0.05	0.47	0.7	0.72
^{55}Mn	0.40 ± 0.14	0.59 ± 0.05	0.28	1.08 ± 0.04	1.04
Fe	0.40 ± 0.14		0.26	1.00 ± 0.05	
^{59}Co	0.26 ± 0.10	0.34 ± 0.04 0.65 ± 0.07 [a])	0.18	1.26 ± 0.06	1.12 1.15 [a])
^{75}As		0.01 ± 0.01	0.044	1.9 ± 0.3	

[a]) 325 MeV.

15) S. A. Steinberg, B. Sc. thesis, Univ. of Illinois, 1963, unpublished (value taken from ref. [17]))
16) J. R. Tatarczuk and H. A. Medicus, Phys. Rev. 143 (1966) 818
17) T. Kato and Y. Oka, Talanta 19 (1972) 515
18) R. Völpel, Nucl. Phys. A182 (1972) 411
19) W. B. Walters and J. P. Hummel, Phys. Rev. 150 (1966) 867
20) B. Bülow, Lund, private communication (preliminary results)
21) R. A. Meyer, thesis, Univ. of Illinois, 1963, unpublished

REF.

A. S. Danagulyan, N. A. Demekhina
Yad. Fiz. 24, 681 (1976)
Sov. J. Nucl. Phys. 24, 355 (1976)

ELEM. SYM.	A	Z
Mn	55	25

METHOD

REF. NO.: 76 Da 4 hmg

REACTION	RESULT	EXCITATION ENERGY	SOURCE		DETECTOR		ANGLE
			TYPE	RANGE	TYPE	RANGE	
G,NA24	ABX	THR* 5	C	2* 5	ACT-I		4PI

*ENERGY, GEV

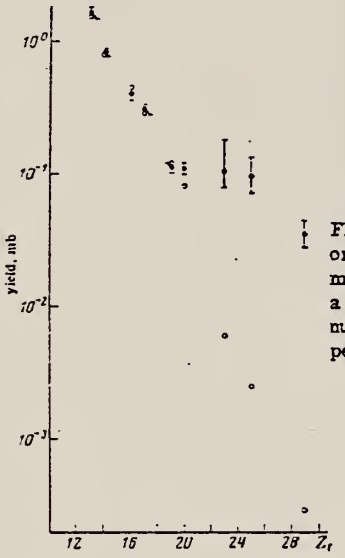

FIG. 2. Yield values and theoretical values according to the modified Rudstam formula as a function of the target charge number Z_t. Points: ●—experiment, ○—theory.

TABLE I. Experimental yields and reaction cross sections obtained in the measurements at the Erevan electron accelerator.

Target nucleus	Reaction yield, mb, $E_{\gamma\,max}$, GeV					Reaction cross section, mb
	2	3	4	4.5	5	
^{27}Al	0.81±0.08	0.87		0.87		0.07215±0.0346
^{28}Si	0.27±0.02	0.28		0.29		0.0267±0.013
^{32}S	0.24±0.02	0.22		0.27		0.0323±0.0155
Cl	0.28±0.03	0.30		0.28		–
^{39}K	0.1±0.01	0.125		0.15		0.06±0.0288
^{40}Ca	0.086±0.01	0.09		0.115		0.035±0.0168
^{51}V	0.085±0.02	0.094±0.02	0.038±0.02		0.082±0.025	0.019
^{55}Mn	0.079±0.02	0.075±0.02	0.087±0.017		0.068±0.015	0.01076±0.0056
Cu	0.029±0.006	0.037±0.007	0.036±0.007		0.034±0.007	0.00547±0.0028

Note. The reaction cross sections have been calculated in the $1/E$ approximation of the bremsstrahlung spectrum.

A.S. Danagulyan, N.A. Demekhina and G.A. Vartapetyan
Nucl. Phys. A285, 482 (1977)

ELEV. SYM.	A	Z
Mn	55	25

METHOD

REF. NO.: 77 Da 3 | egf

REACTION	RESULT	EXCITATION ENERGY	SOURCE		DETECTOR		ANGLE
			TYPE	RANGE	TYPE	RANGE	
G,SPL	ABY	THR * 5	C	2*5	ACT-I		4PI

*ENERGY,GEV

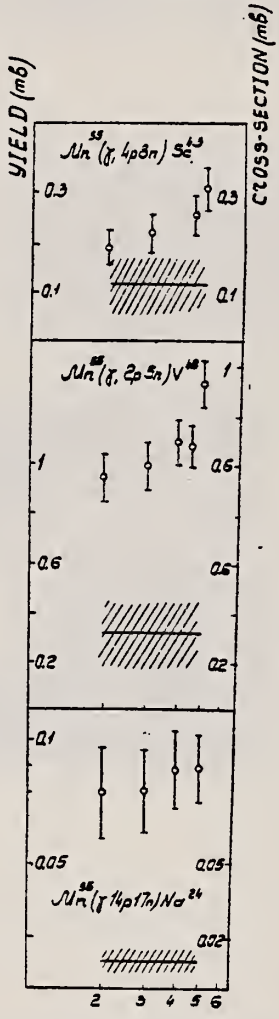

Fig. 2. Yields of some spallation reactions in ^{51}V, ^{55}Mn and Cu targets. The cross section estimates are obtained in the $1/E$ approximation for bremsstrahlung.

TABLE 2

Photospallation reaction yields (mb per eq. quantum)

Residual nuclei	Reaction yields (mb)					Reaction cross sections (mb)
	$E_{\gamma max}$ = 2 GeV (exp)	3 GeV (exp)	4 GeV (exp)	5 GeV (exp)	5 GeV (cal)	
			^{55}Mn target			
^{54}Mn	43	43	43	43		
^{52}Mn	0.55	0.55	0.55	0.55	1.34	
^{52m}Mn	0.48 ±0.05	0.43 ±0.04	0.6 ±0.06	0.48 ±0.05		
^{51}Cr	3.74 ±0.4	3.94 ±0.4	3.75 ±0.4	3.9 ±0.4	3.8	0.0253±0.012
^{49}Cr	0.26 ±0.03	0.25 ±0.03	0.26 ±0.03	0.26 ±0.03	0.31	
^{48}Cr			0.027±0.004	0.027±0.005	0.04	
^{48}V	0.95 ±0.1	1.0 ±0.1	1.1 ±0.1	1.34 ±0.1	1.18	0.318 ±0.152
^{48}Sc	0.1 ±0.01	0.098±0.01	0.11 ±0.01	0.134±0.01	0.167	0.0329±0.016
^{47}Sc	0.53 ±0.05	0.56 ±0.05	0.48 ±0.05	0.55 ±0.05	0.53	
^{46}Sc	1.2 ±0.2	1.1 ±0.15	1.2 ±0.2	1.2 ±0.1	1.3	0.0687±0.033
^{44}Sc	0.42 ±0.04	0.42 ±0.04	0.55 ±0.1	0.48 ±0.05	0.9	0.072 ±0.034
^{44m}Sc	0.45 ±0.04	0.47 ±0.04	0.42 ±0.05	0.55 ±0.05		0.034 ±0.016
^{43}Sc	0.19 ±0.04	0.22 ±0.04	0.26 ±0.05	0.31 ±0.06	0.27	0.115 ±0.055
^{44}K		0.065±0.01		0.065±0.01	0.04	
^{43}K	0.208±0.02	0.214±0.02	0.18 ±0.02	0.214±0.02	0.14	
^{42}K	0.39 ±0.04	0.34 ±0.07	0.36 ±0.07	0.34 ±0.07	0.38	
^{41}Ar	0.071±0.01	0.062±0.01	0.082±0.01	0.066±0.01	0.07	0.003 ±0.0014
^{39}Cl		0.06 ±0.01		0.057±0.01	0.05	
^{38}Cl		0.08 ±0.02		0.11 ±0.02	0.15	
^{24}Na	0.079±0.02	0.079±0.02	0.087±0.017	0.088±0.015	0.033	0.0117±0.005

Calculated values are obtained using Rudstam's formula. Cross section estimates are made in the $1/E$ approximation.

REF. H. Hirayama and T. Nakamura
Nucl. Inst. Meth. 147, 563 (1977)

ELEM. SYM.	A	Z
55	Mn	25

METHOD

REF. NO. 77 Hi 5 hmg

REACTION	RESULT	EXCITATION ENERGY	SOURCE		DETECTOR		ANGLE
			TYPE	RANGE	TYPE	RANGE	
G,N	ABI	10-30	C	18-30	ACT-I		4PI
		(10.2)					

THICK BREMS TARGET

The integral experiment for a sensitivity check of photonuclear cross section data of C, Mn, Fe, In and Au was performed by using the bremsstrahlung produced in a thick iron target by 18, 22, 26 and 30 MeV electrons from a linear accelerator. The cross section data measured by the activation method showed better results for all incident electron energies than those by the photoneutron method, because the latter include the competing (γ, np) reaction above its threshold energy. It is necessary to obtain the cross section data of (γ, n), (γ, np), (γ, 2n), (γ, p2n) reactions etc., separately by the activation method.

The effective energy range and effective cross section in the giant resonance region were determined for C, Mn, Fe and Au. By using these quantities, the gross structure of the bremsstrahlung spectrum was obtained in good agreement with the theoretical calculation.

TABLE 3

Ratio of measured and calculated saturated activities at 9°, $R_i = A_i^{exp}/A_i^{cal}$.

Reaction	Reference	Detector	Electron energy 18 MeV	22 MeV	26 MeV	30 MeV	Threshold energy of competing (γ, np) reaction (MeV)
$^{12}C(\gamma, n)^{11}C$	6	ACT[a]	–	1.205	1.09	0.824	
	7	BF3[b]	–	0.757	0.931	–	27.4
	8	BF3	–	1.492	1.189	0.914	
	9	BF3	–	1.418	1.159	–	
$^{55}Mn(\gamma, n)^{54}Mn$	10	BF3	0.575	0.810	0.598	–	17.8
	11		0.595	0.875	0.654	0.609	
$^{54}Fe(\gamma, n)^{53}Fe$	12	ACT	0.542	0.783	0.722	1.12	20.9
$^{115}In(\gamma, n)^{114m}In$	13	BF3	0.448	0.511	–	–	15.9
	14	BF3	0.603	0.672	0.586	1.00	
$^{115}In(\gamma, \gamma')^{115m}In$	15	ACT	0.829	1.00	0.852	0.995	
$^{197}Au(\gamma, n)^{196}Au$	16	BF3	0.743	0.553	0.529		13.7
	17	BF3	0.842	0.628	0.608	0.476	

[a] ACT: measurement of radioactivity of the target.
[b] BF3: BF_3 neutron counter with moderator.

(OVER)

TABLE 4

Effective cross section and effective energy range.

Reaction	Effective energy range (MeV)	Effective cross section (mb) Electron energy 22 MeV	26 MeV	30 MeV	Average
$^{12}C(\gamma, n)^{11}C$	20.5–24.5	–	5.98	5.28	5.63±0.35
$^{55}Mn(\gamma, n)^{54}Mn$	15.0–20.5	–	56.2	52.7	54.5±1.7
$^{54}Fe(\gamma, n)^{53}Fe$	17.0–24.0	–	33.6	47.9	40.8±7.2
$^{197}Au(\gamma, n)^{196}Au$	12.5–15.0	553.5	532.5	415.0	500±85

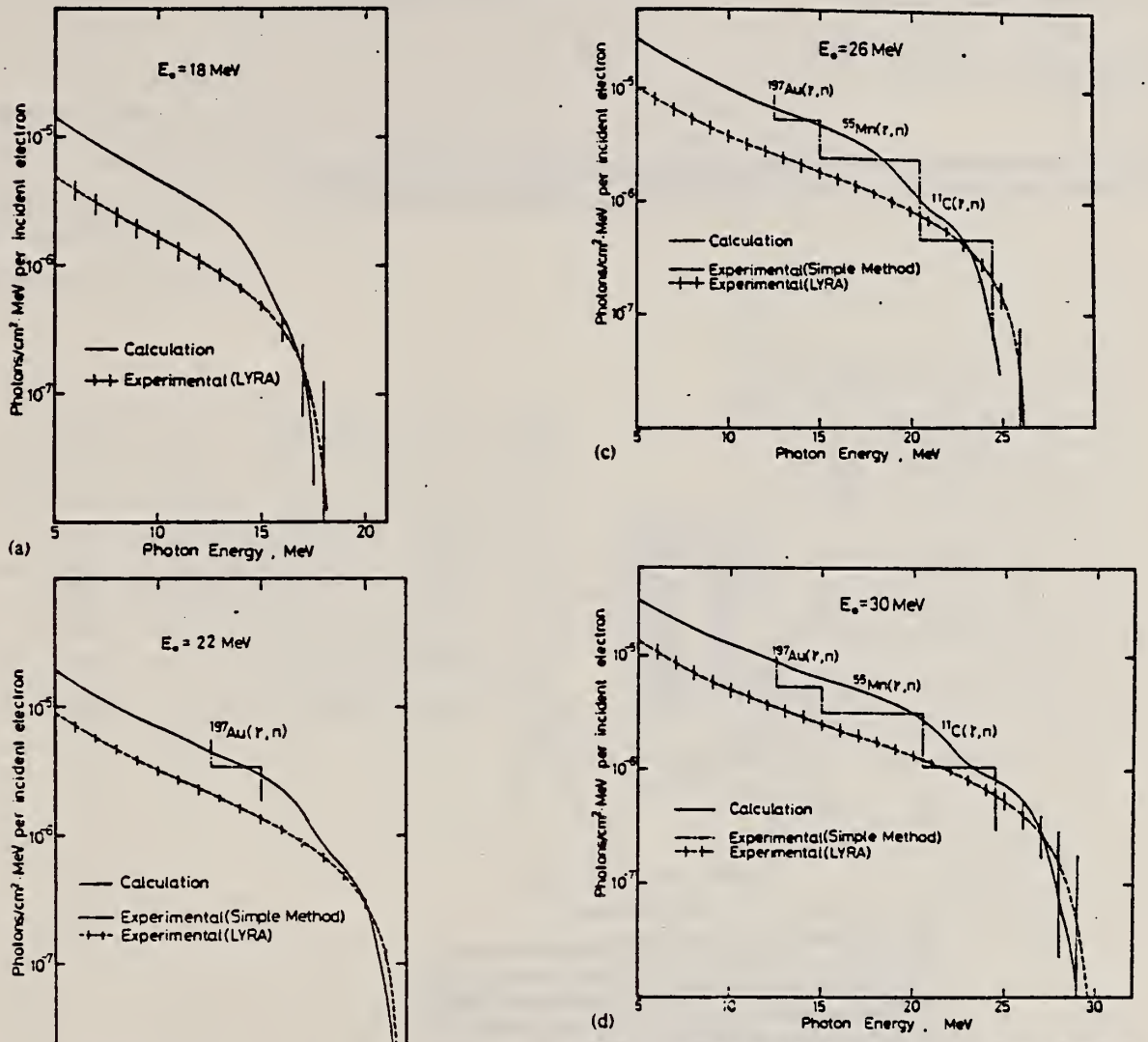

Fig. 3. Comparison of experimental and calculated bremsstrahlung spectra emitted from an iron target in the 9° direction by (a) 18 MeV electrons, (b) 22 MeV electrons, (c) 26 MeV electrons, (d) 30 MeV electrons.

REF. Z. Berant and R. Moreh
Phys. Lett. 73B, 142 (1978)

ELEM. SYM.	A	Z
Mn	55	25

METHOD

REF. NO.	
78 Be 6	rs

REACTION	RESULT	EXCITATION ENERGY	SOURCE		DETECTOR		ANGLE
			TYPE	RANGE	TYPE	RANGE	
G,G	ABX	6- 10	D	6- 10	SCD-D		140
G,G	ABX	11	D	11	NAI-D		140

The elastic differential scattering cross section from ^{55}Mn has been measured at $\theta = 140°$ with $E_\gamma = 5.5$–11.4 MeV photons. Evidence for destructive interference between nuclear resonance (NR) scattering and nuclear Thomson (NT) scattering has been obtained.

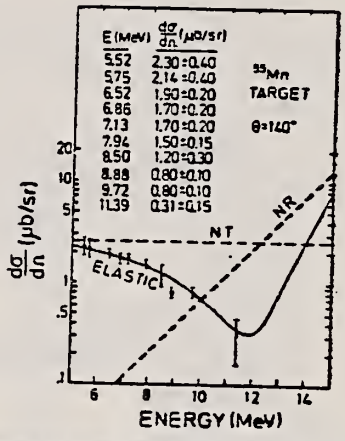

Fig. 1. Differential cross section (μb/sr) for elastic scattering of photons from ^{55}Mn at $\theta = 140°$. The solid curve represents the values obtained by including the incoherent and coherent contributions of the NT, NR and D scattering amplitudes. The dashed curves denoted NT and NR represent the pure contributions of nuclear Thomson and nuclear resonance scattering, respectively.

REF. A.S. Danagulyan, N.A. Demekhina
Yad. Fiz. 27, 877 (1978)
Sov. J. Nucl. Phys. 27, 466 (1978)

ELEM. SYM.	A	Z
Mn	55	25

METHOD

REF. NO. 78 Da 13 hg

REACTION	RESULT	EXCITATION ENERGY	SOURCE		DETECTOR		ANGLE
			TYPE	RANGE	TYPE	RANGE	
G,4P7N	ABY	THR*5	C	2*5	ACT-D		4PI

*GEV, ISOMER YLD

We discuss data concerning the ratios of the yields of different isomeric states in the elements ^{44}Sc and ^{52}Mn. Experimental results are presented for measurement of the yields of ^{44g,m}Sc and ^{52g,m}Mn in disintegration of targets of ^{51}V, ^{55}Mn, and Cu by photons with energies from 2 to 5 GeV; theoretical values of yields for these elements were obtained by means of the five-parameter Rudstam formula. The pattern of formation of high-spin states in photodisintegration reactions is discussed in terms of the cascade-evaporative model.

PACS numbers: 25.20. + y, 27.40. + z

TABLE I.

Type of target	Isomeric states	Yield ratio: Experiment $E_{\gamma max}$ = 3 GeV	Experiment 3 GeV	Experiment 4 GeV	Experiment 5 GeV	Theory 5 GeV
^{51}V	^{44m}Sc ^{44g}Sc	0.47±0.03 0.55±0.06	0.47±0.03 0.45±0.06	0.44±0.04 0.37±0.07	0.46±0.04 0.58±0.07	1.03
^{55}Mn	^{44m}Sc ^{44g}Sc	0.45±0.04 0.42±0.04	0.47±0.04 0.42±0.04	0.42±0.05 0.55±0.1	0.55±0.05 0.45±0.05	1.3
^{55}Mn	^{52m}Mn ^{52g}Mn	0.48±0.05 0.55	0.43±0.04 0.55	0.6±0.06 0.55	0.48±0.05 0.55	1.34
Cu	^{44m}Sc ^{44g}Sc	0.25±0.03 –	0.27±0.03 0.13±0.01	0.26±0.026 0.15±0.02	0.24±0.03 0.14±0.05	0.35
Cu	^{52m}Mn ^{52g}Mn	– 0.55±0.05	– 0.47±0.05	0.128±0.01 0.525±0.05	 0.473±0.05	0.55

TABLE II.

Type of target	Photon energy, MeV	Isomeric yield ratio	Remarks
		^{44m}Sc/^{44g}Sc	
^{51}V	65–300 100–800 2000–5000	0.75±0.03 0.88 0.87±0.04	[11] [10] Present work
^{54,56}Fe	250 250–800	0.61±0.02 1.03±0.05	[7] [8]
^{55}Mn	225 300 250–800 2000–5000	0.72 0.64 1.09±0.04 1.02±0.02	[7] [7] [8] Present work
^{59}Co Cu	250–800 2000–5000	1.24±0.06 1.84±0.16	[8] Present work
^{75}As	250–800	1.9±0.3	[8]
		^{52g}Mn/^{52m}Mn	
^{54,56}Fe	70 100–250	0.47 0.56	[7] [7]
^{55}Mn	100–300 2000–5000	0.88 1.12±0.1	[7] Present work
^{59}Co Cu	150 4000	1.62 4.1±0.4	[7] Present work

REF. V. di Napoli, F. Salvetti, M. L. Terranova, H. G. de Carvalho, J. B. Martins, O. A. P. Tavares
J. Inorg. Nucl. Chem. 40, 175 (1978)

ELEM. SYM.	A	Z
Mn	55	25

METHOD

REF. NO. 78Di12 hg

REACTION	RESULT	EXCITATION ENERGY	SOURCE TYPE	SOURCE RANGE	DETECTOR TYPE	DETECTOR RANGE	ANGLE
G, SPL	ABY	THR-999	C	300-999	ACT-I		4PI

Abstract—Cross sections per equivalent quantum, in the energy range 0.3–1.0 GeV, have been measured for spallation residuals from ^{51}V, ^{55}Mn, natural Fe, and ^{59}Co targets. Mean cross sections per photon have been deduced in this energy range and the data analysed in terms of charge-dispersion curves and mass-yield distributions. The mean cross sections per photon have also been compared with a semiempirical Rudstam's formula. A satisfactorily good agreement has been found with the calculated yields within a factor of two.

YLDS 24NA TO 51CR

Table 3. Yields of radionuclides in units of μb per equivalent quantum. Manganese target

Nuclide	E_0(GeV) 0.30	0.40	0.50	0.60	0.75	0.90	1.00
$^{24}_{11}$Na	3.0 ± 0.3	6.0 ± 0.6	8.0 ± 0.8	10.0 ± 1.0	12.0 ± 1.0	14.0 ± 1.0	15.0 ± 1.0
$^{27}_{12}$Mg	5 ± 1	6 ± 1	9 ± 1	11 ± 1	13 ± 1	14 ± 1	15 ± 1
$^{28}_{12}$Mg		0.5 ± 0.2	1.0 ± 0.3	1.5 ± 0.4	2.2 ± 0.5	2.8 ± 0.5	3.0 ± 0.5
$^{28}_{13}$Al	15 ± 3	25 ± 5	30 ± 4	35 ± 4	45 ± 4	45 ± 4	50 ± 4
$^{29}_{13}$Al	6 ± 1	10 ± 2	12 ± 2	15 ± 3	16 ± 2	18 ± 2	20 ± 2
$^{34}_{17}$Cl^m	34 ± 7	42 ± 5	50 ± 4	55 ± 4	60 ± 4	67 ± 4	70 ± 4
$^{38}_{17}$Cl	16 ± 4	28 ± 6	38 ± 8	47 ± 8	57 ± 8	65 ± 8	70 ± 8
$^{39}_{17}$Cl	20 ± 4	23 ± 3	25 ± 2	28 ± 2	31 ± 2	33 ± 2	34 ± 2
$^{41}_{18}$Ar	18 ± 5	28 ± 4	36 ± 4	42 ± 4	50 ± 4	56 ± 5	60 ± 5
$^{42}_{19}$K	50 ± 15	76 ± 15	100 ± 17	115 ± 17	135 ± 16	150 ± 16	165 ± 17
$^{43}_{19}$K	5 ± 2	15 ± 5	25 ± 6	35 ± 7	45 ± 7	50 ± 7	53 ± 7
$^{44}_{19}$K	17 ± 5	19 ± 4	21 ± 4	24 ± 4	26 ± 4	28 ± 4	30 ± 4
$^{45}_{19}$K	1.0 ± 0.5	1.0 ± 0.5	1.2 ± 0.5	1.4 ± 0.5	1.7 ± 0.5	2.0 ± 0.5	2.0 ± 0.5
$^{47}_{20}$Ca	10 ± 3	12 ± 3	13 ± 3	15 ± 2	16 ± 2	17 ± 2	18 ± 2
$^{43}_{21}$Sc	16 ± 5	17 ± 5	40 ± 7	60 ± 7	75 ± 7	90 ± 7	92 ± 7
$^{44}_{21}$Sc^m	135 ± 15	170 ± 15	200 ± 15	215 ± 15	245 ± 15	265 ± 16	273 ± 16
$^{44}_{21}$Sc^g	140 ± 20	170 ± 20	200 ± 20	220 ± 20	250 ± 20	270 ± 20	275 ± 20
$^{46}_{21}$Sc	190 ± 40	210 ± 40	290 ± 40	350 ± 45	420 ± 45	460 ± 46	465 ± 47
$^{47}_{21}$Sc	170 ± 40	180 ± 40	260 ± 45	300 ± 45	340 ± 45	380 ± 45	384 ± 45
$^{48}_{21}$Sc	1.0 ± 0.5	2 ± 1	15 ± 4	24 ± 5	35 ± 5	50 ± 6	53 ± 6
$^{48}_{23}$V	410 ± 50	470 ± 50	520 ± 50	550 ± 50	600 ± 60	630 ± 60	650 ± 60
$^{48}_{24}$Cr	12 ± 3	13 ± 3	15 ± 3	17 ± 3	18 ± 3	19 ± 3	20 ± 3
$^{49}_{24}$Cr	132 ± 15	144 ± 15	153 ± 15	160 ± 15	170 ± 16	176 ± 18	180 ± 18
$^{51}_{24}$Cr	2000 ± 150	2150 ± 150	2250 ± 150	2340 ± 150	2450 ± 150	2530 ± 150	2580 ± 160

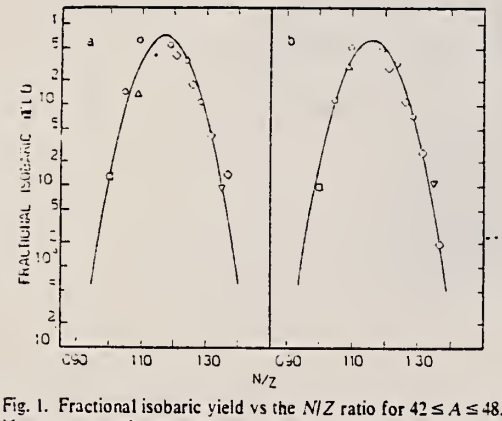

Fig. 1. Fractional isobaric yield vs the N/Z ratio for $42 \le A \le 48$. Mean cross sections per photon in the energy range 0.3–1 GeV. Graph (a): ^{51}V target; (b): ^{55}Mn target. The symbols are: □, for Cr; ○, for Sc; △, for V; ◇, for K; ▽, for Ca isotopes.

Table 6. Mean cross sections in the energy range 0.3–1 GeV in units of μb

Produced radionuclide	Target nucleus: Vanadium Present work	Vanadium Bülow *et al.*[26]	Manganese	Iron	Cobalt
$^{24}_{10}$Ne	2.0 ± 0.4				
$^{22}_{11}$Na	16 ± 4				
$^{24}_{11}$Na	30 ± 2	--18 ± 2	10 ± 1	10 ± 1	7 ± 1
$^{27}_{12}$Mg	22 ± 2	18 ± 3	9 ± 1	10 ± 1	8 ± 1
$^{28}_{12}$Mg	6 ± 1	6 ± 1	2.7 ± 0.5	2.7 ± 0.5	2.2 ± 0.3
$^{28}_{13}$Al	58 ± 7	59 ± 4	29 ± 4	35 ± 4	25 ± 3
$^{29}_{13}$Al	25 ± 4	32 ± 2	11 ± 2	15 ± 2	16 ± 3
$^{34}_{17}$Cl^m	16 ± 2	14 ± 2	30 ± 4	30 ± 4	19 ± 3
$^{38}_{17}$Cl	75 ± 13	96 ± 5	45 ± 8	50 ± 8	37 ± 7
$^{39}_{17}$Cl	37 ± 7	35 ± 1	12 ± 2	19 ± 3	13 ± 2
$^{41}_{18}$Ar	65 ± 6	54 ± 2	35 ± 4	28 ± 3	12 ± 2
$^{42}_{19}$K	280 ± 50	243 ± 11	94 ± 17	80 ± 15	66 ± 12
$^{43}_{19}$K	128 ± 20	128 ± 4	43 ± 7	30 ± 5	28 ± 5
$^{44}_{19}$K	33 ± 12	30 ± 3	11 ± 4	10 ± 4	9.5 ± 4
$^{45}_{19}$K	12 ± 2	8 ± 1	1.0 ± 0.5	1.2 ± 0.5	1.0 ± 0.5
$^{47}_{20}$Ca	12 ± 4	15 ± 1	6.5 ± 2.4	6 ± 2	2.2 ± 0.8
$^{43}_{21}$Sc	104 ± 10	109 ± 6	72 ± 7	77 ± 8	52 ± 6
$^{44}_{21}$Sc^m	260 ± 30	243 ± 14	115 ± 15	100 ± 12	84 ± 10
$^{44}_{21}$Sc^g	230 ± 40	218 ± 13	116 ± 20	90 ± 16	71 ± 13
$^{46}_{21}$Sc	575 ± 100	605 ± 18	260 ± 45	214 ± 35	220 ± 40
$^{47}_{21}$Sc	457 ± 100	540 ± 33	200 ± 45	160 ± 30	127 ± 30
$^{48}_{21}$Sc	165 ± 15	138 ± 8	50 ± 5	30 ± 3	25 ± 3
$^{48}_{23}$V	210 ± 50	307 ± 12	200 ± 50	184 ± 45	100 ± 25
$^{48}_{24}$Cr	20 ± 10		7 ± 3	8 ± 4	5.0 ± 2.5
$^{49}_{24}$Cr	13 ± 5	16 ± 2	40 ± 15	64 ± 25	20 ± 8
$^{51}_{24}$Cr			480 ± 150	570 ± 150	330 ± 150
$^{51}_{25}$Mn				25 ± 5	
$^{52}_{25}$Mn^m				75 ± 40	49 ± 25
$^{52}_{25}$Mn^g				96 ± 40	84 ± 25
$^{54}_{25}$Mn				944 ± 300	584 ± 100
$^{52}_{26}$Fe					1.6 ± 0.8

Table 7. N/Z dispersion parameters of the mean cross sections per photon†

Target nucleus	Mass region	A_m	N/Z_p	Z_p	FWHM	ΔZ	Ref.
^{51}V	42–48	45	1.16	20.8	0.143	1.36	Present work
			1.16	20.8	0.142	1.37	[26]
			1.16	20.9	0.168	1.63	[35]
^{55}Mn	42–48	45	1.16	20.8	0.142	1.37	Present work
^{nat}Fe	42–48	45	1.16	20.8	0.140	1.35	Present work
	48–54	51	1.16	23.6	0.126	1.38	Present work
^{59}Co	42–48	45	1.16	20.8	0.141	1.36	Present work
	48–54	51	1.16	23.6	0.124	1.36	Present work

†A_m is the median mass of the mass region under consideration. N/Z_p is the neutron/proton ratio for the most probable nuclear charge Z_p of A_m. FWHM is the full width at half-maximum of the CD curves. ΔZ is the spread in Z as calculated from the FWHM for the two abscissas N/Z_1 and N/Z_2 (see also Refs. [26] and [35]).

REF. K. Masumoto, T. Kato, N. Suzuki
Nucl. Inst. Meth. 157, 567 (1978)

ELEM. SYM.	A	Z
Mn	55	25

METHOD

REF. NO.	
78 Ma 10	hg

REACTION	RESULT	EXCITATION ENERGY	SOURCE		DETECTOR		ANGLE
			TYPE	RANGE	TYPE	RANGE	
G,N	ABY	10-68	C	30-68	ACT		4PI

Analysis is made of reactions interfering with photon activation analysis procedures.

The activation yield curves have been presented for a number of photonuclear reactions in the energy range from 30 to 68 MeV, in order to evaluate quantitatively the interferences due to competing reactions in multielement photon activation analysis. The general features of the yields as functions of both target mass number and excitation energy were elucidated from the data obtained, discussion being given on the results in terms of the reaction mechanism.

Simultaneous neutron activation due to appreciable neutron production from the converter and surrounding materials has also been studied, and, finally, the magnitudes of interferences in real multielement analysis were given in the form of their energy dependences.

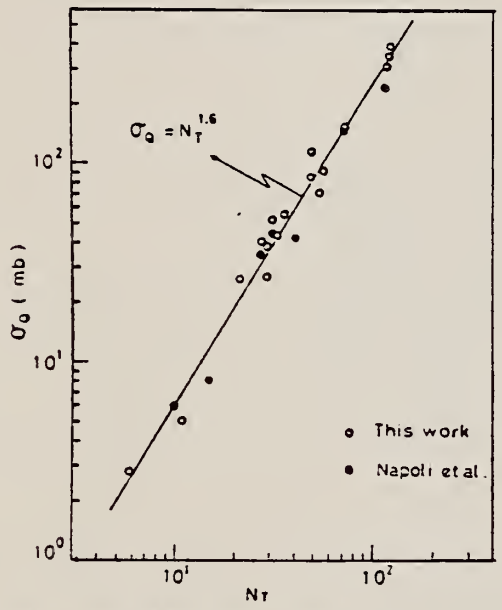

Fig. 2. Yield per equivalent quanta versus target neutron number.

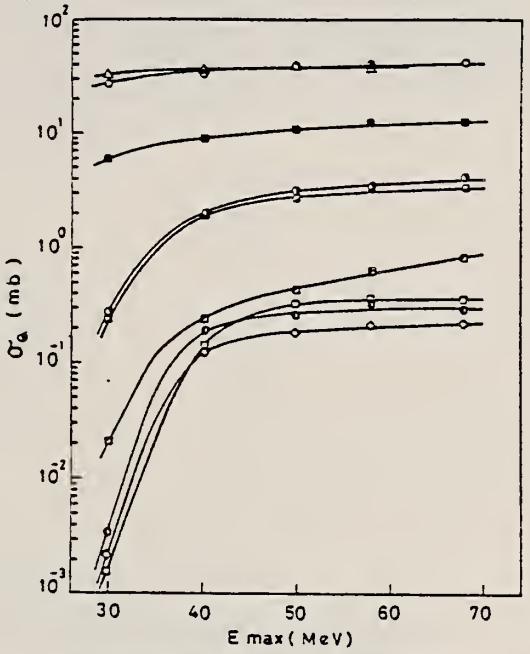

Fig. 5. Activation yield curves for the reactions on Cr, Mn and Fe.
○ $^{52}Cr(\gamma, n)^{51}Cr$, ◑ $^{50}Cr(\gamma, pn)^{48}V$, ◐ $^{50}Cr(\gamma, 2n)^{48}Cr$,
△ $^{55}Mn(\gamma, n)^{54}Mn$, ◪ $^{57}Fe(\gamma, p)^{56}Mn$, ◩ $^{54}Fe(\gamma, pn)^{52g}Mn$,
◪ $^{56}Fe(\gamma, pn)^{54}Mn$, □ $^{56}Fe(\gamma, \alpha n)^{51}Cr$, ◇ $^{54}Fe(\gamma, 2n)^{52}Fe$.

(over)

FORM NBS-418
REV. 7-1-4-4)
U.S. DEPARTMENT OF COMMERCE

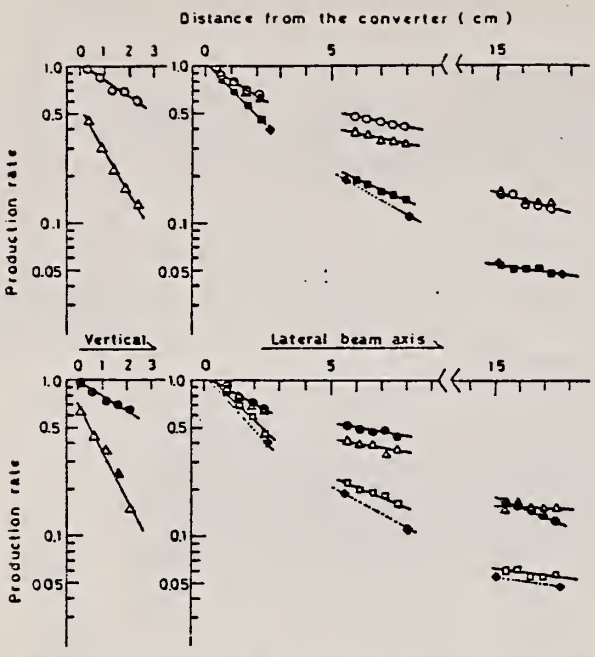

Fig. 13. Production rates of the neutron reactions and the photonuclear reactions as a function of distance from the converter in vertical and lateral directions.
○ ^{55}Mn(n, γ)^{56}Mn. ● ^{23}Na(n, γ)^{24}Na, △ ^{27}Al(n, α)^{24}Na,
■ ^{55}Mn(γ, n)^{54}Mn. □ ^{23}Na(γ, n)^{22}Na. ◆ ^{65}Cu(γ, n)^{64}Cu.

REF. J. L. Zyskind, J. M. Davidson, M. T. Esat, M. H. Shapiro and R. H. Spear
Nucl. Phys. A301, 179 (1978)

ELEM. SYM.	A	Z
Mn	55	25

METHOD

REF. NO. 78 Zy 1 rs

REACTION	RESULT	EXCITATION ENERGY	SOURCE		DETECTOR		ANGLE
			TYPE	RANGE	TYPE	RANGE	
P,G/	ABX	9-13	D	1-4	SCD-D		55

WIGNER CUSP

Abstract: Absolute cross sections for the reactions ^{54}Cr(p, γ)^{55}Mn and ^{54}Cr(p, n)^{54}Mn are presented for effective bombarding energies E_p from 0.830 to 3.606 MeV. A substantial cusp is observed in the ^{54}Cr(p, γ)^{55}Mn excitation function. The data are compared with the predictions of global Hauser-Feshbach models in order to evaluate their applicability to nucleosynthesis calculations.

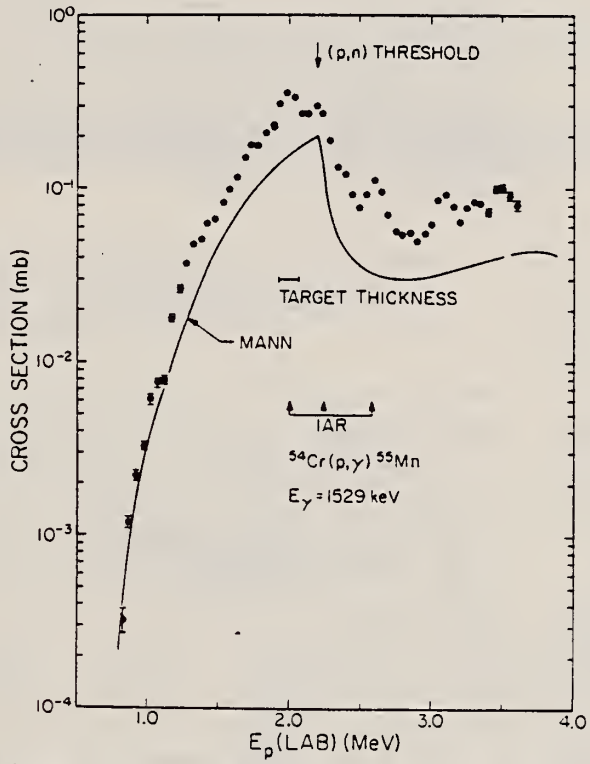

Fig. 1. Excitation function for production of 1529 keV γ-rays in the reaction ^{54}Cr(p, γ)^{55}Mn. Error bars shown are statistical only. The curve shows the results of a Hauser-Feshbach calculation performed using Mann's Code [3]. The arrows labelled IAR indicate proton energies for isobaric-analogue resonances which have been previously observed [20].

3) F. M. Mann, Hanford Engineering Department Laboratory report HEDL-TME 76-80 (1976)

20) J. D. Moses, H. W. Newson, E. G. Bilpuch and G. E. Mitchell, Nucl. Phys. A175 (1971) 556

(OVER)

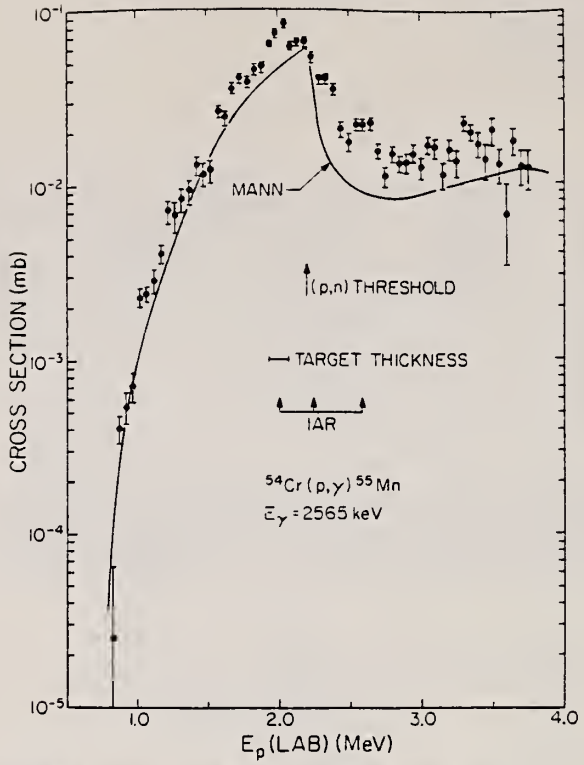

Fig. 2. Excitation function for production of 2565 keV γ-rays in the reaction ^{54}Cr(p, γ)^{55}Mn. Error bars shown are statistical only. The curve shows the results of a Hauser-Feshbach calculation performed using Mann's code [3]. The arrows labelled IAR indicate proton energies for isobaric-analogue resonances which have been previously observed [20].

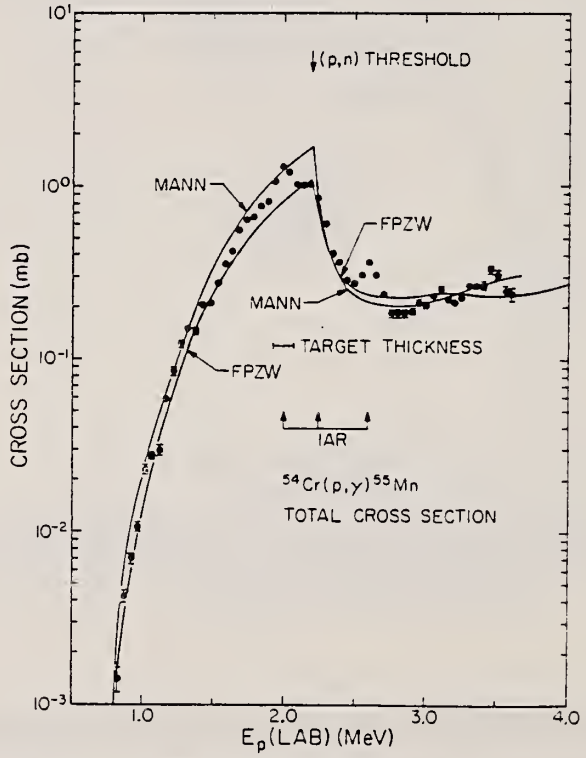

Fig. 3. Excitation function for all primary γ-rays emitted in the reaction ^{54}Cr(p, γ)^{55}Mn. Error bars shown are statistical only. The curves show the results of Hauser-Feshbach calculations performed using the codes of Mann [3] and Fowler *et al.* (FPZW) [18]. The arrows labelled IAR indicate proton energies for isobaric-analogue resonances which have been previously observed [20].

18) W. A. Fowler, J. Powelson, B. A. Zimmerman and S. E. Wooslev, private communication

REF. R.A. Alvarez, B.L. Berman, D.D. Faul, F.H. Lewis, Jr., P. Meyer
Phys. Rev. C20, 128 (1979)

ELEM. SYM.	A	Z
Mn	55	25

METHOD

REF. NO. 79 A1 2 hg

REACTION	RESULT	EXCITATION ENERGY	SOURCE TYPE	SOURCE RANGE	DETECTOR TYPE	DETECTOR RANGE	ANGLE
G,1N	ABX	10-37	D	10-37	BF3-I		4PI
G,2N	ABX	19-37	D	17-37	BF3-I		4PI
G,3N	ABX	31-37	D	29-37	BF3-I		4PI

Data fits given use Lorentz Lines, Kerman & Quang, & Dynamic Collective Models

Photoneutron cross sections, including $\sigma[(\gamma,n)+(\gamma,pn)]$, $\sigma(\gamma,2n)$, and $\sigma(\gamma,3n)$, were measured for ^{55}Mn and ^{59}Co from threshold to 36.5 MeV, with a photon energy resolution which varied from 80 keV at the lowest to 170 keV at the highest energies measured. The source of radiation was the monoenergetic photon beam obtained from the annihilation in flight of fast positrons. The partial photoneutron cross sections were determined by neutron multiplicity counting, and the average neutron energies for $(\gamma,1n)$ and $(\gamma,2n)$ events were determined simultaneously with the cross-section data by the ring-ratio technique. The cross sections exhibit considerable but weak structure. Other nuclear information extracted from the data includes parameters of the giant dipole resonance, integrated cross sections and their moments, and nuclear symmetry energies. A comparison is made with previous experimental data for these nuclei as well as with theoretical predictions based upon hydrodynamic, vibrational, and dynamic collective models. None of these models fits the data for these odd-even nuclei satisfactorily; more theoretical work is needed for this nuclear mass region.

[NUCLEAR REACTIONS ^{55}Mn, ^{59}Co$(\gamma, n, 2n, 3n)$, $E_\gamma = 10-36.5$ MeV; measured 4π neutron yield, multiplicities, average energies for monoenergetic photons; $\sigma(E_\gamma, 1n)$, $\sigma(E_\gamma, 2n)$, $\sigma(E_\gamma, 3n)$, GDR parameters, integrated cross sections and moments, nuclear symmetry energies.]

TABLE II. Parameters of two-component Lorentz-curve fits to the GDR. The fitting interval used is 14 to 21 MeV.

Nucleus	$E_m(1)$ (MeV)	$\sigma_m(1)$[a] (mb)	$\Gamma(1)$ (MeV)	$E_m(2)$ (MeV)	$\sigma_m(2)$[a] (mb)	$\Gamma(2)$ (MeV)	χ^2
^{55}Mn	16.82 ± 0.10	51.4 ± 4.1	4.33 ± 0.63	20.09 ± 0.12	45.2 ± 2.6	4.09 ± 1.07	1.14
^{59}Co	16.43 ± 0.08	28.3 ± 5.4	2.73 ± 1.08	18.66 ± 0.25	58.4 ± 4.4	7.38 ± 0.79	1.11

[a] Uncertainties for σ_m given here are relative. The absolute uncertainties are 7%.

TABLE III. Integrated cross sections. $\sigma_{int}(\gamma,x) = \int \sigma(\gamma,x)dE_\gamma$, integrated from threshold to $E_{\gamma max}$.

Nucleus	$E_{\gamma max}$ (MeV)	$\sigma_{int}(\gamma,1n)$ (MeV-mb)	$\sigma_{int}(\gamma,2n)$ (MeV-mb)	$\sigma_{int}(\gamma,3n)$ (MeV-mb)	$\frac{\sigma_{int}(\gamma,2n)}{\sigma_{int}(\gamma,n_t)}$	$\frac{\sigma_{int}(\gamma,n_t)}{60NZ/A}$	$\frac{\frac{1}{2}\pi[\sigma_m(1)\Gamma(1)+\sigma_m(2)\Gamma(2)]}{60NZ/A}$
^{55}Mn	36.5	567	163	3	0.222	0.90	0.78
^{59}Co	36.5	653	150	4	0.186	0.92	0.91

TABLE IV. Integrated cross-section moments. $\sigma_{-1} = \int \sigma(\gamma,n_t)E_\gamma^{-1}dE_\gamma$ and $\sigma_{-2} = \int \sigma(\gamma,n_t)E_\gamma^{-2}dE_\gamma$, integrated from threshold to $E_{\gamma max}$.

Nucleus	σ_{-1} (mb)	$\sigma_{-1}A^{-4/3}$ (mb)	σ_{-2} (mb-MeV^{-1})	$\frac{\sigma_{-2}}{0.00225A^{5/3}}$	$\frac{\sigma_{-2}K}{0.05175A^{5/3}}$	$\frac{0.05175A^{5/3}}{\sigma_{-2}}$ (MeV)
^{55}Mn	36.4	0.174	1.93	1.08	0.91[a]	21.3
^{59}Co	40.1	0.174	2.14	1.06	0.90[a]	21.7

[a] The values used for the nuclear symmetry energy K are from Table VI.

(over)

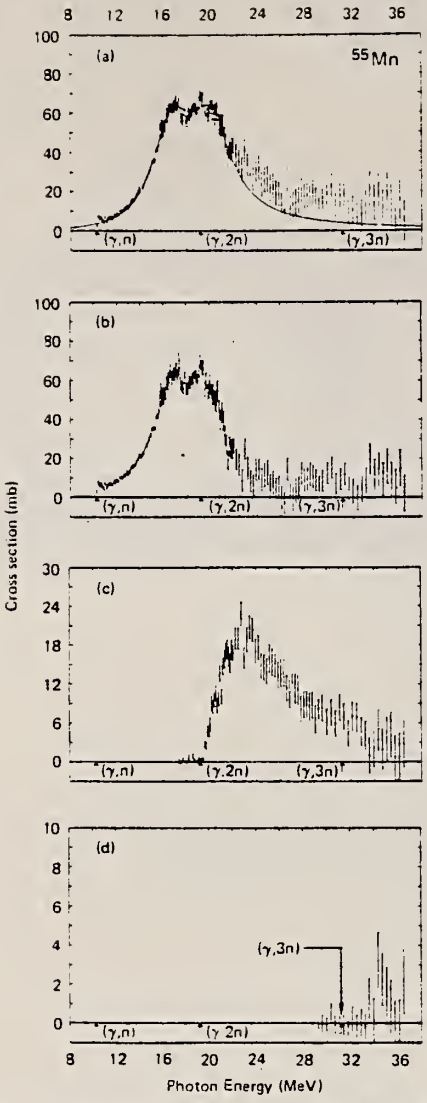

FIG. 2. Photoneutron cross sections for ^{55}Mn: (a) total photoneutron cross section $\sigma(\gamma,n_t)=\sigma[(\gamma,1n)+(\gamma,2n)+(\gamma,3n)]$, together with a two-component Lorentz-curve fit to the data (solid line); (b) single-photoneutron cross section $\sigma(\gamma,1n)=\sigma[(\gamma,n)+(\gamma,pn)]$; (c) double-photoneutron cross section $\sigma(\gamma,2n)$; (d) triple-photoneutron cross section $\sigma(\gamma,3n)$.

Error bars show statistical uncertainties only.

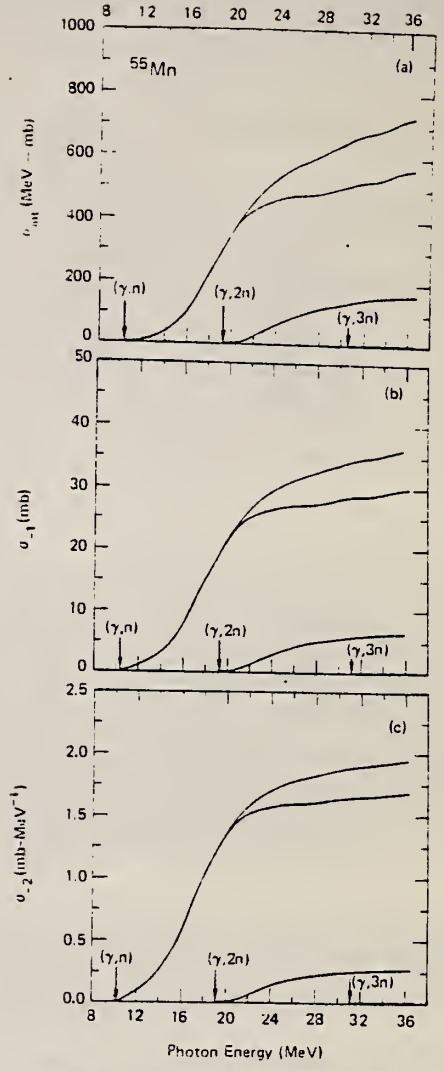

FIG. 4. Running sums of integrated photoneutron cross sections and their moments for ^{55}Mn: (a) $\sigma_{-1}=\int\sigma dE$ for $\sigma(\gamma,n_t)$ (top), $\sigma(\gamma,1n)$ (next to top), $\sigma(\gamma,2n)$ (next to bottom), and $\sigma(\gamma,3n)$ (bottom); (b) $\sigma_{-1}=\int\sigma E_\gamma^{-1}dE_\gamma$; (c) $\sigma_{-2}=\int\sigma E_\gamma^{-2}dE_\gamma$.

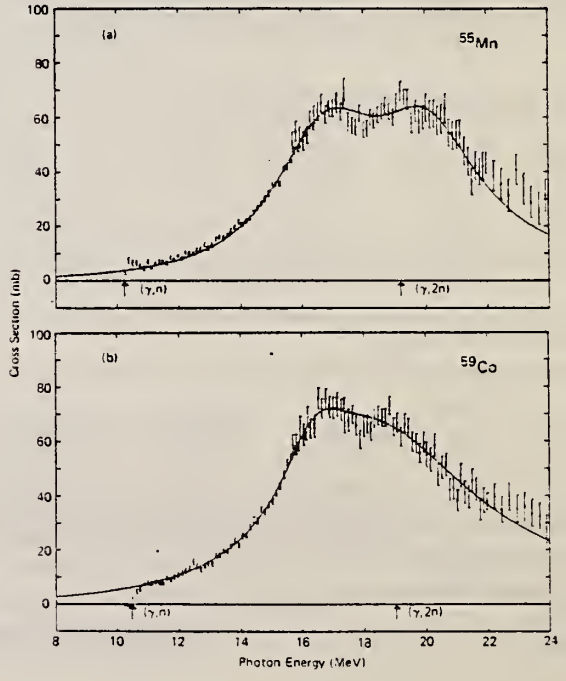

FIG. 6. Total photoneutron cross sections, with two-component Lorentz-curve fits: (a) for ^{55}Mn; (b) for ^{59}Co. Although the theoretical model is strictly valid only for $\sigma(\gamma,\mathrm{tot})$, the curve shown here was scaled to fit the measured $\sigma(\gamma,n_t)$ data (see Sec. III B in the text and Table III).

Mn
A=56

Mn
A=56

Mn
A=56

Ref. J.H. Carver, G.A. Jones
Nuclear Phys. 24, 607 (1961)

Elem. Sym.	A	Z
Mn	56	25

Method: Radioactivity

Ref. No.: 61 Ca 1 JOC

Reaction	E or ΔE	E_o	Γ	$\int \sigma dE$	Jπ	Notes
$Cr^{54}(d,\gamma)$	3.5-4.5					At E_d = 4.5 MeV, $\sigma(d,\gamma)$= 295±45 μb.

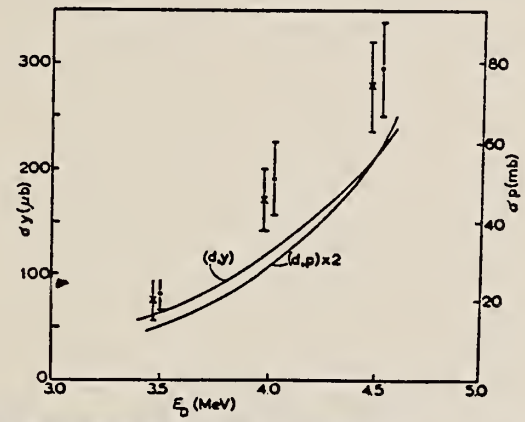

Fig. 2. Cross-sections for the reactions $Cr^{54}(d, \gamma)$ – denoted by dots – and $Cr^{54}(d, p)$ – denoted by crosses – as a function of deuteron energy. The full curves are given by the statistical theory; the theoretical cross-section for (d, p) has been doubled to show the constancy of the ratio of the cross-sections.

TABLE 1

Results for 4.5 MeV deuterons

Initial nucleus	Reaction	σ_{exp}(±15 %)	$\sigma_{stat\ theor}$	σ_{rel} (direct capture)
Ni^{58}	(d, γ)	61 μb	48 μb	61 μb (assuming the measured σ to be totally accounted for by this process)
	(d, n)	85 mb	64 mb	
	$\frac{(d,\gamma)}{(d,n)}$	0.7×10^{-3}	0.75×10^{-3}	
Zn^{64}	(d, γ)	80 μb	86 μb	192 μb
	(d, n) + (d, p)	160 mb	175 mb	
	$\frac{(d,\gamma)}{(d,n)\times(d,p)}$	0.5×10^{-6}	0.49×10^{-3}	
Cr^{54}	(d, γ)	295 μb	215 μb	1280 μb
	(d, p)	75 mb	29 mb	
	$\frac{(d,\gamma)}{(d,p)}$	3.9×10^{-3}	7.4×10^{-3}	

† There is a misprint in eq. (5) of ref. [1]), the right side of which should be divided by π. Eq. (1) of ref. [1]) is correct.

Ref 1: Carver & Jones - Nuclear Phys. 11, 400, (1959)

# IRON
Z=26

Iron has the chemical symbol Fe from the Latin "*ferrum*" and has been known since prehistoric times. Writings of most of the earliest civilizations refer to it and there is evidence that it was known in the ancient world over 8000 years ago. However, prior to 2000 B. C., iron was a rare metal, apparently derived from meteorites. From this time onward, iron derived from ore became an increasingly used metal. Its smelting and fabrication were practied all over the civilized world by processes similar to those used now.

Fe

Fe

Ref. W.R. Dixon
Can. J. Phys. 33, 785 (1955)

Elem. Sym.	A	Z
Fe		26

Method: Synchrotron; neutron angular distribution; scintillator; ion chamber

Ref. No.: 55 Di 1 NVB

Reaction	E or ΔE	E_o	Γ	$\int \sigma dE$	Jπ	Notes
Fe(γ,xn)	70					Isotropy suggests evaporation in heavy nuclei. Curves fitted to a + b $\sin^2\theta$

TABLE II

EXPERIMENTAL VALUES FOR b/a

Target	Correction factor for self-scattering	Corrected b/a
Lead	1.10	-0.08 ± 0.08
Tin	1.08	0.12 ± 0.17
Copper	1.48	0.23 ± 0.15
Iron	1.35	0.09 ± 0.25
Aluminum	1.17	0.36 ± 0.29
Carbon	1.8	1.6 ± 0.8
Beryllium (1)	2.6	1.2 ± 0.4
Beryllium (2)	1.35	

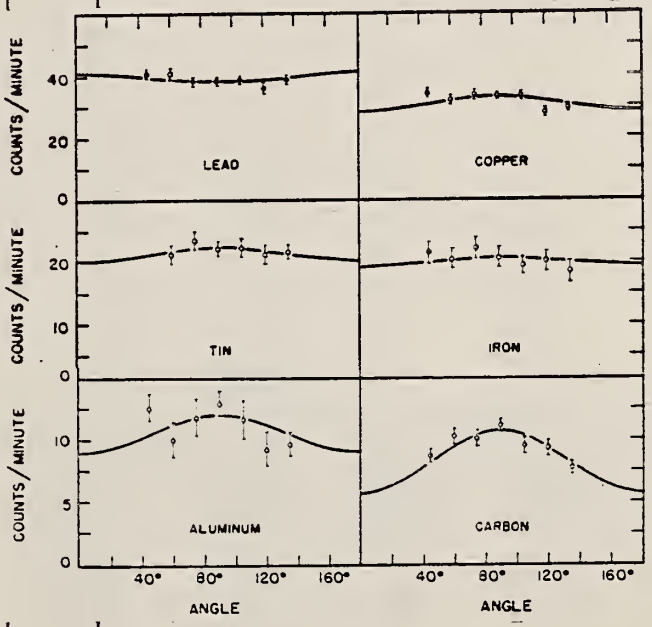

Ref. K. Reibel, A.K. Mann
Phys. Rev. 118, 701 (1960)

Elem. Sym.	A	Z
Fe	.	26

Method
γ's from $F^{19}(p,\alpha\gamma)$ reaction; protons from Vande Graaff; NaI.

Ref. No 60 Re 1 JHH

Reaction	E or ΔE	E_o	Γ	$\int \sigma dE$	$J\pi$	Notes
(γ,γ)	E_γ~7MeV					$\langle\bar{\sigma}\rangle$ (E_p = 2.05 MeV) = 0.40 ± .06 mb

Ref. M. Kregar, B. Povh
Nuclear Phys. 43, 170 (1963)
Erratum in Nuclear Phys. 47, 528 (1963)

Elem. Sym.	A	Z
Fe		26

Method: Betatron; α yields; solid state detectors; NBS chamber monitor

Ref. No.: 63 Kr 1 JHH

Reaction	E or ΔE	E_o	Γ	$\int \sigma dE$	$J\pi$	Notes
Fe(γ,α)	Bremss.					
	21					
	30					

TABLE 1
Relative yields

Element	21 MeV		30 MeV	
	Number of alphas	Relative yield at 90°	Number of alphas	Relative yield at 90°
Ni	1209	40	536	13
Cu	1124	13	590	7
Fe	1108	4.5	653	1.7
V	372	1	363	1
Cd	136	0.7		

Ref. W.H. Hartley, W.E. Stephens, E.J. Winhold
Phys. Rev. 104, 178 (1956)

Elem. Sym.	A	Z
Fe		26

Method: Li(p,γ) source; 480 keV protons; BF_3 counter

Ref. No.: 56 Ha 1 | EGF

Reaction	E or ΔE	E_o	Γ	$\int \sigma dE$	Jπ	Notes
Fe(γ,xn)						Average Li cross section is 38 mb; cross section with detector response weighted for low energy neutrons, 33 mb. Assumed ratio 17.6/14.8 = 1.7. Calculated cross section at 14.8 and 17.6 MeV assuming cross section curves measured at Pennsylvania and Saskatchewan (refer Table I).

[3] McDaniel, Walker, and Stearns, Phys. Rev. 80, 807 (1950).
[4] J. S. Levinger and H. A. Bethe, Phys. Rev. 78, 115 (1950).
[23] Montalbetti, Katz, and Goldemberg, Phys. Rev. 91, 659 (1953).
[24] R. Nathans and J. Halpern, Phys. Rev. 93, 437 (1954).
[32] J. Goldemberg and L. Katz, Can. J. Phys. 32, 49 (1954).

TABLE I. Cross sections for photoneutron emission induced by the lithium gamma rays. The results are compared with previous data.

Element	Present cross-section data: Counter Group A	Present cross-section data: Counter Group B	Data of McDaniel et al.[a]	Betatron data: Pennsylvania σ_{Av}[b]	Pennsylvania $\sigma_{14.8}/\sigma_{17.6}$	Saskatchewan σ_{Av}[b]	Saskatchewan $\sigma_{14.8}/\sigma_{17.6}$	$\sigma_{14.8}$[b]	$\sigma_{17.6}$[b]
$_{26}$Fe	38 mb	33 mb	37 mb			60[f] mb	0.5	23 mb	47 mb
$_{27}$Co	49	49	47	60[e] mb	0.5	95[f]	0.5	30	60
$_{28}$Ni	28	25	23			40[g]	0.7	22	32
$_{29}$Cu	64	61	55±12			95[f]	0.6	45	75
$_{30}$Zn	48	45	48			90[f]	0.7	38	54
$_{47}$Ag	175	170	135			240[f]	1.0	175	175
$_{50}$Sn	200	190	180						
$_{73}$Ta	355	360	260	350[d]	1.3	420[g]	2.3	420[i] 550[j]	320[i] 240[j]
$_{74}$W	365	355	325						
$_{79}$Au	330	295		315[e]	1.7	480[f]	1.9	460	255
$_{80}$Hg	365	340	290						
$_{82}$Pb	310	295	250	320[e]	1.6	440[f]	2.5	400[i] 500[j]	250[i] 200[j]
$_{83}$Bi	305	280	250	270[d]	2.6	550[f]	2.4	490	195

[a] See reference 3.
[b] Average of 14.8- and 17.6-Mev cross sections weighted with relative intensities of the lithium gamma-ray lines.
[c] See reference 24.
[d] R. Nathans, Ph.D. thesis, University of Pennsylvania, 1954 (unpublished).
[e] J. Halpern (private communication).
[f] See reference 23.
[g] See reference 32.
[h] Separate cross sections at 14.8 and 17.6 Mev as obtained from Group A data and 14.8/17.6 betatron cross-section ratios.
[i] Obtained using 14.8/17.6 cross-section ratio from Pennsylvania betatron data.
[j] Obtained using 14.8/17.6 cross-section ratio from Saskatchewan betatron data.

Ref. M.E. Toms, J. McElhinney
Phys. Rev. 111, 561 (1958)

Elem. Sym.	A	Z
Fe		26

Method: Betatron; alpha yield; nuclear emulsion

Ref. No.: 58 To 2 | NVB

Reaction	E or ΔE	E_o	Γ	$\int \sigma dE$	Jπ	Notes
Fe(γ,α)	Bremss. 22					Yield = 1.9×10^{4} alpha/mole/roentgen

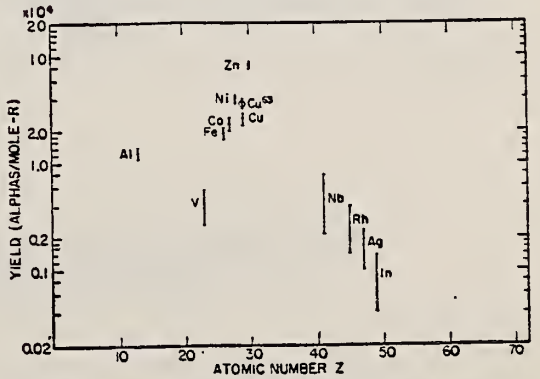

FIG. 8. Photo-alpha yields plotted against atomic numbers for the exposures of the survey.

REF. J. Kockum, N. Starfelt
Nucl. Instruments 5, 37 (1959)

ELEM. SYM.	A	Z
Fe		26

METHOD
30 MeV synchrotron; NaI(Tℓ) scintillator spectrometer; photon

REF. NO.	
59 Ko 1	EH

REACTION	RESULT	EXCITATION ENERGY	SOURCE		DETECTOR		ANGLE
			TYPE	RANGE	TYPE	RANGE	
$Fe(\sigma_t)$		10 - 27	C	10-27	NAI		

TABLE 2

Experimentally determined giant resonance data; peak energy, E_{max}, width at half height, ΔE, and integrated cross section, $\int_{10\,MeV}^{27\,MeV} \sigma dE$, and values of $\int_0^\infty \sigma dE$ predicted by the dipole sum rule.

Absorber	E_{max} (MeV)	ΔE (MeV)	$\int_{10\,MeV}^{27\,MeV} \sigma dE$	$\int_0^\infty \sigma dE$
Carbon	23	4.6	0.12	0.18
Aluminium	21.5	7.8	0.24	0.40
Sulphur	21	6.6	0.30	0.48
Iron	19.5	9.4	0.76	0.84

[17]) J. Halpern and A. K. Mann, Phys. Rev. 83 (1951) 370.
[18]) R. Montalbetti, L. Katz and J. Goldemberg, Phys. Rev. 91 (1953) 659.
[19]) L. W. Jones and K. M. Terwilliger, Phys. Rev. 91 (1953) 699.
[20]) W. C. Barber, W. D. George and D. D. Reagan, Phys. Rev. 98 (1955) 73.
[21]) F. Ferrero, R. Malvano, S. Menardi and O. Terracini, Nuclear Physics 9 (1958) 32.
[22]) L. Katz and A. S. Penfold, Phys. Rev. 81 (1951) 815.
[23]) S. A. E. Johansson, Phys. Rev. 97 (1955) 1186.

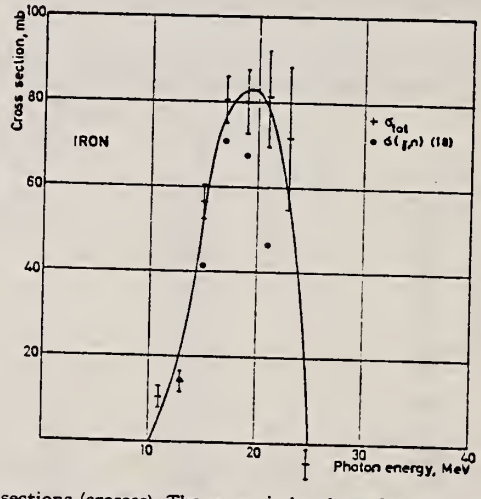

Fig. 4. Experimentally determined photonuclear absorption cross sections (crosses). The open circles show the sum of the (γ,n), and (γ,p) cross sections and the filled squares the (γ,np) + (γ,d) cross section where available[17,18,20–22]). The filled circles give the total photonuclear absorption cross section as measured by Ziegler[9]).

[9]) B. Ziegler, Z. Physik 152 (1958) 566.

REF. R. G. Baker and K. G. McNeill
Can. J. Phys. 39, 1158 (1961)

ELEM. SYM.	A	Z
Fe		26

METHOD Betatron; fast neutron yield; angular distribution; Si threshold detector; ion chamber.

REF. NO. 61 Ba 2 NVB

REACTION	RESULT	EXCITATION ENERGY	SOURCE		DETECTOR		ANGLE
			TYPE	RANGE	TYPE	RANGE	
G,XN	ABY	THR- 22	C	22	THR-I		DST

In Table IV: $\bar{\sigma}$ = average cross section of detector weighted with neutron spectrum;

Φ = neutrons/100 roentgen/mole

$$W(\theta) = a_0 \sum_{n=1}^{\infty} (1 + a_n P_n(\cos\theta))$$

TABLE IV

I Element	II a_0	III a_1	IV a_2	V $(\bar{\sigma}\Phi)\times 10^{29}$	VI Φ_{total} (22 Mev)$\times 10^{3}$	VII Φ_{fast}/Φ_{total}
Vanadium	245 (1±0.06)	0.01±0.08	−0.00±0.10	6.05	0.21	0.12
Chromium	164 (1±0.03)	0.04±0.04	−0.05±0.05	4.05	0.17	0.10
Manganese	308 (1±0.02)	0.07±0.03	−0.09±0.04	7.61	0.25	0.12
Iron	200 (1±0.03)	0.05±0.04	−0.17±0.05	4.94	0.18	0.11
Cobalt	390 (1±0.02)	0.08±0.03	−0.22±0.04	9.63	0.26	0.15
Nickel	145 (1±0.05)	0.07±0.07	−0.23±0.09	3.58	0.12	0.12
Copper	347 (1±0.02)	0.05±0.03	−0.29±0.04	8.57	0.30	0.12
Arsenic	482 (1±0.03)	0.11±0.04	−0.24±0.05	11.91	0.33	0.15
Rubidium	638 (1±0.05)	0.13±0.06	−0.14±0.08	15.76		
Strontium	409 (1±0.05)	0.10±0.06	−0.17±0.08	10.10		
Yttrium	290 (1±0.10)	0.08±0.12	−0.12±0.15	7.16		
Silver	590 (1±0.01)	0.10±0.06	−0.22±0.08	14.57	0.87	0.07
Cadmium	905 (1±0.02)	0.02±0.02	−0.26±0.03	22.35		
Iodine	1133 (1±0.03)	0.04±0.04	−0.29±0.05	27.99	1.42	0.08
Barium	1048 (1±0.01)	0.10±0.06	−0.38±0.08	25.89		
Lanthanum	1595 (1±0.02)	0.02±0.03	−0.42±0.01	39.40	1.01	0.15
Cerium	1316 (1±0.05)	0.05±0.06	−0.39±0.08	32.50		
Dysprosium	1652 (1±0.08)	0.04±0.10	−0.34±0.13	40.80		
Tantalum	1558 (1±0.02)	0.04±0.03	−0.22±0.04	38.48	2.50	0.06
Tungsten	1365 (1±0.02)	−0.07±0.03	−0.24±0.01	33.71		
Mercury	1345 (1±0.02)	0.04±0.03	−0.31±0.04	33.22		
Lead	2274 (1±0.01)	0.02±0.02	−0.42±0.03	56.17	2.72	0.08
Bismuth	2162 (1±0.02)	0.05±0.03	−0.45±0.04	53.40	3.36	0.06
Thorium	3031 (1±0.04)	0.06±0.05	−0.32±0.07	74.87		
Uranium	4630 (1±0.02)	0.05±0.03	−0.17±0.04	114.36		

*$(\bar{\sigma}\Phi)$ = 2.47×10³ a_0 millibarn-neutron. Errors are standard errors due to counting statistics only.

Ref. O.M.M. Mitchell, K.G. McNeill
Can. J. Phys. 41, 871 (1963)

Elem. Sym.	A	Z
Fe		26

Method: Betatron; proton yields; angular distribution; scintillator; ion chamber

Ref. No.: 63 Mi 5 NVB

Reaction	E or ΔE	E_o	Γ	$\int \sigma dE$	Jπ	Notes
Fe(γ,xp)	Bremss. 22					Angular distribution: $Y(\theta) = a + b \sin^2\theta (1 + p \cos\theta)^2$ where a = 74±13; b = 31±17; p = -0.2±0.3 and b/a = 0.4±0.2. Yield (E_p > 8 MeV) = (1.1±0.2) 10^5 protons/mole-r Yield (3.7< E_p < 14): (11±1) 10^5

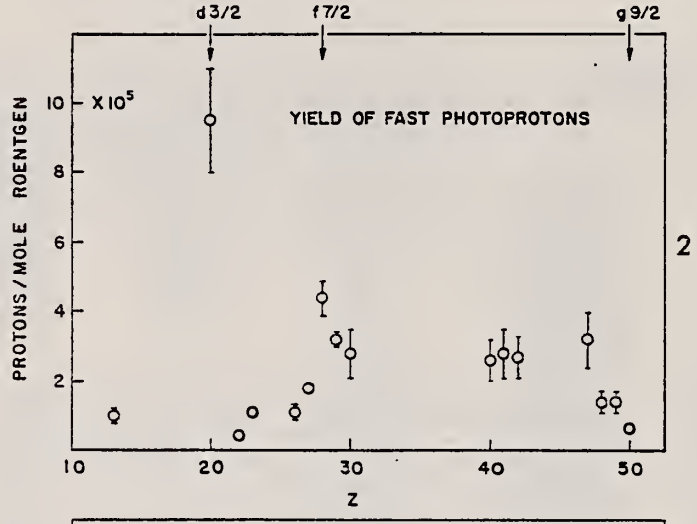

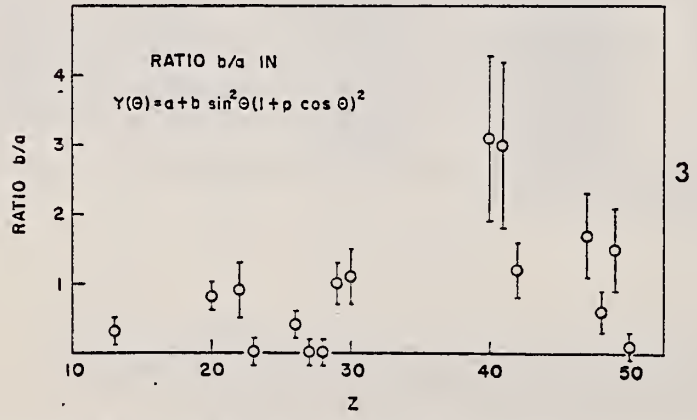

FIG. 2. The yields of fast photoprotons ($E_p > 8$ Mev) obtained from targets of various elements when irradiated with 22-Mev bremsstrahlung. The target thicknesses range from 351 to 572 mg/cm² (about 8 Mev for protons). The errors noted are statistical.
FIG. 3. The anisotropy coefficient b/a for fast photoprotons ($E_p > 8$ Mev) from 16 elements. The errors noted are statistical.

(OVER)

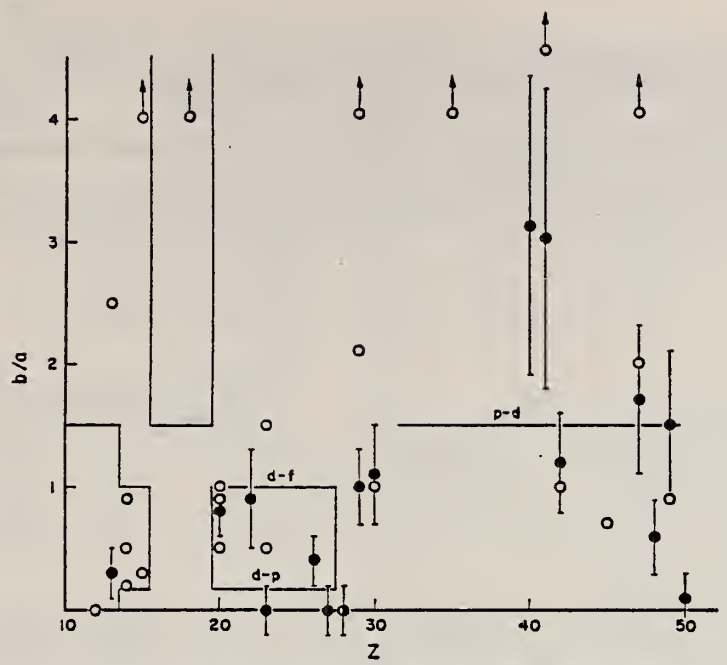

FIG. 4. The values of the fast photoproton anisotropy coefficient b/a found by the present authors (●) and other workers (○) in the region of the periodic table $10 < Z < 50$. Arrows indicate off-scale points. The references to the results of other workers are given in Table II. The demarcations are explained in the text.

Ref. M. Sugawara, S. Mori, A. Ono, A. Hotta, M. Kimura
J. Phys. Soc. Japan 18, 17 (1963)

Elem. Sym.	A	Z
Fe		26

Method: 25 MeV betatron; photon scattering; NaI spectrometer; NBS chamber

Ref. No.: 63 Su 1 NVB

Reaction	E or ΔE	E_o	Γ	$\int \sigma dE$	Jπ	Notes
Fe(γ,γ)	Bremss. 4-14					Detector at 120° σ_{max} = 1.3 mb [Corrects results of J. Phys. Soc. Japan 16, 1657 (1961)]

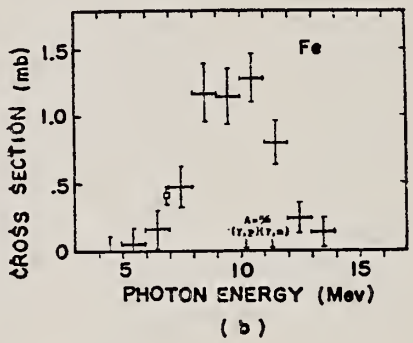

Fig. 2. The elastic scattering cross sections for Mg, Fe, Zn, As, Cd, Sb and Bi. The indicated spread in energy is the width of the sum-up channels, and the vertical lines are the statistical errors including background counts. The arrows represent the positions of the threshold energies of (γ, p) or (γ, n) reaction taken from Ref. 16. The open squares at 7 Mev are Reibel and Mann's data[9]. In Fig. 2(c), the cross section values, which are analyzed by displacing the sum-up channels by five channels to lower energy side than the positions generally used, are indicated by the closed triangles.

9) K. Reibel and A. K. Mann: Phys. Rev. 118 (1960) 701.
10) J. S. Pruitt and S. R. Domen: NBS Monograph 48 (1962).
11) E. G. Fuller and E. Hayward: J. Research
15) J. A. Stratton: *Electromagnetic Theory* (McGraw-Hill Book Co., New York, 1941).
16) *Nuclear Data Sheets*, National Academy o Sciences (N. R. C.).

E. C. Booth, B. Chasan and K. A. Wright
Nucl. Phys. 57, 403-420 (1964)

Fe		26

METHOD
Van de Graaff; resonance fluorescence

REF. NO.
64 Bo 1 | NVB

REACTION	RESULT	EXCITATION ENERGY	SOURCE		DETECTOR		ANGLE
			TYPE	RANGE	TYPE	RANGE	
G,G	LFT	1-3	C	1 - 3	NAI-D		100
		(0.5 - 3.0)		(0.5 - 3.0)			

ABI

TABLE 1
Cases of observed resonance fluorescence

Nucleus multipol.	State (MeV)	Spin	Γ_0/Γ	$T(g w \Gamma_0^2/\Gamma^2)^{-1}$ (sec).	Mean lifetime T BCW (sec)	Mean lifetime T other (sec)	Ref.	Γ_0/Γ_W BCW
Fe^{56}	0.00	0^+						
E2[a])	0.85	2^+	1	$2.5 \pm 1.2 \times 10^{-13}$	$8 \pm 4 \times 10^{-13}$	$8.5 \pm 2.9 \times 10^{-13}$	[16])	16

Synchrotron; $C^{12}(\gamma,n)$ monitor

REACTION	RESULT	EXCITATION ENERGY	SOURCE TYPE	SOURCE RANGE	DETECTOR TYPE	DETECTOR RANGE	ANGLE
G,XN	ABY	THR - 80	C	80	BF3-I		4 PI

Table 1

Element	Yield (36) eV cm^2 mol MeV	60 NZ/A (mb MeV)	Σ_0^{30}	Σ_0^{80}	$\Sigma_0^{30} / \Sigma_0^{80}$	E_m (MeV)	σ_m (mb)
$_{24}Cr$	83×10^{-5}	777	1.21	2.1	0.58	18.5	97
$_{25}Mn$	108×10^{-5}	818	1.52	2.33	0.65	18.5	114
$_{26}Fe$	68×10^{-5}	832	0.88	1.46	0.60	17.5	75
$_{27}Co$	89×10^{-5}	878	1.08	1.82	0.59	17.5	92
$_{28}Ni$	44×10^{-5}	879	0.55	1.07	0.51	18.5	56
$_{29}Cu$	95×10^{-5}	947	1.06	1.99	0.53	17.5	98
$_{30}Zn$	88×10^{-5}	975	0.94	1.68	0.56	17.5	86
$_{31}Ga$	130×10^{-5}	1034	1.29	2.18	0.59	17.5	151
$_{32}Ge$	139×10^{-5}	1064	1.35	2.29	0.59	17.5	158
$_{33}As$	137×10^{-5}	1109	1.22	2.18	0.56	17.5	127

$$\Sigma_0^{30} = \frac{\int_0^{30} \sigma(\gamma,xn)dE}{60\ NZ/A}$$

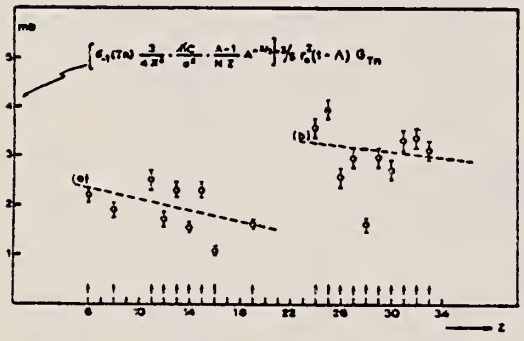

Fig. 2. Bremsstrahlung weighted cross sections, $\sigma_{-1}(Tn)$, conveniently normalized, versus Z.

Table 2

Element	maximum yield ($\times 10^{-5}$)	$\sigma_{-1}(Tn)$	$\sigma_{-1}(Tn) \times \left[\frac{3}{4\pi^2}\frac{\hbar c}{c^2}\left(\frac{A-1}{NZ}\right)A^{-\frac{2}{3}}\right]$
$_6C$	4.0	3.54	2.18
$_8O$	5.2	4.95	1.92
$_{11}Na$	13.6	11.60	2.49
$_{12}Mg$	10.0	8.81	1.73
$_{13}Al$	15.9	13.92	2.30
$_{14}Si$	11.6	9.96	1.55
$_{15}P$	19.8	17.56	2.32
$_{16}S$	9.5	8.55	1.07
$_{19}K$	19.6	17.90	1.61
$_{20}Ca$	12.1	11.68	1.02
$_{24}Cr$	86	61.6	3.56
$_{25}Mn$	115	76.1	3.96
$_{26}Fe$	71	50.5	2.55
$_{27}Co$	94	63.5	2.94
$_{28}Ni$	46	34.2	1.59
$_{29}Cu$	102	72.3	2.96
$_{30}Zn$	93	65.7	2.68
$_{31}Ga$	140	93.6	3.31
$_{32}Ge$	150	101.5	3.36
$_{33}As$	151	99.8	3.12

B. MacDonald, J. A. Diaz, S. N. Kaplan, and R. V. Pyle
Phys. Rev. 139, B1253 (1965)

ELEM. SYM.	A	Z
Fe		26

METHOD

Cyclotron; μ^- capture

REF. NO. 65 Ma 2 NVB

REACTION	RESULT	EXCITATION ENERGY	SOURCE TYPE	SOURCE RANGE	DETECTOR TYPE	DETECTOR RANGE	ANGLE
MU-,XN	NØX	10 - 20	D	0	SCI-I		4PI
		[DO NOT PUT	IN DATA INDEX]				

Tries to fit data with Fermi gas and Gaussian momentum distributions.

NEUT MULTIPLICITY

TABLE IV. Corrected experimental results.

Target	Average multiplicity, $\langle n \rangle$	Multiplicity distribution (adjusted to 0.543 efficiency) F_0	F_1	F_2	F_3	F_4	F_5	F_6	F_7
Al	1.262 ±0.059	0.449 ±0.027	0.464 ±0.028	0.052 ±0.013	0.036 ±0.007	−0.0023 ±0.004	−0.001 ±0.004	0.003 ±0.004	
Si	0.864 ±0.072	0.611 ±0.042	0.338 ±0.042	0.045 ±0.018	−0.002 ±0.008	0.003 ±0.005	0.002 ±0.005	0.005 ±0.006	
Ca	0.746 ±0.032	0.633 ±0.021	0.335 ±0.022	0.025 ±0.009	0.004 ±0.006	0.003 ±0.003			
Fe	1.125 ±0.041	0.495 ±0.018	0.416 ±0.019	0.074 ±0.011	0.014 ±0.005	−0.0001 ±0.003	0.002 ±0.003		
Ag	1.615 ±0.060	0.360 ±0.021	0.436 ±0.023	0.144 ±0.017	0.031 ±0.009	0.007 ±0.005	0.002 ±0.004	0.001 ±0.003	
I	1.436 ±0.056	0.396 ±0.021	0.474 ±0.023	0.087 ±0.015	0.035 ±0.009	0.007 ±0.005	0.0002 ±0.004		
As	1.662 ±0.044	0.370 ±0.015	0.425 ±0.016	0.156 ±0.012	0.032 ±0.006	0.014 ±0.004	0.003 ±0.003	0.0003 ±0.003	
Pb	1.709 ±0.066	0.324 ±0.022	0.483 ±0.025	0.137 ±0.018	0.045 ±0.010	0.011 ±0.006			
Ag[a]	1.60 ±0.18	0.389 ±0.100	0.455 ±0.075	0.120 ±0.035	0.030 ±0.015	0.001 ±0.003	0.009 ±0.006	0.000 ±0.007	0.010 ±0.007
Pb[a]	1.64 ±0.16	0.348 ±0.100	0.479 ±0.057	0.137 ±0.027	0.018 ±0.012	0.010 ±0.005	0.005 ±0.004	0.003 ±0.002	0.002 ±0.002

[a] Results of Kaplan, Moyer, and Pyle (Ref. 1).

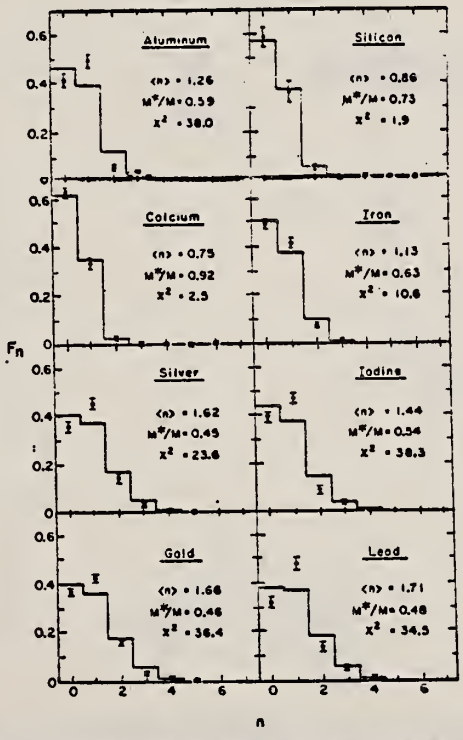

FIG. 11. Comparison of the observed neutron multiplicities with histograms calculated by using the Gaussian momentum distribution, $\alpha^2/2M = 20$ MeV.

REF.

I. Bergqvist, B. Lundberg, L. Nilsson and N. Starfelt
Phys. Letters 19, 670 (1966)

ELEM. SYM.	A	Z
Fe		26

METHOD

Van de Graaff

REF. NO.

66 Be 1 EGF

REACTION	RESULT	EXCITATION ENERGY	SOURCE		DETECTOR		ANGLE
			TYPE	RANGE	TYPE	RANGE	
N,G	SPC	15	D	7	NAI-D	8-18	

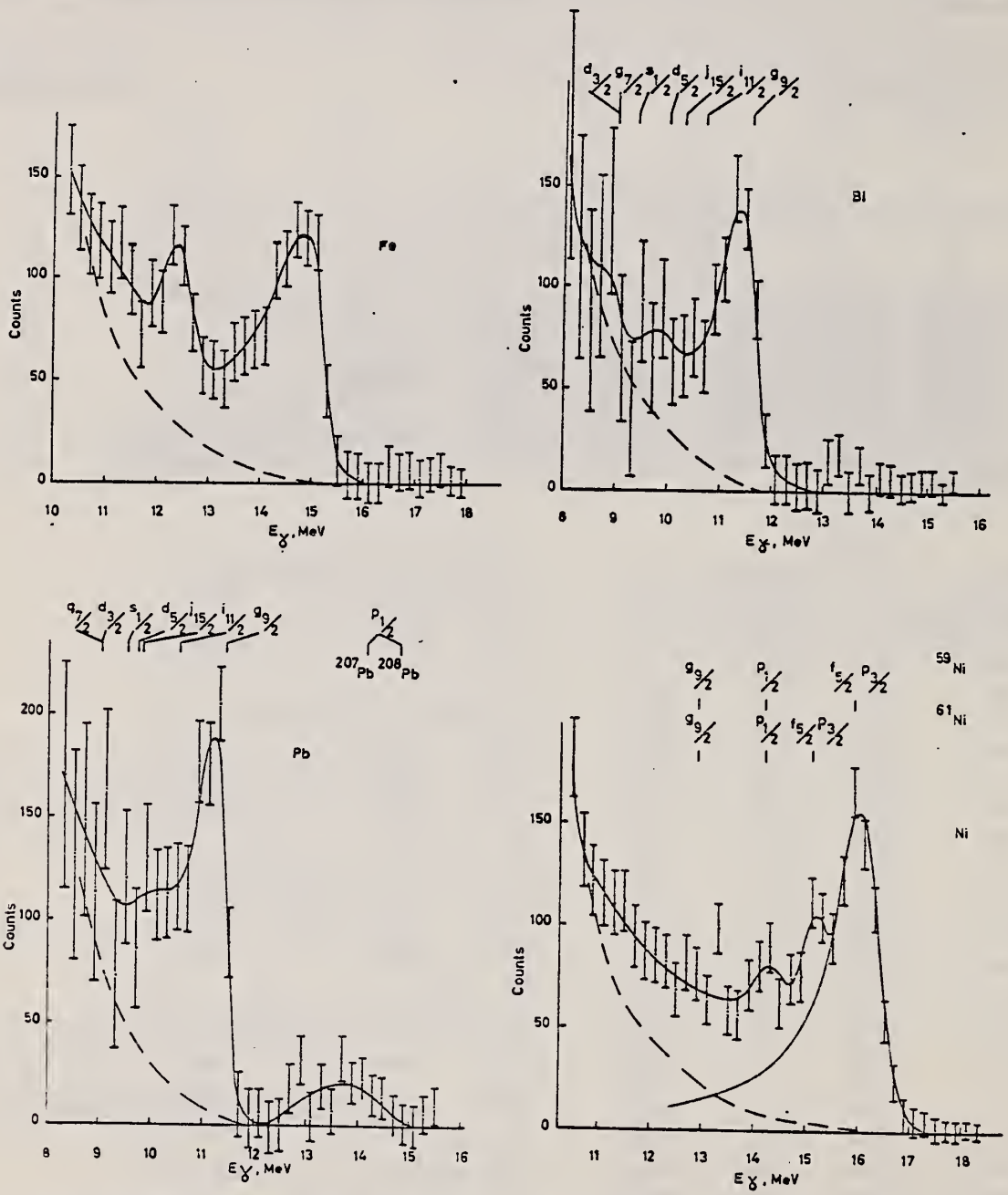

Fig. 1. Gamma-ray spectra emitted in the capture of 7.4 MeV neutrons. The dashed line is the spectrum calculated for the decay of a compound nucleus. The dot-dashed line is the response function of the gamma-ray spectrometer for 16.0 MeV γ rays. Single-particle states as determined from (d,p) reactions are shown.

REF.

W. B. Walters and J. P. Hummel
Phys. Rev. 150, 867 (1966)

ELEM. SYM.	A	Z
Fe		26

METHOD

Betatron

REF. NO.

66 Wa 1

JDM

REACTION	RESULT	EXCITATION ENERGY	SOURCE		DETECTOR		ANGLE
			TYPE	RANGE	TYPE	RANGE	
G,5PXN	RLY	THR-250	C	100-250	ACT-I		4PI
G,PXN	RLY	THR-250	C	100-250	ACT-I		4PI

Measured isomeric yield ratios.

TABLE III. Summary of the results for the photoproduction of the Mn^{52} isomers (spins 2 and 6).

Target isotope and spin	Bremsstrahlung energy (MeV)	Fraction of yield to high-spin isomer
$Fe^{54,56}$ $(I=0)$[a]	100	0.39±0.03
	150	0.36±0.02
	200	0.35±0.02
	250	0.37±0.02
Mn^{55} $(I=\frac{5}{2})$	100	0.44±0.04
	150	0.48±0.02
	225	0.47±0.02
	300	0.47±0.02
Co^{59} $(I=\frac{7}{2})$	150	0.62±0.02

[a] It is assumed that most of the yield is due to reactions involving the two lightest isotopes present in natural iron (Fe^{54} and Fe^{56}).

TABLE II. Summary of the results for the photoproduction of the Sc^{44} isomers (spins 2 and 6).

Target isotope and spin	Bremsstrahlung energy (MeV)	Fraction of yield to high-spin isomer
Sc^{45} $(I=\frac{7}{2})$	50	0.21±0.04
	75	0.21±0.03
	175	0.20±0.02
	223	0.18±0.01
	264	0.17±0.02
	300	0.21±0.02
$Fe^{54,56}$ $(I=0)$[a]	250	0.38±0.02
Mn^{55} $(I=\frac{5}{2})$	225	0.42±0.04
	300	0.39±0.02

[a] It is assumed that most of the yield is due to reactions involving the two lightest isotopes present in natural iron (Fe^{54} and Fe^{56}).

REF. S. Costa, F. Ferrero, C. Manfredotti, L. Pasqualini, C. Piragino, H. Arenhovel
Nuovo Cimento, 51B, 199 (1967)

ELEM. SYM.	A	Z
Fe		26

METHOD

REF. NO.	
67 Co 2	EGF

REACTION	RESULT	EXCITATION ENERGY	SOURCE		DETECTOR		ANGLE
			TYPE	RANGE	TYPE	RANGE	
G,XN	ABX	THR-24	C	11-24	BF3-I		4PI

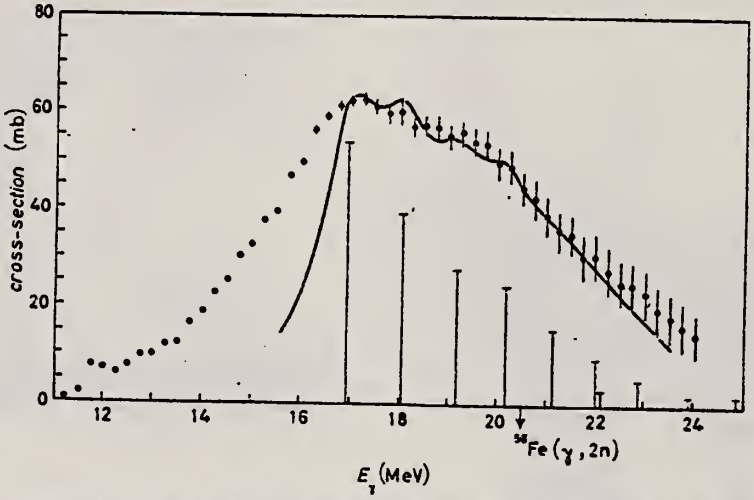

Fig. 2. – Corrected (γ, Tn) cross-section for Fe. The dipole strengths, calculated for ^{56}Fe, are indicated by the vertical bars.

REF.

C. B. Fulmer, I. R. Williams, T. H. Handley, G. F. Dell, and L. N. Blumberg
Phys. Rev. Letters 19, 522 (1967)

ELEM. SYM.	A	Z
Fe		26

METHOD

REF. NO.	
67 Fu 1	egf

REACTION	RESULT	EXCITATION ENERGY	SOURCE		DETECTOR		ANGLE
			TYPE	RANGE	TYPE	RANGE	
G,F	ABY	THR-999	D	999	ACT-I		4PI

999=3 GEV

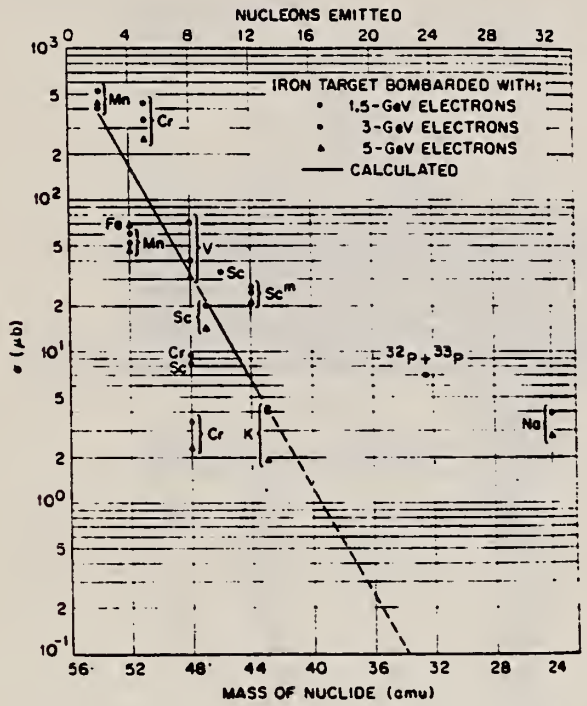

FIG. 1. Yields of radionuclides identified in iron samples that were exposed to a beam of 3-GeV electrons. The values of σ are based on the integrated electron beam intensity.

REF. N. N. Kaushal, E. J. Winhold, P. F. Yergin, H. A. Medicus and R. H. Augustson
Phys. Rev. 175, 1330 (1968)

ELEM. SYM.	A	Z
Fe		26

METHOD

REF. NO.	
68 Ka 1	HMG

REACTION	RESULT	EXCITATION ENERGY	SOURCE		DETECTOR		ANGLE
			TYPE	RANGE	TYPE	RANGE	
G,N	ABX	50-85	C	55,85	TOF-D	10-85	67
							(67.5)

NEUT ENGY SPEC

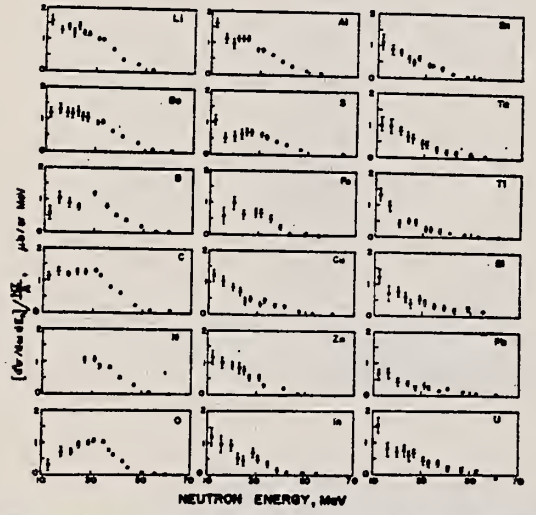

FIG. 6. Observed neutron spectra due to 55–85-MeV difference photon spectra. The effective cross sections have been divided by NZ/A.

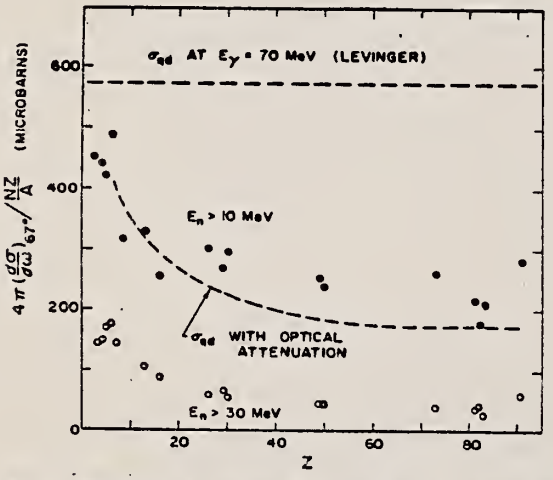

FIG. 7. Effective cross sections for production of fast neutrons with energies greater than 10 MeV (solid circles) and 30 MeV (open circles) by the 55–85-MeV photon difference spectrum. The dashed curves are modified quasideuteron model predictions as discussed in the text.

TABLE I. Comparison of present cross-section values in mb for production of high-energy photoneutrons by 55–85-MeV photons with measured cross sections $\sigma(\gamma,Tn)$, also in mb, for total photoneutron production. The present cross-section values are uncertain by 8 to 10% because of counting statistics and normalization errors; in addition all values depend on an absolute normalization in terms of the deuteron photodisintegration cross section, which is known to about 10% at these energies.

Target	$4\pi(d\sigma/d\omega)_{\pi^0}$ (E_γ > 10 MeV) [Present experiment]	$\sigma(\gamma,Tn)$ Jones and Terwilliger[a]	Costa *et al.*[b]	Other results
Li	0.75		1.0	
Be	1.0	2.7	2.3	2.3[c]
B	1.0		1.4	
C	1.5	1.3	1.4	2.4[d]
O	1.3		1.6	
Al	2.8	5.5	4.6	8[d]
S	2.1		4.4	6.5[d]
Fe	4.2	16	12	
Cu	4.3	20	19	
Zn	4.4		15	
In	7.4			
Sn	7.0			
Ta	10.7	95		
Tl	10.7			
Pb	8.3	100		
Bi	13			
U	16	65		

[a] Average cross sections between 55 and 85 MeV, as read from Figs. 4 and 5 of Ref. 4.
[b] $\int_0^{\infty}\sigma dE - \int_0^{30}\sigma dE/50$, as taken from Fig. 4 of Ref. 5 and Table I of Ref. 6.
[c] S. Costa, L. Pasqualini, G. Piragino, and L. Roasio, Nuovo Cimento 42, 306 (1966).
[d] G. Bishop, S. Costa, S. Ferroni, R. Malvano, and G. Ricco, Nuovo Cimento 42, 148 (1966).

REF.

B. S. Dolbilkin, A. I. Isakov, V. I. Korin, L. E. Lazareva, N. V. Lin'kova, and B. A. Tulupov
Yad. Fiz. 9, 675 (1969)
Sov. J. Nucl. Phys. 9, 391 (1969)

ELEM. SYM.	A	Z
Fe		26

METHOD

REF. NO.	
69 Do 2	hmg

REACTION	RESULT	EXCITATION ENERGY	SOURCE		DETECTOR		ANGLE
			TYPE	RANGE	TYPE	RANGE	
G,MU-T	ABX	10-27	C	THR-260	MGP-D		4PI
		(26.5)					

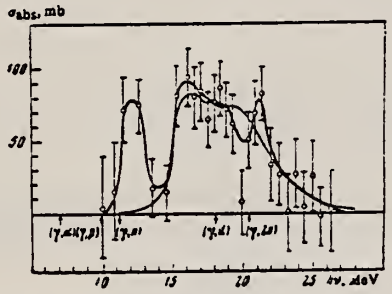

FIG. 1. γ-ray absorption cross section for Fe^{56}. The thin line shows the theoretical calculation.

Integrated cross section for photodisintegration of Fe^{56}

Experiment	δ, MeV	Γ, MeV	σ_0, mb-MeV
Present work	12.2	~2	~100
	18.1	~7	575
			$+120$ -50
(γ, Tn), [9]	18	~7	~450
(γ, Tn), [8]	18	~7	470
(γ, tot), [7]	18	9.4	760

REF.

C. B. Fulmer, I. R. Williams, K. S. Toth, G. F. Dell
Phys. Rev. 188, 1752 (1969)

ELEM. SYM.	A	Z
Fe		26

METHOD

REF. NO. 69 Fu 2 hmg

REACTION	RESULT	EXCITATION ENERGY	SOURCE TYPE	SOURCE RANGE	DETECTOR TYPE	DETECTOR RANGE	ANGLE
G,SPL	RLY	THR-999	D	999	ACT-I		DST
		(THR-3 GEV)		(3 GEV)			

Relative thick target yield as a function of target thickness. 999 = 3 GEV

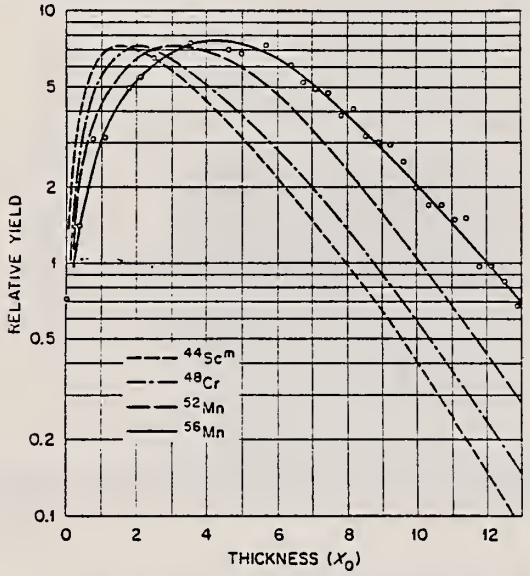

FIG. 1. Relative yields for some nuclides produced in a thick iron target bombarded with 3.0-GeV electrons. The data points shown for ^{56}Mn are typical of the data. The curves are normalized to the same ordinate value at the peaks.

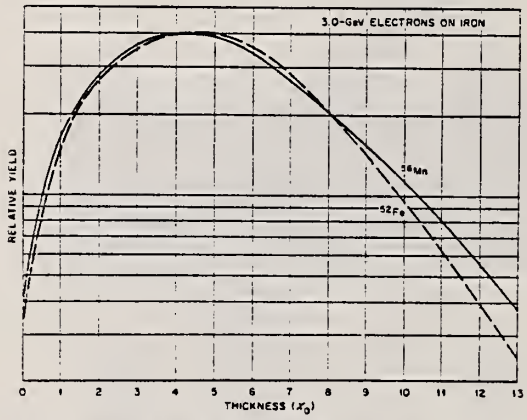

FIG. 2. Relative yields of ^{56}Mn and ^{52}Fe in a thick iron target bombarded with 3.0-GeV electrons. The curves are normalized at the peaks.

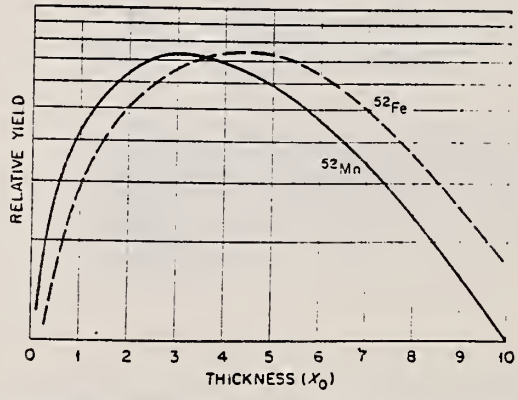

FIG. 4. Relative yields of ^{52}Fe and ^{52}Mn in a thick iron target bombarded with 3.0-GeV electrons. The curves are normalized at the peaks.

(over)

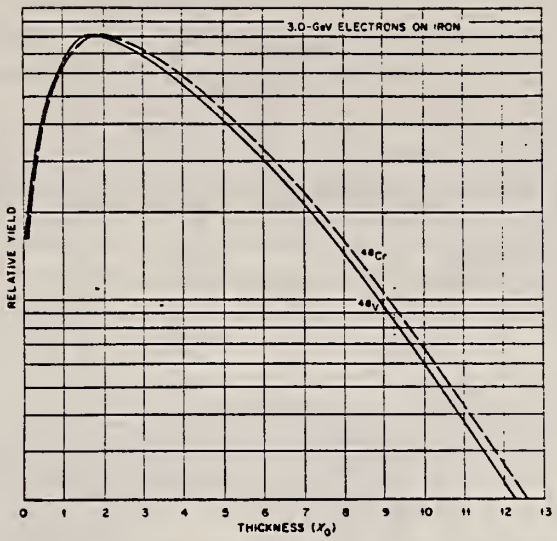

FIG. 3. Relative yields of ^{48}Cr and ^{48}V in a thick iron target bombarded with 3.0-GeV electrons. The curves are normalized at the peaks.

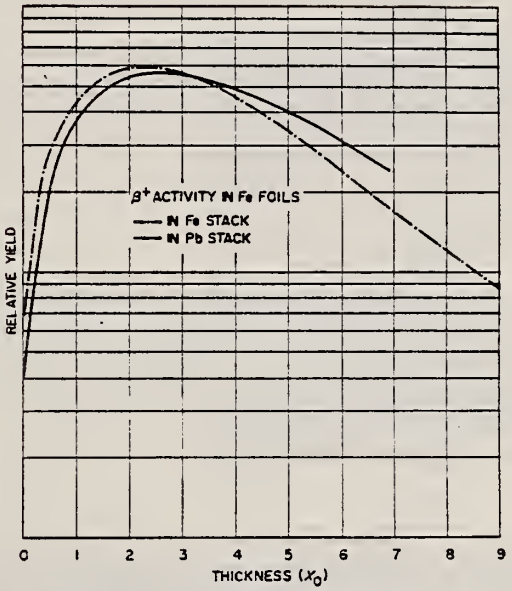

FIG. 7. Relative β^+ activity produced in iron foils in thick targets bombarded with 3.0-GeV electrons.

REF. C. B. Fulmer, K. S. Toth, I. R. Williams, T. H. Handley, G. F. Dell, E. L. Callis, T. M. Jenkins, and J. M. Wyckoff
Phys. Rev. C2, 1371 (1970)

ELEM. SYM.	A	Z
Fe		26

METHOD

REF. NO. 70 Fu 1 hmg

REACTION	RESULT	EXCITATION ENERGY	SOURCE TYPE	SOURCE RANGE	DETECTOR TYPE	DETECTOR RANGE	ANGLE
E,F	RLY	999	D	999	ACT-D		4PI

999 = 1.5-16.0 GEV

Evidence of a fissionlike process for nuclides with a mass < 35.

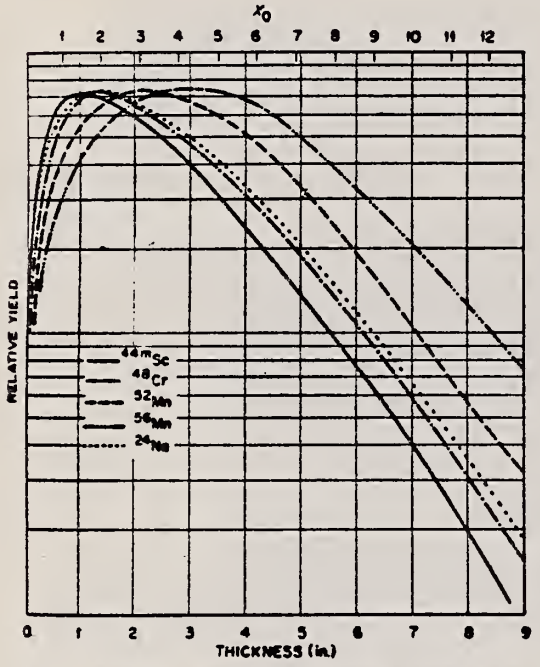

FIG. 2. Relative yields of some nuclides produced in a thick iron target bombarded with 3.0-GeV electrons. The curves are normalized to the same ordinate value at the peaks.

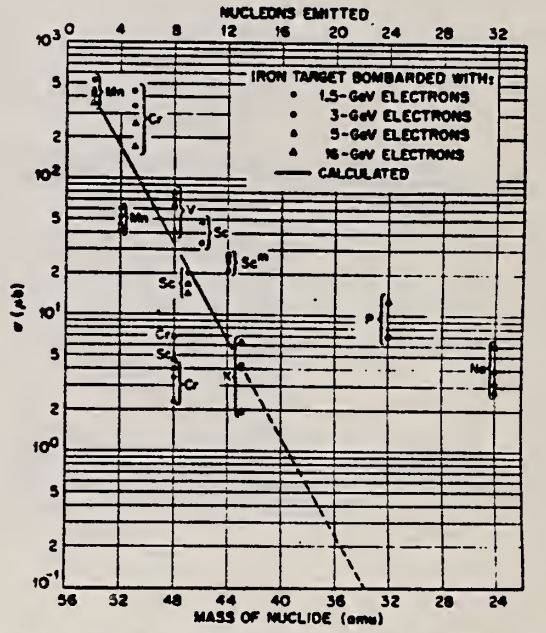

FIG. 1. Yields of radionuclides identified in iron samples that were exposed to beams of 1.5- to 16-GeV electrons. The values of σ are based on the integrated electron beam intensity. The "calculated" line is, in reality, a "calculated slope" as is described in the text.

TABLE I. Ratio of yields of nuclides used to determine values of K. ^{44}Sc yields include 4.0-h ^{44}Sc and 2.4-day ^{44}Sc^m, which for the 1.5-, 3.0-, and 5.0-GeV data were assumed to be twice the yield of ^{44}Sc^m.

Energy (GeV)	Target	Nuclides	Ratio of yields (experimental)	$\Delta Z_1 - \Delta Z_2$	K
1.5	iron	^{51}Cr/^{44}Sc	6.2	3	1.86
3.0	iron	^{51}Cr/^{44}Sc	8.4	3	2.03
5.0	iron	^{51}Cr/^{44}Sc	5.95	3	1.82
16	iron	^{51}Cr/^{44}Sc	4.0	3	1.59
16	aluminum	^{22}Na/^{18}F	2.7	2	1.64
0.32	arsenic		(Halpern *et al.*)[a]		2.3

[a] See Ref. 19. I. Halpern, R. J. Debs, J. T. Eisinger, A. W. Fairhall, and H. G. Richter, Phys. Rev. 97, 1327 (1955).

[over]

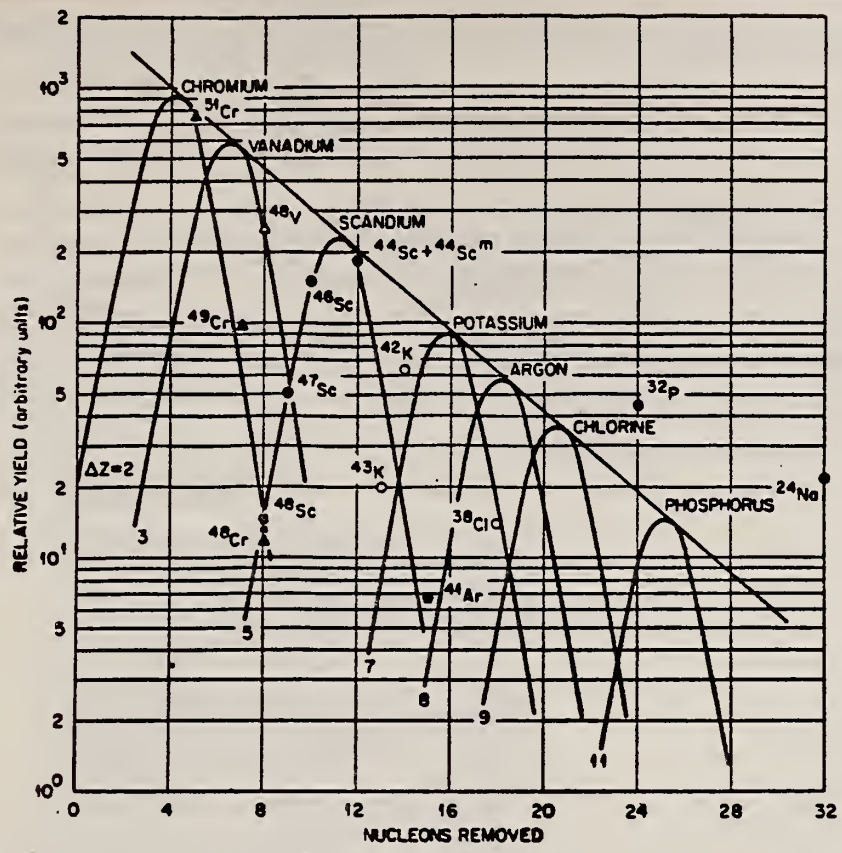

FIG. 3. Yields of radionuclides observed in a thin iron target bombarded with 16.0-GeV electrons versus the number of nucleons removed. The abscissa scale refers to ^{56}Fe.

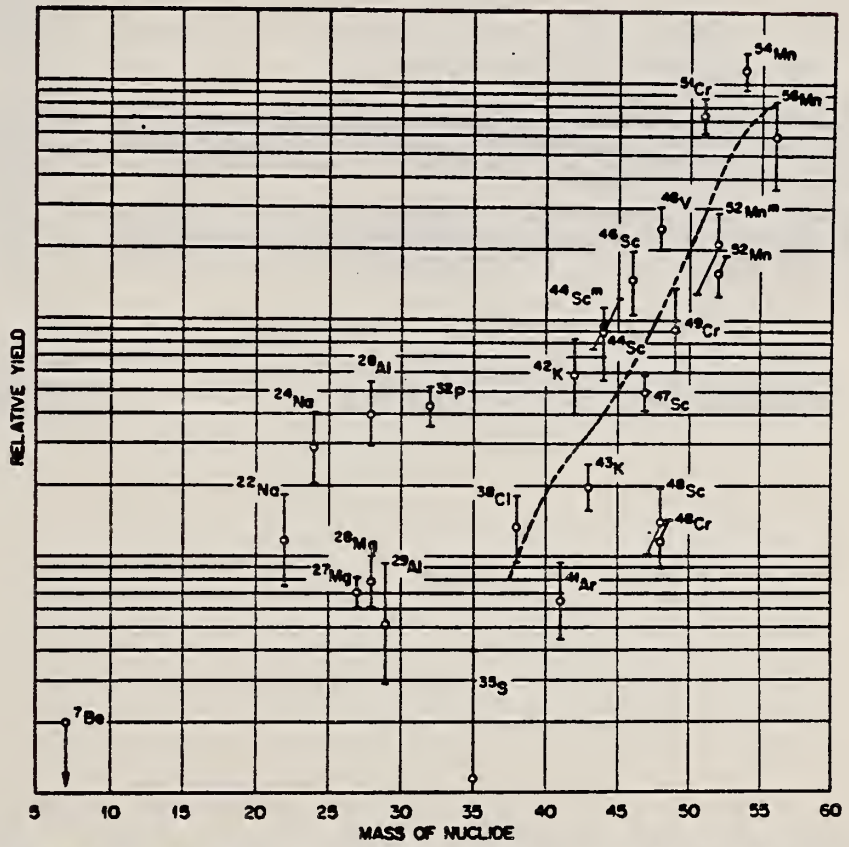

FIG. 5. Yield of radionuclides observed in a thin iron target bombarded with 16-GeV electrons versus mass of the nuclide. The dashed curve is the prediction of a nuclear evaporation theory (Ref. 20).

[20] I. Dostrovsky, Z. Fraenkel, and G. Friedlander, Phys. Rev. 116, 683 (1959).

S. Costa, L. Ferrero, L. Pasqualini, and E. Mancini
Lettere al Nuovo Cimento 2, 665 (1971)

ELEM. SYM.	A	Z
Fe	.	26

METHOD

REF. NO.	
71 Co 2	egf

REACTION	RESULT	EXCITATION ENERGY	SOURCE		DETECTOR		ANGLE
			TYPE	RANGE	TYPE	RANGE	
G,XN	ABI	36-64	C	10-64	BF3-I		4PI

FAST N YIELD

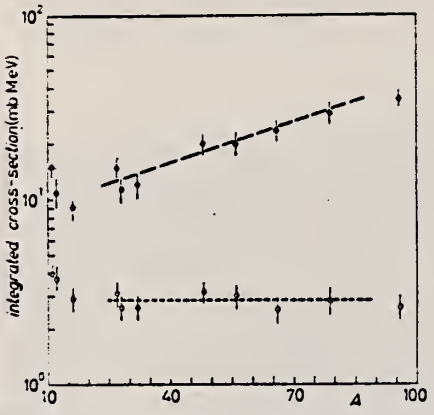

Fig. 2.

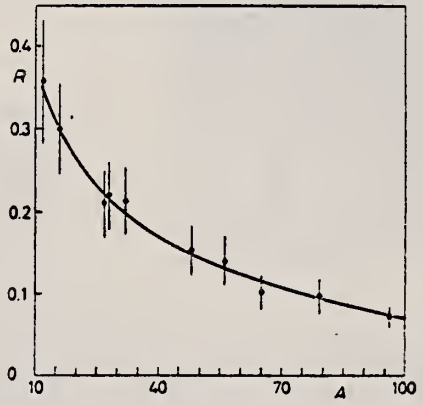

Fig. 3.

Fig 2. – Experimental photoneutron cross-sections integrated over photon energy between 36 and 64 MeV and divided by NZ/A are plotted as a function of the mass number. Black dots are total cross-sections not corrected for neutron multiplicity; open circles represent fast neutron cross-sections (see text). The dashed lines are drawn only to guide the eye.

Fig. 3. – The ratio between « fast » and total photoneutron integrated cross-sections as a function of the mass number A. The solid line represents a fit of the ratios calculated for some nuclei by taking into account the theoretical neutron energy spectra given by GABRIEL and ALSMILLER (*) and the efficiencies of our detector (see Fig. 1).

REF. C.B. Fulmer, K.S. Toth, I.R. Williams, G.F. Dell, T.M. Jenkins
Phys. Rev. C3, 1955 (1971)

ELEM. SYM.	A	Z
Fe		26

METHOD

REF. NO.	
71 Fu 1	hmg

REACTION	RESULT	EXCITATION ENERGY	SOURCE		DETECTOR		ANGLE
			TYPE	RANGE	TYPE	RANGE	
E,SPL	ABI	THR-999	D	40-999	SCD-D		4PI

999 = 16 GEV

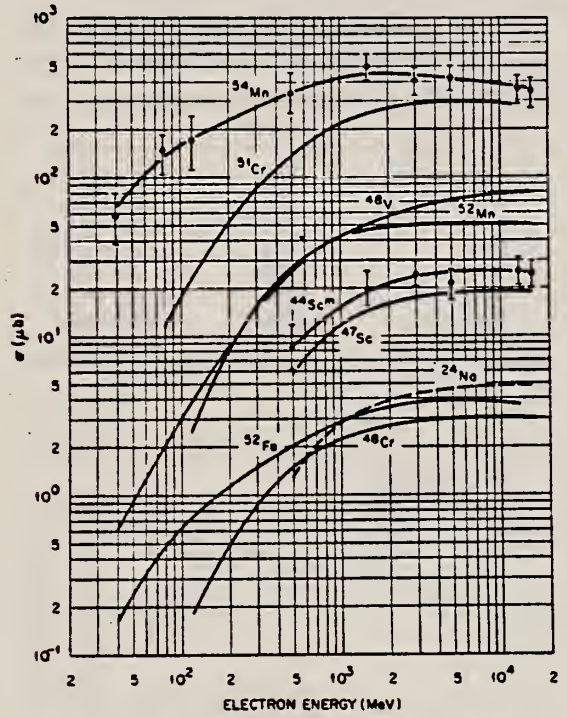

FIG. 1. Yields of some nuclides produced in thin iron targets bombarded with electrons. The yields are plotted as cross sections based on the integrated intensity of the electron beams used.

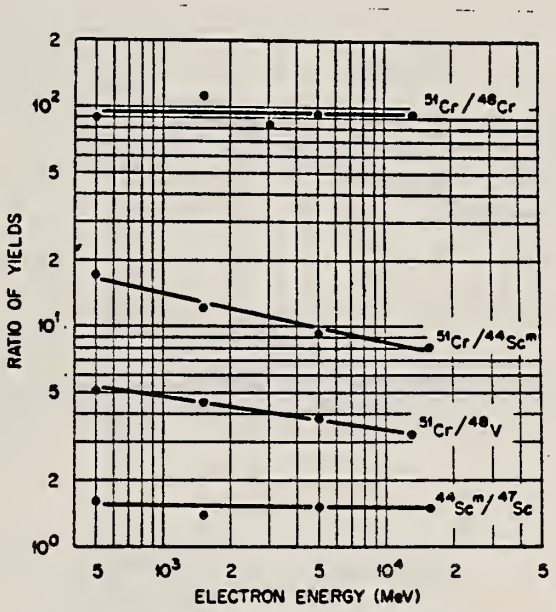

FIG. 2. Ratios of yields of pairs of nuclides produced in thin iron targets bombarded with electrons.

REF.

C. B. Fulmer, K. S. Toth, I. R. Williams, and G. F. Dell
Phys. Rev. C4, 2123 (1971)

ELEM. SYM.	A	Z
Fe		26

METHOD

REF. NO.	
71 Fu 4	hmg

REACTION	RESULT	EXCITATION ENERGY	SOURCE		DETECTOR		ANGLE
			TYPE	RANGE	TYPE	RANGE	
G,SPL	RLX	THR-999	D	999	ACT-I		4PI
		(5 GEV)		(5 GEV)			

Measurement of F values (the ratio of photodisintegration to electrodisintegration cross sections).

999= 5 GEV

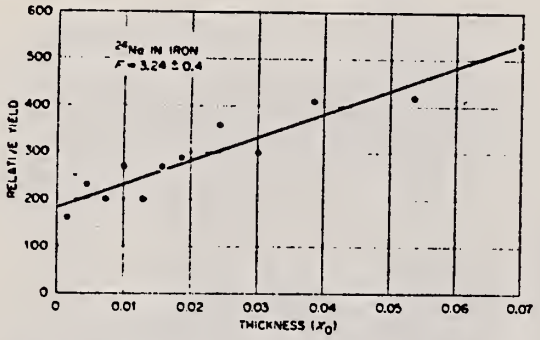

FIG. 3. Relative yields vs target thickness of ^{24}Na in an iron target bombarded with 5-GeV electrons.

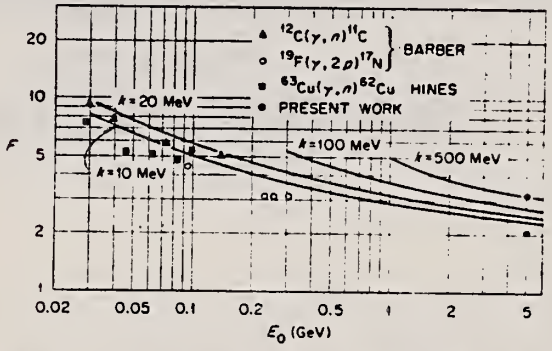

FIG. 5. Calculated F values for $E1$ excitation in iron as a function of incident electron energy. The experimental data for ^{63}Cu are presented in Ref. 1; the experimental data for ^{12}C and ^{19}F are presented in Ref. 3.

TABLE I. Experimentally measured F values for several nuclides produced in targets bombarded with 5-GeV electrons.

Target	Nuclide	F
Aluminum	^{24}Na	2.4 ± 0.4
Aluminum	^{7}Be	3.3 ± 0.5
Iron	^{52}Mn	2.0 ± 0.3
Iron	^{48}Cr	2.0 ± 0.2
Iron	^{44m}Sc	2.4 ± 0.4
Iron	^{24}Na	3.2 ± 0.4
Tantalum	^{175}Hf	2.0 ± 0.3
Tantalum	^{177}Lu	1.9 ± 0.4

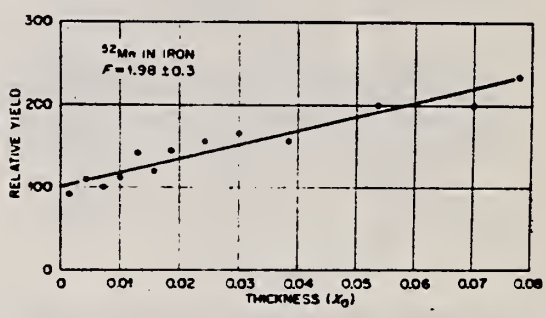

FIG. 1. Relative yields vs target thickness of ^{52}Mn in an iron target bombarded with 5-GeV electrons.

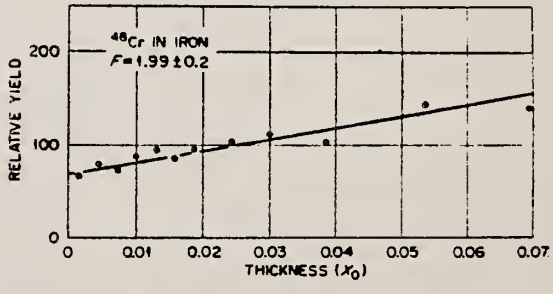

FIG. 2. Relative yields vs target thickness of ^{48}Cr in an iron target bombarded with 5-GeV electrons.

REF. G. J. Kumbartzki, Ung Kim and Ch. K. Kwan
Nucl. Phys. A160, 237 (1971)

ELEM. SYM.	A	Z
Fe		26

METHOD

REF. NO. 71 Ku 2 egf

REACTION	RESULT	EXCITATION ENERGY	SOURCE TYPE	SOURCE RANGE	DETECTOR TYPE	DETECTOR RANGE	ANGLE
G,SPL	ABY	THR-999	C	999	ACT-I		4PI

$\sigma_q(A,Z) = K\exp\left[PA-R(A-SZ+TZ^2)^2\right]$, cross section per equivalent quantum. 999 = 1.5 GEV

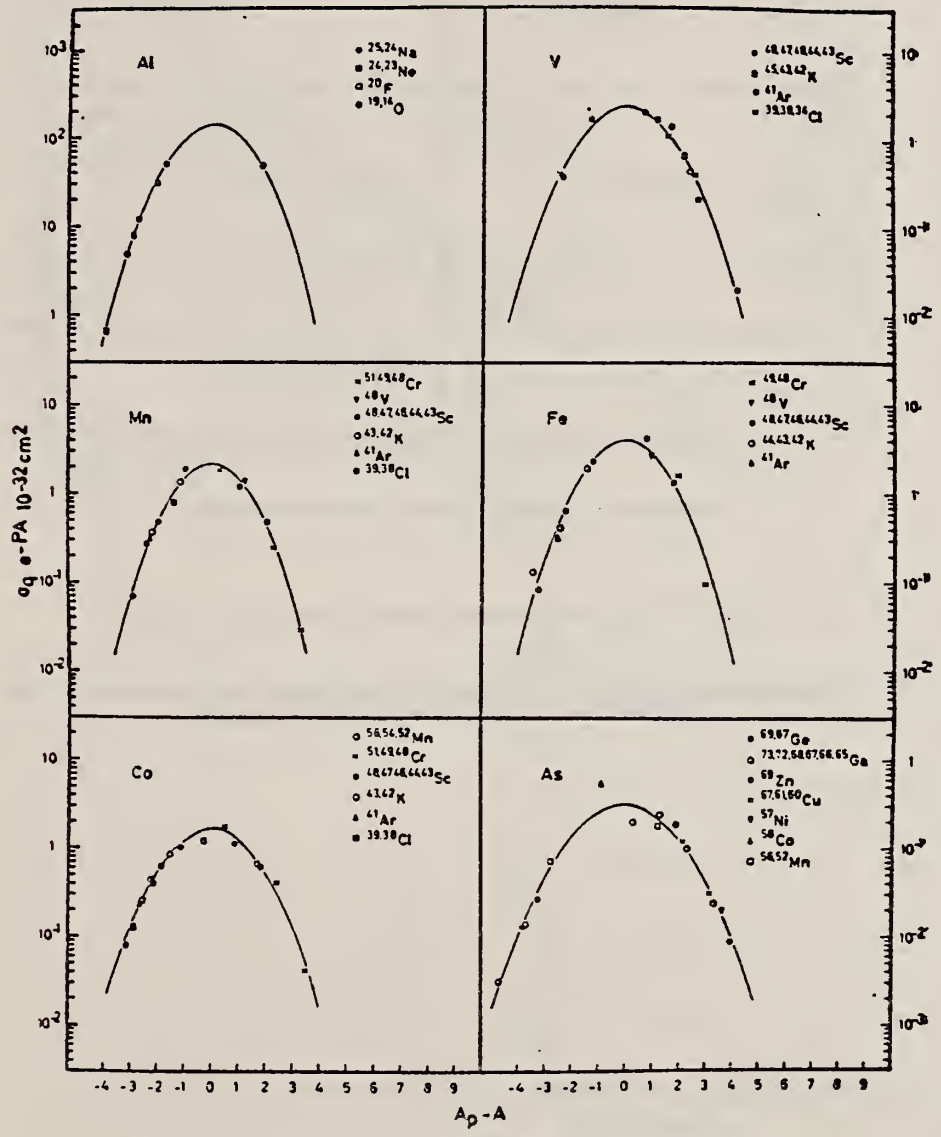

Fig. 4. Yield distributions from various targets with bremsstrahlung of 1.5 GeV.

[over]

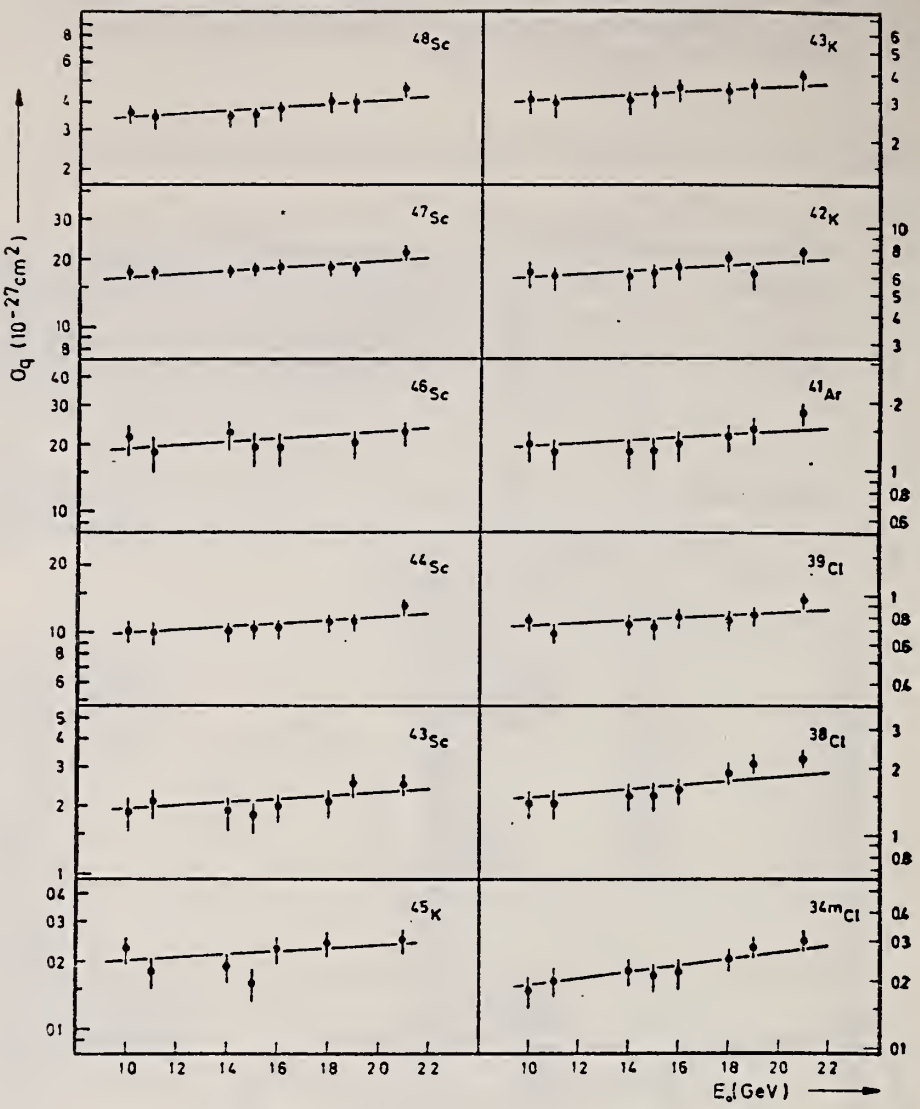

Fig. 5. Yields of spallation products using vanadium targets.

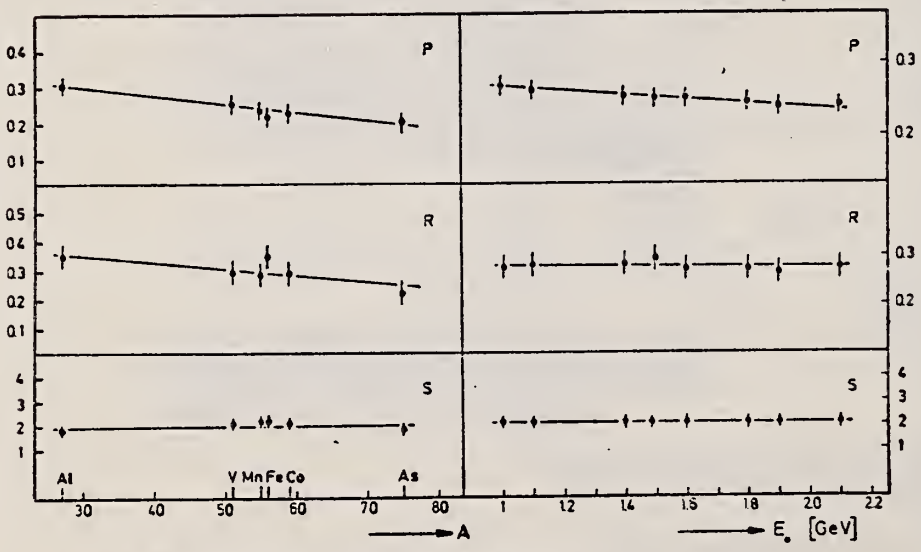

Fig. 6. Behaviour of the parameters P, R and S as functions of A and E_o.

REF.

G. Kumbartzki and U. Kim
Nucl. Phys. A176, 23 (1971)

ELEM. SYM.	A	Z
Fe		26

METHOD

REF. NO.	
71 Ku 5	egf

	REACTION	RESULT	EXCITATION ENERGY	SOURCE		DETECTOR		ANGLE
				TYPE	RANGE	TYPE	RANGE	
*	G,SPL	ABY	THR-999	C	999	ACT-I		4PI
**	G,PI+	ABY	THR-999	C	200-999	ACT-I		4PI

* 999= 1.5 GEV
** 999= 2.2 GEV

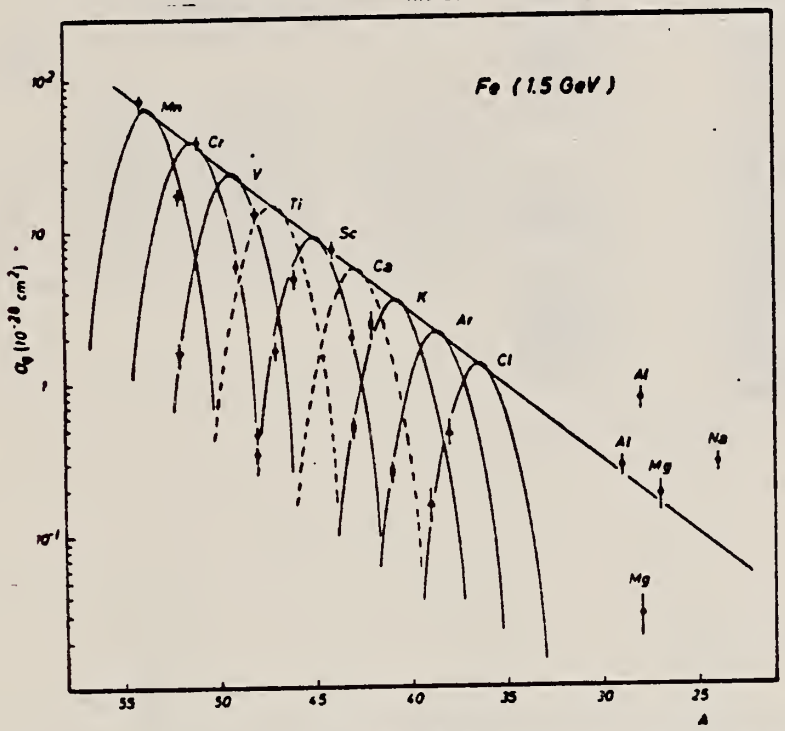

Fig. 3. Photonuclear yields obtained from iron target with 1.5 GeV bremsstrahlung are plotted as a function of the mass number *A* of the residual nucleides.

(over)

TABLE I

Decay data and yields of radioactive nucleides in vanadium and iron at 1.5 GeV bremsstrahlung energy

Nuclide	Half-life	Gamma-energy (keV)	Intensity	σ_q (10^{-28} cm^2) (vanadium)	σ_q (10^{-28} cm^2) (iron)
^{53}Fe	8.6 min	380.0	32		12.6 ±1.6
^{52}Fe	8.2 h	168.1	100		0.40±0.05
^{56}Mn	2.57 h	846.7	100		3.5 ±0.4
^{54}Mn	312 d	834.8	100		72.0 ±9.0
^{52m}Mn	21 min	1434.4	98		9.1 ±1.0
^{52}Mn	5.7 d	1434.4	100		7.9 ±0.9
^{51}Cr	27.8 d	320.1	9		39 ±4
^{49}Cr	42 min	153.6	13	0.77±0.09	5.9 ±0.6
^{48}Cr	23 h	307.8	99		0.46±0.6
^{48}V	16 d	983.7	100	10.2 ±1.3	12.8 ±1.4
^{52}V	3.8 min	1434.4	100		1.6 ±0.3
^{51}Ti	5.8 min	320.1	95	0.31±0.07	
^{48}Sc	1.83 d	1038.5	100	3.49±0.43	0.34±0.06
^{47}Sc	3.4 d	159.4	70	18.2 ±2.7	1.63±0.20
^{46}Sc	83.9 d	1120.0	100	19.4 ±3.3	4.8 ±0.7
^{44m}Sc	2.44 d	270.8	86	5.2 ±0.7	3.8 ±0.4
^{44}Sc	3.92 h	1156.9	100	5.2 ±0.8	4.1 ±0.5
^{43}Sc	3.92 h	372.8	22	1.8 ±0.2	1.9 ±0.3
^{43}K	22.4 h	617.2	81	3.1 ±0.4	0.51±0.08
^{42}K	12.4 h	1524.7	18	6.2 ±0.9	2.4 ±0.5
^{44}K	22 min	1156.9	61	1.7 ±0.3	
^{45}K	20 min	175	80	0.20±0.05	
^{41}Ar	1.83 h	1293.0	99	1.24±0.23	0.26±0.04
^{39}Cl	55.5 min	1266.4	50	0.71±0.12	0.16±0.04
^{38}Cl	37.3 min	1642.2	33	1.47±0.21	0.48±0.09
^{34m}Cl	32 min	147.2	45	0.21±0.04	
^{29}Al	6.6 min	1273.1	94	0.41±0.09	0.28±0.08
^{28}Al	2.3 min	1778.7	100	0.86±0.15	0.78±0.12
^{28}Mg	21 h	1342.0	70	0.09±0.03	0.03±0.01
^{27}Mg	9.5 min	843.2	70	0.42±0.07	0.18±0.04
^{24}Na	15 h	1368.5	100	0.51±0.08	0.29±0.04
^{24}Ne	3.4 min	472.0	100	0.04±0.01	

REF.

N. A. Keller and D. B. McConnell
Can. J. Phys. 50, 1554 (1972)

ELEM. SYM.	A	Z
Fe		26

METHOD

REF. NO.
72 Ke 4 hmg

REACTION	RESULT	EXCITATION ENERGY	SOURCE		DETECTOR		ANGLE
			TYPE	RANGE	TYPE	RANGE	
G,A	RLY	7-32	C	32	SCD-D		DST

TABLE 3. Observed angular distribution parameters for 32 MeV electron energy

Element	A_0	A_1/A_0	A_2/A_0
Ti	7.03 ± 0.15	0.073 ± 0.052	−0.286 ± 0.073
V	2.58 ± 0.06	0.037 ± 0.042	−0.126 ± 0.069
Fe	10.22 ± 0.30	0.006 ± 0.043	−0.333 ± 0.072
Co	6.80 ± 0.20	0.022 ± 0.048	+0.016 ± 0.077
Ni	15.95 ± 0.49	0.051 ± 0.048	−0.213 ± 0.074
Cu	8.37 ± 0.28	0.076 ± 0.056	−0.035 ± 0.081
Zn	17.87 ± 0.61	0.004 ± 0.045	−0.270 ± 0.073
Ag	0.39 ± 0.01	0.115 ± 0.049	+0.093 ± 0.074

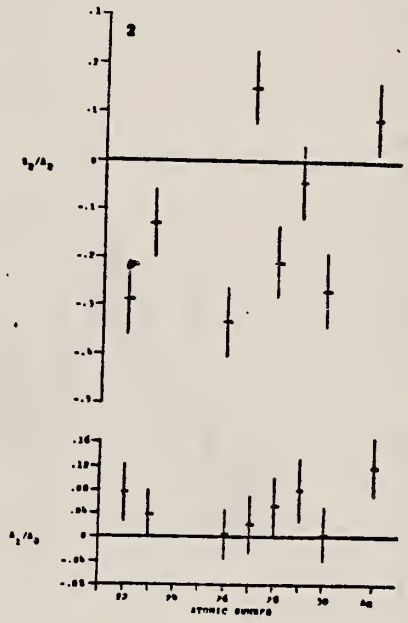

FIG. 2. Angular distributions for 32 MeV electron energy.

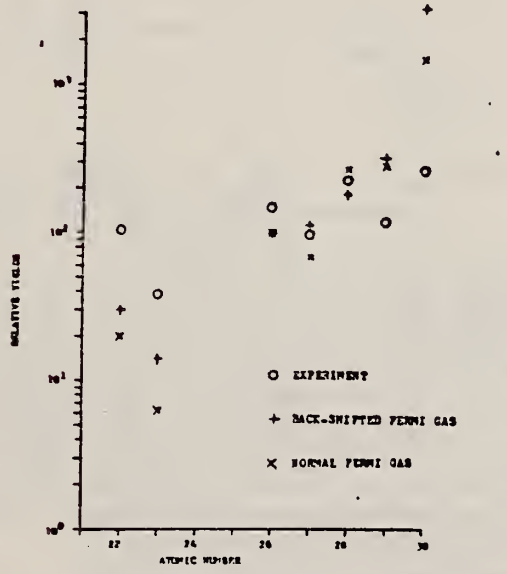

FIG. 13. Experimental and theoretical relative photo-alpha yields for 32 MeV electron beam energy.

R.F. Barrett, J.R. Birkelund, B.J. Thomas, K.S. Lam, and H.H. Thies
Nucl. Phys. A210, 355 (1973)

ELEM. SYM.	A	Z
Fe		26

METHOD	REF. NO.	
	73 Ba 20	egf

REACTION	RESULT	EXCITATION ENERGY	SOURCE		DETECTOR		ANGLE
			TYPE	RANGE	TYPE	RANGE	
G,N	NOX	THR- 27	C	10- 27	BF3-I		4PI

MEAN NEUT ENERGY

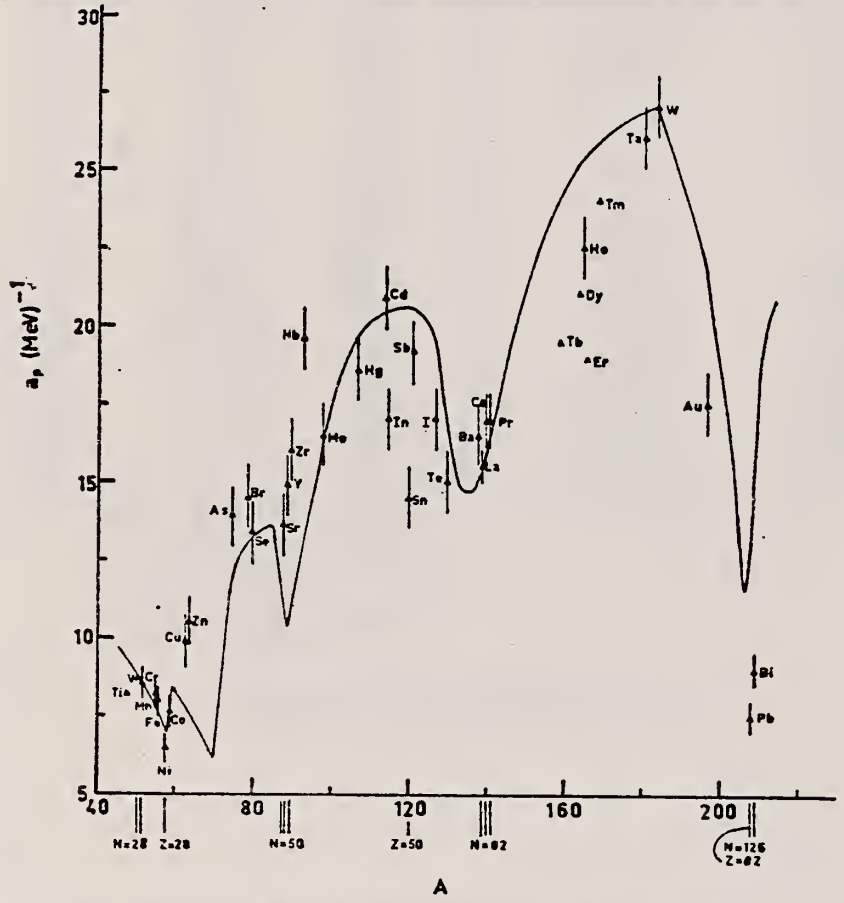

Fig. 12. Experimental values of the level density parameter a_p (Fermi gas formula plus pairing correction) versus atomic number A. The continuous curve is a least-squares fit to the data of a theoretical calculation from Newton [15]).

1
H. Baba and S. Baba, Japan Atomic Energy Research Institute report JAERI-1183 (1969).
2
H. Baba, Nucl. Phys. A159, 625 (1970).
15
T.D. Newton, Can. J. Phys. 34, 804 (1956).

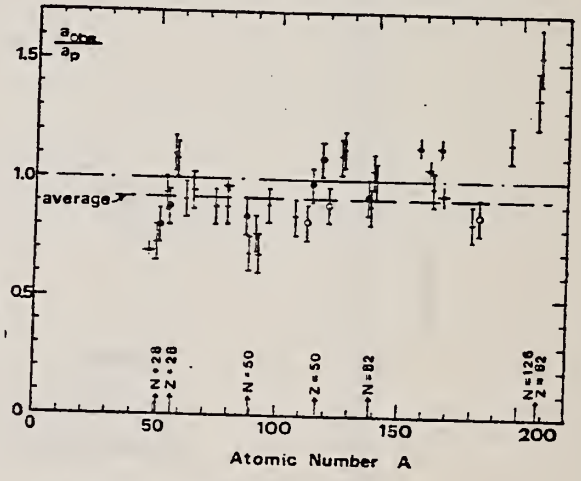

Fig. 15. Ratio a_{obs}/a_p versus atomic number A. Here a_{obs} is the level density parameter taken from the neutron resonance work of refs. [1,2]), and a_p is the level density parameter derived from the present (γ, n) work. Filled circles represent points where nuclei in the neutron resonance and in the (γ, n) experiment were the same. Open circles represent points where the respective nuclei were approximately matched. Triangles represent points which are based on measurement of neutron mean energies at two bremsstrahlung energies only.

(over)

TABLE 3

Comparison of experimental and theoretical data on nuclear level densities with Fermi gas formulae, and comparison of nuclear level density parameters from (γ, n) and n-resonance absorption experiments

Target	N (residual nucleus) [a]		Goodness of fit [b]		$\hat{E}_n(24)$ (MeV) [c]	T (MeV) [d]	a_p (MeV^{-1}) [e]	a_{obs} (MeV^{-1}) [f]	a_{obs}/a_p
			no p.c.	with p.c.					
Ti [g]	23	8%			1.93		8.1–^{47}Ti	6.41–^{47}Ti	0.79
	24	8%							
	25	73%							
	26	5%							
	27	5%							
V [g]	27	100%			1.96		8.7–^{50}V	6.35–^{51}V	0.73
Cr	25	4%	P	G	1.89		8.6–^{51}Cr	6.9 –^{51}Cr	0.80
	27	84%							
	28	10%							
	29	2%							
Mn	29	100%	V.P.	G	2.1		8.2–^{54}Mn	7.82–^{56}Mn	0.94
Fe	27	6%	F	G	1.96		8.0–^{55}Fe	7.06–^{55}Fe	0.88
	29	92%							
	30	2%							
Co	31	100%	P	F	2.12		7.7–^{58}Co	8.35–^{60}Co	1.08
Ni ($Z = 28$)	29	68%	V.P.	P	2.04	1.4	6.5–$^{57.7}$Ni	7.19–^{59}Ni	1.10
	31	26%							
	32	1%							
	33	4%							
	35	1%							
Cu	33	69%	V.P.	P	1.78	1.0	9.8–^{62}Cu	8.90–^{64}Cu	0.91
	35	31%							
Zn	33	49%	F	F	1.61		10.5–$^{64.4}$Zn	10.0–^{65}Zn	0.95
	35	28%							
	36	4%							
	37	19%							
As	41	100%	V.P.	F	1.44		14.5–^{74}As	12.81–^{76}As	0.88
Se [g]	41	9%			1.39		13.3–^{78}Se	12.8 –^{78}Se	0.97
	42	8%							
	43	24%							
	45	50%							
	47	9%							
Br	43	45%	V.P.	V.P.	1.41		14.5–^{79}Br	12.69–^{80}Br	0.88
	45	49%							
Sr	47	10%	F	G	1.31		13.6–^{87}Sr	11.4 –^{87}Sr	0.84
	48	7%							
	49	83%							

[a]) Neutron numbers and abundances of respective residual nuclei in (γ, n) experiments.

[b]) These give an assessment of the goodness of fit of a calculated $\hat{E}_n$ versus E_0 curve to the observed data, using the Fermi gas level density formula both without and with pairing corrections.

[c]) Bremsstrahlung photoneutron mean energies $\hat{E}_n$ for peak bremsstrahlung energy $E_0 = 24$ MeV.

[d]) Nuclear temperature from fit with constant-temperature formula.

[e]) Level density parameter a_p derived from the present (γ, n) experiment, using a Fermi gas formula plus pairing correction, and corresponding residual nucleus (the atomic weight shown is the weighted average of atomic weights of the respective isotopes present).

[f]) As column 7, but using data on n-resonance absorption from refs. [1, 2]).

[g]) Measurements of $\hat{E}_n(E_0)$ for these nuclei were made only for $E_0 = 21$, 23 and 24 MeV.

REF. A. I. Abramov, V. Ya. Kitaev, M. G. Yutkin
Yad. Fiz. 20, 438 (1974)
Sov. J. Nucl. Phys. 20, 236 (1975)

ELEM. SYM.	A	Z
Fe		26

METHOD

REF. NO. 74 Ab 11 hmg

REACTION	RESULT	EXCITATION ENERGY	SOURCE TYPE	SOURCE RANGE	DETECTOR TYPE	DETECTOR RANGE	ANGLE
G,N	ABX	11 - 13	C	11, 13	TOF-D		78
		(11.2-12.5)		(11.5,12.5)			

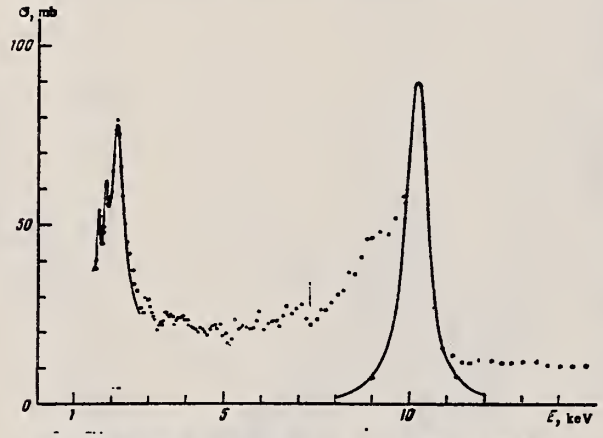

FIG. 3. Differential cross sections for the (γ,n) reaction in iron, measured for E_γ^{max} = 12.5 MeV at an angle of 70° and multiplied by 4π; the smooth curve is a fit by the Breit-Wigner formula (in the vicinity of the peak at ~10 keV the experimental points lie satisfactorily on a Breit-Wigner curve).

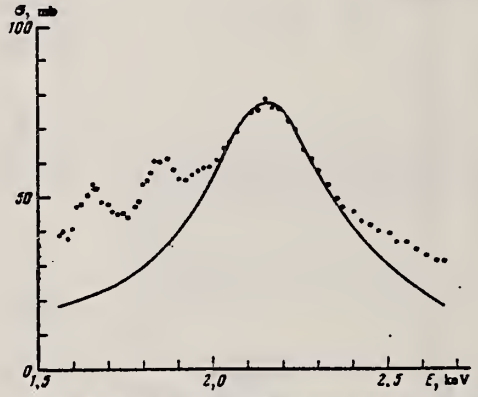

FIG. 4. The same data as in Fig. 3 in the neutron-energy region from 1.5 to 3 keV. The solid curve shows the result of describing the resonance at E_L^0 = 2.16 keV by a Breit-Wigner formula with a constant component σ_C = 10 mb.

TABLE I

E_L^0, keV		E_C^0, keV		E_L^0, keV		E_C^0, keV	
Present work	[2, 4]	Present work	[2, 4]	Present work	[2, 4]	Present work	[2, 4]
—	1.05	—	1.28	—	14.7	—	15.9
1.65	1.25	1.62	1.51	20.5	21.0	20.6	22.3
1.86	1.65	1.83	1.94	—	23.5	—	24.9
2.16	1.92	2.13	2.22	26.5	—	26.7	—
—	2.20	—	2.54	—	27.0	—	28.5
—	2.95	—	2.95	31.6	31.0	31.8	32.6
—	3.40	—	3.40	43.5	(43)	44.0	(45.1)
—	4.0	—	4.0	49.8	(50)	50.0	(52.4)
—	5.35	—	5.35	63.8	—	64.5	—
6.85	—	6.83	—	—	83.1	—	86.6
9.59	8.80	9.59	9.55	—	97.6	—	101.5
10.15	9.80	10.16	10.62	109.6	105	111	109
—	10.65	—	11.5	—	124	—	129
—	11.30	—	12.2	136	132	138	137

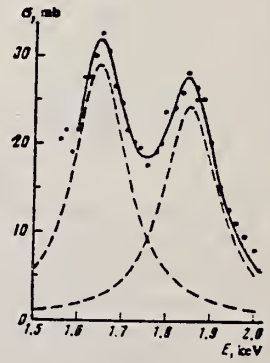

FIG. 5. Results of analysis of the resonances at E_L^0 = 1.65 and 1.86 keV.

[2] C.D. Bowman et al., Phys. Rev. 163, 951 (1967)
[4] R.J. Baglan et al., Phys. Rev. C3, 672 (1971)

TABLE II

E_L^0, keV	Γ, eV		σ_0, mb		$g_J\Gamma_n\Gamma_\gamma/\Gamma$, eV	
	Present work	[2]	Present work	[2]	Present work	[2]
1.65	145±32	—	29.6±4.2	—	0.11±0.03	—
1.86	148±27	—	24.7±2.7	—	0.092±0.019	—
2.16	451±78	415	68±12	75	0.79±0.18	0.80
10.15	536±54	560^{+100}_{-80}	118±15	136	1.62±0.23	1.93

REF. A.I. Abramov, V.Ya. Kitaev, and M.G. Yutkin
Izv. Akad. Nauk SSSR. Ser. Fiz. 38, 2112 (1974)
Bull. Acad. Sci. USSR Phys. Ser. 38, 85 (1974)

ELEM. SYM.	A	Z
Fe		26

METHOD

REF. NO. 74 Ab 12 hmg

REACTION	RESULT	EXCITATION ENERGY	SOURCE		DETECTOR		ANGLE
			TYPE	RANGE	TYPE	RANGE	
G,N	ABX	11- 13	C	11, 13	TOF-D		78
		(11.2-12.5)		(11.5-12.5)			

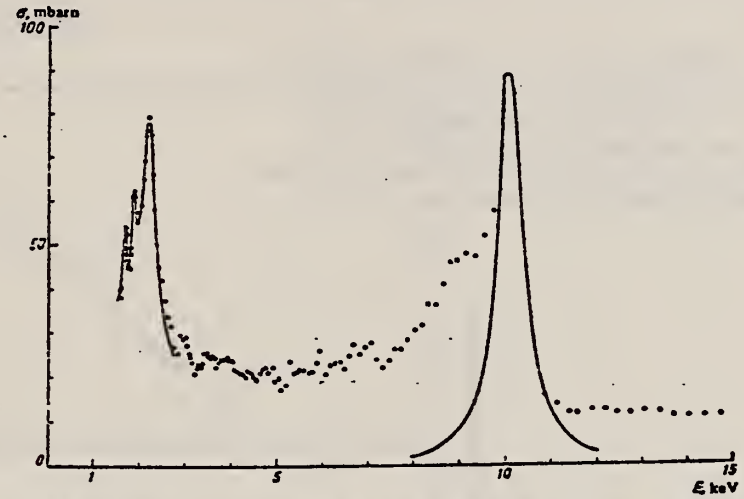

Fig. 2. Differential (γ, n) cross sections for iron at E_{γ}^{max} = 12.5 MeV at 78° and multiplied by 4π.

TABLE 1

Energy Levels of ^{56}Fe

E_L^0, keV	E_c, keV		E, MeV **	E_L^0, keV	E_c, keV		E, MeV **
	our results	[1, 2] *			our results	[1, 2] *	
1,65	1,62	1,51	11,2036	26,5	26,7	—	11,229
1,86	1,83	1,94	11,2039	31,6	31,8	32,6	11,234
2,16	2,13	2,22	11,2042	43,5	44,0	(45,1)	11,247
6,85	6,83	—	11,2089	49,8	50,0	(52,4)	11,253
9,59	9,59	9,55	11,2118	63,8	64,5	—	11,268
10,15	10,16	10,62	11,2124	109,6	111	109	11,313
20,5	20,6	22,3	11,223	136	138	137	11,342

*The results of [1, 2] have been taken selectively. The values in parentheses are for levels shown in the figures in [1] but without numerical data.
**On the assumption that all the observed resonances relate to ^{56}Fe, for which Q_n = 11.202 MeV [9].

TABLE 2

Resonance Parameters of Four Levels of ^{56}Fe

E_L^0, keV	Γ, eV		σ_0, mbarn		$g_\gamma\Gamma_{\gamma 0}$, eV	
	our results	[1]	our results	[1]	our results	[1]
1,65	145±32	—	29,6±4,2	—	0,11±0,03	—
1,88	148±27	—	24,7±2,7	—	0,092±0,019	—
2,16	451±76	415	68±12	75	0,79±0,18	0,80
10,15	536±54	560^{+100}_{+60}	118±15	136	1,62±0,23	1,93

[1] C.D. Bowman et al., Phys. Rev. 163, 951 (1967).
[2] R.J. Baglin et al., Phys. Rev. C3, 672 (1971).
[9] N.B. Gove et al., Nucl. Data Tables, Vol. II, 127 (1972).

REF.		ELEM. SYM.	A	Z
	M. Eriksson and G. G. Jonsson Nucl. Phys. A242, 507 (1975)	Fe		26
METHOD		REF. NO.		
		75 Er 2		egf

REACTION	RESULT	EXCITATION ENERGY	SOURCE		DETECTOR		ANGLE
			TYPE	RANGE	TYPE	RANGE	
G,SC44	ABY	THR-800	C	250-800	ACT-I		4PI

ISOMER RATIO

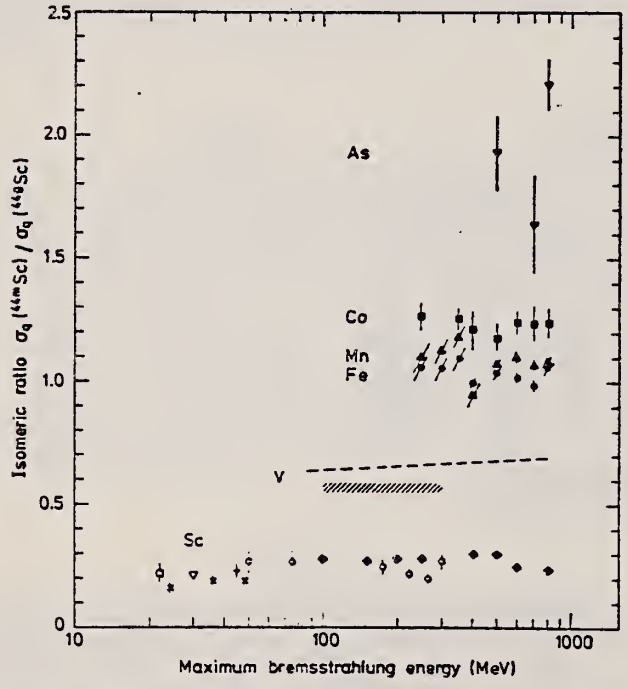

Fig. 6. Isomeric ratio $\sigma_q(^{44m}Sc)/\sigma_q(^{44g}Sc)$ versus bremsstrahlung end-point energy for the different targets. Sc target: ◆ – this work, □ – ref. [15], × – ref. [16]), ▽ – ref. [17]), + – ref. [18]), ○ – ref. [19]); V target: dashed curve – ref. [20]), dashed area – ref. [21]); Fe target: ● – this work; Mn target: ▲ – this work; Co target: ■ – this work; As target: ▼ – this work.

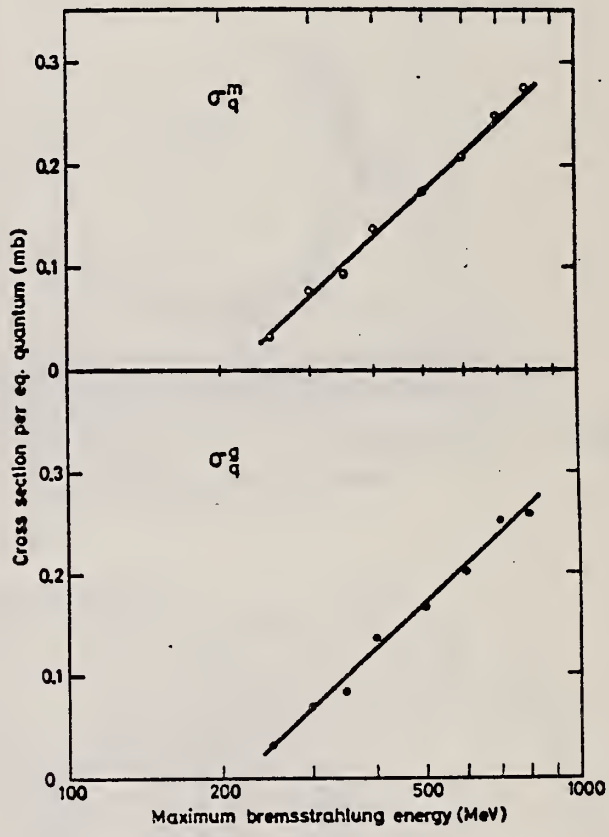

Fig. 4. Yield curves for the reaction $\gamma + Fe \rightarrow {}^{44}Sc$.

(over)

TABLE 2

Comparison between experimental and calculated cross sections and isomeric ratios

Target	$\bar{\sigma}_{exp}$ (mb) 250–800 MeV	σ_{MC} (mb) 400 MeV	$\bar{\sigma}_{SE}$ (mb) 250–800 MeV	$\sigma(m)/\sigma(g)_{exp}$ 250–800 MeV	$\sigma(m)/\sigma(g)_{calc}$ 400 MeV
^{45}Sc	≈ 0.5	0.58 ± 0.05		≈ 0	0.05
^{51}V	≈ 0.5	0.48 ± 0.05	0.47	0.7	0.72
^{55}Mn	0.40 ± 0.14	0.59 ± 0.05	0.28	1.08 ± 0.04	1.04
Fe	0.40 ± 0.14		0.26	1.00 ± 0.05	
^{59}Co	0.26 ± 0.10	0.34 ± 0.04 0.65 ± 0.07 a)	0.18	1.26 ± 0.06	1.12 1.15 a)
^{75}As		0.01 ± 0.01	0.044	1.9 ± 0.3	

a) 325 MeV.

15) S. A. Steinberg, B. Sc. thesis, Univ. of Illinois, 1963, unpublished (value taken from ref. [19])
16) J. R. Tatarczuk and H. A. Medicus, Phys. Rev. 143 (1966) 818
17) T. Kato and Y. Oka, Talanta 19 (1972) 515
18) R. Völpel, Nucl. Phys. A182 (1972) 411
19) W. B. Walters and J. P. Hummel, Phys. Rev. 150 (1966) 867
20) B. Bülow, Lund, private communication (preliminary results)
21) R. A. Meyer, thesis, Univ. of Illinois, 1963, unpublished

REF.

V. Emma, S. Lo Nigro, C. Milone
Nucl. Phys. A257, 438 (1976)

ELEM. SYM.	A	Z
Fe		26

METHOD

REF. NO.	
76 Em 2	egf

REACTION	RESULT	EXCITATION ENERGY	SOURCE		DETECTOR		ANGLE
			TYPE	RANGE	TYPE	RANGE	
G,F	ABY	THR-999	C	999	TRK-I		4PI

999 = 1 GEV

TABLE 1

Measured values of σ_q at $E = 1000$ MeV and deduced values of σ_k assumed constant from E_0 to 1000 MeV

Element	Z^2/A	σ_q (mb)	E_0 (MeV)	σ_k (mb)
Bi	32.96	12.3 ± 0.6	200	7.6 ± 0.6
Pb	32.45	5.4 ± 0.4	220	3.6 ± 0.3
Tl	32.10	4.1 ± 0.3	230	2.8 ± 0.3
Au	31.68	2.0 ± 0.15	240	1.4 ± 0.2
Pt	31.18	1.1 ± 0.08	255	$(8 \pm 0.7) \times 10^{-1}$
Re	30.21	$(3.7 \pm 0.3) \times 10^{-1}$	280	$(2.9 \pm 0.3) \times 10^{-1}$
W	29.78	$(3.5 \pm 0.3) \times 10^{-1}$	290	$(2.8 \pm 0.3) \times 10^{-1}$
Ta	29.45	$(3.3 \pm 0.3) \times 10^{-1}$	300	$(2.7 \pm 0.3) \times 10^{-1}$
Hf	29.04	$(1.7 \pm 0.2) \times 10^{-1}$	310	$(1.4 \pm 0.2) \times 10^{-1}$
Yb	28.31	$(1.3 \pm 0.1) \times 10^{-1}$	330	$(1.2 \pm 0.1) \times 10^{-1}$
Tm	28.18	$(7.5 \pm 0.8) \times 10^{-2}$	335	$(6.8 \pm 0.8) \times 10^{-2}$
Ho	27.21	$(3.6 \pm 0.4) \times 10^{-2}$	355	$(3.5 \pm 0.4) \times 10^{-2}$
Dy	26.80	$(2.6 \pm 0.3) \times 10^{-2}$	360	$(2.5 \pm 0.3) \times 10^{-2}$
Tb	26.58	$(2.5 \pm 0.3) \times 10^{-2}$	370	$(2.5 \pm 0.3) \times 10^{-2}$
Gd	26.04	$(1.6 \pm 0.2) \times 10^{-2}$	380	$(1.7 \pm 0.2) \times 10^{-2}$
Sm	25.56	$(1.3 \pm 0.2) \times 10^{-2}$	390	$(1.4 \pm 0.2) \times 10^{-2}$
Nd	24.96	$(9.2 \pm 0.9) \times 10^{-3}$	405	$(1 \pm 0.1) \times 10^{-2}$
Ce	24.00	$(8 \pm 0.9) \times 10^{-3}$	420	$(9 \pm 1) \times 10^{-3}$
La	23.39	$(8.4 \pm 0.9) \times 10^{-3}$	430	$(1 \pm 0.1) \times 10^{-3}$
Sb	21.36	$(1.2 \pm 0.2) \times 10^{-2}$	460	$(1.5 \pm 0.3) \times 10^{-2}$
Te	21.19	$(8.8 \pm 1) \times 10^{-3}$	465	$(1.2 \pm 0.2) \times 10^{-2}$
Sn	21.06	$(1.3 \pm 0.2) \times 10^{-2}$	465	$(1.7 \pm 0.3) \times 10^{-2}$
Cd	20.49	$(1.7 \pm 0.3) \times 10^{-2}$	470	$(2.2 \pm 0.4) \times 10^{-2}$
Ag	20.47	$(2 \pm 0.3) \times 10^{-2}$	470	$(2.6 \pm 0.4) \times 10^{-2}$
Zn	13.76	$(2 \pm 0.4) \times 10^{-1}$	515	$(3 \pm 0.6) \times 10^{-1}$
Cu	13.44	$(2.4 \pm 0.5) \times 10^{-1}$	515	$(3.6 \pm 0.8) \times 10^{-1}$
Ni	13.35	$(2.4 \pm 0.5) \times 10^{-1}$	510	$(3.6 \pm 0.8) \times 10^{-1}$
Fe	12.10	$(3 \pm 0.6) \times 10^{-1}$	510	$(4.4 \pm 0.9) \times 10^{-1}$

4 A.V. Mitrofanova et al. Sov. J. Nucl. Phys. 6, 512 (1968).

7 T. Methasiri et al., Nucl. Phys. A167, 97 (1971).

12 J.R. Nix et al., Nucl. Phys. 81, 61 (1966).

20 N.A. Perifilov et al., JETP (Sov. Phys.) 14, 623 (1962); Proc. Symp. on the physics & chemistry of fission, Salzburg 1965, vol. 2 (IAEA) Vienna, 1965, p.283.

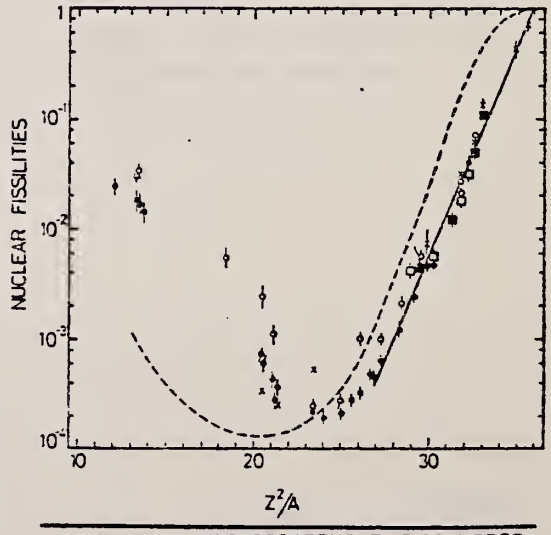

Fig. 2. Nuclear fissilities as a function of Z^2/A. Experimental points: solid circles represent our data; squares, the data from ref. [4]); open circles, the data from ref. [7]); and crosses, the data from (p,f) experiments[20]). The straight line is the best fit calculated from our data for $Z^2/A > 26$. The dashed curve is the curve VI calculated by Nix and Sassi[12]).

REF. V. Ya. Kitaev, A. I. Abramov, A. V. Rogov, and M. G. Yutkin
Bull. of the Acad. of Sci. of the USSR. Phys. Series 40, 218
Izvestiya Akademii Nauk SSSR. Seriya Fizicheskaya 40, 2274 (1976)

ELEM. SYM.	A	Z
Fe		26

METHOD

Remarks: Target 91.9% ^{58}Fe, 8.1% ^{57}Fe

REF. NO. 76 Ki 7

hmg

REACTION	RESULT	EXCITATION ENERGY	SOURCE		DETECTOR		ANGLE
			TYPE	RANGE	TYPE	RANGE	
G,N	ABX	10- 11	C	11- 14	TOF-D	-	78
				(11.25-13.25)			

11.25-13.25 BREMS

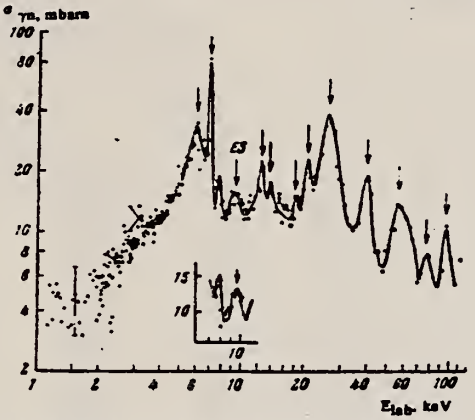

Fig. 1. Differential cross section of the (γn) reaction on ^{58}Fe measured for E_γ^{max} = 13.25 MeV and multiplied by 4π. The insert shows the results of measurements in the E_n ~ 10 keV region for E_γ^{max} = 11.25 MeV. The energies of the peaks are denoted by vertical arrows, and their values are given in the table. The index ES denotes the resonance caused by the transition to the excited level of the final ^{57}Fe nucleus.

TABLE 1

Energies of the Resonances (Peaks) in the Cross Sections of the ^{58}Fe(γn)^{57}Fe and ^{57}Fe(nγ)^{58}Fe Reactions

E_{lab} keV (γn)	E^{calc}, keV (nγ)	E^{exp}, keV (nγ)	E_{lab}, keV (γn)	E^{calc}, keV (nγ)	E_0^{exp}, keV (nγ)
–	–	1,63	21,3	21,4	21,3
–	–	3,92	27,0	27,2	29,0
–	–	4,75	41,0	41,4	41,0
6,25	6,24	6,21	–	–	45,5
7,20	7,19	7,22	58,0	58,8	55,8
7,85	7,85	7,90			61,0
9,70	9,72	–	78,5	79,4	77,2
12,70	12,70	12,80	98,0	99,2	93,7
13,9	14,0	13,9			109,6
18,8	18,7	17,7			110,15

Note. The calculated values are given in the center-of-mass system.

REF. V. di Napoli, F. Salvetti, M. L. Terranova, H. G. de Carvalho, J. B. Martins, O. A. P. Tavares
J. Inorg. Nucl. Chem. 40, 175 (1978).

ELEM. SYM.	A	Z
Fe		26

METHOD	REF. NO.	
	78Di12	hg

REACTION	RESULT	EXCITATION ENERGY	SOURCE TYPE	SOURCE RANGE	DETECTOR TYPE	DETECTOR RANGE	ANGLE
G,SPL	ABY	THR-999	C	300-999	ACT-I		4PI

Abstract—Cross sections per equivalent quantum, in the energy range 0.3–1.0 GeV, have been measured for spallation residuals from ^{51}V, ^{55}Mn, natural Fe, and ^{59}Co targets. Mean cross sections per photon have been deduced in this energy range and the data analysed in terms of charge-dispersion curves and mass-yield distributions. The mean cross sections per photon have also been compared with a semiempirical Rudstam's formula. A satisfactorily good agreement has been found with the calculated yields within a factor of two.

YLDS 24NA TO 54MN

Table 4. Yields of radionuclides in units of μb per equivalent quantum. Iron target

Nuclide	E_0(GeV) 0.30	0.40	0.50	0.60	0.75	0.90	1.00
^{24}Na		3.0 ± 0.3	6.0 ± 0.6	8 ± 1	10 ± 1	12 ± 1	13 ± 1
^{27}Mg	3 ± 1	6 ± 1	8 ± 1	10 ± 1	12 ± 1	14 ± 1	15 ± 1
^{28}Mg			0.7 ± 0.2	1.2 ± 0.4	1.8 ± 0.5	2.2 ± 0.5	2.5 ± 0.5
^{28}Al	8 ± 3	18 ± 4	26 ± 4	32 ± 4	40 ± 4	45 ± 4	50 ± 4
^{29}Al	2 ± 1	6 ± 2	10 ± 2	12 ± 2	16 ± 2	18 ± 2	20 ± 2
^{34}Cl^m		8 ± 4	15 ± 4.	20 ± 4	27 ± 4	32 ± 4	35 ± 4
^{38}Cl		15 ± 4	25 ± 5	35 ± 7	45 ± 8	55 ± 8	60 ± 8
^{39}Cl		5 ± 2	10 ± 3	13 ± 3	18 ± 3	21 ± 3	23 ± 3
^{41}Ar		2 ± 1	8 ± 2	13 ± 3	20 ± 3	25 ± 3	20 ± 3
^{42}K	20 ± 8	40 ± 10	60 ± 15	70 ± 15	90 ± 15	105 ± 15	115 ± 15
^{43}K		2 ± 1	5 ± 2	15 ± 5	24 ± 5	30 ± 5	34 ± 5
^{44}K	8 ± 4	11 ± 4	13 ± 4	15 ± 4	17 ± 4	19 ± 4	20 ± 4
^{45}K	1.6 ± 0.5	1.9 ± 0.5	2.2 ± 0.5	2.4 ± 0.5	2.7 ± 0.5	2.9 ± 0.5	3.0 ± 0.5
^{47}Ca	3.0 ± 1.0	4.0 ± 1.0	6.0 ± 2.0	7.0 ± 2.0	8.5 ± 2.0	9.4 ± 2.0	10.0 ± 2.0
^{43}Sc	30 ± 8	55 ± 8	80 ± 8	85 ± 8	100 ± 8	100 ± 8	140 ± 8
^{44}Sc^m	140 ± 12	170 ± 12	180 ± 12	204 ± 12	230 ± 12	250 ± 12	260 ± 13
^{44}Sc^g	145 ± 16	170 ± 16	180 ± 16	200 ± 16	230 ± 16	245 ± 16	250 ± 16
^{46}Sc	100 ± 30	100 ± 30	170 ± 35	220 ± 35	260 ± 37	330 ± 38	324 ± 40
^{47}Sc	70 ± 20	80 ± 20	154 ± 30	180 ± 30	210 ± 30	235 ± 30	246 ± 30
^{48}Sc	2 ± 1	2 ± 1	15 ± 3	20 ± 3	28 ± 3	32 ± 3	34 ± 3
^{48}V	490 ± 45	540 ± 45	580 ± 45	620 ± 45	660 ± 45	690 ± 45	710 ± 45
^{48}Cr	24 ± 4	27 ± 4	28 ± 4	30 ± 4	31 ± 4	33 ± 4	34 ± 4
^{49}Cr	142 ± 25	160 ± 25	175 ± 25	187 ± 25	200 ± 25	212 ± 25	220 ± 25
^{51}Cr	2700 ± 130	2900 ± 150	3000 ± 150	3100 ± 150	3200 ± 200	3350 ± 200	3400 ± 200
^{51}Mn	20 ± 5	28 ± 5	35 ± 5	38 ± 5	45 ± 5	47 ± 5	50 ± 5
^{52}Mn^m	410 ± 40	430 ± 40	450 ± 40	460 ± 40	480 ± 40	490 ± 40	500 ± 40
^{52}Mn^g	390 ± 40	415 ± 40	435 ± 40	450 ± 40	475 ± 40	490 ± 40	500 ± 40
^{52}Mn	4670 ± 300	4900 ± 300	5150 ± 300	5300 ± 300	5500 ± 300	5700 ± 300	5800 ± 300

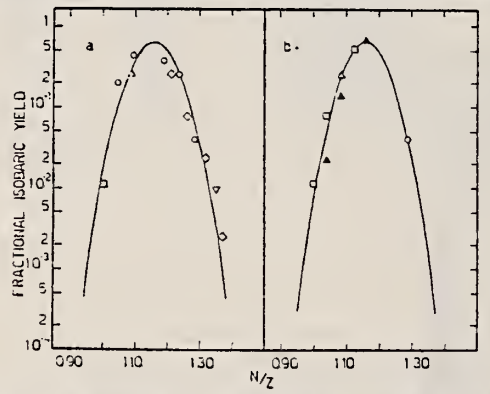

Fig. 2. The same as Fig. 1. Natural Fe target. Graph (a): $42 \le A \le 48$; (b): $48 \le A \le 54$. The symbols are the same used in Fig. 1 plus ▲, for Mn isotopes.

Fig. 1. Fractional isobaric yield vs the N/Z ratio for $42 \le A \le 48$. Mean cross sections per photon in the energy range 0.3–1 GeV. Graph (a): ^{51}V target; (b): ^{55}Mn target. The symbols are: □, for Cr; ○, for Sc; △, for V; ◇, for K; ▽, for Ca isotopes.

Table 6. Mean cross sections in the energy range 0.3–1 GeV in units of μb

Produced radionuclide	Target nucleus: Vanadium, Present work	Vanadium, Bülow *et al.* [26]	Manganese	Iron	Cobalt
^{24}Ne	2.0 ± 0.4				
^{24}Na	16 ± 4				
^{24}Na	30 ± 2	18 ± 2	10 ± 1	10 ± 1	7 ± 1
^{27}Mg	22 ± 2	18 ± 3	9 ± 1	10 ± 1	8 ± 1
^{28}Mg	6 ± 1	6 ± 1	2.7 ± 0.5	2.7 ± 0.5	2.2 ± 0.3
^{28}Al	58 ± 7	59 ± 4	29 ± 4	35 ± 4	25 ± 3
^{29}Al	25 ± 4	32 ± 2	11 ± 2	15 ± 2	16 ± 3
^{34}Cl^m	16 ± 2	14 ± 2	30 ± 4	30 ± 4	19 ± 3
^{38}Cl	75 ± 13	96 ± 5	45 ± 8	50 ± 8	37 ± 7
^{39}Cl	37 ± 7	35 ± 1	12 ± 2	19 ± 3	13 ± 2
^{41}Ar	65 ± 6	54 ± 2	35 ± 4	28 ± 3	12 ± 2
^{42}K	280 ± 50	243 ± 11	94 ± 17	80 ± 15	66 ± 12
^{43}K	128 ± 20	128 ± 4	43 ± 7	30 ± 5	28 ± 5
^{44}K	33 ± 12	30 ± 3	11 ± 4	10 ± 4	9.5 ± 4
^{45}K	12 ± 2	8 ± 1	1.0 ± 0.5	1.2 ± 0.5	1.0 ± 0.5
^{47}Ca	12 ± 4	15 ± 1	6.5 ± 2.4	6 ± 2	2.2 ± 0.8
^{43}Sc	104 ± 10	109 ± 6	72 ± 7	77 ± 8	52 ± 6
^{44}Sc^m	260 ± 30	243 ± 14	115 ± 15	100 ± 12	84 ± 10
^{44}Sc^g	230 ± 40	218 ± 13	116 ± 20	90 ± 16	71 ± 13
^{46}Sc	575 ± 100	605 ± 18	260 ± 45	214 ± 35	220 ± 40
^{47}Sc	457 ± 100	540 ± 33	200 ± 45	160 ± 30	127 ± 30
^{48}Sc	165 ± 15	138 ± 8	50 ± 5	30 ± 3	25 ± 3
^{48}V	210 ± 50	307 ± 12	200 ± 50	184 ± 45	100 ± 25
^{48}Cr	20 ± 10		7 ± 3	8 ± 4	5.0 ± 2.5
^{49}Cr	13 ± 5	16 ± 2	40 ± 15	64 ± 25	20 ± 8
^{51}Cr			480 ± 150	570 ± 150	330 ± 150
^{51}Mn				25 ± 5	
^{52}Mn^m				75 ± 40	49 ± 25
^{52}Mn^g				96 ± 40	84 ± 25
^{54}Mn				944 ± 300	584 ± 100
^{52}Fe					1.6 ± 0.8

Table 7. N/Z dispersion parameters of the mean cross sections per photon†

Target nucleus	Mass region	A_m	N/Z_p	Z_p	FWHM	ΔZ	Ref.
^{51}V	42–48	45	1.16	20.8	0.143	1.36	Present work
			1.16	20.8	0.142	1.37	[26]
			1.16	20.9	0.168	1.63	[35]
^{55}Mn	42–48	45	1.16	20.8	0.142	1.37	Present work
^{nat}Fe	42–48	45	1.16	20.8	0.140	1.35	Present work
	48–54	51	1.16	23.6	0.126	1.38	Present work
^{59}Co	42–48	45	1.16	20.8	0.141	1.36	Present work
	48–54	51	1.16	23.6	0.124	1.36	Present work

†A_m is the median mass of the mass region under consideration. N/Z_p is the neutron/proton ratio for the most probable nuclear charge Z_p of A_m. FWHM is the full width at half-maximum of the CD curves. ΔZ is the spread in Z as calculated from the FWHM for the two abscissas N/Z_1 and N/Z_2 (see also Refs. [26] and [35]).

FE
A=54

FE
A=54

FE
A=54

REF. M.D. DeSouze Santos, J. Goldemberg, R.R. Pieroni, E. Silva, O.A. Borello, S.S. Villaca, J.L. Lopes
Int. Conf. Peaceful Uses of Atomic Energy II (UN, NY), 169 (1955)

ELEM. SYM.	A	Z
Fe	54	26

METHOD

REF. NO.	
55 De 1	EGF

REACTION	RESULT	EXCITATION ENERGY	SOURCE		DETECTOR		ANGLE
			TYPE	RANGE	TYPE	RANGE	
G,N	ABX	11-24	C	11-24	ACT-I		4PI

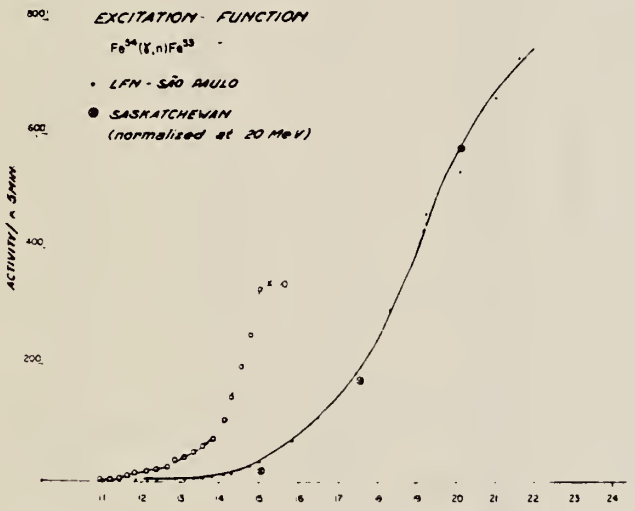

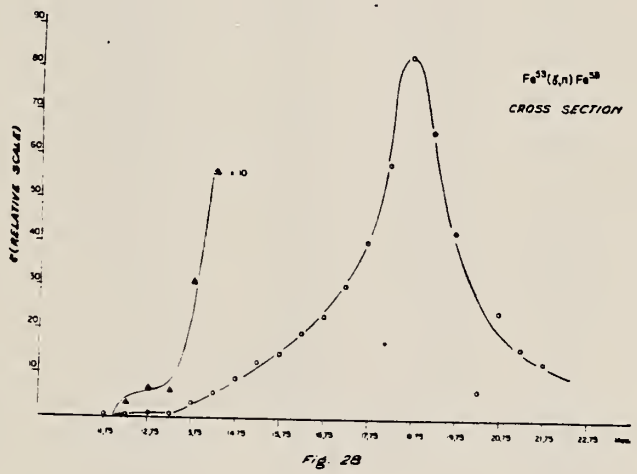

Fig. 28

Ref. J.H. Carver, K.H. Lokan
Australian J. Phys. 10, 312 (1957)

Elem. Sym.	A	Z
Fe	54	26

Method: 33 MeV electron synchrotron; neutron yield; radioactivity; $Cu^{63}(\gamma,n)$ reaction (Berman and Brown)

Ref. No.: 57 Ca 2 EH

Reaction	E or ΔE	E_o	Γ	$\int \sigma dE$	Jπ	Notes
Fe^{54} (γ,n)	Bremss. 13-30	19	$\Gamma_{1/2}$: 6.9 MeV	$\int_{}^{31}$ = 290±50 MeV-mb		

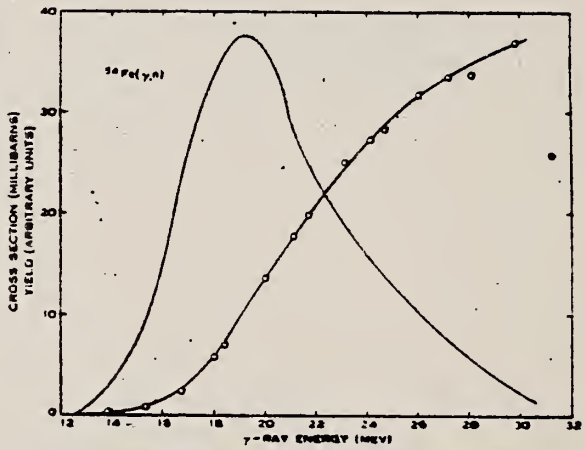

Fig. 4.—The measured yield curve and the derived cross section curve for the reaction ^{54}Fe (γ,n).

TABLE 2

PARAMETERS OF THE MEASURED (γ,n) CROSS SECTIONS

Reaction	Peak Energy (MeV)	Width at Half Maximum (MeV)	Integrated Cross Section to 31 MeV (MeV mb)
^{12}C (γ,n)	23	4·2	42±7
^{16}O (γ,n)	24	3·4	46±7
^{54}Fe (γ,n)	19	6·9	290±50

Ref. J. Goldemberg, L. Marquez
Nuclear Phys. 7, 202 (1958)

Elem. Sym.	A	Z
Fe	54	26

Method
activation; 22 MeV Betatron

Ref. No. 58 Go 3 EH

Reaction	E or ΔE	E_o	Γ	$\int \sigma dE$	Jπ	Notes
(γ,d) + (γ,np)	16-22					Yield less than 1/30 of that found for Zn.

Ref. W.E. Del Bianco, W.E. Stephens
Phys. Rev. 126, 709 (1962)

Elem. Sym.	A	Z
Fe	54	26

Method Electrostatic generator, $H^3(p,\gamma)He^4$ reaction; activation of positron emitter; 2 NaI in coincidence.

Ref. No. 62 De 1 JHH

Reaction	E or ΔE	E_o	Γ	$\int \sigma dE$	Jπ	Notes
(γ,n)	20.48					σ(γ,n) = 30.0±4.8 mb

REF. W. B. Walters, J. R. Van Hise, W. L. Switzer, J. P. Hummel
Nucl. Phys. A157, 73 (1970)

ELEM. SYM.	A	Z
Fe	54	26

METHOD

REF. NO.: 70 Wa 3 egf

REACTION	RESULT	EXCITATION ENERGY	SOURCE TYPE	SOURCE RANGE	DETECTOR TYPE	DETECTOR RANGE	ANGLE
G,2N	RLY	THR-305	C	150-305	ACT-I		4PI
G,PN	RLY	THR-305	C	150-305	ACT-I		4PI

TABLE 1
Summary of measured yield ratios

Target	Bremsstrahlung energy (MeV)	Measured yield ratio
natural Cr	150	$^{48}Cr/^{48}V = 0.043 \pm 0.002$
	250	0.047 ± 0.009
	305	0.042 ± 0.002
enriched ^{52}Cr	250	0.025 ± 0.005
natural Fe	250	$^{52}Fe/^{52}Mn = 0.037 \pm 0.003$
enriched ^{56}Fe	250	0.024 ± 0.005
		$^{52g}Mn/(^{52m}Mn + ^{25g}Mn) = 0.47 \pm 0.02$
natural Y	150	$^{87}Y/^{87m}Sr = 12.9 \pm 1.6$
natural Mo	150	$^{90}Mo/^{90}Nb = 0.41 \pm 0.05$
	280	0.49 ± 0.05

TABLE 2
Summary of experimental and theoretical ratios of (γ, 2n) to (γ, pn) yields

Target isotope	Bremsstrahlung energy (MeV)	Experimental (γ, 2n)/(γ, pn) yield ratio	Calculated (γ, 2n)/(γ, pn) yield ratio
^{50}Cr	250	0.095 ± 0.025	0.14
^{54}Fe	250	0.10 ± 0.03	0.07
^{89}Y	150	7.4 ± 1.0	6.7
^{92}Mo	150	0.41 ± 0.05	0.15
	280	0.49 ± 0.05	0.16

REF. A. S. Litvinenko, N. G. Shevchenko, A. Yu. Buki, P. L. Kondrat'ev, G. A. Savitskii, A. A. Khomich, V. M. Khvastunov, I. I. Chkalov
Ukr. Fiz. Zhur. 17, 1197 (1972)

ELEM. SYM.	A	Z
Fe	54	26

METHOD

REF. NO. 72 Li 3 hmg

REACTION	RESULT	EXCITATION ENERGY	SOURCE TYPE	SOURCE RANGE	DETECTOR TYPE	DETECTOR RANGE	ANGLE
E,E/	FMF	1, 5	D	150,225	MAG-D		DST

B(EL) LEV 1.17,3.75

Таблица 1

Параметры фермиевского распределения плотности заряда (c—радиус полуспада плотности, t—диффузионность ядра)

Ядро	c, ф	t, ф
Fe^{54}	4,012±0,007	2,346±0,011
Fe^{56}	3,971±0,013	2,608±0,020
Fe^{58}	4,027±0,019	2,530±0,031
Ni^{62}	4,149±0,011	2,506±0,016

[1] Институт ядерных исследований АН СССР.

Таблица 2

Ядро	E_λ, Мэв	J^π	Данные настоящей работы: $B(E\lambda)\uparrow$, $e^2\lambda\phi^{2\lambda}$	Данные других работ: $B(E\lambda)\uparrow$, $e^2\lambda\phi^{2\lambda}$	Тип эксперимента и метод определения	Литература
Fe^{54}	1.4	2^+	531,9±32,4	533	(ee′), борновское приближение	[6]
	4.85	3^-	4563±410	4390		
Fe^{56}	0.85	2^+	678,1±47,5	720	(ee′), борновское приближение	»
				1250±270	искаженные волны	[7]
				1240	борновское приближение	»
				900±100	кулоновское возбуждение	[8]
Fe^{58}	0.81	2^+	943,2±79			
	3.86	3^-	13880±1260			
Ni^{62}	1.17	2^+	618,6±42,1	877± 11	(ee′), искаженные волны	[9]
	3.75	3^-	14359±962	20100±540		

REF. Phan Xuan Ho, J. Bellicard, Ph. Leconte, I. Sick
Nucl. Phys. A210, 189 (1973)

ELEM. SYM.	A	Z
Fe	54	26

METHOD

REF. NO. 73 Ho 4 egf

REACTION	RESULT	EXCITATION ENERGY	SOURCE TYPE	SOURCE RANGE	DETECTOR TYPE	DETECTOR RANGE	ANGLE
E,E/	FMF	1- 5	D	209	MAG-D		DST

1.41, 2.54, 4.78

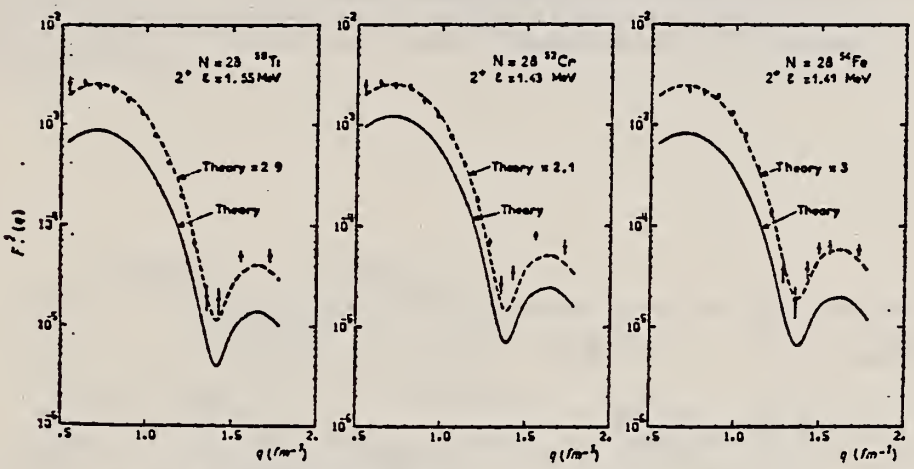

Fig. 5a. Squared inelastic form factor for 2^+ states of the $N = 28$ isotones.

TABLE 4

Inelastic cross sections for $E_e = 209$ MeV on ^{54}Fe

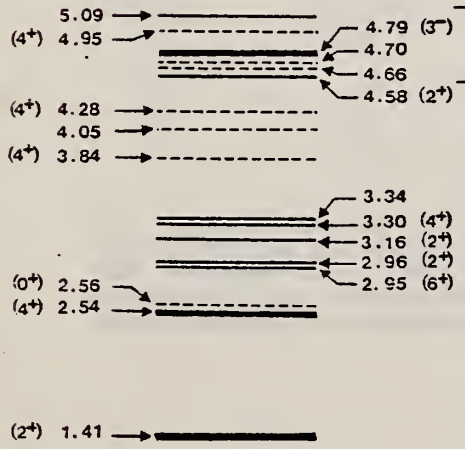

θ (deg.)	$(2^+)\varepsilon = 1.41$ MeV $d\sigma/d\Omega$ (mb/sr)	$(3^-)\varepsilon = 4.78$ MeV $d\sigma/d\Omega$ (mb/sr)	$(4^+)\varepsilon = 2.54$ MeV $d\sigma/d\Omega$ (mb/sr)
35		0.168 E−2±0.940 E−3	
40	0.119 E−1±0.100 E−2	0.156 E−2±0.420 E−3	
45	0.683 E−2±0.430 E−3	0.117 E−2±0.160 E−3	
50	0.401 E−2±0.210 E−3	0.831 E−3±0.670 E−4	0.191 E−3±0.320 E−4
55	0.183 E−2±0.100 E−3	0.571 E−3±0.400 E−4	0.215 E−3±0.150 E−4
60	0.766 E−3±0.410 E−4	0.412 E−3±0.300 E−4	0.174 E−3±0.100 E−4
65	0.256 E−3±0.170 E−4	0.270 E−3±0.180 E−4	0.140 E−3±0.900 E−5
70	0.687 E−4±0.740 E−5	0.157 E−3±0.110 E−4	0.106 E−3±0.700 E−5
75	0.138 E−4±0.360 E−5	0.951 E−4±0.820 E−5	0.764 E−4±0.550 E−5
80	0.509 E−5±0.174 E−5	0.453 E−4±0.380 E−5	0.523 E−4±0.320 E−5
85	0.781 E−5±0.142 E−5	0.151 E−4±0.210 E−5	0.311 E−4±0.210 E−5
90	0.974 E−5±0.120 E−5	0.752 E−5±0.126 E−5	0.220 E−4±0.140 E−5
95	0.781 E−5±0.113 E−5	0.184 E−5±0.960 E−6	0.116 E−4±0.100 E−5
110	0.342 E−5±0.390 E−6	0.174 E−6±0.107 E−6	0.194 E−5±0.230 E−6

Energy level diagram given by ref. [24]). Levels excited in our experiment are shown with solid lines, dashed lines correspond to other levels. The experimental values are normalized on our elastic cross sections considered as reference values.

(over)

[24] Nuclear Data Sheets B (1970).

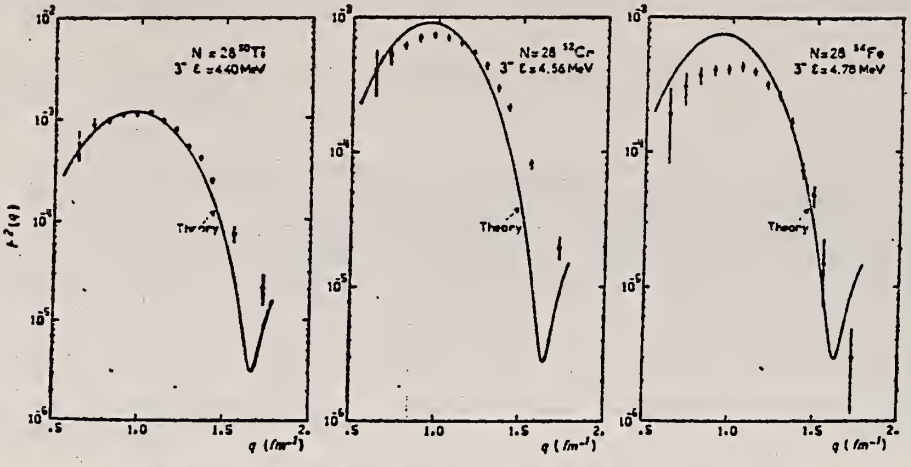

Fig. 6a. Squared inelastic form factor for 3^- states of the $N = 28$ isotones.

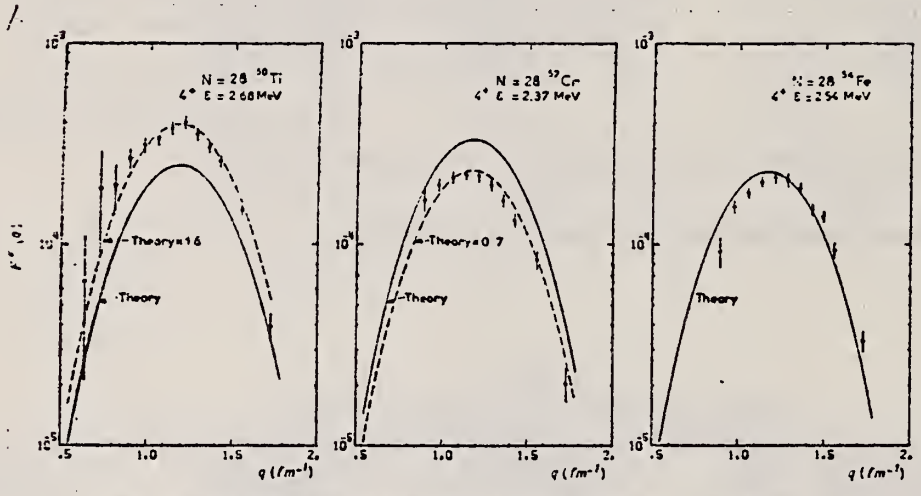

Fig. 7a. Squared inelastic form factor for 4^+ states of the $N = 28$ isotones.

REF. I. A. Grishaev, N. I. Lapin, G. D. Pugachev
Yad. Fiz. 24, 335 (1976)
Sov. J. Nucl. Phys. 24, 175 (1976)

ELEM. SYM.	A	Z
Fe	54	26

METHOD

REF. NO. 76 Gr 3 hmg

REACTION	RESULT	EXCITATION ENERGY	SOURCE		DETECTOR		ANGLE
			TYPE	RANGE	TYPE	RANGE	
G,PI+	SPC	150-500	C	500	EMU-I		DST
G,PI-	SPC	150-500	C	500	EMU-I		DST

The energy spectra of charged photopions from ^{54}Fe, ^{56}Fe, and ^{58}Ni targets irradiated with bremsstrahlung of maximum energy 500 MeV have been measured at photopion-emission angles of 30, 60, 90, 120, and 150° in the lab system over the kinetic-energy range from 15 to 80 MeV. Isotope effects are found in the π^- yields at 30, 60, and 90°. At all angles and energies, the π^+ yields are the same for all three targets within the experimental error.

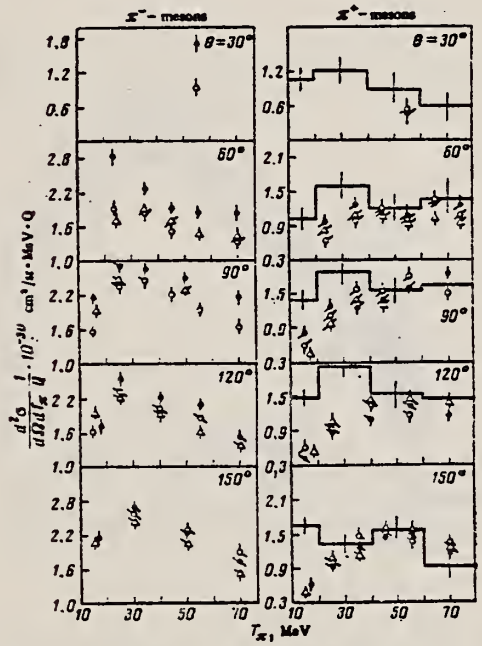

FIG. 1. Energy spectra of charged photopions from ^{54}Fe, ^{56}Fe, and ^{58}Ni targets (open circles, black circles, and triangles, respectively) at E_0=500 MeV. The error bars represent statistical errors. The histograms on the π^+-meson plots represent the results of cascade-model calculations for ^{56}Fe.

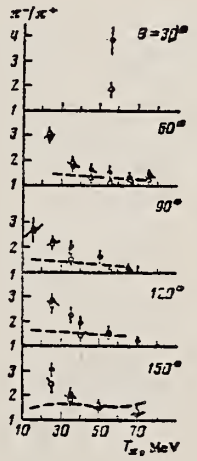

FIG. 2. The π^-/π^+ yield ratios for ^{56}Fe (black circles) and ^{54}Fe (open circles) targets vs photopion kinetic energy. The dashed curves were calculated with Eq. (4).

REF.

H. Lancman, R. J. Sparks, C. Van der Leun
Nucl. Phys. A257, 29 (1976)

ELEM. SYM.	A	Z
Fe	54	26

METHOD

REF. NO.: 76 La 1 egf

REACTION	RESULT	EXCITATION ENERGY	SOURCE		DETECTOR		ANGLE
			TYPE	RANGE	TYPE	RANGE	
G,G	LFT	6	D	6	SCD-D		DST

6=6.13

Abstract: The narrow 6.13 MeV γ-line from the $^{19}F(p, \alpha\gamma)^{16}O$ reaction was used to excite a level of ^{54}Fe. Resonance fluorescence spectra, angular distributions and the temperature dependence of the intensity of the scattered photons were measured. In addition to the decay scheme of the ^{54}Fe level, its following characteristics were determined: $E_x = 6129.0 \pm 0.2$ keV, $J = 1$, $\Gamma = 27 \pm 4$ meV, $\Gamma_0/\Gamma = 0.93 \pm 0.01$. The separation energy between the incident line and the absorption line was found to be 17.0 ± 1.0 eV.

REF. S.S. Verbitskii, B.S. Ratner, A.N. Sergievskii
JETP Lett. 23, 492 (1976)

ELEM. SYM.	A	Z
Fe	54	26

METHOD

REF. NO. 76 Ve 3 hg

REACTION	RESULT	EXCITATION ENERGY	SOURCE		DETECTOR		ANGLE
			TYPE	RANGE	TYPE	RANGE	
G,N	RLX	13-27	C	13-27	SCI-D		UKN

The pre-equilibrium nuclear decay, with which the existence of the intermediate structures seems to be connected, leads to predominate emission of high-energy neutrons.[1] There are therefore grounds for expecting the structure and the cross section of the (γ, n) reaction due to the emission of the high-energy component of the neutron spectrum to become manifest most distinctly.

We have investigated the yield of the (γ, n) reaction for the nucleus Fe^{54} at different values of the minimum energy of the registered neutrons, and also

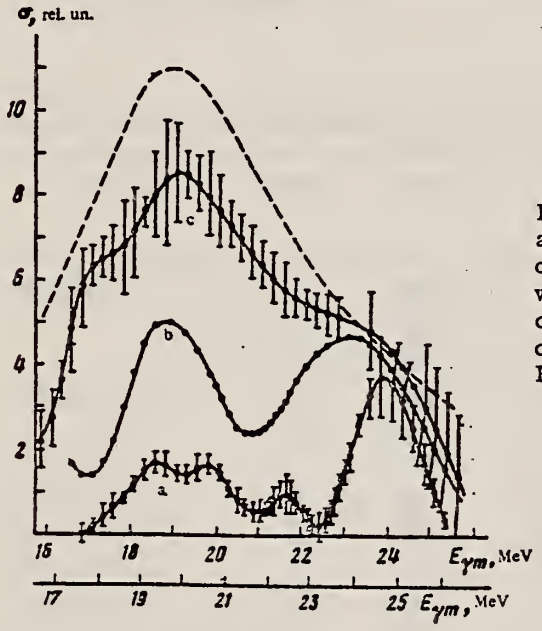

FIG. 1. Cross section of the reaction $Fe^{54}(\gamma, n)Fe^{53}$. The threshold for the neutron registration was: a) 3.7 MeV, b) 3.2 MeV, c) 0.9 MeV. Dashed curve—cross section of the reaction $Fe^{54}(\gamma, n)$ from[4].

(over)

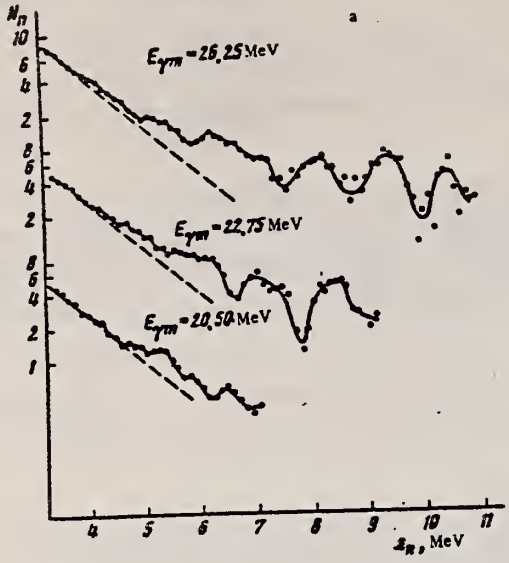

FIG. 2. Energy spectra of photoneutrons from the $Fe^{54}(\gamma, n)$ reaction.

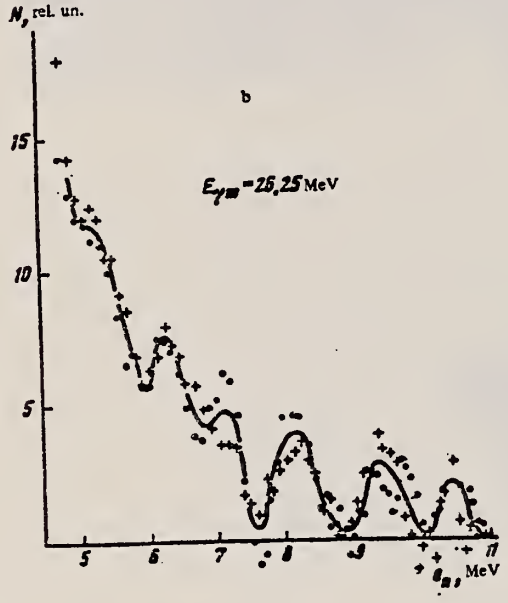

Position of the peak in the energy spectrum of the neutrons ϵ_m, MeV			Position of Fe^{54} resonance	Position of Fe^{53} levels $E = E_R - \bar{\epsilon}_m - \epsilon_{n_0}$, MeV		
$E_{\gamma m}$ = 20.5 MeV	$E_{\gamma m}$ = 22.75 MeV	$E_{\gamma m}$ = 26.25 MeV	E_R, MeV			
4.1	4.1	4.1	19.5	–	1.9	–
4.7	4.7	4.6	19.5	–	–	1.2
5.3	5.1	5.2	19.5	0.7	–	–
6.4	6.1	6.2	20.7	0.9	–	–
–	7.0	7.2	22.5	–	1.8	–
–	8.4	8.1	22.5	0.7	–	–
–	–	9.5	24.8	–	1.7	–
–	–	10.5	24.8	0.8	–	–
				Average		
				0.8	1.8	1.2

ϵ_{n_0} –is the neutron binding energy 13.6 MeV.

REF. H. Hirayama and T. Nakamura
Nucl. Inst. Meth. 147, 563 (1977)

EL EM. SYM.	A	Z
Fe	54	26

METHOD

REF. NO.: 77 Hi 5 | hmg

REACTION	RESULT	EXCITATION ENERGY	SOURCE		DETECTOR		ANGLE
			TYPE	RANGE	TYPE	RANGE	
G,N	ABI	13-30 (13.4)	C	18-30	ACT-I		4PI

THICK BREMS TARGET

The integral experiment for a sensitivity check of photonuclear cross section data of C, Mn, Fe, In and Au was performed by using the bremsstrahlung produced in a thick iron target by 18, 22, 26 and 30 MeV electrons from a linear accelerator. The cross section data measured by the activation method showed better results for all incident electron energies than those by the photoneutron method, because the latter include the competing (γ, np) reaction above its threshold energy. It is necessary to obtain the cross section data of (γ, n), (γ, np), $(\gamma, 2n)$, $(\gamma, p2n)$ reactions etc., separately by the activation method.

The effective energy range and effective cross section in the giant resonance region were determined for C, Mn, Fe and Au. By using these quantities, the gross structure of the bremsstrahlung spectrum was obtained in good agreement with the theoretical calculation.

TABLE 3

Ratio of measured and calculated saturated activities at 9°, $R_i = A_i^{exp}/A_i^{cal}$.

Reaction	Reference	Detector	Electron energy 18 MeV	22 MeV	26 MeV	30 MeV	Threshold energy of competing (γ, np) reaction (MeV)
$^{12}C(\gamma, n)^{11}C$	6	ACT[a]	–	1.205	1.09	0.824	
	7	BF3[b]	–	0.757	0.931	–	27.4
	8	BF3	–	1.492	1.189	0.914	
	9	BF3	–	1.418	1.159	–	
$^{55}Mn(\gamma, n)^{54}Mn$	10	BF3	0.575	0.810	0.598	–	17.8
	11		0.595	0.875	0.654	0.609	
$^{54}Fe(\gamma, n)^{53}Fe$	12	ACT	0.542	0.783	0.722	1.12	20.9
$^{115}In(\gamma, n)^{114m}In$	13	BF3	0.448	0.511	–	–	15.9
	14	BF3	0.603	0.672	0.586	1.00	
$^{115}In(\gamma, \gamma')^{115m}In$	15	ACT	0.829	1.00	0.852	0.995	
$^{197}Au(\gamma, n)^{196}Au$	16	BF3	0.743	0.553	0.529		13.7
	17	BF3	0.842	0.628	0.608	0.476	

[a] ACT: measurement of radioactivity of the target.
[b] BF3: BF_3 neutron counter with moderator.

TABLE 4

Effective cross section and effective energy range.

Reaction	Effective energy range (MeV)	Effective cross section (mb) Electron energy 22 MeV	26 MeV	30 MeV	Average
$^{12}C(\gamma, n)^{11}C$	20.5–24.5	–	5.98	5.28	5.63±0.35
$^{55}Mn(\gamma, n)^{54}Mn$	15.0–20.5	–	56.2	52.7	54.5±1.7
$^{54}Fe(\gamma, n)^{53}Fe$	17.0–24.0	–	33.6	47.9	40.8±7.2
$^{197}Au(\gamma, n)^{196}Au$	12.5–15.0	553.5	532.5	415.0	500±85

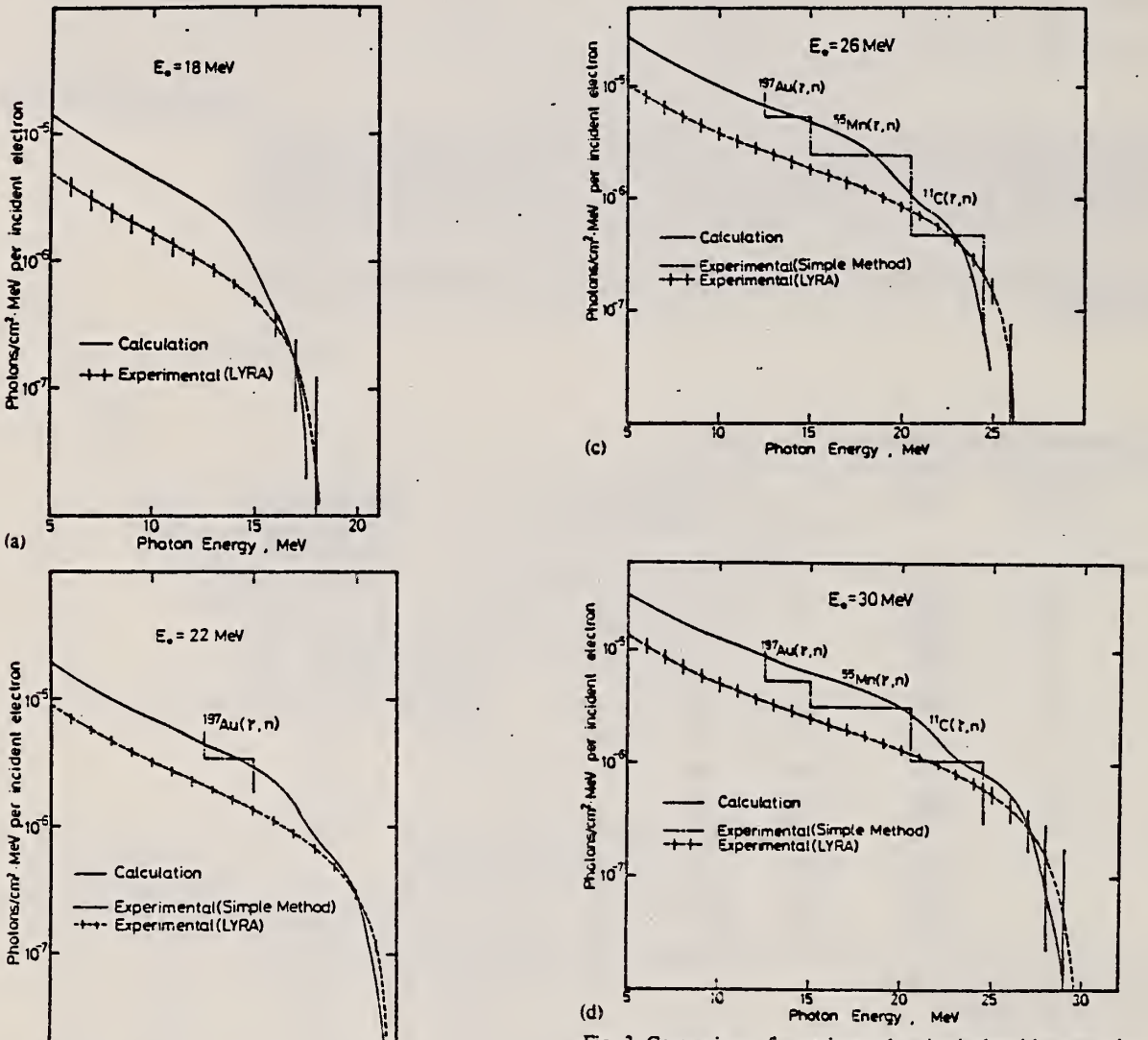

Fig. 3. Comparison of experimental and calculated bremsstrahlung spectra emitted from an iron target in the 9° direction by (a) 18 MeV electrons, (b) 22 MeV electrons, (c) 26 MeV electrons, (d) 30 MeV electrons.

REF. B.S. Ratner, A.N. Sergiyevsky and S.S. Verbitsky
Nucl. Phys. A285, 71 (1977)

ELEM. SYM.	A	Z
Fe	54	26

METHOD

REF. NO. 77 Ra 3 efg

REACTION	RESULT	EXCITATION ENERGY	SOURCE		DETECTOR		ANGLE
			TYPE	RANGE	TYPE	RANGE	
G,N	SPC	16-26	C	15-26	SCI-D		UKN

FAST NEUTS

TABLE 2

Relationship between the structure in the energy spectra and the structure in the photoneutron cross section for ^{54}Fe

Position of peak in neutron energy spectrum ε (MeV) $E_{\gamma\,max}$ (MeV)					Position of resonance ^{54}Fe E_R (MeV)	Position of level ^{53}Fe [a] $E = E_R - \bar{\varepsilon} - E_{n_0}$ [b]		
18.75	19.75	20.50	22.75	26.25				
4.7	4.8	4.7	4.7	4.6	18.4	0		
(4.1)	(4.1)	4.1	4.1	4.1	19.5 (18.4)		(0.6)	1.7
	5.4	5.3	5.1	5.2	19.5		0.65	
		6.4	6.1	6.2	20.7		0.8	
			7.1	7.0	22.5			1.8
			8.3	8.0	22.5		0.65	
				9.5	24.8			1.5
				10.4	24.8		0.6	
						mean value:		
						0	0.68	1.67
						spectroscopic data:		
						0	0.74	1.70

[a]) A nuclear recoil correction has been introduced.
[b]) $\bar{\varepsilon}$ is ε averaged by $E_{\gamma\,max}$.

REF. K. Masumoto, T. Kato, N. Suzuki
Nucl. Inst. Meth. 157, 567 (1978)

ELEM. SYM.	A	Z
Fe	54	26

METHOD

REF. NO. 78 Ma 10 hg

REACTION	RESULT	EXCITATION ENERGY	SOURCE TYPE	SOURCE RANGE	DETECTOR TYPE	DETECTOR RANGE	ANGLE
G,2N	ABY	24-68	C	30-68	ACT - I		4PI
G,PN	ABY	21-68	C	30-68	ACT - I		4PI

Analysis is made of reactions interfering with photon activation analysis procedures. (G,PN) TO MN-52G

The activation yield curves have been presented for a number of photonuclear reactions in the energy range from 30 to 68 MeV, in order to evaluate quantitatively the interferences due to competing reactions in multielement photon activation analysis. The general features of the yields as functions of both target mass number and excitation energy were elucidated from the data obtained, discussion being given on the results in terms of the reaction mechanism.

Simultaneous neutron activation due to appreciable neutron production from the converter and surrounding materials has also been studied, and, finally, the magnitudes of interferences in real multielement analysis were given in the form of their energy dependences.

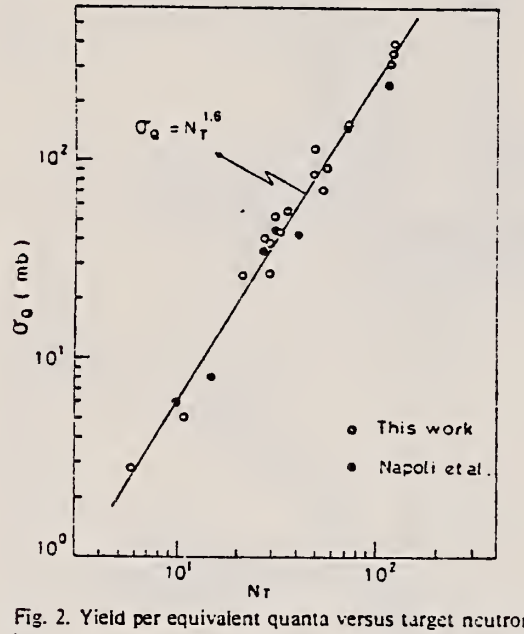

Fig. 2. Yield per equivalent quanta versus target neutron number.

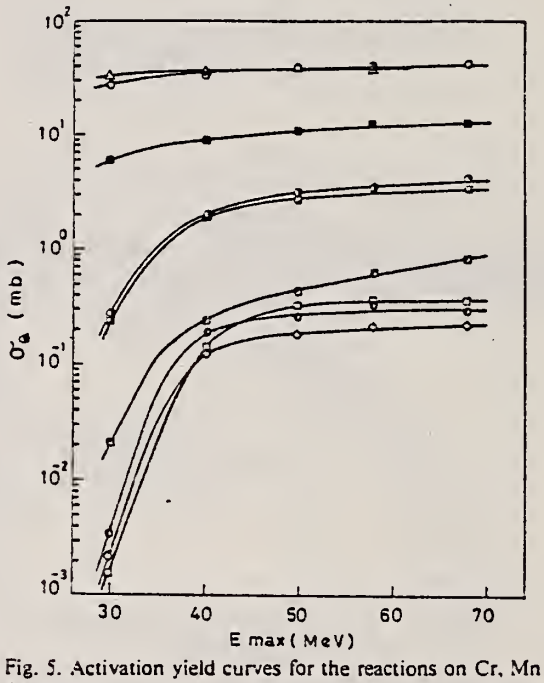

Fig. 5. Activation yield curves for the reactions on Cr, Mn and Fe.
○ $^{52}Cr(\gamma, n)^{51}Cr$, ◑ $^{50}Cr(\gamma, pn)^{48}V$, ◐ $^{50}Cr(\gamma, 2n)^{48}Cr$,
△ $^{55}Mn(\gamma, n)^{54}Mn$, ◪ $^{57}Fe(\gamma, p)^{56}Mn$, ◩ $^{54}Fe(\gamma, pn)^{52g}Mn$,
◪ $^{56}Fe(\gamma, pn)^{54}Mn$, □ $^{56}Fe(\gamma, \alpha n)^{51}Cr$, ◇ $^{54}Fe(\gamma, 2n)^{52}Fe$.

(over)

FORM N3S-418
REV. 7-1[illegible]
U.S. DEPARTMENT OF COMMERCE

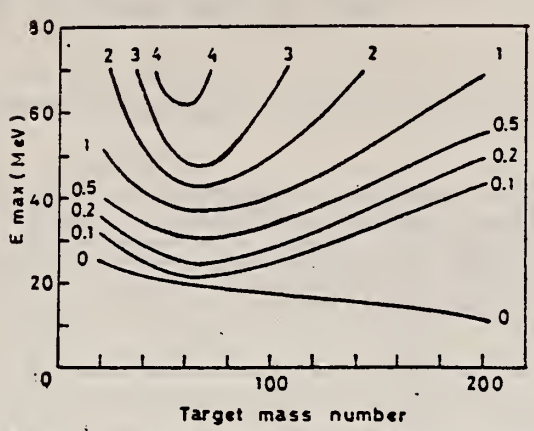

Fig. 11. Yields of the (γ, pn) reactions as a function of bremsstrahlung maximum energy. and target mass number. The numerical values in the figure are yields per equivalent quanta in mb.

REF. J.W. Norbury, M.N. Thompson, K. Shoda, H. Tsubota
Aust. J. Phys. 31, 471 (1978)

ELEM. SYM.	A	Z
Fe	54	26

METHOD

REF. NO. 78 No 2 hg

REACTION	RESULT	EXCITATION ENERGY	SOURCE		DETECTOR		ANGLE
			TYPE	RANGE	TYPE	RANGE	
G,N	ABX	13-25	C	12-18	ACT-I		4PI

Abstract

A high resolution measurement of the $^{54}Fe(\gamma, n)$ cross section is reported. This and a previously measured $^{54}Fe(\gamma, p)$ cross section are discussed in terms of the isospin splitting of the E1 giant dipole.

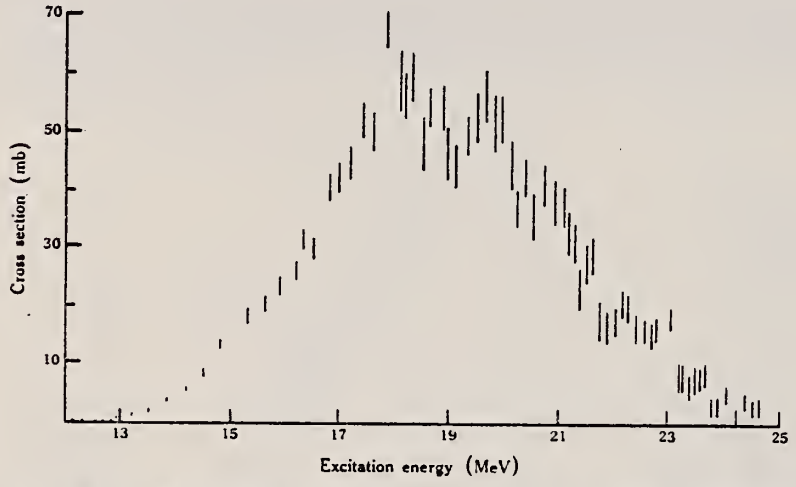

Fig. 1. $^{54}Fe(\gamma, n)^{53}Fe$ cross section obtained from the present high resolution measurement.

REF. R.A. Lindgren, J.B. Flanz, R.S. Hicks, B. Parker, G.A. Peterson, R.D. Lawson, W. Teeters, C.F. Williamson, S. Kowalski, X.K. Maruyama
Phys. Rev. Lett. 46, 706 (1981)

ELEM. SYM.	A	Z
Fe	54	26

METHOD

REF. NO.	
81 Li 2	hg

REACTION	RESULT	EXCITATION ENERGY	SOURCE		DETECTOR		ANGLE
			TYPE	RANGE	TYPE	RANGE	
E,E/	FMF	13	D	131-338	MAG-D		DST
		(13.263)					

5 M8 STATES 8-14 MEV

Inelastic electron scattering is used to identify $M8$ transitions and assign $J^\pi = 8^-$ to states at $E_x = 8.314$, 8.949, 9.974, 10.677, and 13.263 MeV excitations. Shell-model calculations within the model space $[g_{9/2} \otimes (f_{7/2}^{-3})]_{8^-}$ suggest that the four lowest states are $T = 1$ and the strongest excitation, to the state at 13.263 MeV, is $T = 2$.

PACS numbers: 25.30.Cq, 27.40.+z

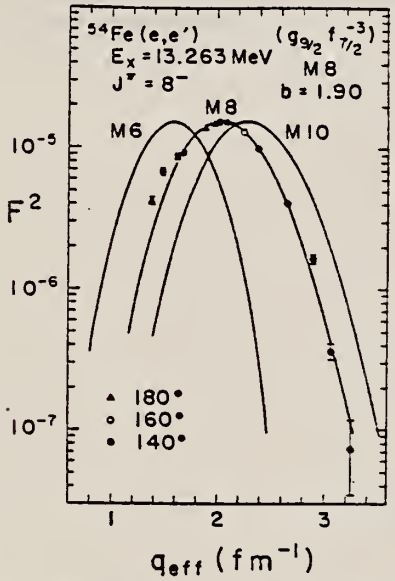

FIG. 2. The form factor squared, F^2, is plotted vs the effective momentum transfer, q_{eff}. Here, $F^2 = \eta(d\sigma/d\Omega)_{exp}/Z^2\sigma_M(\frac{1}{2} + \tan^2\frac{1}{2}\theta)$, where η is the usual recoil factor, $(d\sigma/d\Omega)_{exp}$ is the measured cross section at angle θ, and σ_M is the Mott scattering cross section. In plane-wave Born approximation, $q_{eff} = q(1 + \frac{3}{2}Z\alpha\hbar c/E_0R)$, where $R = \frac{5}{3}\langle r^2\rangle^{1/2}$ and $\langle r^2\rangle^{1/2} = 3.681$ fm, the rms radius of the ground-state charge distribution of ^{54}Fe (Ref. 10).

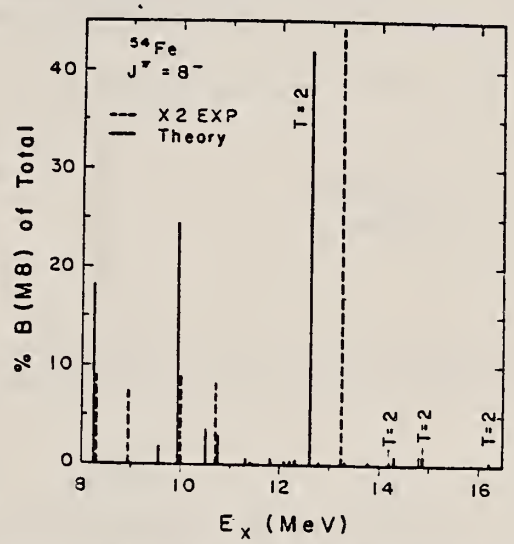

FIG. 3. Experimentally determined and calculated $M8$ transition strength plotted as a fraction of the total $M8$ strength. The total $M8$ strength or $M8$ sum rule is obtained by taking Eq. (3) with ($\alpha = 1$, $\beta = 0$) and with ($\alpha = 0$, $\beta = 1$) and adding both to Eq. (4) with $\gamma = 1$. The result is $F^2 = \frac{1}{8}(7M_1^2 + 2M_0M_1 + 7M_0^2)$. The $T = 2$ $M8$ sum rule is obtained from Eq. (4) with $\gamma = 1$.

REF. G. Eulenberg, D.I. Sober, W. Steffen, H.-D. Gräf, G. Küchler, A. Richter, E. Spamer, B.C. Metsch, W. Knüpfer
Phys. Lett. 116B, 113 (1982)

ELEM. SYM.	A	Z
Fe	54	26

METHOD

REF. NO. 82 Eu 1 egf

REACTION	RESULT	EXCITATION ENERGY	SOURCE		DETECTOR		ANGLE
			TYPE	RANGE	TYPE	RANGE	
E,E/	ABX	8-12	D	30-58	MAG-D		DST

M1 STRENGTH

Following the recent discovery of a very strong magnetic dipole transition in ^{48}Ca to a state at 10.23 MeV in high-resolution inelastic electron scattering, results of a detailed search for M1 strength in the other $N = 28$ isotones ^{50}Ti, ^{52}Cr and ^{54}Fe are described. The M1 strength found in the investigated region of excitation energy $E_x \approx 7$–12 MeV is very fragmented and considerably quenched in comparison to predictions of shell model calculations in a model space that includes up to 2p–2h excitations.

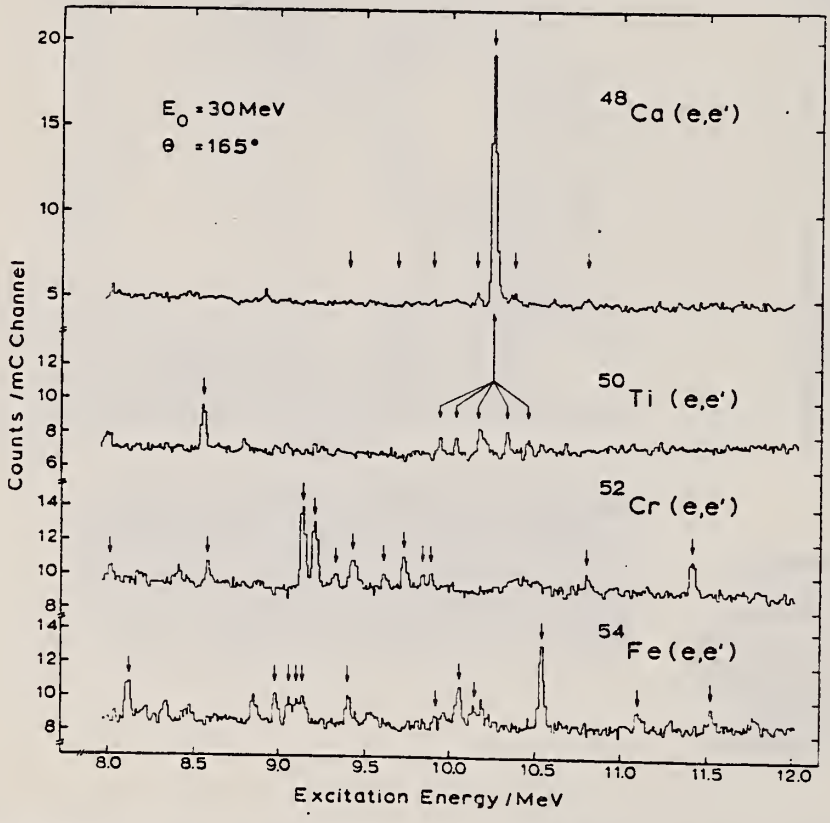

Fig. 1. High-resolution inelastic electron scattering spectra of the $N = 28$ isotones all measured at $E_0 = 30$ MeV and at $\theta = 165°$. The strongest magnetic dipole transitions are indicated by arrows.

(OVER)

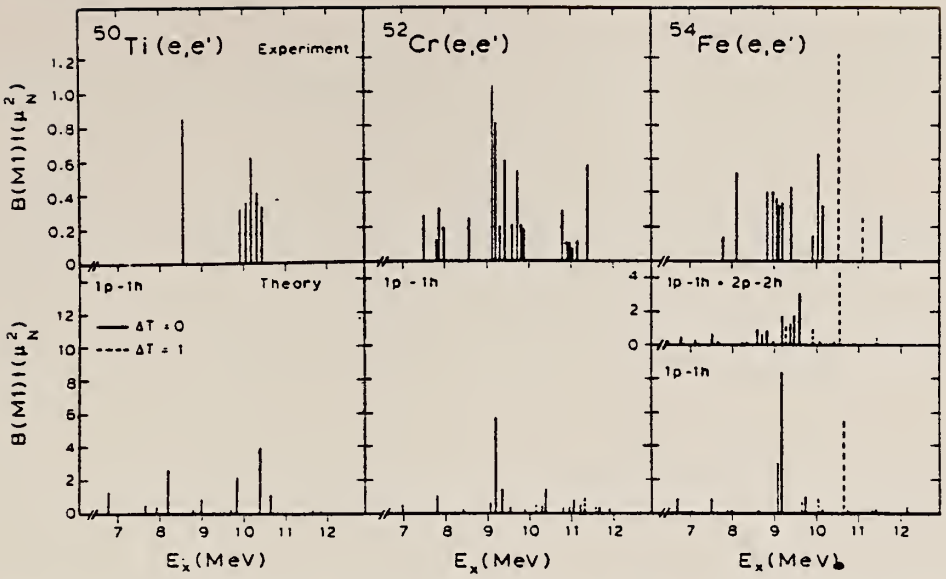

Fig. 3. Comparison of experimental and calculated M1 strength distributions for ^{50}Ti, ^{52}Cr and ^{54}Fe. Note the scale difference. For details, see the main text.

FE
A=56

FE
A=56

FE
A=56

Ref. R. Tobin, J. McElhinney, L. Cohen
Phys. Rev. 110, 1388 (1958)

Elem. Sym.	A	Z
Fe	56	26

Method: 22 MeV betatron; neutron counters

Ref. No.: 58 To 1 | EH

Reaction	E or ΔE	E_o	Γ	$\int \sigma dE$	Jπ	Notes
$Fe^{56}(\gamma,n)$	Bremss. 22					E_{th} = 11.34±0.10

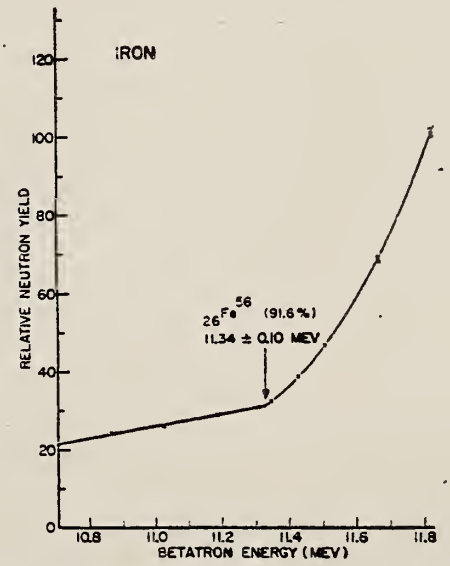

FIG. 3. Photoneutron yield from iron in the betatron-energy range from 10.7 to 11.8 Mev.

K. N. Geller, J. Halpern, and E. G. Muirhead
Phys. Rev. 118, 1302-12 (1960)

ELEM. SYM.	A	Z
Fe	56	26

METHOD	REF. NO.	
Betatron; neutron threshold; ion chamber	60 Ge 3	NVB

REACTION	RESULT	EXCITATION ENERGY	SOURCE		DETECTOR		ANGLE
			TYPE	RANGE	TYPE	RANGE	
G,N	NØX	THR	C THR		BF3-I		4 PI

THRESHØLD

TABLE I. Summary and comparison of neutron separation energies inferred from present threshold measurements with values predicted from mass data and reaction energies. All energies are expressed in the center-of-mass system in Mev.

Reaction	No. runs	Present results	Other results	Method	Reference
$Fe^{56}(\gamma,n)Fe^{55}$	1	11.25 ±0.06	11.159±0.028 11.34 ±0.10	mass data threshold	j k

[j] K. S. Quisenberry, T. T. Scolman, and A. O. Nier, Phys. Rev. 104, 461 (1956).
[k] See reference 2.

Ref. W.H. Kelly, G.B. Beard
Nuclear Phys. 27, 188 (1961)

Elem. Sym.	A	Z
Fe	56	26

Method: Nuclear resonance flourescence; gaseous source (Mn^{56} decay); NaI

Ref. No.: 61 Ke 2 JHH

Reaction	E or ΔE	E_o	Γ	$\int \sigma dE$	Jπ	Notes
(γ,γ)	845kev	845kev	7.3±2.5ev			"Thin absorber approximation" used to determine level width.

REF. S. Costa, F. Ferrero, S. Ferroni and R. Malvano
Proc. Paris Conference 1034 (1964)

ELEM. SYM.	A	Z
Fe	56	26

METHOD: 100 MeV synchrotron

REF. NO.: 64 Co 3 JDM

REACTION	RESULT	EXCITATION ENERGY	SOURCE		DETECTOR		ANGLE
			TYPE	RANGE	TYPE	RANGE	
G,N	ABΣ	THR-80	C	10-80	BF3-I		4PI

TABLE

ELEMENT	Yield (36 MeV) $\left(\frac{\text{n. cm}^2}{\text{mol. MeV}} \times 10^5\right)$	Σ_0^{30}	Σ_0^{80}	$\Sigma_0^{30}/\Sigma_0^{80}$	σ_{-1} (mb)
$_{24}$Cr	83	1.21	2.1	0.58	62
$_{25}$Mn	108	1.52	2.33	0.65	76
$_{26}$Fe	68	0.88	1.46	0.60	50
$_{27}$Co	89	1.08	1.82	0.59	64
$_{28}$Ni	44	0.55	1.07	0.51	34
$_{29}$Cu	95	1.06	1.99	0.53	72
$_{30}$Zn	88	0.94	1.68	0.56	66
$_{31}$Ga	130	1.29	2.18	0.59	94
$_{32}$Ge	139	1.35	2.29	0.59	101
$_{33}$As	137	1.22	2.18	0.56	100

$\sum_a^b = \frac{A}{60\,NZ}\int_a^b \sigma(E)\,dE$ is the integrated cross section measured in units of the classical dipole $60\,NZ/A$ mb. MeV.

REF.

B.L. Berman, G.S. Sidhu, and C.D. Bowman
Phys. Rev. Letters 17, 761 (1966)

EL.EM. SYM.	A	Z
Fe	56	26

METHOD

Linac

REF. NO. 66 Be 4 JDM

REACTION	RESULT	EXCITATION ENERGY	SOURCE		DETECTOR		ANGLE
			TYPE	RANGE	TYPE	RANGE	
G,N	ABX	11	C	13	TOF-D		135

The absolute cross section might contain systematic errors of up to 50%.

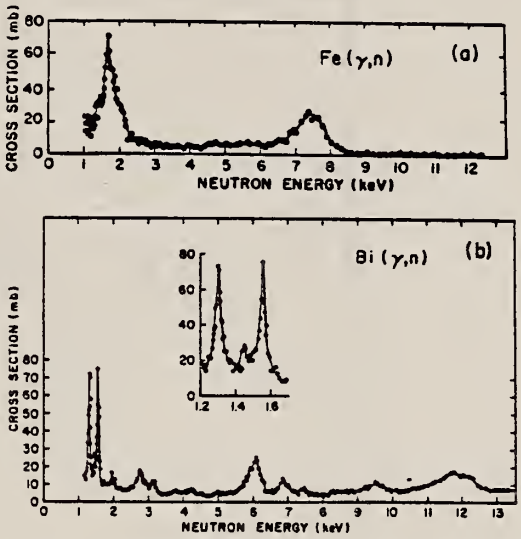

FIG. 2. Absolute cross section for threshold photoneutrons from iron and bismuth as a function of laboratory neutron energy [$\sigma = 4\pi(d\sigma/d\Omega)|_{135°}$].

(OVER)

Table I. Experimental parameters.

Neutron sample	Sample thickness (in.)	$E_{thr}(\gamma,n)$ (MeV)	Bremsstrahlung target	Target thickness (in.)	E_e (MeV)	Bremsstrahlung conversion efficiency (10^{-8} photon/electron sr eV)	Ω_γ (sr)	Average beam current (μA)	W (μsec/channel)	Beam burst width (nsec)	Run time (h)
Fe	1.017	11.21[a]	Al	1.015	12.5	1.57	0.025	36.8	0.125	500	4
Bi	0.502	7.43	Ag	0.249	11.0	4.64	0.133	6.4	0.0625	40-100	34

[a] Fe^{56} (isotopic abundance 91.7 %).

REF.

C. D. Bowman, G. S. Sidhu and B. L. Berman
Phys. Rev. 163, 951 (1967)

ELEM. SYM.	A	Z
Fe	56	26

METHOD

REF. NO.: 67 Bo 2 | HMG

REACTION	RESULT	EXCITATION ENERGY	SOURCE TYPE	SOURCE RANGE	DETECTOR TYPE	DETECTOR RANGE	ANGLE
G,N	ABX	12,13	C	12,13	TOF-D	0-1	135
		(11.6,12.7)		(11.6,12.7)		(0-70 keV)	

Spin of the two major resonances is 1^-.

J-PI

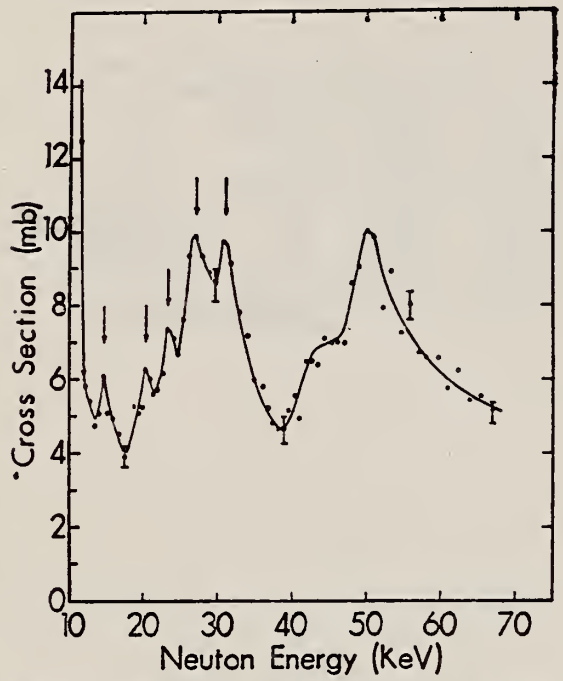

FIG. 6. Absolute photoneutron cross section $\sigma = 4\pi(d\sigma/d\Omega)_{135°}$. The counting statistics for this experiment are shown for a few points by the error bars. The absolute cross-section scale is uncertain to ±30%. The energies of the peaks denoted by the vertical arrows are tabulated in Table I.

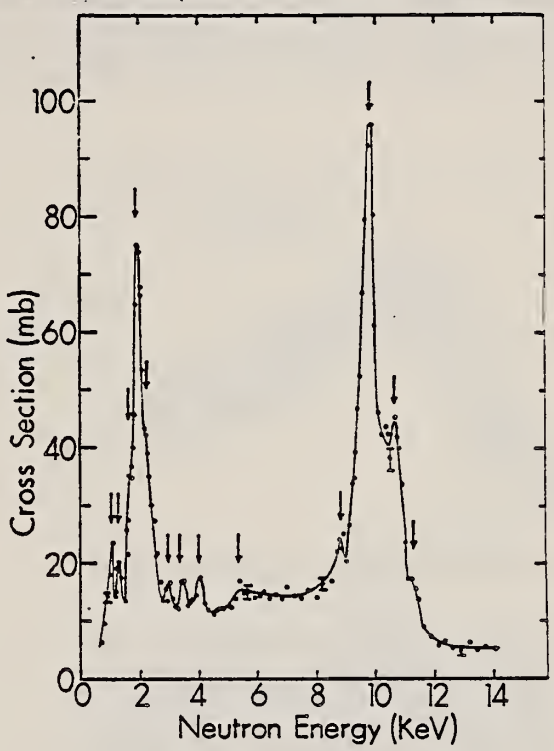

FIG. 5. Absolute photoneutron cross section $\sigma = 4\pi(d\sigma/d\Omega)_{135°}$. The counting statistics for this experiment are shown for a few points by the error bars. The absolute cross-section scale is uncertain to ±30%. The energies of the peaks denoted by the vertical arrows are tabulated in Table I.

TABLE II. Parameters from shape analysis.

E_n (eV)	Resolution (eV)	FWHM[a] (eV)	σ_{obs} (mb)	σ_0 (mb)	$\Gamma \cong \Gamma_n$ (eV)	$g\Gamma_{\gamma 0}$[b] (eV)
1920	66±22	420	73	75	415	0.80
9800	340±120	660	96	136	$560_{+50}{}^{-100}$	$1.93_{-0.15}{}^{+0.1}$

[a] Full width at half maximum.
[b] These numbers do not include the 30% uncertainty in the normalization of the cross section.

TABLE I. Energies of peaks in the cross section.

E_L[a] (keV)	$(E-Q)$[b] (keV)	E_n[c] (keV)
1.05	1.28	1.30
1.25	1.51	1.54
1.65	1.94	1.97
1.92	2.22	2.26
2.20	2.54	2.58
2.95	3.36	3.42
3.40	3.84	3.91
4.00	4.49	4.57
5.35	5.92	2.06
8.80	9.55	9.71
9.80	10.62	10.8
10.65	11.50	11.7
11.30	12.2	12.4
14.70	15.9	16.2
21.0	22.3	22.7
23.5	24.9	25.4
27.0	28.5	29.0
31.0	32.6	33.2

[a] E_L is the energy of the neutrons at the peaks in the cross section measured at 135° in the laboratory system. The uncertainty in flight time, which was 0.25 μsec, corresponds to an uncertainty in energy (not shown in the table) of ±0.01 keV at $E_L = 1$ keV and ±2 keV at 31 keV.
[b] $E-Q$ is the total kinetic energy in the center-of-mass system after photoejection of the neutron from the target nucleus. All resonances were assumed to belong to the Fe^{56} compound nucleus.
[c] E_n is the neutron energy required to excite the same resonance by the $Fe^{55}(n,\gamma_0)$ reaction.

REF.

J. M. Loiseaux, J. M. Maison, and M. Langevin
J. de Physique 28, 11 (1967)

ELEM. SYM.	A	Z
Fe	56	26

METHOD

REF. NO. 67 Lo 1 JOC

REACTION	RESULT	EXCITATION ENERGY	SOURCE		DETECTOR		ANGLE
			TYPE	RANGE	TYPE	RANGE	
G,G/	ABX	14-32	C	34	NAI-D		DST

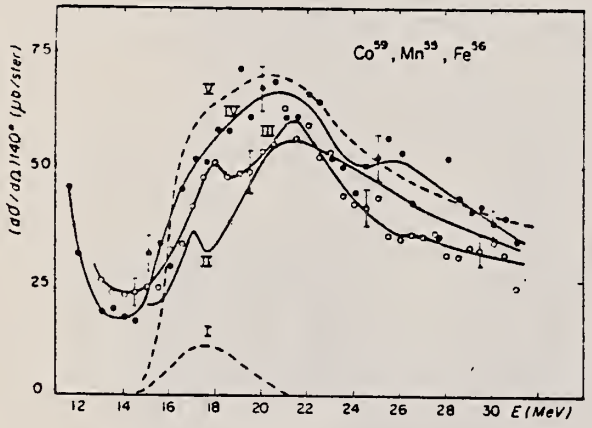

FIG. 10.

Sections efficaces différentielles de diffusion à 140° pour ^{55}Mn (courbe II), ^{56}Fe (courbe III), ^{59}Co (courbe IV). Section efficace de diffusion tenseur (courbe I) et section efficace de diffusion scalaire + tenseur (courbe V) calculées avec les paramètres de Fultz et al. [16] pour ^{59}Co.

Y. Oka, T. Kato, K. Nomura, T. Saito, Hui-Tuh Tsai
Bull. Chem. Soc. Japan 41, 380 (1968)

Fe	56	26

METHOD

REF. NO. 68 Ok 3 egf

REACTION	RESULT	EXCITATION ENERGY	SOURCE		DETECTOR		ANGLE
			TYPE	RANGE	TYPE	RANGE	
G;NP	ABY	THR-20	C	20	ACT-I		4PI

TABLE 2. THE YIELDS OF SOME (γ, pn) REACTIONS WITH 20 MeV BREMSSTRAHLUNG

Reaction	Half-life of product	Specific activity[a] (μCi/mg)	Yield ($mol^{-1} \cdot R^{-1}$)
$^{56}Fe(\gamma, pn)^{55}Mn$	314 d	2.5×10^{-6}	3.6×10^{2}
$^{66}Zn(\gamma, pn)^{65}Cu$	13 hr	7.2×10^{-3}	7.5×10^{2}
$^{104}Pd(\gamma, pn)^{103}Rh$	210 d	1.1×10^{-6}	1.7×10^{3}

a) The value corrected at the end of 1 hr irradiation (9.4×10^{8} R/min).

REF. K. Shoda, K. Abe, T. Ishizuka, N. Kawamura, M. Oyamada, and Baik-Nung Sung
J. Phys. Soc. Japan 25, 664 (1968)

ELEM. SYM.	A	Z
Fe	56	26

METHOD

REF. NO. 68 Sh 3 egf

REACTION	RESULT	EXCITATION ENERGY	SOURCE		DETECTOR		ANGLE
			TYPE	RANGE	TYPE	RANGE	
G,XP	ABX	THR-23	C	13-23	SCI-I		DST

SPECTRA ALSO GIVEN

Table II. Anisotropic factor B/A of angular distributions determined by least-squares fits with $A+B\sin^2\theta$.

^{56}Fe ($E_{\gamma max}$=24.0 MeV)	
E_p(MeV)	B/A
2.8–3.8	−0.4±0.1
3.8–5.7	−0.01±0.05
5.7–6.4	0.5±0.1
6.4–8.1	0.3±0.1
8.1≦	0.7±0.3
2.8≦	0.01±0.06

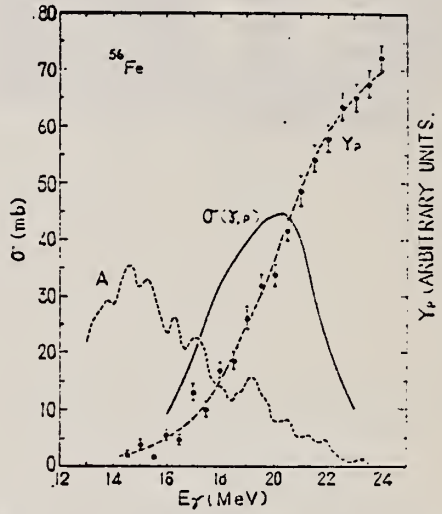

Fig. 15. Comparison among the photoproton cross sections on ^{56}Fe. Curve A is the cross section calculated from the present energy distribution under the assumption that the residual nucleus is completely left in the ground state. Photoproton yield curve using ZnS(Ag) scintillation counters and the cross section calculated from it are indicated by Y_p and $\sigma(\gamma, p)$ respectively.

REF. R. J. Peterson, Horst Theissen and W. J. Alston
Nucl. Phys. A153, 610 (1970)

ELEM. SYM.	A	Z
Fe	56	26

METHOD

REF. NO. 70 Pe 2 egf

REACTION	RESULT	EXCITATION ENERGY	SOURCE		DETECTOR		ANGLE
			TYPE	RANGE	TYPE	RANGE	
E,E/	FMF	0-5	D	60	MAG-D		DST
				(60.2)			

7 2+, 1 3- STATES

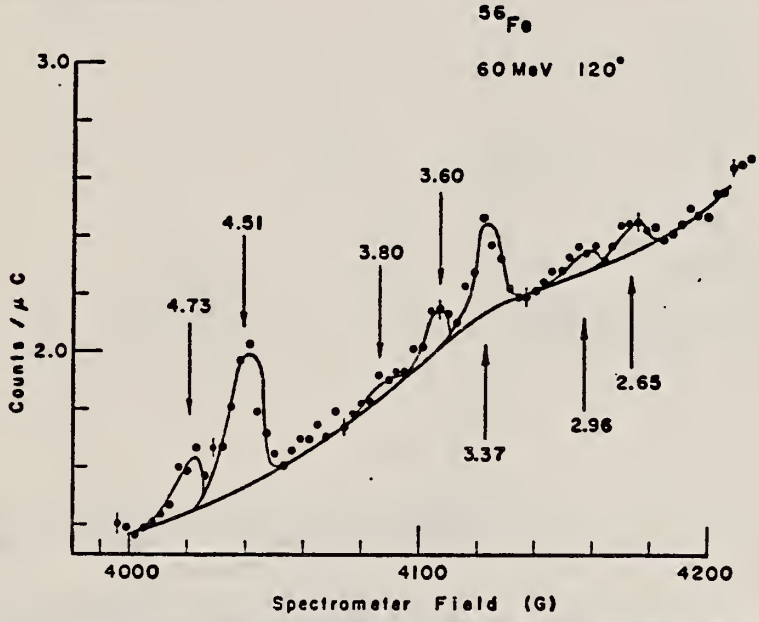

Fig. 2. A typical spectrum of electrons at a beam energy of 60.2 MeV scattered from ^{56}Fe. The bump in the background is due to electron showers generated by the elastic peak striking the spectrometer wall.

TABLE 2

The electromagnetic reduced matrix elements $B(EL)\uparrow$ found in the present study of ^{56}Fe compared to those of the earlier work at a bombarding energy of 150 MeV and the strengths generated by the use of the βR values reported from inelastic proton scattering

	$B(EL)\uparrow$ ($e^2 \cdot fm^{2L}$)				
E2	Present work	Orsay (DWBA)	Orsay [a] (PWBA)	(p, p') [b]	Doppler shift [c]
0.85 MeV	1250	1240	720	1400	892
2.65	37		112	190	17
2.96	21			32	10
3.37	41			30	55
3.60	17			46	13-64
3.80 (doublet)	10			74	8.3
4.73	19			42	

E3	Present work	Orsay (DWBA)	Orsay (PWBA)	(p, p')
4.51	1.66×10^4	1.89×10^4	1.04×10^4	1.79×10^4

[a]) Ref. [4]). [b]) Ref. [3]). [c]) Ref. [22]).

[3]R.J. Peterson, Ann. of Phys. 53, 40 (1969).
[4]J. Bellicard and P. Barreau, Nucl. Phys. 36, 476 (1962).
[22]G. G. Seaman et al., Phys. Rev. 188, 1706 (1969).

REF. R. J. Peterson, Horst Theissen and W. J. Alston
Nucl. Phys. A153, 610 (1970)

ELEM. SYM.	A	Z
Fe	56	26

METHOD

REF. NO. 70 Pe 2 egf

REACTION	RESULT	EXCITATION ENERGY	SOURCE TYPE	SOURCE RANGE	DETECTOR TYPE	DETECTOR RANGE	ANGLE

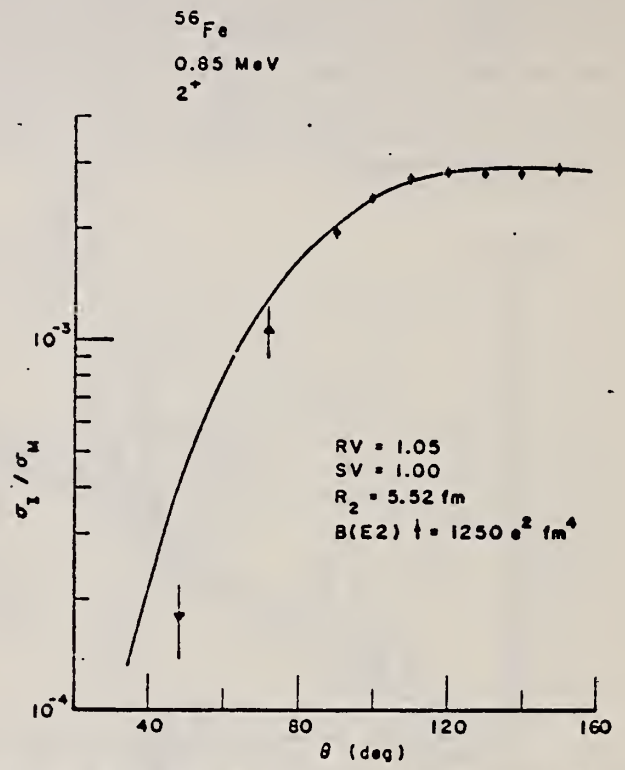

Fig. 5. The ratio of the observed cross section for populating the 0.85 MeV 2^+ state of ^{56}Fe to the Mott prediction is compared to the DWBA prediction. The parameters used for the fit are listed, as is the calculated transition radius. The data points taken at 110° at beam energies of 30.0 MeV and 42.9 MeV are plotted at the angle for which the same momentum transfer is obtained at 60.2 MeV. These two points have been adjusted to a beam energy of 60.2 MeV according to DWBA calculations.

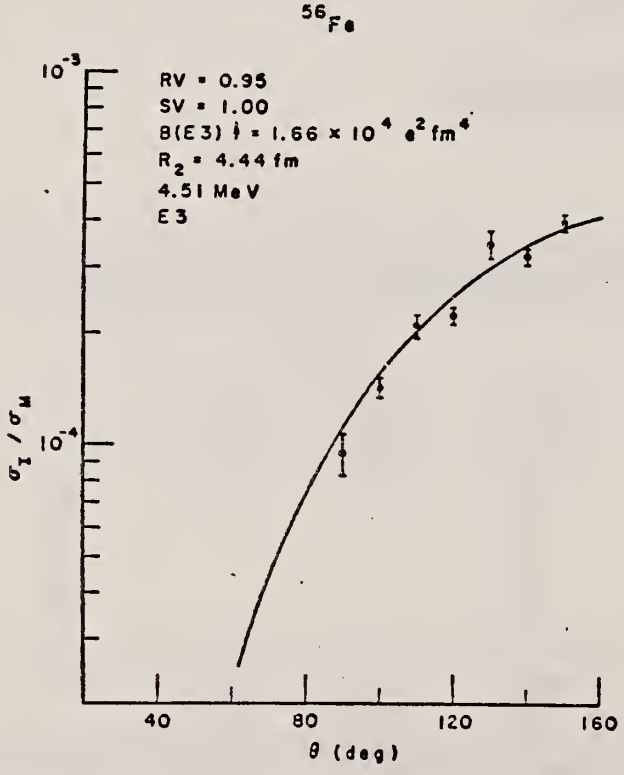

Fig. 7. The angular distribution for populating the 4.51 MeV 3^- state of ^{56}Fe is compared to the DWBA prediction.

U.S. DEPARTMENT OF COMMERCE
NATIONAL BUREAU OF STANDARDS

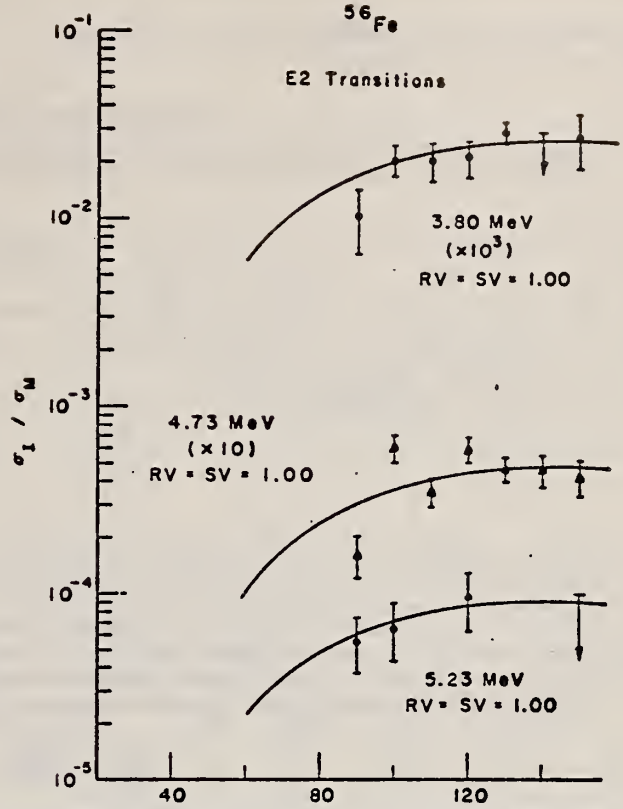

Fig. 9. The angular distributions for populating several probable 2^+ states of ^{56}Fe are shown and compared to DWBA predictions. The parameters used for the fits are listed in table 1.

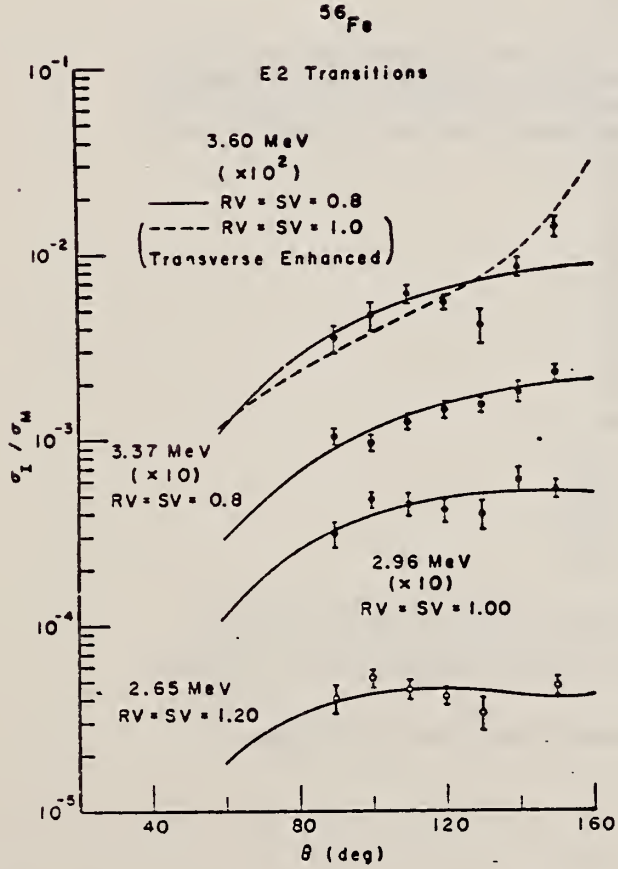

Fig. 8. The angular distributions for exciting four known 2^+ states of ^{56}Fe are shown and compared to DWBA predictions. The predicted shapes are chosen from those of fig. 6. For the 3.60 MeV state we also show the prediction obtained with an enhanced transverse electric excitation.

REF. R. J. Baglan, C. D. Bowman and B. L. Berman
Phys. Rev. C3, 672 (1971)

ELEM. SYM.	A	Z
Fe	56	26

METHOD

REF. NO. 71 Ba 2 hmg

REACTION	RESULT	EXCITATION ENERGY	SOURCE TYPE	SOURCE RANGE	DETECTOR TYPE	DETECTOR RANGE	ANGLE
G,N	ABX	11-13	C	11,13	TOF-D		135
		(11.2-12.7)					

TABLE VI. Resonance parameters for ^{56,57}Fe and ^{52,53}Cr. For all resonances, the area under the peak in the 135° differential cross section is multiplied by 4π to yield approximate values for $g_\gamma\Gamma_{\gamma 0}\Gamma_n/\Gamma \simeq g_\gamma\Gamma_{\gamma 0}$. For those resonances where J^π is known, the differential area is multiplied by the appropriate factor F from Table I to obtain $\Gamma_{\gamma 0}$. E_L is the laboratory neutron energy for the (γ,n) reaction and E_n is the corresponding laboratory neutron energy for a neutron-induced reaction. Column 5 labels the peak as a ground-state (GS) or excited-state (ES) transition as determined in this work alone. Clearly, if a peak is seen in a neutron-induced reaction (columns 9–11), it must be GS.

Nucleus	E_L (keV)	E_{ex} (MeV)	$g_\gamma\Gamma_{\gamma 0}\Gamma_n/\Gamma$ (eV)	GS or ES	J^π	$\Gamma_{\gamma 0}$ (eV)	E_n (keV) (This work)	E_n (keV) from neutron-induced reactions (Ref. a)	(Ref. b)	(Ref. c)
^{56}Fe	83.1	11.290	0.30	GS			88.1			
	97.6	11.304	0.47	GS			103.4			
	105	11.312	0.30				111			
	124	11.332	0.22	GS			131			
	132	11.340	0.23	GS			139			
	138	11.346	0.29	GS			146			
	164	11.373	0.74	GS			173			
	189	11.398	0.73	GS			199			
	195	11.405	0.80	GS			205			
	218	11.428	1.27	GS			229			
	228	11.438	0.31	GS			240			
	267	11.478	0.91	GS			280			
	274	11.485	1.84	GS			288			
	307	11.519	0.47				322			
	316	11.529	0.29				332			
	338	11.551	1.20	GS			354			
	347	11.560	1.13	GS			364			
	374	11.588	2.15	GS			392			
	388	11.602	1.64	GS			407			
	430	11.645	1.04	GS			450			
	450	11.666	0.95	GS			471			
	488	11.705	1.19	GS			511			
	502	11.719	1.03	GS			526			
	543	11.761	0.97	GS			568			
	576	11.795	0.34				602			
	594	11.813	1.89	GS			621			
	627	11.847	2.30	GS			656			
	705	11.927	0.37				737			

17(a) C.D. Bowman, E.G. Bilpuch, and H.W. Newson, Ann. Phys. (N.Y.) 17, 319 (1962).

b) See R.W. Hockenbury, Z.M. Bartolome, J.R. Tatarczuk, W.R. Moyer, and R.C. Block, Phys. Rev. 178, 1746 (1969).

19(c) R.G. Steiglitz, Ph.D. thesis, Rensselaer Polytechnic Institute, 1970, (unpub.)

[over]

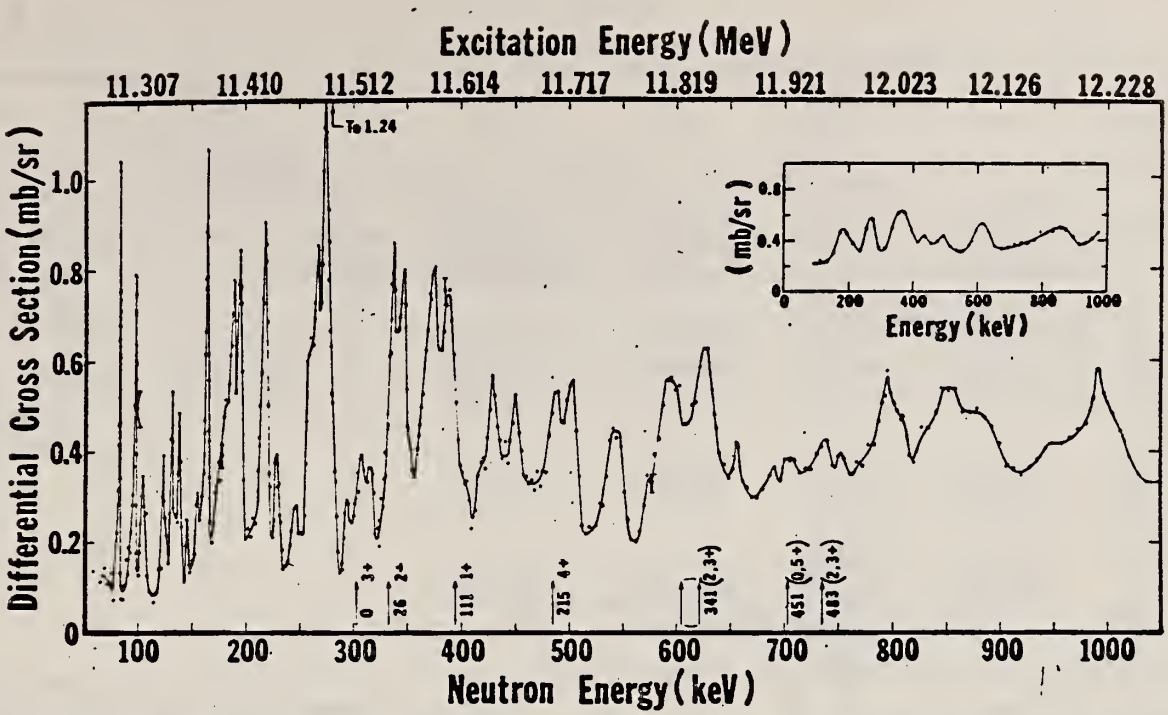

FIG. 11. The 135° differential threshold photoneutron cross section for ^{56}Fe (see caption to Fig. 4). The arrows below the data indicate the positions of isobaric analogs of low-lying states of ^{56}Mn. Next to the arrows are the values of J^{π} and the energy in keV of these low-lying states.

FIG. 4. The 135° differential threshold photoneutron cross section for ^{207}Pb at low energies versus the energy of the emitted neutron (lower scale) and the excitation energy (upper scale). The arrows indicate peaks which decay to excited states of the residual nucleus (ES), or peaks owing to contaminating isotopes in the photoneutron sample. The inset shows the ^{207}Pb(γ, n) cross section averaged with a square 40-keV wide smoothing function.

REF. J. Heisenberg, J. S. McCarthy and I. Sick
Nucl. Phys. A164, 353 (1971)

ELEM. SYM.	A	Z
Fe	56	26

METHOD

REF. NO. 71 He 1 egf

REACTION	RESULT	EXCITATION ENERGY	SOURCE		DETECTOR		ANGLE
			TYPE	RANGE	TYPE	RANGE	
E,E/	FMF	1	D	198-300	MAG-D		DST

1 = .880

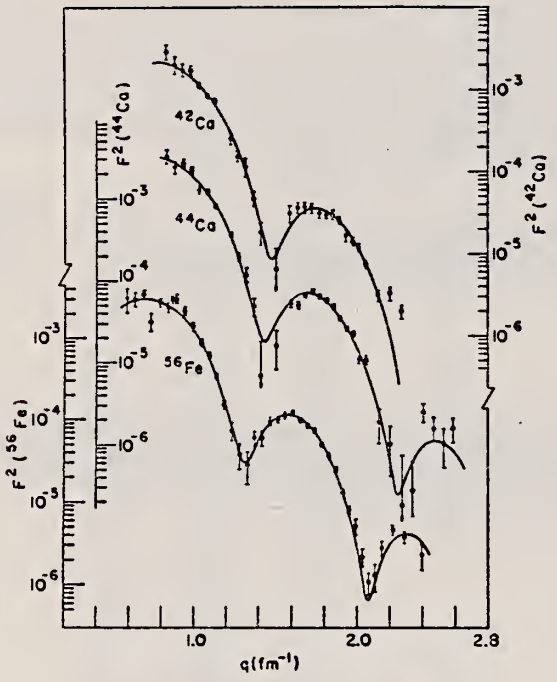

Fig. 1. Fits to the ^{42}Ca, ^{44}Ca and ^{56}Fe 2^+ levels.

FORM NBS-418
(REV. 7-14-64)
USCOMM-DC 26010-P64

U.S. DEPARTMENT OF COMMERCE
NATIONAL BUREAU OF STANDARDS

TABLE 2

Inelastic parameters for 2^+ levels

Isotope	E^* (MeV)	B(E2) Coulomb Excit. ($e^2 \cdot fm^4$)	Shape	c_{tr} [a]) (fm)	z_{tr} [a]) (fm)	Fitted B(E2) ($e^2 \cdot fm^4$) [b])	R_{tr} [a]) (fm)	B(E2)($e^2 \cdot fm^4$) heavy-particle scattering
^{42}Ca	1.520	364± 82 [9])	2	3.541±0.025	1.459±0.020	320±20	4.619±0.030	476± 74 [19])
^{44}Ca	1.160	350± 70 [10])	2	3.691±0.027	1.428±0.020	480±30	4.704±0.030	507±100 [19])
			1	3.454±0.025	0.690±0.010	1270±85	5.553±0.030	
	3.259		2			54±10		
^{46}Ti	0.885	830±170 [14])	2	3.807±0.014	1.397±0.010	740±20	4.763±0.017	867 [20])
		560±100 [13])	1	3.562±0.014	0.669±0.005	1680±50	5.510±0.020	738 [11])
^{48}Ti	0.984	700±140 [14])	2	3.777±0.014	1.340±0.010	537±15	4.671±0.017	788±120 [19])
		310± 70 [13])	1	3.539±0.014	0.633±0.005	1110±30	5.321±0.020	673 [11])
								659 [20])
	2.420		2			49± 8		57± 10 [19])
^{50}Ti	1.550	240± 20 [12])	2	3.768±0.014	1.255±0.010	307±10	4.567±0.017	349 [20])
			1	3.535±0.014	0.576±0.005	515±17	5.047±0.020	260 [21])
								431 [24])
	4.320		2			51± 8		72 [24])
^{56}Fe	0.850	877± 70 [c])	2	4.048±0.024	1.357±0.014	945±45	4.919±0.025	
			1	3.878±0.024	0.651±0.006	1570±70	5.454±0.030	
				Present experiment				—

[a]) Errors do not reflect any model dependence.
[b]) Given errors do not include the 6 % error of normalization.
[c]) Average for B(E2) formed from values of refs. [13–18]).

13) J. Simpson, J. Cookson, D. Eccleshall and M. Yates, Nucl. Phys. 62 (1965) 385
14) G. M. Temmer and N. P. Heydenburg, Phys. Rev. 104 (1956) 967
15) D. S. Andreyev, A. P. Grinberg, K. I. Erokhina and I. Kh. Lemberg, Nucl. Phys. 19 (1960) 400
16) F. R. Metzger, Nucl. Phys. 27 (1961) 612
17) W. H. Kelly and G. B. Beard, Nucl. Phys. 27 (1961) 188
18) R. B. Begzhanov, A. A. Islamov, D. K. Kaipov and Yu. K. Shubnyi, JETP (Sov. Phys.) 17 (1963) 94

REF. A.S. Litvinenko, N.G. Shevchenko, A.Yu. Buki, P.L. Kondrat'ev, G.A. Savitskii, A.A. Khomich, V.M. Khvastunov, I.I. Chkalov
Ukr. Fiz. Zhur. 17, 1197 (1972)

ELEM. SYM.	A	Z
Fe	56	26

METHOD

REF. NO. 72 Li 3 hmg

REACTION	RESULT	EXCITATION ENERGY	SOURCE TYPE	SOURCE RANGE	DETECTOR TYPE	DETECTOR RANGE	ANGLE
E,E/	FMF	1	D	150,225	MAG-D		DST

B(EL) LEV .85

Таблица 1

Параметры фермиевского распределения плотности заряда (*c*—радиус полуспада плотности, *t*—диффузионность ядра)

Ядро	*c*, *ф*	*t*, *ф*
Fe^{54}	4,012±0,007	2,346±0,011
Fe^{56}	3,971±0,013	2,608±0,020
Fe^{58}	4,027±0,019	2,530±0,031
Ni^{62}	4,149±0,011	2,506±0,016

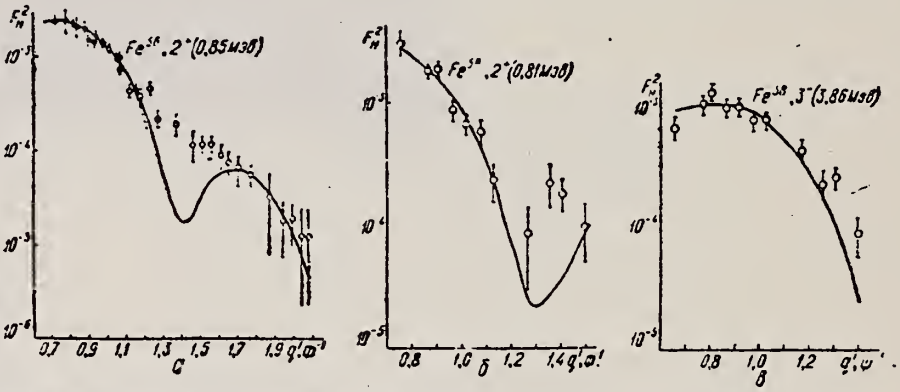

Формфакторы *E*2- и *E*3-переходов в ядрах Fe^{56} (*а*) и Fe^{58} (*б*, *в*). Сплошные кривые — расчет по вибрационной модели в высокоэнергетическом приближении: ⊖ — 150 *Мэв*; ○ — 225 *Мэв*. ▲ — данные работы [6]; пунктирная кривая — расчет в борновском приближении [6].

Таблица 2

Ядро	E_λ, *Мэв*	J^π	Данные настоящей работы $B(E\lambda)\uparrow$, $e^2\lambda^2 R^{2\lambda}$	Данные других работ $B(E\lambda)\uparrow$, $e^2\lambda^2 R^{2\lambda}$	Данные других работ: Тип эксперимента и метод определения	Литература
Fe^{56}	1,4	2^+	531,9±32,4	533	(ee'), борновское приближение	[6]
	4,85	3^-	4563±410	4390		
Fe^{58}	0,85	2^+	678,1±47,5	720	(ee'), борновское приближение	»
				1250±270	искаженные волны	[7]
				1240	борновское приближение	»
				900±100	кулоновское возбуждение	[8]
Fe^{58}	0,81	2^+	943,2±79			
	3,86	3^-	13880±1260			
Ni^{62}	1,17	2^+	618,6±42,1	877± 11	(ee'), искаженные волны	[9]
	3,75	3^-	14359±962	20100±540		

U.S. DEPARTMENT OF COMMERCE
NATIONAL BUREAU OF STANDARDS

REF. Y. Torizuka, Y. Kojima, T. Saito, K. Itoh, A. Nakada, S. Mitsunobu, M. Nagao, K. Hosoyama, S. Fukuda
PICNS-72, p.171 Sendai

ELEM. SYM.	A	Z
Fe	56	26

METHOD

REF. NO.	
72 To 6	hvm

REACTION	RESULT	EXCITATION ENERGY	SOURCE		DETECTOR		ANGLE
			TYPE	RANGE	TYPE	RANGE	
E,E/	SPC	0- 37	D	250	MAG-D		35

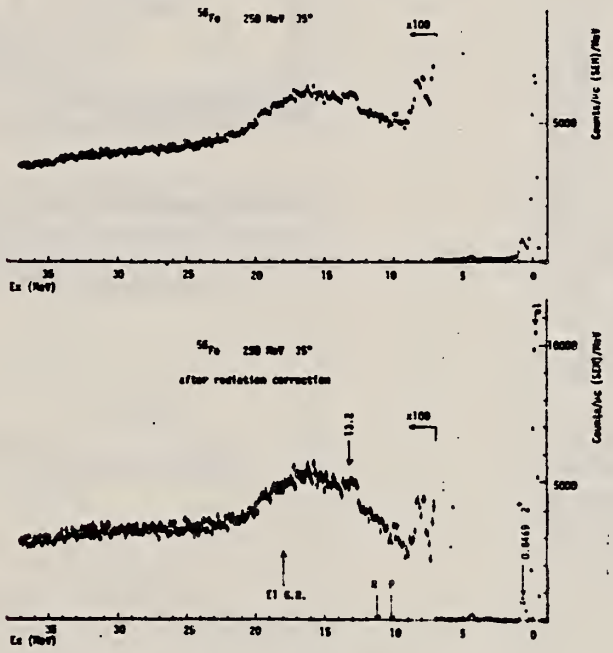

Fig. 1. The spectra of ^{56}Fe obtained at 250 MeV and 35°. The upper figure corresponds to the raw spectrum and the lower one to the spectrum after radiation tail subtraction. The peak of the E1 giant resonance is indicated at 18 MeV and the proton or neutron emission threshold energy is shown by the arrows.

REF. Y. Torizuka, Y. Kojima, T. Saito, K. Itoh, A. Nakada, S. Mitsunobu, M. Nagao, K. Hosoyama, S. Fukuda, H. Miura
PICNS-73, Vol.I, p.675 Asilomar

ELEM. SYM.	A	Z
Fe	56	26

METHOD

REF. NO. 73 To 1 hmg

REACTION	RESULT	EXCITATION ENERGY	SOURCE TYPE	SOURCE RANGE	DETECTOR TYPE	DETECTOR RANGE	ANGLE
E,E/	FMF	10- 35	D	150, 250	MAG-D		DST

FMF OF 16.1 MEV LEV

Table II. B(EL), $|M_{if}|^2$ and fractions of energy-weighted sum rules (EWSR) with T=0 in ^{56}Fe.

E_x (MeV)	J^π	$B(E2)_{or}\|M_{if}\|^2$	$\frac{E_x \cdot B(E2)}{EWSR}$	$\frac{E_x \cdot \|M_{if}\|^2}{EWSR}$
16.1	2^+	672 e^2fm^4	0.80	
16.1	0^+	1370 fm^4		1.43

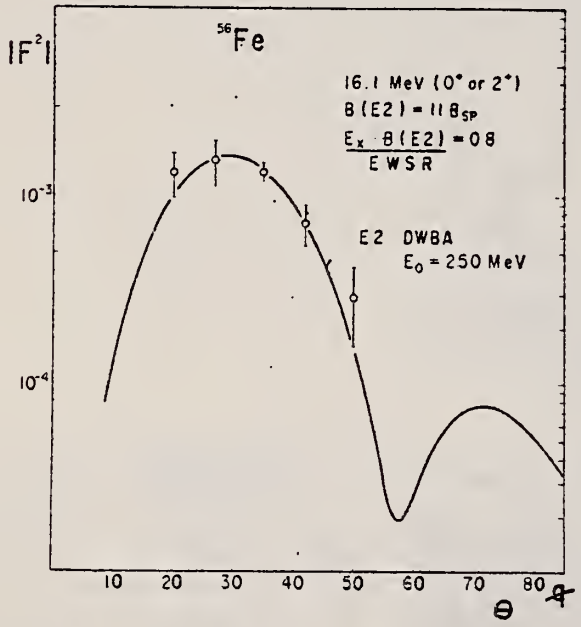

Fig. 4. The form factor for the 16.1-MeV state.

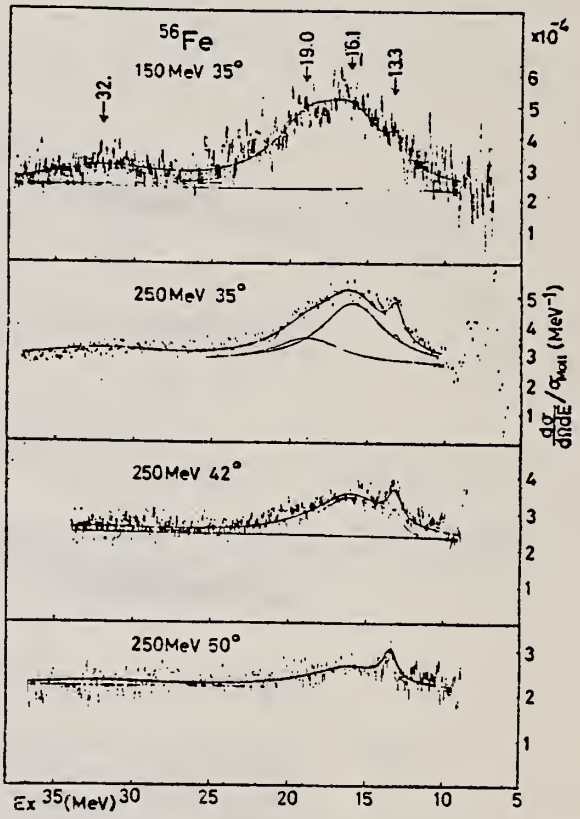

Fig. 3. Inelastic electron scattering spectra of ^{56}Fe in the range from 10 to 35 MeV. The arrows indicate peaks at 13.3, 16.1, 19.0, and ∿32 MeV.

REF. V. V. Verbinski, Hans Weber, and R. E. Sund
Phys. Rev. C8, 1002 (1973)

ELEM. SYM.	A	Z
Fe	56	26

METHOD

REF. NO. 73 Ve 3 hmg

REACTION	RESULT	EXCITATION ENERGY	SOURCE TYPE	SOURCE RANGE	DETECTOR TYPE	DETECTOR RANGE	ANGLE
G,N	ABX	11- 14	C	11, 13	TOF-D		93
		(11.20-13.27)		(11.71, 13.27)			

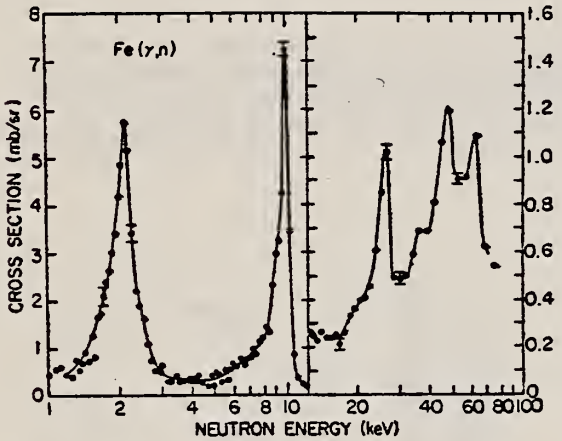

FIG. 4. The 93° differential threshold photoneutron cross section for Fe(γ, n) versus the energy of the emitted neutron. Electrons of 13.27-MeV and 3% resolution were incident on the bremsstrahlung converter, and the time analyzer was set at 250 nsec per channel.

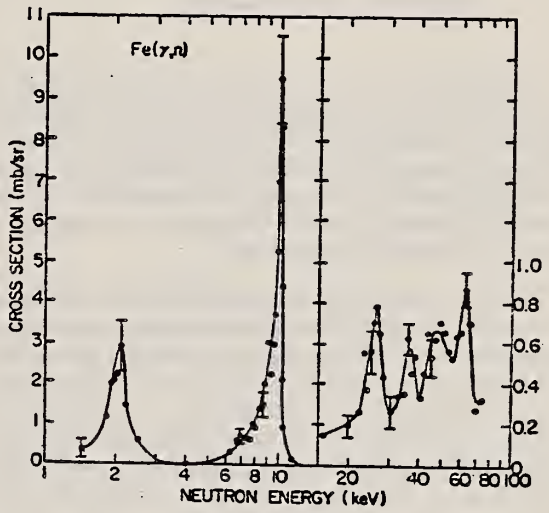

FIG. 5. The 93° differential threshold photoneutron cross section for Fe(γ, n) versus the energy of the emitted neutron. Electrons of 11.71-MeV and 1% resolution were incident on the bremsstrahlung converter, and the time analyzer was set at 62.5 nsec per channel.

TABLE II. Resonance parameters from threshold Fe(γ,n) data.

Neutron energy (keV)	Width at half maximum (keV)	Experimental resolution (keV) Fig. 4	Fig. 5	Deexcitation to ground state (G) or to excited states (E) of ^{55}Fe	$\Gamma \approx \Gamma_n$ (keV)	$g\Gamma_{\gamma 0}\Gamma_n/\Gamma$ (eV)
2.1	0.40 (Fig. 4)	0.052	0.039	E(=0.411 MeV)	0.40	0.68
~2.5		0.066	0.050	?		
10.0	0.4 (Fig. 5)	0.51	0.36	G	~0.17	1.97

REF. A.I. Abramov, V.Ya. Kitaev, A.V. Rogov, M.G. Yutkin
Yad. Fiz. 24, 871 (1976)
Sov. J. Nucl. Phys. 24, 455 (1976)

ELEM. SYM.	A	Z
Fe	56	26

METHOD

REF. NO. 76 Ab 9 hg

REACTION	RESULT	EXCITATION ENERGY	SOURCE		DETECTOR		ANGLE
			TYPE	RANGE	TYPE	RANGE	
G,N	ABX	11-14	C	11-14	TOF-D		78

The reaction $^{56}Fe(\gamma,n)^{55}Fe$ near threshold

A. I. Abramov, V. Ya. Kitaev, A. V. Rogov, and M. G. Yutkin

Physics and Power Engineering Institute
(Submitted February 23, 1976)
Yad. Fiz. 24, 871–872 (October 1976)

PACS numbers: 25.20.+y, 27.40.+z

Experiments on the (γ, n) reaction near threshold in iron nuclei have been carried out repeatedly by various groups of investigators.[1–5] The existence of several strong resonances in the region of neutron energies up to 20 keV makes this reaction very convenient for development of technique and for comparison of results obtained in different laboratories.

Up to this time all of the measurements in this energy region have been carried out exclusively with samples of natural iron. Here it has been assumed that at least the strongest resonances at $E_n \simeq 2$ and 10 keV are due to the (γ, n) reaction in the isotope ^{56}Fe. In regard to the weaker resonances, it has been impossible to exclude with a sufficient degree of reliability their connection with the (γ, n) reactions in the other isotopes of iron, particularly ^{57}Fe, and therefore the assignment of them to the reaction $^{56}Fe(\gamma, n)^{55}Fe$ (as was done in all of the studies cited) is only hypothetical in nature.

In order to check the validity of this assumption, we have measured the cross section for the reaction $^{56}Fe(\gamma, n)^{55}Fe$ with a sample containing the isotope ^{56}Fe in the amount 99.7% (91.7% in natural iron). The sample had the shape of a disk 75 mm in diameter and weight 218.4 grams. The experimental method has been described in detail elsewhere.[5] The figure shows the experimental results in the neutron energy region from 2 to 130 keV, obtained with a bremsstrahlung maximum energy of 13.3 MeV. The arrows denote the location of the resonances according to the data of our earlier work.[5] From the results presented it follows that the previously observed resonances at $E = 2.16$, 10.15, 26.5, 43.5, 49.8, 63.8, and 109.6 eV can be assigned definitely to the (γ, n) reaction in the isotope ^{56}Fe. The resonances at $E_n = 6.85$, 9.59, 20.5, and 31.6 keV did not appear in our measurements. At the same time, in the regions 3–6 and 13–17 keV some structural details appear which can be compared with the resonances of other studies.[1,2,4] However, this question can be finally answered only after a more detailed study.

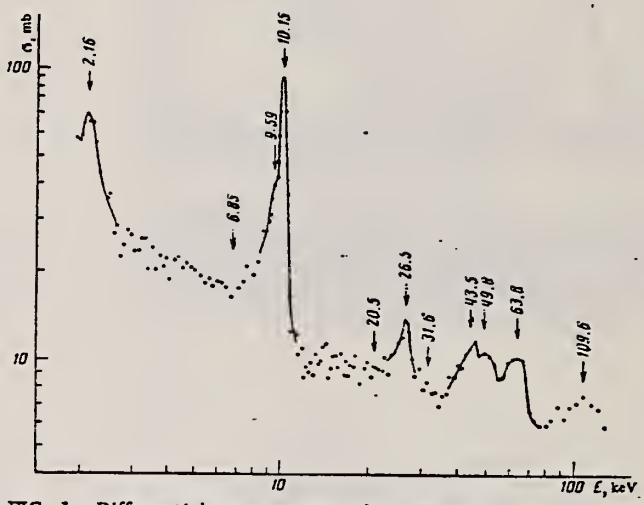

FIG. 1. Differential cross sections for the reaction $^{56}Fe(\gamma, n)^{55}Fe$ for $E_{\gamma max} = 13.3$ MeV, measured at an angle 78° and multiplied by 4π.

[1]C. D. Bowman, G. S. Sidhu, and B. L. Berman, Phys. Rev. 163, 951 (1967).
[2]R. J. Baglan, C. D. Bowman, and B. L. Berman, Phys. Rev. C3, 672 (1971).
[3]A. I. Abramov, V. Ya. Kitaev, Yu. Ya. Stavisskiĭ, and M. G. Yutkin, Neĭtronaya fizika (Neutron Physics), Part I, Kiev, Naukova dumka, 1972, p. 289.
[4]V. V. Verbinski, Hans Weber, and R. E. Sund, Phys. Rev. C8, 1002 (1973).
[5]A. I. Abramov, V. Ya. Kitaev, and M. G. Yutkin, Yad. Fiz. 20, 438 (1974) [Sov. J. Nucl. Phys. 20, 236 (1975)].

Translated by Clark S. Robinson

REF. I. A. Grishaev, N. I. Lapin, G. D. Pugachev
Yad. Fiz. 24, 335 (1976)
Sov. J. Nucl. Phys. 24, 175 (1976)

ELEM. SYM.	A	Z
Fe	56	26

METHOD

REF. NO.	
76 Gr 3	hmg

REACTION	RESULT	EXCITATION ENERGY	SOURCE		DETECTOR		ANGLE
			TYPE	RANGE	TYPE	RANGE	
G,PI+	SPC	150-500	C	500	EMU-I		DST
G,PI-	SPC	150-500	C	500	EMU-I		DST

The energy spectra of charged photopions from ^{54}Fe, ^{56}Fe, and ^{58}Ni targets irradiated with bremsstrahlung of maximum energy 500 MeV have been measured at photopion-emission angles of 30, 60, 90, 120, and 150° in the lab system over the kinetic-energy range from 15 to 80 MeV. Isotope effects are found in the π^- yields at 30, 60, and 90°. At all angles and energies, the π^+ yields are the same for all three targets within the experimental error.

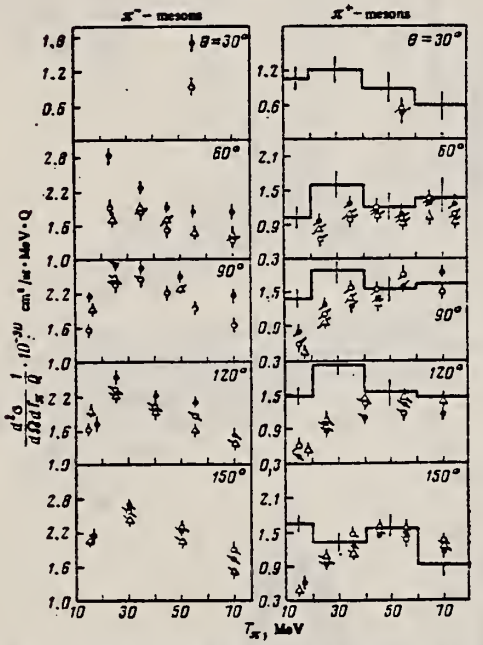

FIG. 1. Energy spectra of charged photopions from ^{54}Fe, ^{56}Fe, and ^{58}Ni targets (open circles, black circles, and triangles, respectively) at E_0=500 MeV. The error bars represent statistical errors. The histograms on the π^+-meson plots represent the results of cascade-model calculations for ^{56}Fe.

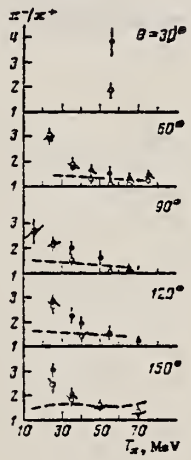

FIG. 2. The π^-/π^+ yield ratios for ^{56}Fe (black circles) and ^{54}Fe (open circles) targets vs photopion kinetic energy. The dashed curves were calculated with Eq. (4).

REF. D.G. Rickel, C.P. Cameron, R.D. Ledford, N.R. Roberson, H.R. Weller, D.R. Tilley
Phys. Rev. C14, 338 (1976)

ELEM. SYM.	A	Z
Fe	56	26

METHOD

REF. NO. 76 Ri 2 hmg

REACTION	RESULT	EXCITATION ENERGY	SOURCE		DETECTOR		ANGLE
			TYPE	RANGE	TYPE	RANGE	
A,G	ABX	14- 22	D	7- 16	NAI-D		90
P,G	ABX	14-22	D	3-12	NAI-D		90

A comparison is made between the yield curves of the measured $^{52}Cr(\alpha,\gamma_0)$ and $^{55}Mn(p,\gamma_0)$ reactions in the giant dipole resonance region of ^{56}Fe ($E_x = 14.0$ to 21.5 MeV) to determine if the gross differences can be interpreted as being due to isospin effects. Above 18 MeV the yield of (γ,α_0), determined by the principle of detailed balance, is observed to drop below the value obtained when the energy dependence of the transmission coefficients is removed. This leads to the conclusion that while the diminished yield in the (γ,α_0) channel may be due to the failure to populate the isospin forbidden $T_>$ states, other effects cannot be ruled out.

TABLE II. Comparison of yields in proposed $T_<$ and $T_>$ regions of the GDR for both proton and α capture. The energy region extends from 14.5 to 21.5 MeV with the division between the $T_<$ and $T_>$ region assumed to occur at 18.7 MeV.

	(γ,p_0) observed (mb MeV)	(γ,α_0) observed (mb MeV)	(γ,α_0) Theory 2 (mb MeV)
$T_<$ yield	2.00	2.31	2.57
$T_>$ yield	0.72	0.29	0.82
$T_>/T_<$	0.36	0.13	0.32

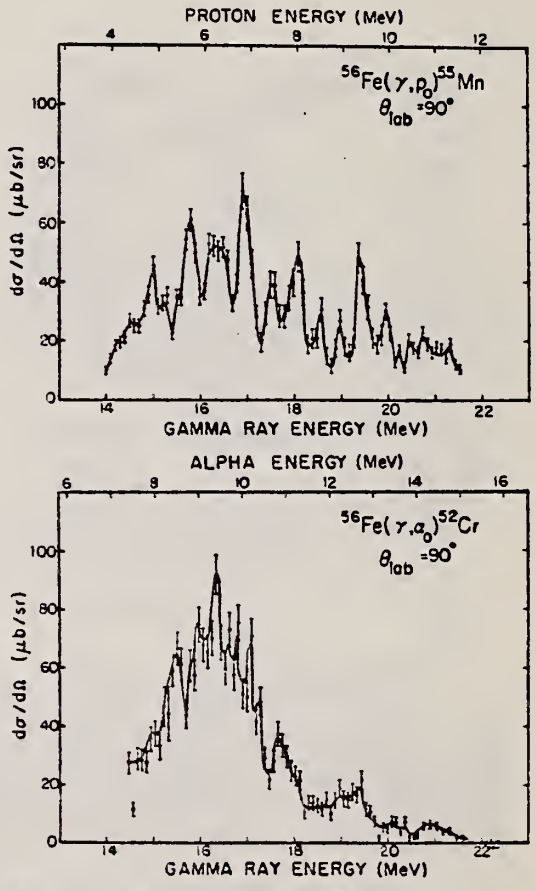

FIG. 2. The 90° yield curves for $^{56}Fe(\gamma,p_0)$ and $^{56}Fe(\gamma,\alpha_0)$ obtained from the data by the principle of detailed balance. The error bars represent the statistical errors of the data points. The solid lines are smooth curves drawn through the data points.

REF. B.S. Ratner, A.N. Sergiyevsky and S.S. Verbitsky
Nucl. Phys. A285, 71 (1977)

ELEM. SYM.	A	Z
Fe	56	26

METHOD

REF. NO. 77 Ra 3 egf

REACTION	RESULT	EXCITATION ENERGY	SOURCE		DETECTOR		ANGLE
			TYPE	RANGE	TYPE	RANGE	
G,N	SPC	14-26	C	15-26	SCI-D		UKN

FAST NEUTS

TABLE 3

Relationship between the structure in the energy spectra and the structure in the photoneutron cross section for ^{56}Fe

Position of peak in neutron energy spectrum ε						Position of resonance ^{56}Fe	Position of level ^{55}Fe [a]			
$E_{\gamma\,max}$ (MeV)							$E = E_R - \bar{\varepsilon}_m - E_{sep}$ [b]			
18.5	20.2	21.2	23.0	25.0	26.2	E_R (MeV)				
4.4	4.5	4.2	4.2	4.2		16.0	0.4			
5.1	5.2	5.3	5.3	5.5	5.4	18.1			1.5	
6.2	6.4		6.4	6.4	6.4	18.1	0.4			
	5.9	6.0	6.0	5.9	6.0	19.8				2.5
	7.1	7.1	7.0	7.4	7.4	19.8			1.3	
		8.6	8.6		8.4	19.8	0.1			
			9.6	9.2	9.4	21.6		0.8		
			10.0	9.9	10.0	21.6	0.2			
				10.9	11.0	24.7				2.3
							mean value:			
							0.1	0.33	0.8	1.4	2.4
							spectroscopic data:			
							0	0.41	0.93	1.32	2.54

[a]) A nuclear recoil correction has been introduced.
[b]) $\bar{\varepsilon}$ is ε averaged by $E_{\gamma\,max}$.

REF. K. Masumoto, T. Kato, N. Suzuki
Nucl. Inst. Meth. 157, 567 (1978)

ELEM. SYM.	A	Z
Fe	56	26

METHOD

REF. NO. 78 Ma 10 hg

REACTION	RESULT	EXCITATION ENERGY	SOURCE		DETECTOR		ANGLE
			TYPE	RANGE	TYPE	RANGE	
G,PN	ABY	20-68	C	30-68	ACT - I		4PI
G,AN	ABY	20-68	C	30-68	ACT - I		4PI

Analysis is made of reactions interfering with photon activation analysis procedures.

The activation yield curves have been presented for a number of photonuclear reactions in the energy range from 30 to 68 MeV, in order to evaluate quantitatively the interferences due to competing reactions in multielement photon activation analysis. The general features of the yields as functions of both target mass number and excitation energy were elucidated from the data obtained, discussion being given on the results in terms of the reaction mechanism.

Simultaneous neutron activation due to appreciable neutron production from the converter and surrounding materials has also been studied, and, finally, the magnitudes of interferences in real multielement analysis were given in the form of their energy dependences.

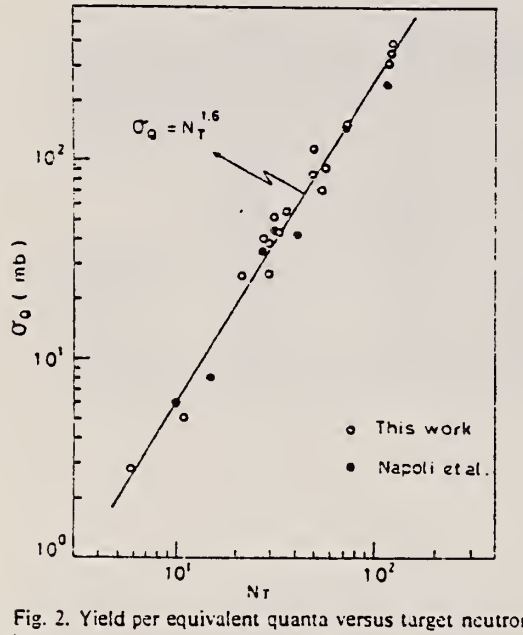

Fig. 2. Yield per equivalent quanta versus target neutron number.

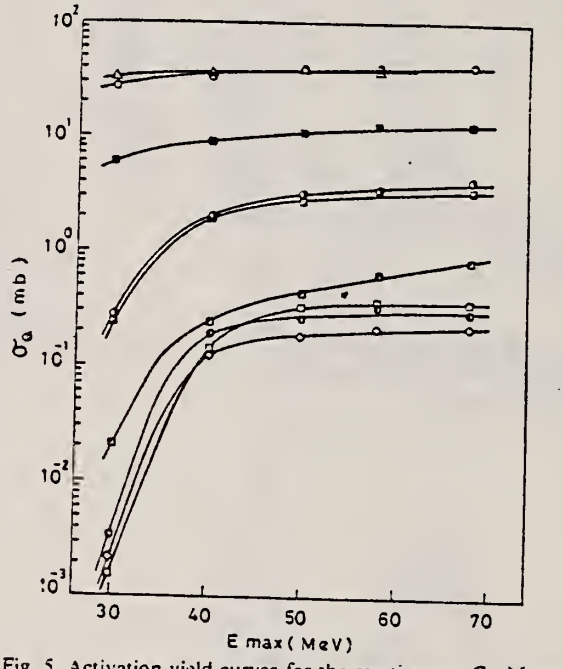

Fig. 5. Activation yield curves for the reactions on Cr, Mn and Fe.
○ $^{52}Cr(\gamma, n)^{51}Cr$, ◑ $^{50}Cr(\gamma, pn)^{48}V$, ◐ $^{50}Cr(\gamma, 2n)^{48}Cr$,
△ $^{55}Mn(\gamma, n)^{54}Mn$, ◪ $^{57}Fe(\gamma, p)^{56}Mn$, ◩ $^{54}Fe(\gamma, pn)^{52g}Mn$,
◪ $^{56}Fe(\gamma, pn)^{54}Mn$, □ $^{56}Fe(\gamma, \alpha n)^{51}Cr$, ◇ $^{54}Fe(\gamma, 2n)^{52}Fe$.

(over)

FORM NBS-418
U.S. DEPARTMENT OF COMMERCE

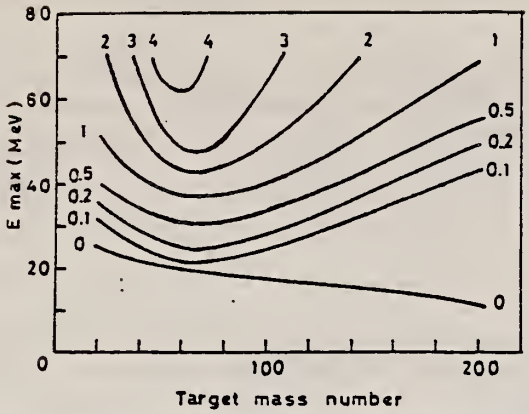

Fig. 11. Yields of the (γ, pn) reactions as a function of bremsstrahlung maximum energy and target mass number. The numerical values in the figure are yields per equivalent quanta in mb.

REF. N. Kumagai, T. Ishimatsu, E. Tanaka, K. Kageyama, G. Isoyama
Nucl. Phys. A329, 205 (1979)

ELEM. SYM.	A	Z
Fe	56	26

METHOD

REF. NO. 79Ku4 hg

REACTION	RESULT	EXCITATION ENERGY	SOURCE		DETECTOR		ANGLE
			TYPE	RANGE	TYPE	RANGE	
G,G	LFT	6-12	C	14	SCD-D		DST

Abstract: The resonance scattering of electron bremsstrahlung from natural chromium and iron targets has been studied for photon energies up to 12 MeV. Seven γ-transitions of energies higher than 7 MeV were observed for each of the targets, which suggests seven resonant levels in each of ^{52}Cr and ^{56}Fe at excitation energies above 7 MeV. The spins of these levels were all assigned to be 1 from the relative yields at scattering angles of 125° and 150°. Radiative widths of these levels were obtained. A discussion is made about the possibility that these levels are $T_<$ components of the M1 giant resonance in ^{52}Cr and ^{56}Fe.

7 LEVELS

E NUCLEAR REACTIONS ^{52}Cr, ^{56}Fe(γ, γ) bremsstrahlung E_e = 14 MeV; measured E_γ, $I_\gamma(\theta = 125°, 150°)$; ^{52}Cr, ^{56}Fe deduced levels, J, Γ_γ. Natural targets.

TABLE 2

Electromagnetic transitions in ^{11}B used for calibration of $N\varepsilon\Omega$ [a])

Initial state	J^π	Γ (eV)	Branching ratios (%) to final states [b])			
			g.s.	2.125	4.445	5.021
4.445	$\frac{1}{2}^-$	0.610±0.030	100 [c])			
5.021	$\frac{1}{2}^-$	1.80 ±0.13 [d])	84±2 [e])	16±2 [f])		
7.286	$\frac{1}{2}^+$	1.17 ±0.26 [d])	87±2		5.5±1	7.5±1
8.920 [g])	$\frac{1}{2}^-$	4.20 ±0.52 [d])	95±1		5 ±0.5	

[a]) Ref. [6]) except where shown.
[b]) Ref. [8]).
[c]) $\delta = -0.19 \pm 0.15$ [ref. [9])].
[d]) Ref. [7]).
[e]) $\delta = 0.03 \pm 0.05$ [ref. [9])].
[f]) $\delta = -0.05 \pm 0.20$ [ref. [9])].
[g]) $\delta = -0.11 \pm 0.04$ [ref. [10])].

TABLE 3

Electromagnetic transtions in ^{24}Mg used for calibration of $N\varepsilon\Omega$ [a])

Initial state	J^π	Γ (eV)	Branching ratios (%) to final states	
			g.s.	1.369
9.966	1^+	8.8±2.3	65±2	35±2
10.712	1^+	19.9±1.8	78±4	22±4

[a]) Ref. [11]).

TABLE 4

Summary of the experimental results of ^{52}Cr

Level energy (MeV)	$I(150°)/I(125°)$	J	Γ [a]) (eV)	$B(M1, 1^+ \rightarrow 0^+)$ [b]) (μ_N^2)
7.524	1.36±0.45	1	0.97±0.23	0.20
7.729	1.29±0.20	1	1.75±0.32	0.33
7.896	1.42±0.15	1	5.68±0.80	1.00
8.091	1.52±0.42	1	1.60±0.35	0.26
9.138	1.36±0.24	1	2.93±0.51	0.33
9.211	1.30±0.34	1	2.76±0.59	0.31
9.783	1.30±0.21	1	4.01±0.61	0.37

[a]) Deduced on the assumption of 100% ground-state transition.
[b]) Deduced on the assumption of even parity.

REF. R. Altemus, A. Cafolla, D. Day, J.S. McCarthy, R.R. Whitney, J.E. Wise
Phys. Rev. Lett. 44, 965 (1980)

ELEM. SYM.	A	Z
Fe	56	26

METHOD

REF. NO. 80 A1 1 hg

REACTION	RESULT	EXCITATION ENERGY	SOURCE		DETECTOR		ANGLE
			TYPE	RANGE	TYPE	RANGE	
E,E/	RLX	0-70	D	100-373	MAG-D		DST

Inelastic-electron-scattering cross sections for ^{56}Fe have been measured in the continuum region. The longitudinal and transverse inelastic response functions have been determined for vector momentum transfers, q, from 210–410 MeV/c and for energy losses $0 < \omega \leq 220$ MeV.

Q 210-410 MEV/C

PACS numbers: 25.30.Cg, 27.40.+z

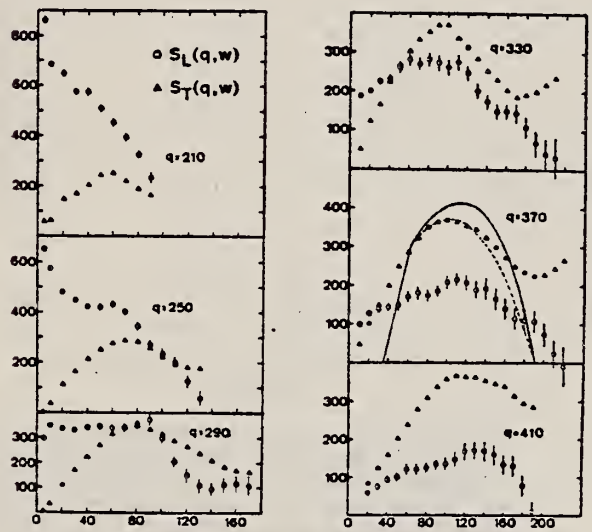

FIG. 1. (a),(b) S_L (circles) and S_T (solid triangles) for Fe. The errors are smaller than the points unless otherwise shown and include statistics only. The overall data has an uncertainty of ±3% coming from the normalization to the proton. All q values are in units of MeV/c; the transverse and longitudinal response functions are dimensionless. For the data at q = 370 MeV/c the results for the Fermi-gas calculations are shown; the dashed line represents S_T, the solid line S_L.

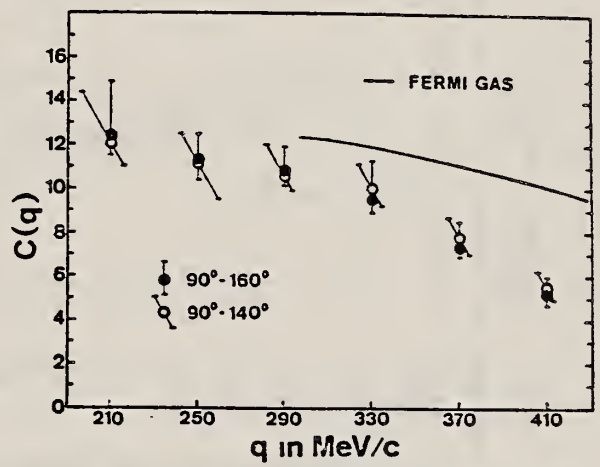

FIG. 2. The Coulomb sum rule $C(q)$ for Fe compared with prediction for a Fermi gas over the range of experimentally available q.

REF. James S. McCarthy
Nucl. Phys. A335, 27 (1980)

ELEM. SYM.	A	Z
Fe	56	26

METHOD

REF. NO. 80 Mc 3 hg

REACTION	RESULT	EXCITATION ENERGY	SOURCE		DETECTOR		ANGLE
			TYPE	RANGE	TYPE	RANGE	
E,E/	ABX	10*200	D	100-999	MAG-D		DST

Abstract: Inclusive electron scattering from the nuclei ^{56}Fe and ^{3}He has been measured over a wide range of incident energy and momentum transfer. The data is used to separate the longitudinal and transverse response functions. The two-nucleon correlation function and the momentum distribution of the internal nucleons is compared to the data.

999=14 GEV, *E LOSS

NUCLEAR REACTIONS: (e,e') on ^{56}Fe, ^{3}He Incident Energies E = 0.1 to 14 GeV; measured scattered electron at energy loss $\omega = E-E'$ of 0-2 GeV. Deduced momentum distribution.

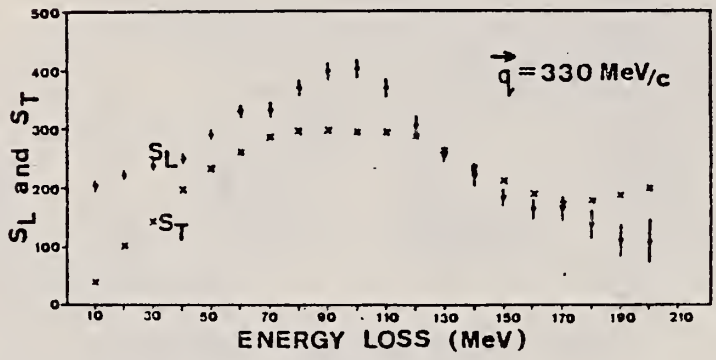

Fig. 3 The transverse (S_T) and longitudinal (S_L) response functions at constant $\vec{q}$ = 330 MeV/c for ^{56}Fe.

REF. D.M. Skopik, J. Asai, J.J. Murphy II
Phys. Rev. C21, 1746 (1980)

ELEM. SYM.	A	Z
Fe	56	26

METHOD

REF. NO. 80 Sk 5 hg

REACTION	RESULT	EXCITATION ENERGY	SOURCE TYPE	SOURCE RANGE	DETECTOR TYPE	DETECTOR RANGE	ANGLE
E,A	ABX	7-50	D	26-50	MAG-D		DST

The cross section ^{56}Fe(e,α) has been measured as a function of α energy, lab angle, and incident electron energy. The analyses of these data using distorted-wave Born approximation virtual photon spectra have been performed in the framework of models suggested by the data. We find that the (e,α) channel exhausts a sizable percentage of the $E2$ isoscalar sum rule.

VIRT PHOTON ANAL

[NUCLEAR REACTIONS ^{56}Fe(e,α) measured $\sigma(E_0, E_\alpha, \theta_\alpha)$, obtained $\sigma(e,\alpha)$ and determined $\sigma^{E1}(\gamma,\alpha)$ and $\sigma^{E2}(\gamma,\alpha)$.]

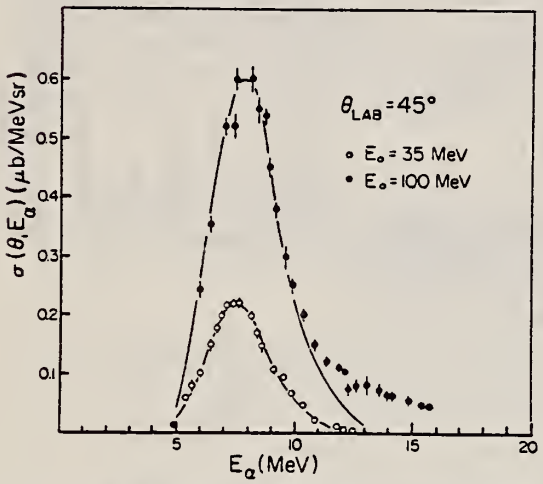

FIG. 2. Measured differential cross sections at θ_{LAB} =45° for incident electron energies of 35 and 100 MeV. The solid lines are fits using the statistical model employed in our earlier studies of the (e,α) reaction from various nuclei. These fits result in a nuclear temperature of 0.3 MeV.

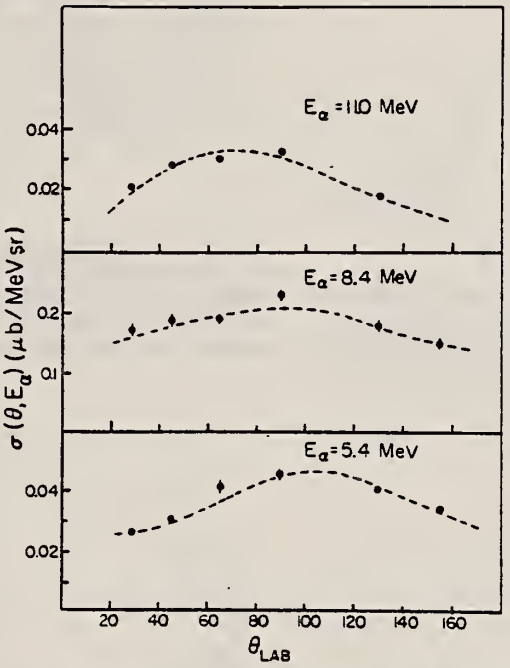

FIG. 3. Representative angular distributions that show the shift from backward to forward angles of α particles.

TABLE I. $E2$ integrated cross sections and resonance parameters determined by the isochromat analysis of Sec. IV B.

	Trapezoidal [a] integration	2nd order fit [a] integration	Lorentz line shape	Breit-Wigner line shape
$\int \sigma dE$ (mb MeV)	3.6 ± 0.3	3.8 ± 0.3	3.9 ± 0.1	3.9 ± 0.1
$\int \frac{\sigma dE}{E^2}$ (μb/MeV)	11.0 ± 1.0	11.3 ± 0.9	11.1 ± 1.6	11.1 ± 1.5
% of $E2$ sum rule [b]	28 ± 3	29 ± 2	29 ± 4	29 ± 4
E_R (MeV)			17.9 ± 0.2	18.1 ± 0.2
Γ (MeV)			2.8 ± 0.3	2.9 ± 0.3
σ_0 (mb)			1.00 ± 0.07	1.00 ± 0.06

[a] Reference 13.
[b] We have used the value $0.22Z^2/A^{1/3}$.

TABLE II. $E2$ integrated cross sections and resonance parameters determined by the total cross section analysis of Sec. IV C.

Line shape		σ_0 (mb)	Γ (MeV)	E_R (MeV)	$\int \sigma dE$ (mb MeV)	$\int \sigma dE/E^2$ (mb/MeV)	χ^2	% of $E2$ sum rule
Lorentz	a	0.72 ± 0.02	3.1	17.6	3.04 ± 1.55	8.74 ± 2.82	3.6	22 ± 7
	b	0.99 ± 0.03	2.2 ± 0.2	17.9 ± 0.4	3.14 ± 0.30	9.12 ± 0.42	3.4	23 ± 1
Breit-Wigner	a	0.75 ± 0.02	3.1	17.6	2.99 ± 1.40	8.92 ± 2.84	3.7	23 ± 7
	b	1.00 ± 0.02	2.3 ± 0.1	18.0 ± 0.6	3.13 ± 0.23	9.27 ± 0.15	3.4	24 ± 1

[a] Fit constrained to the $E2$ values of Γ and E_R found from the angular distribution analysis.
[b] Unconstrained fit.

(over)

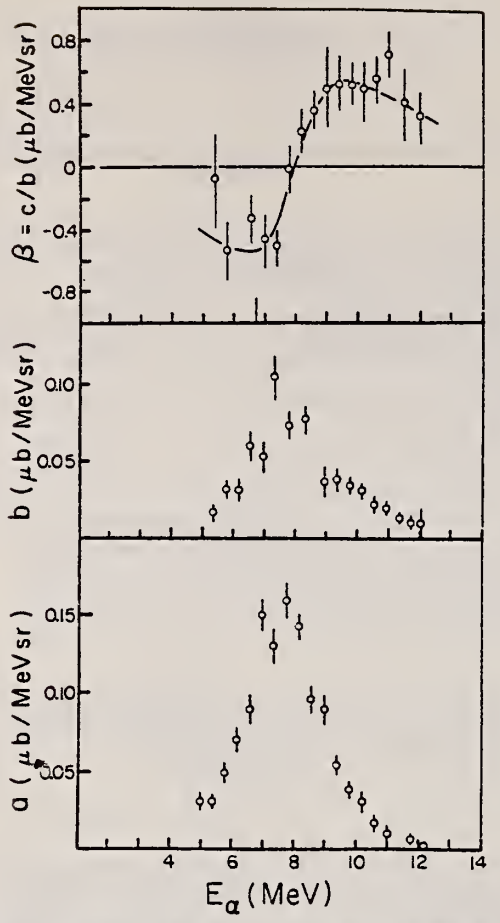

FIG. 4. Angular distribution coefficients (μb/MeV sr) that are found by fitting to Eq. (1). The asymmetry $\beta = c/b$ shows a change in sign that can be associated with resonance interference. The solid line is the result of fitting to an asymmetry defined in the text.

$$\sigma(\theta, E) = a + b\sin^2\theta + c\sin^2\theta\cos\theta + d\sin^2\theta\cos^2\theta . \quad (1)$$

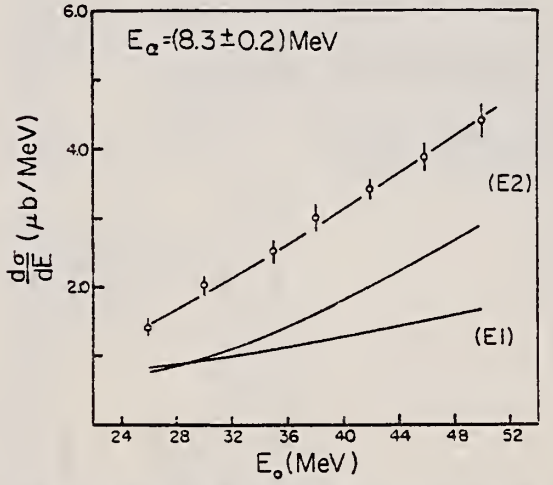

FIG. 5. The cross section $d\sigma/dE$ found by integrating over $d\Omega$ using the angular dependence shown in Fig. 4. These data are analyzed in terms of α particles making transitions to the 2^+ state in ^{52}Cr. The solid lines are the contributions to the cross section from $E1$ and $E2$ cross sections by least squares fitting Eq. (3).

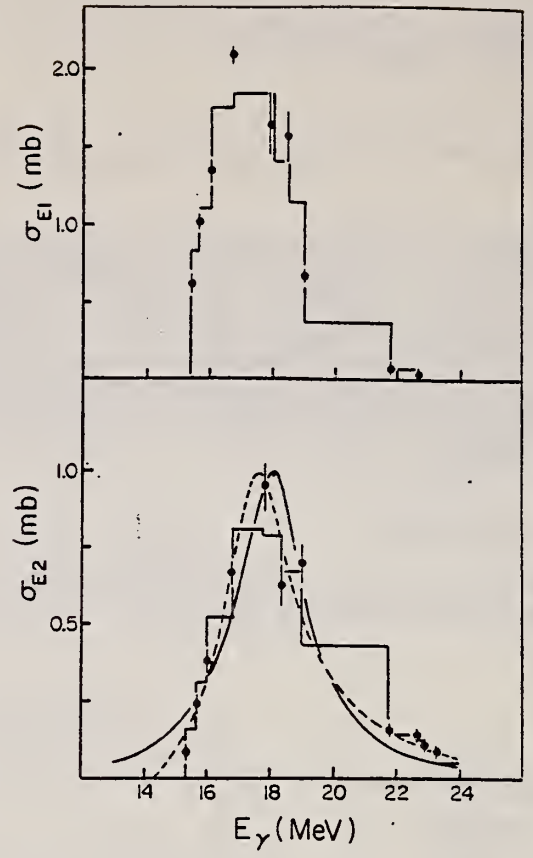

FIG. 8. Total $E1$ and $E2$ cross section determined from the isochromat analysis at seven α energies. The dashed line is the Lorentz line shape fit and the solid line is the Breit-Wigner line shape fit. The resonance parameters are summarized in Table I.

TABLE III. Summary of the $E1$ integrated cross sections for the ^{56}Fe(e,α) reaction and the percentage exhaustion of the sum rule $60NZ/A$.

Analysis		$\int \sigma dE$ (mb MeV)	E_R (MeV)	Γ (MeV)	σ_0 (mb)	% of sum rule
Isochromats		6.41 ± 0.64				0.8 ± 0.1
Lorentz	a	10.51 ± 2.63	16.5 ± 3.1	4.04 ± 0.26	2.19 ± 0.02	1.3 ± 0.3
	b	10.44 ± 0.80	17.0 ± 2.5	4.14 ± 0.30	2.02 ± 0.02	1.2 ± 0.1
Breit-Wigner	a	9.87 ± 3.12	16.7 ± 3.5	4.09 ± 0.3	2.19 ± 0.03	1.2 ± 0.4
	b	9.98 ± 2.19	17.1 ± 2.8	4.25 ± 0.23	2.06 ± 0.02	1.2 ± 0.3

[a] Fit constrained to the $E2$ values of Γ and E_R found from the angular distribution analysis.
[b] Unconstrained fit.

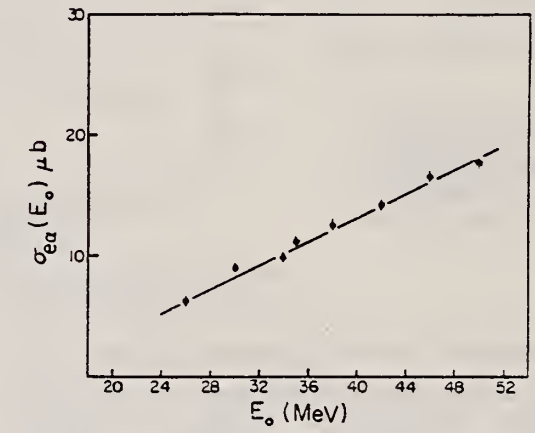

FIG. 9. The total electrodisintegration cross section for the (e,α) channel. The solid line is the result of least square fitting these data with Eq. (1). No appreciable difference was found for Lorentzian and Breit-Wigner line shapes.

REF. T.J. Bowles, R.J. Holt, H.E. Jackson, R.M. Laszewski, R.D. McKeown, A.M. Nathan, J.R. Specht
Phys. Rev. C24, 1940 (1981)

EL EM. SYM.	A	Z
Fe	56	26

METHOD

REF. NO.: 81 Bo 5 hg

REACTION	RESULT	EXCITATION ENERGY	SOURCE		DETECTOR		ANGLE
			TYPE	RANGE	TYPE	RANGE	
G,G	ABX	15-23	D	15-23	NAI-D		90

Quasimonochromatic photons have been used to measure elastic and inelastic photon scattering cross sections in the giant dipole resonance region of ^{52}Cr, Fe, ^{60}Ni, ^{92}Mo, and ^{96}Mo in an experiment in which the elastic and inelastic scattering are resolved. The elastic scattering cross sections show clear evidence for isospin splitting of the giant dipole resonance. The inelastic scattering to low-lying vibrational levels, which is a measure of the coupling between the giant dipole resonance and collective surface vibrations, is in qualitative agreement with the predictions of the dynamic collective model. However, when examined in detail, this model does not provide an adequate description of the scattering data.

[NUCLEAR REACTIONS ^{52}Cr, Fe, ^{60}Ni, ^{92,96}Mo (γ,γ'), $14 \leq E_\gamma \leq 22$ MeV; measured E_γ, $E_{\gamma'}$, $d\sigma/d\Omega$ for γ_0,γ_1. Compared to DCM predictions. Tagged photons.]

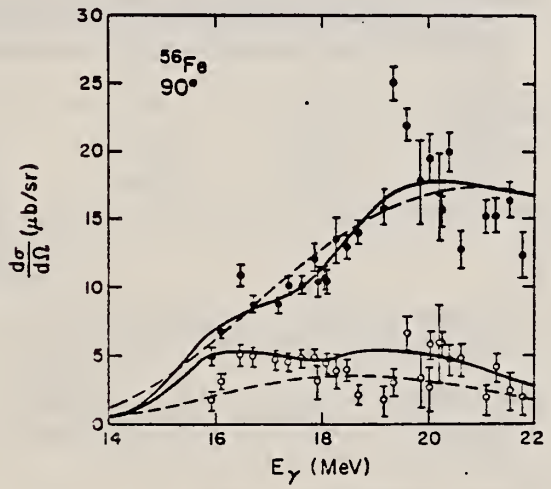

FIG. 7. Elastic (closed circles) and inelastic (open circles) scattering cross sections at $\theta = 90°$ for ^{56}Fe. The error bars represent statistical uncertainties only. The solid (dashed) lines are DCM calculations for the elastic and inelastic cross sections including (not including) the effect of isospin splitting.

REF. W.R. Dodge, R.G. Leicht, E. Hayward, E. Wolynec
Phys. Rev. C24, 1952 (1981)

ELEM. SYM.	A	Z
Fe	56	26

METHOD

REF. NO. 81 Do 2 hg

REACTION	RESULT	EXCITATION ENERGY	SOURCE		DETECTOR		ANGLE
			TYPE	RANGE	TYPE	RANGE	
E,P	ABX	10-100	D.	16-100	MAG-D		DST
E,A	ABX	7-100	D	16-100	MAG-D		DST

The (e,p) and (e,α) cross sections for ^{56}Fe, ^{59}Co, and ^{64}Zn have been measured in the electron energy range 16—100 MeV. They have been analyzed using the distorted-wave Born approximation $E1$ and $E2$ virtual photon spectra. The $E1$ and $E2$ components in the proton and α channels have been obtained.

[NUCLEAR REACTIONS ^{56}Fe(e,p), ^{56}Fe(e,α), ^{59}Co(e,p), ^{59}Co(e,α), ^{64}Zn(e,p), and ^{64}Zn(e,α); measured $\sigma(E_0,E_x,34°)$, $\sigma(E_0,E_x,48°)$, $\sigma(E_0,E_x,62°)$, $\sigma(E_0,E_x,90°)$, $\sigma(E_0,E_x,118°)$, $\sigma(E_0,E_x,132°)$; obtained $\sigma(e,p)$, $\sigma(e,\alpha)$; deduced $\sigma^{E1}_{\gamma,p}(E)$, $\sigma^{E2}_{\gamma,p}(E)$, $\sigma^{E1}_{\gamma,\alpha}(E)$, $\sigma^{E2}_{\gamma,\alpha}(E)$.]

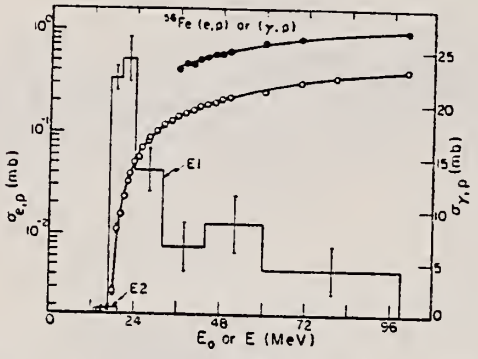

FIG. 3. The measured $\sigma_{e,p}(E_0)$ for ^{56}Fe as a function of total incident electron energy E_0 (open circles). The full circles represent the yield $Y_{e,p}(E_0)$ obtained when a 0.217 g/cm^2 tantalum foil was placed in the electron beam ahead of the target. The smooth curves are the best fits to the data and were obtained by combining the histograms representing the $E1$ and $E2$ (γ,p) cross sections (right-hand scale) in Eqs. (1) and (2) with the $E1$ and $E2$ DWBA virtual photon spectra and by making use of the DBM bremsstrahlung cross section. The size effect correction described in the text has been applied to the virtual photon spectra.

VIRT PHOTON ANAL

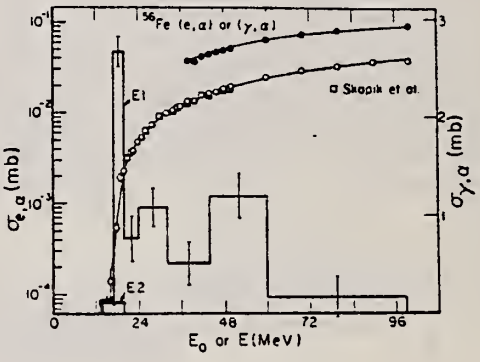

FIG. 6. The $\sigma_{e,\alpha}(E_0)$ for ^{56}Fe. See caption of Fig. 3. The squares represent the data of Ref. 6 and are included to show the good agreement between the two experiments.

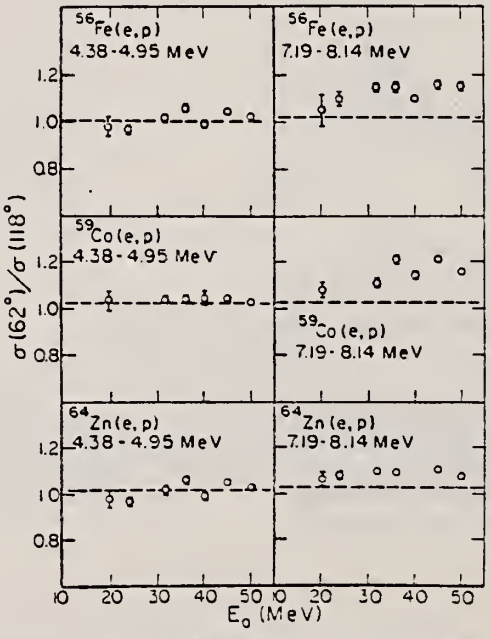

FIG. 9. The ratios of the number of protons observed in the indicated energy bite ΔT_p at 62° to the same number observed at 118°, $\sigma(62°)/\sigma(118°)$, as a function of incident electron energy.

(OVER)

TABLE III. Percentage of the $E2$ sum when only points up to 50 MeV ($E_0=50$ MeV) and when all measured points ($E_0=100$ MeV) are considered in the analysis. The bremsstrahlung cross section used is DBM. $E2$ sum: $0.22Z^2A^{-1/3}$ μb/MeV.

Nucleus	Reaction	Without size effect $E_0=50$ MeV	Without size effect $E_0=100$ MeV	With size effect $E_0=50$ MeV	With size effect $E_0=100$ MeV
^{56}Fe	(e,α)	9± 3	3 ± 1	11± 3	7± 1
	(e,p)	47±30	8±11	61±32	37±15
^{59}Co	(e,α)	7± 2	4 ± 1	8± 2	5± 1
	(e,p)	32±22	4± 8	48±24	28±11
^{64}Zn	(e,α)	26± 6	12± 2	32± 6	25± 3
	(e,p)	29±43	26±15	56±46	77±21

TABLE IV. Percentage of the $E1$ and $E2$ sums in the α and proton channels. $E1$ sum: $60NZ/A$ MeV mb. $E2$ sum: $0.22Z^2A^{-1/3}$ μb/MeV. Integrals to 100 MeV.

Nucleus	Reaction	$E1$ Schiff	$E1$ DMB	$E2$ Schiff	$E2$ DBM
	(e,α)	5± 1	6± 1	10± 1	7± 1
^{56}Fe	(e,p)	67±20	82±19	82±14	37±15
	$(e,\alpha)+(e,p)$	72±20	88±19	92±14	44±15
	(e,α)	5± 1	7± 1	8± 1	5± 1
^{59}Co	(e,p)	52±10	67±12	63±10	28±11
	$(e,\alpha)+(e,p)$	57±10	74±12	71±10	33±11
	(e,α)	16± 4	18± 4	33± 3	25± 3
^{64}Zn	(e,p)	129±28	154±30	137±30	77±21
	$(e,\alpha)+(e,p)$	145±28	172±30	170±20	102±21

TABLE VI. $E1$ strength integrated up to 30 MeV.

Nucleus	$\int_0^{30}\sigma_{\gamma,x}(E)dE$ (MeV mb) α	p	n	Total	Fraction of $E1$ sum
^{56}Fe	18± 3	256±26	735[a]	1009	1.21
^{59}Co	15± 2	211±22	884[b]	1110	1.26
^{64}Zn	66±14	545±75	616[b]	1227	1.28

[a]Reference 13.
[b]Reference 14.

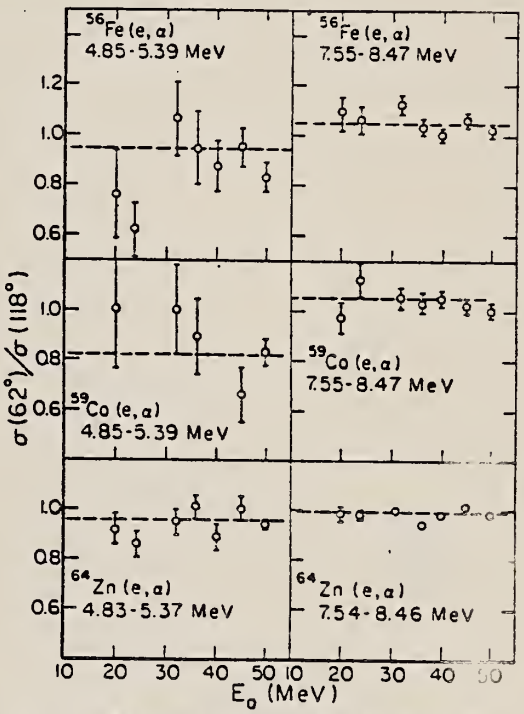

FIG. 10. The ratios of the number of α particles observed in the indicated energy bite ΔT_α at 62° to the same number observed at 118°, $\sigma(62°)/\sigma(118°)$, as a function of incident electron energy.

[13]Y. -W., Lui, P. Bogucki, J. D. Bronson, U. Garg, C. M. Rozsa, and D. H. Youngblood, Phys. Lett. 93B, 31 (1980).

[14]S. Costa, F. Ferrero, S. Ferroni, C. Molino and R. Malvano, Phys. Lett. 11, 324 (1964). 64Co2

FE
A=57

FE
A=57

FE
A=57

Ref. R. Tobin, J. McElhinney, L. Cohen
Phys. Rev. 110, 1388 (1958)

Elem. Sym.	A	Z
Fe	57	26

Method: 22 MeV betatron; neutron counting

Ref. No.: 58 To 1 EH

Reaction	E or ΔE	E_o	Γ	$\int \sigma dE$	Jπ	Notes
$Fe^{57}(\gamma,n)$	Bremss. 22					E_{th} = 7.85±0.13

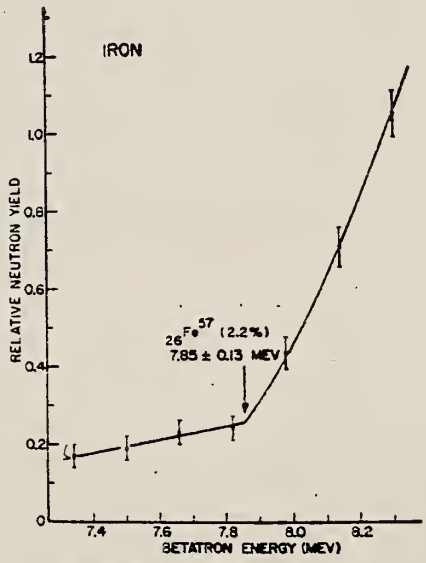

FIG. 2. Photoneutron yield from iron in the betatron-energy range from 7.3 to 8.3 Mev.

K. N. Geller, J. Halpern, and E. G. Muirhead
Phys. Rev. 118, 1302-12 (1960)

ELEM. SYM.	A	Z
Fe	57	26

METHOD

Betatron; neutron threshold; ion chamber

REF. NO. 60 Ge 3 NVB

REACTION	RESULT	EXCITATION ENERGY	SOURCE		DETECTOR		ANGLE
			TYPE	RANGE	TYPE	RANGE	
G,N	NØX	THR	C THR		BF3-I		4 PI

THRESHØLD

TABLE I. Summary and comparison of neutron separation energies inferred from present threshold measurements with values predicted from mass data and reaction energies. All energies are expressed in the center-of-mass system in Mev.

Reaction	No. runs	Present results	Other results	Method	Reference
$Fe^{57}(\gamma,n)Fe^{56}$	1	7.85 ±0.13	7.633±0.007	mass data	j
			7.636±0.010	$Fe^{56}(n,\gamma)Fe^{57}$	e
			7.85 ±0.13	threshold	k

[j] P. M. Van Patter and W. Whaling, Revs. Modern Phys. 26, 402 (1954); 29, 756 (1957).
[k] See reference 2.

REF. Y. Oka, T. Kato, K. Nomura, T. Saito, Hui-Tuh Tsai
Bull. Chem. Soc. Japan 41, 380 (1968)

ELEM. SYM.	A	Z
Fe	57	26

METHOD

REF. NO. 68 Ok 3 egf

REACTION	RESULT	EXCITATION ENERGY	SOURCE		DETECTOR		ANGLE
			TYPE	RANGE	TYPE	RANGE	
G,P	ABY	THR-20	C	20	ACT-I		4PI

TABLE 1. SUMMARY OF DATA ON (γ, p) REACTIONS WITH 20 MeV BREMSSTRAHLUNG

Nuclide: Parent (Natural abundance, %)	Nuclide: Residual (Half-life)	S_p (MeV)	Observed γ-ray: Energy (MeV)	Observed γ-ray: Branching ratio (%)	Observed γ-ray: Type of multipole transition	Yield determined: μCi/mg[a]	Yield determined: Yield/mol·R
^{25}Mg (10.11)	^{24}Na (15 hr)	12.06	1.37	100	$E2$	1.48×10^{-1}	1.7×10^{9}
^{29}Si (4.71)	^{29}Al (2.27 min)	12.33	1.78	100	$E2$	1.91	2.8×10^{9}
^{30}Si (3.12)	^{29}Al (6.56 min)	13.59	1.28	93.8	$E2+M1$	6.51×10^{-1}	1.5×10^{9}
^{44}Ca (2.06)	^{43}K (22.4 hr)	12.17	0.374	85	$E2+M1$	7.86×10^{-3}	1.3×10^{9}
^{47}Ti (7.32)	^{46}Sc (84.1 d)	10.47	0.887	100	$E2$	7.11×10^{-4}	3.1×10^{9}
^{48}Ti (73.99)	^{47}Sc (3.4 d)	11.44	0.160	100	$E2+M1$	6.83×10^{-3}	1.2×10^{9}
^{49}Ti (5.46)	^{48}Sc (1.8 d)	11.35	1.31	100	$E2$	4.40×10^{-3}	5.8×10^{8}
^{53}Cr (9.55)	^{52}V (3.8 min)	11.15	1.43	100	$E2$	5.01×10^{-1}	6.6×10^{8}
^{57}Fe (2.17)	^{56}Mn (2.58 hr)	10.57	1.81	23.5	$E2+M1$	8.10×10^{-3}	2.1×10^{9}
^{76}Ge (36.74)	^{73}Ga (4.8 hr)	10.92	0.295	97	$(E2)$	3.70×10^{-1}	1.3×10^{9}
^{77}Se (7.58)	^{76}As (26.5 hr)	9.61	0.559	41	$E2$	1.48×10^{-3}	1.3×10^{9}
^{87}Sr (7.02)	^{86}Rb (19 d)	9.41	1.08	9	$E2$	5.15×10^{-4}	9.9×10^{8}
^{113}Cd (12.26)	^{112}Ag (3.2 hr)	9.74	1.39	35	$E2$	1.91×10^{-2}	2.1×10^{8}
^{117}Sn (7.57)	^{116m}In (54 min)	9.58	1.27	84	$E2$	9.80×10^{-3}	6.9×10^{8}
^{137}Ba (11.32)	^{136}Cs (13 d)	8.67	0.830	100	$E2$	1.68×10^{-4}	2.2×10^{8}
^{199}Hg (16.84)	^{198}Au (2.7 d)	7.27	0.412	100	$E2$	8.43×10^{-4}	2.2×10^{8}

a) The value corrected at the end of 1 hr irradiation (9.4×10^{6} R/min).

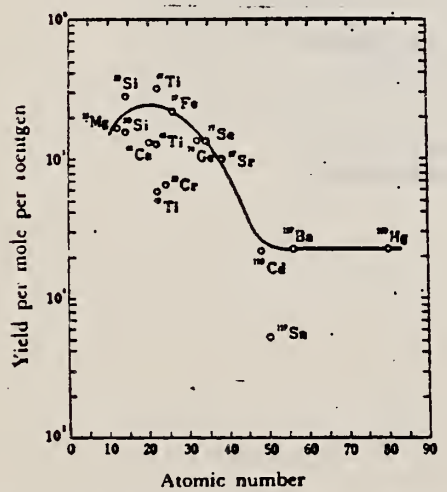

Fig. 2. The yield curve for the (γ, p) reaction with 20 MeV bremsstrahlung.

REF. R. J. Baglan, C. D. Bowman and B. L. Berman
Phys. Rev. C3, 672 (1971)

ELEM. SYM.	A	Z
Fe	57	26

METHOD

REF. NO. 71 Ba 2 hmg

REACTION	RESULT	EXCITATION ENERGY	SOURCE		DETECTOR		ANGLE
			TYPE	RANGE	TYPE	RANGE	
G,N	ABX	7-12	C	8-12	TOF-D		135
		(7.6-11.5)					

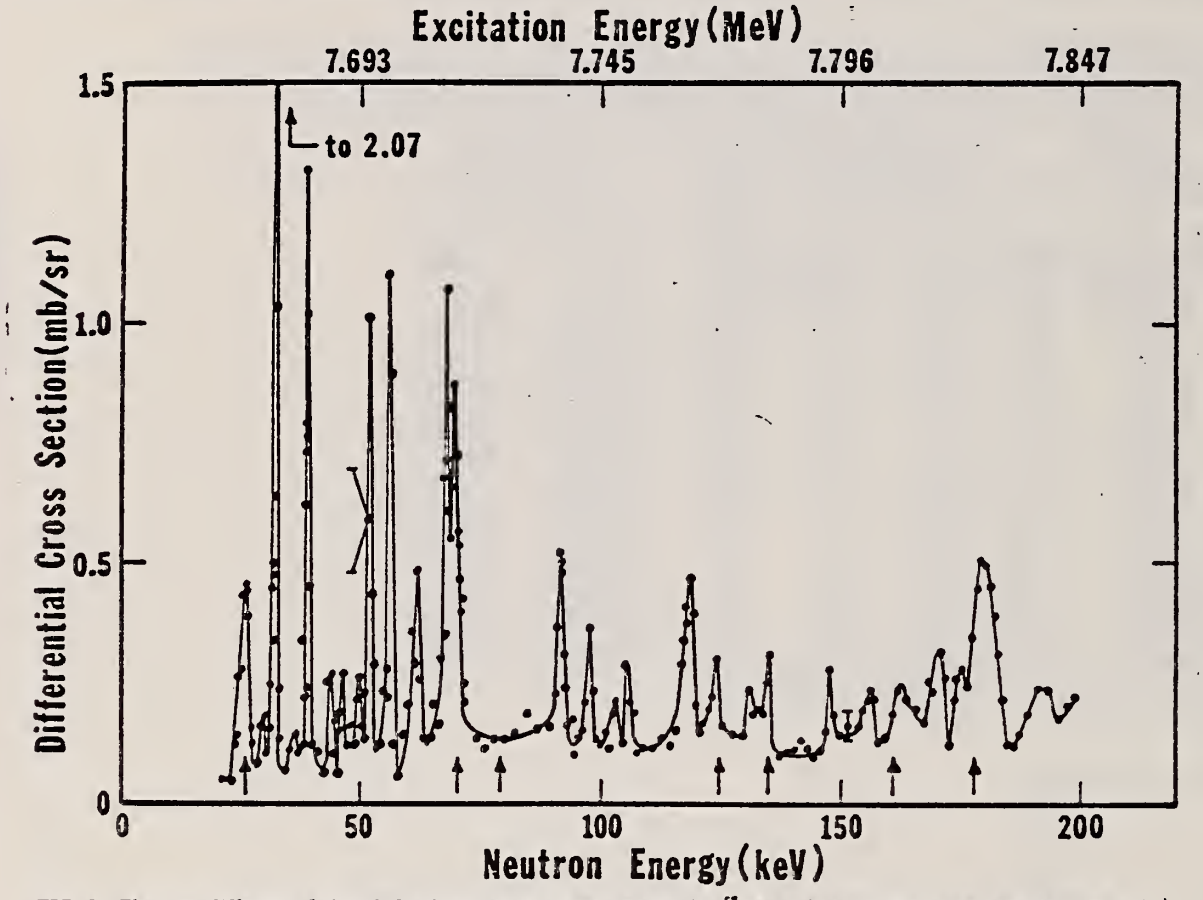

FIG. 9. The 135° differential threshold photoneutron cross section for ^{57}Fe, at low energies (see caption to Fig. 4). The arrows below the data indicate the positions of $J^{\pi} = \frac{1}{2}^{+}$ states obtained from neutron total cross-section measurements on ^{56}Fe. The 26-keV peak is asymmetric.

TABLE VI. Resonance parameters for ^{56,57}Fe and ^{52,53}Cr. For all resonances, the area under the peak in the 135° differential cross section is multiplied by 4π to yield approximate values for $g_\gamma\Gamma_{\gamma 0}\Gamma_n/\Gamma \simeq g_\gamma\Gamma_{\gamma 0}$. For those resonances where J^π is known, the differential area is multiplied by the appropriate factor F from Table I to obtain $\Gamma_{\gamma 0}$. E_L is the laboratory neutron energy for the (γ,n) reaction and E_n is the corresponding laboratory neutron energy for a neutron-induced reaction. Column 5 labels the peak as a ground-state (GS) or excited-state (ES) transition as determined in this work alone. Clearly, if a peak is seen in a neutron-induced reaction (columns 9–11), it must be GS.

Nucleus	E_L (keV)	E_{ex} (MeV)	$g_\gamma\Gamma_{\gamma 0}\Gamma_n/\Gamma$ (eV)	GS or ES	J^π	$\Gamma_{\gamma 0}$ (eV)	E_n (keV) (This work)	E_n (keV) from neutron-induced reactions (Ref. a)	(Ref. b)	(Ref. c)
^{57}Fe	26.0	7.669	0.084		$\frac{1}{2}^{+a}$	0.17	27.7	28	27.7	
	32.3	7.675	0.11				34.3		34.1	
	38.7	7.682	0.055				41.0			
	51.8	7.695	0.080				54.7			
	56.2	7.699	0.12				59.4		59.0	
	61.5	7.705	0.067				64.9		63.1	
	68.2	7.712	0.10				71.8			
	69.1	7.713	0.12		$\frac{1}{2}^{+a}$	0.24	72.8	74	72.6	
	91.6	7.736	0.069				96.3		95.9	
	97.7	7.743	0.031				102.7		102	
	106	7.751	0.022				111		112	
	119	7.764	0.094	GS			125			
	124	7.769	0.028		$\frac{1}{2}^{+a}$	0.056	130	131	129	
	135	7.781	0.036		$\frac{1}{2}^{+a}$	0.072	141	142		
	148	7.794	0.027				155			
	156	7.802	0.044				163	164		
	162	7.808	0.059		$\frac{1}{2}^{+a}$	0.12	170	169		
	171	7.817	0.072				179			
	179	7.826	0.21	GS	$\frac{1}{2}^{+a}$	0.42	187	187		
	192	7.839	0.050				201			
	212	7.859	0.36	GS	$\frac{1}{2}^{+a}$	0.72	222	220		
	223	7.871	0.40				233			
	232	7.880	0.26	GS	$\frac{1}{2}^{+a}$	0.52	243	244		
	245	7.893	0.072				256			
	259	7.907	0.11		$\frac{1}{2}^{+a}$	0.22	271	273		
	274	7.923	0.15				286			
	299	7.948	0.32		$\frac{1}{2}^{+a}$	0.64	312	315		
	330	7.980	0.32				345			
	393	8.045	0.31				410	406		

[a] See Ref. 17.
[b] See R. W. Hockenbury, Z. M. Bartolome, J. R. Tatarczuk, W. R. Moyer, and R. C. Block, Phys. Rev. 178, 1746 (1969).
[c] See Ref. 19.

[17] C.D. Bowman, E.G. Bilpuch, and H.W. Newson, Ann. Phys. (N.Y.) 17, 319 (1962).

[b] See R.W. Hockenbury, Z.M. Bartolome, J.R. Tatarczuk, W.R. Moyer, and R.C. Block, Phys. Rev. 178, 1746 (1969).

[19] R.G. Steiglitz, Ph.D. thesis, Rensselaer Polytechnic Institute, 1970 (unpub.)

REACTION	RESULT	EXCITATION ENERGY	SOURCE		DETECTOR		ANGLE
			TYPE	RANGE	TYPE	RANGE	

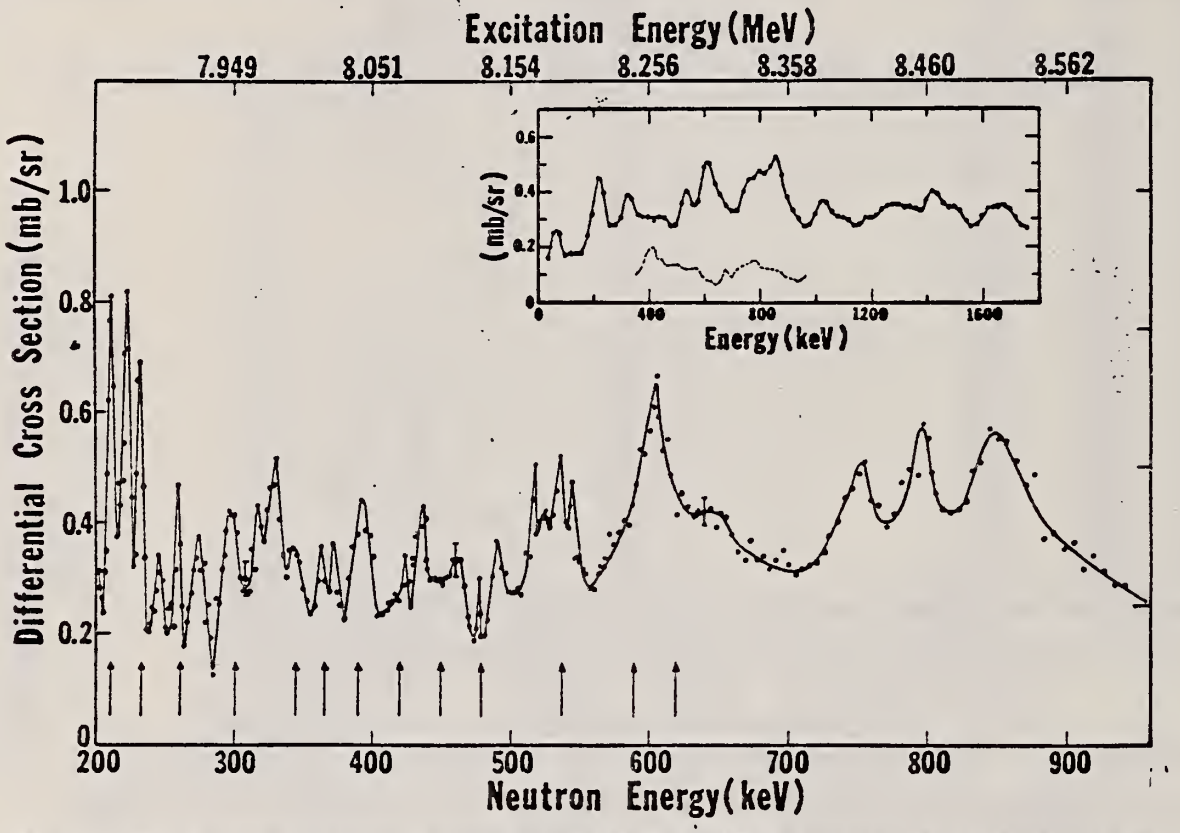

FIG. 10. The 135° differential threshold photoneutron cross section for ^{57}Fe, at high energies (see caption to Fig. 4). The arrows below the data indicate the positions of $J^{\pi} = \frac{1}{2}^{+}$ states obtained from neutron total cross-section measurements on ^{56}Fe. The dashed curve in the inset is the smoothed total cross section for ^{56}Fe.

REF. H. E. Jackson and E. N. Strait
Phys. Rev. C4, 1314 (1971)

ELEM. SYM.	A	Z
Fe	57	26

METHOD

REF. NO. 71 Ja 1 hmg

REACTION	RESULT	EXCITATION ENERGY	SOURCE TYPE	SOURCE RANGE	DETECTOR TYPE	DETECTOR RANGE	ANGLE
G,N	RLX	7-8	C	7-8	TOF-D		DST
		(7.6-8.45)		(7.6-8.45)			

No evidence found near threshold for doorway states.

TABLE III. Energies and parameters for resonances in the reaction $^{57}Fe(\gamma, n)$. The ±20% error in the quantity $\Gamma_{\gamma 0}\Gamma_n/\Gamma$ for all resonances is due mainly to the uncertainty in the absolute normalization of the data. The energies given in column 2 are calculated from those of column 1 by applying a correction for recoil effects. For unassigned levels, column 4 gives $g\Gamma_{\gamma 0}\Gamma_n/\Gamma$.

$E_n(n,\gamma)$ References 19, 22 (keV)	$E_n(\gamma,n)$ at $\theta=90°$ Calc. (keV)	Obs. (keV)	$\Gamma_{\gamma 0}\Gamma_n/\Gamma$ (eV)
	$J=\frac{1}{2}^+$		
27.9	26.9	26.7	0.112
74	71.4	70.2	0.082
83.7	80.8	...	...
123.5	119.2	118.4	0.119
130	125.5	125.1	0.105
141	136	136	0.068
169	163	163	0.066
188	181	181	0.423
220	212	212	0.663
		Total	1.658
	$J=\frac{1}{2}^-$		
34.1	32.9	32.9	0.180
59	56.9	56.9	0.221
...	...	216	0.130
...	...	278	0.208
		Total	0.739
	$J=\frac{1}{2}^-$		
...	...	224	0.364
...	...	235	0.382
...	...	270	0.090
		Total	0.836
	Unassigned levels		
...	...	92.6	0.045
...	...	98.7	0.042
...	...	167	0.032
...	...	247	0.030
...	...	260	0.046
		Total	0.195

TABLE IV. Angular momentum assignments for resonances in the reaction $^{57}Fe(\gamma, n)$.

$E_n(\gamma,n)$ (keV)	$\frac{d\sigma(90°)/d\Omega}{d\sigma(135°)/d\Omega}$	J^π	$E_n(\gamma,n)$ (keV)	$\frac{d\sigma(90°)/d\Omega}{d\sigma(135°)/d\Omega}$	J^π
26.7	s wave	$\frac{1}{2}^+$	181	s wave	$\frac{1}{2}^+$
32.9	1.10 ± 0.08	$\frac{1}{2}^-$	212	s wave	$\frac{1}{2}^+$
56.9	1.08 ± 0.09	$\frac{1}{2}^-$	216	0.90 ± 0.10	$\frac{1}{2}^-$
70.2	s wave, other	$\frac{1}{2}^+$, ?	224	1.32 ± 0.04	$\frac{1}{2}^-$
118.4	s wave	$\frac{1}{2}^+$	235	1.43 ± 0.04	$\frac{1}{2}^-$
125.1	s wave	$\frac{1}{2}^+$	270	1.36 ± 0.09	$\frac{1}{2}^-$
136.	s wave	$\frac{1}{2}^+$	278	0.99 ± 0.07	$\frac{1}{2}^-$
163.	s wave	$\frac{1}{2}^+$			

(over)

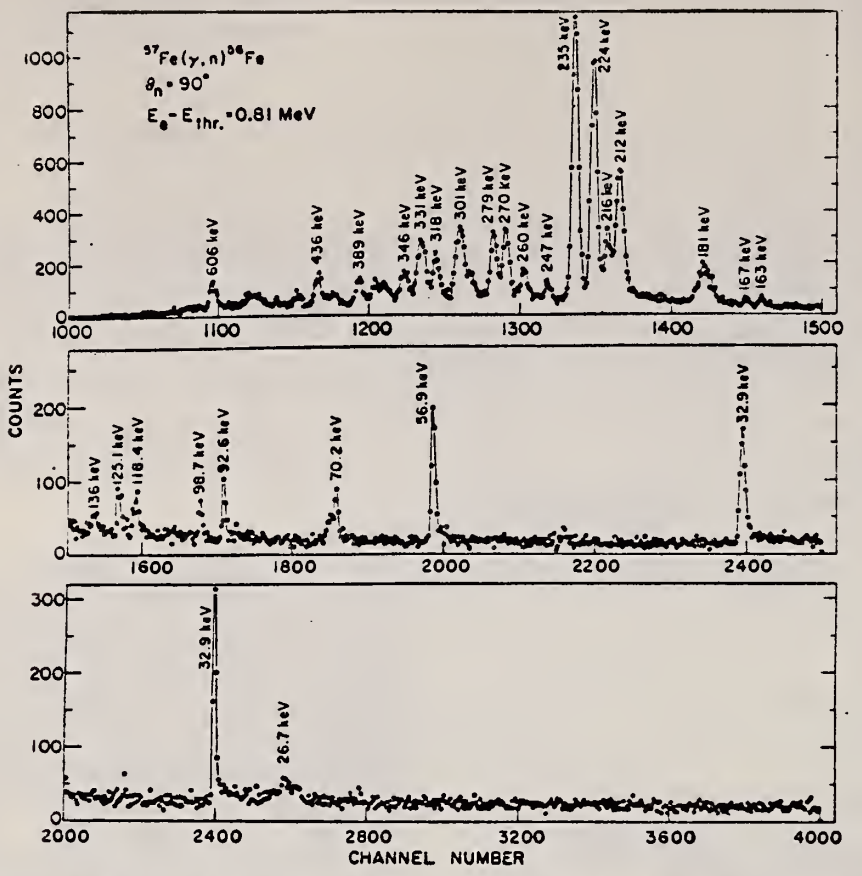

FIG. 6. Photoneutron time-of-flight spectrum for $^{57}Fe(\gamma,n)$. The flight path was 9 m. Each point in the center section represents the sum of two adjacent channels; in the lower section they represent sums of four adjacent channels.

TABLE VII. Integrated yields and reduced widths for electric and magnetic dipole radiation. Integrated yields are given for all resonances observed, but reduced widths for magnetic dipole transitions are calculated only from yields for p-wave levels above 100-keV neutron energy (see discussion in Sec. IV). The number of resonance widths used to obtain each $\bar{k}$ is given by n. The errors given were calculated by assuming that the individual $\Gamma_{\gamma 0}$'s follow a Porter-Thomas distribution.

Target	J^π	$\sum g\Gamma_{\gamma 0}\Gamma_n/\Gamma$ (eV)	$\sum \Gamma_{\gamma 0}\Gamma_n/\Gamma$ (eV)	n	$10^3\times$ reduced width Individual	average
^{53}Cr	$\frac{1}{2}^+$	0.97	3.88	7	$\bar{k}_{E1}=1.7^{+1.7}_{-0.5}$	
	$\frac{1}{2}^-$	1.27	5.06	6	$\bar{k}_{M1}=41$	$\bar{k}_{M1}=28^{+15}_{-8}$
	$\frac{3}{2}^-$	0.86	1.71	10	$\bar{k}_{M1}=16$	
^{57}Fe	$\frac{1}{2}^+$	0.83	1.66	8	$\bar{k}_{E1}=0.86^{+0.8}_{-0.3}$	
	$\frac{1}{2}^-$	0.37	0.74	4	$\bar{k}_{M1}=9$	$\bar{k}_{M1}=10^{+10}_{-3}$
	$\frac{3}{2}^-$	0.84	0.84	3	$\bar{k}_{M1}=10$	
^{61}Ni	$\frac{1}{2}^+$	0.37	1.48	11	$\bar{k}_{E1}=0.96^{+0.42}_{-0.19}$	
	$\frac{1}{2}^-$	0.41	1.65	5	$\bar{k}_{M1}=27$	$\bar{k}_{M1}=20^{+18}_{-7}$
	$\frac{3}{2}^-$	0.54	1.07	3	$\bar{k}_{M1}=12$	

REF.

H.E. Jackson and E.N. Strait
Statistical Properties of Nuclei, ed. J. B. Garg, Plenum Publishing Corporation, New York (1971) p.601

ELEM. SYM.	A	Z
Fe	57	26

METHOD

REF. NO. 71 Ja 2 egf

REACTION	RESULT	EXCITATION ENERGY	SOURCE TYPE	SOURCE RANGE	DETECTOR TYPE	DETECTOR RANGE	ANGLE
G,N	RLX	8-9	C	8	TOF-D		DST
		(7.6-8.45)		(8.45)			

7.6-8.4 MEV, G-WIDTH

TABLE I. Angular-momentum assignments for resonances in the reaction $^{57}Fe(\gamma,n)$.

E_n (keV)	$\frac{d\sigma(90^\circ)/d\Omega}{d\sigma(135^\circ)/d\Omega}$	J^π	E_n (keV)	$\frac{d\sigma(90^\circ)/d\Omega}{d\sigma(135^\circ)/d\Omega}$	J^π
26.7	s-wave	$\frac{1}{2}^+$	181.	1.05 ± 0.07	$\frac{1}{2}^+$
32.9	1.10 ± 0.08	$\frac{1}{2}^-$	212	1.00 ± 0.03	$\frac{1}{2}^+$
56.9	1.08 ± 0.09	$\frac{1}{2}^-$	216	0.90 ± 0.10	$\frac{1}{2}^-$
70.2	s-wave,other	$\frac{1}{2}^+$,?	224	1.32 ± 0.04	$\frac{3}{2}^-$
118.4	s-wave	$\frac{1}{2}^+$	235	1.43 ± 0.04	$\frac{3}{2}^-$
125.1	s-wave	$\frac{1}{2}^+$	270	1.36 ± 0.09	$\frac{3}{2}^-$
136	s-wave	$\frac{1}{2}^+$	278	0.99 ± 0.07	$\frac{1}{2}^-$
163	s-wave	$\frac{1}{2}^+$			

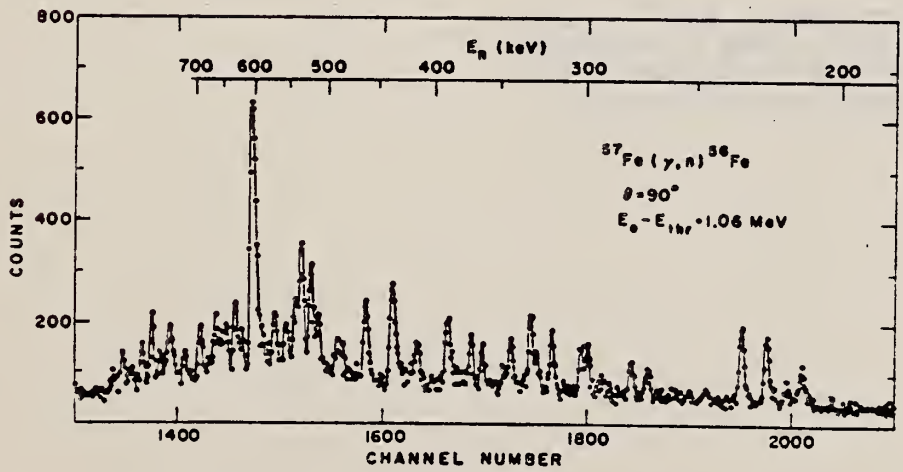

Fig. 4. Photoneutron time-of-flight spectrum for $^{57}Fe(\gamma,n)$ as observed with a proton-recoil neutron detector.

(over)

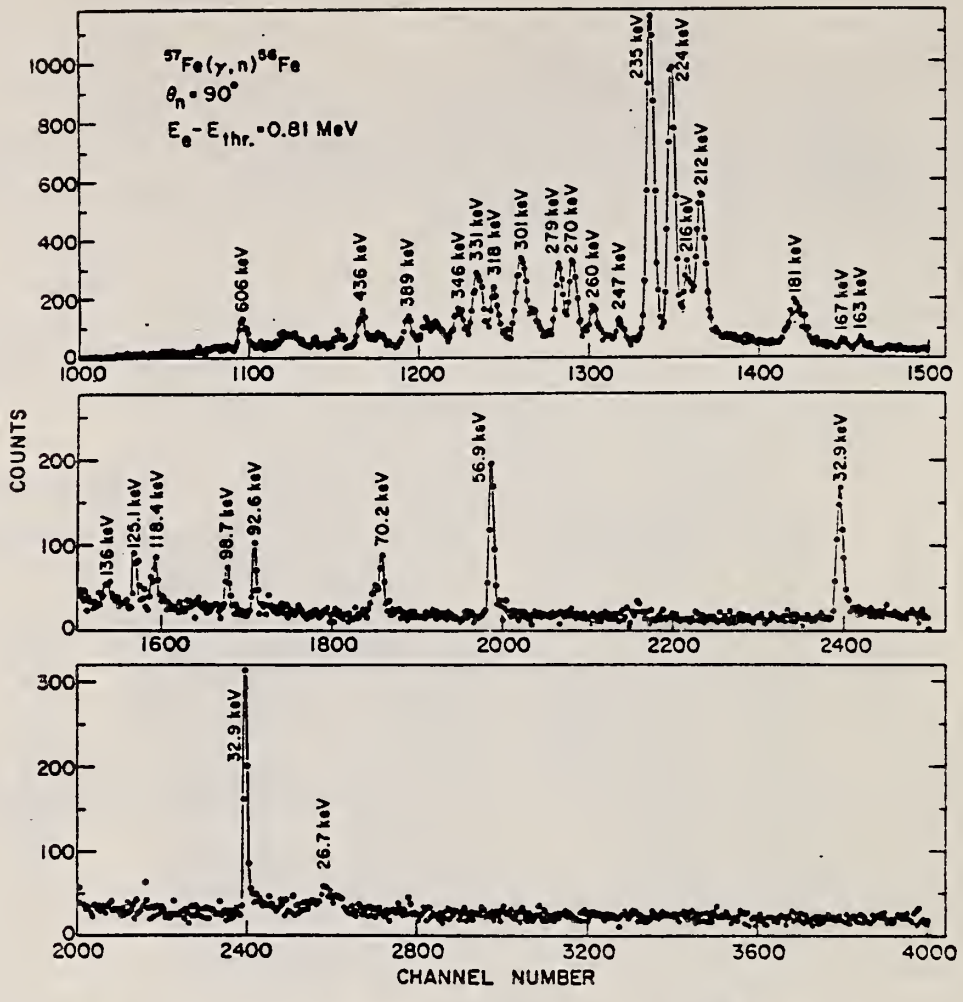

Fig. 2. Photoneutron time-of-flight spectrum for $^{57}Fe(\gamma,n)$. Points in the center section are sums of two adjacent channels; in the lower section they are sums of four adjacent channels. The data were taken with ^{6}Li glass detectors.

FE
A=58

FE
A=58

REF. A.S. Litvinenko, N.G. Shevchenko, A.Yu. Buki, P.L. Kondrat'ev, G.A. Savitskii, A.A. Khomich, V.M. Khvastunov, I.I. Chkalov
Ukr. Fiz. Zhur. 17, 1197 (1972)

ELEM. SYM.	A	Z
Fe	58	26

METHOD

REF. NO. 72 Li 3 hmg

REACTION	RESULT	EXCITATION ENERGY	SOURCE TYPE	SOURCE RANGE	DETECTOR TYPE	DETECTOR RANGE	ANGLE
E,E/	FMF	1, 4	D	150,225	MAG-D		DST

B(EL) LEV .81,3.86

Таблица 1

Параметры фермиевского распределения плотности заряда (*c*—радиус полуспада плотности, *t*—диффузионность ядра)

Ядро	*c*, *ф*	*t*, *ф*
Fe^{54}	4,012±0,007	2,346±0,011
Fe^{56}	3,971±0,013	2,608±0,020
Fe^{58}	4,027±0,019	2,530±0,031
Ni^{62}	4,149±0,011	2,506±0,016

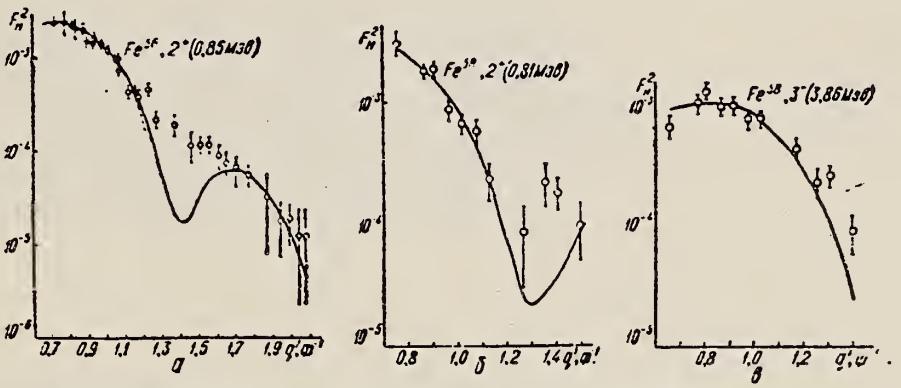

Формфакторы *E*2- и *E*3-переходов в ядрах Fe^{56} (*а*) и Fe^{58} (*б*, *в*). Сплошные кривые — расчет по вибрационной модели в высокоэнергетическом приближении: ⊖ — 150 *Мэв*; ○ — 225 *Мэв*, △ — данные работы [6]; пунктирная кривая — расчет в борновском приближении [6].

Таблица 2

Ядро	E_λ, *Мэв*	J^π	Данные настоящей работы $B(E\lambda)\uparrow$, $e^2\lambda\phi^{2\lambda}$	Данные других работ $B(E\lambda)\uparrow$, $e^2\lambda\phi^{2\lambda}$	Данные других работ: Тип эксперимента и метод определения	Литература
Fe^{54}	1,4	2^+	531,9±32,4	533	(ee'), борновское приближение	[6]
	4.85	3^-	4563±410	4390		
Fe^{56}	0.85	2^+	678,1±47,5	720	(ee'), борновское приближение	»
				1250±270	искаженные волны	[7]
				1240	борновское приближение	»
				900±100	кулоновское возбуждение	[8]
Fe^{58}	0.81	2^+	943.2±79			
	3.86	3^-	13880±1260			
Ni^{62}	1,17	2^+	618.6±42,1	877± 11	(ee'), искаженные волны	[9]
	3,75	3^-	14359±962	20100±540		

U.S. DEPARTMENT OF COMMERCE
NATIONAL BUREAU OF STANDARDS

# COBALT
Z=27

Ores containing cobalt have been used since antiquity as pigments, but without knowledge of the source of the color. The word cobalt is from the Greek word "*cobalos*" meaning mine. Its German form signified a mischievous spirit (gnomes or goblins) and was used by the German miners in Saxony to designate certain ores which injured their hands and feet. These ores were later found to contain arsenical cobalt.

Co
A=55

Co
A=55

REF.

D.J. Martin, J.R. Leslie, W. McLatchie, C.F. Monahan, and L.E. Carlson
Nucl. Phys. A187, 337 (1972)

ELEM. SYM.	A	Z
Co	55	27

METHOD

REF. NO.	
72 Ma 2	egf

REACTION	RESULT	EXCITATION ENERGY	SOURCE		DETECTOR		ANGLE
			TYPE	RANGE	TYPE	RANGE	
P,G	LFT	7	D	2	SCD-D		DST

J-PI

TABLE I

Summary of γ-ray angular distribution coefficients, multipole mixing ratios and spin hypotheses for the E_p = 1803 keV resonance

Transition $E_i \rightarrow E_f$ (MeV)	A_0	a_2	a_4	Spin sequence $J_i \rightarrow J_f$	Mixing ratio δ
6.83 → 0	100±3	−0.30±0.06	0.02±0.06	$\frac{1}{2} \rightarrow \frac{1}{2}$	$-0.09^{+0.02}_{-0.01}$
6.83 → 2.16	8±1	0.34±0.19	−0.02±0.14	$\frac{1}{2} \rightarrow \frac{3}{2}$	$0.36^{+0.16}_{-0.08}$
6.83 → 2.56	4±1	−0.19±0.25	0.24±0.25	$\frac{1}{2} \rightarrow \frac{3}{2}$	$0.30^{+0.23}_{-0.20}$
6.83 → 2.92	8±1	−0.32±0.10	0.11±0.17	$\frac{1}{2} \rightarrow \frac{1}{2}$	$-0.09^{+0.17}_{-0.18}$
				$\frac{3}{2} \rightarrow \frac{1}{2}$	$-0.36^{+0.18}_{-0.15}$
6.83 → 3.32	23±2	−0.62±0.10	0.00±0.10	$\frac{1}{2} \rightarrow \frac{1}{2}$	$0.08^{+0.04}_{0.04}$
				$\frac{1}{2} \rightarrow \frac{3}{2}$	$1.32^{+1.00}_{-0.35}$
6.83 → 3.73	19±2	−0.08±0.13	−0.07±0.13	$\frac{1}{2} \rightarrow \frac{3}{2}$	$0.36^{+0.04}_{-0.06}$
				$\frac{1}{2} \rightarrow \frac{1}{2}$	$0.00^{+0.07}_{-0.08}$
				$\frac{1}{2} \rightarrow \frac{1}{2}$	$-0.17^{+0.05}_{-0.15}$
6.83 → 4.16	8±1	−0.65±0.20	−0.03±0.18	$\frac{1}{2} \rightarrow \frac{1}{2}$	$0.09^{+0.12}_{-0.10}$
				$\frac{1}{2} \rightarrow \frac{3}{2}$	$1.19^{+0.95}_{-0.35}$
6.83 → 4.72	7±1	0.26±0.17	0.00±0.15	$\frac{1}{2} \rightarrow \frac{1}{2}$	$0.09^{+0.09}_{-0.10}$

TABLE 3

Gamma-ray transition probabilities for the strong transitions observed from the E_p = 1803 keV resonance

Transition $E_i \rightarrow E_f$ (MeV)	E_γ (MeV)	Γ_γ (meV)	Spin sequence $J_i \rightarrow J_f$	B(M1) (W.u. × 10^3)	B(E2) (W.u.)
6.83 → 2.92	3.91	20±4	$\frac{1}{2} \rightarrow \frac{1}{2}$	16± 3	
6.83 → 3.32	3.51	57±8	$\frac{1}{2} \rightarrow \frac{1}{2}$	63± 8	
			$\frac{1}{2} \rightarrow \frac{3}{2}$	23^{+9}_{-10}	6^{+3}_{-3}
6.83 → 3.73	3.11	48±8	$\frac{1}{2} \rightarrow \frac{1}{2}$	67±12	2±1
			$\frac{1}{2} \rightarrow \frac{1}{2}$	74±12	
			$\frac{1}{2} \rightarrow \frac{3}{2}$		16±3
6.83 → 4.16	2.67	20±4	$\frac{1}{2} \rightarrow \frac{1}{2}$	51±10	
			$\frac{1}{2} \rightarrow \frac{3}{2}$	23± 6	8^{+4}_{-4}
6.83 → 4.72	2.11	11±3	$\frac{1}{2} \rightarrow \frac{1}{2}$	59±16	1±1

TABLE 4

Gamma-ray transition probabilities for the strong transitions observed from the $E_p = 1887$ keV resonance

Transition $E_i \rightarrow E_f$ (MeV)	E_γ (MeV)	Γ_γ (meV)	Spin sequence $J_i \rightarrow J_f$	B(M1) (W.u. $\times 10^3$)	B(E2) (W.u.)
6.92 → 0	6.92	19 ± 4	$\frac{5}{2} \rightarrow \frac{7}{2}$	2.7 ± 0.5	
6.92 → 2.56	4.35	22 ± 5	$\frac{5}{2} \rightarrow \frac{5}{2}$	13 ± 4	
6.92 → 2.92	3.99	4 ± 2	$\frac{5}{2} \rightarrow \frac{3}{2}$	2.0 ± 1.0	0.08 ± 0.06
6.92 → 3.73	3.19	12 ± 3	$\frac{5}{2} \rightarrow \frac{3}{2}$	17 ± 4	
			$\frac{5}{2} \rightarrow \frac{5}{2}$	14 ± 4	0.5 ± 0.4
			$\frac{5}{2} \rightarrow \frac{7}{2}$	9 ± 3	1.5 ± 0.8
6.92 → 3.86	3.06	11 ± 3	$\frac{5}{2} \rightarrow \frac{3}{2}$	17 ± 4	
			$\frac{5}{2} \rightarrow \frac{5}{2}$	16 ± 4	0.5 ± 0.3
			$\frac{5}{2} \rightarrow \frac{7}{2}$	17 ± 4	
6.92 → 4.18	2.74	7 ± 2	$\frac{5}{2} \rightarrow \frac{3}{2}$	17 ± 4	
			$\frac{5}{2} \rightarrow \frac{7}{2}$	12 ± 3	$1.3^{+1.3}_{-0.6}$
6.92 → 4.72	2.19	14 ± 2	$\frac{5}{2} \rightarrow \frac{1}{2}$	65 ± 9	0.2 ± 0.1

REF.

J.V. Maher, L. Meyer-Schutzmeister, E.L. Sprenkel-Segel, D. von Ehrenstein, R.J. Nemanich, G.C. Kiang, J.F. Tonn, R.E. Segel
Phys. Rev. C9, 1440 (1974)

ELEM. SYM.	A	Z
Co	55	27

METHOD

REF. NO.	
74 Ma 1	hmg

REACTION	RESULT	EXCITATION ENERGY	SOURCE		DETECTOR		ANGLE
			TYPE	RANGE	TYPE	RANGE	
P,G	ABX	9- 22	D	4- 17	NAI-D		DST

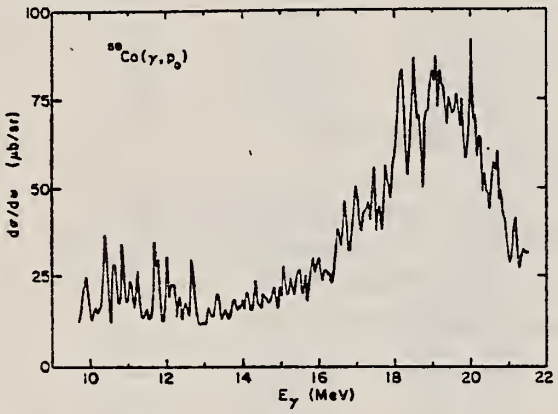

FIG. 3. Yield curve at 90° for the $^{55}Co(\gamma,p_0)^{54}Fe$ reaction obtained by applying detailed balance to the $^{54}Fe(p,\gamma_0)$ measured cross sections.

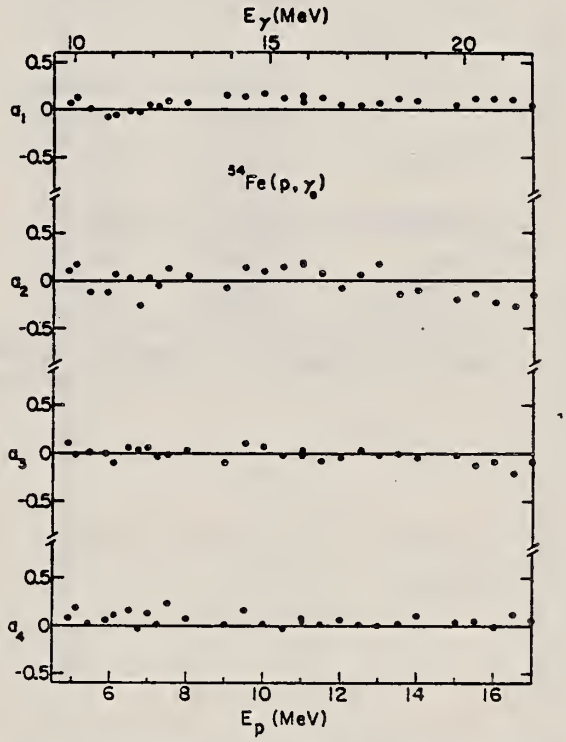

FIG. 7. Coefficients obtained when the $^{54}Fe(p,\gamma_0)$ angular distributions are expressed as a sum of Legendre polynomials.

REF. C.P. Cameron, N.R. Roberson, D.G. Rickel, R.D. Ledford, H.R. Weller, R.A. Blue, D.R. Tilley
Phys. Rev. C14, 553 (1976)

ELEM. SYM.	A	Z
Co	55	27

METHOD

REF. NO. 76 Ca 4 hmg

REACTION	RESULT	EXCITATION ENERGY	SOURCE		DETECTOR		ANGLE
			TYPE	RANGE	TYPE	RANGE	
$ P,G	ABX	14- 22	D	8- 15	NAI-D		DST

POLARIZED PROTONS

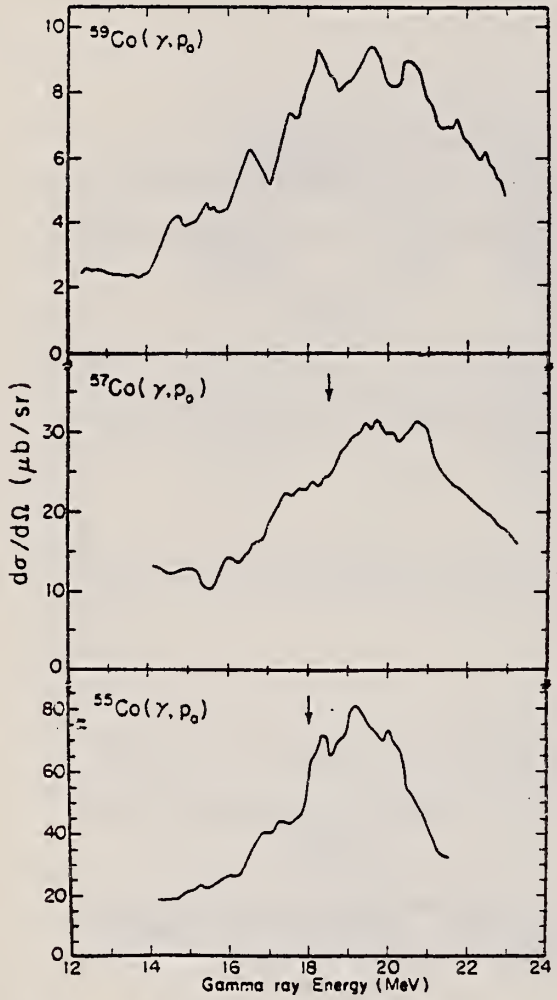

FIG. 3. The 90° yield curves for the ^{54,56,58}Fe(p,γ) reactions after averaging over a 500 keV interval. The arrows indicate the energy of the splitting between the $T_<$ and $T_>$ components of the GDR as suggested in Ref. 1.

$$\sigma(\theta)=a_0\left[1+\sum_k \frac{a_k}{a_0}Q_k P_k(\cos\theta)\right],$$

$$A(\theta)=\left(\frac{N_+-N_-}{N_++N_-}\right)\frac{1}{P}.$$ (Where N_+ and N_- are counts spin up and counts spin down.)

$$A(\theta)\sigma(\theta)/a_0=\sum_k b_k Q_k P_k^1(\cos\theta).$$

[1] J.V. Maher, L. Meyer-Schutzmeister, E.L. Sprenkel-Segel, D. von Ehrenstein, R.J. Nemanich, G.C. Kiang, J.F. Tonn, and R.E. Segel, Phys. C9, 1440 (1974).

(over)

TABLE III. The a and b coefficients obtained from least square fits to the data as described in the text. Higher order coefficients are given only when the criterion of normalized χ^2 justified the use of higher order terms.

E_p (MeV)	a_1/a_0	a_2/a_0	a_3/a_0	b_1	b_2	b_3
			$^{54}Fe(\vec{p},\gamma_0)^{55}Co$			
8.0	0.26± 0.06	0.11± 0.11		−0.03± 0.05	0.00± 0.04	−0.02± 0.04
9.0	0.20± 0.05	0.09± 0.10		−0.07± 0.04		
10.0	0.25± 0.04	0.03± 0.07		0.02± 0.03	−0.09± 0.02	
11.0	0.10± 0.03	0.24± 0.05		0.03± 0.02	−0.07± 0.02	
12.1	0.27± 0.05	0.18± 0.04	0.18± 0.07	0.01± 0.01	−0.12± 0.01	
13.0	0.01± 0.03	−0.09± 0.05		0.03± 0.02	−0.15± 0.01	
14.0	0.07± 0.03	0.0 ± 0.05		−0.02± 0.02	−0.16± 0.02	−0.02± 0.02
15.0	0.18± 0.03	−0.12± 0.06		0.01± 0.02	−0.20± 0.02	−0.03± 0.02
			$^{56}Fe(\vec{p},\gamma_0)^{57}Co$			
8.0	0.27± 0.06	0.03± 0.12		0.08± 0.05	−0.01± 0.04	
9.0	0.07± 0.04	−0.04± 0.08		−0.05± 0.03	−0.06± 0.02	−0.03± 0.02
10.0	0.08± 0.03	0.24± 0.06		0.05± 0.02	−0.08± 0.02	−0.02± 0.02
11.5	0.03± 0.03	0.20± 0.05		−0.08± 0.03	−0.09± 0.02	
13.0	0.14± 0.03	0.15± 0.05		0.02± 0.02	−0.22± 0.02	−0.03± 0.02
14.5	0.14± 0.04	−0.34± 0.08		0.10± 0.03	−0.21± 0.02	−0.04± 0.02
			$^{58}Fe(\vec{p},\gamma_0)^{59}Co$			
7.6	0.19± 0.05	0.19± 0.09		0.04± 0.03	−0.02± 0.03	
9.2	0.12± 0.04	0.28± 0.07		0.01± 0.03	−0.11± 0.02	
9.6	0.04± 0.04	0.26± 0.07		0.06± 0.02	−0.17± 0.02	
10.5	0.12± 0.04	0.15± 0.06		0.04± 0.02	−0.17± 0.02	0.04± 0.02
11.2	0.16± 0.04	0.09± 0.06		0.08± 0.02	−0.18± 0.02	
11.9	0.18± 0.05	−0.14± 0.09		0.03± 0.03	−0.20± 0.03	−0.04± 0.03
12.7	0.13± 0.05	−0.25± 0.09		0.07± 0.03	−0.23± 0.02	
13.5[a]	0.08± 0.09	−0.28± 0.09	0.00± 0.14	0.06± 0.03	−0.22± 0.02	
14.0[a]	0.14± 0.09	−0.47± 0.08	0.00± 0.13	0.08± 0.03	−0.20± 0.02	−0.04± 0.02
15.0[a]	0.08± 0.10	−0.29± 0.08	0.00± 0.15	0.10± 0.03	−0.23± 0.02	−0.03± 0.02

[a] The criterion of normalized χ^2 did not clearly indicate that a fit which included $P_3(\cos\theta)$ was statistically justified for these energies. The error given for a_1 and a_3 reflects this uncertainty.

REF. H.R. Weller, N.R. Roberson & S.R. Cotanch
Phys. Rev. C18, 65 (1978)

ELEM. SYM.	A	Z
Co	55	27

METHOD

REF. NO. 78 We 4 hmg

REACTION	RESULT	EXCITATION ENERGY	SOURCE TYPE	SOURCE RANGE	DETECTOR TYPE	DETECTOR RANGE	ANGLE
$ P,G	RLX	13-20	D	8-15	UKN-D		DST

Analysis of data in reference 3.

POLARIZED PROTONS

Measurements of cross sections and analyzing powers are examined for polarized proton capture on ^{14}C, ^{30}Si, ^{54}Fe, ^{56}Fe, ^{58}Fe, ^{59}Co, and ^{88}Sr at energies which cover the giant dipole resonance region. These data are used to extract the relative amplitudes and phases of the contributing $E1$ T-matrix elements. A typical result exhibits two solutions. Calculations using the direct (or a direct-semidirect) capture model appear to provide a means for choosing the physical solution.

[NUCLEAR REACTIONS: $^{14}C(\vec{p},\gamma_0)$, $^{30}Si(\vec{p},\gamma_0)$, $^{54}Fe(\vec{p},\gamma_0)$, $^{56}Fe(\vec{p},\gamma_0)$, $^{58}Fe(\vec{p},\gamma_0)$, $^{59}Co(\vec{p},\gamma_0)$, $^{88}Sr(\vec{p},\gamma_0)$; measured $\sigma(\theta)$ and $A(\theta)$ over energy region of the giant dipole resonance. Deduced T-matrix amplitudes and phases. Compare results to direct-semidirect model calculations.]

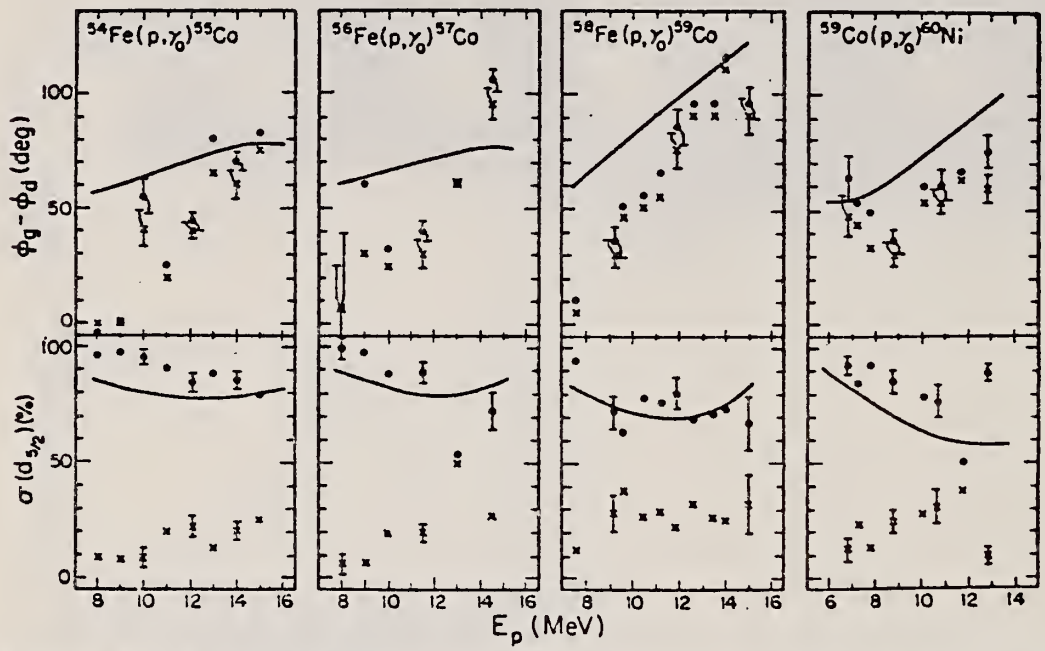

FIG. 2. Same as Fig. 1 for the target nuclei of ^{54}Fe, ^{56}Fe, ^{58}Fe, and ^{59}Co. The remaining cross section is due to the $g_{9/2}$ matrix element.

FIG. 1. The two solutions (dots and x's) resulting from a pure $E1$ analysis of the data are shown along with the results of the calculation for target nuclei of ^{14}C, ^{88}Sr, and ^{30}Si. The remaining cross section in the case of ^{14}C and ^{88}Sr is due to the $s_{1/2}$ matrix element. In the case of ^{30}Si it arises from the $p_{1/2}$ matrix element. The error bars represent typical statistical errors associated with the data points. The amplitudes are presented in terms of the percentage of the total cross section for which they are responsible. The curves represent DSD calculations as described in the text. The dashed curves in the case of ^{88}Sr were obtained using the optical model parameters of Ref. 16 while the solid lines were obtained from the parameters of Ref. 18.

(OVER)

[2]H. R. Weller, R. A. Blue, N. R. Roberson, D. G. Rickel, S. Maripuu, C. P. Cameron, R. D. Ledford, and D. R. Tilley, Phys. Rev. C 13, 922 (1976). (Note: an error exists in the sign of the phase in this paper. The quantity $\phi_s - \phi_d$ should be $\phi_d - \phi_s$ wherever it appears.)
[3]C. P. Cameron, N. R. Roberson, D. G. Rickel, R. D. Ledford, H. R. Weller, R. A. Blue, and D. R. Tilley, Phys. Rev. C 14, 553 (1976).
[4]C. P. Cameron, Ph.D. thesis, Duke University, 1976 (unpublished).
[5]R. D. Ledford, Ph.D. thesis, Duke University, 1976 (unpublished).
[6]J. D. Turner, C. P. Cameron, N. R. Roberson, H. R. Weller, and D. R. Tilley, Phys. Rev. C 17, 1853 (1978).

REF. R. Hanninen, R. Hentela, G.U. Din
Phys. Scripta 22, 451 (1980)

ELEM. SYM.	A	Z
Co	55	27

METHOD

REF. NO. 80 Ha 5 egf

REACTION	RESULT	EXCITATION ENERGY	SOURCE		DETECTOR		ANGLE
			TYPE	RANGE	TYPE	RANGE	
P,G	J PI	6-7	D	1-2	SCD-D		DST

Complete angular distribution and mixing ratio data given in Table 1 for all states listed in Table II. 10 STATES 6.2-7.3 MEV

The Doppler-shift attenuation (DSA) measurements of γ-rays performed on five $^{54}Fe(p,\gamma)^{55}Co$ resonances yielded mean lifetimes of 20 levels in ^{55}Co below 5.5 MeV, seven of them for the first time. Angular distribution measurements were carried out on 17 $^{54}Fe(p,\gamma)^{55}Co$ resonances in the energy range $E_p = 1.1$–2.3 MeV. The analysis of the angular distributions along with the present DSA and available literature data lead to the following unique spin and parity assignments for four bound states: $5/2^-$ ($E_x = 2659$ keV), $5/2^-$ (3725), $3/2^-$ (4164) and $5/2^-$ (4548). The spin of the 3563 keV state was found to be 3/2. The unique spin values of eight resonance states were determined. The present results are compared with recent shell-model calculations.

Table II. *The spin values of ^{55}Co excited states obtained in the present experiment. The energies are from* [22]

	Resonance states			Bound states	
	E_p (keV)	E_x (keV)	J^π	E_x	J^π
→	1162	6205	$5/2^+$	2659	$5/2^-$ [b]
	1226	6268	$5/2^-$	2918	$7/2^-$ [b]
	1288	6328	$3/2^-$	2939	$1/2^-(3/2)^-$
	1329	6369	$5/2^+$	2976	$9/2^-(7/2)^-$ [b]
→	1476	6513	3/2(5/2)	3563	3/2
→	1667	6701	5/2	3725	$5/2^-$ [b]
	1680	6713	$1/2^-(3/2)^-$ [a]	4164	$3/2^-$
→	1722	6755	5/2	4177	$5/2^-$
→	1747	6780	$3/2^-$ [b]	4548	$5/2^-$
	1803	6834	3/2, 5/2 [c]	4748	$3/2^-$ [f]
→	1846	6876	$7/2^-$, $9/2$ [b]		
→	1887	6917	$5/2^-$ [d]		
→	2075	7101	5/2		
→	2168	7193	5/2		
	2245	7269	$3/2^-$ [e]		
	2270	7293	$5/2^-$ [b]		
→	2297	7319	5/2		

[a] Possible analogue of the 1919($1/2^-$) keV state in ^{55}Fe [15, 17].
[b] For the parity assignment see Section 4.1.
[c] This resonance has been suggested to be a doublet [7], the lower member of which is the analogue of the 2051($3/2^-$) keV state in ^{55}Fe.
[d] Analogue of the 2144($5/2^-$) keV state in ^{55}Fe [7, 25].
[e] Possible analogue of the 2471($3/2^-$) keV state in ^{55}Fe [6].
[f] Analogue of the ground state ($J^\pi = 3/2^-$) of ^{55}Fe [11, 15, 17].

ground state gamma transitions observed for states marked with arrows

REF. M.Sana Ullah, H.M. Sen Gupta
Nucl. Phys. A337, 231 (1980)

EL EM. SYM.	A	Z
Co	55	27

METHOD

REF. NO. 80 U1 2 hg

REACTION	RESULT	EXCITATION ENERGY	SOURCE TYPE	SOURCE RANGE	DETECTOR TYPE	DETECTOR RANGE	ANGLE
P,G	RLY	6	D	1	SCD-D		DST
		(6.754)		(1.721)			

Abstract: Excitation functions for the $^{54}Fe(p,\gamma)^{55}Co$ reaction have been recorded in the energy region E_p = 1100–1760 keV. The decay schemes and branching ratios of ten resonances have been investigated. Angular distributions of primary γ-rays have been measured for three resonances to establish resonance spins. Resonance strengths for six resonances and gamma widths for three resonances have been determined. The isobaric analogues of the ground ($J^\pi = \frac{7}{2}^-$) and 1919 keV ($J^\pi = \frac{3}{2}^-$) states of the parent nucleus ^{55}Fe have been identified at 4722 and 6712 keV respectively in ^{55}Co. The Coulomb displacement energies of the observed analogue pairs (0–4722 keV) and (1919–6712 keV) have been obtained. The strengths of the possible analogue-antianalogue transitions for the proton capture state at E_p = 1679 keV have also been determined.

J-PI, 6754 KEV

E NUCLEAR REACTIONS $^{54}Fe(p,\gamma)$, E = 1.100–1.760 MeV; measured $\sigma(E; E_\gamma, \theta)$. ^{55}Co deduced levels, analogue resonances, J, δ, resonance strengths, gamma widths. Enriched target.

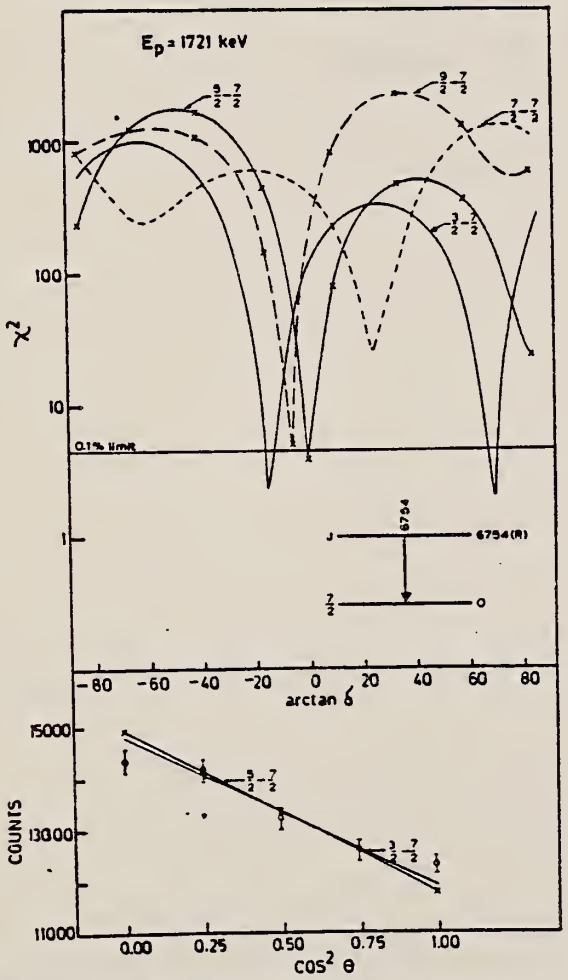

Fig. 5. Angular distribution for the transition from the proton capture state at E_p = 1721 keV to ground state and the corresponding χ^2 plots.

(OVER)

TABLE 3

Results of the angular distributions for the dominant primary transitions

Resonance E_p (keV)	Transition E_i–E_f (keV)	Spin sequence J_i–J_f	χ^2 min	Mixing ratio δ	Legendre polynomial coefficients A_0	a_2	a_4
1747	6780–2167	$\frac{3}{2}$–$\frac{1}{2}$	2.01	$-3.72^{+0.35}_{-1.04}$	1044±21	0.38 ±0.04	0.006±0.04
			1.82	$0.00^{+0.03}_{-0.02}$			
		$\frac{5}{2}$–$\frac{1}{2}$	2.71	$-0.36^{+0.02}_{-0.02}$			
	6780–2566	$\frac{3}{2}$–$\frac{1}{2}$	1.41	$-1.43^{+0.18}_{-0.08}$	1334±23	0.93 ±0.04	0.06 ±0.04
			1.48	$-0.36^{+0.04}_{-0.09}$			
	6780–3324	$\frac{3}{2}$–$\frac{1}{2}$	1.14	$-0.08^{+0.03}_{-0.02}$	788±24	−0.39 ±0.06	0.02 ±0.06
			1.14	$2.14^{+0.12}_{-0.14}$			
		$\frac{5}{2}$–$\frac{1}{2}$	0.96	$0.57^{+0.06}_{-0.03}$			
			1.00	$3.73^{+0.35}_{-0.70}$			
		$\frac{5}{2}$–$\frac{1}{2}$	0.99	$0.00^{+0.01}_{-0.02}$			
			2.60	$1.73^{+1.21}_{-0.45}$			
1721	6754–0	$\frac{3}{2}$–$\frac{7}{2}$	2.32	$-0.27^{+0.02}_{-0.005}$	13691±107	−0.11±0.01	0.003±0.01
			1.89	$2.74^{+0.07}_{-0.14}$			
		$\frac{5}{2}$–$\frac{7}{2}$	3.76	$0.00^{+0.02}_{-0.005}$			
	6754–2167	$\frac{3}{2}$–$\frac{1}{2}$	0.56	$0.46^{+0.03}_{-0.03}$	543±5	0.21 ±0.33	−0.57 ±1.24
			0.52	$5.67^{+1.44}_{-0.65}$			
		$\frac{5}{2}$–$\frac{1}{2}$	0.53	$-0.08^{+0.02}_{-0.02}$			
			14.40	$2.75^{+1.96}_{-1.15}$			
1679	6712–2167	$\frac{3}{2}$–$\frac{1}{2}$	1.23	$0.27^{+0.01}_{-0.04}$	1732±37	0.02 ±0.04	0.04 ±0.04
		$\frac{5}{2}$–$\frac{1}{2}$	1.38	$-0.17^{+0.01}_{-0.04}$			
	6712–2918	$\frac{3}{2}$–$\frac{1}{2}$	0.17	$0.08^{+0.02}_{-0.01}$	1321±41	0.001±0.05	0.04 ±0.05
			0.28	$2.74^{+0.15}_{-0.14}$			
		$\frac{5}{2}$–$\frac{1}{2}$	12.57	$-2.74^{+1.10}_{-1.96}$			
			0.63	$0.36^{+0.02}_{-0.02}$			
	6712–3324	$\frac{3}{2}$–$\frac{1}{2}$	0.68	$-0.36^{+0.02}_{-0.02}$	700±29	0.17 ±0.23	0.51 ±0.69
			0.68	$5.67^{+0.69}_{-0.64}$			
		$\frac{5}{2}$–$\frac{1}{2}$	0.78	$0.17^{+0.02}_{-0.07}$			
		$\frac{5}{2}$–$\frac{1}{2}$	0.61	$-0.27^{+0.12}_{-0.01}$			

Co
A=57

Co
A=57

Co
A=57

REF. M.T. Esat, J.R. Leslie, and W. McLatchie
Nucl. Phys. A232, 139 (1974)

ELEM. SYM.	A	Z
Co	57	27

METHOD

REF. NO. 74 Es 3 egf

REACTION	RESULT	EXCITATION ENERGY	SOURCE TYPE	SOURCE RANGE	DETECTOR TYPE	DETECTOR RANGE	ANGLE
P,G	LFT	7- 8	D	1- 2	SCD-D		DST
				(1.2-1.5)			

TABLE 1
Branching ratios in percent determined in the present work

E_x (keV)	J^π	Resonance proton energy (keV)															
		1223	1275	1280	1301	1311	1328	1345	1351	1372	1403	1408	1416	1420	1452	1458	1465
4685	$\frac{1}{2}^-, \frac{3}{2}^-$															29	11
4251	$\frac{5}{2}^-, \frac{7}{2}^-$																
4197	$\frac{1}{2}^-, \frac{3}{2}^-$																
4064	$\frac{1}{2}^-, \frac{3}{2}^-$										11		3				
3993	$\frac{5}{2}^-$	4										35					
3856									12								
3723		7										5			12		
3701																	7
3467	$\frac{3}{2}^-$												9				13
3357	$\frac{3}{2}^-$			3									7	3			
3262	$\frac{5}{2}^-, \frac{7}{2}^-$		19														
3176	$\frac{5}{2}^-$	11		16								13	5	6		9	
3109	$\frac{1}{2}^-, \frac{3}{2}^-$																8
2981	$\frac{1}{2}^+$		2											8			
2879	$\frac{3}{2}^-$								16			4	8	6			
2803	$\frac{5}{2}^-, \frac{7}{2}^-$										12	8			5		20
2743	$> \frac{7}{2}^-$																
2730	$\frac{3}{2}^-, \frac{5}{2}^-$	4		18							8			9			6
2723	$> \frac{5}{2}^-$																
2611	$\frac{7}{2}^-, \frac{9}{2}^-$				13							10				6	
2560	$> \frac{7}{2}^-$																
2524	$> \frac{7}{2}^-$																
2485	$> \frac{7}{2}^-$																
2311	$\frac{7}{2}^-$				9								20	16		6	
2133	$\frac{5}{2}^-$			5								8	30	26			
1920	$\frac{5}{2}^-$	7				38	13			38	39	4		5	21		
1897	$\frac{7}{2}^-$											4	4			12	
1757	$\frac{3}{2}^-$	19	24			62	87		10			4	5	18	20	14	11
1689	$\frac{1}{2}^-$																
1505	$\frac{1}{2}^-$	35	20	36					13		27		2		42		9
1378	$\frac{3}{2}^-$	12	35	22	20			67	49	62		2	2			5	15
1223	$\frac{3}{2}^-$																
0	$\frac{7}{2}^-$	1			58			33			3	3	5	3		19	

The level energies, spins and parities, are those of ref. [7]). Exceptions are discussed in the text. The resonance at $E_p = 1351$ keV is an unresolved doublet [6]).

TABLE 3
Results of absolute yield measurements for four of the resonances studied

Resonance proton energy (keV)	$(2J+1)\Gamma_p\Gamma_\gamma/(\Gamma_p+\Gamma_\gamma)$ (eV)
1223	0.30
1403	0.20
1408	0.45
1416	0.34

Taking into account uncertainties in the target composition we view these results as uncertain to ±30 % in absolute value. Other sources of uncertainty contribute less than 5 %.

(over)

TABLE 2

Angular distribution results for the dominant primary transitions

Decay	Spin sequence	χ^2	Mixing ratio	Legendre polynomial coefficients A_2	A_4
$E_p = 1223$ keV					
R → 1505	$\frac{3}{2}$-$\frac{1}{2}$	0.6	0.09±0.05	−0.63±0.04	−0.01±0.03
		0.6	1.43±0.05		
$E_p = 1301$ keV					
R → 1377	$\frac{3}{2}$-$\frac{3}{2}$	0.2	−0.05±0.03	−0.27±0.05	−0.04±0.05
		21	0.38±0.4		
	$\frac{1}{2}$-$\frac{3}{2}$	0.2	0.51±0.15		
		0.2	4.71±0.3		
$E_p = 1403$ keV					
R → 1505	$\frac{3}{2}$-$\frac{1}{2}$	0.3	−0.02±0.09	−0.46±0.09	0.02±0.1
		0.3	1.80±0.1		
R → 1920	$\frac{3}{2}$-$\frac{3}{2}$	0.3	−19.1 ±0.05	−0.41±0.03	0.01±0.03
		0.3	−0.29±0.05		
R → g.s.	$\frac{3}{2}$-$\frac{7}{2}$	1.3	0.12±0.3	0.45±0.1	−0.50±0.1
		1.3	1.10±0.3		
R → 4064	$\frac{3}{2}$-$\frac{1}{2}$	0.1	0.02±0.06	−0.50±0.1	−0.00±0.1
		0.1	1.70±0.1		
	$\frac{3}{2}$-$\frac{3}{2}$	0.1	0.84±0.2		
		0.1	2.15±0.2		
$E_p = 1408$ keV					
R → 1757	$\frac{5}{2}$-$\frac{3}{2}$	0.1	−0.02±0.04	−0.35±0.1	0.02±0.05
		18	2.25±0.4		
R → 1920	$\frac{5}{2}$-$\frac{3}{2}$	0.5	−0.75±0.3	0.64±0.06	−0.06±0.07
		0.3	−0.27±0.4		
R → 3993	$\frac{5}{2}$-$\frac{5}{2}$	8.9	−1.28±0.2	0.48±0.03	0.03±0.03
		0.3	−0.04±0.03		
R → g.s.	$\frac{5}{2}$-$\frac{7}{2}$	0.1	−0.05±0.03	−0.18±0.07	−0.03±0.07
		0.8	19.1 ±0.14		
R → 1896	$\frac{5}{2}$-$\frac{7}{2}$	1.4	19.1 ±0.09	−0.30±0.07	−0.04±0.06
		0.4	0.14±0.02		
R → 2131	$\frac{5}{2}$-$\frac{1}{2}$	1.2	0.14±0.4	0.55±0.05	0.10±0.06
$E_p = 1416$ keV					
R → 2879	$\frac{5}{2}$-$\frac{7}{2}$	0.2	0.07±0.04	−0.52±0.09	0.01±0.08
		6.7	1.60±0.2		
R → 1757	$\frac{5}{2}$-$\frac{3}{2}$	0.9	−0.05±0.1	−0.35±0.09	0.13±0.09
		4.3	2.48±0.4		
R → 2131	$\frac{5}{2}$-$\frac{5}{2}$	7.6	−0.1 ±0.6	0.05±0.03	0.01±0.03
		0.1	0.07±0.03		
R → 4064	$\frac{5}{2}$-$\frac{3}{2}$	1.1	0.04±0.15	−0.45±0.2	−0.00±0.2
		4.3	1.80±0.7		
R → 3357	$\frac{5}{2}$-$\frac{3}{2}$	0.1	0.14±0.04	−0.11±0.04	−0.00±0.04
		56	3.5 ±0.4		
R → 3467	$\frac{5}{2}$-$\frac{7}{2}$	0.4	0. ±0.02	−0.41±0.08	0.01±0.1
		54	2.14±0.2		
R → g.s.	$\frac{5}{2}$-$\frac{7}{2}$	0.0	−0.07±0.05	−0.24±0.06	0.00±0.05
		0.9	29.0 ±0.1		
R → 2311	$\frac{5}{2}$-$\frac{7}{2}$	0.1	−0.02±0.03	−0.14±0.04	−0.01±0.04
		2.0	11.4 ±0.14		
$E_p = 1420$ keV					
R → 1757	$\frac{1}{2}$-$\frac{3}{2}$	0.2	0.02±0.02	−0.40±0.06	0.01±0.05
		17	1.90±0.3		
R → 2133	$\frac{1}{2}$-$\frac{5}{2}$	0.6	0.23±0.6	0.63±0.06	0.01±0.07

[6] L.S. August, G.R. Gossett and P.A. Treado, Phys. Rev. 142 (1966) 664

[7] G. Hardie, T.H. Braid, L. Meyer-Schutzmeister and J.W. Smith, Phys. Rev. C5 (1972) 1600

REF.

J.V. Maher, L. Meyer-Schutzmeister, E.L. Sprenkel-Segel,
D. von Ehrenstein, R.J. Nemanich, G.C. Kiang, J.F. Tonn, R.E. Segel
Phys. Rev. C9, 1440 (1974)

ELEM. SYM.	A	Z
Co	57	27

METHOD

REF. NO.	
74 Ma 1	hmg

REACTION	RESULT	EXCITATION ENERGY	SOURCE		DETECTOR		ANGLE
			TYPE	RANGE	TYPE	RANGE	
P,G	ABX	10- 24	D	4- 18	NAI-D		DST

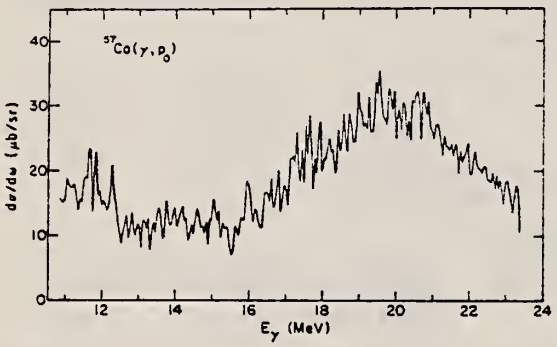

FIG. 4. Yield curve at 90° for the ^{57}Co(γ,p_0) reaction.

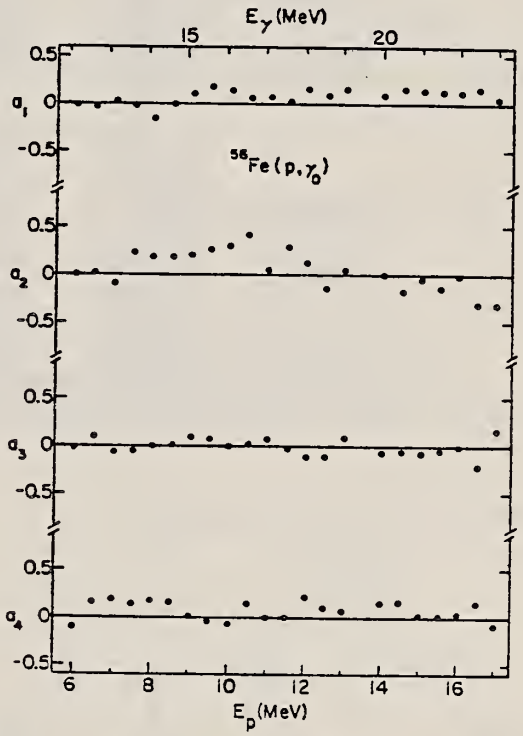

FIG. 8. Angular-distribution coefficients for the ^{56}Fe-(p,γ_0) reaction.

REF. C.P. Cameron, N.R. Roberson, D.G. Rickel, R.D. Ledford, H.R. Weller, R.A. Blue, D.R. Tilley
Phys. Rev. C14, 553 (1976)

ELEM. SYM.	A	Z
Co	57	27

METHOD

REF. NO. 76 Ca 4 hmg

REACTION	RESULT	EXCITATION ENERGY	SOURCE		DETECTOR		ANGLE
			TYPE	RANGE	TYPE	RANGE	
$ P,G	ABX	14- 24	D	8- 15	NAI-D		DST

POLARIZED PROTONS

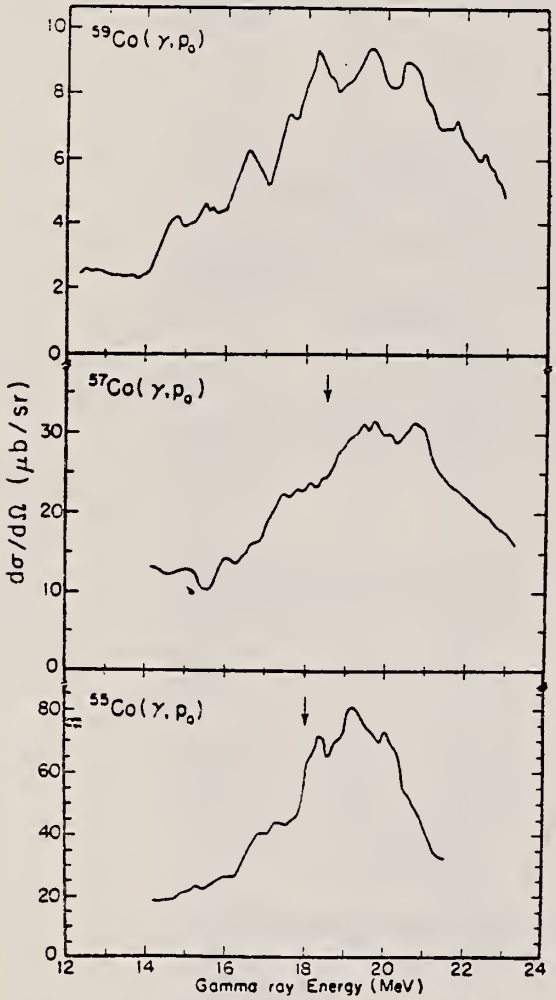

FIG. 3. The 90° yield curves for the $^{54,56,58}Fe(p,\gamma)$ reactions after averaging over a 500 keV interval. The arrows indicate the energy of the splitting between the $T_<$ and $T_>$ components of the GDR as suggested in Ref. 1.

$$\sigma(\theta)=a_0\left[1+\sum_k \frac{a_k}{a_0}Q_k P_k(\cos\theta)\right],$$

$$A(\theta)=\left(\frac{N_+-N_-}{N_++N_-}\right)\frac{1}{P}.$$ (Where N_+ and N_- are counts spin up and counts spin down.)

$$A(\theta)\sigma(\theta)/a_0=\sum_k b_k Q_k P_k^1(\cos\theta).$$

[1] J.V. Maher, L. Meyer-Schutzmeister, E.L. Sprenkel-Segel, D. von Ehrenstein, R.J. Nemanich, G.C. Kiang, J.F. Tonn, and R.E. Segel, Phys. C9, 1440 (1974).

(over)

TABLE III. The a and b coefficients obtained from least square fits to the data as described in the text. Higher order coefficients are given only when the criterion of normalized χ^2 justified the use of higher order terms.

E_p (MeV)	a_1/a_0	a_2/a_0	a_3/a_0	b_1	b_2	b_3
			$^{54}Fe(\vec{p},\gamma_0)^{55}Co$			
8.0	0.26±0.06	0.11±0.11		−0.03±0.05	0.00±0.04	−0.02±0.04
9.0	0.20±0.05	0.09±0.10		−0.07±0.04		
10.0	0.25±0.04	0.03±0.07		0.02±0.03	−0.09±0.02	
11.0	0.10±0.03	0.24±0.05		0.03±0.02	−0.07±0.02	
12.1	0.27±0.05	0.18±0.04	0.18±0.07	0.01±0.01	−0.12±0.01	
13.0	0.01±0.03	−0.09±0.05		0.03±0.02	−0.15±0.01	
14.0	0.07±0.03	0.0 ±0.05		−0.02±0.02	−0.16±0.02	−0.02±0.02
15.0	0.18±0.03	−0.12±0.06		0.01±0.02	−0.20±0.02	−0.03±0.02
			$^{56}Fe(\vec{p},\gamma_0)^{57}Co$			
8.0	0.27±0.06	0.03±0.12		0.08±0.05	−0.01±0.04	
9.0	0.07±0.04	−0.04±0.08		−0.05±0.03	−0.06±0.02	−0.03±0.02
10.0	0.08±0.03	0.24±0.06		0.05±0.02	−0.08±0.02	−0.02±0.02
11.5	0.03±0.03	0.20±0.05		−0.08±0.03	−0.09±0.02	
13.0	0.14±0.03	0.15±0.05		0.02±0.02	−0.22±0.02	−0.03±0.02
14.5	0.14±0.04	−0.34±0.08		0.10±0.03	−0.21±0.02	−0.04±0.02
			$^{58}Fe(\vec{p},\gamma_0)^{57}Co$			
7.6	0.19±0.05	0.19±0.09		0.04±0.03	−0.02±0.03	
9.2	0.12±0.04	0.28±0.07		0.01±0.03	−0.11±0.02	
9.6	0.04±0.04	0.26±0.07		0.06±0.02	−0.17±0.02	
10.5	0.12±0.04	0.15±0.06		0.04±0.02	−0.17±0.02	0.04±0.02
11.2	0.16±0.04	0.09±0.06		0.08±0.02	−0.18±0.02	
11.9	0.18±0.05	−0.14±0.09		0.03±0.03	−0.20±0.03	−0.04±0.03
12.7	0.13±0.05	−0.25±0.09		0.07±0.03	−0.23±0.02	
13.5[a]	0.08±0.09	−0.28±0.09	0.00±0.14	0.06±0.03	−0.22±0.02	
14.0[a]	0.14±0.09	−0.47±0.08	0.00±0.13	0.08±0.03	−0.20±0.02	−0.04±0.02
15.0[a]	0.08±0.10	−0.29±0.08	0.00±0.15	0.10±0.03	−0.23±0.02	−0.03±0.02

[a] The criterion of normalized χ^2 did not clearly indicate that a fit which included $P_3(\cos\theta)$ was statistically justified for these energies. The error given for a_1 and a_3 reflects this uncertainty.

REF. I. Fodor, J. Sziklai, B. Kardon, J. Rao, K. Beckert, F. Herrmann and H. Schobbert
J. Phys. G 4, 1117 (1978)

ELEM. SYM.	A	Z
Co	57	27

METHOD

REF. NO. 78 Fo 3 rs

REACTION	RESULT	EXCITATION ENERGY	SOURCE TYPE	SOURCE RANGE	DETECTOR TYPE	DETECTOR RANGE	ANGLE
P,G	LFT	9	D	4	SCD-D		DST

9=9.689,9.696

Abstract. Resonances consistent with fragmented $g_{9/2}$ analogue resonance have been found in ^{57}Co corresponding to the $E_x = 2{\cdot}454$ MeV level in the ^{57}Fe parent nucleus. The resonance was located through the ^{56}Fe(p, γ) ^{57}Co reaction. Total γ-ray spectra were measured with a Ge(Li) detector in 2 keV steps in the expected proton energy range. Excitation functions for the different primary γ transitions were constructed. The $g_{9/2}$ IAR were found in two components at $E_p = 3728$ and 3735 keV. The angular distributions of γ rays were measured at these two bombarding proton energies. The two resonances were suggested to have spin and parity $J^\pi = \frac{9}{2}^+$ based on the γ-ray excitation functions and angular distribution measurements. The γ-ray branchings and absolute transition probabilities were also determined. The M1 γ transitions from the $g_{9/2}$ IAR components going to the possible anti-analogue level at $E_x = 4{\cdot}585$ MeV excitation energy have absolute transition strengths of $1{\cdot}8 \times 10^{-2}$ Wu and $1{\cdot}2 \times 10^{-2}$ Wu.

Table 1. Summary of the Legendre polynomial coefficients and comparison of the mixing ratio δ with the Weisskopf estimate for the transitions studied.

Proton energy (keV)	Excitation energy (MeV)	Transition $E_i \rightarrow E_f$ (MeV)	Legendre polynomial A_2/A_0	Legendre polynomial A_4/A_0	Transition Character $J_i^\pi \rightarrow J_f^\pi$		Weisskopf estimate for $\lvert\delta\rvert$	Mixing ratio experiment	Assigned spin and parity
3728	9·689	9·689 → 0·000	−0·26 ± 0·09	0·002 ± 0·06	$\frac{9}{2}^+ \rightarrow \frac{7}{2}^-$	E1(M2)	0·003	0·04 ± 0·04	$J_R^\pi = \frac{9}{2}^+$
					$\frac{9}{2}^- \rightarrow \frac{7}{2}^-$	M1(E2)	0·22	0·04 ± 0·04	
					$\frac{7}{2}^- \rightarrow \frac{7}{2}^-$	M1(E2)	0·22	0·90 ± 0·08	
3735	9·696	9·696 → 0·000	−0·39 ± 0·04	0·02 ± 0·06	$\frac{9}{2}^+ \rightarrow \frac{7}{2}^-$	E1(M2)	0·003	−0·04 ± 0·04	$J_R^\pi = \frac{9}{2}^+$
					$\frac{9}{2}^- \rightarrow \frac{7}{2}^-$	M1(E2)	0·22	−0·04 ± 0·04	
					$\frac{7}{2}^- \rightarrow \frac{7}{2}^-$	M1(E2)	0·22	−1·27 ± 0·09	
3728	9·689	9·689 → 4·585	0·46 ± 0·08	−0·02 ± 0·05	$\frac{9}{2}^+ \rightarrow \frac{9}{2}^+$	M1(E2)	0·11	−0·04 ± 0·08	$J_i^\pi = \frac{9}{2}^+$
					$\frac{9}{2}^+ \rightarrow \frac{7}{2}^-$	E1(M2)	0·002	0·40 ± 0·08	
3735	9·696	9·696 → 4·585	0·43 ± 0·08	−0·03 ± 0·10	$\frac{9}{2}^+ \rightarrow \frac{9}{2}^+$	M1(E2)	0·11	−0·07 ± 0·08	$J_i^\pi = \frac{9}{2}^+$
					$\frac{9}{2}^+ \rightarrow \frac{7}{2}^-$	E1(M2)	0·002	−0·40 ± 0·09	

Table 2. γ-ray transition strength leading to different excited states measured on top of the resonances at $E_p = 3728$ and 3735 keV (calculated by thick-target estimate The Γ_γ values were deduced supposing $\Gamma_i \simeq \Gamma_p$.

E_x^{final} (MeV)	J^π	$E_p = 3728$ keV $\omega(\Gamma_p\Gamma_\gamma/\Gamma_i)$ (keV)	$E_p = 3728$ keV Γ_γ(eV)	$E_p = 3728$ keV $\Gamma_\gamma/\Gamma_{wu}$	$E_p = 3735$ keV $\omega(\Gamma_p\Gamma_\gamma/\Gamma_i)$ (keV)	$E_p = 3735$ keV Γ_γ(eV)	$E_p = 3735$ keV $\Gamma_\gamma/\Gamma_{wu}$
0·000	$\frac{7}{2}^-$	$12{\cdot}0 \times 10^{-4}$	0·24	$3{\cdot}0 \times 10^{-4}$	$11{\cdot}0 \times 10^{-4}$	0·23	$3{\cdot}0 \times 10^{-4}$
2·611	$\frac{7}{2}^-, \frac{5}{2}^-$	$1{\cdot}0 \times 10^{-4}$	0·02		$0{\cdot}8 \times 10^{-4}$	0·02	
2·723	$\geq\frac{5}{2}^-$	$0{\cdot}7 \times 10^{-4}$	0·01		$0{\cdot}8 \times 10^{-4}$	0·02	
2·743	$\geq\frac{7}{2}^-$	$0{\cdot}7 \times 10^{-4}$	0·01		$0{\cdot}7 \times 10^{-4}$	0·01	
4·585	$\frac{9}{2}^+$	$3{\cdot}0 \times 10^{-4}$	0·05	$1{\cdot}8 \times 10^{-2}$	$2{\cdot}0 \times 10^{-4}$	0·03	$1{\cdot}2 \times 10^{-2}$

REF. H.R. Weller, N.R. Roberson & S.R. Cotanch
Phys. Rev. C18, 65 (1978)

ELEM. SYM.	A	Z
Co	57	27

METHOD

REF. NO. 78 We 4 hmg

REACTION	RESULT	EXCITATION ENERGY	SOURCE TYPE	SOURCE RANGE	DETECTOR TYPE	DETECTOR RANGE	ANGLE
$ P,G	RLX	14-31	D	8-15	UKN-D		DST

Analysis of data in reference 3.

POLARIZED PROTONS

Measurements of cross sections and analyzing powers are examined for polarized proton capture on ^{14}C, ^{30}Si, ^{54}Fe, ^{56}Fe, ^{58}Fe, ^{59}Co, and ^{88}Sr at energies which cover the giant dipole resonance region. These data are used to extract the relative amplitudes and phases of the contributing $E1$ T-matrix elements. A typical result exhibits two solutions. Calculations using the direct (or a direct-semidirect) capture model appear to provide a means for choosing the physical solution.

[NUCLEAR REACTIONS: $^{14}C(\vec{p},\gamma_0)$, $^{30}Si(\vec{p},\gamma_0)$, $^{54}Fe(\vec{p},\gamma_0)$, $^{56}Fe(\vec{p},\gamma_0)$, $^{58}Fe(\vec{p},\gamma_0)$, $^{59}Co(\vec{p},\gamma_0)$, $^{88}Sr(\vec{p},\gamma_0)$; measured $\sigma(\theta)$ and $A(\theta)$ over energy region of the giant dipole resonance. Deduced T-matrix amplitudes and phases. Compare results to direct-semidirect model calculations.]

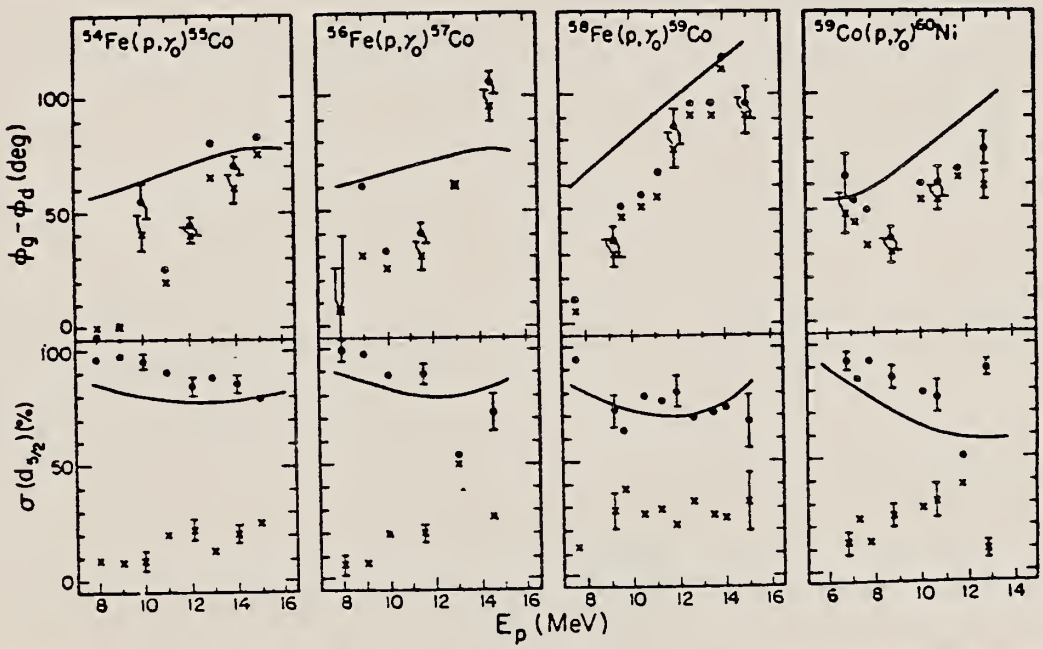

FIG. 2. Same as Fig. 1 for the target nuclei of ^{54}Fe, ^{56}Fe, ^{58}Fe, and ^{59}Co. The remaining cross section is due to the $g_{9/2}$ matrix element.

FIG. 1. The two solutions (dots and x's) resulting from a pure $E1$ analysis of the data are shown along with the results of the calculation for target nuclei of ^{14}C, ^{88}Sr, and ^{30}Si. The remaining cross section in the case of ^{14}C and ^{88}Sr is due to the $s_{1/2}$ matrix element. In the case of ^{30}Si it arises from the $p_{1/2}$ matrix element. The error bars represent typical statistical errors associated with the data points. The amplitudes are presented in terms of the percentage of the total cross section for which they are responsible. The curves represent DSD calculations as described in the text. The dashed curves in the case of ^{88}Sr were obtained using the optical model parameters of Ref. 16 while the solid lines were obtained from the parameters of Ref. 18.

[2]H. R. Weller, R. A. Blue, N. R. Roberson, D. G. Rickel, S. Maripuu, C. P. Cameron, R. D. Ledford, and D. R. Tilley, Phys. Rev. C 13, 922 (1976). (Note: an error exists in the sign of the phase in this paper. The quantity $\phi_s - \phi_d$ should be $\phi_d - \phi_s$ wherever it appears.)
[3]C. P. Cameron, N. R. Roberson, D. G. Rickel, R. D. Ledford, H. R. Weller, R. A. Blue, and D. R. Tilley, Phys. Rev. C 14, 553 (1976).
[4]C. P. Cameron, Ph.D. thesis, Duke University, 1976 (unpublished).
[5]R. D. Ledford, Ph.D. thesis, Duke University, 1976 (unpublished).
[6]J. D. Turner, C. P. Cameron, N. R. Roberson, H. R. Weller, and D. R. Tilley, Phys. Rev. C 17, 1853 (1978).

REF. S. El-Kateb, G.M. Griffiths
Z. Phys. A301, 189 (1981)

ELEM. SYM.	A	Z
Co	57	27

METHOD

REF. NO. 81 El 1 hg

REACTION	RESULT	EXCITATION ENERGY	SOURCE TYPE	SOURCE RANGE	DETECTOR TYPE	DETECTOR RANGE	ANGLE
P,G	LFT	7	D	1	SCD-D		DST
		(7.598)		(1.599)			

The yield curve of the reaction $^{56}Fe(p,\gamma)^{57}Co$ has been measured over the energy range $E_p = 1{,}300$–$1{,}900$ keV and the decay of nine resonances has been investigated. For twelve of the resonances the strengths have been determined. The angular distributions of the gamma rays have been recorded for resonances at $E_p = 1{,}599$, 1,623, 1,643 and 1.649 keV, giving spin-parity assignments $J^\pi = 3/2^-$ for all four resonances. The resonances at $E_p = 1{,}623$, 1,643 and 1.649 keV have been identified as the split analogue resonances of the 367 ($J^\pi = 3/2^-$) states in ^{57}Fe. The $M1$ transition strengths to the corresponding antianalogue states have been measured and compared with theoretical predictions.

LEVEL 7.598, JPI

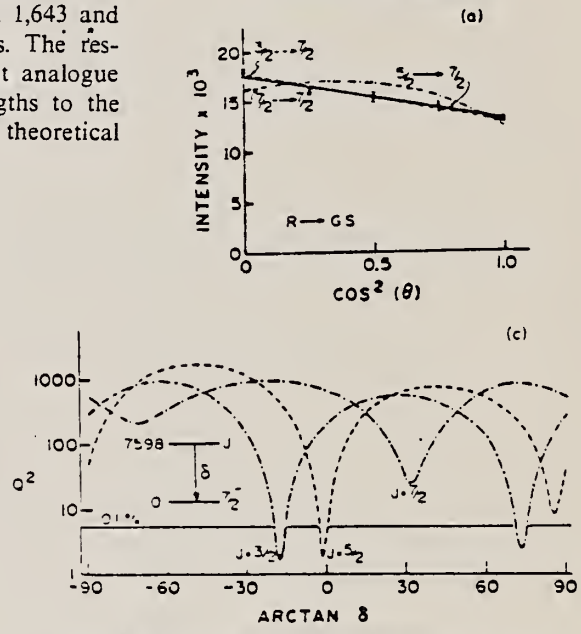

Fig. 3a–d. (a) and (b) Experimental angular distribution data and theoretical fits to transitions from the resonant state to ground state and 1758 respectively. (c) and (d) show Q^2 versus arctan δ from fitting experimental angular distribution to theory for different spin values for γ-rays from the resonant state at 7,598 keV to the ground state and to the 1,758 keV state in ^{57}Co, respectively

Table 3. Resonance strengths for the resonances in the $^{56}Fe(p,\gamma)^{57}Co$

(a) $E_p \pm 2$ (keV)	(a) $\omega\gamma$ ($\pm 35\%$)	(a) J^π	(a) Γ_γ (eV)	(b) E_p (keV)	(b) $\omega\gamma$ ($\pm 30\%$)	(b) J^π	(b) Γ_γ (eV)
1,403	0.30			1.403	0.20	3/2	
1,408	0.42			1,408	0.45	5/2	
1,416	0.39			1,416	0.34	5/2	
1,453	0.43			1,452		(1/2, 3/2)	
1,460	0.38			1,458		(5/2)	
1,466	0.40			1,465		(1/2, 3/2)	
1,525	0.60						
1,557	0.42						
1,599	0.88	$3/2^-$	0.22				
1,623	1.33	$3/2^-$	0.33	1,622.7		3/2, 5/2	
1,643	1.12	$3/2^-$	0.28	1,645.8	0.90	3/2	0.20
1,649	2.30	$3/2^-$	0.58	1,651.9	2.0	3/2	0.50

(a) Present Work (b) Ref. 5, 10

Table 4. Partial radiative widths for transitions in ^{57}Co

Transition resonance to	$E_p = 1.599$ keV Γ_γ' (meV)	$E_p = 1{,}623$ keV Γ_γ' (meV)	$E_p = 1{,}643$ keV Γ_γ' (meV)	$E_p = 1{,}649$ keV Γ_γ' (meV)
G.S.	122			
1,378	9	176	24.4	279
1,505			150	97
1,758	39		8	
1,920		17	57	29
2,133	9			29
2,731	17	27		
2,803		27		
2,879			11	
2,981		31		
3,108			11	40
3,177	22	31	5	
3,268				40
3,357		31	5	17
3,993				40

Table 1. Summary of the Legendre polynomial coefficients for the studied transitions

Proton energy (keV)	Excitation energy (keV)	Transition $E_i \rightarrow E_f$ (keV)	Legendre Polynomial A_2/A_0	A_4/A_0
1.599	7,598	7,598 → g.s.	−0.197 ± 0.015	0.026 ± 0.018
		7,598 → 1,758	−0.223 ± 0.012	−0.017 ± 0.014
1.623	7.622	7.622 → 1.378	0.337 ± 0.022	−0.041 ± 0.025
1.643	7.641	7.641 → 1.378	0.042 ± 0.019	−0.006 ± 0.02
		7.641 → 1.505	−0.201 ± 0.016	−0.004 ± 0.02
		7.641 → 1.920	−0.227 ± 0.015	0.002 ± 0.02
1.649	7.647	7.647 → 1.378	0.285 ± 0.019	−0.039 ± 0.02
		7.647 → 1.505	−0.299 ± 0.054	−0.057 ± 0.064

(over)

Table 2. Experimental mixing ratios δ compared with Weisskopf values for states of ^{57}Co studied here

Resonance $E_p \pm ?$ (keV)	Transition $E_i \rightarrow E_f$ (keV)	Transition $J_i^\pi \rightarrow J_f^\pi$	Character	Weisskopf estimate for $\lvert\delta\rvert$	Experimental mixing ratio δ	Assigned J_i^π
1,599	7,598→0	$3/2^+ \rightarrow 7/2^-$	$M2(E3)$	0.04	-0.325 ± 0.018	$3/2^-$
		$3/2^- \rightarrow 7/2^-$	$E2(M3)$	0.003		
		$5/2^+ \rightarrow 7/2^-$	$E1(M2)$	0.004	-0.035 ± 0.018	
		$5/2^- \rightarrow 7/2^-$	$M1(E2)$	0.249		
	7,598→0	$3/2^- \rightarrow 3/2^-$	$M1(E2)$	0.20	0.445 ± 0.014	
		$3/2^+ \rightarrow 3/2^-$	$E1(M2)$	0.003		
		$5/2^+ \rightarrow 3/2^-$	$E1(M2)$	0.002	-0.07 ± 0.011	
		$5/2^- \rightarrow 3/2^-$	$M1(E2)$	0.20		
1,623	7,622→1,378	$3/2^- \rightarrow 3/2^-$	$M1(E2)$	0.20	0.07 ± 0.018	$3/2^-$
		$3/2^+ \rightarrow 3/2^-$	$E1(M2)$	0.003		
1,643	7,641→1,505	$3/2^- \rightarrow 1/2^-$	$M1(E2)$	0.20	-0.176 ± 0.018	$3/2^-$
		$3/2^+ \rightarrow 1/2^-$	$E1(M2)$	0.003		
	7,641→1,920	$3/2^- \rightarrow 5/2^-$	$M1(E2)$	0.20	-0.105 ± 0.018	
		$3/2^+ \rightarrow 5/2^-$	$E1(M2)$	0.003		
1,649	7,647→1,378	$3/2^- \rightarrow 3/2^-$	$M1(E2)$	0.20	0.07 ± 0.018	$3/2^-$
		$3/2^+ \rightarrow 3/2^-$	$E1(M2)$	0.003		
	7,647→1,505	$3/2^- \rightarrow 1/2^-$	$M1(E2)$	0.20	-0.105 ± 0.012	
		$3/2^+ \rightarrow 1/2^-$	$E1(M2)$	0.003		

Co
A=58

Co
A=58

Co
A=53

REF. B. Erlandsson and A. Marcinkowski
Nucl. Phys. A146, 43 (1970)

ELEM. SYM.	A	Z
Co	58	27

METHOD

REF. NO.	
70 Er 1	egf

REACTION	RESULT	EXCITATION ENERGY	SOURCE		DETECTOR		ANGLE
			TYPE	RANGE	TYPE	RANGE	
P,G	SPC	8-9	D	1-2	SCD-D	1-9	45

DETAILS 4 LEVELS

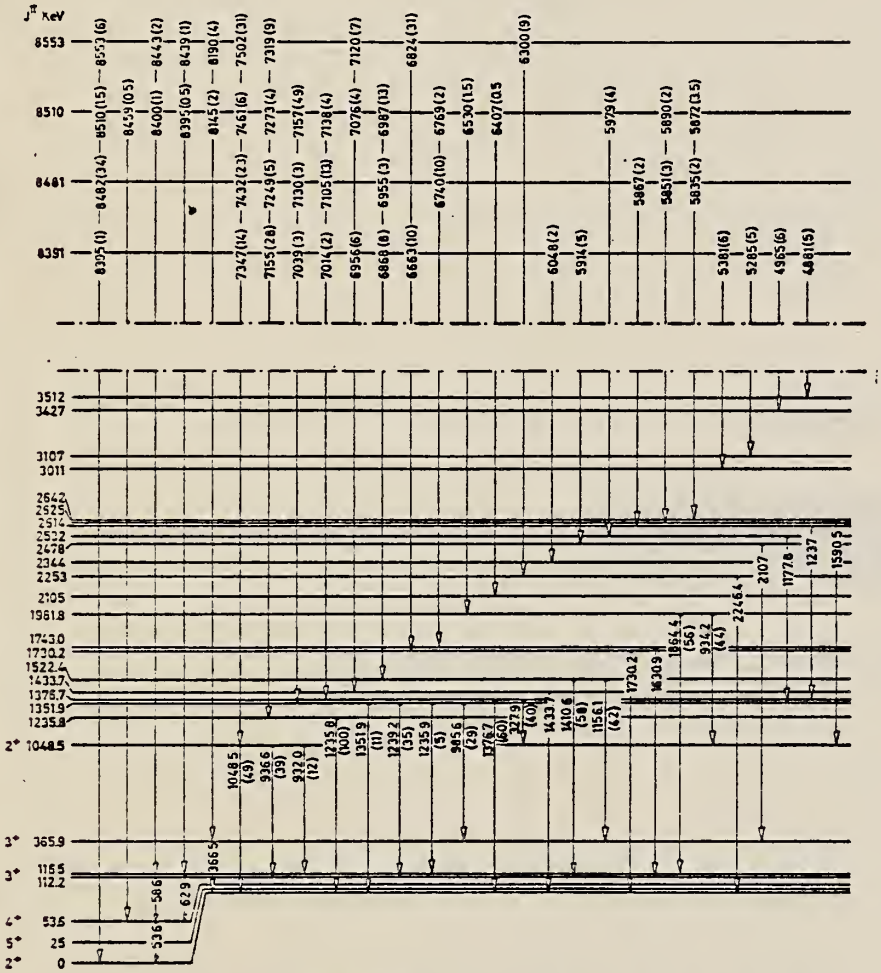

Fig. 5. The proposed decay scheme. Spin and parity values are taken from Trier *et al.* [8]).

[8] A. Trier, J. Rapaport, T. A. Belote and W. E. Dorenbusch, Nucl. Phys. A134 (1969) 396.

[over]

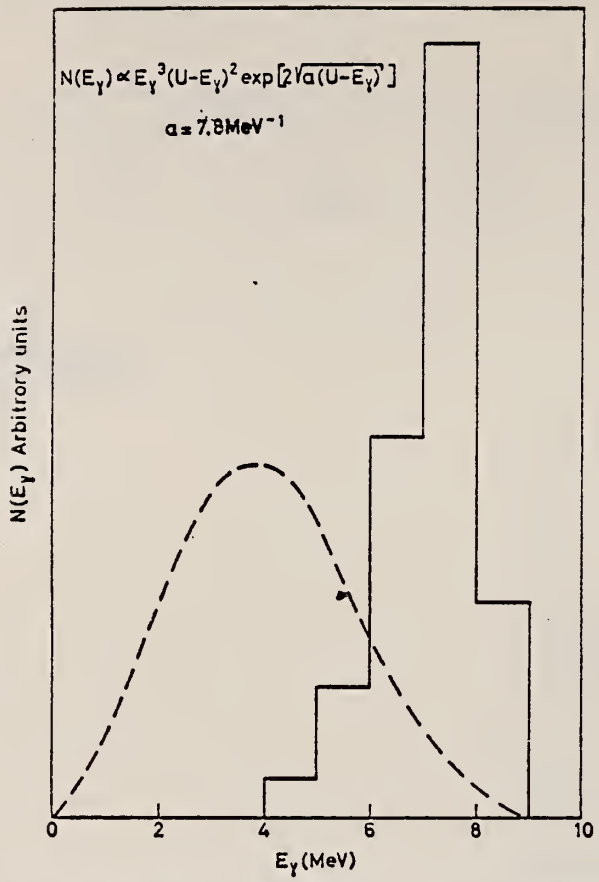

Fig. 7. Integrated spectrum of the primary γ-rays from the proton capture states at the four resonances investigated. The dashed line shows the spectrum according to the formula given in the figure. The constant a is taken from Glower and Purser [28]). The area under the theoretical curve is normalized to the numbers of γ-rays in the experimental curve.

[28] U. Fanger, W. Michaelis, H. Schmidt and H. Ottmar, Nucl. Phys. A128 (1969) 641.

Co
A=59

Co
A=59

REF.

B. Forkman
Arkiv Fysik 11, 265-75 (1956)

ELEM. SYM.	A	Z
Co	59	27

METHOD

Synchrotron; ion chamber

REF. NO.	
56 Fo 1	NVB

	REACTION	RESULT	EXCITATION ENERGY	SOURCE		DETECTOR		ANGLE
				TYPE	RANGE	TYPE	RANGE	
1)	G,D	RLY	15-30	C	30	EMU-D		90
2)	G,P	RLY	7-30	C	30	EMU-D		90

$$\frac{Y(\gamma,d)}{Y(\gamma,p)} = 0.22$$

1) YLD REL TØ G,P

2) YLD REL TØ G,D

Ref. W.H. Hartley, W.E. Stephens, E.J. Winhold
Phys. Rev. 104, 178 (1956)

Elem. Sym.	A	Z
Co	59	27

Method: Li(p,γ) source; 480 keV protons; BF_3 counter

Ref. No.: 56 Ha 1 EGF

Reaction	E or ΔE	E_o	Γ	$\int \sigma dE$	Jπ	Notes
$Co^{59}(\gamma,xn)$						Average Li cross section is 49 mb; cross section with detector response weighted for low energy neutrons, 49 mb. Assumed ratio 17.6/14.8 = 1.7. Calculated cross section at 14.8 and 17.6 MeV assuming cross section curves measured at Pennsylvania and Saskatchewan (refer Table I).

TABLE I. Cross sections for photoneutron emission induced by the lithium gamma rays. The results are compared with previous data.

Element	Present cross-section data: Counter Group A	Present cross-section data: Counter Group B	Data of McDaniel et al.[a]	Betatron data: Pennsylvania $\sigma_{14.8}$[b]	Pennsylvania $\sigma_{14.8}/\sigma_{17.6}$	Saskatchewan $\sigma_{14.8}$[b]	Saskatchewan $\sigma_{14.8}/\sigma_{17.6}$	$\sigma_{14.8}$[b]	$\sigma_{17.6}$[b]
$_{26}$Fe	38 mb	33 mb	37 mb			60[f] mb	0.5	23 mb	47 mb
$_{27}$Co	49	49	47	60[e] mb	0.5	95[f]	0.5	30	60
$_{28}$Ni	28	25	23			40[e]	0.7	22	32
$_{29}$Cu	64	61	55±12			95[f]	0.6	45	75
$_{30}$Zn	48	45	48			90[f]	0.7	38	54
$_{47}$Ag	175	170	135			240[f]	1.0	175	175
$_{50}$Sn	200	190	180						
$_{73}$Ta	355	360	260	350[d]	1.3	420[e]	2.3	420[i] 550[i]	320[i] 240[i]
$_{74}$W	365	355	325						
$_{79}$Au	330	295		315[e]	1.7	480[f]	1.9	460	255
$_{80}$Hg	365	340	290						
$_{82}$Pb	310	295	250	320[e]	1.6	440[f]	2.5	400[i] 500[i]	250[i] 200[i]
$_{83}$Bi	305	280	250	270[d]	2.6	550[f]	2.4	490	195

[a] McDaniel, Walker, and Stearns, Phys. Rev. 80, 807 (1950).
[22] Montalbetti, Katz, and Goldemberg, Phys. Rev. 91, 659 (1953).
[24] R. Nathans and J. Halpern, Phys. Rev. 93, 437 (1954).
[23] J. Goldemberg and L. Katz, Can. J. Phys. 32, 49 (1954).
[25] Burkhardt, Winhold, and Dupree, Phys. Rev. 100, 199 (1955), and references therein.

REF.

F. Heinrich and H. Waffler
Helv. Phys. Acta 29, 232 (1956)

ELEM. SYM.	A	Z
Co	59	27

METHOD

REF. NO.: 56 He 1 | EGF

REACTION	RESULT	EXCITATION ENERGY	SOURCE		DETECTOR		ANGLE
			TYPE	RANGE	TYPE	RANGE	
G,T	RLY	THR-31	C	31	ACT-I		4PI

Yields relative to (G,N) yields.

Tabelle 1.
Experimentelle und theoretische nukleare Ausbeute der (γ, T)-Prozesse.

Element	$\eta_{exp} \times 10^5$	$\eta_{theor} \times 10^5$
Al	240 ± 14	200
Co	$6 \pm 1{,}7$	4
Cu	$4{,}5 \pm 1{,}5$	3

H. Waffler and F. Heinrich
Physica 22, 1146 (1956)

Co	59	27

METHOD

REF. NO. 56 Wa 1 | EGF

REACTION	RESULT	EXCITATION ENERGY	SOURCE		DETECTOR		ANGLE
			TYPE	RANGE	TYPE	RANGE	
G,T	RLY	THR - 31	C	31	ACT-I		4PI

Detected activity of tritium. Yields are relative to $^{63}Cu(\gamma,n)$.

Reaction	Threshold energy MeV	$\eta_{exp} \times 10^5$	$\eta_{theor} \times 10^5$
Al	18.2 ± 0.2	34 ± 2	31
Co	16.5 ± 0.3	7 ± 2	5
^{63}Cu	16.2 ± 0.3	6 ± 2	4
^{65}Cu	15.1 ± 0.3		
^{107}Ag	13.9 ± 0.6	6.5 ± 1	0.4
^{109}Ag	13.1 ± 0.6		

The table shows the calculated yield ratios (according to statistical theory) as well as the measured relative yield

$$\eta = \int_0^{31\ \mathrm{MeV}} N(E_\gamma)\, \sigma^{(x)}(\gamma,t) E_\gamma\, dE_\gamma / \int_0^{31\ \mathrm{MeV}} N(E_\gamma)\, \sigma^{(^{63}Cu)}(\gamma,t)\, E_\gamma\, dE_\gamma$$

taking the (γ, n) yield on ^{63}Cu as unity. The good agreement between the experimental

REF.

Miroslav Rozkoš
Czech. J. Phys. 7, 592 (1957)

ELEM. SYM.	A	Z
Co	59	27

METHOD

[Page 1 of 2]

REF. NO.	
57 Ro 1	EGF

REACTION	RESULT	EXCITATION ENERGY	SOURCE		DETECTOR		ANGLE
			TYPE	RANGE	TYPE	RANGE	
G,P	SPC	15,18	D	15,18	EMU-D	3-7	DST

14.8 and 17.6 MeV photons.

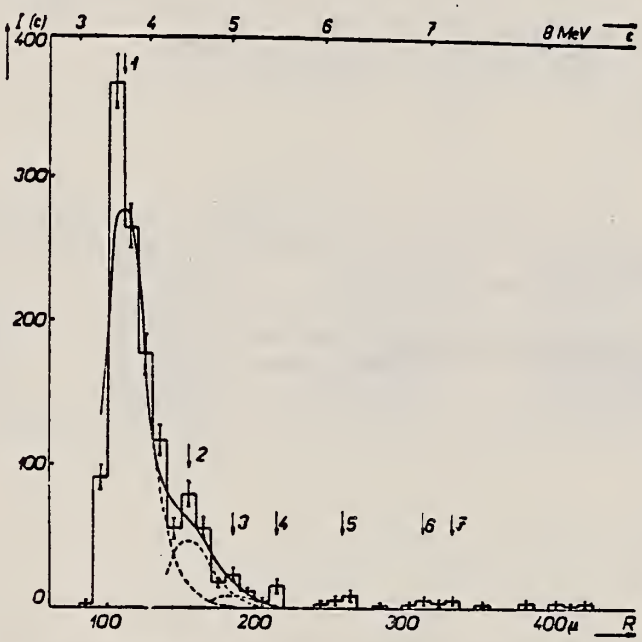

Рис. 1. Энергетическое распределение фотопротонов в интервале $\vartheta \sim 30° - 70°$ (пластинка III). Ось абсцисс нижняя: пролет R протонов в микронах, верхняя: соответствующая энергия ϵ протонов в MeV. Ось ординат: число протонов $I(\epsilon)$. Ломаная линия означает измеренные значения, вертикальные отрезки — экспериментальные ошибки; прерывистая линия удовлетворяет распределению Пуассона, сплошная кривая — сумма отдельных распределений. В целом использовано 1323 следа.

REACTION	RESULT	EXCITATION ENERGY	SOURCE TYPE	SOURCE RANGE	DETECTOR TYPE	DETECTOR RANGE	ANGLE

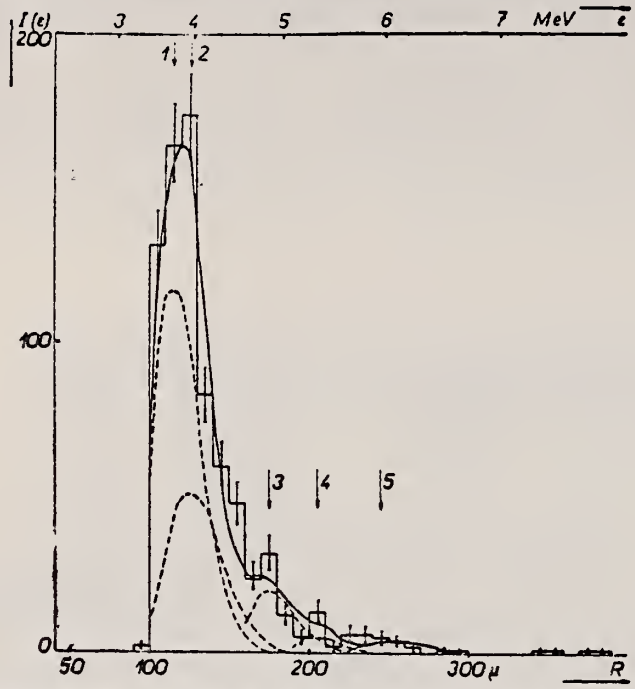

Рис. 2. Энергетическое распределение фотопротонов в интервале углов $\vartheta \sim 60° - 90°$ (пластинки II). На оси вынесены те же величины, что и на рис. 1. В целом использовано 779 следов.

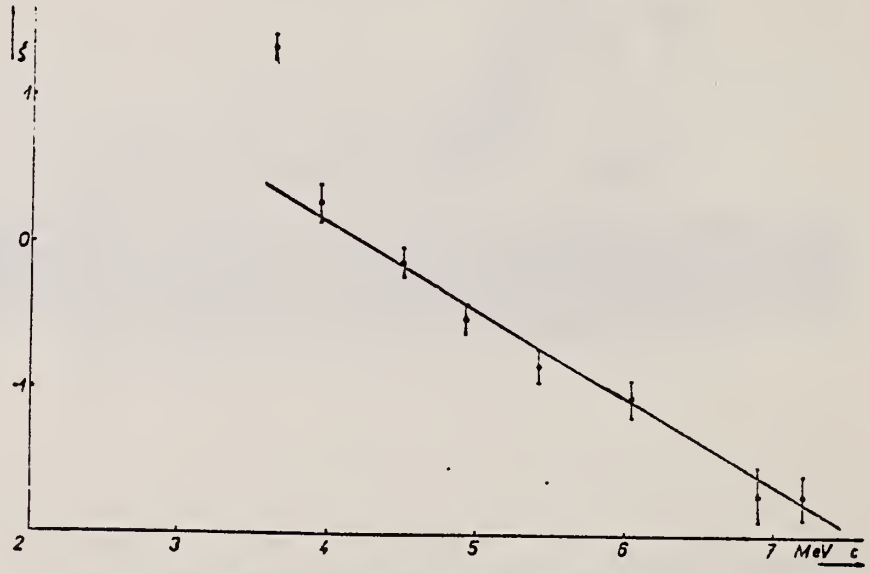

Рис. 3. Энергетическое распределение фотопротонов, обработанное по уравнению (1). Ось абсцисс: ε — энергия протонов в MeV. Ось ординат: $\zeta = \log \frac{I(\varepsilon)}{\varepsilon \cdot \sigma(\varepsilon)}$. Из направляющей прямой определена температура $\Theta = 0{,}74 \pm 0{,}16$ MeV. В целом использовано 2102 следа.

B.G. Chidley, L. Katz, S. Kowalski
Can. J. Phys. 36, 407 (1958)

ELEM. SYM.	A	Z
Co	59	27

Betatron

REF. NO.	
58 Ch 2	NVB

REACTION	RESULT	EXCITATION ENERGY	SOURCE		DETECTOR		ANGLE
			TYPE	RANGE	TYPE	RANGE	
G,N	RLY	THR	C	THR	BF3-I		4PI

See 58 Ka 1 for cross sections

THRESHOLD

TABLE I

MEASURED PHOTONEUTRON THRESHOLDS

Reaction	Measured Q value, Mev.	Other Q values, Mev.	Method	Reference
$Co^{59}(\gamma, n)Co^{58}$	10.44±0.05			
		10.25 ±0.20	Threshold	Sher *et al.* (1951)
		10.491±0.012	Mass data	Duckworth (unpublished)
			Q^+ value	Way *et al.* (1955)
		10.490±0.012	Mass data	Quisenberry *et al.* (1956)

TABLE II

COMPARISON OF THRESHOLDS FROM MASS DATA AND FROM PHOTONEUTRON REACTIONS

Reaction	Photoneutron threshold, Mev.	Mass data threshold, Mev.	Difference, Mev.
$Na^{23}(\gamma, n)Na^{22}$	12.47±0.05	12.417±0.014	−0.05±0.05
$Al^{27}(\gamma, n)Al^{26}$	12.96±0.06	13.03 ±0.06	+0.07±0.08
$P^{31}(\gamma, n)P^{30}$	12.48±0.05	12.39 ±0.03	−0.09±0.06
$Co^{59}(\gamma, n)Co^{58}$	10.44±0.05	10.49 ±0.01	+0.05±0.05
$Pr^{141}(\gamma, n)Pr^{140}$	9.46±0.05	9.30 ±0.06	−0.16±0.08

REACTION	RESULT	EXCITATION ENERGY	SOURCE TYPE	SOURCE RANGE	DETECTOR TYPE	DETECTOR RANGE	ANGLE
G,XN	ABX	10-22	C	10-22	BF3-I		4PI

Таблица 2

Пороги испускания фотонейтронов

Изотоп	B_n, *Мэв*	B_{2n}, *Мэв*	Изотоп	B_n, *Мэв*	B_{2n}, *Мэв*
V^{51}	11,16	20,5	L^{139}	8,81	16,1
Mn^{55}	10,14	19,2	Pr^{141}	9,46	17,6
Co^{59}	10,44	18,6	Tb^{159}	8,16	14,8
As^{75}	10,24	18,1	Ho^{165}	8,10	14,6
Y^{89}	11,82	20,7	Tm^{169}	8,00	14,7
Nb^{93}	8,86	17,1	Lu^{175}	7,77	14,2
Rh^{103}	9,46	16,8	Ta^{181}	7,66	13,8
J^{127}	9,14	16,2	Au^{197}	7,96	13,3
Cs^{133}	9,11	16,5	Bi^{209}	7,43	14,5

THRESHOLDS

не приведены, поскольку они превышают 22 *Мэв* во всех случаях, кроме золота, для которого B_{2n}=21 *Мэв*. Свойства сечений $\sigma_C(\gamma)$ сведены в табл. 3.

Таблица 1

Изотоп	$E_{макс}$, *Мэв*	$\sigma_n(E_\gamma)$, барн	Γ, *Мэв*	Γ^{int}, *Мэв·барн*	Y(22), 10^8 нейтрон/100 р·моль
V^{51}	18,4	0,062	5,2	0,33	1,62
Mn^{55}	20,2	0,060	7,0	0,39	2,01
Co^{59}	18,3	0,068	6,3	0,44	2,30
As^{75}	16,4	0,090	9,5	0,74	4,25
Y^{89}	17,1	0,172	5,2	0,93	5,33
Nb^{93}	18,0	0,156	7,5	1,17	6,80
Rh^{103}	17,5	0,160	9,4	1,40	8,28
J^{127}	15,2	0,273	6,8	1,76	11,9
Cs^{133}	16,5	0,238	7,7	1,59	10,7
La^{139}	15,5	0,325	3,8	1,55	11,2
Pr^{141}	15,0	0,320	4,9	1,93	13,1
Tb^{159}	15,6	0,274	9,8	2,49	18,1
Ho^{165}	13,5	0,305	8,9	2,52	18,7
Tm^{169}	16,4	0,250	8,4	1,91	14,9
Lu^{175}	16,0	0,225	8,4	1,90	23,0
Ta^{181}	14,5	0,380	8,5	3,15	22,0
Au^{197}	13,8	0,475	4,7	3,04	22,6
Bi^{209}	13,2	0,455	5,9	2,89	23,2

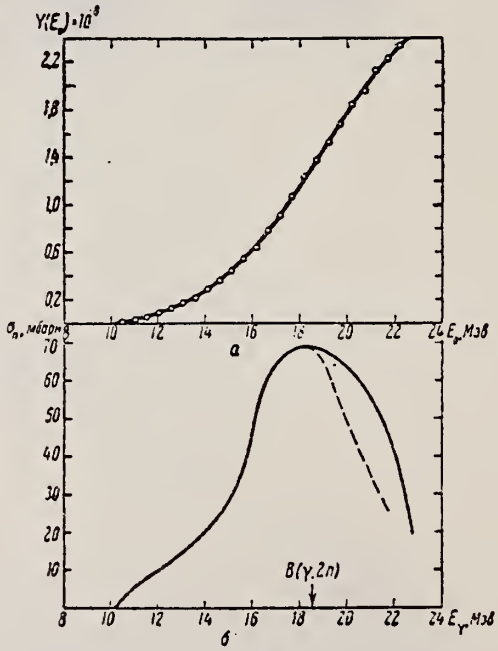

Рис. 3.
а — Выход фотонейтронов для Co; б — $\sigma_n(E_\gamma)$ и $\sigma_C(\gamma)$ для Co

Ref. M.E. Toms, J. McElhinney
Phys. Rev. 111, 561 (1958)

Elem. Sym.	A	Z
Co	59	27

Method: Betatron; alpha yield; nuclear emulsion

Ref. No.: 58 To 2 | NVB

Reaction	E or ΔE	E_o	Γ	$\int \sigma dE$	Jπ	Notes
$Co^{59}(\gamma,\alpha)$	Bremss. 22					Yield = 2.3×10^{4} alpha/mole/roentgen

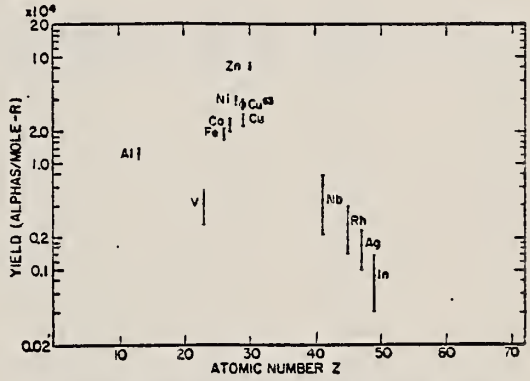

FIG. 8. Photo-alpha yields plotted against atomic numbers for the exposures of the survey.

Ref. V.P. Chizhov
Zhur. Eksp. i Teoret. Fiz. 38, 809 (1960)
Soviet Phys. JETP 11, 587 (1960)

Elem. Sym.	A	Z
Co	59	27

Method: 90 MeV Bremsstrahlung; scintillator counter telescope

Ref. No.: 60 Ch 1 JHH

Reaction	E or ΔE	E_o	Γ	$\int \sigma dE$	Jπ	Notes
$Co^{59}(\gamma,p)$ $Co^{59}(\gamma,d)$ $Co^{59}(\gamma,t)$						Energy Range of particles detected: E_d - 15.5-30 MeV E_p - 15.5-30 MeV E_t - 17-30 MeV Ratios: $\sigma(\gamma,d)/\sigma(\gamma,p)$ } at $\theta = 90^\circ$ $\sigma(\gamma,t)/\sigma(\gamma,d)$

TABLE I

Element	$100N_t/N_d$	Element	$100N_t/N_d$	Element	$100N_t/N_d$	Element	$100N_t/N_d$
Li^6	30±3	B	39±8	Ni	10±4	In	5±2.5
Li^7	22.5±2.5	Si	10±4	Co	2.5±2	Ta	10±4
Be	13±2.6	S	N 4	Cu	2.2±2	Au	3±3

(over)

METHOD

REF. NO.

REACTION	RESULT	EXCITATION ENERGY	SOURCE		DETECTOR		ANGLE
			TYPE	RANGE	TYPE	RANGE	

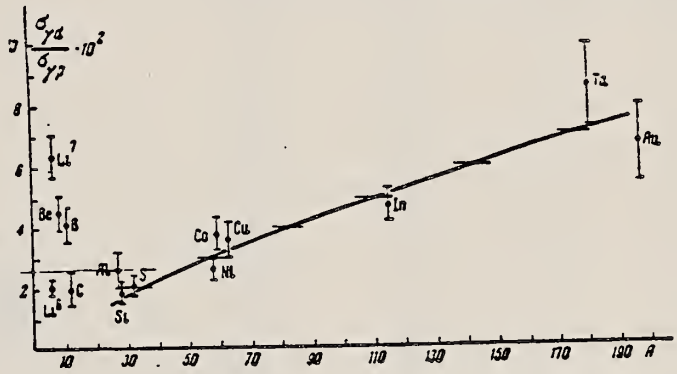

FIG. 3. Ratio of (γ, d) to (γ, p) cross sections for protons and deuterons of energies 15.5–30 Mev as function of atomic weight A. The solid curve shows the dependence given by Eq. (2), arbitrarily normalized.

Ref. P.A. Flournoy, R.S. Tickle, W.D. Whitehead
Phys. Rev. 120, 1424 (1960)

Elem. Sym.	A	Z
Co	59	27

Method: Synchrotron; BF_3 counters in 4π geom.

Ref. No.: 60 F1 1 JHH

Reaction	E or ΔE	E_o	Γ	$\int \sigma dE$	Jπ	Notes
(γ,xn)	12-30	16.75±.25	2.0	25 MeV 709 MeV-mb 12		σ_{max}(16.75 MeV) = 109 mb
		18.75±.25	4.0			σ_{max}(18.75 MeV) = 92 mb
			(From Brent-Wigner Fit; see Table I)			Intrinsic quadrupole moment Q_o = +0.76±0.11 barn if $\sigma_{total} \cong \sigma(\gamma,n) + \sigma(\gamma,2n)$ in this region, using $R_o = 1.2 \times 10^{-13}$ cm.
						In Figure 5, open circles are uncorrected data; closed circles are corrected for neutron multiplicity.
						Integrated cross section is $\sigma(\gamma,n) + \sigma(\gamma,pn) + \sigma(\gamma,2n) + \ldots$

TABLE I. Parameters of Breit-Wigner fit to data.

Element	E_o (Mev)	Γ_o (Mev)	σ_o (mb)	E_1 (Mev)	Γ_1 (Mev)	σ_1 (mb)	$\Gamma_{n\sigma}/\Gamma_{\sigma\sigma}$
Manganese	16.8	2.7	70	19.75	4.0	64	1.35
Cobalt	16.5	2.0	78	19.0	4.0	78	2.00

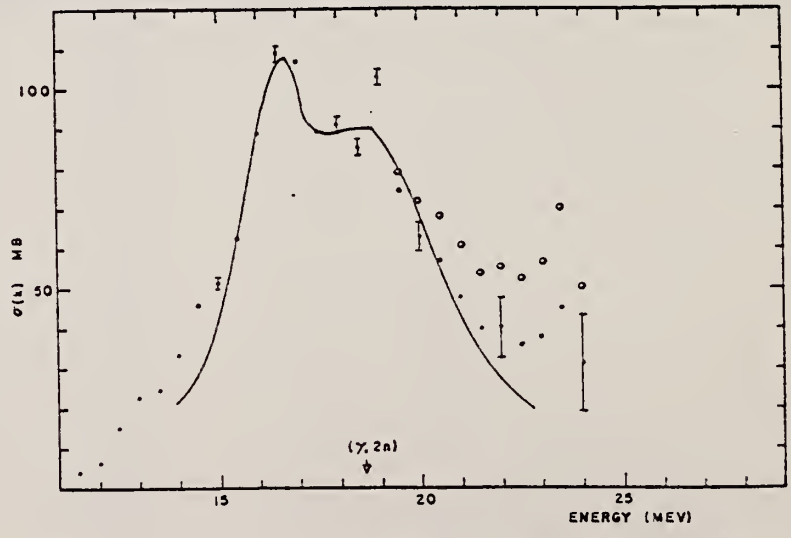

Figure 5: Neutron cross section of colbalt.

REF.

K. N. Geller, J. Halpern, and E. G. Muirhead
Phys. Rev. 118, 1302-12 (1960)

ELEM. SYM.		
Co	59	27

METHOD

Betatron; neutron threshold; ion chamber

REF. NO.	
60 Ge 3	NVB

REACTION	RESULT	EXCITATION ENERGY	SOURCE		DETECTOR		ANGLE
			TYPE	RANGE	TYPE	RANGE	
G,N	NØX	THR	C THR		BF3-I		4 PI

: THRESHØLD

TABLE I. Summary and comparison of neutron separation energies inferred from present threshold measurements with values predicted from mass data and reaction energies. All energies are expressed in the center-of-mass system in Mev.

Reaction	No. runs	Present results	Other results	Method	Reference
$Co^{59}(\gamma,n)Co^{58}$	4	10.441±0.026	10.490±0.010	mass data	j
			10.44 ±0.05	threshold	f

[f] See reference 4.
[g] C. F. Giese and J. L. Benson, Phys. Rev. 110, 712 (1958).
[h] P. M. Endt et al., Phys. Rev. 105, 1002 (1957).
[i] M. Mazari, W. W. Buechner, and A. Sperduto, Phys. Rev. 112, 1691 (1958).
[j] K. S. Quisenberry, T. T. Scolman, and A. O. Nier, Phys. Rev. 104, 461 (1956).

Ref.		Elem. Sym.	A	Z
	A.N. Gorbunov, F.P. Denisov, V.A. Kolutkhin Zhur. Eksp. i Teoret. Fiz. 38, 1084 (1960) Soviet Phys. JETP 11, 783 (1960)	Co	59	27

Method	Ref. No.	
260 MeV Synchrotron; activation; B ctrs. "photon difference"	60 Go 2	JHH

Reaction	E or ΔE	E_o	Γ	$\int \sigma dE$	Jπ	Notes
$Co^{59}(\gamma,?)Mn^{56}$	30-260			~6 MeV-mb (frm graph: E.H.) [150]		Activation probably mostly due to (γ,dp), $(\gamma,2pn)$. (γ,He^3) also possible. Refers to "quasi-neutron mechanism."

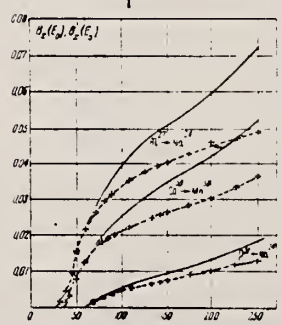

FIG. 1. Active yields of the $Al^{27} \rightarrow Na^{24}$, $Co^{59} \rightarrow Mn^{56}$, and $P^{31} \rightarrow Na^{24}$ reactions as a function of the peak bremsstrahlung energy. The values of $B_\gamma'(E_0)$ are given by the continuous curves, of $B_\gamma(E_0)$ – by the dashed curves (the values of $B_\gamma(E_0)$ are given in arbitrary units).

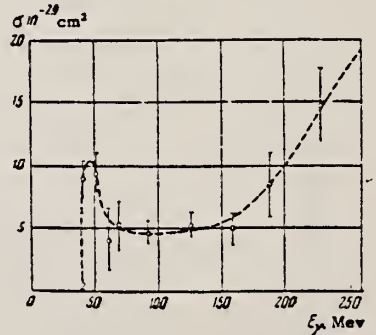

FIG. 3. Effective cross section for the $Co^{59} \rightarrow Na^{24}$ reaction.

K. Reibel, A.K. Mann
Phys. Rev. 118, 701 (1960)

Elem. Sym.	A	Z
Co	59	27

Method: γ's from $F^{19}(\gamma,\alpha\gamma)$ reaction; protons from Van de Graaff; ~~NaI~~

Ref. No. 60 Re 1 JHH

Reaction	E or ΔE	E_o	Γ	$\int \sigma dE$	Jπ	Notes
$Co^{59}(\gamma,\gamma)$	~ 7					$\langle \bar{\sigma} \rangle$ (E_p = 2.05 MeV) = 0.29±0.04 mb Detector at 90°.

REF. R. G. Baker, K. G. McNeill
Can. J. Phys. 39, 1158 (1961)

ELEM. SYM.	A	Z
Co	59	27

METHOD
Betatron; fast neutron yield, angular distribution; Si threshold detector; ion chamber

REF. NO. 61 Ba 2 NVB

REACTION	RESULT	EXCITATION ENERGY	SOURCE		DETECTOR		ANGLE
			TYPE	RANGE	TYPE	RANGE	
G,XN	ABY	THR-22	C	22	THR-I	5-+	DST

In Table 4:

$\bar{\sigma}$ = average cross section of detector weighted with neutron spectrum

Φ = neutrons/100 roentgen/mole

$$W(\theta) = a_0 \left[1 + \sum_{n=1}^{\infty} A_n P_n (\cos\theta)\right]$$

TABLE IV

I Element	II a_0	III a_1	IV a_2	V $(\bar{\sigma}\Phi)\times 10^{28}$	VI Φ_{total} (22 Mev) $\times 10^{9}$	VII Φ_{fast}/Φ_{total}
Vanadium	245 (1±0.06)	0.01±0.08	−0.00±0.10	6.05	0.21	0.12
Chromium	164 (1±0.03)	0.04±0.04	−0.05±0.05	4.05	0.17	0.10
Manganese	308 (1±0.02)	0.07±0.03	−0.09±0.04	7.61	0.25	0.12
Iron	200 (1±0.03)	0.05±0.04	−0.17±0.05	4.94	0.18	0.11
Cobalt	390 (1±0.02)	0.08±0.03	−0.22±0.04	9.63	0.26	0.15
Nickel	145 (1±0.05)	0.07±0.07	−0.23±0.09	3.58	0.12	0.12
Copper	347 (1±0.02)	0.05±0.03	−0.29±0.04	8.57	0.30	0.12
Arsenic	482 (1±0.03)	0.11±0.04	−0.24±0.05	11.91	0.33	0.15
Rubidium	638 (1±0.05)	0.13±0.06	−0.14±0.08	15.76		
Strontium	409 (1±0.05)	0.10±0.06	−0.17±0.08	10.10		
Yttrium	290 (1±0.10)	0.08±0.12	−0.12±0.15	7.16		
Silver	590 (1±0.04)	0.10±0.06	−0.22±0.08	14.57	0.87	0.07
Cadmium	905 (1±0.02)	0.02±0.02	−0.26±0.03	22.35		
Iodine	1133 (1±0.03)	0.04±0.04	−0.29±0.05	27.99	1.42	0.08
Barium	1048 (1±0.04)	0.10±0.06	−0.38±0.08	25.80		
Lanthanum	1595 (1±0.02)	0.02±0.03	−0.42±0.04	39.40	1.04	0 15
Cerium	1316 (1±0.05)	0.05±0.06	−0.39±0.08	32.50		
Dysprosium	1652 (1±0.08)	0.04±0.10	−0.34±0.13	40.80		
Tantalum	1558 (1±0.02)	0.04±0.03	−0.22±0.04	38.48	2.50	0.06
Tungsten	1365 (1±0.02)	−0.07±0.03	−0.24±0.04	33.71		
Mercury	1345 (1±0.02)	0.04±0.03	−0.31±0.04	33.22		
Lead	2274 (1±0.01)	0.02±0.02	−0.42±0.03	56.17	2.72	0.08
Bismuth	2162 (1±0.02)	0.05±0.03	−0.45±0.04	53.40	3.36	0.06
Thorium	3031 (1±0.04)	0.06±0.05	−0.32±0.07	74.87		
Uranium	4630 (1±0.02)	0.05±0.03	−0.17±0.04	114.36		

*$(\bar{\sigma}\Phi) = 2.47\times 10^{7}\, a_0$ millibarn-neutron. Errors are standard errors due to counting statistics only.

Ref. H. Crannell, R. Helm, H. Kendall, J. Oeser, M. Yearian
Phys. Rev. 123, 923 (1961)

Elem. Sym.	A	Z
Co	59	27

Method
Linac; Cerenkov counter telescope; inelastic electron scattering 40°-90° in lab.

Ref. No. 61 Cr 1 JHH

Reaction	E or ΔE	E_o	Γ	$\int \sigma dE$	Jπ	Notes
$(e^-,e^{-\prime})$	183	1.30				Measured γ transition rate, Γ_m: $\Gamma_m = (7.4\pm0.95)10^{12}$ sec^{-1}; (E2); $G = \Gamma_m/\Gamma_{sp} = 44\pm5.7$
		2.70				$\Gamma_m = (1.1\pm0.46)10^{5}$ sec^{-1}; (E4); $G = \Gamma_m/\Gamma_{sp} = 14.0\pm5.9$
		3.95				$\Gamma_m = (5.0\pm0.96)10^{10}$ sec^{-1}; (E3); $G = \Gamma_m/\Gamma_{sp} = 16.5\pm3.1$
						[Γ_{sp} = single-particle estimate of the γ transition rate.]
						Fits R_o = 1.20 fermi

FIG. 13. In this and the following four figures are shown portions of the energy-level structures of the nuclei investigated in the present experiment. The information is, for the most part, taken from reference 15. The γ-ray transitions shown are those whose decay rates were determined directly in the present experiment or inferred from a knowledge of the γ-ray branching ratios in de-excitation of the nucleus. The spin and parity of each level are shown at the left, where known, and the energy of the excited states in Mev on the right. The best assignments of the transition multipolarities are indicated. This figure shows the energy-level structure of Ni^{58}.

Ref 15: Data on the decay schemes are taken principally from Nuclear Data Sheets, National Academy of Sciences - National Research Council (U.S. Government Printing Office, Washington, D.C., 1959)

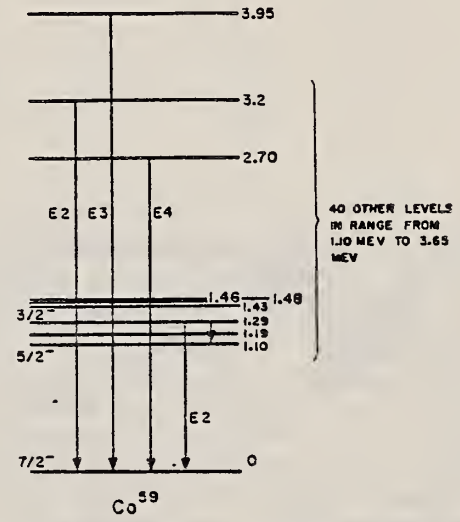

FIG. 14. Energy-level diagram for Co^{59}. A large number of the energy levels are omitted (see reference 16). We have identified the 1.30-Mev transition induced by inelastic electron scattering with the 1.29-Mev transition known from other studies (see references 15 and 16). It is expected, from other considerations discussed in the text, that each observed electron-induced transition may excite a number of levels spaced less than about 200 kev apart. This possibility adds some uncertainty to the level scheme and to the measurements of the gamma transition rate for the 0.19-Mev ray from the 1.29-Mev level. See caption for Fig. 13.

Ref 16: Mazari et al - Phys. Rev. 107 365 (1957).

Ref. V. Emma, C. Milone, A. Rubbino, S. Janelli, F. Mezzanores
Nuovo Cimento 22, 135 (1961)

Elem. Sym.	A	Z
Co	59	27

Method: Betatron; emulsions

Ref. No.: 61 Em 1 | EGF

Reaction	E or ΔE	E_o	Γ	$\int \sigma dE$	Jπ	Notes
$Co^{59}(\gamma, xn)$	Bremss. 30					90° spectra. Neutron measurement cut off at 2 MeV.

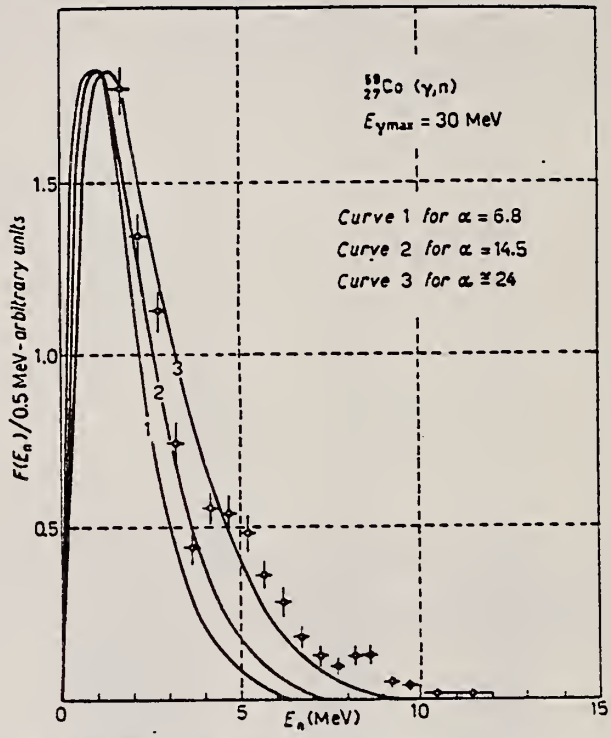

Fig. 3. – Points: experimental photoneutron spectrum from cobalt. The curves represent evaporation spectra calculated according to expression (1). For $\omega(E_R)$ given by (2): curve (1) for $\alpha=6.8$; curve (2) for $\alpha=14.5$; curve (3) for $\alpha=24$ using $\omega(E_B)$ given by (3).

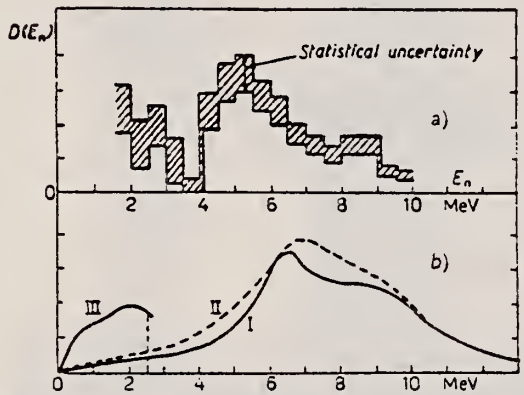

Fig. 7. – *a*) Expected photoneutron distribution for transition to the ground state for the (γ, n) process, curves I and II and for the (γ, 2n) process, curve III (see text). Abscissae: $E_\gamma - E_{th}$ (d, n) for curves I and II; $\frac{1}{2}[E_\gamma - E_{th}(\gamma, 2n)]$ for curve III. Ordinates: $\sigma(\gamma, n)\cdot I(E_\gamma, E_\beta)$ for curves I and II; $2\sigma(\gamma, 2n)\cdot I(E_\gamma, E_\beta)$ for curve III. *b*) $D(E_n)$ = difference between the experimental spectrum and the evaporation curve 2 of Fig. 3.

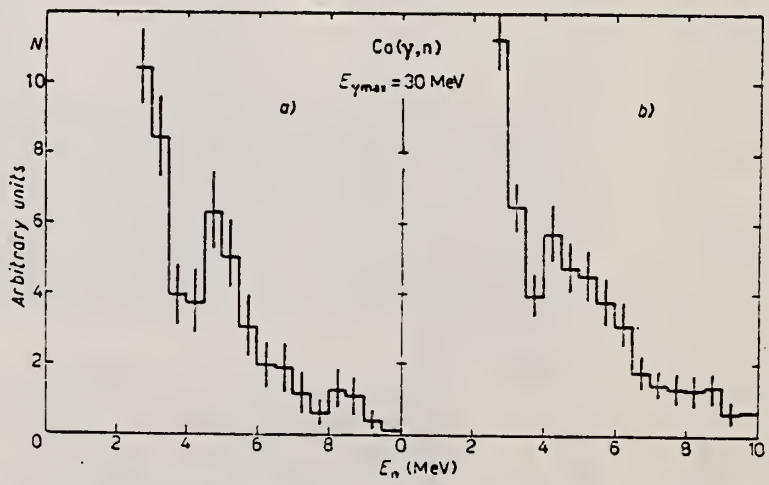

Fig. 4. – Partial photoneutron spectra from Co as measured independently at Catania (*a*) and Messina (*b*) laboratories.

Ref. B. Forkman
Nuclear Phys. 23, 269 (1961)

Elem. Sym.	A	Z
Co	59	27

Method: 30 MeV electron synchrotron; emulsions; magnetic analysis

Ref. No.: 61 Fo 1 JHH

Reaction	E or ΔE	E_o	Γ	$\int \sigma dE$	Jπ	Notes
$Co^{59}(\gamma,d)$	Bremss.			Angle Unknown		No significant (γ,d) yield detected. Ratio of yields: $\frac{(\gamma,\alpha)}{(\gamma,p)} = 0.09$
$Co^{59}(\gamma,\alpha)$	30					

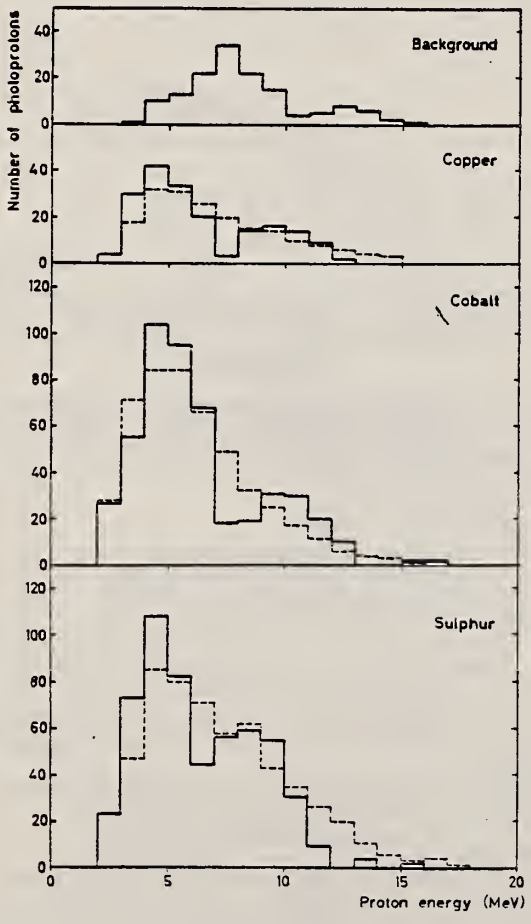

Figure 8: Energy distribution of the photoproton tracks giving intersection points in the area -8.4> x_t> -11.6 and -3.0 <x_t< 3.0.

The lowest section shows the photoprotons from the sulphur exposure. The dashed line is the expected distribution from ref. 19 [Cujec-Dobovisek, Congr. Intern. de Physiq. Nucleaire 634, (1958)]. The second section shows the photoprotons from the colbalt exposure. The dashed line is the expected distribution from ref. 20 [Toms and Stephens, Phys. Rev. 95, 1209 (1954)]. The third section shows the photoprotons from the copper exposure. The dashed line is the expected distribution from ref. 21 [Lin'kova et al, Soviet JETP 38, 780 (1960)]. The background is subtracted in these 3 sections, but shown in the uppermost section. It originates from the entrance window.

Ref. J.H. Carver, G.E. Coote, T.R. Sherwood
Nuclear Phys. 37, 449 (1962)

Elem. Sym.	A	Z
Co	59	27

Method: 30 MeV electron synchrotron; activation; NaI

Ref. No.: 62 Ca 1 | JHH

Reaction	E or ΔE	E_0	Γ	$\int \sigma dE$	Jπ	Notes
Co^{59} (γ,n)	Bremss. 30					

TABLE 1

Isomeric ratios from (γ, n) reactions

Target nucleus	J_0	Residual nucleus: Ground state Spin	Ground state Half-life	Metastable state Spin	Metastable state Half-life	Intermediate state Spin	Isomer ratio $Y_1/(Y_1+Y_2)$	σ
Co^{59}	$\frac{7}{2}^-$ Co^{58}	2+	71.3 d	5+	9.2 h		0.44±0.02	3.2±0.2
Ge^{76}	0^+ Ge^{75}	$\frac{1}{2}^-$	82 min	$\frac{7}{2}^+$	49 s		0.48±0.07	2.8±0.5
Br^{81}	$\frac{3}{2}^-$ Br^{80}	1+	18 min	5−	4.4 h	2−	0.32±0.02	6.5±1.0
Sr^{86}	0^+ Sr^{85}	$\frac{9}{2}^+$	64 d	$\frac{1}{2}^-$	70 min	$\frac{1}{2}^+$	0.36±0.07	2.2±0.4
Zr^{90}	0^+ Zr^{89}	$\frac{9}{2}^+$	79 h	$\frac{1}{2}^-$	4.4 min		0.33±0.10	2.3±0.7
Mo^{92}	0 Mo^{91}	$\frac{9}{2}^+$	15.7 min	$\frac{1}{2}^-$	66 s		0.46±0.04	6^{+4}_{-2}
Ag^{107}	$\frac{1}{2}^-$ Ag^{106}	1+	24 min	6	8.3 d		0.04±0.02	2.0±0.3
In^{113}	$\frac{9}{2}^+$ In^{112}	1+	14.5 min	4+	20.7 min	7−	0.8±0.1	3.1±0.7
Cd^{116}	0^+ Cd^{115}	$\frac{1}{2}^+$	53 h	$\frac{11}{2}^-$	43 d		≦ 0.2	≦ 3
Ce^{140}	0^+ Ce^{139}	$\frac{3}{2}^+$	140 d	$\frac{11}{2}^-$	55 s		0.08±0.01	2.5±0.2
Hg^{198}	0^+ Hg^{197}	$\frac{1}{2}^-$	65 h	$\frac{13}{2}^+$	24 h	$\frac{3}{2}^-$, $\frac{5}{2}^-$	0.05±0.01	3.4±0.5

	Ref.	J_0		Previous work: Ground state Spin	Ground state Half-life	Metastable state Spin	Metastable state Half-life	Intermediate state Spin	Isomer ratio $Y_1/(Y_1+Y_2)$	σ
Br^{81}	10)	$\frac{3}{2}^-$	Br^{80}	1+	18 min	5−	4.4 h	2−	0.33	6.5
Sc^{82}	12)	0^+	Sc^{81}	$\frac{1}{2}^-$	18 min	$\frac{7}{2}^+$	57 min		0.5	3.0
Zr^{90}	11)	0^+	Zr^{89}	$\frac{9}{2}^+$	79 h	$\frac{1}{2}^-$	4.3 min		0.44±0.06	4.5±1
In^{115}	23)	$\frac{9}{2}^+$	In^{114}	1+	72 s	5+	50 d	8 ($T_{\frac{1}{2}}$ = 2.5 s)	0.85	5.0

The yields Y_1 and Y_2 are for (γ, n) reactions ending in the isomeric- or ground-state. The yield Y_1 is for the higher-spin state.

References

1) J. R. Huizenga and R. Vandenbosch, Phys. Rev. 120 (1960) 1305
2) T. Ericson, Advances in Physics 9 (1960) 425
3) D. L. Allan, Nuclear Physics 24 (1961) 274
4) C. T. Hibdon, Phys. Rev. 114 (1959) 179
5) C. T. Hibdon, Phys. Rev. 122 (1961) 1235
6) T. Ericson, Nuclear Physics 11 (1959) 481
7) J. H. Carver, and G. A. Jones, Nuclear Physics 19 (1960) 184
8) A. C. Douglas and N. MacDonald, Nuclear Physics 13 (1959) 382
9) T. Ericson and V. M. Scrutinski, Nuclear Physics 8 (1958) 284
10) L. Katz, L. Pease and H. Moody, Can. J. Phys. 30 (1952) 476
11) L. Katz, R. G. Baker and R. Montalbetti, Can. J. Phys. 31 (1953) 250
12) E. Silva and J. Goldemberg, An Acad. Brasil Ciencc 28 (1956) 275
13) J. H. Carver and D. C. Peaslee, Phys. Rev. 120 (1960) 2155
14) J. M. Blatt and V. F. Weisskopf, Theoretical nuclear physics (John Wiley, New York, 1952)
15) S. H. Vegors, L. L. Marsden and R. L. Heath, U. S. Atomic Energy Commission Report IDO-16370 (1958)
16) Nuclear Data Sheets (National Research Council, Washington, 1960) sets 1-5 inclusive
17) R. Vandenbosch and J. R. Huizenga, Phys. Rev. 120 (1960) 1313
18) E. Weigold and R. N. Glover, Nuclear Physics 32 (1962) 106
19) K. J. Le Couteur and D. W. Lang, Nuclear Physics 13 (1959) 32
20) T. D. Newton, Can. J. Phys. 34 (1956) 804
21) D. W. Lang, Nuclear Physics 26 (1961) 434
22) M. E. Rose, Internal conversion coefficients (North Holland Publ. Co., Amsterdam, 1958)
23) J. Goldemberg and L. Katz, Phys. Rev. 90 (1953) 308

Ref. S.C.Fultz, R.L.Bramblett, J.T.Caldwell, N.E.Hansen, C.P.Jupiter

Phys.Rev. 128, 2345 (1962)

Elem. Sym.	A	Z
Co	59	27

Method

e^+ annihilation - ion chamber, BF_3

Ref. No. 62Ful BG

Reaction	E or ΔE	E_o	Γ	$\int \sigma dE$	Jπ	Notes
(γ,n)	8.5-28	17.5	5.9	$.447 \pm .044)_0^{28}$		435+
(γ,2n)	(444)	23.5		$.139 \pm .014)_0^{28}$		
(γ,n)+(γ,2n) +(γ,np)	(441)			$.586 \pm .058)_0^{28}$		
(γ,n)+2(γ,2n) +3(γ,3n) + (γ,np)		17.5	11.5			

It is estimated that σ(γ,p) would add 20% to formation cross section, i.e.:

$$\int [\sigma(\gamma,n)+\sigma(\gamma,2n)+\sigma(\gamma,np)+\sigma(\gamma,p)]dE = .70 \text{ Mev-b}$$

$$\sigma_{-2} = \int_o^{28} \sigma(E)E^{-2}dE = 1.82 \text{ mb-MeV}^{-1}$$

$$Q_o = .94 \pm 0.13 \text{b}$$

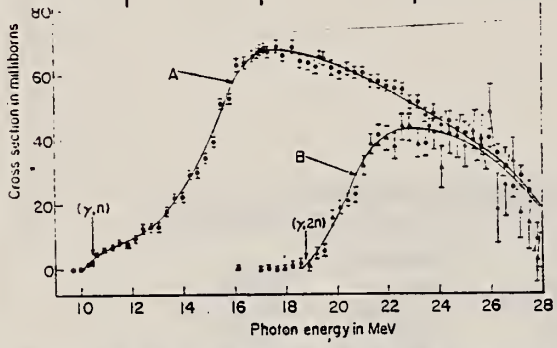

FIG. 1. Cross sections for Co from neutron yield data. Curve A consists of $\sigma(\gamma,n)+2\sigma(\gamma,2n)+\sigma(\gamma,np)+3\sigma(\gamma,3n)$ and was obtained from single-neutron counting data. Curve B consists of $2\sigma(\gamma,2n)+6\sigma(\gamma,3n)$ and was obtained from double-neutron counting data.

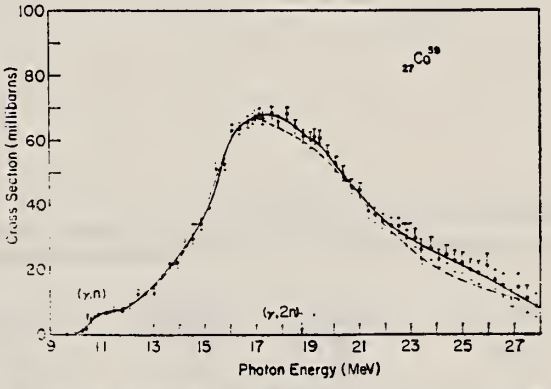

FIG. 3. The formation cross section, $\sigma(\gamma,n)+\sigma(\gamma,2n)+\sigma(\gamma,np)$ for the compound nucleus Co^{59}. The solid curve represents an average line through the data points. The dashed curve is the sum of two Lorentz lines with parameters given in Table I.

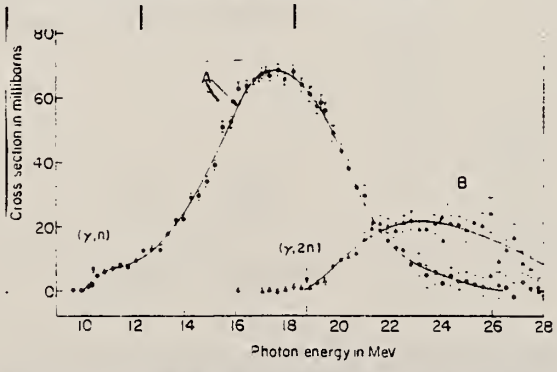

FIG. 2. Partial cross-section curves for Co. Curve A consists of $\sigma(\gamma,n)+\sigma(\gamma,np)$. Curve B consists of $\sigma(\gamma,2n)+3\sigma(\gamma,3n)$.

(over)

TABLE I. Lorentz line and nuclear shape parameters for Co and V.

Element	σ_a (mb)	Γ_a (MeV)	E_a (MeV)	σ_b (mb)	Γ_b (MeV)	E_b (MeV)	Q_0 (b)	α (10^{-13} cm)	β (10^{-13} cm)	ϵ
Co^{59}	40	3.75	16.5	43.4	7.0	19.25	0.94	5.53	4.68	0.355
V^{51}	41	3.60	17.5	46	6.5	20.25	0.66	4.40	5.15	0.338

TABLE II. Integrated cross sections and nuclear level density parameters. σ_{tot} includes estimated contributions for (γ,p) reactions.

Element	$\sigma_{-\frac{1}{2}}$ (mb/MeV)	$0.00225A^{5/3}$ (mb/MeV)	a (MeV^{-1})	$\int_0^{28}\sigma dE$ (MeV-b)	$\int_0^{28}\sigma_{tot}dE+W$ (MeV-b)	$0.06\,NZ/A$ (MeV-b)
Co^{59}	1.82	2.014	5.49	0.586	0.87	0.879
V^{51}	1.56	1.564	6.18	0.557	0.84	0.758

Ref. O.M.M. Mitchell, K.G. McNeill
Can. J. Phys. 41, 871 (1963)

Elem. Sym.	A	Z
Co	59	27

Method: Betatron; proton yield, angular distribution; scintillator; ion chamber

Ref. No.: 63 Mi 5 25 | NVB

Reaction	E or ΔE	E_o	Γ	$\int \sigma dE$	Jπ	Notes
$Co^{59}(\gamma,xp)$	Bremss. 22					Angular distribution: $Y(\theta) = a + b \sin^2\theta (1 + p \cos\theta)^2$ where a = 98±8; b = 3±10 and b/a = 0.0±0.2. Yield (E_p > 8 MeV): (1.8±0.1) 10^5 protons/mole-r Yield (3.7 < E_p < 14): (11±1) 10^5

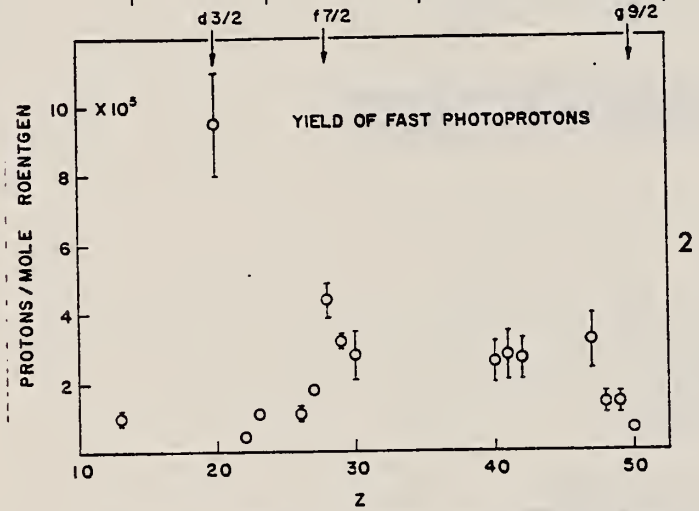

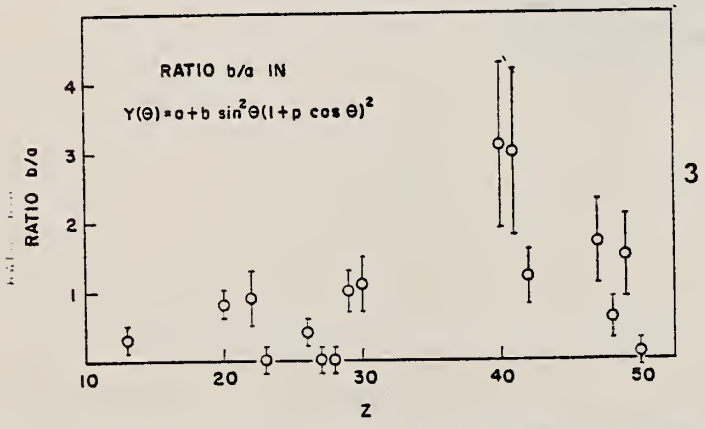

FIG. 2. The yields of fast photoprotons (E_p > 8 Mev) obtained from targets of various elements when irradiated with 22-Mev bremsstrahlung. The target thicknesses range from 351 to 572 mg/cm² (about 8 Mev for protons). The errors noted are statistical.
FIG. 3. The anisotropy coefficient *b/a* for fast photoprotons (E_p > 8 Mev) from 16 elements. The errors noted are statistical.

(over)

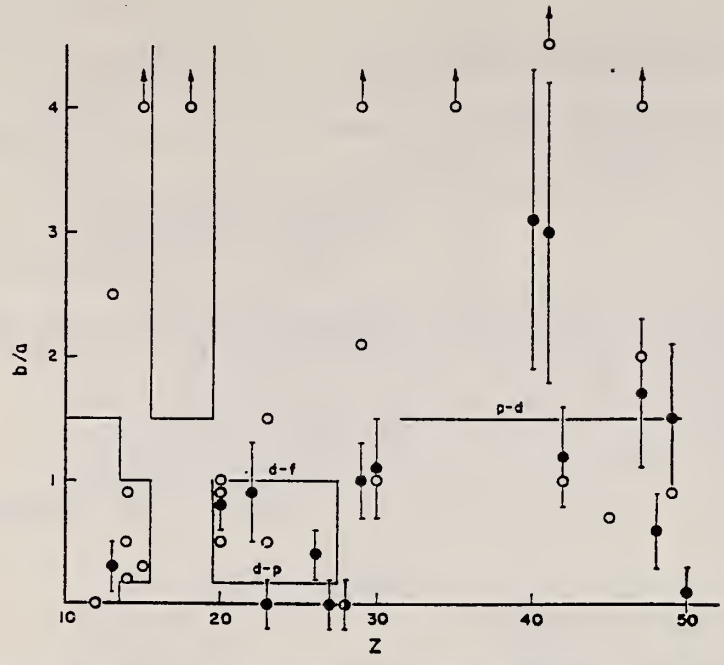

FIG. 4. The values of the fast photoproton anisotropy coefficient b/a found by the present authors (●) and other workers (○) in the region of the periodic table $10 < Z < 50$. Arrows indicate off-scale points. The references to the results of other workers are given in Table II. The demarcations are explained in the text.

REF.

E.B. Bazhanov, A.P. Komar, A.V. Kulikov
Zhur. Eksp. i Teoret. Fiz. 46, 1497-1499 (1964)
Soviet Phys. JETP 19, 1014 (1964)

ELEM. SYM.	A	Z
Co	59	27

METHOD

Synchrotron

REF. NO. 64 Ba 2 NVB

REACTION	RESULT	EXCITATION ENERGY	SOURCE		DETECTOR		ANGLE
			TYPE	RANGE	TYPE	RANGE	
G,XN	ABX	10-30	C	10-30	BF3-I		4PI

$$\int_0^{29} \sigma(\gamma,xn)dE = 701(\pm 13\%)\text{MeV-mb}$$

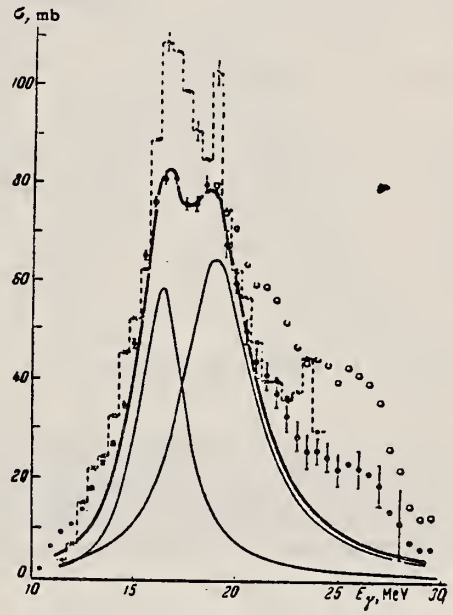

FIG. 2. Variation of photoneutron cross section with γ-ray energy for Co^{59}. Statistical errors are indicated. The light circles show the behavior of the cross section before correction is made for the multiplicity of neutrons.

G. Baciu, A. Bonazzola, B. Minetti, C. Molino, L. Pasqualini and G. Piragino
Rev. Roum. Phys. 9, 977 (1964)

ELEM. SYM.	A	Z
Co	59	27

METHOD

REF. NO. 64 Ba 4 egf

REACTION	RESULT	EXCITATION ENERGY	SOURCE		DETECTOR		ANGLE
			TYPE	RANGE	TYPE	RANGE	
G,XN	ABX	10-27	C	10-27	BF3-I		4PI

65 BA3 SAME DATA

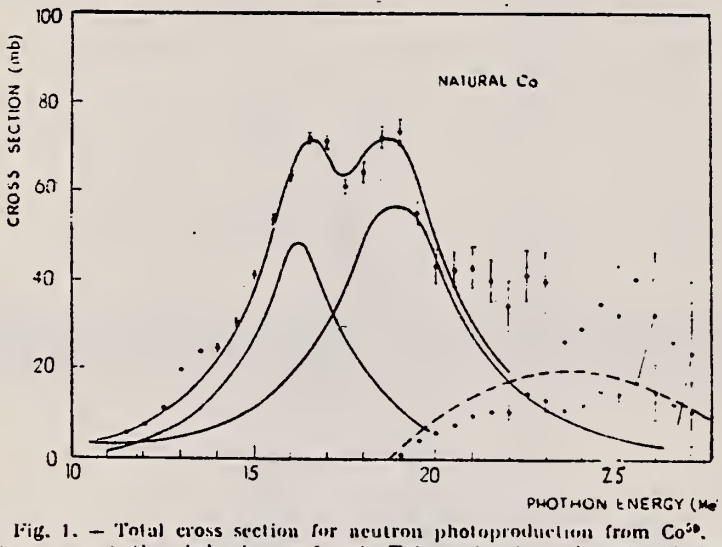

Fig. 1. — Total cross section for neutron photoproduction from Co^{59}.
The points represent the behaviour of $\sigma(\gamma, Tn) = \sigma(\gamma, n) + \sigma(\gamma, np) + 2\sigma(\gamma, 2n) + \ldots$
The circles represent the values for $\sigma(\gamma, 2n)$ estimated by the statistical method, taking as parameter of the density level the value $a = 6.5\ MeV^{-1}$.
The full line is the resultant of two Lorentzians corresponding to the parameters of Table I.
The dotted line represents the behaviour of $\sigma(\gamma, 2n)$ measured by Fultz et al. [6].

METHOD

Van de Graaff; resonance fluorescence

REF. NO. 64 Bo 1 NP3

REACTION	RESULT	EXCITATION ENERGY	SOURCE TYPE	SOURCE RANGE	DETECTOR TYPE	DETECTOR RANGE	ANGLE
G,G	LFT	1-3	C	1 - 3	NAI-D		100
		(0.5 - 3.0)		(0.5 - 3.0)			

ABT

TABLE 1
Cases of observed resonance fluorescence

Nucleus multipol.	State (MeV)	Spin	Γ_0/Γ	$T(g\omega\Gamma_0^2/\Gamma^2)^{-1}$ (sec).	Mean lifetime T BCW (sec)	Mean lifetime T other (sec)	Ref.	Γ_0/Γ_W BCW
Co^{59}	0.00	$\frac{7}{2}^-$						
(E2)[a]	1.19	$(\frac{11}{2})$	(1)	$8\pm2\times10^{-14}$	$11.5\pm5\times10^{-14}$			57
[M1][a]	1.46 1.48	$[\frac{5}{2}]$	?	$4\pm1.3\times10^{-13}$				$0.34\Gamma/\Gamma_0$
[M1][a]	2.48 2.54	$[\frac{5}{2}]$	?	$7.5^{+3}_{-2}\times10^{-14}$				$0.04\Gamma/\Gamma_0$

S. Costa, F. Ferroni, S. Ferroni and C. Molino
Phys. Letters 11, 324 (1964)

Co	59	27

METHOD

Synchrotron; $C^{12}(\gamma,n)$ monitor

REF. NO.: 64 Co 2 | JOC

REACTION	RESULT	EXCITATION ENERGY	SOURCE		DETECTOR		ANGLE
			TYPE	RANGE	TYPE	RANGE	
C.XN	ABY	THR - 80	C	80	BF3-I		4 PI

Table 1

Element	Yield (36) eV cm^2 mol MeV	60 NZ/A (mb MeV)	Σ_0^{30}	Σ_0^{80}	$\Sigma_0^{30}/\Sigma_0^{80}$	E_m (MeV)	σ_m (mb)
$_{24}Cr$	83 x10^{-5}	777	1.21	2.1	0.58	18.5	97
$_{25}Mn$	108 x10^{-5}	818	1.32	2.33	0.65	18.5	114
$_{26}Fe$	68 x10^{-5}	832	0.88	1.46	0.60	17.5	75
$_{27}Co$	89 x10^{-5}	878	1.08	1.82	0.59	17.5	92
$_{28}Ni$	44 x10^{-5}	879	0.55	1.07	0.51	18.5	56
$_{29}Cu$	95 x10^{-5}	947	1.06	1.99	0.53	17.5	98
$_{30}Zn$	88 x10^{-5}	975	0.94	1.68	0.56	17.5	86
$_{31}Ga$	130 x10^{-5}	1034	1.29	2.18	0.59	17.5	151
$_{32}Ge$	139 x10^{-5}	1064	1.35	2.29	0.59	17.5	158
$_{33}As$	137 x10^{-5}	1109	1.22	2.18	0.56	17.5	127

$$\Sigma_0^{30} = \frac{\int_0^{30} \sigma(\gamma,xn)dE}{60\ NZ/A}$$

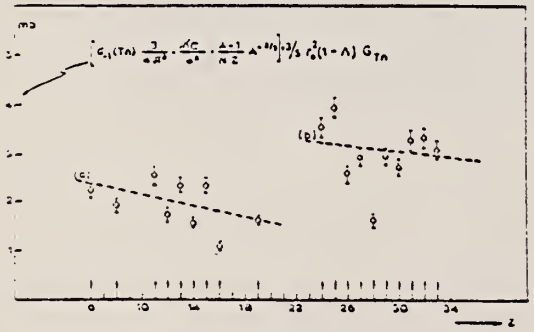

Fig. 2. Bremsstrahlung weighted cross sections, $\sigma_{-1}(Tm)$, conveniently normalized, versus Z.

Table 2

Element	maximum yield (x 10^{-5})	$\sigma_{-1}(Tm)$	$\sigma_{-1}(Tm) \times \left[\frac{3}{4\pi^2}\frac{\hbar c}{e^2}\left(\frac{A-1}{NZ}\right)A^{-\frac{2}{3}}\right]$
$_6C$	4.0	3.54	2.13
$_8O$	5.2	4.95	1.92
$_{11}Na$	13.6	11.60	2.49
$_{12}Mg$	10.0	8.81	1.73
$_{13}Al$	15.9	13.92	2.30
$_{14}Si$	11.6	9.96	1.55
$_{15}P$	19.8	17.56	2.32
$_{16}S$	9.5	8.35	1.07
$_{19}K$	19.6	17.90	1.61
$_{20}Ca$	12.1	11.68	1.02
$_{24}Cr$	86	61.6	3.56
$_{25}Mn$	115	78.1	3.96
$_{26}Fe$	71	50.5	2.55
$_{27}Co$	94	63.5	2.94
$_{28}Ni$	46	34.2	1.59
$_{29}Cu$	102	72.3	2.96
$_{30}Zn$	93	65.7	2.68
$_{31}Ga$	140	93.6	3.31
$_{32}Ge$	150	101.5	3.36
$_{33}As$	151	99.3	3.12

REF.

S. Costa, F. Ferrero, S. Ferroni and R. Malvano
Proc. Paris Conference 1034 (1964)

ELEM. SYM.	A	Z
Co	59	27

METHOD

100 MeV synchrotron

REF. NO. 64 Co 3 JDM

REACTION	RESULT	EXCITATION ENERGY	SOURCE		DETECTOR		ANGLE
			TYPE	RANGE	TYPE	RANGE	
G,N	ABΣ	THR-80	C	10-80	BF3-I		4PI

TABLE

ELEMENT	Yield (36 MeV) $\left(\frac{\text{n. cm}^2}{\text{mol. MeV}} \times 10^6\right)$	Σ_0^{30}	Σ_0^{80}	$\Sigma_0^{30}/\Sigma_0^{80}$	σ_{-1} (mb)
$_{24}$Cr	83	1.21	2.1	0.58	62
$_{25}$Mn	108	1.52	2.33	0.65	76
$_{26}$Fe	68	0.88	1.46	0.60	50
$_{27}$Co	89	1.08	1.82	0.59	64
$_{28}$Ni	44	0.55	1.07	0.51	34
$_{29}$Cu	95	1.06	1.99	0.53	72
$_{30}$Zn	88	0.94	1.68	0.56	66
$_{31}$Ga	130	1.29	2.18	0.59	94
$_{32}$Ge	139	1.35	2.29	0.59	101
$_{33}$As	137	1.22	2.18	0.56	100

$\sum_a^b = \frac{A}{60\,NZ}\int_a^b \sigma(E)\,dE$ is the integrated cross section measured in units of the classical dipole $60\,NZ/A$ mb. MeV.

G. Baciu, G. C. Bonazzola, B. Minetti, C. Molino, L. Pasqualini, and G. Piragino

ELEM. SYM.	A	Z
Co	59	27

METHOD

NBS Monitor

REF. NO. 65 Ba 3 EGF

REACTION	RESULT	EXCITATION ENERGY	SOURCE TYPE	SOURCE RANGE	DETECTOR TYPE	DETECTOR RANGE	ANGLE
G,XN	ABX	THR - 28	C	10-30	BF3-I		4PI

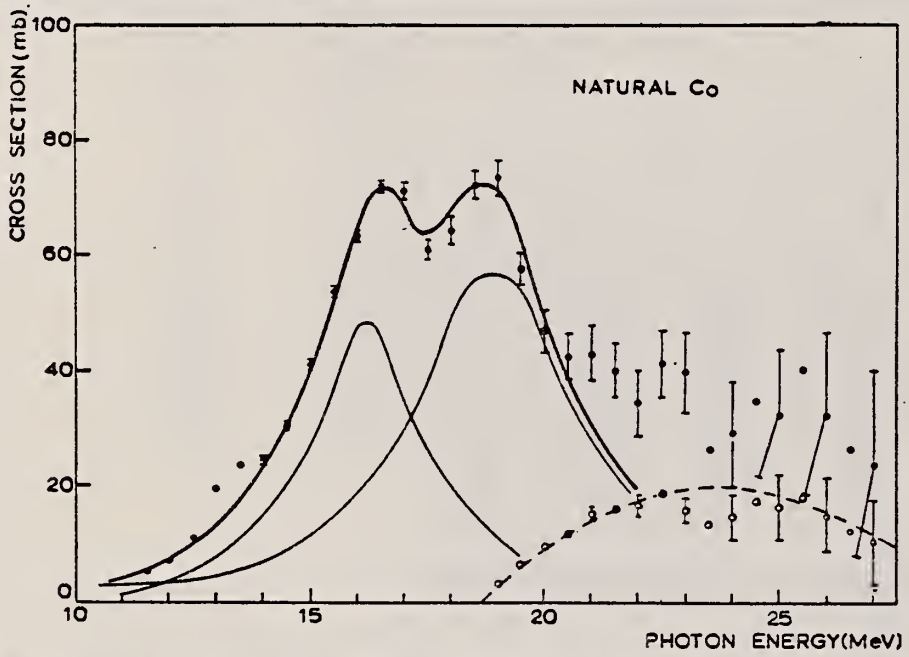

Fig. 1. Total photoneutron cross section for cobalt. The points represent the values of the $\sigma(\gamma, \mathrm{Tn}) = \sigma(\gamma, \mathrm{n}) + \sigma(\gamma, \mathrm{np}) + 2\sigma(\gamma, 2\mathrm{n})$. The open circles represent the $\sigma(\gamma, 2\mathrm{n})$ values calculated with the statistical model taking $a = 6.5\ \mathrm{MeV}^{-1}$ as found in sect. 4. The two Lorentz lines, having the parameters given in table 1, are such that their sum gives the heavier line drawn through the data points. The dashed line gives the $\sigma(\gamma, 2\mathrm{n})$ measured by Fultz *et al.* [6]).

TABLE 1

Lorentz line and nuclear shape parameters for cobalt obtained in the present work compared with those given by Fultz *et al.* [6])

E_m (MeV)	σ_m (mb)	Γ (MeV)	Q_0 (b)	ε	a (fm)	b (fm)	Ref.
16.2	46	3.0	0.86	0.344	5.26	4.47	this work
18.8	57	4.6					
16.5	40	3.75	0.94	0.355	5.53	4.68	
19.25	43.4	7.0					[6])

REACTION	RESULT	EXCITATION ENERGY	SOURCE TYPE	SOURCE RANGE	DETECTOR TYPE	DETECTOR RANGE	ANGLE
G,XN	ABX	THR - 28	C	10-30	BF3-I		4PI

TABLE 2
Cross sections for Co, Ni, Cu and Ga

	E_m (MeV)	σ_m (mb)	$\int_0^x \sigma(E)dE$ (mb · MeV)	Ref.
Co^{59}	16.9	130	750(24)	a)
	16.75 19	110 103	709(25)	a)
	17.5	68	725±72(28)	a)
	16.5 19	82 80	701±91(29)	10)
	16.5 19	72 74	657±89(28)	this work
			537±34(24)	this work
			445±48(24)	a)
Ni	16.5	50	340(24)	11)
	16.5	46±1	313±48(28)	this work
			276±25(24)	this work
Ni^{58}	18.5	60	330(24)	12)
		30	180(24)	a 12)
	20.5	21	160(24)	13)
	19.0	32	220±30(32)	14)
Ni^{60}	16.5	85	440(±20 %)(24)	b)
Cu	19.5	120	870(20)	a)
			904(27)	15)
	17.2	126	930(27)	16)
	17	90	450±15(19,6)	17)
	16.75	71±7	745±74(28)	18)
	17.0	86±2	733±105(28)	this work
			451±18(20)	this work
Ga	16.5	115±3	947±98(28)	this work

σ_m is the peak value of the cross section, E_m is the peak energy and $\int_0^x \sigma(E)dE$ is the integrated cross section. The upper limit of the integration is indicated in parentheses.

a) Value obtained subtracting the $(\gamma, 2n)$ reaction contribution from the $\sigma(\gamma, Tn)$.
b) Value obtained by subtracting the $Ni^{58}(\gamma, n)Ni^{57}$ reaction contribution from the $\sigma(\gamma, Tn)$ for natural nickel corrected for the $(\gamma, 2n)$ reaction contribution.

6) S. C. Fultz *et al.*, Phys. Rev. 128 (1962) 2345
7) C. R. Hatcher, R. L. Bramblett, N. E. Hansen and S. C. Fultz, Nucl. Instr. 14 (1961) 337
8) R. Montalbetti, L. Katz and J. Goldenberg, Phys. Rev. 91 (1953) 659
9) P. A. Flurnoy, R. S. Ticle and W. D. Whitehead, Phys. Rev. 120 (1960) 1424
10) E. B. Bazhanov, A. P. Komar and A. V. Kulikov, JETP 46 (1964) 1497

REF.

J.M. Wyckoff, B. Ziegler, H.W. Koch, and R. Uhlig
Phys. Rev. 137, B576-94 (1965)

ELEM. SYM.	A	Z
Co	59	27

METHOD

Synchrotron; ion chamber monitor

REF. NO.

65 Wy 1 NVB

REACTION	RESULT	EXCITATION ENERGY	SOURCE		DETECTOR		ANGLE
			TYPE	RANGE	TYPE	RANGE	
G,MU-T	ABX	10-35	-C	90	SCI-D		4PI

EC

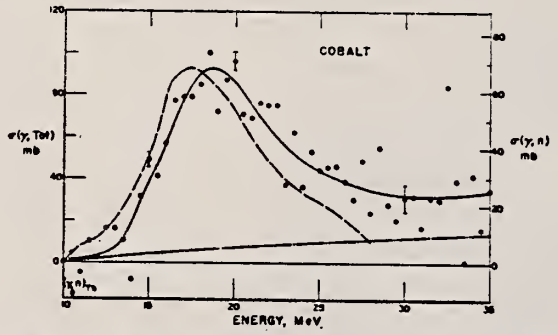

FIG. 23. Cobalt total photonuclear cross section. The solid line is drawn as the best approximation to the experimental points. The dashed line represents the $\sigma(\gamma,n)$ data of the Livermore group.

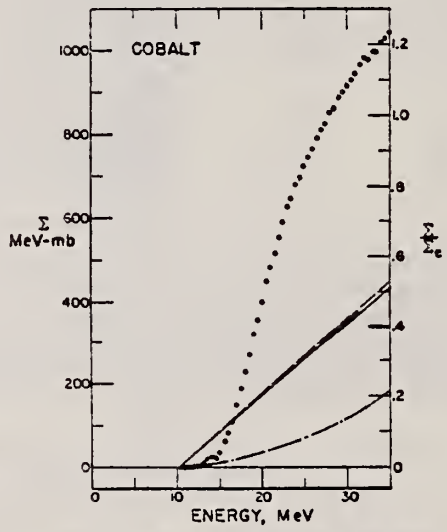

FIG. 24. Cobalt total photonuclear cross section integrated over energy. The solid, dashed, and dot-dashed lines have the same meaning as in Fig. 16.

REF.

F. W. K. Firk
Proc. Gatlinburg Conference 352 (1966)

ELEM. SYM.	A	Z
Co	59	27

METHOD

REF. NO.	
66 Fi 2	hmg

REACTION	RESULT	EXCITATION ENERGY	SOURCE		DETECTOR		ANGLE
			TYPE	RANGE	TYPE	RANGE	
G,XN	SPC	THR-60	C	60	TOF-D	5-40	90

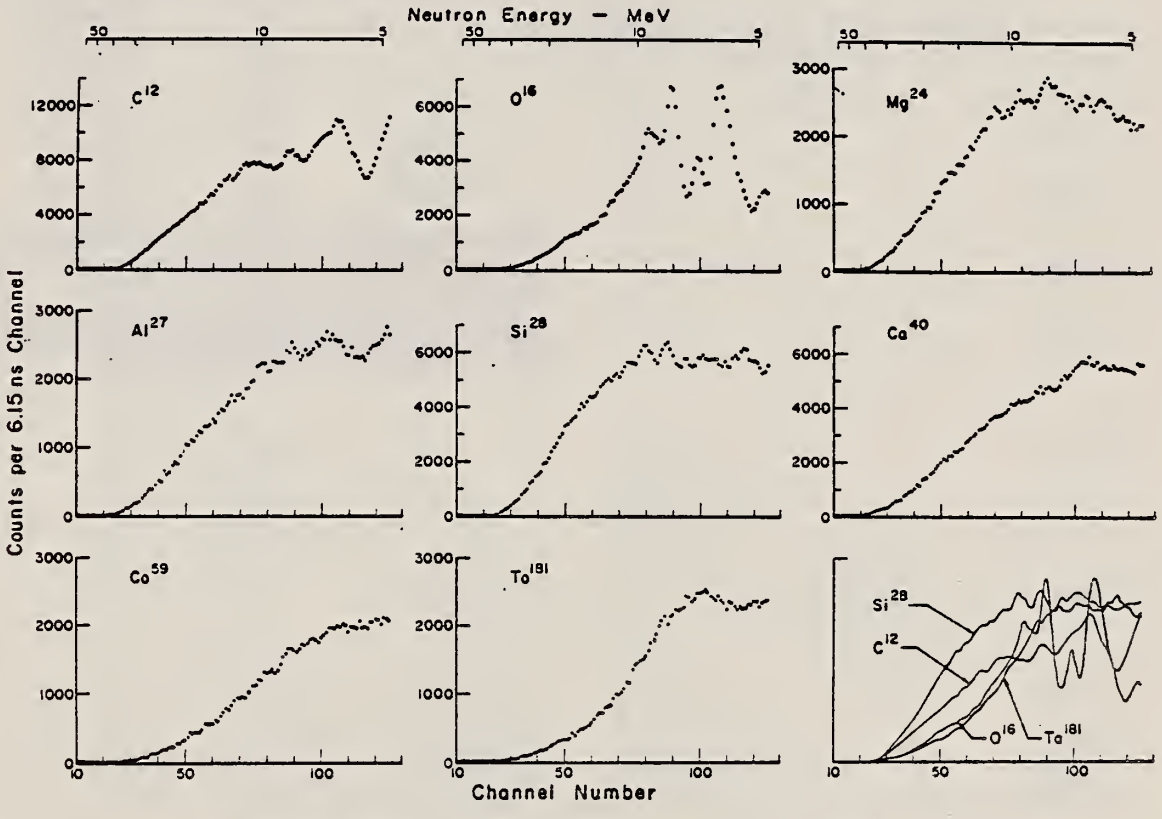

Fig. 1. Observed photoneutron time-of-flight spectra of C, O, Mg, Si, Ca, Co, V, and Ta.

REF.

W. B. Walters and J. P. Hummel
Phys. Rev. 150, 867 (1966)

ELEM. SYM.	A	Z
Co	59	27

METHOD

Betatron

REF. NO.

66 Wa 1

JDM

REACTION	RESULT	EXCITATION ENERGY	SOURCE		DETECTOR		ANGLE
			TYPE	RANGE	TYPE	RANGE	
G,2P5N	RLY	THR-150	C	150	ACT-I		4PI

Measured isomeric yield ratios.

TABLE II. Summary of the results for the photoproduction of the Sc^{44} isomers (spins 2 and 6).

Target isotope and spin	Bremsstrahlung energy (MeV)	Fraction of yield to high-spin isomer
Sc^{45} ($I=\frac{7}{2}$)	50	0.21±0.04
	75	0.21±0.03
	175	0.20±0.02
	223	0.18±0.01
	264	0.17±0.02
	300	0.21±0.02
$Fe^{54,56}$ ($I=0$)[a]	250	0.38±0.02
Mn^{55} ($I=\frac{5}{2}$)	225	0.42±0.04
	300	0.39±0.02

[a] It is assumed that most of the yield is due to reactions involving the two lightest isotopes present in natural iron (Fe^{54} and Fe^{56}).

[19] The least-squares fitting program was supplied to us by G. Moscati. It was based on a program described in J. L. Need and T. E. Fessler, National Aeronautics and Space Administration Report No. NASA TND-1453, 1962 (unpublished).

REF. H. M. Gerstenberg and E. G. Fuller
NBS Tech. Note 416, June 1967

ELEM. SYM.	A	Z
Co	59	27

METHOD

REF. NO. 67 Ge 2 HMG

REACTION	RESULT	EXCITATION ENERGY	SOURCE		DETECTOR		ANGLE
			TYPE	RANGE	TYPE	RANGE	
G,N	ABY	THR-27	C	22,27	BF3-I		4PI

Table 7. Comparison of neutron yields. Yields are given in units of (neutron cm^2/MeV nucleus)$\times 10^{-28}$. The estimated uncertainties in Y and Y_c are of the order of 6% and 10%, respectively.

Element	E_o	$Y(E_o)$	Y_c UCRL	Y_c Saclay	Y_c Va.	Y_c NBS(Old)	Y_c/Y UCRL Exp	Y_c/Y Saclay Exp	Y_c/Y Va. Exp	Y_c/Y NBS(Old) Exp	Ref.
Pb	27	103	86				0.83				26,30
	22	111	92	116			0.83	1.05			
Au	27	89	97				1.09				24,30,
	22	92	98	88		115	1.07	0.96		1.25	38
Ta	27	81	82	77			1.01	0.95			27,30,
	22	85	79	80		113	0.93	0.94		1.33	38
Ho	27	67	75				1.12				27,31,
	22	69	77	82		103	1.12	1.19		1.49	39
Ag	27	36									
	22	34.8									
Cu	27	14.4	13.2				0.92				28,30
	22	12.6	11.5	12.4			0.91	0.98			
Co	27	12.7	12.1				0.95				29,34
	22	10.6	9.9		13.5		0.94		1.27		
Cd	27	1.69		1.13	1.01			0.67	0.60		32,35
P	27	2.35			1.76				0.75		36
Al	27	1.92	1.62		1.38		0.84		0.72		25,37
O^{18}	27	0.54	0.42	0.48	0.42		0.78	0.89			16,32, 37
C	27	0.50	0.35	0.33	0.46		0.70	0.66			25,32, 33

(OVER)

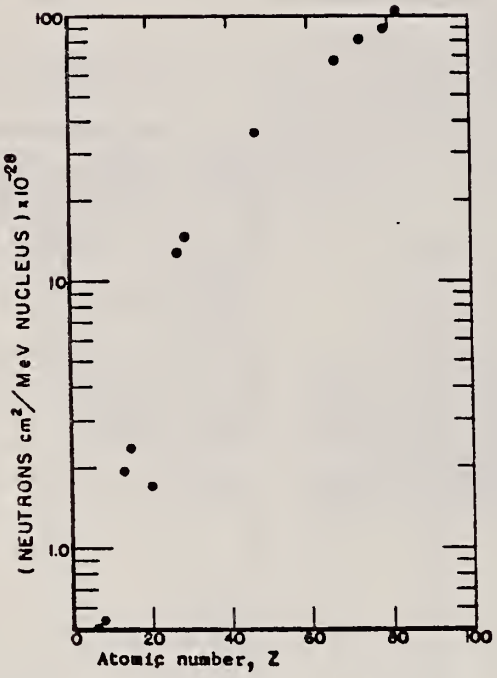

Fig. 31. Absolute neutron yield as a function of atomic number. The neutron yield from calcium (Z = 20) is particularly low in comparison with the other elements because its (γ,n) threshold is high compared to the mean energy of the giant resonance.

REF.

R. R. Hurst and D. J. Donahue
Nucl. Phys. A91, 365 (1967)

ELEM. SYM.	A	Z
Co	59	27

METHOD

Neutron capture gamma rays

REF. NO.

67 Hu 1

EGF

REACTION	RESULT	EXCITATION ENERGY	SOURCE		DETECTOR		ANGLE
			TYPE	RANGE	TYPE	RANGE	
G,N	ABX	11	D	11	BF3-I		4PI

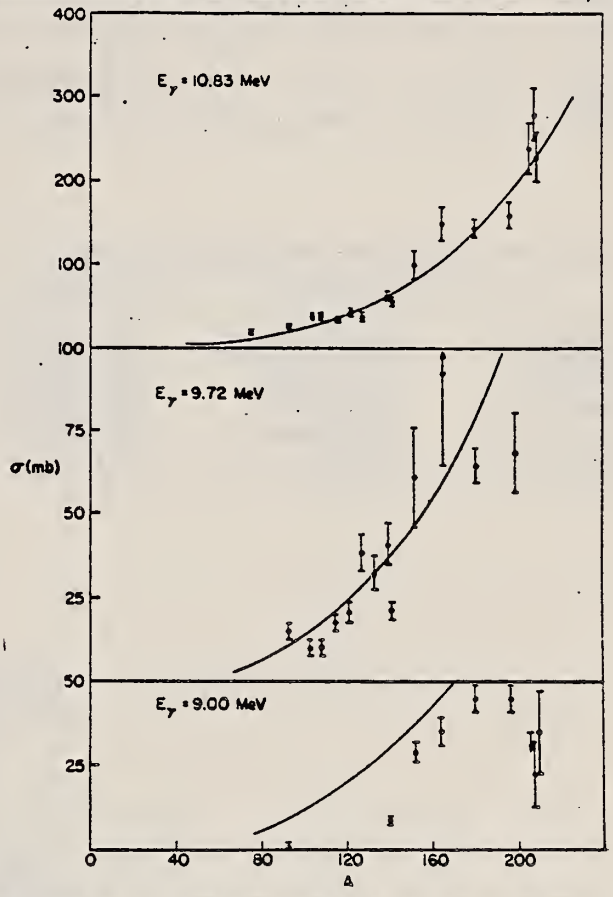

Fig. 1. Cross section (in mb) versus mass number of the target for gamma-ray energies of 9.00 9.72 and 10.83 MeV. The solid lines are plots of eq. (1) in the text.

TABLE 1
Photoneutron cross sections (mb)

Target	7.72 MeV	9.00 MeV	9.72 MeV	10.83 MeV
^{59}Co				9.0± 0.8
^{75}As				20.4± 1.7
^{93}Nb		0.53± 0.10	14.6± 2.2	25.8± 2.1
^{103}Rh			10.6± 1.7	38.8± 3.1
^{107}Ag, ^{109}Ag			10.0± 1.5	37.6± 2.9
^{115}In			17.1± 2.6	33.3± 2.7
^{121}Sb, ^{123}Sb			20.7± 3.1	42.5± 3.6
^{127}I			38.7± 5.8	38.8± 3.1
^{133}Cs			31.7± 4.8	52.5± 3.8
^{139}La		8.61± 0.86	40.8± 6.5	63.0± 5.0
^{141}Pr			21.5± 3.2	58.3± 4.1
^{151}Eu, ^{153}Eu		28.9 ± 3.2	61.3±14.7	102 ±18
^{165}Ho		35.6 ± 4.3	92.2±27.6	150 ±20
^{181}Ta	4.14±0.36	45.4 ± 3.7	65.0± 5.5	146 ±12
^{197}Au		44.5 ± 3.6	68.4±13.5	160 ±15
^{206}Pb		<34.3		238 ±29
^{208}Pb		22.6 ±11.3		280 ±31
^{209}Bi		36.1 ±12.0		226 ±27

U.S. DEPARTMENT OF COMMERCE
NATIONAL BUREAU OF STANDARDS

REF.	ELEM. SYM.	A	Z
H. Lichtblau and A. Goldmann Z. Physik 205, 47 (1967)	Co	59	27

METHOD	REF. NO.
	67 Li 1 egf

REACTION	RESULT	EXCITATION ENERGY	SOURCE		DETECTOR		ANGLE
			TYPE	RANGE	TYPE	RANGE	
G,2N	RLY	THR-54	C	35,54	ACT-I		4PI
G,3N							
G,4N							
G,XNYP							

ISOMER RATIO (G,N)

Table 2. *Yield ratios at end point energies E_m=35 and 54 MeV*

Yield ratio	E_m=35 MeV	E_m=54 MeV
$Y[Co(\gamma, 2n)]/Y[Co(\gamma, n)]$	$(1.63\pm0.11)\,10^{-1}$	$(1.86\pm0.13)\,10^{-1}$
$Y[Co(\gamma, 3n)]/[Co(\gamma, n)]$	$(1.24\pm0.12)\,10^{-3}$	$(6.34\pm0.25)\,10^{-3}$
$Y[Co(\gamma, 4n)]/[Co(\gamma, n)]$	below threshold	$(1.02\pm0.08)\,10^{-4}$
$Y[Co(\gamma, x)^{56}Mn]/[Co(\gamma, n)]$	$(3.7\pm0.7)\,10^{-5}$	$(1.26\pm0.05)\,10^{-3}$
$Y_m/(Y_m+Y_g)$	$(5.70\pm0.20)\,10^{-1}$	$(5.77\pm0.20)\,10^{-1}$
$Y[Co(\gamma, n)]/Y[C(\gamma, n)\,^{11}C]$	16.1 ± 1.3	13.5 ± 1.1

Table 3. *Values of σ_γ in* mb *calculated from the yield ratios of Table 2, based on the $^{12}C(\gamma, n)$ cross section of* Barber *et al.*[26] *(see also footnote *). An additional error of 4.5%, due to uncertainties in the calibration of the methane counter*[21], *which applies equally to all listed values of σ_γ, is not included in the quoted errors*

E_m	Reaction				
	(γ, n)	$(\gamma, 2n)$	$(\gamma, 3n)$	$(\gamma, 4n)$	$(\gamma, x)\,^{56}Mn$
35 MeV	28.3 ± 1.0	4.6 ± 0.2	$(3.5\pm0.3)10^{-2}$	—	$(1.1\pm0.2)10^{-3}$
54 MeV	31.7 ± 1.2	5.9 ± 0.3	$(2.0\pm0.15)10^{-1}$	$(3.2\pm0.3)10^{-3}$	$(4.0\pm0.3)10^{-3}$

* Reference to the $C(\gamma, n)$ cross section measured by Cook *et al.*[28] has the effect of increasing the values listed in table 3 by 8% at E_m=35 MeV and by 10% at E_m=54 MeV.

[21] Krämer, K., H.v.Buttlar, A.Goldmann, B.Huber: Z.Physik 207, 1 (1967).
[26] Howerton, R.J.: UCRL-Report 5573 (1961).

REF.

J. M. Loiseaux, J. M. Maison, and M. Langevin
J. de Physique 28, 11 (1967)

ELEM. SYM.	A	Z
Co	59	27

METHOD

REF. NO.	
67 Lo 1	JOC

REACTION	RESULT	EXCITATION ENERGY	SOURCE		DETECTOR		ANGLE
			TYPE	RANGE	TYPE	RANGE	
G,G/	ABX	14-32	C	34	NAI-D		DST

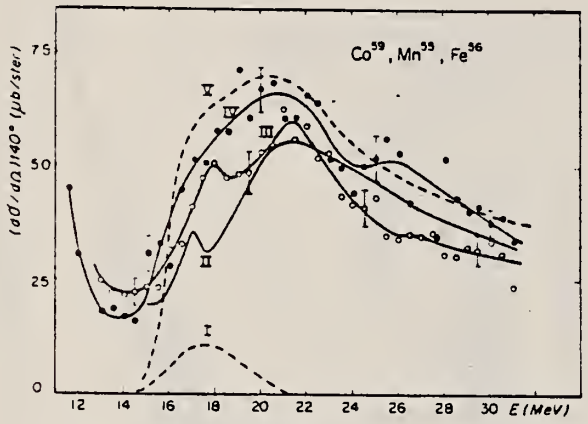

FIG. 10.

Sections efficaces différentielles de diffusion à 140° pour ^{55}Mn (courbe II), ^{56}Fe (courbe III), ^{59}Co (courbe IV). Section efficace de diffusion tenseur (courbe I) et section efficace de diffusion scalaire + tenseur (courbe V) calculées avec les paramètres de Fultz et al. [16] pour ^{59}Co.

REF. W. J. Alston III, H. H. Wilson and E. C. Booth
Nucl. Phys. A116, 281 (1968)

ELEM. SYM.	A	Z
Co	59	27

METHOD

REF. NO.	
68 Al 1	egf

REACTION	RESULT	EXCITATION ENERGY	SOURCE		DETECTOR		ANGLE
			TYPE	RANGE	TYPE	RANGE	
G,G	LFT	0 - 1	C	4	SCD-D	0-3	130
		(1.19)					

Angle greater than 90° for all measurements.

SELF-ABSORPTION

TABLE 1
Direct and absorption measurements of resonance fluorescence

Nucleus	E_r (MeV)	J_r	Γ_0/Γ	$gW\Gamma_0\Gamma_0/\Gamma$ (meV)	Error (%)	This work Γ_0 (meV)	Other work Γ_0
^{55}Mn	0.000	$\frac{5}{2}^-$					
	1.527	$(\frac{3}{2}^-)$	0.9	5.2	25	8–12	
				abs [a]	40	8.0	
	1.884	?	0.82 [b]	41	25	$50/gW$	
				abs [a]	10	$55/g$	
	2.197	?	(0.8) [c]	17	25	$21/gW$	
				abs	20	$17/g$	
	2.252	?	(0.9) [c]	17	25	$19/gW$	
				abs	20	$13/g$	
	2.365	?	?	3.5	36	$(2–6)\Gamma/\Gamma_0$	
	2.564	?	(1.0)	50	25	$50/gW$	
				abs [a]	20	$61/g$	
	2.751	?	?	6.7	42	$6.7(\Gamma/\Gamma_0)/gW$	
^{59}Co	0.000	$\frac{7}{2}^-$					
	1.187	$(\frac{7}{2}^-)$	(1.0)	6.8	25	7.5	0.33(E2) [d]
				abs	25 [a]	12	
		$(\frac{9}{2}^-)$	(1.0)	6.8	25	(5.4–6.5)	0.27(E2)
				abs	25 [a]	9.6	
^{63}Cu	0.000	$\frac{3}{2}^-$					
	1.414	$\frac{5}{2}^-$	?	1.6	30	$(1.1–1.7)\Gamma/\Gamma_0$	
	1.551	$\frac{3}{2}^-$	?	1.7	37	$(1.7–2.5)\Gamma/\Gamma_0$	0.1(E2) [e]
^{69}Ga	0.000	$\frac{3}{2}^-$					
	0.872	$(\frac{1}{2}^-)$	0.95	1.1	35	$0.8/W$	
	1.107	$(\frac{3}{2}^-)$	0.95	8.0	20	$8.4/W$	
^{75}As	0.000	$\frac{3}{2}^-$					
	0.86	?	?	1.7	20	$1.7\,\Gamma/gW\Gamma_0$	
	1.07	?	?	2.6	30	$2.6\,\Gamma/gW\Gamma_0$	
	1.35	?	?	3.6	20	$3.6\,\Gamma/gW\Gamma_0$	
^{89}Y	0.000	$\frac{1}{2}^-$					
	1.51	$\frac{3}{2}^-$	(1.0)	52 [a]	30	28	0.37(E2) [f]
				abs [a]	15	22	

[a] Measured with NaI.
[b] Ref. [24].
[c] Measured with a Ge(Li) detector to ±10 %.
[d] Ref. [13]. [e] Ref. [14]. [f] Ref. [23].

[13] D.G. Alkhazov, K.I. Erokhina and I.K. Lemberg, Izv.Akad.Nauk.SSSR(ser.fiz.) 28 (1964) 1667.
[14] B.G. Harvey, J.R. Meriwether and A.Bussiere, Nucl. Phys. 70 (1965) 305.
[23] G.A. Peterson and J.Alster, Phys.Rev. 166 (1968) 136.
[24] N. Nath, M.A. Rothman, D.M. Van Patter and C.E. Mandeville, Nucl. Phys. 13 (1959) 74.

REF. R. Garfagnini and G. Piragino
Nucl. Phys. A122, 49 (1968)

ELEM. SYM.	A	Z
Co	59	27

METHOD

REF. NO.	
68 Ga 1	egf

REACTION	RESULT	EXCITATION ENERGY	SOURCE		DETECTOR		ANGLE
			TYPE	RANGE	TYPE	RANGE	
$G,XN	SPC	THR-85	C	85	CCH	1-15	135

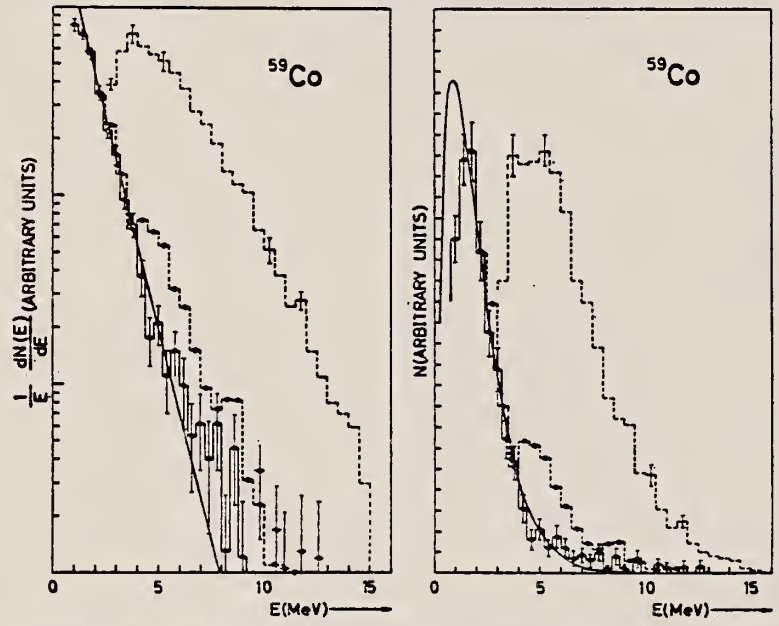

Fig. 5. Energy spectrum of photoneutrons from ^{59}Co compared with the spectrum of photoprotons for $E_{\gamma\,max} = 24$ MeV of ref. [11]) (dashed histogram). The dotted histogram represents the photoneutron spectrum deduced by Emma *et al.* [16]) at 90° with $E_{\gamma\,max} = 30$ MeV (open circles). The spectra are normalized to the maximum value of *N*. The full line has the same meaning as in fig. 2.

[16] V. Emma, C. Milone, A. Rubbino, S. Jannelli and Mezzanares, Nuovo Cim. 22, 135 (1961).

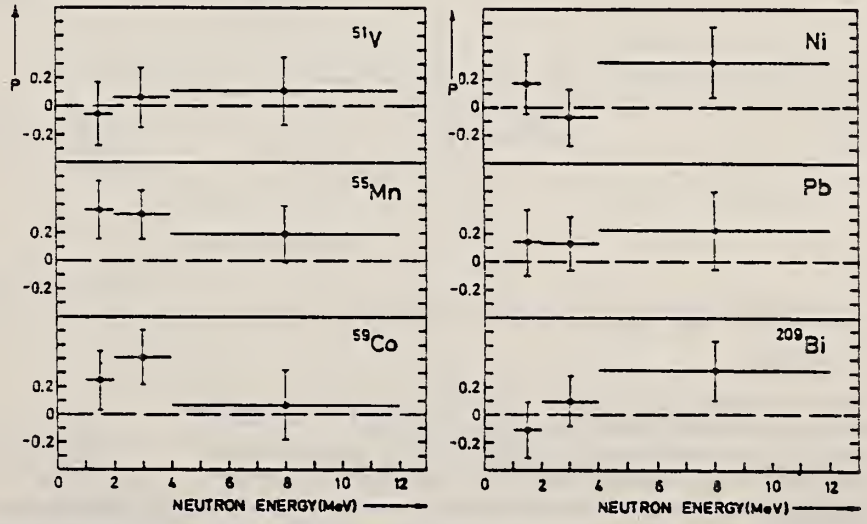

Fig. 7. Polarization of photoneutrons from ^{51}V, ^{55}Mn, ^{59}Co, natural Ni, natural Pb and ^{209}Bi.

REF. C. E. Rhoades, Jr., and H. A. Medicus
Phys. Rev. 167, 1049 (1968)

ELEM. SYM.	A	Z
Co	59	27

METHOD

REF. NO. 68 Rh 1 egf

REACTION	RESULT	EXCITATION ENERGY	SOURCE		DETECTOR		ANGLE
			TYPE	RANGE	TYPE	RANGE	
G,XN	NOX	THR-48	C	48	ACT-I		4PI

TABLE I. ^{59}Co isomer ratios.

Reaction	Reference	Bremsstrahlung endpoint energy (MeV)	Experimental isomer yield (ground-state/total)
^{59}Co(γ,n)	7	30	0.56±0.02
	8	30	0.55±0.02
	9	35	0.43±0.02
	This work	43	0.43±0.03
	9	54	0.43±0.02
	10	68	0.38±0.02
^{60}Ni(γ,np)	This work	48	0.68±0.03

REF.

R. Garfagnini, G. Piragino & A. Zanini
Atti Accad. Naz. Lincei, Rend.
Cl. Sci. Fis. Mat. Natur. 47, 33 (1969)

ELEM. SYM.	A	Z
Co	59	27

METHOD

REF. NO.	
69 Ga 3	egf

REACTION	RESULT	EXCITATION ENERGY	SOURCE		DETECTOR		ANGLE
			TYPE	RANGE	TYPE	RANGE	
G,XN	SPC	11-85	C	85	CCH-D		135

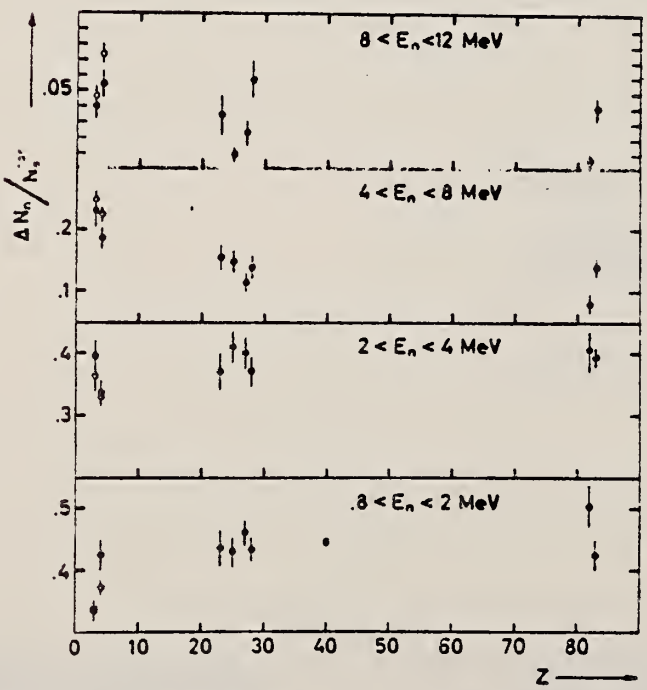

Fig. 1. – Percentage of the photoneutrons emitted at 135°, in the respective energy interval as a function of Z, by a γ-ray bremsstrahlung beam with $E_{\gamma max}$ = = 85 MeV. The open circles represent the values obtained at 60° for ^{7}Li and ^{9}Be.

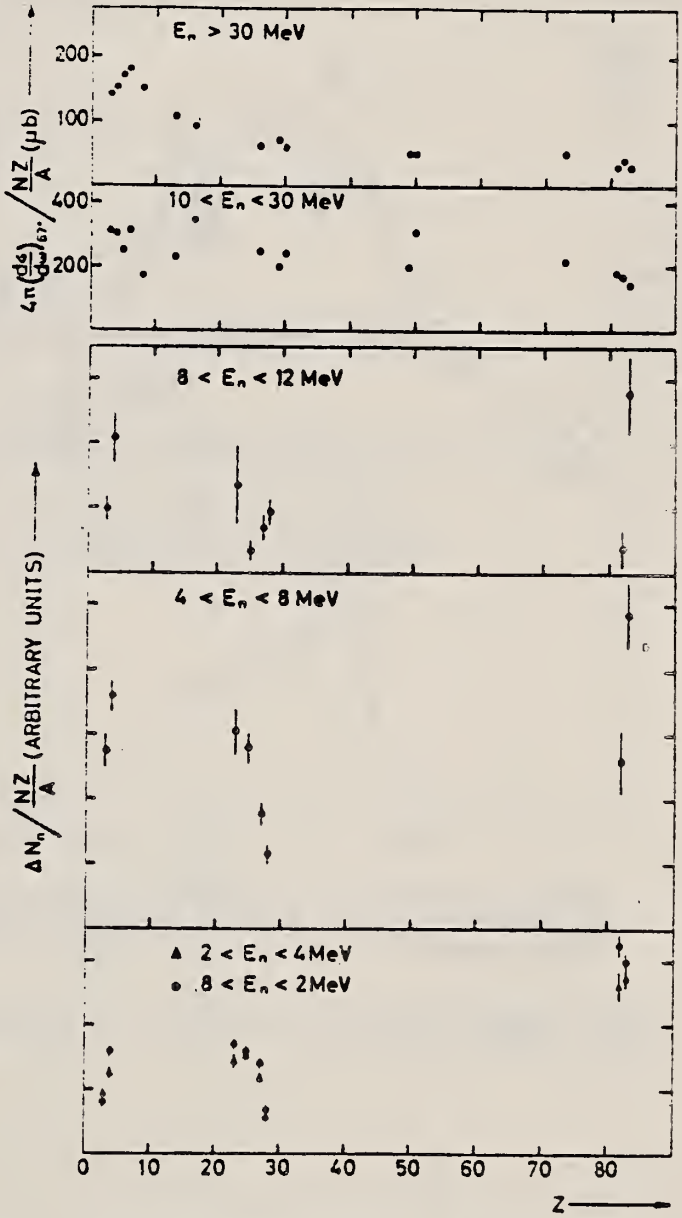

Fig. 2. – Number of photoneutrons emitted at 135°, normalized to the sum rule factor NZ/A, as a function of Z. In the upper part is reported the effective cross section divided by NZ/A for photoproduction of fast neutrons by 55–85 MeV bremsstrahlung photons as deduced by Kaushal *et al.* [1].

[1] N.N. Kaushal et al., Phys. Rev. 175, 557 1330 (1968).

B.I. Goryachev, B.S. Ishkhanov, I.M. Kapitonov, I.M. Piskarev, V.G. Shevchenko & O.P. Shevchenko
Izv. Akad. Nauk. Fiz. 33, 1736 (1969)
Bull. Acad. Sci. USSR-Phys. 33, 1588

Co	59	27

METHOD

REF. NO. 69 Go 3 hmg

REACTION	RESULT	EXCITATION ENERGY	SOURCE		DETECTOR		ANGLE
			TYPE	RANGE	TYPE	RANGE	
G,XN	ABX	10-30	C	10-30	BF3-I		4PI

450

450

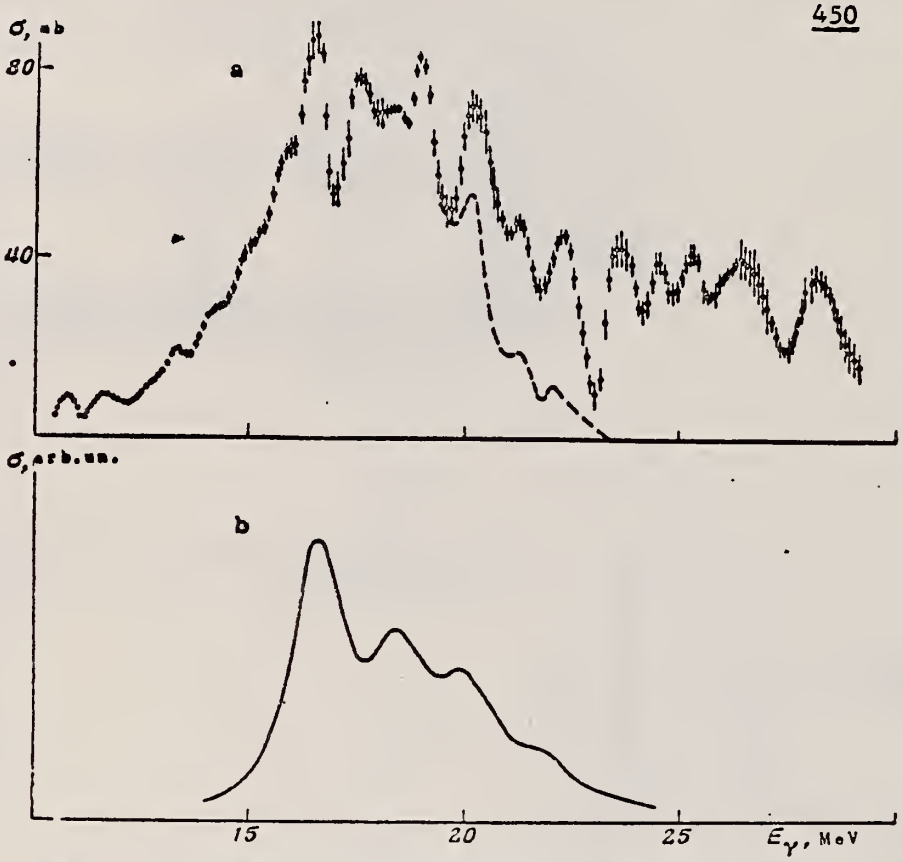

Fig.3. a - The $(\gamma,n) + (\gamma,2n)$ cross section for ^{59}Co, b - absorption cross section implied by the collective dynamic model[6].

[6] M.G. Huber, M. Danos, H.J. Weber & W. Greiner, Phys. Rev. 155, 1073 (1967).

(over)

Characteristics of the Photoneutron Cross Sections (in MeV-mb)

Nuclei	Integral cross sections*				Center of gravity $\sigma(\gamma n)+\sigma(\gamma, 2n)$, MeV	Refs.	Dipole sum rule $60NZ/A$, MeV·mb
	$\sigma(\gamma n)+2\sigma(\gamma, 2n)$	$\sigma(\gamma n)+\sigma(\gamma, 2n)$	$\sigma(\gamma n)$	$\sigma(\gamma, 2n)$			
^{51}V	820 (30)	600 (30)	380 (30)	220 (30)	21,3	Our work	760
	670 (28)	560 28)	450 (28)	110 (28)		[9]	
	590 (24)					[10]	
	560 (25)					[11]	
^{52}Cr	950 (30)	740	530 (30)	210 (30)	20,4	Our work	775
	600 (24)					[10]	
^{59}Co	1030 (30)	740 (30)	450 (30)	290 (30)	20,2	Our work	880
	730 (28)	590 (28)	450 (28)	140 (28)		[9]	
	870 (29)					[12]	
	840 (25)					[13]	
	660 (28)					[14]	
	630 (25)					[11]	

*The upper integration limits are given in parentheses.

9. S.C.Fultz, R.L.Bramblett, I.T.Caldwell, N.E.Hansen & C.P.Jupiter, Phys. Rev. 128, 2345 (1962).

10. J.Goldemberg & L.Katz, Canadian J. Phys. 32, 49 (1954).

11. B.Nathans & J.Halpern, Phys. Rev. 93, 437 (1954).

12. E.B.Bazhanov, A.P.Komar & A.V.Kulikov, Zh. Eksperim. i teor. fiz. 46, 1497 (1964). (Trans. Soviet Physics - JETP.)

13. P.A.Flournoy, R.S.Tickle & W.D.Whitehead, Phys. Rev. 120, 1424 (1960).

14. G.Baciu, G.C.Bonazzola, B.Minetti, C.Molino, L.Pasqualini & G.Piragino, Nuclear Phys. 68, 178 (1965).

REF. G. Baciu, D. Catana, C. Deberth, C. Iliescu, B. Carstoiu
Nucl. Phys. A167, 177 (1971)

ELEM. SYM.	A	Z
Co	59	27

METHOD

REF. NO. 71 Ba 1 egf

REACTION	RESULT	EXCITATION ENERGY	SOURCE TYPE	SOURCE RANGE	DETECTOR TYPE	DETECTOR RANGE	ANGLE
G,XN 251+	ABX	10-22	C	10-22	BF3-I		4PI

247+

TABLE 1
Results

E_m (MeV)		σ_m (mb)		$\int_0^x \sigma(w)dw$ (mb · MeV)	Ref.
16.9		130		750 (24)	[18]
16.75	19	110	103	709 (25)	[19]
17.5		68		725 ±72 (28)	[20]
16.5	19	82	80	701 ±91 (29)	[21]
16.5	19	72	74	657 ±89 (28)	[22]
17.44	19.29	120.0	102.9	598.7± 0.9 (22)	this work

Here σ_m is the peak value of the cross section, E_m is the peak energy and $\int_0^x \sigma(w)dw$ is the integrated cross section. The upper limit of the integration is indicated in parentheses.

[16] M.G. Huber, M. Danos, H.J. Weber and W. Greiner, Phys. Rev. 155 (1967) 1073

[18] R. Montalbetti, L. Katz and J. Goldemberg, Phys. Rev. 91 (1953) 659

[19] P.A. Flurnoy, R.S. Ticle and W.D. Whitehead, Phys. Rev. 120 (1960) 1424

[20] S.C. Fultz, R. L. Bramblett, J. T. Caldwell, N.E. Hansen and C.P. Jupiter, Phys, Rev. 128 (1962) 2345

[21] E.B. Bazhanov, A.P. Komar and A.V. Kulikov, JETP (Sov. Phys.) 46 (1964) 1497

[22] G. Baciu, G.C. Bonazzola, B. Minetti, C. Molino, L. Pasqualini and G. Piragino, Nucl. Phys. 67 (1965) 178

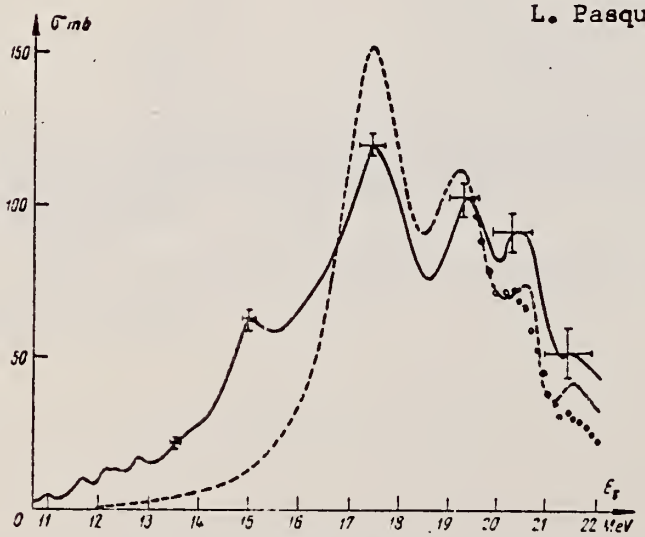

Fig. 1. Least-structure solution for $^{59}Co(\gamma, \Sigma n)$ cross section (full line). The statistical errors and resolution are shown at representative energies (at cross-section peak values). The points at higher energies represent an estimate for multiplicity correction. The dashed line illustrates the calculation by using the appropriate parameters [16].

U.S. DEPARTMENT OF COMMERCE
NATIONAL BUREAU OF STANDARDS

REF. G. J. Kumbartzki, Ung Kim and Ch. K. Kwan
Nucl. Phys. A160, 237 (1971)

ELEM. SYM.	A	Z
Co	59	27

METHOD

REF. NO. 71 Ku 2 egf

REACTION	RESULT	EXCITATION ENERGY	SOURCE		DETECTOR		ANGLE
			TYPE	RANGE	TYPE	RANGE	
G,SPL	ABY	THR-999	C	999	ACT-I		4PI

$\sigma_q(A,Z) = K\exp\left[PA-R(A-SZ+TZ^2)^2\right]$, cross section per equivalent quantum. 999 = 1.5 GEV

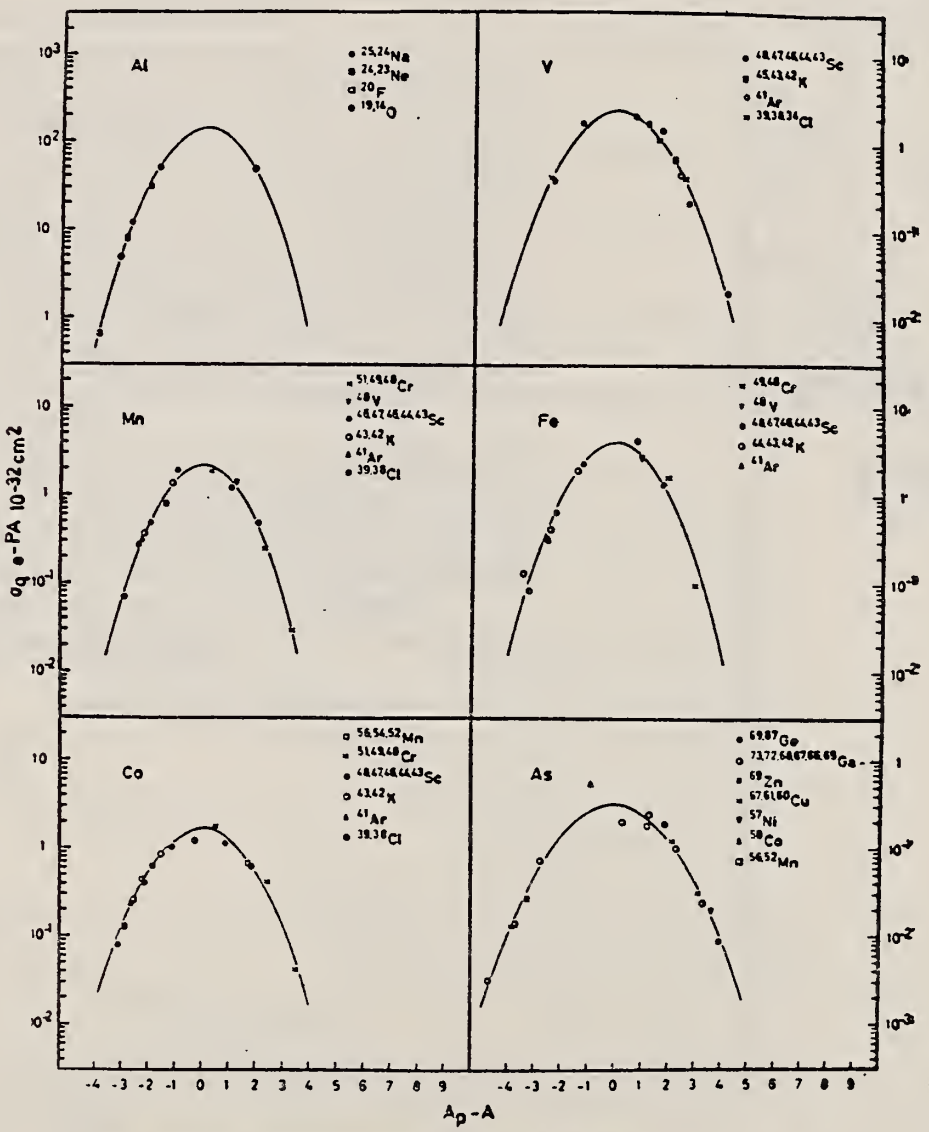

Fig. 4. Yield distributions from various targets with bremsstrahlung of 1.5 GeV.

[over]

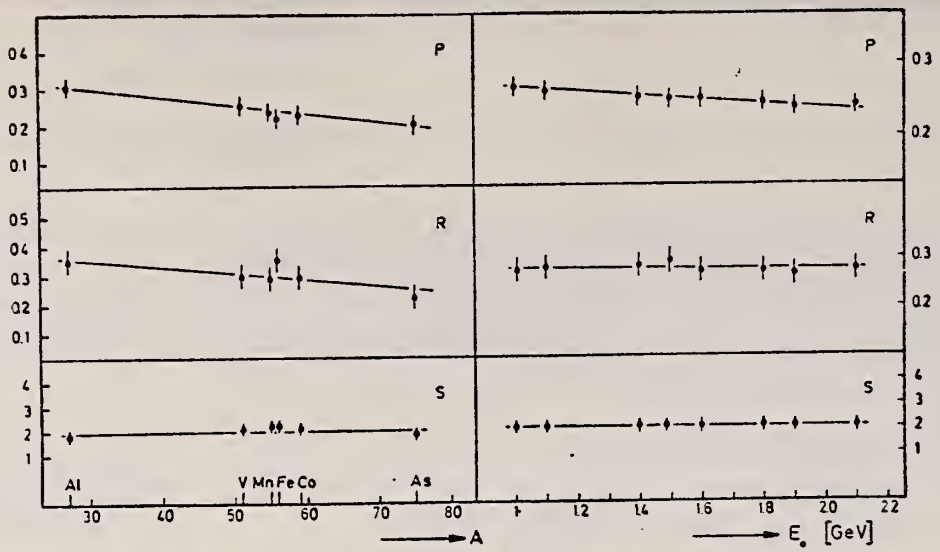

Fig. 6. Behaviour of the parameters P, R and S as functions of A and E_0.

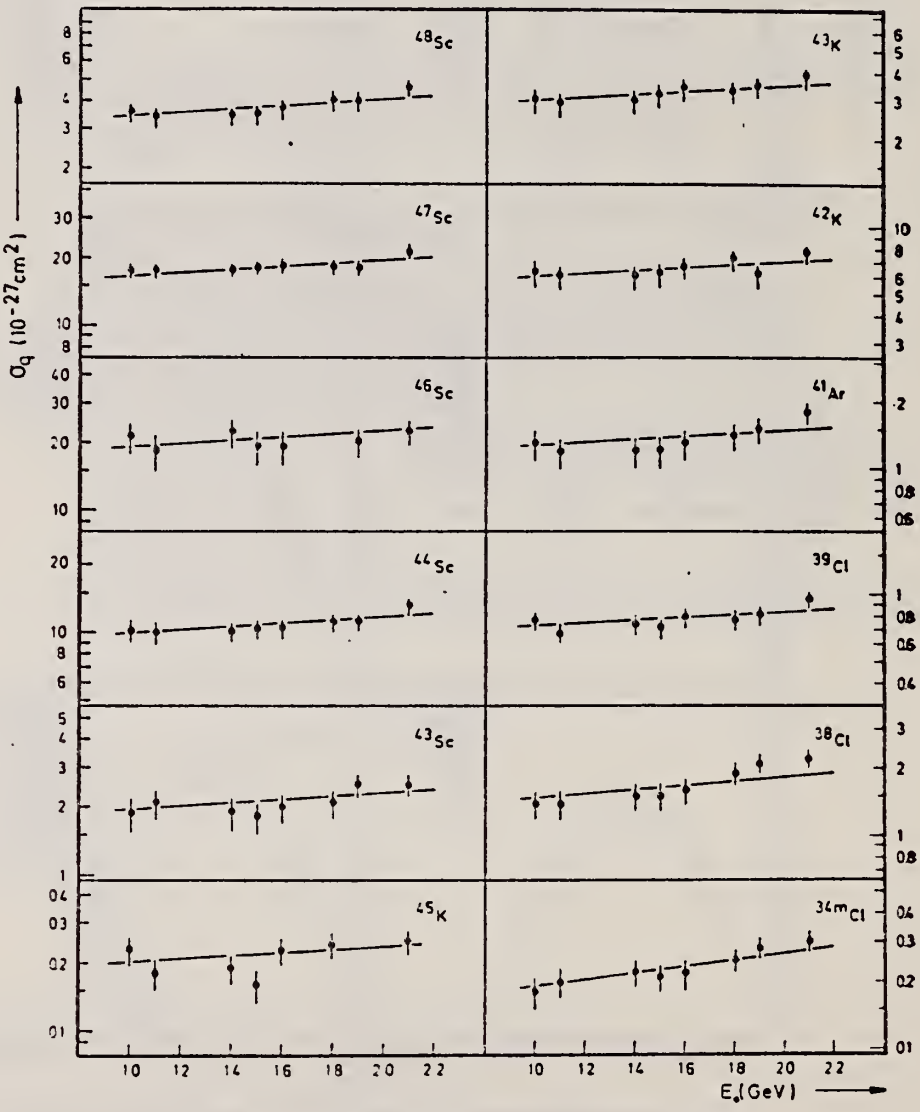

Fig. 5. Yields of spallation products using vanadium targets.

REF.

Tatsuya Saito
Nippon Kagaku Zasshi 92, 164 (1971)

ELEM. SYM.	A	Z
Co	59	27

METHOD

REF. NO. 71 Sa 1 egf

REACTION	RESULT	EXCITATION ENERGY	SOURCE		DETECTOR		ANGLE
			TYPE	RANGE	TYPE	RANGE	
G,N	ABY	10-68	C	10-68	ACT-I		4PI

Nippon Kagaku Zasshi, 92, 164~168(1971)

The Yields of Radioactivities Induced by (γ, n) Reactions with Bremsstrahlung up to 68 MeV

by Tatsuya SAITO

The (γ, n) yields of 12 target nuclides have been measured at 10, 13, 16, 30, 45 and 68 MeV bremsstrahlung by observing the induced activities.

The energy dependence of the yields has been investigated extensively in the same way as in the previous work at 20 MeV bremsstrahlung.

In the case of heavy nuclides, the yields rise greatly as a function of maximum bombarding energy up to 20 MeV, and rise gradually from 20 MeV up to 68 MeV. However, in the case of light nuclides, the yields rise greatly up to 30 MeV, because the neutron separation energies of light ones are larger than those of heavy ones, and the bremsstrahlung spectrum covers the giant resonance and so the yields rise gradually from 30 MeV up to 68 MeV.

The yields have approximately been estimated from the parameter of the giant resonance, that is the peak cross section and the half width, in order to compare with the experimental data. As a result, the experimental data of light nuclides and heavy ones are nearly in agreement with the estimated data of Nathans et al., Johns et al. and Montalbetti et al., but those of medium weight ones are relatively lower values.

Department of Chemistry, Faculty of Science, Tohoku University; Katahira-cho, Sendai-shi, Japan

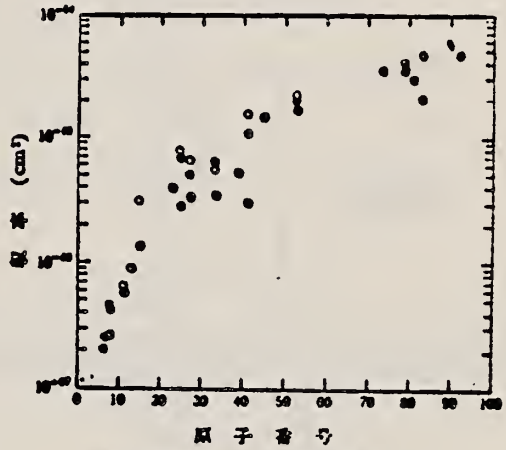

●: 実験値, ⊕: Johns ら,
◑: Nathans ら, ○: Monlalbetti ら

図 4 (γ, n)反応の収率の比較

C. P. Swann
Nucl. Phys. A172, 569 (1971)

ELEM. SYM.	A	Z
Co	59	27

METHOD

REF. NO.	
71 Sw 3	egf

REACTION	RESULT	EXCITATION ENERGY	SOURCE		DETECTOR		ANGLE
			TYPE	RANGE	TYPE	RANGE	
G,G	LFT	1-5	C	5	SCD-D		DST

15 LEVELS, J-PI

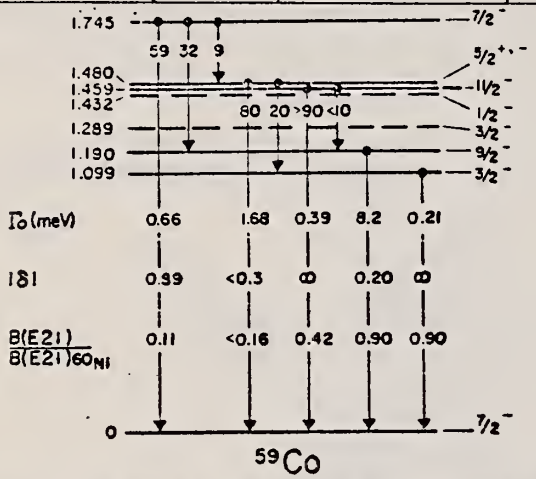

Fig. 4. Decay scheme of the first five levels observed in ^{59}Co. Also given are the ground state transition widths, the amplitude mixing ratios and the $B(E2\downarrow)$ values relative to that for the 1330 keV state of ^{60}Ni.

Table 1
Properties of the observed levels

Level (keV)	J^π	$W(\theta)g\,\Gamma_0^2/\Gamma$ [a] (meV)	Γ_0/Γ [b]	Γ_0 (meV) present	Γ_0 (meV) others	$\lvert\delta\rvert$ present	$\lvert\delta\rvert$ others
1098.7±0.5	$\frac{3}{2}^-$	0.11±0.02	1.0	0.21±0.04	0.12±0.03 [c]		
1189.6±0.5	$\frac{3}{2}^-$	10.25±0.50	1.0	8.2 ±0.4	8.2 ±1.0 [c]	0.16±0.09	0.20 [c]) 0.25±0.05 [b])
1458.8±0.3	$\frac{1}{2}^-$	0.62±0.06 [a])	> 0.9	0.39±0.04	0.44±0.08 [a])		
1480.4±0.3	$\frac{1}{2}^{+,-}$	1.06±0.11 [d])	0.8	1.68±0.17		< 0.35	
1745 ±1	$\frac{7}{2}^-$	0.39±0.12	0.59	0.66±0.19			$0.89^{+0.33}_{-0.17}$ [b])
2479 ±1		11.5 ±0.5 [d])	> 0.9				
2783 ±1		15.0 ±1.0					
2825 ±1	$(\frac{1}{2}^-)$ [e])	4.8 ±0.6					
2966 ±1		2.7 ±0.8					
3328 ±2		6.2 ±1.2					
3625 ±2		8.5 ±2.2					
3667 ±2		16.6 ±2.4					
3954 ±3		12.3 ±2.4					
4303 ±3		17.1 ±4.7					
4467 ±3		42.2 ±6.3					

[a]) Errors given in this column are statistical and do not include an estimated error of 10 % on $N(E_\gamma)$.
[b]) See ref. [4]).
[c]) See ref. [3]).
[d]) Booth *et al.* [22]) observed lines at about 1.47 and 2.5 MeV. The cross sections they give agree well with the values we obtained for the combined 1.459 and 1.480 MeV levels and for the 2.479 MeV level respectively.
[e]) See ref. [20]).

[3] R. Nordhagen, B. Elbek and B. Herskind, Nucl. Phys. A104, 353 (1967).
[4] K. L. Coop, I. G. Graham and E. W. Titterton, Nucl. Phys. A150, 346 (1970).
[20] M. Mazari, A. Sperduto and W. W. Buechner, Phys. Rev. 107, 365 (1957)
[22] E. C. Booth, B. Chasan and K. A. Wright, Nucl. Phys. 57, 403 (1964).

REF.

N. A. Keller and D. B. McConnell
Can. J. Phys. 50, 1554 (1972)

ELEM. SYM.	A	Z
Co	59	27

METHOD

REF. NO.	
72 Ke 4	hmg

REACTION	RESULT	EXCITATION ENERGY	SOURCE		DETECTOR		ANGLE
			TYPE	RANGE	TYPE	RANGE	
G,A	RLY	7-32	C	32	SCD-D		DST

TABLE 3. Observed angular distribution parameters for 32 MeV electron energy

Element	A_0	A_1/A_0	A_2/A_0
Ti	7.03 ± 0.15	0.073 ± 0.052	−0.286 ± 0.073
V	2.58 ± 0.06	0.037 ± 0.042	−0.126 ± 0.069
Fe	10.22 ± 0.30	0.006 ± 0.043	−0.333 ± 0.072
Co	6.80 ± 0.20	0.022 ± 0.048	+0.016 ± 0.077
Ni	15.95 ± 0.49	0.051 ± 0.048	−0.213 ± 0.074
Cu	8.37 ± 0.28	0.076 ± 0.056	−0.035 ± 0.081
Zn	17.87 ± 0.61	0.004 ± 0.045	−0.270 ± 0.073
Ag	0.39 ± 0.01	0.115 ± 0.049	+0.093 ± 0.074

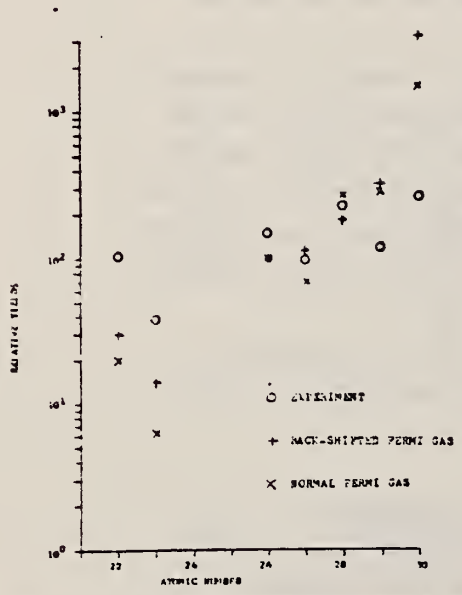

FIG. 13. Experimental and theoretical relative photo-alpha yields for 32 MeV electron beam energy.

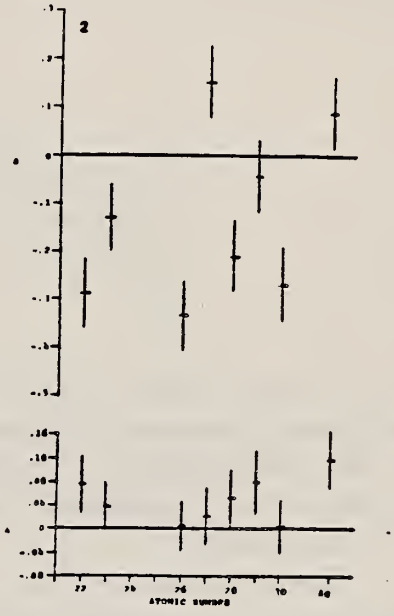

FIG. 2 Angular distributions for 32 MeV electron energy.

REF. R.A. Alvarez, B.L. Berman, F.H. Lewis, P. Meyer
PICNS-73, Vol.I, p.547 Asilomar

ELEM. SYM.	A	Z
Co	59	27

METHOD

REF. NO. 73 A1 7 hmg

REACTION	RESULT	EXCITATION ENERGY	SOURCE TYPE	SOURCE RANGE	DETECTOR TYPE	DETECTOR RANGE	ANGLE
G,N	ABX	10- 37	D	10- 37	BF3-I		4PI
G,2N	ABX	17- 37	D	17- 37	BF3-I		4PI
G,3N	ABX	29- 37	D	29- 37	BF3-I		4PI

525†

We report here the results of measurements of the ^{59}Co photoneutron cross sections with nearly monoenergetic photons obtained simultaneously with those for ^{55}Mn reported in the preceding paper.[1] Our results are shown in Fig. 1. The error bars are statistical only; the systematic errors and photon energy resolution are the same as for the ^{55}Mn measurement.[1]

As was the case for ^{55}Mn, the giant resonance of ^{59}Co is very broad, with considerable strength in the region of 24 MeV in addition to the two main peaks near 17 and 19 MeV The latter both have peak cross sections of about 75 mb, about 10% larger than the peak value found in a previous low-resolution measurement at this laboratory.[2] Both the total photoneutron cross section and the (γ,2n) cross section (which has a peak value of 17 mb at 22 MeV) exhibit considerable fine structure, including a well-defined shoulder just above the (γ,n) threshold.

The integrated total photoneutron cross section, up to 36.5 MeV is 894 MeV mb, while that for the (γ,2n) reactions is 139 MeV mb. The (γ,3n) cross section, up to 37 MeV, is quite small, as indicated in Fig. 1d.

† Work performed under the auspices of the U. S. Atomic Energy Commission.

1 R. A. Alvarez, B. L. Berman, F. H. Lewis, P. Meyer: preceding paper.

2 S. C. Fultz, R. L. Bramblett, J. T. Caldwell, N. E. Hansen, and C. P. Jupiter, Phys. Rev. 128, 2345 (1962).

(over)

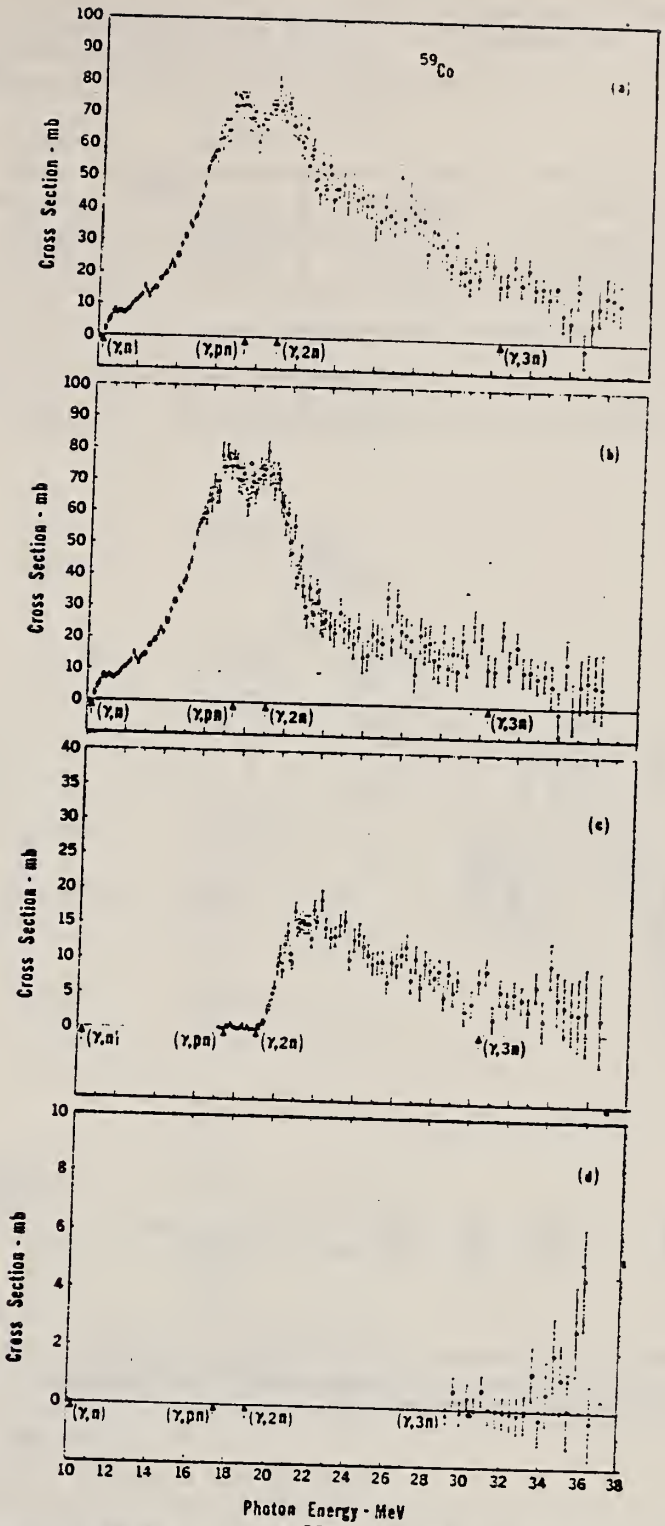

Figure 1. Photoneutron cross sections of ^{59}Co. Thresholds are indicated by arrows. (a) Total photoneutron cross section: $\sigma[(\gamma,n) + (\gamma,pn) + (\gamma,2n) + (\gamma,3n)]$; (b) $\sigma[(\gamma,n) + (\gamma,pn)]$; (c) $\sigma(\gamma,2n)$; (d) $\sigma(\gamma,3n)$.

R.F. Barrett, J.R. Birkelund, B.J. Thomas, K.S. Lam, and H.H. Thies
Nucl. Phys. A210 , 355 (1973)

Co	59	27

METHOD

REF. NO. 73 Ba 20 egf

REACTION	RESULT	EXCITATION ENERGY	SOURCE TYPE	SOURCE RANGE	DETECTOR TYPE	DETECTOR RANGE	ANGLE
G,N	NOX	THR- 27	C	10- 27	BF3-I		4PI

MEAN NEUT ENERGY

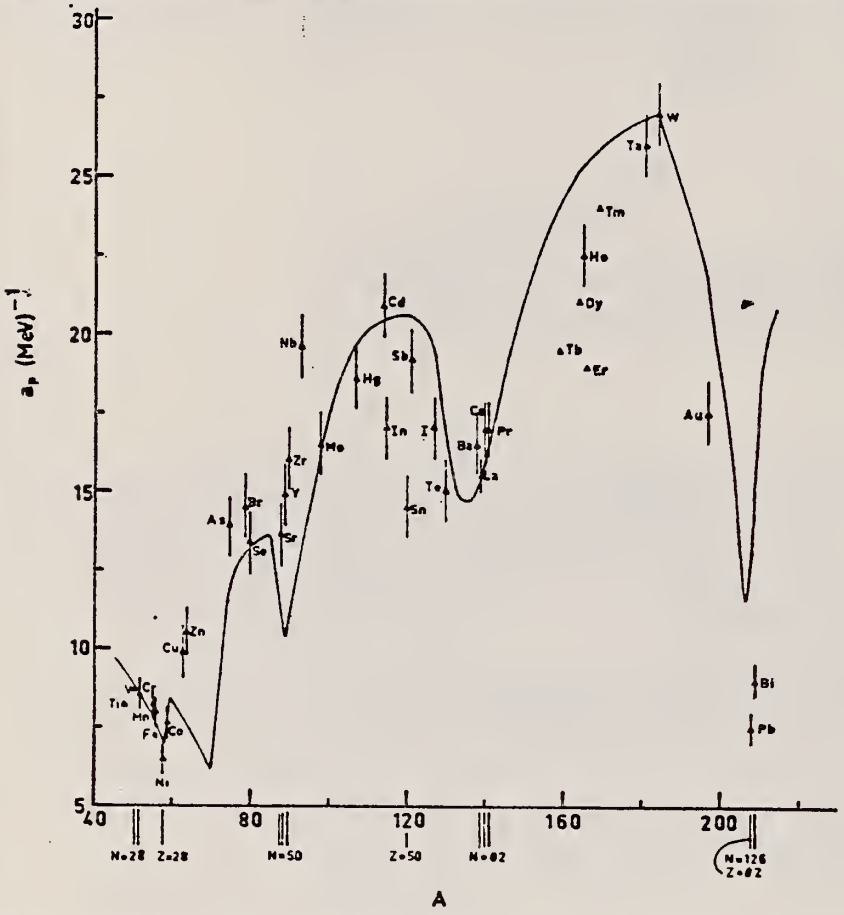

Fig. 12. Experimental values of the level density parameter a_p (Fermi gas formula plus pairing correction) versus atomic number A. The continuous curve is a least-squares fit to the data of a theoretical calculation from Newton [15].

1
H. Baba and S. Baba, Japan Atomic Energy Research Institute report JAERI-1183 (1969).
2
H. Baba, Nucl. Phys. A159, 625 (1970).
15
T.D. Newton, Can. J. Phys. 34, 804 (1956).

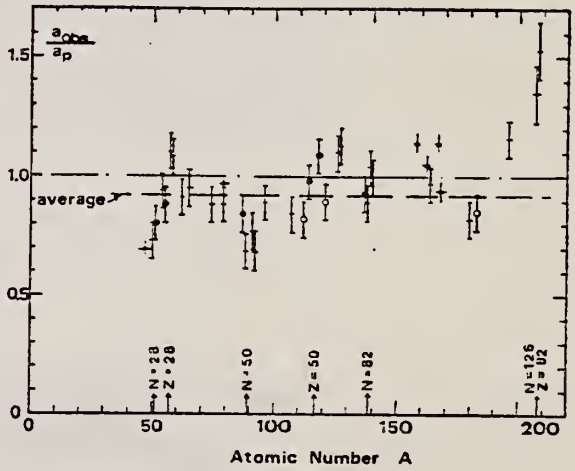

Fig. 15. Ratio a_{obs}/a_p versus atomic number A. Here a_{obs} is the level density parameter taken from the neutron resonance work of refs. [1,2]), and a_p is the level density parameter derived from the present (γ, n) work. Filled circles represent points where nuclei in the neutron resonance and in the (γ, n) experiment were the same. Open circles represent points where the respective nuclei were approximately matched. Triangles represent points which are based on measurement of neutron mean energies at two bremsstrahlung energies only.

(over)

TABLE 3

Comparison of experimental and theoretical data on nuclear level densities with Fermi gas formulae, and comparison of nuclear level density parameters from (γ, n) and n-resonance absorption experiments

Target	N (residual nucleus) [a]		Goodness of fit [b]		$\hat{E}_0(24)$ (MeV) [c]	T (MeV) [d]	a_p (MeV^{-1}) [e]	a_{obs} (MeV^{-1}) [f]	a_{obs}/a_p
			no p.c.	with p.c.					
Ti [g]	23	8%			1.93		8.1–^{47}Ti	6.41–^{47}Ti	0.79
	24	8%							
	25	73%							
	26	5%							
	27	5%							
V [g]	27	100%			1.96		8.7–^{50}V	6.35–^{51}V	0.73
Cr	25	4%	P	G	1.89		8.6–^{51}Cr	6.9 –^{51}Cr	0.80
	27	84%							
	28	10%							
	29	2%							
Mn	29	100%	V.P.	G	2.1		8.2–^{54}Mn	7.82–^{56}Mn	0.94
Fe	27	6%	F	G	1.96		8.0–^{55}Fe	7.06–^{55}Fe	0.88
	29	92%							
	30	2%							
Co	31	100%	P	F	2.12		7.7–^{58}Co	8.35–^{60}Co	1.08
Ni	29	68%	V.P.	P	2.04	1.4	6.5–$^{57.7}$Ni	7.19–^{59}Ni	1.10
($Z = 28$)	31	26%							
	32	1%							
	33	4%							
	35	1%							
Cu	33	69%	V.P.	P	1.78	1.0	9.8–^{62}Cu	8.90–^{64}Cu	0.91
	35	31%							
Zn	33	49%	F	F	1.61		10.5–$^{64.4}$Zn	10.0–^{65}Zn	0.95
	35	28%							
	36	4%							
	37	19%							
As	41	100%	V.P.	F	1.44		14.5–^{74}As	12.81–^{76}As	0.88
Se [g]	41	9%			1.39		13.3–^{78}Se	12.8 –^{78}Se	0.97
	42	8%							
	43	24%							
	45	50%							
	47	9%							
Br	43	45%	V.P.	V.P.	1.41		14.5–^{79}Br	12.69–^{80}Br	0.88
	45	49%							
Sr	47	10%	F	G	1.31		13.6–^{87}Sr	11.4 –^{87}Sr	0.84
	48	7%							
	49	83%							

[a]) Neutron numbers and abundances of respective residual nuclei in (γ, n) experiments.

[b]) These give an assessment of the goodness of fit of a calculated $\hat{E}_n$ versus E_0 curve to the observed data, using the Fermi gas level density formula both without and with pairing corrections.

[c]) Bremsstrahlung photoneutron mean energies $\hat{E}_n$ for peak bremsstrahlung energy $E_0 = 24$ MeV.

[d]) Nuclear temperature from fit with constant-temperature formula.

[e]) Level density parameter a_p derived from the present (γ, n) experiment, using a Fermi gas formula plus pairing correction, and corresponding residual nucleus (the atomic weight shown is the weighted average of atomic weights of the respective isotopes present).

[f]) As column 7, but using data on n-resonance absorption from refs. [1,2]).

[g]) Measurements of $\hat{E}_0(E_0)$ for these nuclei were made only for $E_0 = 21$, 23 and 24 MeV.

REF. M. Eriksson and G. G. Jonsson
PICNS-73, Vol.II, p.995 (1973) Asilomar

ELEM. SYM.	A	Z
Co	59	27

METHOD

REF. NO.	
73 Er 1	egf

REACTION	RESULT	EXCITATION ENERGY	SOURCE		DETECTOR		ANGLE
			TYPE	RANGE	TYPE	RANGE	
G,SPL	NOX	0-800	C	100-800	ACT-I		4PI

SC-44 ISOMER RATIO

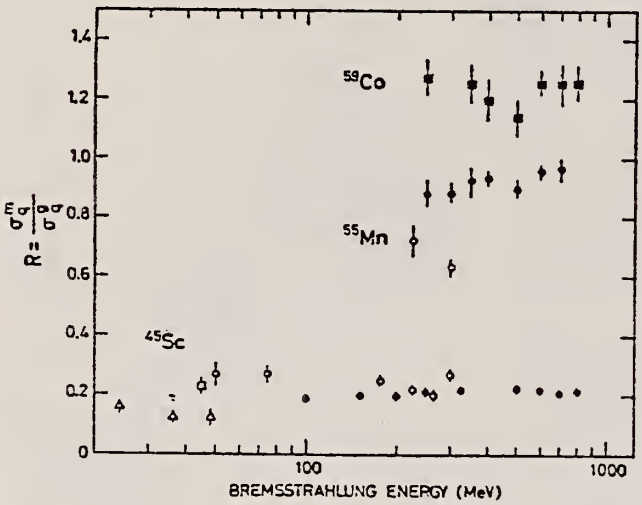

Isomeric yield ratio, $^{44}Sc^{m}(6+)/^{44}Sc^{g}(2+)$, versus bremsstrahlung end point energy.
●, ■ this work, Δ ref 1, O ref 2, □ ref 3.

[1] J.R. Tatarczuk and H.A. Medicus, Phys. Rev. 143 (1966) 818.
[2] W.B. Walters and J.P. Hummel, Phys. Rev. 150 (1966) 867.
[3] R. Völpel, Nucl. Phys. A182 (1972) 311.

REF. A. Järund, B. Friberg, and B. Forkman
Z. Physik 262, 15 (1973)

ELEM. SYM.	A	Z
Co	59	27

METHOD

REF. NO. 73 Ja 3 egf

REACTION	RESULT	EXCITATION ENERGY	SOURCE TYPE	SOURCE RANGE	DETECTOR TYPE	DETECTOR RANGE	ANGLE
G,NA24	ABY	THR-999	C	100-999	ACT-I		4PI

999=1 GEV

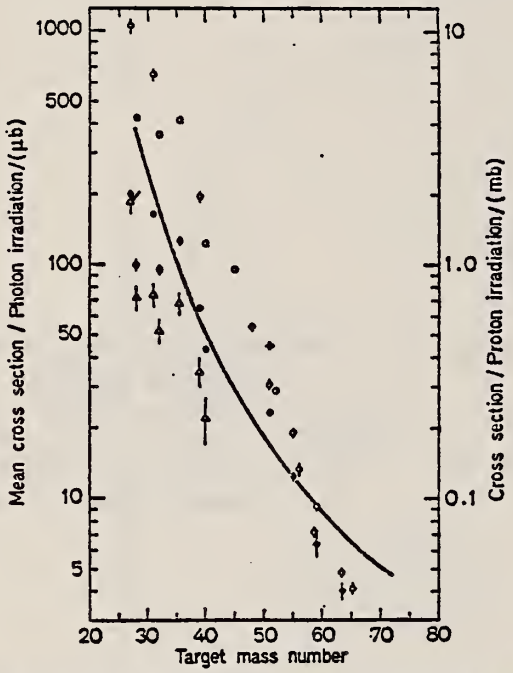

Fig. 7. Mean cross sections for ^{24}Na production as a function of target mass number. Present work filled circles. Noga *et al.* [3] open triangles, Kumbartzki *et al.* [13] cross and Korteling *et al.* [1] 400 MeV protons open circles. The solid line gives the mean cross sections calculated by Jonsson *et al.* [17]

[1] Korteling, R.G. et al., J. Inorg. Nucl. Chem. 29, 2863 (1967).

[3] Noga, V.I. et al., Sov. J. Nucl. Phys. 9, 637 (1969).

[13] Kumbartzki, G. et al., Nucl. Phys. A176, 23 (1971).

[17] Jonsson, G.G. et al., LUNP7212, Oct. 1972, to be published in Physica Scripta.

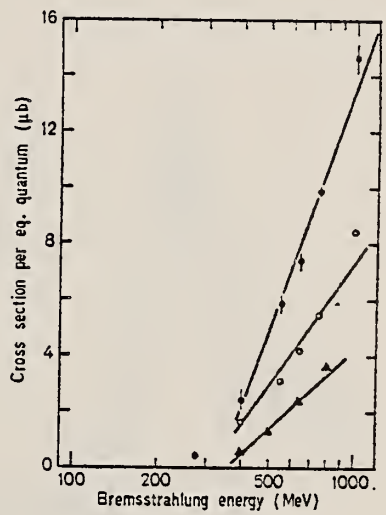

Fig. 6

Fig. 6. The determined yields for the reactions ^{55}Mn → ^{24}Na (filled circles), ^{59}Co → ^{24}Na (open circles) and ^{63,65}Cu → ^{24}Na (filled triangles)

REF. A.I. Abramov, V.Ya. Kitaev, and M.G. Yutkin
Izv. Akad. Nauk SSSR. Ser. Fiz. 38, 2112 (1974)
Bull. Acad. Sci. USSR Phys. Ser. 38, 85 (1974)

ELEM. SYM.	A	Z
Co	59	27

METHOD

REF. NO.	
74 Ab 12	hmg

REACTION	RESULT	EXCITATION ENERGY	SOURCE		DETECTOR		ANGLE
			TYPE	RANGE	TYPE	RANGE	
G,N	ABX	10- 13	C	11, 13	TOF-D		78
		(10.5-12.5)		(11.5-12.5)			

TABLE 3

Energy Levels of ^{59}Co

E_L^0, keV	E_c, keV	E, MeV*	E_L^0, keV	E_c, keV	E, MeV*	E_L^0, keV	E_c, keV	E, MeV*
2,06	2,02	10,4622	7,83	7,79	10,4680	20,5	20,6	10,4808
2,34	2,29	10,4625	9,3	9,3	10,4695	23,9	24,0	10,4842
2,53	2,53	10,4627	11,6	11,6	10,4718	29,4	29,6	10,4898
2,84	2,79	10,4630	15,1	15,1	10,4753	45,5	45,8	10,5060
3,60	3,55	10,4638	16,2	16,2	10,4764	75,2	75,8	10,5360
4,70	4,65	10,4649						

*On the assumption that all the observed resonances correspond to transitions to the ground state of ^{58}Co, for which Q_n = 10.4602 MeV [9].

[9] N.B. Gove et al., Nucl. Data Tables, Vol. II, 127 (1972).

TABLE 4

Parameters of the 3.6 keV Resonance of ^{59}Co

E_L^0, keV	σ_m, mbarn	Γ, ev	$g_\gamma\Gamma_{\gamma 0}$, ev
3,6	54,8±9,6	915±92	1,27±0,23

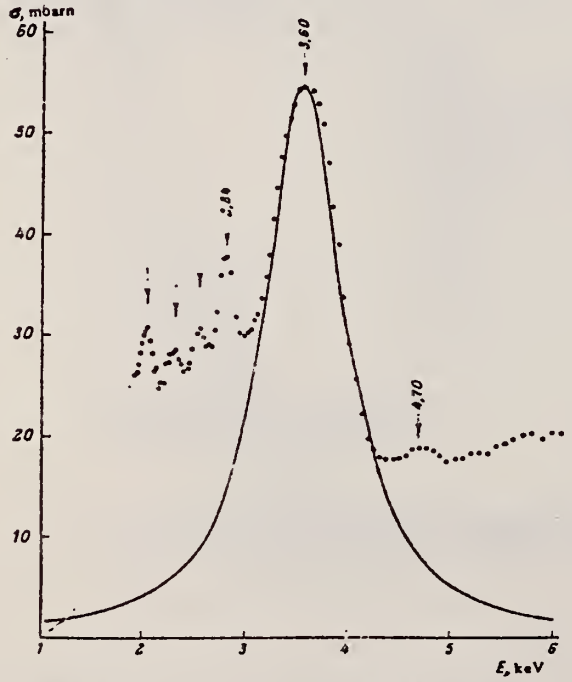

Fig. 5. Differential (γ, n) cross sections for cobalt measured at E_γ^{max} = 11.5 MeV at 78° and multiplied by 4π.

U.S. DEPARTMENT OF COMMERCE
NATIONAL BUREAU OF STANDARDS

REF.

P. David, J. Debrus, F. Lubke, H. Mommsen, R. Schoenmackers, and G. Stein
Nucl. Phys. A221, 145 (1974)

ELEM. SYM.	A	Z
Co	59	27

METHOD

REF. NO.	
74 Da 2	egf

REACTION	RESULT	EXCITATION ENERGY	SOURCE		DETECTOR		ANGLE
			TYPE	RANGE	TYPE	RANGE	
G,P	ABY	10-450	C	450	TEL-D		90
G,T	ABY	22-450	C	450	TEL-D		90
G,HE*	ABY	30-450	C	450	TEL-D		90
G,A	ABY	17-450	C	450	TEL-D		90

* HE=HE3

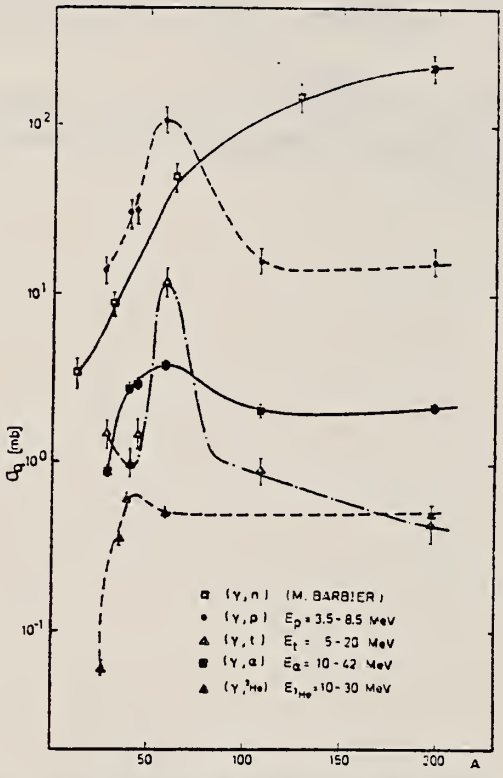

Fig. 5. Yield of protons, tritons, ^{3}He and ^{4}He depending on mass number A [ref. [23]]. The lines through the points are to guide the eye.

23) M. Barbier, Induced Radioactivity (North-Holland, Amsterdam, 1969)

(over)

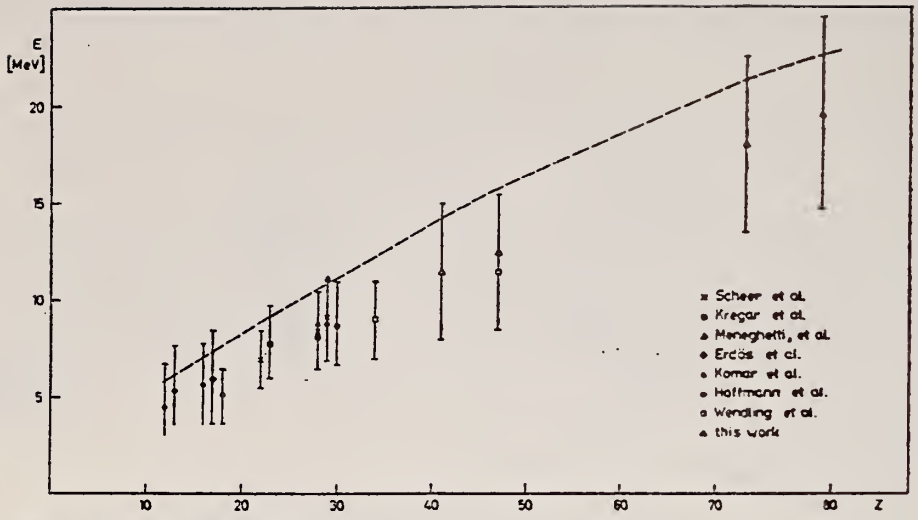

Fig. 8. The position of maxima of the (γ, α) spectra and the width of the spectra at half height. The broken line gives the height of the Coulomb barrier.

REF. M. Boivin, Y. Cauchois, Y. Heno, C. Schloesing-Moller, V. Zecevic
C.R. Acad. Sc. Paris 281B, 201 (1975)

ELEM. SYM.	A	Z
Co	59	27

METHOD

REF. NO. 75 Bo 11 egf

REACTION	RESULT	EXCITATION ENERGY	SOURCE		DETECTOR		ANGLE
			TYPE	RANGE	TYPE	RANGE	
G,G	LFT	1	C	2	UKN		UKN

1190 KEV

TABLEAU

Niveau....	^{63}Cu 670	^{65}Cu 771	^{63}Cu 962	^{65}Cu 1115	^{115}In 1133	^{59}Co 1190
τ(ps).....	0,28 ± 8 %	0,15 ± 12,5 %	0,76 ± 15 %	0,38 ± 14 %	0,094 ± 4,5 %	0,074 ± 3 %

REF. M. Eriksson and G. G. Jonsson
Nucl. Phys. A242, 507 (1975)

ELEM. SYM.	A	Z
Co	59	27

METHOD

REF. NO. 75 Er 2 egf

REACTION	RESULT	EXCITATION ENERGY	SOURCE		DETECTOR		ANGLE
			TYPE	RANGE	TYPE	RANGE	
G,SC44	ABY	THR-800	C	250-800	ACT-I		4PI

ISOMER RATIO

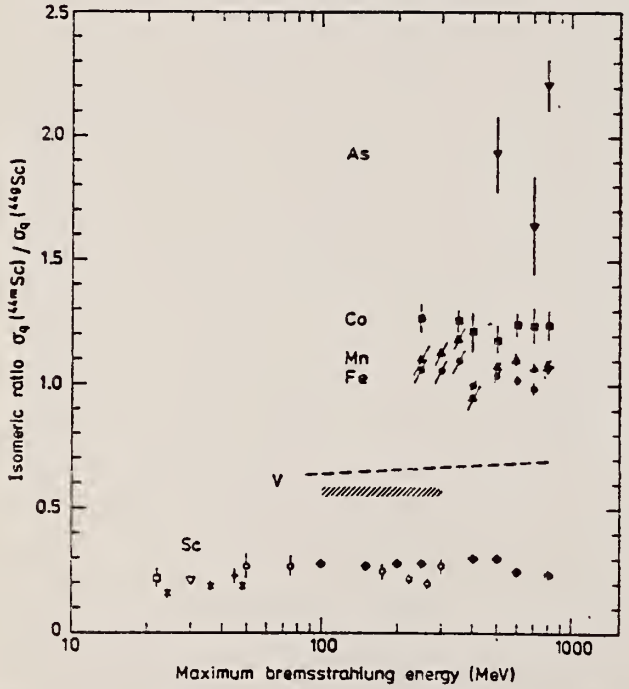

Fig. 6. Isomeric ratio $\sigma_q(^{44m}Sc)/\sigma_q(^{44g}Sc)$ versus bremsstrahlung end-point energy for the different targets. Sc target: ◆ – this work, □ – ref. [15]), × – ref. [16]), ▽ – ref. [17]), + – ref. [18]), ○ – ref. [19]); V target: dashed curve – ref. [20]), dashed area – ref. [21]); Fe target: ● – this work; Mn target: ▲ – this work; Co target: ■ – this work; As target: ▼ – this work.

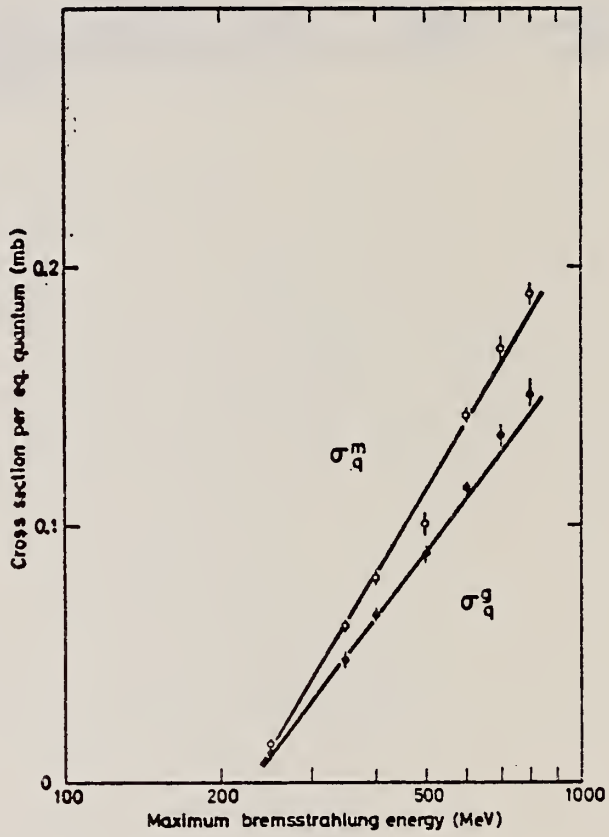

Fig. 5. Yield curves for the reaction $^{59}Co(\gamma, 6p9n)^{44}Sc$.

(over)

TABLE 2

Comparison between experimental and calculated cross sections and isomeric ratios

Target	$\tilde{\sigma}_{exp}$ (mb) 250–800 MeV	σ_{MC} (mb) 400 MeV	$\tilde{\sigma}_{SE}$ (mb) 250–800 MeV	$\sigma(m)/\sigma(g)_{exp}$ 250–800 MeV	$\sigma(m)/\sigma(g)_{calc}$ 400 MeV
^{45}Sc	≈ 0.5	0.58 ± 0.05		≈ 0	0.05
^{51}V	≈ 0.5	0.48 ± 0.05	0.47	0.7	0.72
^{55}Mn	0.40 ± 0.14	0.59 ± 0.05	0.28	1.08 ± 0.04	1.04
Fe	0.40 ± 0.14		0.26	1.00 ± 0.05	
^{59}Co	0.26 ± 0.10	0.34 ± 0.04 0.65 ± 0.07 [a])	0.18	1.26 ± 0.06	1.12 1.15 [a])
^{75}As		0.01 ± 0.01	0.044	1.9 ± 0.3	

[a]) 325 MeV.

15) S. A. Steinberg, B. Sc. thesis, Univ. of Illinois, 1963, unpublished (value taken from ref. [19]))
16) J. R. Tatarczuk and H. A. Medicus, Phys. Rev. 143 (1966) 818
17) T. Kato and Y. Oka, Talanta 19 (1972) 515
18) R. Völpel, Nucl. Phys. A182 (1972) 411
19) W. B. Walters and J. P. Hummel, Phys. Rev. 150 (1966) 867
20) B. Bülow, Lund, private communication (preliminary results)
21) R. A. Meyer, thesis, Univ. of Illinois, 1963, unpublished

REF.

C. O. Wene
Z. Phys. A272, 77 (1975)

ELEM. SYM.	A	Z
Co	59	27

METHOD

REF. NO.	
75 We 4	egf

REACTION	RESULT	EXCITATION ENERGY	SOURCE		DETECTOR		ANGLE
			TYPE	RANGE	TYPE	RANGE	
G,P	ABX	18	D	18	SCD-D		90

18 = 17.6 MEV

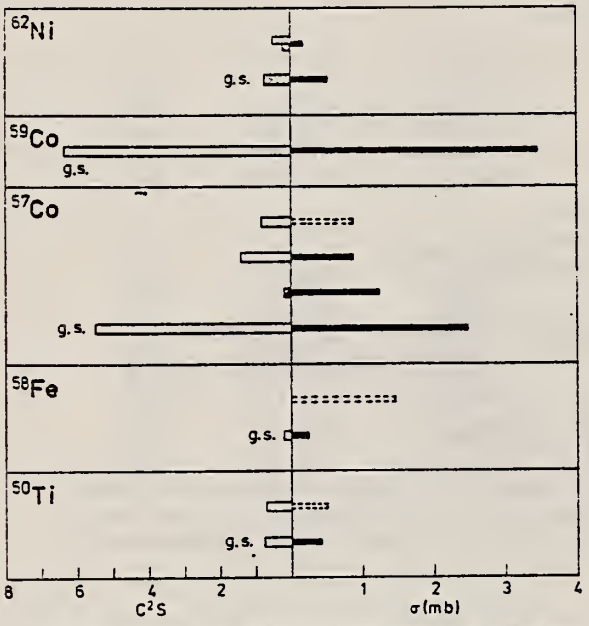

Fig. 5. Correlation between the spectroscopic factors and the cross-sections measured in this work. Open staples indicate $\ell_p = 3$ pick-up and cross hatched staples $\ell_p = 1$ pick-up. Dashed staples indicate that the cross section is uncertain due to the subtraction of a large back-ground

Table 2

Daughter nucleus	Level (MeV)	J^a	σ^a (mb)
^{44}Ca	0	0^+	$\leqq 0.2^b$
	1.16	2^+	$\leqq 0.5^b$
^{50}Ti	0	0^+	0.41 ± 0.05
	2.68	4^+	$(0.5)^c$
^{58}Fe	0	0^+	0.23 ± 0.08
	3.24?	0^+?	$(1.5)^c$
^{57}Co	0	$7/2^-$	2.5 ± 0.2^d
	1.76	$3/2^-$	1.2 ± 0.3
	1.90	$7/2^-$	0.9 ± 0.2
	2.31	$7/2^-$	$(0.9)^c$
^{59}Co	0	$7/2^-$	3.5 ± 0.8
^{62}Ni	0	0^+	0.51 ± 0.09
	1.18	2^+	0.2 ± 0.1

[a] The quoted errors are only those due to counting statistics.
[b] Confidence level 95%.
[c] Uncertain because of large background.
[d] $\sigma = 2.4$ mb from [43].

43. Miyase, H., Oikawa, S., Suzuki, A., Uegaki, J., Saito, T., Sugawara, M., Shoda, K.: The photoproton reactions of Ni-isotopes. In: Proc. Int. Conf. Photonuclear Reactions and Applications, Vol. I, p. 553. Livermore, USA 1973 (see Ref. 13)

REF. C.P. Cameron, N.R. Roberson, D.G. Rickel, R.D. Ledford, H.R. Weller, R.A. Blue, D.R. Tilley
Phys. Rev. C14, 553 (1976)

ELEM. SYM.	A	Z
Co	59	27

METHOD

REF. NO. 76 Ca 4 hmg

REACTION	RESULT	EXCITATION ENERGY	SOURCE		DETECTOR		ANGLE
			TYPE	RANGE	TYPE	RANGE	
$ P,G	ABX	12- 23	D	5- 15	NAI-D		DST

POLARIZED PROTONS

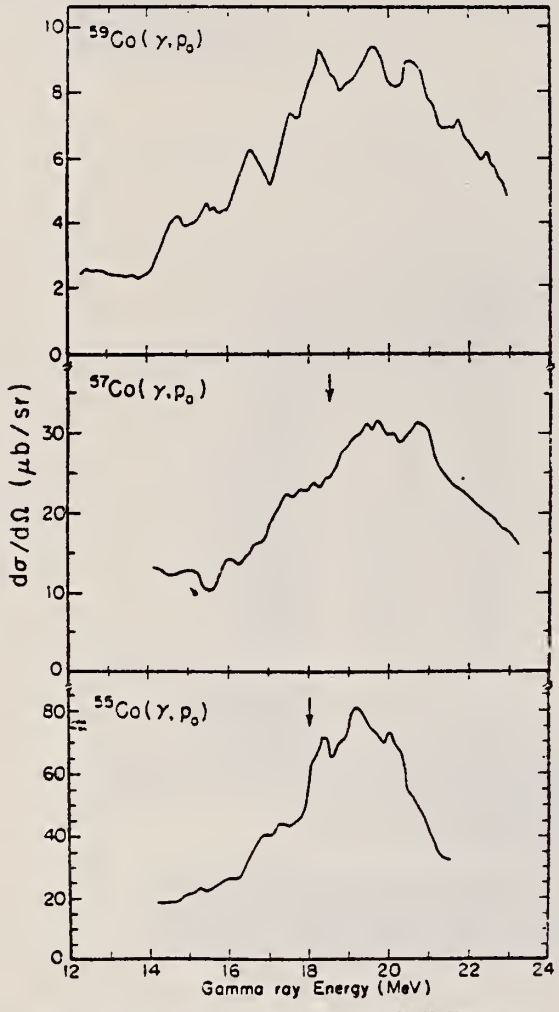

FIG. 3. The 90° yield curves for the $^{54,56,58}Fe(p,\gamma)$ reactions after averaging over a 500 keV interval. The arrows indicate the energy of the splitting between the $T_<$ and $T_>$ components of the GDR as suggested in Ref. 1.

$$\sigma(\theta)=a_0\left[1+\sum_k \frac{a_k}{a_0}Q_k P_k(\cos\theta)\right],$$

$$A(\theta)=\left(\frac{N_+-N_-}{N_++N_-}\right)\frac{1}{P}.$$ (Where N_+ and N_- are counts spin up and counts spin down.)

$$A(\theta)\sigma(\theta)/a_0=\sum_k b_k Q_k P_k^1(\cos\theta).$$

[1] J.V. Maher, L. Meyer-Schutzmeister, E.L. Sprenkel-Segel, D. von Ehrenstein, R.J. Nemanich, G.C. Kiang, J.F. Tonn, and R.E. Segel, Phys. C9, 1440 (1974).

(over)

TABLE III. The a and b coefficients obtained from least-square fits to the data as described in the text. Higher order coefficients are given only when the criterion of normalized χ^2 justified the use of higher order terms.

E_p (MeV)	a_1/a_0	a_2/a_0	a_3/a_0	b_1	b_2	b_3
			$^{54}Fe(\vec{p},\gamma_0)^{55}Co$			
8.0	0.26±0.06	0.11±0.11		−0.03±0.05	0.00±0.04	−0.02±0.04
9.0	0.20±0.05	0.09±0.10		−0.07±0.04		
10.0	0.25±0.04	0.03±0.07		0.02±0.03	−0.09±0.02	
11.0	0.10±0.03	0.24±0.05		0.03±0.02	−0.07±0.02	
12.1	0.27±0.05	0.18±0.04	0.18±0.07	0.01±0.01	−0.12±0.01	
13.0	0.01±0.03	−0.09±0.05		0.03±0.02	−0.15±0.01	
14.0	0.07±0.03	0.0 ±0.05		−0.02±0.02	−0.16±0.02	−0.02±0.02
15.0	0.18±0.03	−0.12±0.06		0.01±0.02	−0.20±0.02	−0.03±0.02
			$^{56}Fe(\vec{p},\gamma_0)^{57}Co$			
8.0	0.27±0.06	0.03±0.12		0.08±0.05	−0.01±0.04	
9.0	0.07±0.04	−0.04±0.08		−0.05±0.03	−0.06±0.02	−0.03±0.02
10.0	0.08±0.03	0.24±0.06		0.05±0.02	−0.08±0.02	−0.02±0.02
11.5	0.03±0.03	0.20±0.05		−0.08±0.03	−0.09±0.02	
13.0	0.14±0.03	0.15±0.05		0.02±0.02	−0.22±0.02	−0.03±0.02
14.5	0.14±0.04	−0.34±0.08		0.10±0.03	−0.21±0.02	−0.04±0.02
			$^{58}Fe(\vec{p},\gamma_0)^{57}Co$			
7.6	0.19±0.05	0.19±0.09		0.04±0.03	−0.02±0.03	
9.2	0.12±0.04	0.28±0.07		0.01±0.03	−0.11±0.02	
9.6	0.04±0.04	0.26±0.07		0.06±0.02	−0.17±0.02	
10.5	0.12±0.04	0.15±0.06		0.04±0.02	−0.17±0.02	0.04±0.02
11.2	0.16±0.04	0.09±0.06		0.08±0.02	−0.18±0.02	
11.9	0.18±0.05	−0.14±0.09		0.03±0.03	−0.20±0.03	−0.04±0.03
12.7	0.13±0.05	−0.25±0.09		0.07±0.03	−0.23±0.02	
13.5[a]	0.08±0.09	−0.28±0.09	0.00±0.14	0.06±0.03	−0.22±0.02	
14.0[a]	0.14±0.09	−0.47±0.08	0.00±0.13	0.08±0.03	−0.20±0.02	−0.04±0.02
15.0[a]	0.08±0.10	−0.29±0.08	0.00±0.15	0.10±0.03	−0.23±0.02	−0.03±0.02

[a] The criterion of normalized χ^2 did not clearly indicate that a fit which included $P_3(\cos\theta)$ was statistically justified for these energies. The error given for a_1 and a_3 reflects this uncertainty.

REF. V. di Napoli, M.L. Terranova, H.G. de Carvalho, J.B. Martins, J.D. Pinheiro Filo and O.A.P. Tavares
J. Inorg. Nucl. Chem. 39, 1727 (1977)

ELEM. SYM.	A	Z
Co	59	27

METHOD

REF. NO. 77 Di 6 egf

REACTION	RESULT	EXCITATION ENERGY	SOURCE TYPE	SOURCE RANGE	DETECTOR TYPE	DETECTOR RANGE	ANGLE
G,2N	ABY	THR-999	C	300-999	ACT-I		4PI
G,3N	ABY	THR-999	C	300-999	ACT-I		4PI
G,4N	ABY	THR-999	C	300-999	ACT-I		4PI

999=1 GeV

Abstract—Cross sections per equivalent quantum, in the energy range 0.3–1.0 GeV, have been measured for $^{209}Bi(\gamma, 2n)$, $^{209}Bi(\gamma, 3n)$, $^{209}Bi(\gamma, 4n)$, $^{59}Co(\gamma, 2n)$, $^{59}Co(\gamma, 3n)$, $^{59}Co(\gamma, 4n)$ and $^{51}V(\gamma, 3n)$ reactions. From the calculated mean absolute cross sections and the data already available in literature for (γ, xn) reactions ($x \geq 1$), a cross section formula has been deduced which reproduces, within a factor of two, most of the experimental cross sections for target nuclei ranging between ^{9}Be and ^{238}U.

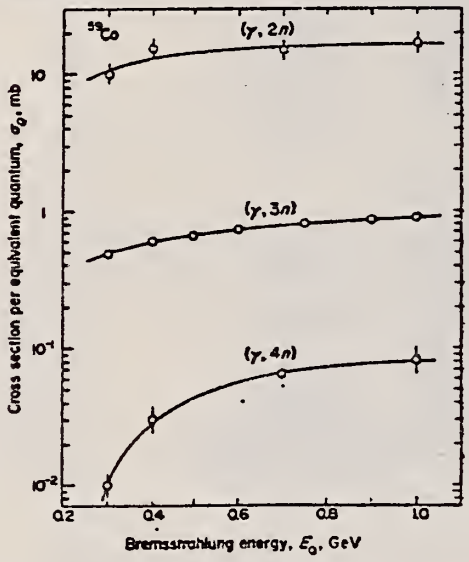

Fig. 2. Yields for the $^{59}Co(\gamma, xn)$ reactions ($1 < x < 5$). Smooth curves are drawn "by eye" through the experimental points.

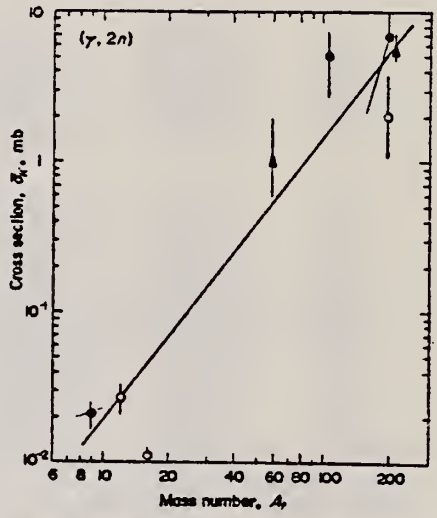

Fig. 4. Experimentally determined mean absolute cross sections, $\bar{\sigma}_{\gamma}$, for the $(\gamma, 2n)$ reactions vs the mass number, A_t, of the target nucleus. Filled circles are taken from our earlier experiments: ^{9}Be, Ref. [8]; ^{103}Rh, Ref. [4, 6]; ^{197}Au, Ref. [5]. Open circles: ^{12}C and ^{16}O, Ref. [16]; ^{197}Au, Ref. [15]. Filled triangles are the results of the present work for ^{59}Co and ^{209}Bi. The straight line is a least-squares fit of the experimental points.

REFERENCES

1. V. di Napoli, F. Salvetti, M. L. Terranova, H. G. de Carvalho, J. B. Martins and O. A. P. Tavares, *Gazz. Chim. Ital.* 105, 317 (1975). This review article reports all existing data in literature on cross-section of (γ, n) reactions in complex nuclei at intermediate energies.
3. V. di Napoli, F. Dobici, F. Salvetti and H. G. de Carvalho, *Nuovo Cimento* 48B, 1 (1967).
4. V. di Napoli, D. Margadonna, F. Salvetti, H. G. de Carvalho and J. B. Martins, *Lett. Nuovo Cimento* 1, 308 (1969).
5. V. di Napoli, A. M. Lacerenza, D. Margadonna, F. Salvetti, H. G. de Carvalho and J. B. Martins, *Lett. Nuovo Cimento* 1, 65 (1971).
6. C. Aurisicchio, V. di Napoli, F. Salvetti and M. L. Terranova, *Gazz. Chim. Ital.* 102, 378 (1972).
7. H. G. de Carvalho, J. B. Martins, O. A. P. Tavares, V. di Napoli, F. Salvetti, *Proceedings of the International Conference on Photonuclear Reactions and Applications*, Pacific Grove, Cal., Sect 8C5-1 (1973); V. di Napoli, J. B. Martins, G. Persichelli and M. L. Terranova, *Lett. Nuovo Cimento* 11, 179 (1974).
8. V. di Napoli, M. L. Terranova, H. G. de Carvalho and J. B. Martins, *Gazz. Chim. Ital.* 104, 463 (1974).
9. G. G. Jonsson and B. Forkman, *Nucl. Phys.* A107, 52 (1968).
10. G. G. Jonsson, B. Forkman and K. Lindgren, *Phys. Lett.* 26B, 508 (1968).
11. G. Andersson, B. Forkman and B. Friberg, Report LUNP 6901, Lund Institute of Technology, Lund University, p. 4, Sect. 8, 1969 (unpublished).
12. G. Andersson and B. Forkman, Annual Report, University of Lund, Lund Institute of Technology, p. 48, (1970) (unpublished).
13. G. G. Jonsson and B. Persson, *Nucl. Phys.* A153, 32 (1970).
14. J. Sternby, Report LUNP 7011, Lund Institute of Technology, Lund University, September 1970 (unpublished). Also quoted in G. G. Jonsson and K. Lindgren, *Phys. Scr.* 7, 49 (1973).
15. K. Lindgren and G. G. Jonsson, *Nucl. Phys.* A166, 643, (1971).
16. B. Johnsson, M. Nilsson and K. Lindgren, University of Lund Report LUNFD6/NFFR-3005/1-18/, LUTFD 6/(TFKF-3003/1-18/, October (1976).
17. I. Blomqvist, P. Janeček, G. G. Jonsson, R. Petersson, H. Dinter and K. Tesch, *Z. Physik* A278, 83 (1976).
18. B. Bülow, B. Johnsson, M. Nilsson and B. Forkman, *Z. Physik* A278, 89 (1976).

over

FORM NBS-418 (REV. 7-1-64) USCOMM-NBS-DC
OF COMMERCE OF STANDARDS

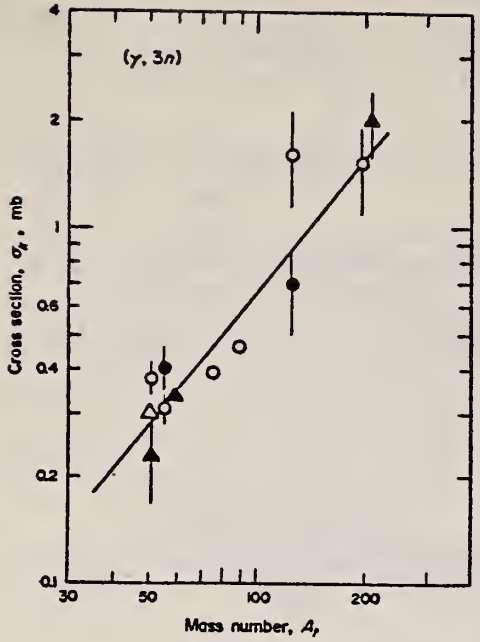

Fig. 5. The same as in Fig. 4 for the $(\gamma, 3n)$ reactions. Filled circles are taken from our earlier experiments: ^{55}Mn, Ref. [7]; ^{127}I, Ref. [3]. Open circles: ^{51}V, Ref. [17]; ^{55}Mn, Ref. [11]; ^{75}As, Ref. [12]; ^{89}Y, Ref. [14]; ^{127}I, Ref. [9, 10, 13]; ^{197}Au, Ref. [15]. Open triangle: ^{51}V, Ref. [18]. Filled triangles are the results of the present work for ^{51}V, ^{59}Co and ^{209}Bi. The straight line is a least-squares fit of the experimental points.

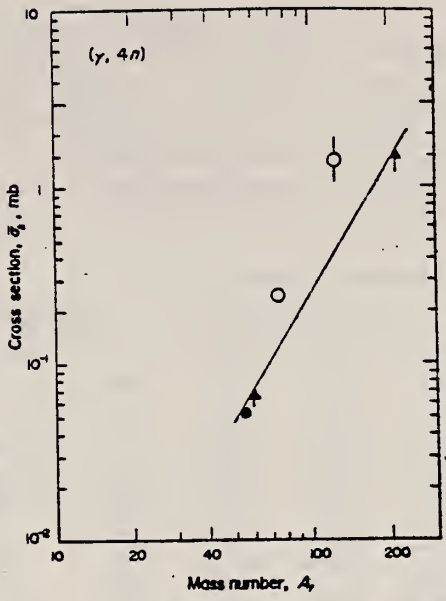

Fig. 6. The same as in Fig. 4 for the $(\gamma, 4n)$ reactions. Filled circle is taken from our earlier experiment: ^{55}Mn, Ref. [7]. Open circles: ^{75}As, Ref. [12]; ^{127}I, Ref. [9, 10,13]. Filled triangles are the results of the present work for ^{59}Co and ^{209}Bi. The straight line is a least-squares fit of the experimental points.

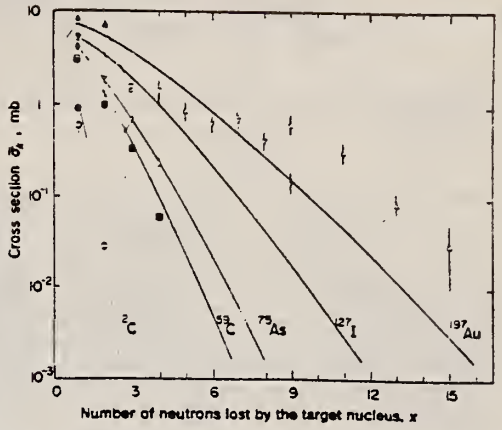

Fig. 7. Cross section distributions for the (γ, xn) reactions $(x \geq 1)$ at intermediate energies (0.2–1.0 GeV). Experimental data are taken from: filled circle: ^{12}C Ref. [1]; open circles: ^{12}C, Ref. [1, 16]; filled squares: ^{59}Co, this work and Ref. [1]; open square; ^{59}Co, Ref. [1]; filled rhomb: ^{75}As, Ref. [1]; open rhombs: ^{75}As, Ref. [12]; filled reversed triangles: ^{127}I, Ref. [1, 3]; open reversed triangles: ^{127}I, Ref. [1, 9, 10, 13]; filled triangles: ^{197}Au, Ref. [1, 5]; open triangles: ^{197}Au, Ref. [15]. The full lines represent the calculated cross section distributions according to eqn (12).

Table 2. Mean absolute cross sections for the (γ, xn) reactions, with $1 < x < 5$, in complex nuclei at intermediate energies.

Target nucleus	Reaction	Energy-range (GeV)	Ref.	Cross section, $\bar{\sigma}_x$(mb) (Experimental)	(Calc.†)
^{9}Be	$(\gamma, 2n)$	0.3–1.0	8	0.021 ± 0.002	0.007
^{12}C	$(\gamma, 2n)$	0.2–0.8	16	0.0277 ± 0.0004	0.025
^{16}O	$(\gamma, 2n)$	0.2–0.8	16	0.0113 ± 0.0003	0.072
^{51}V	$(\gamma, 3n)$	0.3–1.0	This work	0.23 ± 0.06	0.268
		0.25–0.60	17	0.38 ± 0.04	0.268
		0.25–0.80	18	0.307 ± 0.012	0.268
^{55}Mn	$(\gamma, 3n)$	0.3–1.0	7	0.41 ± 0.05	0.33
		0.3–0.8	11	0.311 ± 0.016	0.33
	$(\gamma, 4n)$	0.3–1.0	7	0.053 ± 0.004	0.079
^{59}Co	$(\gamma, 2n)$	0.4–1.0	This work	1 ± 1	1.3
	$(\gamma, 3n)$	0.3–1.0	This work	0.337 ± 0.007	0.4
	$(\gamma, 4n)$	0.3–1.0	This work	0.06 ± 0.01	0.1
^{75}As	$(\gamma, 3n)$	0.2–0.9	12	0.39	0.7
	$(\gamma, 4n)$	0.2–0.9	12	0.24	0.24
^{89}Y	$(\gamma, 3n)$	0.25–1.0	14	0.47	1.0
^{103}Rh	$(\gamma, 2n)$	0.4–0.9	4, 6	5.1 ± 2.4	2.7
^{127}I	$(\gamma, 2n)$	0.1–0.8	9	7.4‡	3.4
		0.3–1.0	3	20 ± 7	3.4
	$(\gamma, 3n)$	0.3–1.0	3	0.7 ± 0.2	1.9
		0.25–0.9	9, 10, 13	1.6 ± 0.5	1.9
	$(\gamma, 4n)$	0.25–0.9	9, 10, 13	1.4 ± 0.4	1.0
^{197}Au	$(\gamma, 2n)$	0.3–0.9	15	2 ± 2	5.2
		0.3–1.0	5	7 ± 5	5.2
	$(\gamma, 3n)$	0.3–0.9	15	1.5 ± 0.4	3.6
^{209}Bi	$(\gamma, 2n)$	0.3–1.0	This work	6 ± 1	5.5
	$(\gamma, 3n)$	0.3–1.0	This work	2.0 ± 0.4	3.8
	$(\gamma, 4n)$	0.3–1.0	This work	1.3 ± 0.2	2.5

†Calculated values according to eqn (12)
‡Deduced value from the interpolated σ_Q curve as indicated in Ref. [9].

REF. V. di Napoli, F. Salvetti, M. L. Terranova, H. G. de Carvalho, J. B. Martins, O. A. P. Tavares
J. Inorg. Nucl. Chem. 40, 175 (1978)

ELEM. SYM.	A	Z
Co	59	27

METHOD

REF. NO. 78Di12 hg

REACTION	RESULT	EXCITATION ENERGY	SOURCE TYPE	SOURCE RANGE	DETECTOR TYPE	DETECTOR RANGE	ANGLE
G,SPL	ABY	THR-999	C	300-999	ACT-I		4PI

Abstract—Cross sections per equivalent quantum, in the energy range 0.3–1.0 GeV, have been measured for spallation residuals from ^{51}V, ^{55}Mn, natural Fe, and ^{59}Co targets. Mean cross sections per photon have been deduced in this energy range and the data analysed in terms of charge-dispersion curves and mass-yield distributions. The mean cross sections per photon have also been compared with a semiempirical Rudstam's formula. A satisfactorily good agreement has been found with the calculated yields within a factor of two.

Table 5. Yields of radionuclides in units of μb per equivalent quantum. Cobalt target

Nuclide	E_0(GeV) 0.30	0.40	0.50	0.60	0.75	0.90	1.00
$^{24}_{11}$Na		2 ± 1	3 ± 1	5 ± 1	7 ± 1	8 ± 1	8 ± 1
$^{27}_{12}$Mg		3 ± 1	4 ± 1	6 ± 1	8 ± 1	9 ± 1	10 ± 1
$^{28}_{12}$Mg			0.5 ± 0.2	1.0 ± 0.3	1.4 ± 0.3	1.8 ± 0.3	2.0 ± 0.3
$^{28}_{13}$Al	50 ± 3	57 ± 3	64 ± 3	67 ± 3	72 ± 3	77 ± 4	80 ± 4
$^{29}_{13}$Al		5 ± 2	10 ± 3	12 ± 3	16 ± 3	18 ± 3	20 ± 3
$^{34m}_{17}$Cl		1 ± 1	5 ± 2	10 ± 3	15 ± 3	20 ± 3	20 ± 3
$^{38}_{17}$Cl		11 ± 5	20 ± 6	30 ± 6	35 ± 7	45 ± 7	40 ± 7
$^{39}_{17}$Cl	35 ± 2	40 ± 2	42 ± 2	45 ± 2	48 ± 3	50 ± 3	50 ± 3
$^{41}_{18}$Ar			2.5 ± 1.0	5.0 ± 1.5	9.6 ± 2.0	11.0 ± 2.0	10.0 ± 2.0
$^{42}_{19}$K	2 ± 1	2 ± 1	10 ± 5	20 ± 5	50 ± 15	70 ± 20	71 ± 20
$^{43}_{19}$K		2 ± 1	5 ± 2	10 ± 3	28 ± 5	30 ± 5	26 ± 5
$^{44}_{19}$K	2.0 ± 1.0	2.0 ± 1.0	5.0 ± 2.0	7.0 ± 3.0	9.0 ± 4.0	11.5 ± 4.0	12.0 ± 4.0
$^{45}_{19}$K	0.8 ± 0.4	1.1 ± 0.5	1.3 ± 0.5	1.5 ± 0.5	1.7 ± 0.5	1.9 ± 0.5	2.0 ± 0.5
$^{47}_{20}$Ca		0.5 ± 0.3	0.5 ± 0.3	1.5 ± 0.8	2.0 ± 0.8	3.0 ± 0.8	2.0 ± 0.8
$^{43}_{21}$Sc	10 ± 4	20 ± 5	40 ± 6	40 ± 6	56 ± 6	65 ± 6	72 ± 6
$^{44m}_{21}$Sc	120 ± 10	140 ± 10	150 ± 10	160 ± 10	190 ± 10	210 ± 10	220 ± 10
$^{44g}_{21}$Sc	130 ± 13	145 ± 13	160 ± 13	160 ± 13	190 ± 13	210 ± 13	210 ± 13
$^{46}_{21}$Sc	100 ± 30	140 ± 30	200 ± 40	260 ± 40	295 ± 40	335 ± 40	340 ± 40
$^{47}_{21}$Sc	63 ± 20	134 ± 20	130 ± 25	160 ± 30	190 ± 30	214 ± 30	228 ± 30
$^{48}_{21}$Sc	1.0 ± 0.5	7.0 ± 2.0	14.0 ± 3.0	19.0 ± 3.0	23.0 ± 3.0	28.0 ± 3.0	30.0 ± 3.0
$^{48}_{23}$V	300 ± 25	325 ± 25	350 ± 25	370 ± 25	390 ± 25	410 ± 25	420 ± 25
$^{48}_{24}$Cr	10.0 ± 2.5	11.5 ± 2.5	12.6 ± 2.5	13.5 ± 2.5	14.6 ± 2.5	15.6 ± 2.5	16.0 ± 2.5
$^{51}_{24}$Cr	126 ± 8	132 ± 8	136 ± 8	140 ± 8	144 ± 8	148 ± 8	150 ± 8
$^{51}_{24}$Cr	1600 ± 150	1700 ± 150	1800 ± 150	1800 ± 150	1900 ± 150	1960 ± 150	2000 ± 150
$^{52m}_{25}$Mn	280 ± 25	320 ± 25	320 ± 25	330 ± 25	340 ± 25	340 ± 25	350 ± 25
$^{52g}_{25}$Mn	260 ± 26	260 ± 25	300 ± 25	330 ± 25	300 ± 25	360 ± 25	360 ± 25
$^{54}_{25}$Mn	1200 ± 100	1400 ± 100	1500 ± 100	1600 ± 100	1780 ± 100	1850 ± 100	1900 ± 100
$^{52}_{26}$Fe	14.0 ± 0.8	14.5 ± 0.8	15.0 ± 0.8	15.0 ± 0.8	15.5 ± 0.8	15.8 ± 0.8	16.0 ± 0.8

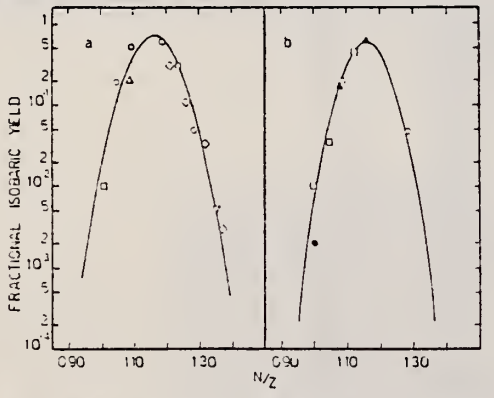

Fig. 3. The same as Fig. 2. ^{59}Co target. Graph (a): $42 \le A \le 48$; (b): $48 \le A \le 54$. The symbols are the same used in Fig. 2 plus ●. for Fe isotopes.

Fig. 1. Fractional isobaric yield vs the N/Z ratio for $42 \le A \le 48$. Mean cross sections per photon in the energy range 0.3–1 GeV. Graph (a): ^{51}V target; (b): ^{55}Mn target. The symbols are: □, for Cr; ○, for Sc; △, for V; ◇, for K; ▽, for Ca isotopes.

YLDS 24NA TO 52FE

Table 6. Mean cross sections in the energy range 0.3–1 GeV in units of μb

Produced radionuclide	Target nucleus: Vanadium Present work	Vanadium Bülow *et al.*[26]	Manganese	Iron	Cobalt
$^{24}_{10}$Ne	2.0 ± 0.4				
$^{22}_{11}$Na	16 ± 4				
$^{24}_{11}$Na	30 ± 2	18 ± 2	10 ± 1	10 ± 1	7 ± 1
$^{27}_{12}$Mg	22 ± 2	18 ± 3	9 ± 1	10 ± 1	8 ± 1
$^{28}_{12}$Mg	6 ± 1	6 ± 1	2.7 ± 0.5	2.7 ± 0.5	2.2 ± 0.3
$^{28}_{13}$Al	58 ± 7	59 ± 4	29 ± 4	35 ± 4	25 ± 3
$^{29}_{13}$Al	25 ± 4	32 ± 2	11 ± 2	15 ± 2	16 ± 3
$^{34m}_{17}$Cl	16 ± 2	14 ± 2	30 ± 4	30 ± 4	19 ± 3
$^{38}_{17}$Cl	75 ± 13	96 ± 5	45 ± 8	50 ± 8	37 ± 7
$^{39}_{17}$Cl	37 ± 7	35 ± 1	12 ± 2	19 ± 3	13 ± 2
$^{41}_{18}$Ar	65 ± 6	54 ± 2	35 ± 4	28 ± 3	12 ± 2
$^{42}_{19}$K	280 ± 50	243 ± 11	94 ± 17	80 ± 15	66 ± 12
$^{43}_{19}$K	128 ± 20	128 ± 4	43 ± 7	30 ± 5	28 ± 5
$^{44}_{19}$K	33 ± 12	30 ± 3	11 ± 4	10 ± 4	9.5 ± 4
$^{45}_{19}$K	12 ± 2	8 ± 1	1.0 ± 0.5	1.2 ± 0.5	1.0 ± 0.5
$^{47}_{20}$Ca	12 ± 4	15 ± 1	6.5 ± 2.4	6 ± 2	2.2 ± 0.8
$^{43}_{21}$Sc	104 ± 10	109 ± 6	72 ± 7	77 ± 8	52 ± 6
$^{44m}_{21}$Sc	260 ± 30	243 ± 14	115 ± 15	100 ± 12	84 ± 10
$^{44g}_{21}$Sc	230 ± 40	218 ± 13	116 ± 20	90 ± 16	71 ± 13
$^{46}_{21}$Sc	575 ± 100	605 ± 18	260 ± 45	214 ± 35	220 ± 40
$^{47}_{21}$Sc	457 ± 100	540 ± 33	200 ± 45	160 ± 30	127 ± 30
$^{48}_{21}$Sc	165 ± 15	138 ± 8	50 ± 5	30 ± 3	25 ± 3
$^{48}_{23}$V	210 ± 50	307 ± 12	200 ± 50	184 ± 45	100 ± 25
$^{48}_{24}$Cr	20 ± 10		7 ± 3	8 ± 4	5.0 ± 2.5
$^{49}_{24}$Cr	13 ± 5	16 ± 2	40 ± 15	64 ± 25	20 ± 8
$^{51}_{24}$Cr			480 ± 150	570 ± 150	330 ± 150
$^{52}_{25}$Mn				25 ± 5	
$^{52m}_{25}$Mn				75 ± 40	49 ± 25
$^{52g}_{25}$Mg				96 ± 40	84 ± 25
$^{54}_{25}$Mn				944 ± 300	584 ± 100
$^{52}_{26}$Fe					1.6 ± 0.8

Table 7. N/Z dispersion parameters of the mean cross sections per photon†

Target nucleus	Mass region	A_m	N/Z_p	Z_p	FWHM	ΔZ	Ref.
^{51}V	42–48	45	1.16	20.8	0.143	1.36	Present work
			1.16	20.8	0.142	1.37	[26]
			1.16	20.9	0.168	1.63	[35]
^{55}Mn	42–48	45	1.16	20.8	0.142	1.37	Present work
^{nat}Fe	42–48	45	1.16	20.8	0.140	1.35	Present work
	48–54	51	1.16	23.6	0.126	1.38	Present work
^{59}Co	42–48	45	1.16	20.8	0.141	1.36	Present work
	48–54	51	1.16	23.6	0.124	1.36	Present work

†A_m is the median mass of the mass region under consideration. N/Z_p is the neutron/proton ratio for the most probable nuclear charge Z_p of A_m. FWHM is the full width at half-maximum of the CD curves. ΔZ is the spread in Z as calculated from the FWHM for the two abscissas N/Z_1 and N/Z_2 (see also Refs. [26] and [35]).

REF. D.J.S. Findlay, D.J. Gibson, R.O. Owens, J.L. Matthews
Phys. Lett. 79B, 356 (1978)

ELEM. SYM.	A	Z
Co	59	27

METHOD

REF. NO. 78 Fi 7

REACTION	RESULT	EXCITATION ENERGY	SOURCE		DETECTOR		ANGLE
			TYPE	RANGE	TYPE	RANGE	
G,P	NOX	45-85	C	60-100	MAG-D		DST

Experimental data on the (γ, p) reaction at $E_\gamma = 60$–100 MeV for targets in the range $A = 7$–93 are compared with predictions based on a single-particle knock-out mechanism using shell model wavefunctions. The results show that this mechanism is more important than has generally been believed

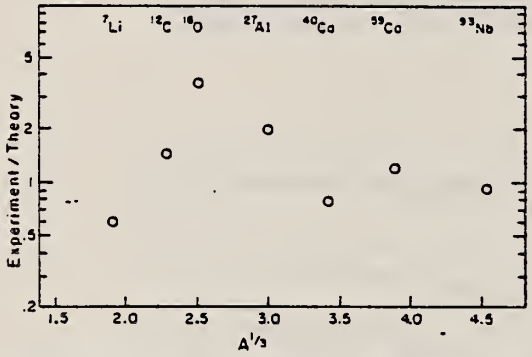

Fig. 2. The ratio of the measured photoproton emission populating low-lying states to the single-particle direct knock-out predictions is shown as a function of nuclear mass A for 80 MeV bremsstrahlung. Errors in the ratio, due to uncertainties in our calculations, are estimated to be a factor of ≈ 1.5. Errors in the experimental data are negligible.

REF. K. Masumoto, T. Kato, N. Suzuki
Nucl. Inst. Meth. 157, 567 (1978)

ELEM. SYM.	A	Z
Co	59	27

METHOD

REF. NO. 78 Ma 10 hg

REACTION	RESULT	EXCITATION ENERGY	SOURCE		DETECTOR		ANGLE
			TYPE	RANGE	TYPE	RANGE	
G,N	ABY	10-68	C	30-68	ACT-I		4PI
G,2N	ABY	19-68	C	30-68	ACT-I		4PI

Analysis is made of reactions interfering with photon activation analysis procedures.

The activation yield curves have been presented for a number of photonuclear reactions in the energy range from 30 to 68 MeV, in order to evaluate quantitatively the interferences due to competing reactions in multielement photon activation analysis. The general features of the yields as functions of both target mass number and excitation energy were elucidated from the data obtained, discussion being given on the results in terms of the reaction mechanism.

Simultaneous neutron activation due to appreciable neutron production from the converter and surrounding materials has also been studied, and, finally, the magnitudes of interferences in real multielement analysis were given in the form of their energy dependences.

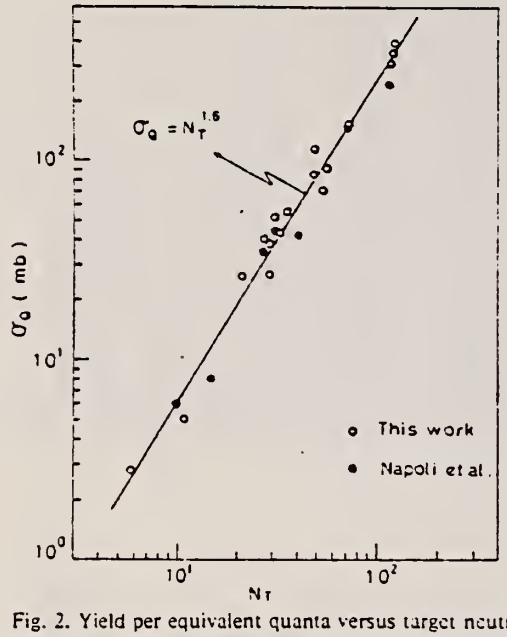

Fig. 2. Yield per equivalent quanta versus target neutron number.

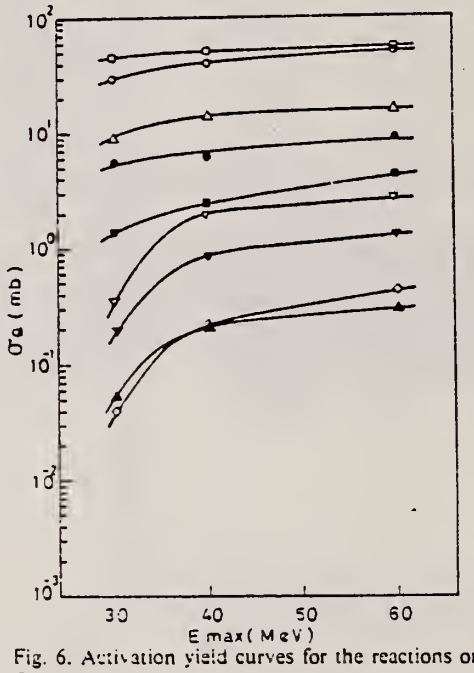

Fig. 6. Activation yield curves for the reactions on Co, Ni and Cu.
○ $^{59}Co(\gamma, n)^{58}Co$. ● $^{59}Co(\gamma, 2n)^{57}Co$. △ $^{58}Ni(\gamma, n)^{57}Ni$.
▽ $^{58}Ni(\gamma, pn)^{56}Co$. ▼ $^{60}Ni(\gamma, pn)^{58}Co$. ▲ $^{59}Ni(\gamma, 2n)^{56}Ni$.
□ $^{65}Cu(\gamma, n)^{64}Cu$. ■ $^{63}Cu(\gamma, 2n)^{61}Cu$. ◇ $^{63}Cu(\gamma, xn)^{53}Co$.

(over)

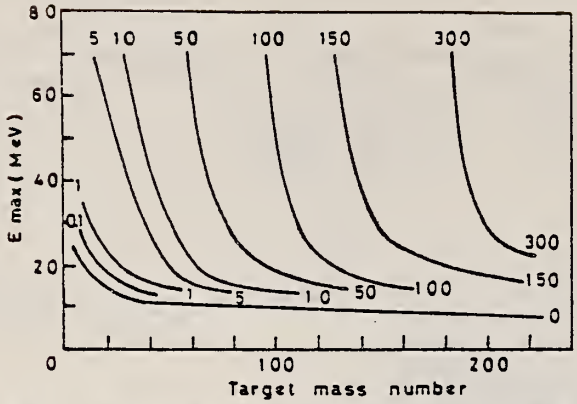

Fig. 9. Yields of the (γ, n) reactions as a function of bremsstrahlung maximum energy and target mass number. The numerical values in the figure are yields per equivalent quanta in mb.

REF. H. Tsubota, S. Oikawa, J. Uegaki and T. Tamas
Nucl. Phys. A303, 333 (1978)

ELEM. SYM.	A	Z
Co	59	27

METHOD

REF. NO. 78 Ts 1

REACTION	RESULT	EXCITATION ENERGY	SOURCE		DETECTOR		ANGLE
			TYPE	RANGE	TYPE	RANGE	
E,XP	ABX	15- 29	D	15- 29	MAG-D		90

Abstract: The differential cross sections of the (e, e'p) reactions for ^{51}V and ^{59}Co have been measured at 90° over the region of excitation corresponding to the electric giant dipole resonance. The (γ, p) cross sections of these nuclei were deduced from differential cross sections assuming isotropic angular distributions of protons. The results are compared with the (γ, n) cross sections, and are used to obtain strengths of the $T_<$ and $T_>$ giant dipole states separately by using the statistical theory. For each nucleus the ratio of the separated strengths and the splitting energy are consistent with those expected by the isospin formalism.

G,XP E1-VIRTUAL PHOT

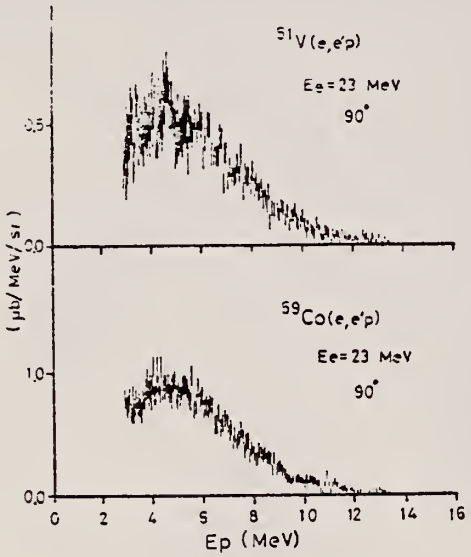

Fig. 2. Typical proton energy spectra of the (e, e'p) reactions of ^{51}V and ^{59}Co nuclei at 23.0 MeV of the incident electron energy.

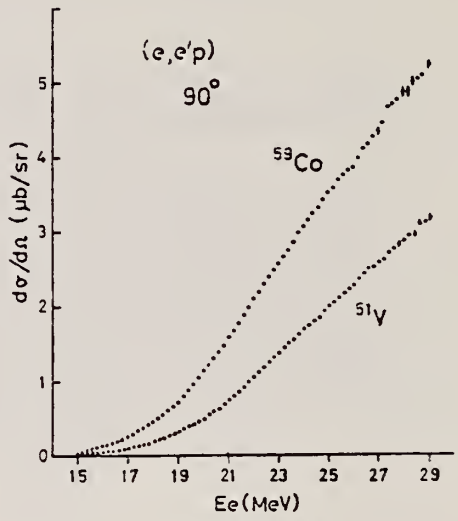

Fig. 3. Proton yield curves of the (e, e'p) reactions of ^{51}V and ^{59}Co nuclei at 90°.

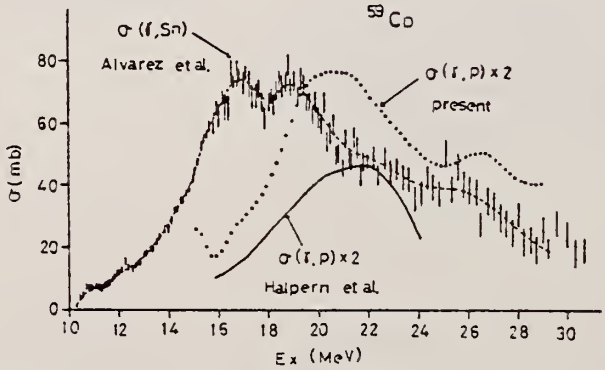

Fig. 6. Comparison between (γ, p) and (γ, Sn) cross sections of ^{59}Co (see the caption to fig. 5).

over

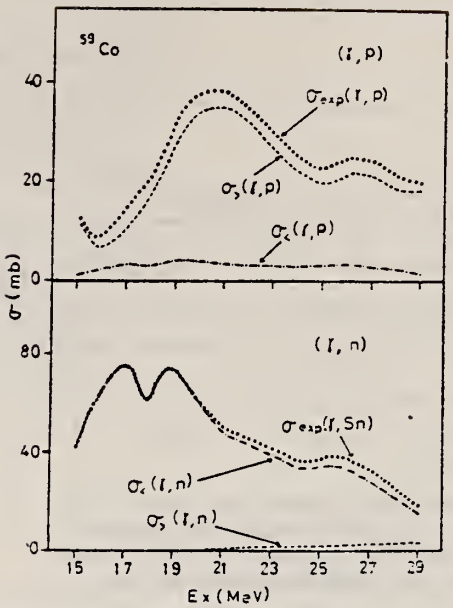

Fig. 9. Comparison between experimental cross sections and separated isospin components of ^{59}Co. Notations are explained in the text.

TABLE 2

Summary of the parameters obtained from the differential cross sections at 90° for ^{51}V and ^{59}Co

	Range of measurement (MeV)	$\int \frac{d\sigma(\gamma, p)}{d\Omega} dE$ (MeV · mb/sr)	$4\pi \int \frac{d\sigma(\gamma, p)}{d\Omega} dE$ (MeV · mb)
^{51}V	15.0–29.0	16.32 ± 1.39	205 ± 17
^{59}Co	15.0–29.0	28.10 ± 2.00	353 ± 25

REF. H.R. Weller, N.R. Roberson & S.R. Cotanch
Phys. Rev. C18, 65 (1978)

ELEM. SYM.	A	Z
Co	59	27

METHOD

REF. NO. 78 We 4 hmg

REACTION	RESULT	EXCITATION ENERGY	SOURCE		DETECTOR		ANGLE
			TYPE	RANGE	TYPE	RANGE	
$ P,G	RLX	14-23	D	7-15	UKN-D		DST

Analysis of data in reference 3.

POLARIZED PROTONS

Measurements of cross sections and analyzing powers are examined for polarized proton capture on ^{14}C, ^{30}Si, ^{54}Fe, ^{56}Fe, ^{58}Fe, ^{59}Co, and ^{88}Sr at energies which cover the giant dipole resonance region. These data are used to extract the relative amplitudes and phases of the contributing $E1$ T-matrix elements. A typical result exhibits two solutions. Calculations using the direct (or a direct-semidirect) capture model appear to provide a means for choosing the physical solution.

[NUCLEAR REACTIONS: $^{14}C(\vec{p},\gamma_0)$, $^{30}Si(\vec{p},\gamma_0)$, $^{54}Fe(\vec{p},\gamma_0)$, $^{56}Fe(\vec{p},\gamma_0)$, $^{58}Fe(\vec{p},\gamma_0)$, $^{59}Co(\vec{p},\gamma_0)$, $^{88}Sr(\vec{p},\gamma_0)$; measured $\sigma(\theta)$ and $A(\theta)$ over energy region of the giant dipole resonance. Deduced T-matrix amplitudes and phases. Compare results to direct-semidirect model calculations.]

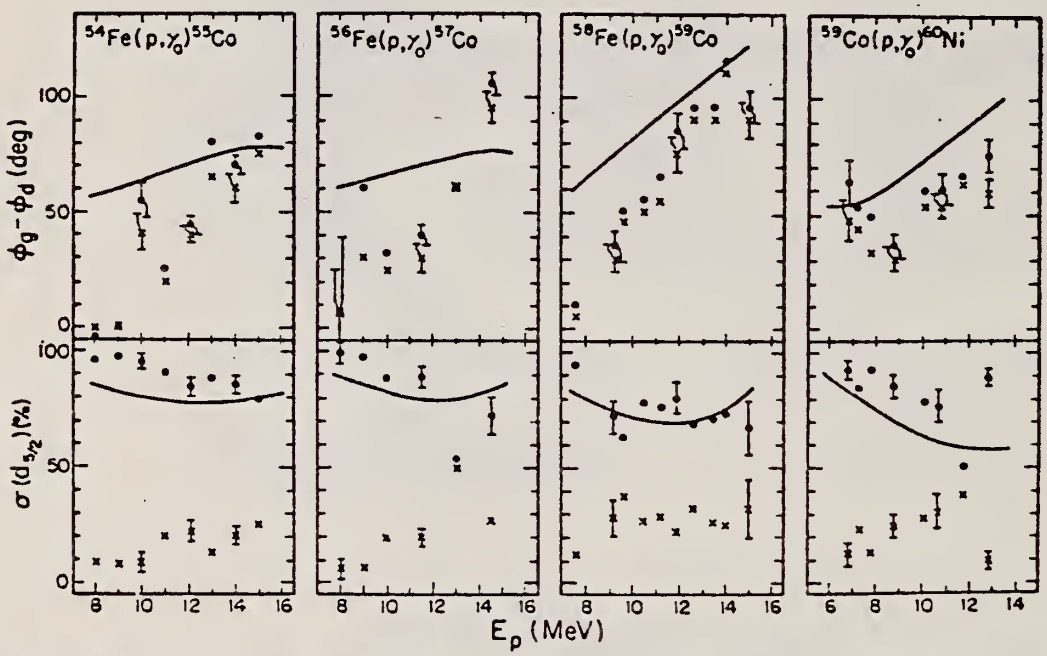

FIG. 2. Same as Fig. 1 for the target nuclei of ^{54}Fe, ^{56}Fe, ^{58}Fe, and ^{59}Co. The remaining cross section is due to the $s_{1/2}$ matrix element.

FIG. 1. The two solutions (dots and x's) resulting from a pure $E1$ analysis of the data are shown along with the results of the calculation for target nuclei of ^{14}C, ^{88}Sr, and ^{30}Si. The remaining cross section in the case of ^{14}C and ^{88}Sr is due to the $s_{1/2}$ matrix element. In the case of ^{30}Si it arises from the $p_{1/2}$ matrix element. The error bars represent typical statistical errors associated with the data points. The amplitudes are presented in terms of the percentage of the total cross section for which they are responsible. The curves represent DSD calculations as described in the text. The dashed curves in the case of ^{88}Sr were obtained using the optical model parameters of Ref. 16 while the solid lines were obtained from the parameters of Ref. 18.

(over)

[2]H. R. Weller, R. A. Blue, N. R. Roberson, D. G. Rickel, S. Maripuu, C. P. Cameron, R. D. Ledford, and D. R. Tilley, Phys. Rev. C 13, 922 (1976). (Note: an error exists in the sign of the phase in this paper. The quantity $\phi_s - \phi_d$ should be $\phi_d - \phi_s$ wherever it appears.)
[3]C. P. Cameron, N. R. Roberson, D. G. Rickel, R. D. Ledford, H. R. Weller, R. A. Blue, and D. R. Tilley, Phys. Rev. C 14, 553 (1976).
[4]C. P. Cameron, Ph.D. thesis, Duke University, 1976 (unpublished).
[5]R. D. Ledford, Ph.D. thesis, Duke University, 1976 (unpublished).
[6]J. D. Turner, C. P. Cameron, N. R. Roberson, H. R. Weller, and D. R. Tilley, Phys. Rev. C 17, 1853 (1978).

REF. R.A. Alvarez, B.L. Berman, D.D. Faul, F.H. Lewis, Jr., P. Meyer
Phys. Rev. C20, 128 (1979)

ELEM. SYM.	A	Z
Co	59	27

METHOD

REF. NO. 79 Al 2 hg

REACTION	RESULT	EXCITATION ENERGY	SOURCE		DETECTOR		ANGLE
			TYPE	RANGE	TYPE	RANGE	
G,1N	ABX	10-37	D	10-37	BF3-I		4PI
G,2N	ABX	19-37	D	17-37	BF3-I		4PI
G,3N	ABX	30-37	D	29-37	BF3-I		4PI

Data fits given use Lorentz Lines, Kerman & Quang, & Dynamic Collective Models

Photoneutron cross sections, including $\sigma[(\gamma,n)+(\gamma,pn)]$, $\sigma(\gamma,2n)$, and $\sigma(\gamma,3n)$, were measured for ^{55}Mn and ^{59}Co from threshold to 36.5 MeV, with a photon energy resolution which varied from 80 keV at the lowest to 170 keV at the highest energies measured. The source of radiation was the monoenergetic photon beam obtained from the annihilation in flight of fast positrons. The partial photoneutron cross sections were determined by neutron multiplicity counting, and the average neutron energies for $(\gamma,1n)$ and $(\gamma,2n)$ events were determined simultaneously with the cross-section data by the ring-ratio technique. The cross sections exhibit considerable but weak structure. Other nuclear information extracted from the data includes parameters of the giant dipole resonance, integrated cross sections and their moments, and nuclear symmetry energies. A comparison is made with previous experimental data for these nuclei as well as with theoretical predictions based upon hydrodynamic, vibrational, and dynamic collective models. None of these models fits the data for these odd-even nuclei satisfactorily; more theoretical work is needed for this nuclear mass region.

[NUCLEAR REACTIONS ^{55}Mn, ^{59}Co$(\gamma, n, 2n, 3n)$, $E_\gamma = 10-36.5$ MeV; measured 4π neutron yield, multiplicities, average energies for monoenergetic photons; $\sigma(E_\gamma, 1n)$, $\sigma(E_\gamma, 2n)$, $\sigma(E_\gamma, 3n)$, GDR parameters, integrated cross sections and moments, nuclear symmetry energies.]

TABLE II. Parameters of two-component Lorentz-curve fits to the GDR. The fitting interval used is 14 to 21 MeV.

Nucleus	$E_m(1)$ (MeV)	$\sigma_m(1)$[a] (mb)	$\Gamma(1)$ (MeV)	$E_m(2)$ (MeV)	$\sigma_m(2)$[a] (mb)	$\Gamma(2)$ (MeV)	χ^2
^{55}Mn	16.82 ±0.10	51.4 ±4.1	4.33 ±0.63	20.09 ±0.12	45.2 ±2.6	4.09 ±1.07	1.14
^{59}Co	16.43 ±0.08	28.3 ±5.4	2.73 ±1.08	18.66 ±0.25	58.4 ±4.4	7.38 ±0.79	1.11

[a] Uncertainties for σ_m given here are relative. The absolute uncertainties are 7%.

TABLE III. Integrated cross sections. $\sigma_{int}(\gamma,x)=\int\sigma(\gamma,x)dE_\gamma$, integrated from threshold to $E_{\gamma max}$.

Nucleus	$E_{\gamma max}$ (MeV)	$\sigma_{int}(\gamma,1n)$ (MeV-mb)	$\sigma_{int}(\gamma,2n)$ (MeV-mb)	$\sigma_{int}(\gamma,3n)$ (MeV-mb)	$\frac{\sigma_{int}(\gamma,2n)}{\sigma_{int}(\gamma,n_t)}$	$\frac{\sigma_{int}(\gamma,n_t)}{60NZ/A}$	$\frac{\frac{1}{2}\pi[\sigma_m(1)\Gamma(1)+\sigma_m(2)\Gamma(2)]}{60NZ/A}$
^{55}Mn	36.5	567	163	3	0.222	0.90	0.78
^{59}Co	36.5	653	150	4	0.186	0.92	0.91

TABLE IV. Integrated cross-section moments. $\sigma_{-1}=\int\sigma(\gamma,n_t)E_\gamma^{-1}dE_\gamma$ and $\sigma_{-2}=\int\sigma(\gamma,n_t)E_\gamma^{-2}dE_\gamma$, integrated from threshold to $E_{\gamma max}$.

Nucleus	σ_{-1} (mb)	$\sigma_{-1}A^{-1/3}$ (mb)	σ_{-2} (mb-MeV^{-1})	$\frac{\sigma_{-2}}{0.00225A^{5/3}}$	$\frac{\sigma_{-2}K}{0.05175A^{5/3}}$	$\frac{0.05175A^{5/3}}{\sigma_{-2}}$ (MeV)
^{55}Mn	36.4	0.174	1.93	1.08	0.91[a]	21.3
^{59}Co	40.1	0.174	2.14	1.06	0.90[a]	21.7

[a] The values used for the nuclear symmetry energy K are from Table VI.

(over)

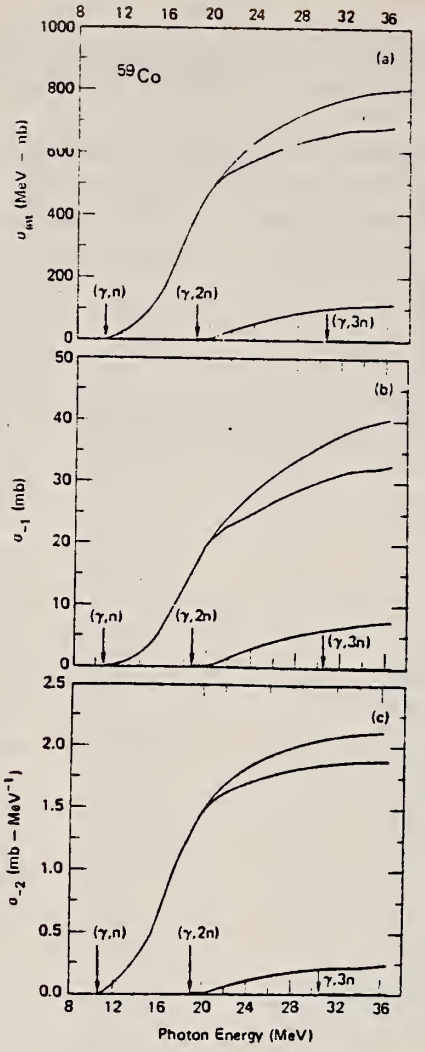

FIG. 5. Running sums of integrated cross sections for ^{59}Co: (a) σ_{int}; (b) σ_{-1}; (c) σ_{-2}.

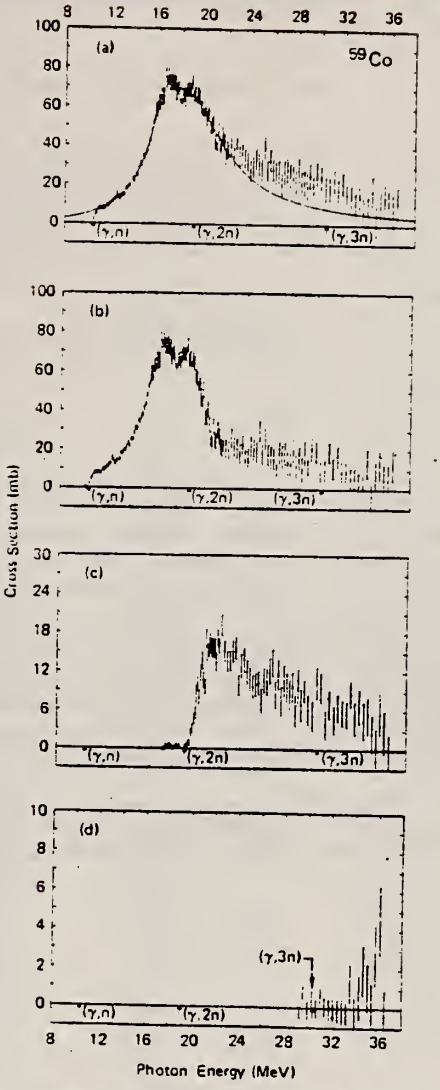

FIG. 3. Photoneutron cross sections for ^{59}Co: (a) $\sigma(\gamma, n_t)$, with a two-component Lorentz-curve fit; (b) $\sigma(\gamma, 1n)$; (c) $\sigma(\gamma, 2n)$; (d) $\sigma(\gamma, 3n)$.

Error bars show statistical uncertainties only.

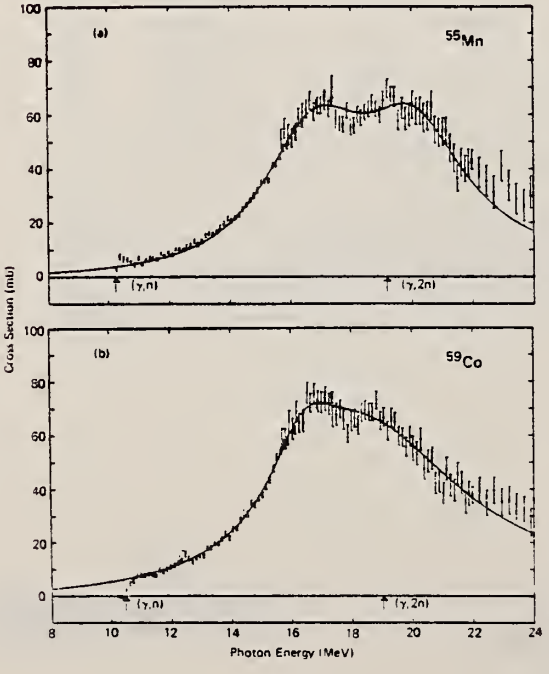

FIG. 6. Total photoneutron cross sections, with two-component Lorentz-curve fits: (a) for ^{55}Mn; (b) for ^{59}Co. Although the theoretical model is strictly valid only for $\sigma(\gamma, \text{tot})$, the curve shown here was scaled to fit the measured $\sigma(\gamma, n_t)$ data (see Sec. III B in the text and Table III).

Y. Cauchois, H. Ben Abdelaziz, R. Khérouf, C. Schloesing-Möller
J. Phys. G7, 1539 (1981)

ELEM. SYM.	A	Z
Co	59	27

METHOD

REF. NO. 81 Ca 2 hg

REACTION	RESULT	EXCITATION ENERGY	SOURCE TYPE	SOURCE RANGE	DETECTOR TYPE	DETECTOR RANGE	ANGLE
G,G	LFT	1 - 2	C	0 - 2	SCD-D		
		(1.099 - 1.481)					

1.10, 1.46, 1.48 MEV

Abstract. Lifetimes of 49 excited states below 1.65 MeV have been measured in ^{24}Mg, ^{27}Al, ^{48}Ti, ^{58}Ni, ^{59}Co, ^{61,62}Ni, ^{63,65}Cu, ^{64,66,68}Zn, ^{75}As, ^{103}Rh, ^{113,115}In, ^{116,118,120}Sn and ^{121,123}Sb by means of nuclear resonance fluorescence experiments. The levels are excited by bremsstrahlung x-ray photons. The self-absorption technique applied to suitable cases provides nuclear absorption cross sections, widths and lifetimes from which the x-ray spectral distributions are also obtained. Scattering experiments are performed for all other cases in order to obtain widths and lifetimes from these x-ray photon curves. The Compton effect in the sample is taken into account. Self-absorption provides $g\Gamma_0$ from which Γ is deduced using adopted J^π and Γ_0/Γ values; scattering provides $u = g(\Gamma_0^2/\Gamma)W(\theta)$ from which Γ is also deduced with J, Γ_0/Γ and mixing ratios taken from the literature. Thanks to simultaneous determination of the x-ray spectra all the lifetimes as given by our programs with their statistical errors form an unusually coherent set of values.

NUCLEAR REACTIONS (γ, γ'), bremsstrahlung excitation; natural isotopes; ^{24}Mg, ^{27}Al, ^{48}Ti, ^{58}Ni, ^{59}Co, ^{61,62}Ni, ^{63,65}Cu, ^{64,66,68}Zn, ^{75}As, ^{103}Rh, ^{113,115}In, ^{116,118,120}Sn and ^{121,123}Sb; $E \simeq 0.5$–1.65 MeV; measured $g\Gamma_0$ or $g(\Gamma_0^2/\Gamma)W(\theta)$; deduced $T_{1/2}$.

(OVER)

Tableau 3. Résultats des mesures des niveaux étudiés par diffusion.

Table 3. Results obtained using the diffusion method.

Isotope	Energie (keV)	J^π	J_0^π	Γ_0/Γ	δ	$u=g(\Gamma_0^2/\Gamma)W(\theta)$ (meV)	τ (ps) ce travail	τ_{ref} (ps)	Références†
^{24}Mg	1368.59(4)	2^+	0^+	1	E2	1,08(13)	1,76(21)	1,98(4)	Endt et van der Leun (1978)
^{27}Al	1014.45(3)	$\frac{1}{2}^+$	$\frac{5}{2}^+$	0.971	+0.351(12)	0,186(13)	2.20(16)	2.12(8)	Endt et van der Leun (1978)
^{48}Ti	983.512(3)	2^+	0^+	1	E2	0,282(23)	6,74(55)	6,1(13)	Been (1978)
^{58}Ni	1454.45(15)	2^+	0^+	1	E2	2,11(26)	0,90(11)	0.92(3)	Kocher et Auble (1976)
^{59}Co	1099,224(25)	$\frac{3}{2}^-$	$\frac{7}{2}^-$	1	(E2)	0,069(8)	4,79(55)	3,17(58)	Kim (1976)
^{59}Co	1458.8(3)	$\frac{1}{2}^-$	$\frac{7}{2}^-$	0.91	(E2)	0,68(8)	1,17(14)	1.52(16)	Kim (1976)
^{59}Co	1480.9(3)	$\frac{5}{2}^-$	$\frac{7}{2}^-$	0.8	$<0.35^a$	1,23(15)	0.254(31)	0,31(3)	Kim (1976)
^{61}Ni	1185.7(6)	$\frac{3}{2}^-$	$\frac{1}{2}^-$	$0.77(8)^i$	$\lvert 0.14\rvert$	1,88(49)	0,21(5)	0,16(3)	Andreev *et al* (1974)
^{62}Ni	1172,91(9)	2^+	0^+	1	E2	0.88(17)	2,15(42)	2.09(3)	Halbert (1979a)
^{63}Cu	1327.00(7)	$\frac{7}{2}^-$	$\frac{3}{2}^-$	0.84	(E2)	1,04(14)	0,84(11)	0.88(4)	Auble (1979b)
^{63}Cu	1412,05(4)	$\frac{5}{2}^-$	$\frac{3}{2}^-$	0.72	$+0.61\{^{+9}_{-8}\}$	0,260(38)	1,90(28)	1,61(3)	Auble (1979b)
^{64}Zn	991.54(7)	2^+	0^+	1	E2	0,640(54)	2,97(25)	2,60(13)	Halbert (1979b)
^{65}Cu	1481.83(5)	$\frac{7}{2}^-$	$\frac{3}{2}^-$	0,85	(E2)	1,13(19)	0,79(13)	0,49(5)	Auble (1975a)
^{66}Zn	1039,37(6)	2^+	0^+	1	E2	0,70(6)	2,71(23)	2.25(15)	Auble (1975b)
^{68}Zn	1077,38(5)	2^+	0^+	1	E2	0,70(6)	2,71(23)	2,34(23)	Lewis (1975)
^{75}As	572,5(10)	$\frac{5}{2}^-$	$\frac{3}{2}^-$	1[d]	0,39[b]	0,236(26)	4,14(46)	3,5(9)	Horen et Lewis (1975)
^{75}As	823,0(10)	$\frac{7}{2}^-$	$\frac{3}{2}^-$	0,86[d]	(E2)	0,214(22)	4,27(43)	3,5(3)	Robinson *et al* (1967)
^{75}As	865,5(10)	$\frac{5}{2}^+$	$\frac{3}{2}^-$	0,83[d]	—[c]	0,78(6)	0,863(68)	0,60(12)	Celliers *et al* (1977)
^{75}As	1076,0(10)	$\frac{7}{2}^-$	$\frac{3}{2}^-$	0,94[d]	0,38[d]	1,97(13)	0,287(19)	0,32(7)	Celliers *et al* (1977)
^{75}As	1128,5(10)	$\frac{1}{2}^+$	$\frac{3}{2}^-$	1	E1[d]	0,224(24)	1,47(16)	—	
^{75}As	1349.0(10)	$\frac{3}{2}^-$	$\frac{3}{2}^-$	0,67[d]	0.20[d]	1,61(29)	0,180(32)	0,12(3)	Wilson (1970)
^{75}As	1370.0(10)	$\frac{1}{2}^-$	$\frac{3}{2}^-$	0.47[d]	0,47[d]	0.64(13)	0,218(44)	—	
^{103}Rh	803.1(2)	$\frac{1}{2}^-$	$\frac{1}{2}^-$	0,70	M1	1,85(16)	0,174(15)	—	Harmatz (1979)
^{103}Rh	1277.0(2)	$\frac{3}{2}^-$	$\frac{1}{2}^-$	0.75	−0.62(30)[e]	0,81(9)	0,87(10)	1.3(9)	Harmatz (1979)
^{113}In	1177(1)	$\frac{11}{2}^+$	$\frac{9}{2}^+$	1	+0.5(2)	9,1(8)	0.086(8)	0,10(6)	Tuttle *et al* (1976)
^{113}In	1510(1)	$\frac{7}{2}^+$	$\frac{9}{2}^+$	0.935	$-0.5\{^{+11}_{-25}\}$	6,4(9)	0,071(10)	$0,11\{^{+41}_{-23}\}$	Tuttle *et al* (1976)
^{115}In	1077.7(10)	$\frac{5}{2}^+$	$\frac{9}{2}^+$	0.81[j]	(E2)	0.159(24)	1,61(24)	1,23(7)	Tuttle *et al* (1976)
^{115}In	1290.59(3)	$\frac{11}{2}^+$	$\frac{9}{2}^+$	0.98[j]	(E2)	1.31(11)	0.66(6)	0.55(4)	Tuttle *et al* (1976)
^{115}In*	1448.78(3)	$\frac{7}{2}^+$	$\frac{9}{2}^+$	0.86	−8[f]	0,90(11)	0.50(6)	0.52(20)	Tuttle *et al* (1976)
^{115}In	1486.1(1)	$\frac{9}{2}^-$	$\frac{9}{2}^+$	0,787	−0.8[f]	0,63(9)	0,63(9)	0.4(3)	Tuttle *et al* (1976)
^{115}In	1497.2(4)	$(\frac{5}{2}^+)$	$\frac{9}{2}^+$	<1	(E2)	1,33(16)	<0,30(4)	—	
^{115}In	1607.8(15)	$(\frac{5}{2}^+)$	$\frac{9}{2}^+$	⩽1	(E2)	1,54(24)	⩽0.26(4)	—	
^{116}Sn	1293.54(2)	2^+	0^+	1	E2	3,58(37)	0,53(6)	0.522(14)	Carlson *et al* (1975)
^{118}Sn	1229.64(4)	2^+	0^+	1	E2	2,75(28)	0.69(7)	0.67(2)	Carlson *et al* (1976)
^{120}Sn	1171.6(2)	2^+	0^+	1	E2	1.83(16)	1,04(9)	0,91(2)	Kocher (1976)
^{121}Sb	1023.5(10)	$\frac{7}{2}^+$	$\frac{5}{2}^+$	1	$\lvert 0.57\rvert$[g]	3.69(34)	0.228(21)	0.20(7)[h]	Tamura *et al* (1979)
^{121}Sb	1105.5(10)	$\frac{9}{2}^+$	$\frac{7}{2}^+$	0.4	—	0,47(4)	0.42(4)	—	
^{121}Sb	1142.5(10)	$\frac{9}{2}^+$	$\frac{5}{2}^+$	0.6	(E2)	0.85(8)	0,449(40)	0,41(8)[h]	Booth *et al* (1973)
^{121}Sb	1384.0(10)	$\frac{7}{2}^+$	$\frac{5}{2}^+$	1	$\lvert 0.45\rvert$[g]	4,7(5)	0.092(10)	0,088(14)[h]	Booth *et al* (1973)
^{123}Sb	1029.5(10)	$\frac{9}{2}^+$	$\frac{7}{2}^+$	1	$\lvert 0,57\rvert$[g]	2,96(27)	0,272(25)	0,26(4)[h]	Booth *et al* (1973)
^{123}Sb	1086.5(10)	$\frac{9}{2}^+$	$\frac{7}{2}^+$	1	$\lvert\delta\rvert > 1,26$[g]	1,06(9)	0,67(6)	0,72(15)[h]	Booth *et al* (1973)

† Références pour les colonnes 3, 4, 5, 6 et 9 de chaque ligne, sauf indication appelée au bas de ce tableau. Pour les autres données se reporter au texte.

Remarque. Pour calculer δ^2 quand nous ne disposons que de $B(E2)$, pour un mélange (E2) + (M1), nous déduisons $g\Gamma_0(E2) \propto B(E2)E_\gamma^5$; en admettant $W(\theta)=1$ et connaissant Γ_0/Γ, notre détermination de u donne une première approximation de $g\Gamma_0$ d'où une valeur de $\delta^2=(g\Gamma_0(E2))/(g\Gamma_0-g\Gamma_0(E2))$ qui permet d'améliorer $W(\theta)$ et $g\Gamma_0$ de proche en proche.

[a] Swann (1971); [b] Robinson *et al* (1967); [c] $W(\theta)=0.99$ calculé d'après la formule de Celliers *et al* (1977); [d] Abbondanno *et al* (1978); [e] Sayer *et al* (1972); [f] Tuttle *et al* (1976); [g] d'après $B(E2)$ de Barnes *et al* (1966); [h] calculé d'après Booth *et al* (1973); [i] Williams *et al* (1975); [j] Dietrich *et al* (1970).

REF. W.R. Dodge, R.G. Leicht, E. Hayward, E. Wolynec
Phys. Rev. C24, 1952 (1981)

ELEM. SYM.	A	Z
Co	59	27

METHOD

REF. NO. 81 Do 2 hg

REACTION	RESULT	EXCITATION ENERGY	SOURCE		DETECTOR		ANGLE
			TYPE	RANGE	TYPE	RANGE	
E,P	ABX	7-100	D	16-100	MAG-D		DST
E,A	ABX	7-100	D	16-100	MAG-D		DST

The (e,p) and (e,α) cross sections for ^{56}Fe, ^{59}Co, and ^{64}Zn have been measured in the electron energy range 16—100 MeV. They have been analyzed using the distorted-wave Born approximation $E1$ and $E2$ virtual photon spectra. The $E1$ and $E2$ components in the proton and α channels have been obtained.

VIRT PHOTON ANAL

NUCLEAR REACTIONS ^{56}Fe(e,p), ^{56}Fe(e,α), ^{59}Co(e,p), ^{59}Co(e,α), ^{64}Zn(e,p), and ^{64}Zn(e,α); measured $\sigma(E_0,E_x,34°)$, $\sigma(E_0,E_x,48°)$, $\sigma(E_0,E_x,62°)$, $\sigma(E_0,E_x,90°)$, $\sigma(E_0,E_x,118°)$; $\sigma(E_0,E_x,132°)$; obtained $\sigma(e,p)$, $\sigma(e,\alpha)$; deduced $\sigma_{\gamma,p}^{E1}(E)$, $\sigma_{\gamma,p}^{E2}(E)$, $\sigma_{\gamma,\alpha}^{E1}(E)$, $\sigma_{\gamma,\alpha}^{E2}(E)$.

[13]Y. -W., Lui, P. Bogucki, J. D. Bronson, U. Garg, C. M. Rozsa, and D. H. Youngblood, Phys. Lett. 93B, 31 (1980).

[14]S. Costa, F. Ferrero, S. Ferroni, C. Molino and R. Malvano, Phys. Lett. 11, 324 (1964). 64 Co 2

TABLE III. Percentage of the $E2$ sum when only points up to 50 MeV ($E_0=50$ MeV) and when all measured points ($E_0=100$ MeV) are considered in the analysis. The bremsstrahlung cross section used is DBM. $E2$ sum: $0.22Z^2A^{-1/3}$ μb/MeV.

Nucleus	Reaction	Without size effect $E_0=50$ MeV	Without size effect $E_0=100$ MeV	With size effect $E_0=50$ MeV	With size effect $E_0=100$ MeV
^{56}Fe	(e,α)	9± 3	3 ± 1	11± 3	7± 1
	(e,p)	47±30	8±11	61±32	37±15
^{59}Co	(e,α)	7± 2	4 ± 1	8± 2	5± 1
	(e,p)	32±22	4± 8	48±24	28±11
^{64}Zn	(e,α)	26± 6	12± 2	32± 6	25± 3
	(e,p)	29±43	26±15	56±46	77±21

TABLE IV. Percentage of the $E1$ and $E2$ sums in the α and proton channels. $E1$ sum: $60NZ/A$ MeV mb. $E2$ sum: $0.22Z^2A^{-1/3}$ μb/MeV. Integrals to 100 MeV.

Nucleus	Reaction	$E1$ Schiff	$E1$ DMB	$E2$ Schiff	$E2$ DBM
^{56}Fe	(e,α)	5± 1	6± 1	10± 1	7± 1
	(e,p)	67±20	82±19	82±14	37±15
	$(e,\alpha)+(e,p)$	72±20	88±19	92±14	44±15
^{59}Co	(e,α)	5± 1	7± 1	8± 1	5± 1
	(e,p)	52±10	67±12	63±10	28±11
	$(e,\alpha)+(e,p)$	57±10	74±12	71±10	33±11
^{64}Zn	(e,α)	16± 4	18± 4	33± 3	25± 3
	(e,p)	129±28	154±30	137±30	77±21
	$(e,\alpha)+(e,p)$	145±28	172±30	170±20	102±21

OVER

TABLE VI. $E1$ strength integrated up to 30 MeV.

Nucleus	$\int_0^{30} \sigma_{\gamma,x}(E)dE$ (MeV mb)				Fraction
	α	p	n	Total	of $E1$ sum
^{56}Fe	18± 3	256±26	735[a]	1009	1.21
^{59}Co	15± 2	211±22	884[b]	1110	1.26
^{64}Zn	66±14	545±75	616[b]	1227	1.28

[a]Reference 13.
[b]Reference 14.

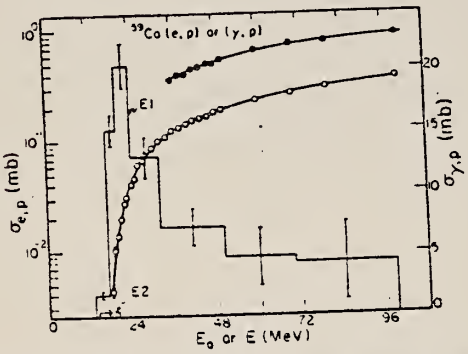

FIG. 4. The $\sigma_{e,p}(E_0)$ for ^{59}Co. See caption of Fig. 3.

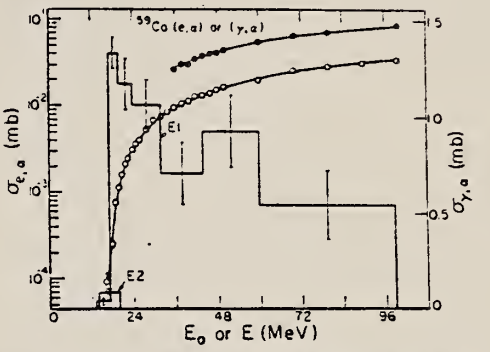

FIG. 7. The $\sigma_{e,\alpha}(E_0)$ for ^{59}Co. See caption of Fig. 3.

FIG. 3. The measured $\sigma_{e,p}(E_0)$ for ^{56}Fe as a function of total incident electron energy E_0 (open circles). The full circles represent the yield $Y_{e,p}(E_0)$ obtained when a 0.217 g/cm^2 tantalum foil was placed in the electron beam ahead of the target. The smooth curves are the best fits to the data and were obtained by combining the histograms representing the $E1$ and $E2$ (γ,p) cross sections (right-hand scale) in Eqs. (1) and (2) with the $E1$ and $E2$ DWBA virtual photon spectra and by making use of the DBM bremsstrahlung cross section. The size effect correction described in the text has been applied to the virtual photon spectra.

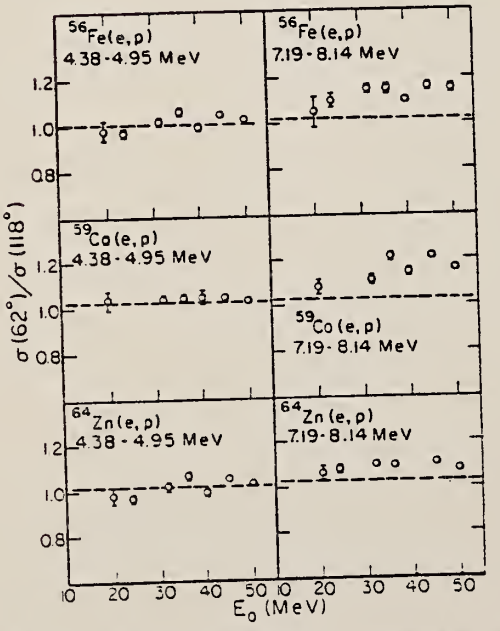

FIG. 9. The ratios of the number of protons observed in the indicated energy bite ΔT_p at 62° to the same number observed at 118°, $\sigma(62°)/\sigma(118°)$, as a function of incident electron energy.

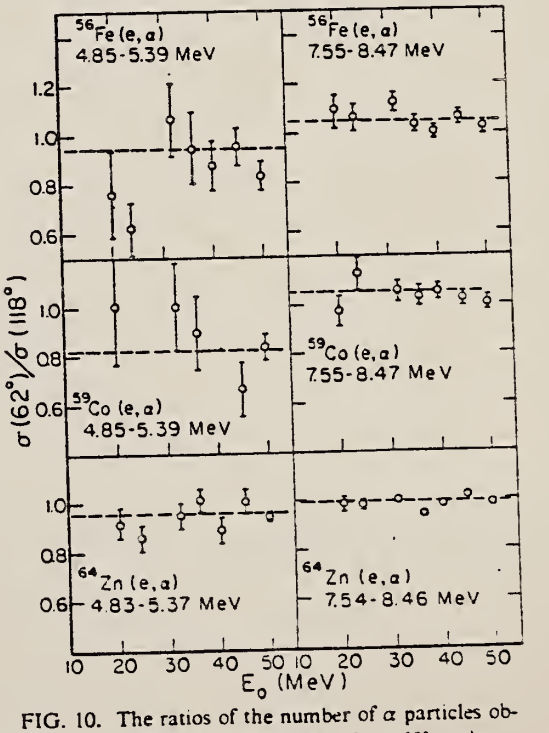

FIG. 10. The ratios of the number of α particles observed in the indicated energy bite ΔT_α at 62° to the same number observed at 118°, $\sigma(62°)/\sigma(118°)$, as a function of incident electron energy.

Co
A=60

Co
A=60

Co
A=60

REF. O. A. Wasson, M. R. Bhat, R. E. Chrien, M. A. Lone, and M. Beer
Phys. Rev. Letters 17, 1220 (1966)

ELEM. SYM.	A	Z
Co	60	27

METHOD

REF. NO.	
66 Wa 2	EGF

REACTION	RESULT	EXCITATION ENERGY	SOURCE		DETECTOR		ANGLE
			TYPE	RANGE	TYPE	RANGE	
N,G	RLX	7	D	0	SCD-D	5-3	45
		(7.49)					

$\sigma_{n\gamma_1}$ = Ground-state capture γ's for 3-500 eV neutrons.

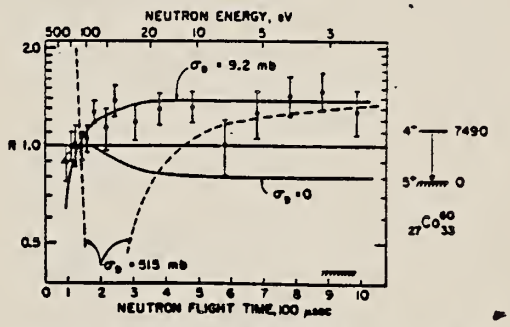

FIG. 2. The energy variation of $R \propto \sigma_{n\gamma_1}/\sigma_{n\gamma}$ for the ground-state transition. The curve $\sigma_D = 0$ would be the expected variation after correction for the presence of the 3^- bound state, with no interference assumed between the resonance and direct reaction amplitudes. The curves $\sigma_D = 9.2$ mb and $\sigma_D = 515$ mb result from constructive and destructive interference below the 132-eV resonance.

DEFINITIONS OF ABBREVIATIONS AND SYMBOLS

Note: In this list definitions are given for various photoneutron reactions in which the following symbols are used: N, NL, nN, SN and XN. Corresponding definitions apply for reactions involving other nuclear particles where the symbols N (neutron) is replaced by, e.g. P, D, T, HE, A etc. Where unknown reactions result in the production of a specific radionuclide, the chemical symbol and mass number is listed as the reaction product, e.g. a G,NA22 reaction in ^{59}Co.

A	alpha particle
ANAL	analysis
ABI	absolute integrated cross-section data
ABX	absolute cross-section data
ABY	absolute yield data. Often means cross-section per equivalent quantum is listed.
ACT	measurement of induced radioactivity of the target
ASM	asymmetric, asymmetry
AVG	average
BBL	bubble chamber
BEL B(EL)	reduced electric radiative transition probability
BF3	BF_3 neutron counter with moderator e.g., Halpern detector, long counter
BML	reduced magnetic radiative transition probability, B(ML)
BREAKS	levels located by "breaks" in the yield curve
BRKUP	breakup
BRMS	bremsstrahlung
BTW	between
C	continuous. Used to describe a photon source or a detector response function. Contrast with D = discrete.
CCH	cloud chamber
CF	compared with
CHRGD	charged
CMPT	Compton
COIN COINC	coincidence, coincide
COH	coherent
CK	Cerenkov
D	deuteron or discrete. When discrete, it is used to describe a photon source or a detector response function. Contrast with C = continuous.
DLTE	energy loss
DLTQ	momentum transfer
DST	distribution
DT BAL	detailed balance
E	electron
E/	inelastically scattered electron
E+	positron
EDST	energy distribution or spectrum
E/N	used only to indicate a coincidence experiment as in (E,E/N).

	N stands for any outgoing particle measured in coincidence with an inelastically scattered electron. Distinguish from eg., (E,N) which is used to represent an electron induced reaction when only the outgoing particle N is detected.
EMU	emulsions (photographic plates)
EXCIT	excited
F	fission
FMF	form factor
FM-1	inverse femtometers
FRAG	fragment
G	photon
G/	inelastically scattered photon
G-WIDTH	gamma-ray transition width
HAD	hadrons, hadron production
HE He3	^{3}He particle
INT	interaction, integral, intensity
INC	includes
ION	ionization chamber
ISOB	isobaric
ISM	isomer
J	multiplicity of particle defined by following symbol e.g. (G,PJN) with remark J = 2,3,5,7
JPI J-PI	spin and parity of a nuclear state
K	second multiplicity index, e.g. (G,JPKN) with both J & K positive integers greater than 1
KE	kinetic energy
L	may be an integer or zero that always follows a reaction product symbol. This is used to indicate transitions to specific states in the residual nuclide. When the letter is used as in (G,NL) the cross section given is that for the sum of transitions to two or more specific final states.
LFT	excited state lifetime
LIM	limit
LV,LVS	level, levels
LQD	liquid
MAG	magnetic spectrometer
MEAS	measurement(s)
MGC	magnetic Compton spectrometer
MGP	magnetic pair spectrometer
MOD	moderated neutron detector <u>not</u> employing a BF_3 counter, e.g. rhodium foil, Szilard-Chalmers reaction, ^{3}He, ^{6}Li reactions, GD loaded liquid scintillator, etc.
MSP	mass spectrometer
MULT	multiple, multipole, multiplicity
MU-T	used only in combination with G to indicate a total photon absorption cross section measurement, i.e. (G,MU-T)
N	neutron (see also XN and SN). The notation (G,N) is used to indicate a reaction in which only a single neutron is emitted, i.e. the reaction that can, in many cases, be measured by observing the radioactive decay of the residual nuclide.

nN	where n is any integer. (G,nN) indicates the sum over all reaction cross sections in which n neutrons are emitted.
NAI	NaI(Tl) spectrometer
NEUT	neutron(s)
NOX	no cross-section data
P	proton (see also XP)
PART	particle(s)
PHOT	photon(s)
PI	pion, usually written as PI+, PI-, PIO to indicate charge
POL	polarized or polarization
Q-SQUAR	momentum transfer squared (q^2)
RCL	recoil
REL	relative
RLI	relative integrated cross-section data
RLX	relative cross-section data
RSP	reaction spectrometer
RLY	relative yield data
SCTD	scattered
SCD	semiconductor (solid state) detector
SCI	scintillator detector other than NaI, e.g., CsI, KI, organic (liquid or solid), stilbene, He
SEP	separation
SEP ISOTP	separated isotope used
SIG	SIGMA (cross section)
SN	sum of neutron producing reactions, $\sigma(\gamma,SN)=\sigma(\gamma,N) + \sigma(\gamma,NP) + \sigma(\gamma,2N) + \sigma(\gamma,3N)$ + etc.
SPC	photon or particle energy spectrum
SPK	spark chamber
SPL	spallation
STAT	statistical
SYM	symetric, symmetry
T	triton
TEL	counter telescope
THR	threshold for reaction or threshold detector, e.g., $^{29}Si(n,p)^{29}Al$.
TOF	time-of-flight detector
TRK	tracks of particles or fragments observed in solid materials (glass, mylar, etc.)
TRNS	transition
UKN UNK	unknown
VIB	vibrational
VIR PHOT	virtual photon(s)
XN	all neutrons, total neutron yield, $\sigma(\gamma,XN) = \sigma(\gamma,N) + 2\sigma(\gamma,2N) + 3\sigma(\gamma,3N) + \sigma(\gamma,NP)$ + etc.
XP	all protons, total proton yield $\sigma(\gamma,XP) = \sigma(\gamma,P) + \sigma(\gamma,NP) + 2\sigma(\gamma,2P)$ + etc.
XX XXX	reaction products defined in REMARKS
YLD	yield

4PI	a 4π geometry was used or a method like radioactivity or a total absorption measurement		products was determined. The polarized particle is indicated in REMARKS.
999	energy defined in REMARKS	* or @	symbols used to indicate that the units associated with the numerals on one or both sides of the symbol in a specific column are not MeV. The units are defined in REMARKS.
$	indicates the measurement involved beams or targets that were either polarized or aligned, or that the polarization of the reaction		

NBS-114A (REV. 2-8C)

U.S. DEPT. OF COMM. BIBLIOGRAPHIC DATA SHEET (See instructions)	1. PUBLICATION OR REPORT NO.	2. Performing Organ. Report No.	3. Publication Date

4. TITLE AND SUBTITLE

Photonuclear Data-Abstract Sheets
1955-1982

5. AUTHOR(S)

E.G. Fuller and Henry Gerstenberg

6. PERFORMING ORGANIZATION (If joint or other than NBS, see instructions)

NATIONAL BUREAU OF STANDARDS
DEPARTMENT OF COMMERCE
WASHINGTON, D.C. 20234

7. Contract/Grant No.

8. Type of Report & Period Covered

9. SPONSORING ORGANIZATION NAME AND COMPLETE ADDRESS (Street, City, State, ZIP)

10. SUPPLEMENTARY NOTES

☐ Document describes a computer program; SF-185, FIPS Software Summary, is attached.

11. ABSTRACT (A 200-word or less factual summary of most significant information. If document includes a significant bibliography or literature survey, mention it here)

These abstract sheets cover most classes of experimental photonuclear data leading to information of the electromagnetic matrix element between the ground and excited states of a given nucleus. This fifteen volume work contains nearly 7200 abstract sheets and covers 89 chemical elements from hydrogen through americium. It represents a twenty-seven year history of the study of electromagnetic interactions. The sheets are ordered by target element, target isotope, and by an assigned bibliographic reference code. Information is given on the type of measurement, excitation energies studied, source type and energies, detector type, and angular ranges covered in the measurement. For a given reference, the relevant figures and tables are mounted on a separate sheet for each nuclide studied.

12. KEY WORDS (Six to twelve entries; alphabetical order; capitalize only proper names; and separate key words by semicolons)

data-abstract sheets, elements, experimental, isotopes, nuclear physics, photonuclear reactions

13. AVAILABILITY

☐ Unlimited

☒ For Official Distribution. Do Not Release to NTIS

☐ Order From Superintendent of Documents, U.S. Government Printing Office, Washington, D.C. 20402.

☐ Order From National Technical Information Service (NTIS), Springfield, VA. 22161

14. NO. OF PRINTED PAGES

15. Price